UNIVERSITAT de
BARCELONA

NMDA receptor mutations associated with neurodevelopmental disorders: pathophysiological impact and personalized pharmacotherapy

Ana Santos Gómez

UNIVERSITAT de BARCELONA

Programa de Doctorat en Biomedicina de la Universitat de Barcelona

Tesis doctoral:

NMDA receptor mutations associated with neurodevelopmental disorders: pathophysiological impact and personalized pharmacotherapy

Presentada por:

Ana Santos Gómez

2017-2020

iGluRs lab
Neuropharmacology and pain
IDIBELL

2020-2021
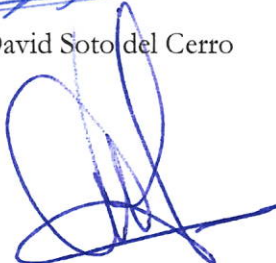
Neurophysiology
Biomedicine
Universitat de Barcelona

Directores de Tesis:

Dr. Xavier Altafaj Tardío

Dr. David Soto del Cerro

Tutor:

Francisco Ciruela Alférez

Doctorando:

Ana Santos Gómez

Founding

The studies presented in this thesis were supported by the PhD fellowship 'Tatiana Pérez de Gúzman el Bueno'.

FUNDACIÓN
TATIANA PÉREZ DE GUZMÁN EL BUENO

These studies were supported by the Spanish and European communities of GRD individuals and their families (Asociación Española de Grinpatías' and '*GRIN2B* Europe')

These studies were conducted in the iGluRs (Ionotropic glutamate receptors) lab, Genetic department, Neuropharmacology and Pain Unit, (IDIBELL, Universitat de Barcelona, L'Hospitalet de Llobregat) from 2017 to 2020; and Neurophisiology Unit, Biomedicine Departament (IDIBAPS, Medicine Faculty, Universitat de Barcelona) from 2020 to 2021.

Acknowledgements
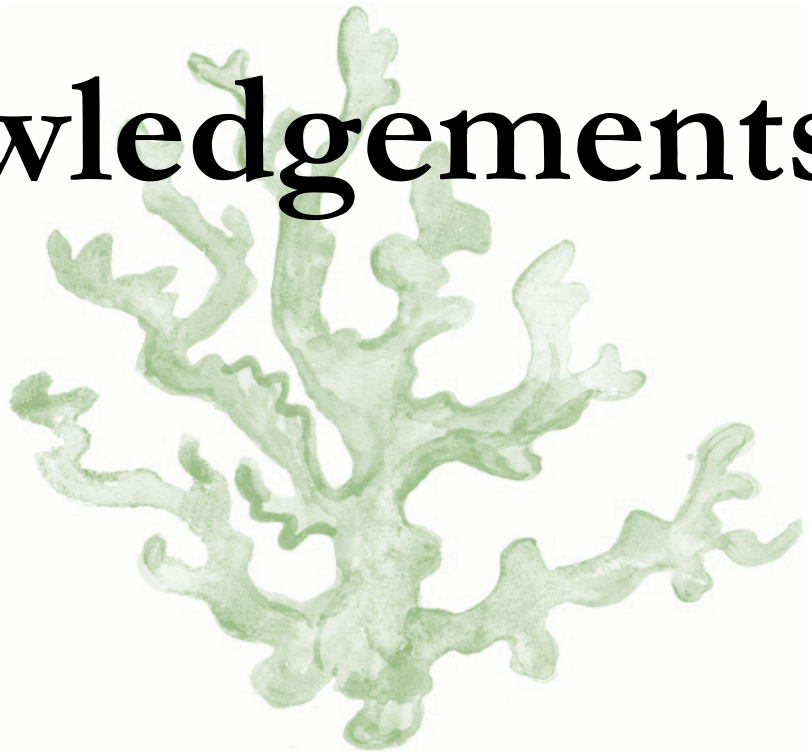
Bueno, la parte de la tesis que más curiosidad le causa al público general. Quiero decir que he intentado acordarme de todo el mundo que ha contribuido de una u otra forma a que esto saliera adelante, pero escribo estos agradecimientos después de un mes intensivo escribiendo la tesis a contrarreloj y con un poco de falta de sueño, así que pido perdón de antemano si alguien siente que debería estar aquí y no está.

En primer lugar, gracias a los miembros de la Fundación Tatiana Pérez de Guzmán por escuchar a esa chiquilla hace cuatro años y darle la oportunidad de recorrer este camino que me he transformado en la persona que soy hoy.

También gracias a las fundaciones de pacientes. El proyecto de esta tesis es fascinante, no cabe duda, pero el haber tenido contacto cercano con vosotros, y el hecho de que pusiera caras y nombres a tantas de las variantes, me ha motivado a intentar dejarme la piel en el proyecto para poder aportar lo máximo posible y ayudar, aunque solo sea un poco. Así que esta tesis va por vosotros.

Luego me gustaría dar las gracias a los miembros del tribunal. Sé como funciona la ciencia y lo liados que iréis, pero gracias por aceptar sin dudarlo y por formar parte de una parte tan importante del proceso, como es la lectura de la tesis. Espero que disfrutéis de lo que hay aquí escrito.

Gracias a mis codirectores, Xavier Altafaj y David Soto agradecerles el esfuerzo titánico que han tenido que hacer en estos meses finales, que se que ha sido una época complicada de mucho trabajo y circunstancias excepcionales que han dificultado un poco todo el proceso. A Xavi agradecerle que me abriera las puertas del iGluRs lab. Creo que llegué siendo una persona y me voy siendo una persona totalmente distinta, y es que esa cabeza caótica tuya ha hecho que tuviera que adquirir habilidades de superhéroe, pero también tu cercanía y tu confianza ha hecho que seas un gran apoyo en un camino tan duro como es este. Gracias también por tu motivación por los *GRIN* que han hecho que este proyecto se enriquezca tanto. A David darle las gracias por llegar en esta etapa final, porque el team Pili y Mili funciona mejor así que por separado. Gracias también por haberme apoyado y animado tanto, definitivamente, has sido la mamá de esta tesis.

Gracias a mi grupo burbuja. Cuando tu jefe te dice, a falta de un año para acabar, que el lab se muda de centro, le quieres matar, por el estrés y porque tú te has hecho tu hueco en el sitio en el que estás y las perspectivas de integrarse en otro sitio nuevo solo por un año imponen una mijita. Pero lo habéis puesto tan pero tan fácil. Gracias a Esther, porque a pesar de que coincidimos poco, me enseñaste donde estaba y como funcionaba todo. Gracias a Roberto, a Fede, y a Marija, por enseñarme tantas cosas del mundo de la electrofisiología, y por tantos ratos compartidos, charlando sobre quien vive en Groenlandia y cómo o pretendiendo que vamos a cambiar el mundo. Gracias también a Nuria Comes, a Anna Pujol, a Irene, a Guillem, a Anna Pérez y a Sara, porque a pesar de que no hayamos compartido tanto la parte experimental, me habéis transmitido mucho ánimo, me habéis dejado que me desahogue algún que otro día, habéis ofrecido vuestra ayuda siempre que habéis podido y habéis sido un apoyo increíble, sobre todo en esta fase final. Gracias a Xavi Gasull, por las cervezas y charlas a las 8 de la tarde que hacen que no te deprima tanto estar en el lab aún a esas horas y por motivarme y apoyarme a escribir esta tesis en tiempo record cuando todo el mundo me decía que estaba loca. Gracias a Mar, porque no he conocido en mi vida persona que transmita más buen rollo que tú, ha sido un placer compartir el despacho con alguien tan especial, que me alegrara los ratos de escritura con temazos musicales y que me dejara invadir su rinconcito para poder escribir más inspirada. Y gracias a 'miarma', porque me has montado un chiringuito buenísimo para escribir la tesis, pero sobre todo gracias por estar ahí y hacerme sentir que podía hablar contigo de cualquier cosa con total franqueza, por preocuparte por mi y por mis horarios, por apoyarme y animarme cuando había días que ya había petado y no podía más, y por intentar hacerme ver que valgo más de lo que yo pienso.

Gracias a las 'eméritas' del lab. Gracias a Silvia por la luz que tienes. Entramos casi juntas en esto y mantenía la esperanza de que, en algún momento, volvieras a casa por Navidad, como el turrón. No obstante, me alegro mucho de que hayas conseguido tu huequito y estoy segura de que harás una tesis increíble porque tu motivación y tu vocación son abrumadoras. Gracias a Maca, porque, aunque hemos tenido nuestros más y nuestros menos, ya que somos dos personas con personalidades potentes, considero que fuiste un gran apoyo para mi y hoy desde otra punta del continente sigues siéndolo. Y a Cris muchas gracias por todo, me hacía mucho bien tenerte en el lab, y este tramo final hubiera sido mucho más fácil, lo que las circunstancias son las que son, pero eres una persona increíble y sé que conseguirás lo que quieras cuando quieras.

De entre todos los estudiantes que han pasado por el lab durante estos cuatro años, a los que he intentado enseñar algo, gracias a los que han puesto todo de su parte y me han hecho el trabajo más fácil. Gracias a Pablo, el primero de todos y el que probablemente más sufrió mi inexperiencia. Gracias a Andrea, una de las pocas con las que aún mantengo el contacto de vez en cuando, por transmitir tanto buen rollo. Y gracias a Vanessa, porque a pesar de haber sido una experiencia corta y accidentada, me has hecho recuperar un poco la fe en los estudiantes en prácticas.

Gracias a Paco, por aceptar en su día, ser mi tutor por si pasaba algo y por la eficiencia a la hora de conceder autógrafos siempre que lo necesitaba. Y gracias a todos los que estáis en su lab, por todo el tiempo compartido, en especial a aquellos con los que más tiempo he pasado. Gracias a Marc y Marta porque siempre eran una dosis de alegría cuando llegabas al laboratorio, también a personas increíbles que ya no están como Jaume, Andrea o Rene, y por supuesto, gracias a las dos personas, en las que más me he apoyado, Xavi y Héctor. Sois increíbles y os esperan cosas grandes. Ojalá pudiéramos haber compartido más tiempo juntos durante esta tesis.

Gracias a Mireia y a Adrián por la colaboración estrecha y por contagiaros del espíritu de las Grinpatías. Sin vosotros, muchas de las cosas en esta tesis no hubieran sido posibles. De hecho, si podéis mirar las visitas que tiene la base de datos, me juego lo que sea a que al menos un 30 % de esas visitas (probablemente tirando por lo bajo) son mías.

Gracias a Aihnoa Mielgo Iza por darme la primera oportunidad de pisar un laboratorio y en una ciudad tan increíble como es Liverpool. Muchas gracias a Francisco Gómez Scholl, por inmiscuirme en el mundo de la neurociencia y de la sinapsis glutamatérgica, y por permitirme estar en un laboratorio en el que aprendí muchísimo y que sentó las bases para llegar a este punto en el que me encuentro ahora.

Y hablando de esta primera etapa científica, no puedo pasar sin dar las gracias a todas las personas increíbles que conocí en el IBiS como Estefanía, Enriqueta, Víctor y Álvaro. Y en especial, (porque eres especial), a Ana Sánchez, porque te debo un millón de cosas. Tú hiciste que mi primera experiencia en un laboratorio fuese BESTIAL, y eso que yo era una pipiola que no tenía idea ni de rotular y tú eras la *predoc* NÚMERO 1. Gracias por enseñarme tantas cosas y por tratarme como amiga más que alumna. Y gracias por seguir aguantando lo pesada que he podido llegar a ser para poner todo el comportamiento de ratones a punto conexión Sevilla-Barcelona vía WhatsApp, porque esto es una parte muy importante de la tesis que no habría sido posible sin ti.

Gracias a toda la gente de genética en el IDIBELL. La mayor parte de la tesis ha sido aquí y hemos compartido muchas Flamas y eso une mucho. En particular, dar las gracias a Clara, Leire, Laura, Ana Luque, Cris, Edgar, Inma, Juanjo, y a todos los 'worms' que me adoptaron en el grupo y me hicieron sentir una más de la familia. Al IDIBELL le tengo que dar las gracias también por poner a Nadia en mi vida. Ya no tenemos nuestros almuerzos, pero te he seguido teniendo presente y echándote de menos porque nadie me ha cuidado y apoyado tanto desde que llegué aquí como tú.

Gracias a Albert Giralt por compartir con nosotros todo su equipamiento para hacer comportamiento con los ratones. También a Mercé Masana, como experta en comportamiento, por reunirse con nosotros y aconsejarnos para proceder de forma correcta. Y a efectos prácticos, gracias a Sara y sobre todo a Ened, por estar siempre dispuesta a ayudarme cuando necesitaba aparatos o salas, mucho ánimo con tu tesis también.

Gracias a Roger, Nuria y Raquel, por ayudarme a optimizar la secuenciación y por abrirme tantas veces la puerta del laboratorio en el PRBB para dejar muestras a primera hora de la mañana, sin dejaros hacer ni el café. Creo que esto ha sido lo más cerca de la Barceloneta que he estado estos años.

Aunque los resultados no fueron los esperados, gracias a Michel Ronjat y a Michel De Waard por dejarme realizar una estancia en su laboratorio. Gracias a todos los miembros del laboratorio (Thomas, Justine, Antoine, Benjamin...), y en especial a Jerome, Ludivine y Sebastien por ayudarme tanto y por hacer que me sintiera menos lejos de casa, a pesar de mi penoso francés.

Gracias a los técnicos y veterinarios del estabulario (Pep, Sergi, David, Víctor e Ignacio), donde he pasado tantas horas. Gracias por vuestra amabilidad y por estar ahí siempre dispuestos a ayudarme y a hacer que el trabajo fuera fácil.

Gracias también a los técnicos de microscopía del CCitUB. En la facultad de Medicina, gracias a María, Gemma y Elisenda, por explicarme tan bien como funciona todo, y por estar disponibles siempre para ayudarme y para ofrecerme el microscopio en cualquier ratito libre de imprevisto porque saben que casi siempre lo necesito. Por la parte Bellvitge, muchas gracias a Bea y a Esther por intentar sacar el 'sorting' adelante conmigo, aunque no fuera posible al final. Y hablando de abordajes que tampoco han salido, muchísimas gracias a Benja por todo, por estar siempre ahí, por alegrarme los ratitos de confo, y por haberte estado horas y horas conmigo peleándote con un protocolo, el cual no había forma de sacar adelante.

Y tocando un poco la parte más alejada de lo profesional, pero no menos importante, muchas gracias a toda mi familia. Aunque siempre he sido la 'médica' de la familia, creo que ya más o menos sabéis que yo no receto nada y que mi trabajo es algo distinto. Gracias a mi padre y a mi madre, por ayudarme a conseguir todas las ideas locas que se me pasan por la cabeza (salvo la de ser actriz, esa no cuajó), por motivarme siempre a seguir y a luchar para llegar lo más lejos que se pueda. Gracias a mi hermana y a churrete por animarme, distraerme y alegrarme cuando más lo necesito. Y gracias a las morenillas, a la familia Santos, y a mi familia política, porque sé que, aunque no entendáis la mitad de lo que haya aquí escrito os hace ilusión ver un minilibro escrito por mí.

Gracias a mi familia del sur, a domin, a agu, a seri y a mi tocaya. Sé que nuestra relación con miles de kilómetros de distancia hace lo que puede, pero el hecho de que sigamos en contacto y que pisé tierras onubenses y no tarde ni 30 segundos en avisaros para veros, ya dice todo lo que significáis para mi. Ojalá haberos tenido aquí en Barcelona, que eso hubiera hecho que todo este camino hubiera sido mucho más fácil y divertido, aunque igual también habría currado menos y la tesis sería la mitad de gruesa.

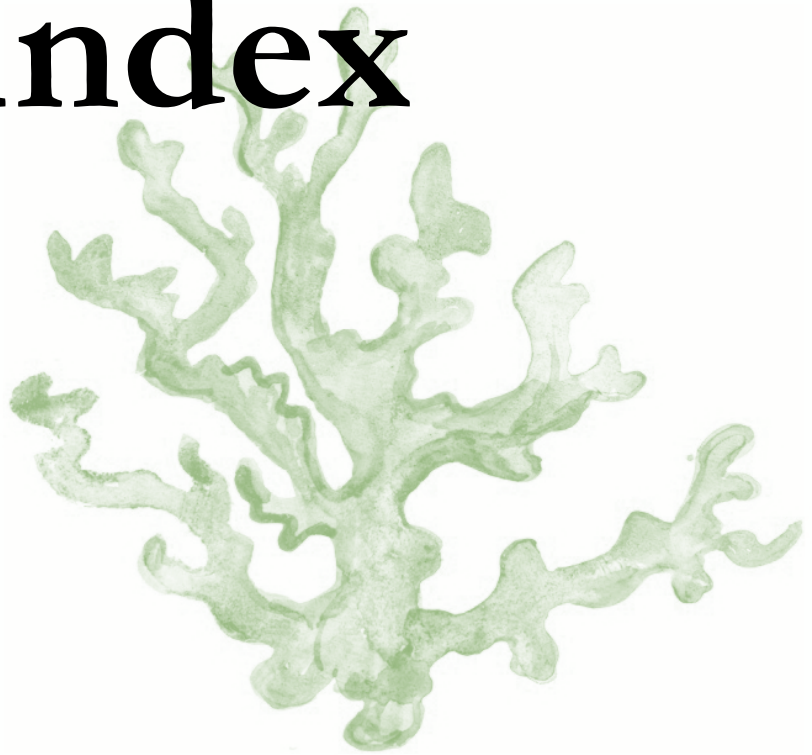Menos mal que mi vicius si que está en Barcelona. Lo malo ha sido que nos dedicáramos las dos a la ciencia y que tengamos una agenda que ni Florentino Pérez y Laporta, porque a veces ha parecido que una vivía en Londres y la otra en California. Aún así gracias por el primer año juntas que hizo que la llegada a Barcelona fuera mucho más fácil y por los ratitos que hemos sabido encontrar después.

Y hablando de personas que hicieron la transición Sevilla-Barcelona más fácil. Muchas gracias a personas importantes que me han apoyado y que han compartido parte del camino conmigo como Bea o María Barceló. También muchas gracias a Anika, Marcos, y Sergi, que habría hecho sin vosotros, os convertisteis en mi familia aquí en Barcelona. Ahora todo es más difícil, pero quiero que sepáis que me tendréis aquí siempre para tomar una cerveza.

El lado bueno de tener a mucha de tu gente lejos es que te permite encontrar personas maravillosas en el sitio en el que estás. Y en este aspecto tengo que dar las gracias a Geri y Vio, porque nos han integrado como nadie en Barcelona y nos han hecho sentir como si fuéramos amigos de toda la vida, con nuestras comidas y cenas, con excursiones y siendo un gran apoyo, espero seguir teniéndoos en nuestras vidas por mucho tiempo. También dar las gracias al resto de la familia Holded, a Toni, a Bea, a Ignasi, a Marc, a Javi, a Laura, y a Pol, que siempre te tienen preparada una silla para tomar una cerveza y pasar un buen rato. Y muchas gracias a Malak y Judith y a nuestros miércoles de birra, porque, aunque se pierdan las tradiciones, habéis sido también una parte importante de este camino.

Y muchas gracias a Ignacio, al cual le dedico mi último párrafo. Somos dos tornados a punto de colisionar continuamente. De hecho, a veces te quiero matar y a veces me quieres matar tú, pero a pesar de todo eres mi apoyo incondicional, y la persona a la que busco cuando necesito ayuda. Sin haberte tenido a mi lado estos años, esta tesis no estaría aquí y sabes que no lo digo por decir. No solo has colaborado en lo científico permitiendo que hiciera los experimentos de comportamiento a ciegas sin tener ni idea de a qué jugaba con mis 'mascotas', si no que también estabas en esos días en los que uno llega tan quemado que lo mandaba todo a la mierda. Gracias por hacerme ver lo grandes que son mis alas y por estar a mi lado en este arduo

Index

Hypothesis and objectives

Materials and methods

Phenotypic assessment of Grinb⁺/⁻ mouse model

Grin2b⁺/⁻ mice therapeutic interventions

Statistical analysis

Results

List of abbreviations (A-Z)

A

- AAV, adeno-associated virus
- AADC, aromatic L-aminoacid decarboxylase
- Aβ, amyloid-beta
- AC, adenylyl cyclase
- ACBC, 1-aminocyclobutane-1-carboxylic acid
- ACBD, 1-aminocyclobutane-1,3-dicarboxylic acid
- ACPC, 1-aminocyclopropane-1-carboxylic acid
- ACPD, 1-aminocyclopentane-1,3-dicarboxylic acid
- ACTH, adrenocorticotropic hormone
- aCSF, artificial cerebrospinal fluid
- AD, Alzheimer disease
- ADA, azetidine-2,4-dicarboxylic acid
- ADC, azetidine-2,3-dicarboxylic acid
- ADHD, attention deficit and hyperactivity disorder
- ALS, amyotrophic lateral sclerosis
- AMPA, -amino-3-hydroxy-5-methyl-4-isoxazolepropionic acid
- AMPAR, AMPA receptor
- ANOVA, One-way Analysis of Variance
- AP1, activator protein 1
- AP5, 2-amino-7-phosphonopentanoate
- AP7, 2-amino-7-phosphonopentanoate
- Apaf-1, protease activating factor 1
- APP, amyloid precursor protein
- ARF3, ADP-ribosylation factor 3
- ASEBA, Achenbach System of Empirically Based Assessment
- ASO, antisense oligonucleotide
- ATA2, amino acid transporter A2
- ATD, amino-terminal domain
- Atf3, activating transcription factor 3
- ATP, adenosine triphosphate
- ATPase, adenosine triphosphate hydrolase

B

- BAD, Bcl-2-associated death promoter
- BBB, blood brain barrier
- BCA, bicinchonic acid
- Bcl2l11, Bcl2-like protein 11
- Bcl6, B-cell lymphoma 6
- BDNF, brain-derived neurotrophic factor
- bFGF, basic fibroblast growth factor
- bp, base pair(s)
- BSID, Bayley Scale of Infant and toddler Development
- Btg2, B-cell translocation gene 2

C

- CA, cysteic acid/cysteate
- CA1, cornu ammonis 1
- CA3, cornu ammonis 3
- CamKII, Ca^{2+}/calmodulin-dependent protein kinase II
- cAMP, cyclic adenosine monophosphate
- CASK, calcium/calmodulin-dependent serine protein kinase
- CBIO, 5-Chlorobenzo[d]isoxazol-3-ol
- CGG, 2-carboxycyclopropylglycine
- 7-CK, 7-chlorokynurenic acid
- cLTP, glycine-mediated chemical long-term potentiation assay
- cm, centimeter
- CNS, central nervous system
- CPP, 3-(2-carboxypiperazin-4-yl)propyl-1-phosphonic acid
- CREB, cAMP response element binding protein
- CRF, corticotropin releasing factor
- CSA, cystein sulfinic acid/cystein sulfinate
- CSF, cerebrospinal fluid
- CSWS, continuous spike and wave during sleep
- CTD, carboxyl-terminal domain
- CVI, cortical visual impairment

D

- DAG, diacylglycerol
- DAO/DAAO, D-aminoacid oxidase
- DD, developmental delay
- DDO, D-asparte oxidase
- D-AP5, D(−)-2-Amino-5-phosphonopentanoic acid NMDA receptor antagonist
- 5,7-dCK, 5,7-dichlorokynurenic acid
- DCS, D-cycloserine
- 2-DG, ^{14}C-2-deoxyglucose
- DIV, day in vitro
- DL-TBOA, DL-threo-beta-benzyloxyaspartic acid

E

- EAAC, excitatory amino acid carriers
- EAAT, excitatory amino acid transporters
- EC50, half maximal efficacy concentration
- EEG, electroencephalogram
- EGF, epidermal growth factor
- ENS, enteric nervous system
- EPSP, excitatory postsynaptic potential
- ER, endoplasmic reticulum
- ERK1/2, extracellular signal-regulated kinases 1/2
- Extra, extrasynaptic fraction

F

- FBS$_i$, heat-inactivated fetal bovine serum
- FDA, Food and Drug Administration
- FMT, fecal microbiota transplantation
- FOXO, forkhead box O

G

- g, grams
- GABA, γ-aminobutyric acid
- GAD, glutamic acid decarboxylase
- GADD45, growth arrest and DNA damage induced gene 45
- GCP II, glutamate carboxypeptidase II
- GDNF, glial-derived neurotrophic factor
- GI, gastrointestinal
- GLAST, glutamate-Aspartate transporter 1
- Gln, glutamine
- Glt1, glutamate transporter 1
- GLYT1, glycine transporter type 1
- GMFM, Gross Motor Function Measure
- GOT, glutamic oxalacetic aminotransferase

H

- HCA, homocysteic acid/homocysteate
- HCSA, homocystein sulfinic acid/homocysteine sulfinate
- HEK, human embryonic kidney
- HPA, hypothalamus-pituitary-adrenal axis
- HSP, heat-shock protein

I

- IB, isolating buffer
- ID, intelectual disability
- IF, immunofluorescence
- Ifi202B, Interferon activated gene 202B
- IGF-1, insulin-like growth factor 1
- iGluR, ionotropic glutamate receptor
- Inhba, Inhibin beta-A
- IP3, inositol-1,4,5-trisphosphate

K

- KAR, kainate receptor
- kb, kilobase(s)
- KD, knock-down
- KI, knock-in
- kif, kinesins
- Kir, inward-rectifier potassium channel
- KN, kynurenine pathway
- KO, knock-out

L

- LBD, ligand-binding domain
- LGP, lateral globus pallidus
- LIVBP, leucine, isoleucine, valine binding protein
- LKS, Landau-Kleffner syndrome
- LTD, long-term depression
- LTM, long-term memory
- LTP, long-term potentiation
- PDC, pyrrolidine-2,4-dicarboxylic acid

M

- M1-M4, transmembrane domains of ionotropic glutamatergic receptors
- MAGUK, membrane-associated guanylate kinase
- MALS, mammalian lin-seven protein
- MAM, microbial-associated metabolite
- MAPK, mitogen-activated protein kinase
- MDD, major depressive disorder
- mGluR, metabotropic glutamate receptor
- MGP, medial globus pallidus
- min, minutes
- Mint1, munc18-1-interacting protein 1
- MLCK, myosin light-chain kinase
- Mm, milimeter
- mPins, mammalian homologue of *Drosophila melanogaster* partner of inscuteable
- MTR, missense tolerance ratio

N

- NAA, N-acetylaspartic acid/N-acetylaspartate
- NAAG, N-acetylaspartylglutamic acid/N-acetylaspartylglutamate
- NAALADase, N-acetylated α-linked acidic dipeptidase
- NAM, negative allosteric modulator
- NHP4G, N-hydroxypyrazol-4-yl glycine
- NHP5G, N-hydroxypyrazol-5-yl glycine
- NMDA, *N*-methyl-D-aspartate/N-methyl-D-aspartic acid
- NMDAR, NMDA receptor
- NO, nitric oxide
- NOR, novel object recognition
- Npas4, neuronal PAS domain protein 4
- NPC, neural progenitor cell
- Nr4a1, nerve growth factor IB
- NS, nervous system

O

- OCD, obsessive-compulsive disorder
- O/N, overnight

P

- P2, synaptosomal fraction
- P2-pannexin, complex of purinergic receptors P2 with pannexin channel
- PACAP, pituitary adenylate cyclase-activating polypeptide
- PAM, positive allosteric modulator
- PBPD, 1-(biphenyl-4-carbonyl)piperazine-2,3-dicarboxylic acid
- PCA, 1-phenylcyclohexylamine
- PCP, phencyclidine
- PCR, polymerase chain reaction
- PD, Parkinson disease
- PDA, piperidinedicarboxylic acid
- PDC, pyrrolidine-2,4-dicarboxylic acid
- PDZ, postsynaptic density 95/disc-large (Dlg)/zona occludens (ZO)
- PEI, polyethylenimine
- PFA, paraformaldehyde
- PI3K, phosphatidyl-inositol 3 kinase
- PKA, protein kinase A
- PKC, protein kinase C
- PLCβ, phospholipase C Beta
- PMPA, phosphonomethylpentanedioic acid
- PNS, peripheral nervous system
- Post, postsynaptic fraction
- PP1, protein phosphatase 1
- PPDA, 1-(phenanthren-2-carbonyl)piperazine-2,3-dicarboxylic acid
- PPIC, Proteases and Phosphatase Inhibitor cocktail
- Pre, presynaptic fraction
- PSD, postsynaptic density
- PTEN, phosphatidylinositol 3,4,5-trisphosphate 3-phosphatase
- PTM, post-translational modification
- PTSD, post-traumatic stress disorder
- PVC, polyvinyl chloride

Q

- QPRT, quinolinate phosphoribosyl transferase

R

- RE, Rolandic epilepsy
- RNA$_i$, RNA interference
- RPM, rotations per minute
- RT, room temperature
- RVIS, residual variation intolerance score

S

- SA1, system A transporter 1
- SAAs, sulfu-containing aminoacids
  SAM, silent allosteric modulator
- SAP90, 102, synapse-associated protein 90, 102
- SAT2, system A amino acid transporter 2
- SCFA, short-chain fatty acids
- SCQ, Social Communication Questionnaire
- SDS, sodium dodecyl sulfate
- SDSC, Sleep Disturbance Scale for Children
- SDS-PAGE, sodium dodecyl sulfate polyacrylamide gel electrophoresis
- Sec8, exocyst component
- Serpinb2, serine protease inhibitor B2
- Sesn2, sestrin 2
- SH3-GK domains, src-homology-3 (SH3)–guanylate kinase (GK) domains
- SHANK, SH3 and multiple ankyrin repeat domains protein
- SHMT, serine hydroxymethyltransferase
- shRNA, short-hairpin RNA
- SLC38, sodium-coupled neutral amino acid transporter
- SN1,2, system N transporter 1,2
- SNAP25, synaptosome associated protein 25
- SNAT2,3,5, system N amino acid transporter 2,3,5
- SNpc, substantia nigra pars compacta
- SNr, substantia nigra pars reticulata
- SR, serine racemase
- Srxn1, sulfiredoxin
- SSAT, spermidine/spermine N-acetyltransferase
- STM, short-term memory
- STN, sub-thalamic nucleus
- STP, short-term potentiation
- SynGAP, Synaptic Ras GTPase-activating protein

T

- TBS-T, Tris-base plus Tween
- TCA, tricarboxylic acid cycle
- TGN, trans-golgi network
- TMD, transmembrane domain
- TRPC, transient receptor potential cation channels
- T-SNARE, target soluble NSF attachment protein
- TTX, tetrodotoxin
- Txnip, thioredoxin-interacting protein

U

- μL, microliter

V

- VABS, Vineland Adaptive Behavior Scale
- VAMP, vesicle-associated membrane protein
- Veli, vertebrate lin-seven homolog
- VIP, vasoactive intestinal peptide
- V-SNARE, vesicle soluble NSF attachment protein
- VGLUT, vesicular glutamate transporters

W
- WB, western blot
- WISC, Wechsler Intelligence Scale
- WT, wild-type

Summary
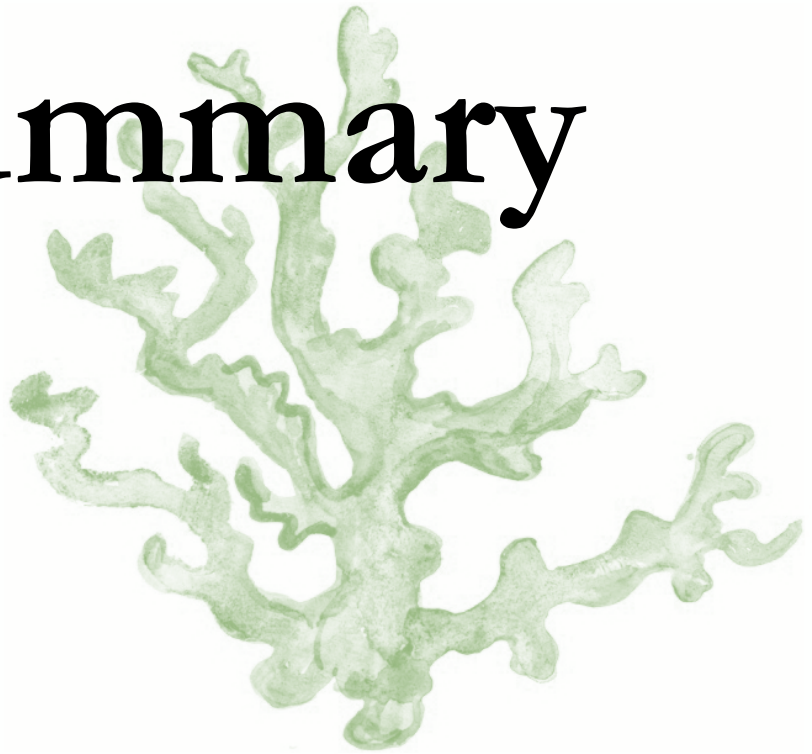
English version

N-methyl-D-aspartate receptors (NMDARs) are glutamate-gated ion channels that play a central role in learning and memory processes. Recent developments on Next-Generation Sequencing have identified a growing number of *de novo* genetic variants affecting *GRIN* genes (encoding for NMDAR subunits), with a high prevalence of *GRIN1*, *GRIN2A* and *GRIN2B* mutations associated with severe neurodevelopmental disorders, the so-called *GRIN*-related disorders (GRDs; ORPHA: 101685, 289266, 178469). However, the study of *GRIN* variants pathogenicity in these neurological conditions is very scarce, and the therapeutic options are practically unmet. These *GRIN* variants could potentially affect NMDAR stability, surface trafficking and/or biophysical properties, leading to neurodevelopmental and psychiatric disorders. In this Thesis, we hypothesized that GRIN *de novo* mutations could be functionally grouped and stratified, for further design of personalized therapies. Ninety-five GRD patients have been recruited, and their respective *GRIN* variants have been annotated *in vitro*, to shed light in a potential genotype-phenotype correlation in the disease. Further, since most frequent outcome of *GRIN* disease-associated variants lead to NMDAR loss-of-function, in addition to cellular models, a constitutive haploinsufficient *Grin2b*$^{+/-}$ mouse model has been characterized (behavior, biochemistry and electrophysiology). Finally, we used both cellular and animal models to investigate the therapeutic benefit of different therapeutic strategies (genetic, nutraceutical/pharmacological and microbiota manipulation) to rescue NMDAR loss-of-function.

Spanish version

Los receptores ionotrópicos de tipo N-metil-D-aspartato (NMDAR) son canales iónicos activados por glutamato que juegan un papel clave en la fisiología neuronal. Los avances en la secuenciación masiva han identificado un número creciente de variantes genéticas *de novo* que afectan a los genes *GRIN,* codificantes de las subunidades del receptor NMDA. Las mutaciones que afectan a los genes *GRIN* están relacionadas con trastornos del neurodesarrollo severos, conocidos como Grinpatías (ORPHA: 101685, 289266, 178469). No obstante, el estudio de la patogenicidad de las mutaciones *GRIN* aún es escaso, al igual que las opciones terapéuticas para los pacientes con Grinpatías. A nivel funcional, las mutaciones *GRIN* pueden afectar distintos procesos de la fisiología del receptor (estabilidad proteica, tráfico a superficie y/o propiedades biofísicas del canal), provocando trastornos del neurodesarrollo. En este Tesis, hipotetizamos que las mutaciones *GRIN* podrían estratificarse en distintos grupos funcionales y que esto permitiría la aplicación de tratamientos personalizados. A lo largo de la Tesis, se han reclutado 95 pacientes con Grinpatías, y se ha realizado la anotación funcional y estratificación de 57 mutaciones *GRIN,* observando una predominancia de variantes de tipo pérdida de función. Posteriormente, se han evaluado distintas estrategias terapéuticas (genética, dietética/farmacológica y manipulación de la flora intestinal) para la corrección de la hipofuncionalidad de los receptores NMDA, en modelos celulares y/o en el modelo de ratón heterocigoto para la subunidad GluN2B.

Introduction
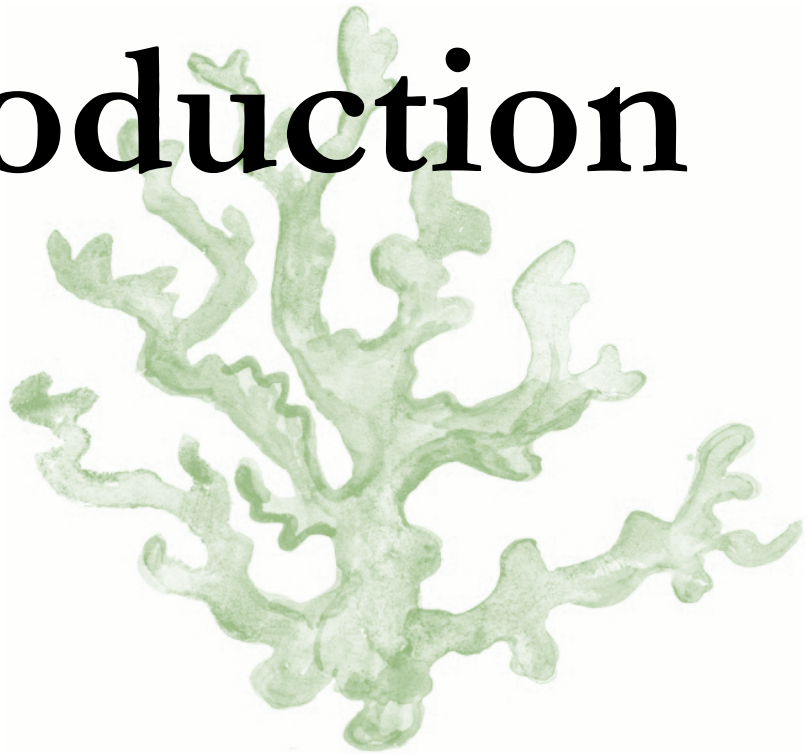
Chapter 1.

The glutamatergic system

1.1. The glutamatergic system: biodistribution, glutamate roles and synthesis

1.1.1.   Glutamatergic system biodistribution

The glutamatergic neurotransmission system is the main excitatory network in the nervous system (NS). Glutamate-mediated neurotransmission is widely present in the central and the peripheral nervous systems (CNS and PNS, respectively), both in neuronal and non-neuronal cells, with a particular prominence in the circuitry connecting: a) Cortex – Brain stem centers (raphe, locus coeruleus, ventral tegmental area), controlling the neurotransmitter release; b) Prefrontal cortex – Striatum, controlling the dopamine system and consequently, motor outputs; c) Thalamus – Cortex, d) Prefrontal Cortex – Thalamus, controlling sensory processing; e) Septum – Hippocampus, controlling cognitive processes such as learning and memory and f) Cortex – Cortex (Schwartz et *al.*, 2012; Khakpai F. et al., 2013) (see **figure 1**). Besides its pivotal role in the NS, glutamatergic system players are also expressed in heart, immune cells, testis, ovary, kidney, bone, bone marrow, pancreatic β-cells, intestine, esophagus, hepatocytes, lung and keratinocytes (reviewed by Hogan Cann AD. and Anderson CM., 2016).
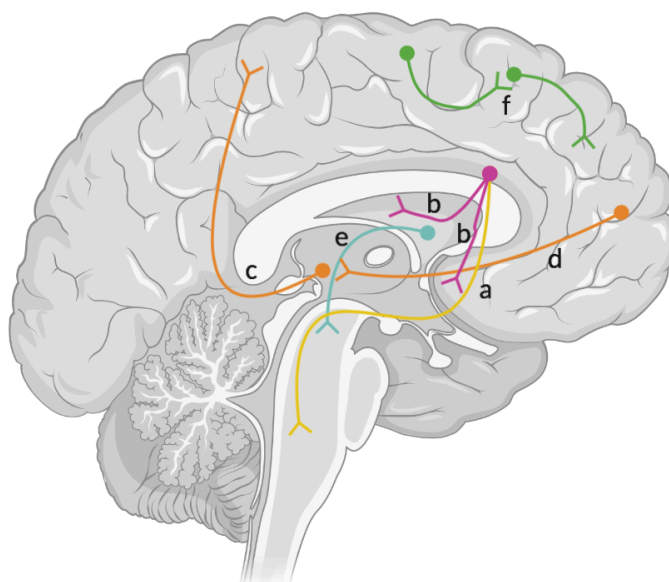
Figure 1. Glutamate neurotransmission pathways in the central nervous system: a) Cortex – Brain stem b) Prefrontal cortex – Striatum, c) Thalamus – Cortex, d) Prefrontal Cortex – Thalamus, e) Septum – Hippocampus, f) Cortex – Cortex.

1.1.2.   Glutamate roles

Glutamatergic neurotransmission uses glutamate as the primary signaling molecule. Glutamate functions may vary, based on the heterogenicity of cell types synthetizing and releasing glutamate, in combination with their relative target cells/receptors (see **table 1**) (Chenu C. et al., 1998; Yano S. et al., 1998; Genever PG. et al., 1999; Gill S. and Pulido O., 2001; Gill S. et al., 2007; Mckenna M., 2007; Mattson M. et al., 2008; Anaparti V. et al., 2015; Du J. et al., 2016; Tomé D., 2018; Takahashi H. et al., 2019).

Tissue	Glutamate roles	References
Gut	- Energy production - Intestinal motility - Salivation - Food preference (chemosensing) - Precursor (GABA, gluthatione, proline, arginine, ornithine, L-alanine, 2-oxoglutarate)	Du J. et al., 2016; Tomé D., 2018
Reproductive system	- Ejaculation - Erection - Spermatogenesis - Spermatozoa motility and maturation - Ovulation - Fertilization - Implantation of the ovum - Uterus excitability	Gill S. and Pulido O., 2001
Heart	- Cardiac rhythm - Heart excitation - Heart contraction - Coronary circulation	Gill S. and Pulido O., 2001; Gill S. et al., 2007; Du J. et al., 2016
Pancreas	- Insulin secretion and regulation - Glucagon and somatostatin release	Gill S. and Pulido O., 2001; Takahashi H. et al., 2019
Kidneys	- Electrolytes and water homeostasis - Renin release (blood pressure)	Gill S. and Pulido O., 2001; Du J. et al., 2016
Respiratory system	Airway smooth muscle contraction	Gill S. and Pulido O., 2001; Anaparti V. et al., 2015; Du J. et al., 2016
Skin	Epidermal renewal and wound healing (proliferation and differentiation)	Genever PG. et al., 1999
Bone	Bone resorption	Chenu C. et al., 1998
Immune system	Innate and adaptative immune response (activation and proliferation of B-cells, T-cells, dendritic cells and macrophages)	Du J. et al., 2016
Nervous system	- Neurotrophic factors synthesis (bFGF, EGF, BDNF, IGF-1) - Neuronal differentiation from NPCs, proliferation, migration and survival (via bFGF, EGF, BDNF, IGF-1) - Neurite growth (via bFGF, EGF) - Sensory processing (thalamus-cortex and cortex-thalamus) - Control of consciousness (thalamus-cortex and cortex-thalamus) - Motor control (basal ganglia) - Learning and memory (hippocampus) - Energy production (oxidation) - Protein synthesis - GABA, gluthatione and glutamine precursor	Yano S. et al., 1998; Nedergaard M. et al., 2002; Mckenna M., 2007; Mattson M. et al., 2008

Table 1. Table summarizing the different glutamate roles in distinct body systems where this molecule is expressed. Abbreviations: GABA, gamma-aminobutyric acid; bFGF, basic fibroblast growth factor; EGF, epidermal growth factor; NPCs, neural progenitor cells; BDNF, brain-derived neurotrophic factor; IGF-1, insulin-like growth factor 1.

1.1.3. Glutamate synthesis

Based on the high abundance of glutamate concentration in brain, this aminoacid was initially considered as a metabolite. However, the identification of GABA effects on neurons (Curtis DR., Phillis JW. and Watkins JC., 1959) and the metabolic relationship between GABA and glutamate suggested that, rather than playing a role in metabolic processes (protein synthesis), glutamate could control neuronal function. The pioneering studies of Curtis DR. et al. (Curtis DR., Phillis JW. and Watkins JC., 1959) identified glutamate effects on the control of neuronal activity, playing a role as a neurotransmitter.

In neurons, glutamate is synthetized de novo from alpha ketoglutarate, by the enzymatic activity of glutamate dehydrogenase along the tricarboxylic acid cycle (TCA, also known as Krebs cycle) (see **figure 2**), the common pathway for oxidation of carbohydrates, lipids and proteins (Akram M, 2014).
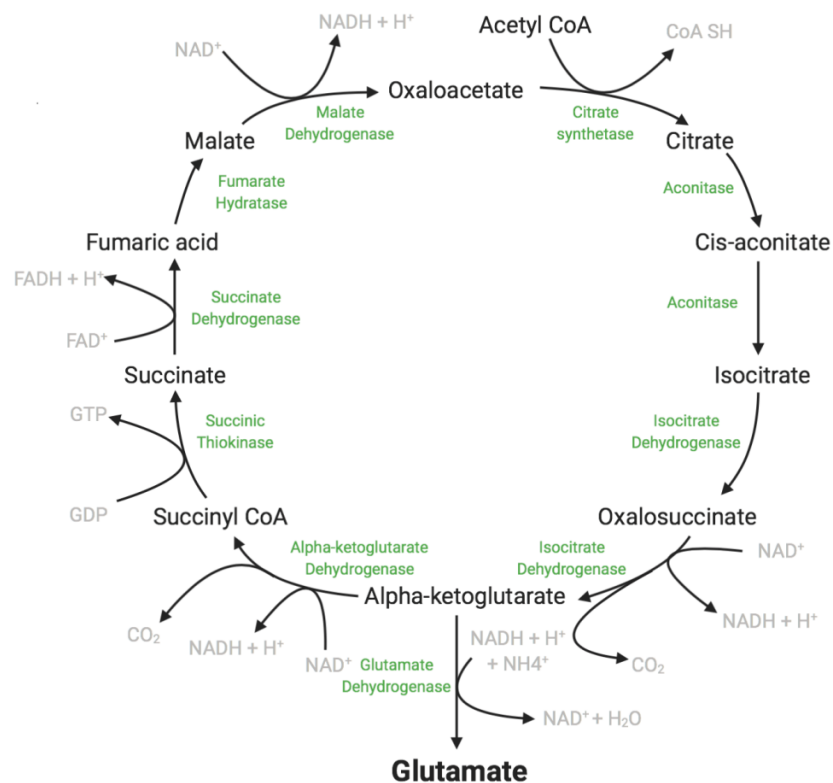
Figure 2. Krebs cycle and its association with glutamate synthesis. The different substrates/products are indicated in black, the enzymes in green and the cofactors in gray.

Upon glutamate release (from the presynaptic neuron) in the synaptic cleft, neurotransmitter glutamate is mainly uptaken by surrounding astrocytes (see next paragraph) subsequent to interaction with receptors in the synapse. In the astrocyte, glutamate is converted into glutamine (Gln, catalyzed by glutamine synthetase, exclusively expressed in astrocytes) and transported to glutamatergic neurons, to be further converted into glutamate by phosphate-activated glutaminase (Yu-Ying et al., 2018) (see **figure 3**).

Glutamine uptake by neurons occurs via SAT2/ATA2/SNAT2/SA1 transporter (System A amino acid transporter 2, Amino acid transporter A2, System N amino acid transporter 2, System A transporter 1) from SLC38 (Sodium-coupled neutral amino acid transporter) family (see **figure 7**), using electrical and chemical gradients of Na^+ (Chaudhry FA. et al. 2002) (see **figure 8**).
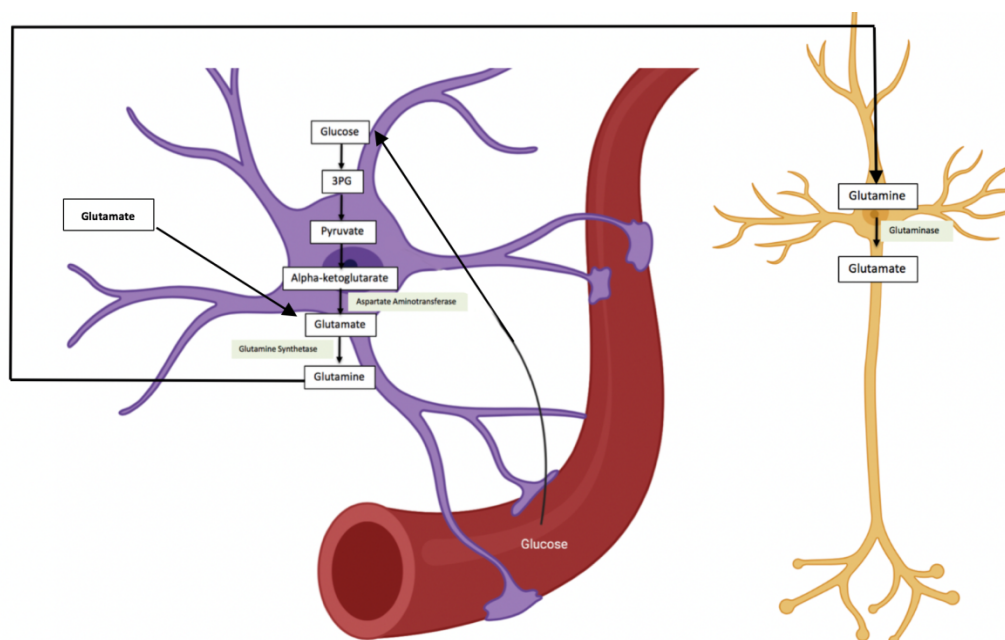
Figure 3. Glutamate synthesis from astrocyte-released glutamine. In astrocyte, glucose is transformed into 3PG which is converted to pyruvate and consequently, to alpha-ketoglutarate. Alpha-ketoglutarate is then converted to glutamate by aspartate aminotransferase. There are additional sources of glutamate for the astrocyte. Finally, glutamate is converted to glutamine by glutamine synthetase.

1.2. <u>The glutamatergic tripartite synapse</u>

Traditionally, synapses were thought to be dependent on two cellular players' communication, with information flowing from pre-synaptic neurons to post-synaptic neurons. However, the current consensus view, includes, in addition to the presence of the pre-synaptic and post-synaptic neurons, the role of a third player, namely the astrocyte. Indeed, astrocytes also exchange information with the two neuronal actors, having a regulatory role in neurotransmission, and forming the so-called 'tripartite synapse' (Perea G. et al., 2009). The glutamatergic synapse is a tripartite synapse, and the following paragraph describes their different actors.

1.2.1. <u>Pre-synaptic neuron</u>

Upon glutamate synthesis in the pre-synaptic neuron (using one of the mechanisms previously described), the neurotransmitter is transported (via vesicular glutamate transporters, VGLUT) and stored in synaptic vesicles. This glutamate transport is driven, firstly by chloride ions uptaken during vesicles recycling after those vesicles have been fused to the pre-synaptic membrane, and also by a proton ATPase in the vesicular membrane that creates a positive gradient that facilitates glutamate (a negatively charged molecule) transport into the vesicles (Martineau M. et al., 2017) (see **figure 4**).

The fine regulation of glutamate exocytosis as for other neurotransmitters release, requires the arrival of an action potential to the pre-synaptic neuron. This action potential is translated into a transient Ca^{2+} increase via activation of voltage-gated calcium channels. In synaptic vesicles, there are distinct proteins like synaptobrevin or VAMP (vesicle-associated membrane protein) that is a V-SNARE (Vesicle Soluble NSF Attachment Protein) which binds to syntaxin and SNAP25 (Synaptosome associated protein 25), that are T-SNAREs (Target Soluble NSF Attachment Protein) in the plasma membrane of neuron terminals, resulting in the vesicle-membrane fusion, and consequently, the glutamate release, via Ca^{2+} binding to V-SNARE (Lodish H. et al., 2000) (see **figure 4**).

This calcium also mediates phosphorylation of different protein kinases (cAMP- or Ca^{2+}-calmodulin-dependent) that act in some proteins located in the synaptic vesicles' membrane, such as synapsins and Rab3A (a GTP-binding protein) leading to the vesicles' recruitment to the active zone (see **figure 4**).
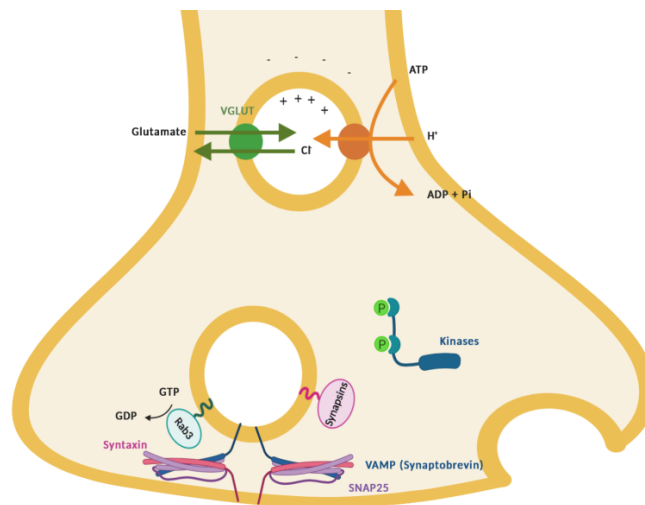
Figure 4. Schematic representation of glutamate transport into vesicles through VGLUT transporter (coupled to chloride transport and an ATPase pump) and glutamate vesicles fusion with membrane to release the neurotransmitter via SNARE complex (kinases phosphorylate synapsins and Rab3, recruiting synaptic vesicles to active zone, where synaptobrevin/VAMP binds to syntaxin and SNAP25, and allow vesicles fusion).

Although the precise mechanisms remain elusive, experimental data support the release (in addition to glutamate) of D-serine from the pre-synaptic glutamatergic neurons. In brain, D-serine can be *de novo* synthetized from its precursor L-serine by the action of serine racemase (SR) and act as a co-agonist together with glutamate. Traditionally, SR was thought to be exclusively expressed in astrocytes, but recent data showed SR expression in neurons as well. Neuronal release of D-serine is Ca^{2+} dependent (Kartvelishvily E. et al., 2006). Another molecule which act as co-agonist is glycine. In order to control the glycine concentration in the synaptic cleft, there is a glycine transporter GLYT1 (glycine transporter type 1), coupling the glycine transport with the transport of 2 Na^+ ions and 1 Cl^- ion (see **figures 7-8**) (Tsai G. et al., 2004; Cubelos B. et al., 2005, Erdem FA. et al., 2019).

Additionally, in the pre-synaptic neuron, there are some glutamate receptors regulating the release process and consequently, having an impact on some critical process such as neuronal plasticity. These receptors are known as autoreceptors. Ionotropic pre-synaptic receptors (Kainate, AMPA and NMDA) mainly facilitate neurotransmission whereas metabotropic receptors might be facilitating (Group I) or inhibiting (Group II and III) depending on the signaling and the coupled G-protein (Pinheiro PS. et al., 2008) (see **figure 7**).

1.2.2.   Post-synaptic neuron

Released glutamate in the synaptic cleft can bind to the agonist (glutamate) binding site of the glutamate receptors, which are predominantly present in the post-synaptic neuron. Glutamate receptors are functionally classified in two main families: metabotropic receptors (mGluRs), a class of ligand-dependent receptors coupled to G-proteins; and ionotropic receptors (iGluRs) which are voltage-dependent channels that allow direct cations movement. These cations depolarize the post-synaptic neuron from a negative resting potential to a more positive potential, that when achieving a threshold, generates an action potential that propagates.

1.2.1.1.   Metabotropic glutamate receptors

Metabotropic receptors responding to glutamate consist on seven transmembrane domains receptors that form dimers and are divided in three different groups: Group I (mGluR1 and mGluR5), Group II (mGluR2 and mGluR3) and Group III (mGluR4, mGluR6, mGluR7 and mGluR8). Whereas Group I receptors are coupled to $G_q/11$ protein, Group II and III receptors bind to G_i/G_o protein (Nicoletti F. et al., 2011). Activation of metabotropic receptors is associated with slow responses (minutes, hours), in contrast to the fast activation and responses triggered by ionotropic receptors (few milliseconds). Further, the signaling pathways activated by mGluRs are dependent on the identity of the target (mGluR) and the associated G-protein. Glutamate binding to mGluRs coupled to G_q proteins stimulates phospholipase Cb (PCb) resulting in the cleavage of phosphatidylinositol-4,5-bisphosphate and the formation of inositol-1,4,5-trisphosphate (IP3) and diacylglycerol (DAG). In turn, IP3 increase promotes Ca^{2+} release from intracellular stores whereas DAG activates protein kinase C (PKC), which regulates several second messengers and signaling pathways, such as cAMP (cyclic adenosine monophosphate) synthesis, arachidonic acid release, the mitogen-activated protein kinase (MAPK) pathway, and L-type voltage-sensitive Ca^{2+} channels. In the other hand, receptors binding to G_i/G_o proteins, inhibit adenylyl cyclase (AC) and cAMP formation and directly regulate ion channels (inhibiting Ca^{2+} channels or activating K^+ channels) and other signaling pathways, like the activation of the MAPK and PI3K (phosphatidyl-inositol 3 kinase) pathways (Nicoletti F. et al., 2011) (see **figure 5**).
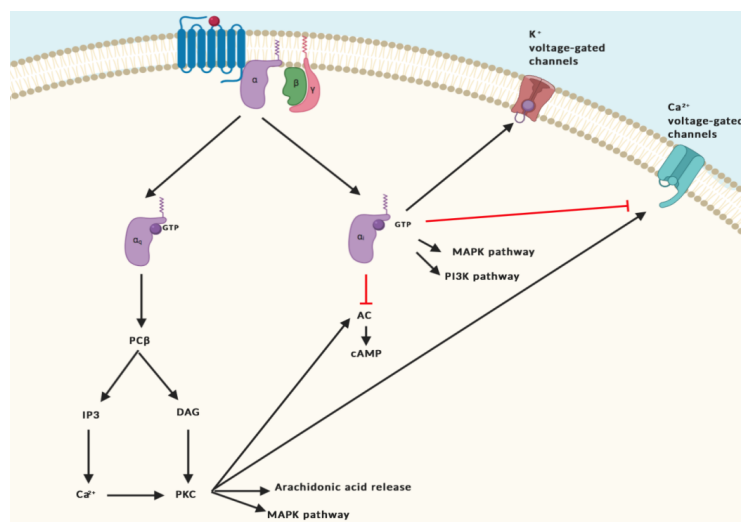
Figure 5. Signaling pathways modulation by glutamate metabotropic receptor activation. Activation of metabotropic receptors containing G_q proteins result in PLCβ activation and IP3 production, which in turn increases calcium and DAG. Increased DAG and Ca^{2+} levels activate PKC which activates AC, calcium voltage-gated channels, arachidonic acid release and the MAPK pathway. Metabotropic receptors containing G_i proteins inactivate AC (decreasing cAMP production), and calcium voltage-gated channels while activating potassium voltage-gated channels, MAPK and PI3K pathway.

Metabotropic receptors can be located either in the post-synaptic neuron (mGluR1,5 and 3), or in the pre-synaptic terminal acting as autorreceptors (mGluR1, 2, 3, 4, 5, 7 and 8). Besides, they are also found in astrocytic cells (mGluR3 and 5) (Nicoletti F. et al., 2011) (see **figure 7**).

1.2.1.2.   Ionotropic glutamate receptors

Ionotropic glutamate receptors are ion channels that are pharmacologically divided in three groups based on their response to glutamate analogues: AMPA receptors (AMPARs, which respond to α-amino-3-hydroxy-5-methyl-4-isoxazol-propionate, AMPA), kainate receptors (KARs, which respond to kainic acid), and NMDA receptors (NMDARs, which respond to N-methyl-D-aspartate). Ionotropic receptors are tetrameric structures (homotetramers or heterotetramers). Each tetramer is composed by four large transmembrane subunits (900-1500 residues) with a central channel pore permeable to cations. iGluR subunits are encoded by different genes, named according to the functional type of receptor they are forming (Collingridge GL. et al 2009; Traynelis SF. et al., 2010) (see **table 2**).

Receptor	Protein subunit names (Gene genes)
AMPA	**GluA1**, GluR1, GluRA (*GRIA1*)
	GluA2, GluR2, GluRB (*GRIA2*)
	GluA3, GluR3, GluRC (*GRIA3*)
	GluA4, GluR4, GluRD (*GRIA4*)
Kainate	**GluK1**, GluR5 (*GRIK1*)
	GluK2, GluR6 (*GRIK2*)
	GluK3, GluR7 (*GRIK3*)
	GluK4, KA1 (*GRIK4*)
	GluK5, KA2 (*GRIK5*)
NMDA	**GluN1**, NMDAR1, NR1, GluRx1 (*GRIN1*)
	GluN2A, NMDAR2A, NR2A, GluRe1 (*GRIN2A*)
	GluN2B, NMDAR2B, NR2B, GluRe2 (*GRIN2B*)
	GluN2C, NMDAR2C, NR2C, GluRe3 (*GRIN2C*)
	GluN2D, NMDAR2D, NR2D, GluRe4 (*GRIN2D*)
	GluN3A, NR3A (*GRIN3A*)
	GluN3B, NR3B (*GRIN3B*)

Table 2. Glutamate ionotropic receptor subunits classification: AMPAR (GluA1-GluA4), kainate (GluK1-GluK5) and NMDA (GluN1, GluN2A-D, GluN3-A,B) with different historical nomenclatures of the codifying genes and proteins. In bold, the current IUPHAR nomenclature (Collingridge GL. et al 2009).

Each of these subunits is composed by a large extracellular amino-terminal domain (ATD), an extracellular ligand-binding domain (LBD), a transmembrane domain (TMD) with three transmembrane helices (M1, M3 and M4) and a re-entrant loop (M2), and an intracellular carboxyl-terminal domain (CTD) (Traynelis SF. et al., 2010).

Upon agonist(s) binding, ionotropic glutamate receptors permeability to monovalent cations (Na^+, K^+) and, additionally, to Ca^{2+} (for some iGluRs, including NMDARs, and calcium permeable AMPA and Kainate receptors) change, resulting in an ion influx through them. The influx of positive charges depolarizes the cell and consequently, produces an excitatory postsynaptic potential (EPSP) that activates the postsynaptic neuron and leads to activation of different signaling pathways (Traynelis SF. et al., 2010).

Subunits conforming Kainate receptors (GluK1-K5) are further divided into low- (GluK1-K3) and high-affinity (GluK4-K5) subunits. Low-affinity subunits might form homomers whereas high-affinity subunits should heteromerize with one low-affinity subunit. The most common subunits in the adult hippocampus are GluK2 and GluK5. Kainate receptors are activated upon glutamate binding leading to small currents and their activation and deactivation kinetics are slow. However, KARs also present a non-canonical activation pathway via a G_o protein through an adaptor protein (same pathway than $G_q/11$ protein) (Valbuena S. et al., 2020).

AMPA receptors are composed by GluA1-GluA4 subunits, with the majority of them in adult hippocampus containing the GluA1 and GluA2 subunit (leading to Ca^{2+} impermeability) and they mediate the fastest excitatory transmission, when glutamate is released, which has a larger amplitude than KAR and decays rapidly (Traynelis SF. et al., 2010).

NMDAR subunit composition and physiology will be further discussed in the next sections.

1.2.1.3.   Additional molecular and structural elements of the glutamatergic synapse: Glutamate transporters, glycine transporters and the post-synaptic density

When glutamate is released from the pre-synaptic terminal, it must be cleared out to avoid diffusion, overactivation of glutamate receptors and hence the excitotoxicity derived from this excess of glutamatergic signaling (Hardingham GE. and Bading H., 2010). The majority of glutamate clearance is carried out by astrocytes. However, there are also glutamate transporters in the post-synaptic neurons (EAAT3/EAAC1) that might remove the excess of glutamate (Zhou Y. et al., 2014) (see **figure 7**). These EAAT (excitatory amino acid transporters/carriers) glutamate transporters allow glutamate transport by coupling to the cotransport of two Na^+ ions, and the opposite transport of one K^+ ion and one H^+. In addition to the coupled ions, glutamate transporters allow an uncoupled anion chloride flux (Wadiche JI. et al., 1995) (see **figure 8**).

In the post-synaptic neuron, the glycine transporter (GLYT1) is also expressed. This transporter controls glycine concentration in the synaptic cleft, likely working in the same direction than GLYT1 in the pre-synaptic terminal.

The complex molecular machinery (membrane proteins) of the post-synaptic neuron, is organized in a dynamic subcellular compartment known as postsynaptic density (PSD). This structure comprises a plethora of proteins, that are dynamically regulated and compose the so-called synaptoproteome (SynGO, https://www.syngoportal.org) and can directly or indirectly interact with GluRs (Sheng M. et al., 2007, Kennedy MB., 2018) (see **figure 6**). The ensemble of these proteins is responsible of maintaining the synapse structure and the different signaling cascades (upon receptors activation) involved in synaptic plasticity. Functionally, these proteins are grouped into the following categories: scaffold proteins (*e.g.* MAGUKs, including PSD-95/SAP90, PSD-93/Chapsyn, SAP97, and SAP102; proteins from the SHANK and Homer families), cell adhesion molecules (*e.g.* neurexins, neuroligins, cadherins, catenins), kinases (*e.g.* CaMKII, PKA, PKC), phosphatases (*e.g.* PTEN, PP1), GTPases (*e.g.* SynGAP, ARF3), motor proteins (*e.g.* dynein, myosin), trafficking proteins (*e.g.* clathrin, AP1, synapsin, SNAP5), chaperones (HSP40), ubiquitins, cytoskeleton proteins (actin, tubulin, ankyrins…) and proteases. These proteins in the PSD interact with the glutamatergic receptors through the carboxy-terminal domain (Sheng M. et al., 2007, Kennedy MB., 2018) (see **figure 6**).
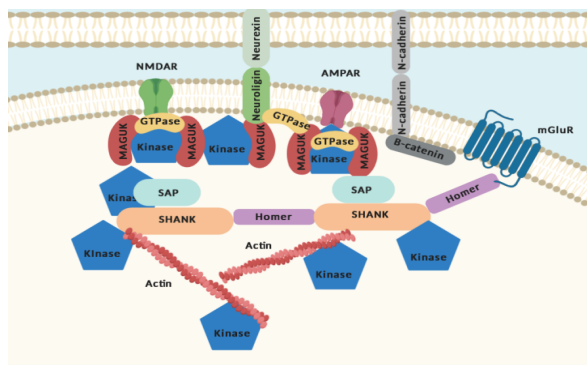
Figure 6. A simplified scheme of postsynaptic density components: NMDAR, AMPAR, mGluR, neurexin-neuroligin, N-cadherin-B-catenin, GTPases, MAGUKs, Kinases, SAP, SHANK, Homer, Actin.

1.2.3. Astrocytic cells

Astrocytes represent a major group of glial cells with crucial role in CNS. Among other important roles, astrocytes are part of the structure of the blood brain barrier, regulate extracellular K^+ levels and can release gliotransmitters that modulate the tripartite synapse. Regarding their role in the glutamatergic transmission, after glutamate release and glutamatergic receptor activation, glutamate must be cleared from the synaptic cleft to avoid diffusion to neighbor synapses and excitotoxicity. This clearance is principally made by astrocytes, thanks to GLAST (Glutamate-Aspartate transporter 1)/EAAT1 and Glt1(Glutamate transporter 1)/EAAT2, and allow the conversion of uptaken glutamate into glutamine that will be released from astrocytes and uptaken by neurons, ultimately entering neurons and being used for glutamate synthesis (Zhou Y. et al., 2014) (see **figure 7**). Glutamine release from astrocytes is carried out via SN1 (System N transporter 1)/SNAT3 and SN2/SNAT5 thanks to a cotransport of 1 Na^+ ion and the opposite transport of 1 H^+. It is known that this system might act in both directions depending on the substrates and the ionic gradients (Rubio-Aliaga I. et al., 2016) (see **figures 7-8**).

Additionally, astrocytes also express GLYT1 for the regulation of glycine concentration in the synaptic cleft, similar to pre-synaptic and post-synaptic terminals GLYT1 in the pre-and the post-synaptic terminals (see **figure 7**). In astrocytes, glycine can be released by different mechanisms: 1, through SNAT5 transporter; 2, via GLYT1 reverse transport (when astrocytic intracellular glycine increases); or 3, due to an increase in Na^+ intracellular concentration, after acute depolarization (Hamdani EH. et al., 2012, Shibasaki K. et al., 2017) (see **figure 7**). Astrocytes might also release D-serine when they are depolarized. D-serine is released from astrocytes by Ca^{2+}-dependent mechanism through SNARE complex and/or Ca^{2+}-independent machineries through complexes between purinergic receptors P2 (activated by adenosine triphosphate, ATP) and pannexins channels (see **figures 7-8**) (Mothet JP. et al., 2005, Pan HC. et al., 2015).
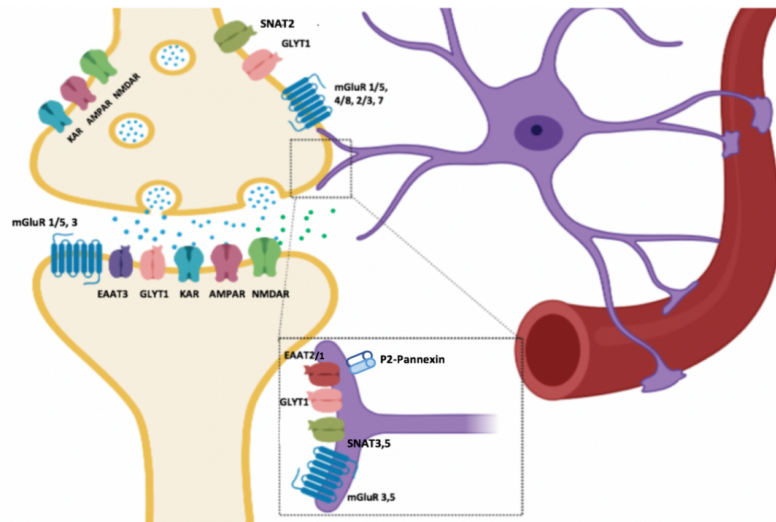
Figure 7. Schematic representation of the tripartite glutamatergic synapse depicting the distribution pattern of the different glutamatergic receptors and transporters; *Pre-synaptic neuron*: Autoreceptors (KAR, AMPAR, NMDAR, mGluR 1/5, 4/8, 2/3 and 7), GLYT1 transporter (glycine clearance), SNAT2 transporter (glutamine uptake); *Post-synaptic neuron*: Metabotropic receptors (mGluR 1/5 and 3) and ionotropic receptors (KAR, AMPAR and NMDAR), GLYT1 transporter (glycine clearance) and EAAT3 transporter (glutamate clearance); *Astrocyte:* P2-Pannexin complex (serine release), EAAT1 and EAAT2 transporter (glutamate clearance), GLYT1 transporter (glycine clearance and release), SNAT3 and 5 transporter (glutamine and glycine release) and mGluR3,5
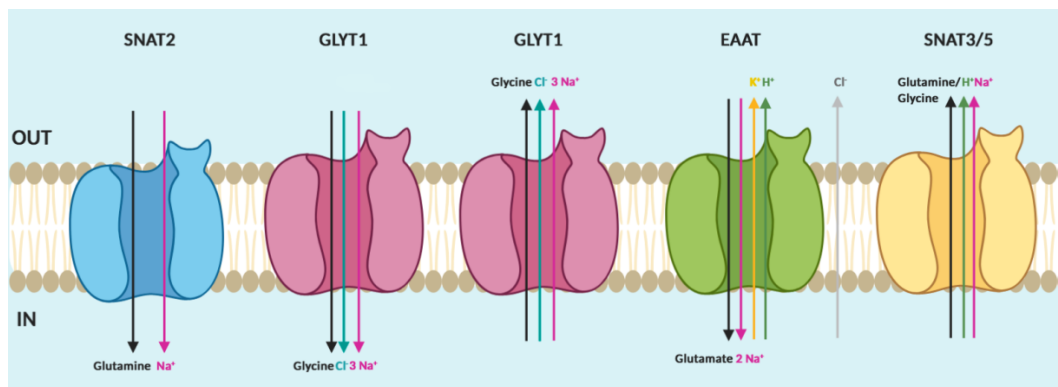
Figure 8. Summary of substrates/ions fluxes through the different transporters in the glutamatergic synapse: SNAT2 (influx of glutamine and sodium), GLYT1 (influx or outflux of glycine, chloride and sodium), EAAT (influx of glutamate and sodium; outflux of potassium and protons, coupled to chloride transport) and SNAT3/5 (outflux of glutamine, glycine, protons and sodium).

Chapter 2.

The NMDA receptor

2.1. Structure and composition of the NMDA receptor

NMDA receptors (NMDARs) are tetrameric structures of 4 GluN subunits (see **table 1**). NMDARs are formed by the combination of two obligatory GluN1 subunits and 2 variable GluN subunits (GluN2A-D, or GluN3A-B). Furthermore, several isoforms (resulting from alternative splicing) have been described for GluN1, GluN2A and GluN3A subunits. In the GluN2A and GluN3A subunits, the alternative splicing affects the C-terminal domain, resulting in two distinct GluN2A or GluN3A isoforms (GluN2A-1 or GluN2A-2, GluN3A-1 or GluN3A-2) whereas in the GluN1 subunit, alternative splicing might occur in the amino-terminal domain (ATD) or the carboxy-terminal domain (CTD). Alternative splicing in the ATD (particularly, in exon 5, N1 cassette) distinguish GluN1a (without N1 cassette) and GluN1b (with N1 cassette). Moreover, CTD splicing determines the inclusion/exclusion of different cassettes: exon 21 (C1 cassette), exon 22 (C2 cassette), and exon 22' (C2' cassette) and, in combination with ATD splicing, might result in 8 different GluN1 isoforms (see **figure 9**) (Paoletti P. et al., 2013; Warming H. et al., 2019).
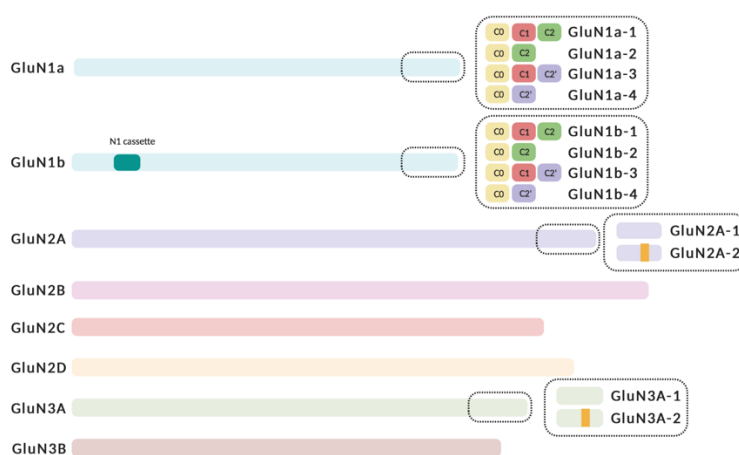
Figure 9. The different GluN subunits resulting from *GRIN* genes and the alternative splicing (adapted from Paoletti P. et al., 2013; Warming H. et al., 2019).

The two obligatory GluN1 subunits might be identical or different (although GluN1-1a and GluN1-1b do not seem to coexist within the same tetrameric receptor). Based on the identity of GluN variable subunits, NMDAR might form di-heteromeric complexes when both variable subunits are the same or tri-heteromeric complexes when variable subunits are different from each other (for instance, GluN3 subunits do not form functional glutamate-gated channels unless they combine with a GluN2 subunit where the glutamate-binding site is) (see **figure 10**) (Paoletti P. et al., 2013; Pérez-Otaño I. et al., 2016).
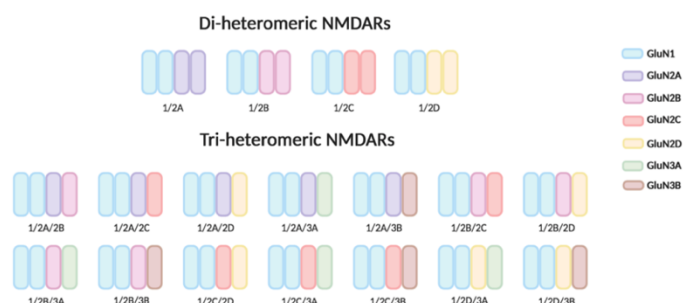
Figure 10. The different populations of di-heteromeric o tri-heteromeric NMDARs that might be formed based on the distinct possibilities of combination.

Thus, the possibilities for subunit combination are very diverse, and result on a large repertoire of NMDAR sub-populations. Functionally, NMDAR molecular composition heterogeneity is crucial, since NMDAR composition determines the biophysical and pharmacological properties of the channel as well as the receptor subcellular distribution, its interactions with other proteins and their physiological role.

2.2. Topology of NMDARs

As other ionotropic glutamate receptors, NMDARs are composed by different domains: an extracellular amino-terminal domain (ATD), a ligand-binding domain (LBD), a transmembrane domain (TMD), and an intracellular carboxy-terminal domain (CTD) (Traynelis SF. et al., 2010) (see **figure 11**).

The ATD is a clamshell-like structure with two parts (R1 and R2) and a pocket in the middle (see **figure 11**). This domain differs the most among GluN subunits (Traynelis SF. et al., 2010) and binds different endogenous ligands that regulates NMDAR function, such Zn^{2+} or NMDAR allosteric modulators that regulate NMDAR activity (see **note[1]**) (Karakas E. et al., 2009). In addition, ATD also mediates initial dimer formation of NMDAR subunits through disulfide bonds formation (Papadakis M. et al., 2004; Hansen KB. et al., 2010) and also regulates NMDARs trafficking- Regarding the latter, the ATD contains a short signal peptide targeting the receptor to the membrane (Hansen KB. et al., 2010), retention signals that prevent release from the endoplasmic reticulum unless the subunits correctly assemble (Horak M. et al., 2008; Qiu S. et al., 2009), and several N-glycosylation sites (Standley S. and Baudry M., 2000; Lichnerova K. et al., 2015). Biophysically, the ATD also influences NMDAR deactivation kinetics and open probability (Gielen et al., 2009; Yuan H. et al., 2009). In summary, the ATD plays a very important role in NMDAR assembly and trafficking, although being also involved in the modulation of NMDAR channel gating.

Following ATD through a linker region, there is the LBD. Phylogenetically, the LBD is more conserved than the ATD and its topology contains a clamshell-like structure (formed by two lobes, S1 and S2) and a pocket for natural agonists binding (Traynelis SF. et al., 2010) (see **figure 11**). Thus, this domain is critical for agonist binding, and consequently, NMDARs gating and activation. The LBD is connected to TMD via three linkers and it is composed by 3 transmembrane helices M1, M3 and M4 and a re-entrant loop M2. Together, the M1-4 of the different GluN subunits constitute the NMDAR channel (see **figure 11**). Within this pore, there is the 'selectivity filter' that controls permeation and ion selectivity and it is susceptible to be blocked by open channel blockers. This structure determines that NMDARs are permeant to monovalent ions (*e.g.* Na^+ and K^+) and divalent ions (*e.g.* Ca^{2+}) while blocked by Mg^{2+} depending on membrane potential, and several blocking drugs (Traynelis SF. et al., 2010). Besides its predominant role in NMDAR biophysics, the TMD also plays a role in NMDARs trafficking (Kaniakova M. et al., 2012).

The M4 segment of the TMD is adjacent to the CTD of the NMDAR (see **figure 11**). CTD contains binding motifs for intracellular binding proteins (Sheng M. et al., 2007, Kennedy MB., 2018), that play a role in NMDAR post-translational modifications (Tingley WG. et al., 1997; Choi Y-B. et al., 2000; Nakazawa T. et al., 2001; Scott DB. et al., 2001; Vissel B. et al., 2001; Yang M. and Leonard JP., 2001; Krupp JJ. et al., 2002; Lavezzari G. et al., 2003; Szklarczyk A. et al., 2008; Yuan H. et al., 2009; Sanz-Clemente A. et al., 2010; Traynelis SF. et al, 2010; Qiu S. et al., 2011; Farinelli M. et al., 2012; Lussier MP. et al., 2015; Sinitskiy AV. et al., 2017; Hayashi T., 2020; Yong XLH. et al., 2021), NMDAR trafficking and docking (Standley S. et al., 2000; Hawkins LM. et al., 2004; Horak M. et al., 2008; Horak M. and Wenthold RJ., 2009), conductance and gating (Maki BA. et al., 2012). Concomitant to the large interactome and domain flexibility, the crystallographic structure of the CTD cannot be resolved.

> **Note[1]:** Allosteric modulators are compounds that bind to an allosteric site within a receptor. Allosteric binding sites are different from the endogenous agonist binding-site, also known as orthosteric site. These compounds modulate the receptor response to the agonist in a positive way (positive allosteric modulators, PAMs, increasing ligand affinity and/or channel activity), negative way (negative allosteric modulators, NAMs, decreasing ligand affinity and/or channel activity) or a neutral way (through blockade of other modulators' binding to the agonist-binding site).
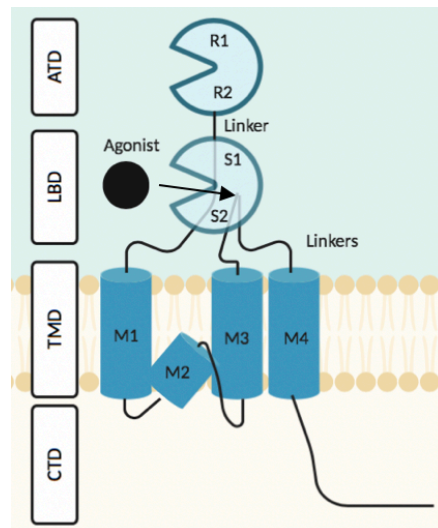
Figure 11. Topological domains of the NMDA receptor: amino-terminal domain (ATD, R1 and R2 regions), ligand-binding domain (LBD, S1 and S2 lobes), transmembrane domain (TMD, M1-M4 transmembrane regions), carboxy-terminal domain (CTD) and linker regions. Agonist (glutamate or glycine/D-serine) is represented as a black dot.

2.3. Assembly, trafficking and docking of NMDARs

Several working models have been proposed to explain GluN subunits assembly into the tetrameric NMDAR structure. Some studies suggest that GluN1-GluN1 and GluN2-GluN2 homodimers would be initially formed, for further formation of the functional tetramers (Qiu S. et al., 2005) (see **model 1, figure 12**). Another theory proposed that GluN2 and GluN3 subunits might only form oligomers in the presence of GluN1 in order to later constitute tetrameric receptors (Schüler T. et al., 2008) (see **model 2, figure 12**). Finally, it has also been proposed the formation of a GluN1-GluN1 homodimer complex followed by sequential assembly of two GluN2 monomers to form the NMDAR tetramer (Atlason PT. et al., 2007) (see **model 3, figure 12**).
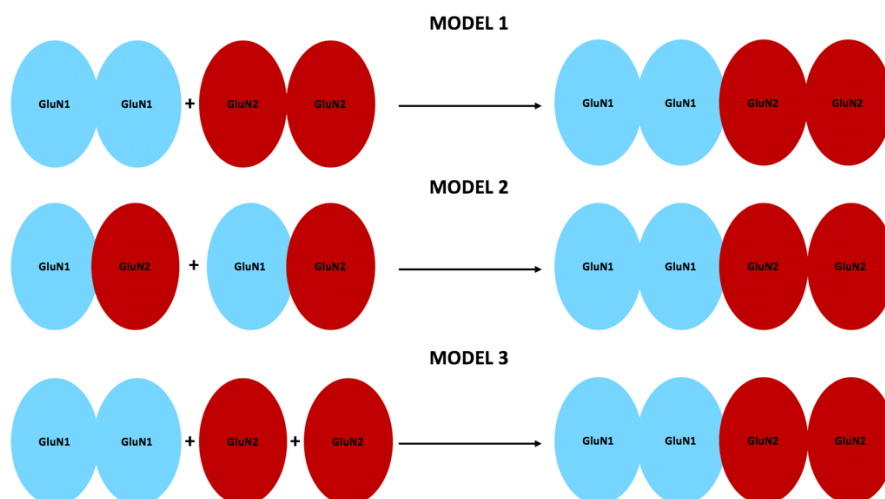
Figure 12. Current working models of GluN subunits assembly for the constitution of tetrameric NMDARs.

Despite the possible/s mechanism/s involved in NMDAR tetramerization, there are several residues which have a role in the interaction between human GluN1 and GluN2 subunits. These residues are GluN1-1a-I519, A524, K531, P532, Y535, R755, L777, GluN2A-I514, F524, V526, P527, E530, L777, L780 and their equivalent positions in other GluN2 subunits such as GluN2B (Furukawa H. et al., 2005) (see **figure 13**).
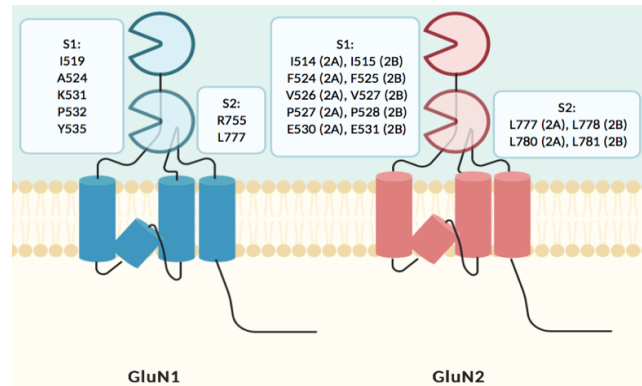
Figure 13. Aminoacid residues in the human GluN1-1a and GluN2A-B subunits with a role in the interaction between both subunits, and NMDAR oligomerization.

The understanding of NMDAR biogenesis mechanisms benefited from the use of heterologous expression systems. In these models, individual expression of GluN subunits (single GluN subunit type) resulted on the retention in the endoplasmic reticulum (ER). This finding reflected a quality control mechanism, suggesting its participation to ensure that only fully assembled and properly folded complexes reach the cell surface. Retention of GluN subunits is due to degradation of misfolded proteins and the presence of retention signals in particular human GluN1 isoforms (RRR or KKK in the C1 cassette), the configuration of a fragment in the human GluN2A ATD and GluN2 C-termini retention signal (unknown sequence), as well as, the integrity of M3 loop in the transmembrane domain of GluN1 and GluN2B (Standley S. et al, 2000; Scott DB. et al., 2001; Hawkins LM. et al., 2004; Horak M. et al., 2008; Horak M. and Wenthold RJ., 2008; Kenny AV. et al., 2009; Qiu S. et al., 2009; Kaniakova M. et al., 2012) (see **figure 14**).
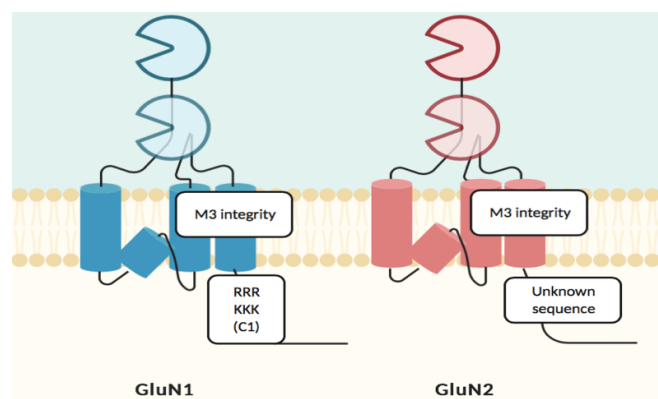
Figure 14. Retention signals located in the M3 transmembrane fragment and the C-terminal domain in the human GluN1 and GluN2 subunits of NMDA receptors.

Mechanistically, the assembly of GluN subunits results on ER retention signals maskings, allowing further trafficking of the NMDAR to the plasma membrane. For instance, in the human GluN2, the presence of at least 3 aminoacid length sequence within the C-termini of GluN2 subunits sequences immediately following the fourth transmembrane domain (EHL), is able to mask the human GluN1 C1 retention signals, as well as some human GluN1 isoforms containing the C2' cassette last 6 aminoacids including

the PDZ-binding motif (PSD-95/Dlg/ZO-1). Also, the human GluN2A M3 domain (Ser-644 and Tyr-645) and the human GluN2B M3 domain (Trp-635, Ser-645, Tyr-646, Thr-647) is involved in masking human GluN1 M3 retention signals, whereas the human GluN1 M4 domain is necessary for masking human GluN1 M3 and GluN2B M3 retention signals, and human GluN1 M3 (in GluN1-1a: Trp-636, Tyr-647 and Thr-648) also participates on masking human GluN2 retention signals. Besides this masking mechanism, additional control checkpoints participate in the control of tetrameric NMDAR exit from the intracellular compartments. In this regard, the proximal region of the C0 cassette in human GluN1 regulates the structure of the M4 domain and other surrounding regions of the GluN1 subunit. Another structure which is important for the release of functional NMDARs from the ER is the integrity of the glycine binding site in the human GluN1 subunit (*e.g.* GRIN1(p.D732A) variant, within the LBD, abolishes NMDAR surface trafficking) (Standley S. et al, 2000; Scott DB. et al., 2001; Hawkins LM. et al., 2004; Horak M. et al., 2008; Horak M. and Wenthold RJ., 2008; Kenny AV. et al., 2009; Qiu S. et al., 2009; Kaniakova M. et al., 2012) (see **figure 15**).
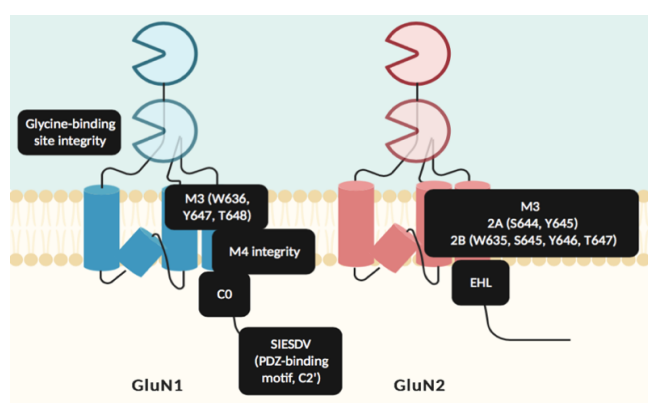
Figure 15. Masking mechanisms of retention signals located in the N-terminal, M3 and M4 transmembrane fragments, and C-terminal domains in the human GluN1-1a and GluN2 subunits of NMDA receptors.

After NMDAR-containing complexes exit the endoplasmic reticulum (ER), they are modified at the Golgi apparatus. Some of these post-translational modifications also play a role in the receptor trafficking such as N-glycosylation of GluN1-1a subunit (at residues N203 and N368) or protein kinase C-mediated phosphorylation of GluN2 subunit (GluN-S896) (Standley S. and Baudry M., 2000; Scott DB. et al., 2001; Horak M. and Wenthold RJ., 2008; Lichnerova K. et al., 2015) (see **figure 16**).
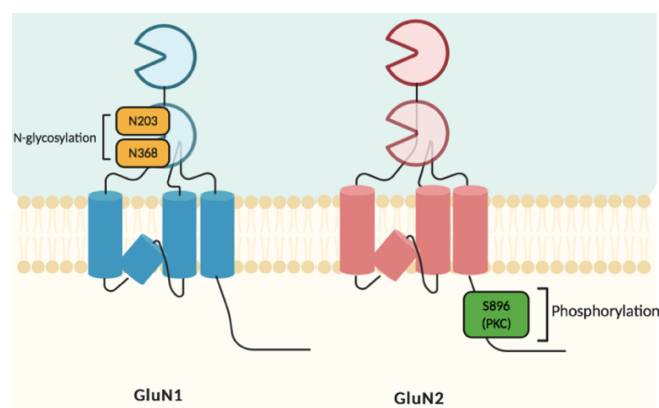
Figure 16. Schematic representation of GluN subunits post-translational modifications involved in surface trafficking control of the NMDAR.

Once the receptor is modified, it is sorted in the trans-Golgi network (TGN). NMDARs are carried on transport vesicles, bound to MAGUKs that in turn bind the exocyst component Sec8 and mPins (mammalian homologue of Drosophila melanogaster partner of inscuteable) that binds to the G protein subunit Gα. Both Sec8 and the NMDARs subunits bind to the same region of MAGUKs primarily within the first and second PDZ domains. MAGUKs-NMDARs interaction occurs via the E(S/T)XV motif GluN2-CTD. mPins–MAGUK complex may promote efficient targeting of NMDARs to cell surfaces and the interaction of $G\alpha_i$ with mPins contributes in the stabilization of the complex. NMDAR subunits can bind to a complex of other proteins (mLin-7/MALS (mammalian lin-seven protein) /Veli (vertebrate lin-seven homolog), mLin-2/CASK (calcium/calmodulin-dependent serine protein kinase), mLin-10/Mint1 (munc18-1-interacting protein 1)/X11) linking the NMDAR to the kinesins through their C-termini and mediating the transport of the NMDAR along the dendrite (see **figure 17**). NMDAR traveling via kinesins (kif) on microtubule tracks may switch to myosin motors on actin filaments for final transport to cell surfaces and transport within postsynaptic spines although this last motor protein identity remains elusive (Setou M. et al., 2000; Sans N. et al., 2003; Sans N. et al., 2005).
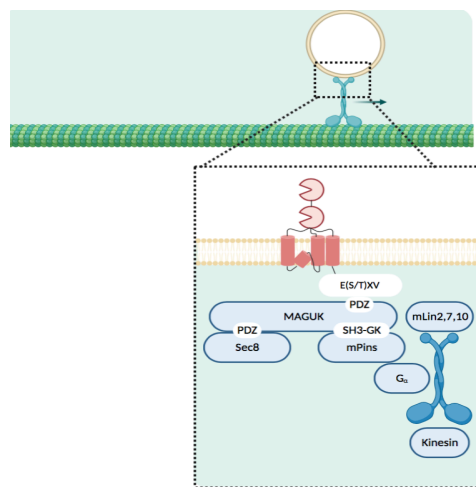
Figure 17. NMDAR transport along the dendrite via kinesin transport in microtubules and underlying multimeric protein complex (NMDAR, MAGUK, SEC8, mPins, mLins, G_α and kinesin).

2.4. NMDARs as coincidence detectors: NMDAR activation process

For their activation, NMDARs require simultaneous binding of co-agonists: glutamate to the GluN2 subunits and glycine/D-serine to GluN1 and/or GluN3 subunits (Johnson and Ascher, 1987; Mothet JP. et al., 2000). Regarding glycine/D-serine co-agonist activity, their role on NMDAR activation varies within the brain region, with D-serine playing a role in the forebrain and glycine being most predominant in the cerebellum (Matsui T-A. et al., 1995). Moreover, D-serine preferentially binds to synaptic receptors while glycine predominantly binds to extra-synaptic receptors (Papouin T. et al., 2012). Co-agonists binding mechanism differ, with glutamate binding based on the interaction with positively charged chains (outside the binding pocket), guiding glutamate binding to the LBD, whereas glycine/D-serine binding is independent of electrostatic interactions (Yu A. and Lau AY., 2018).

Under basal conditions, neurons have a negative resting membrane potential (-60/-80 mV) and thus NMDARs are blocked by a Mg^{2+} ion (Nowak L. et al., 1984). This blockade is voltage-dependent, in such a way that the blockade disappears at positive membrane potentials, with the release of Mg^{2+}. Thus, for their activation NMDARs behave as coincidence detectors, considering the obligatory and simultaneous presence of two sine qua non events. Indeed, NMDARs activation requires glutamate release (from the depolarized pre-synaptic terminal) and the depolarization of the post-synaptic terminal (at the same time or shortly after pre-synaptic neuron depolarization) allowing Mg^{2+} release from the channel pore.

Depolarization of the post-synaptic neuron results from the activation of non-NMDARs (e.g. AMPARs) with fast and transient voltage-independent response (Blanke ML. and Van Dongen AMJ., 2009) (see **figure 18**). Once the NMDAR is unblocked, and agonist and co-agonist bind to the receptor, NMDAR gating occurs. NMDAR gating results in a conformational change in the LBD, causing the two lobes to close around the ligand, preventing its dissociation (Dolino DM. et al., 2016).
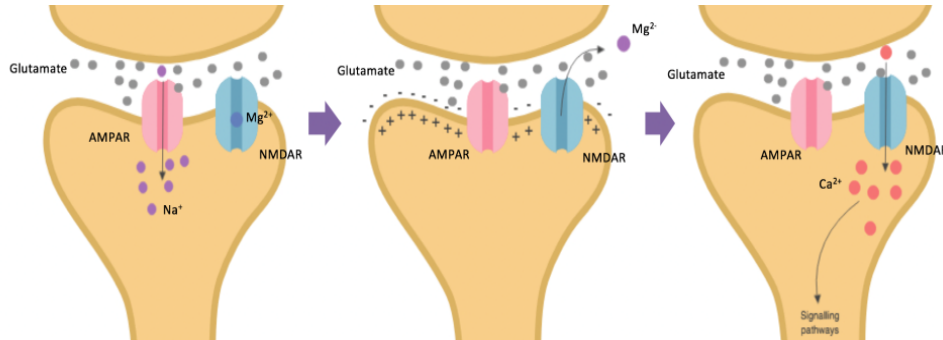
Figure 18. NMDAR activation via pre-synaptic terminal depolarization (resulting in glutamate release) and post-synaptic neuron stimulation (due to AMPARs activation) which releases Mg^{2+} blockade and allows Ca2+ influx through the NMDAR.

The identity of the amino acid residues involved in co-agonists binding to the NMDAR have been the object of multiple studies, ranging from structural and computational studies to the characterization of disease-associated *GRIN* variants. Several amino acid residues involved in the interaction between glycine or D-serine and the human GluN1-1a subunit of the NMDAR (*e.g.* GluN1-1a-K483, F484, G485, E488, N499, P516, T518, E522, R523, Q686, S688, R694, R695, E712, R722, D732). In parallel, there are also residues which are important for glutamate binding to the human GluN2 binding-site (*e.g.* GluN2A-H485, S511, T513, E517, R518, S689, T690, R692, R695, Y730, D731, Y761 and their respective equivalent positions in other GluN2 subunits like GluN2B) (Furukawa H. et al., 2005; Dai J. and Zhou H-X., 2016; Yu A. and Lau AY., 2018) (see **figure 19).**
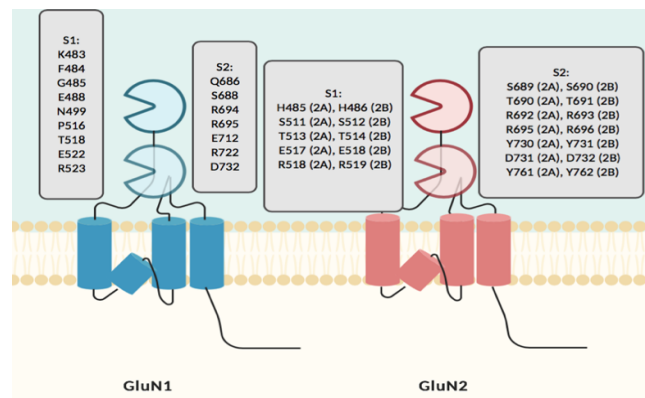
Figure 19. Aminoacid residues of human GluN1-1a and GluN2A/B subunits with a role in agonist binding.

Co-agonists binding probably triggers the movement of the linkers between TMD and LBD, and consequently, a rearrangement of M3 segment, resulting in the channel opening (Furukawa H. et al., 2005) allowing ion fluxes through the channel pore, including Na^+, K^+ and specially a Ca^{2+}transient that is transduced and activates multiple signaling cascades.

 Missense mutations affecting amino acid residues involved on co-agonists binding (see **figure 19**) might affect the agonist affinity and/or efficacy (see **note²**), depending on their topological location: if these variants affect residues whose role is related with agonist-binding affect both affinity and efficacy, while variants occurring in residues that are associated with the stabilization of the LBD conformation only affect efficacy (Kalbaugh TL. et al., 2004).

Ionic selectivity and conductance are dictated by the residues lining NMDAR channel pore. In particular, GluN1-1a-N616 (within the M2 re-entrant loop) determines Ca^{2+} permeability (Chen N. et al., 2004) (see **figure 20**). Additionally, GluN1-1-N616 and orthologous GluN2 subunit (*e.g.* GluN2A-N614 and GluN2B-N615) also play role in Mg^{2+} blockade (Mori H. et al., 1992) (see **figure 20**).
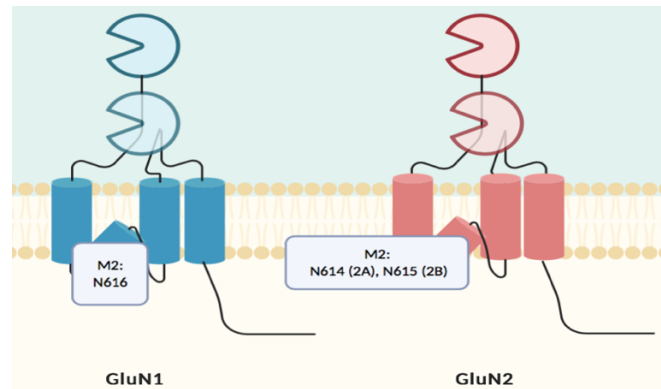
Figure 20. Aminoacid residues in human GluN1-1a and GluN2A/B subunits with a role in Ca^{2+} permeability and Mg^{2+} blockade.

In relation with the movement of the LBD-TMD linkers, there are a group of residues which are known as the 'TTTT gate' in the channel pore (human GluN1-1a-T648, GluN2A-T646 and GluN2B-T647) and the 'LILI gate' which is located in the S2-M3 linker (human GluN1-1a-L657, GluN2A-I654 and GluN2B-I655) and control NMDAR gating (Ladislav M. et al., 2018) (see **figure 21**). However, there is a subunit-specific effect in these linkers' regulation because GluN1 is responsible of controlling the duration of channel opening while GluN2 has a role in the regulation of the opening frequency (Kazi R. et al., 2014).
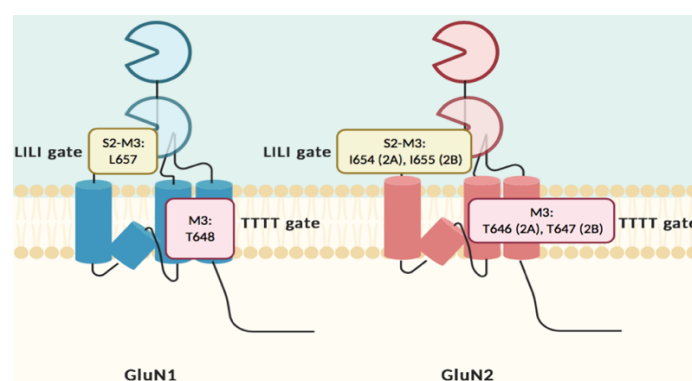
Figure 21. Aminoacid residues in human GluN1-1a and GluN2A/B subunits with a role in the regulation of NMDAR gating.

Note²: Agonist binding depends on two properties: affinity which determines how strong is the interaction agonist-receptor, and efficacy that defines the ability to activate the receptor

2.5. NMDAR activity control by deactivation, desensitization, internalization or degradation

After the agonists are rapidly cleared from the synaptic cleft, NMDARs undergoes in a closed non-permeable state (deactivation). This closing is due to a rearrangement in the receptor extracellular domains, particularly by ATD rotation that approaches GluN2 amino-terminal domains while separating the GluN1 ATD (see **figure 22**) (Černý J. et al., 2019). NMDAR gating is stationary, meaning that NMDA receptors stochastically oscillates between two states, open and closed, to allow conductance while avoiding permeation (Dai J. and Zhou H-X., 2016).

Nevertheless, when there is a sustained agonist exposition, NMDARs do not deactivate but might enter in a desensitization state where these receptors are less responsive. Currently, desensitization is explained by different mechanisms: 1) weakening of co-agonists affinities (Nahum-Levy R. et al., 2001); 2) calcium/calmodulin and α-actinin binding to the GluN1 CTD C0 segment (human GluN1-1a R859-Q863) via Ca^{2+} increase, resulting in a decreased open probability (Krupp JJ. et al., 1999); 3) pH-dependent allosteric interaction between GluN2 LBD and Zn^{2+} (Paoletti P. et al., 2000; Erreger F. and Traynelis SF., 2005); or 4) PSD95 direct interaction with GluN2 CTD (PDZ-binding motif) (see **figure 22**) (Sornarajah L. et al., 2011).

In addition to deactivation and/or desensitization biophysical properties, another control mechanism of NMDARs activity is the receptor internalization. NMDARs are internalized via AP2 adaptor that allows the binding of the receptor to clathrin. This internalization is driven by specific motifs present in GluN1 and GluN2 subunits, located in the intracellular CTDs (*e.g.* GluN1-Y838, K861 in C0 cassette, the proximal GluN2 CTD and YEKL motif in the distal GluN2B CTD) (Roche KW. et al., 2001; Scott DB. et al., 2004) (see **figure 22**). These internalized receptors might be recycled and re-inserted in the plasma membrane (determined by the proximal CTD of GluN2) or degraded (influenced by GluN1 endocytic motifs) (Scott DB. et al., 2004). This endocytosis process is promoted by the co-agonist site stimulation in the GluN1 subunit, that promotes recruitment of the endocytic machinery but needs the NMDAR receptor activation to occur (Nong Y. et al., 2003).

Furthermore, due to synaptic activation, NMDARs might be targeted to degradation, ultimately controlling NMDARs density and consequently, NMDARs global activity. This occurs via a F-box protein which binds to glycosylated regions of the GluN1 ATD, promoting its ubiquitination and consequently, its degradation via the ubiquitin-proteasome system (see **figure 22**) (Kato A. et al., 2005).
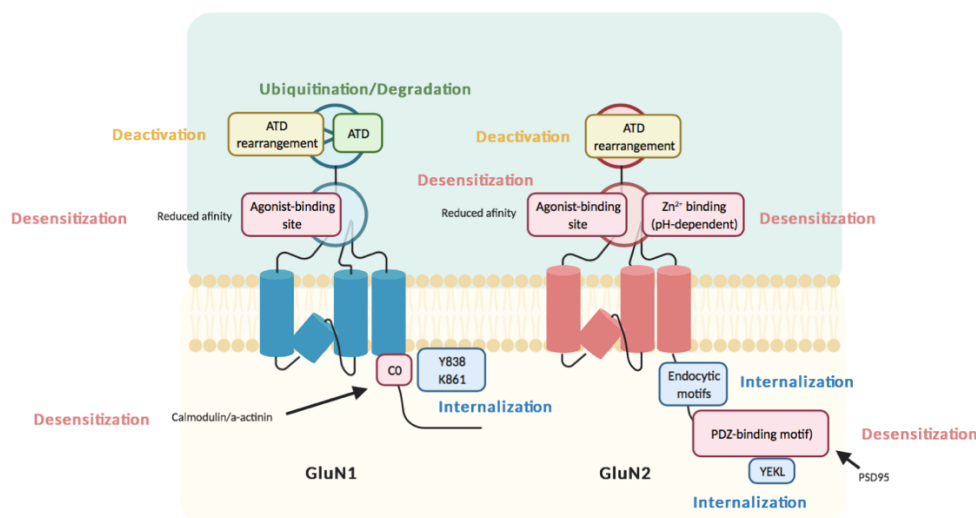
Figure 22. Critical domains and amino acid residues of GluN1-1a, GluN2A and GluN2B subunits participating in the regulation of NMDARs deactivation, desensitization, internalization or ubiquitination/degradation.

2.6. Anatomical, biophysical and pharmacological differences based on the NMDARs composition

NMDARs composition is spatio-temporally regulated. Indeed, the precise composition of NMDAR depends on the developmental stage, on the brain region or on neuronal activity, and can also be modified under pathophysiological conditions. All these data indicate that specific NMDAR subtypes might carry particular functions in the central nervous system (Paoletti P. et al., 2013).

GluN1 subunit is expressed from embryonic stages to adulthood, since it is the obligatory subunit and needs to be present on NMDARs for the correct function of the receptor. Yet, the regional distribution depends on the isoform. Whereas GluN1-1b is ubiquitous, GluN1-1a is highly represented in the cortex and the hippocampus (Paoletti P. et al., 2013). On the contrary, GluN2A-D and GluN3A, B subunits expression is more variable. Shortly after birth, there are only GluN2B in frontal and cerebellar regions, GluN2D in caudal regions and GluN3A subunits, in rostral brain, suggesting an important role in synaptogenesis and synapses maturation for these subunits. While these subunits decrease after birth (some of them more than others), GluN2A expression increases after birth until being the most prominent GluN2 subunit in the adult brain (Bar-Shira O. et al., 2015). GluN2D subunit expression is restricted to few brain areas, while GluN3A subunit expression practically disappears in the adult brain. GluN2B subunit presence in adult brain is more preserved, being one of the predominant subunits along with GluN2A. In the other hand, GluN2C appears few weeks after birth in very restricted areas like cerebellum and olfactory bulb, GluN3B is essentially limited to motoneurons in spinal cord and brainstem (Chatterton JE. Et al., 2002; Paoletti P. et al., 2013) (see **figure 23**).

Figure 23. Developmental changes on NMDAR GluN2 and GluN3 subunits distribution shortly after birth (GluN2B-frontal brain and cerebellum; GluN2D-caudal brain; GluN3A-rostral brain), few weeks later (GluN2B-to-GluN2A switch, both subunits spread along the whole brain; GluN2C in frontal brain and cerebellum; GluN2D-caudal brain; GluN3A-rostral and caudal brain) and in adulthood (GluN2A is predominant and spread in the whole brain; there are some remaining GluN2B subunits which appear in different regions; GluN2C remain in frontal brain and cerebellum; GluN2D remain in caudal regions; GluN3A disappear; and GluN3B appear in brainstem).

GluN subunits might also vary among cell types (neurons, astrocytes, oligodendrocytes) or subcellular localization (extrasynaptic or synaptic sites) (Papouin T. et al., 2012; Paoletti P. et al. 2013).

Nevertheless, not only regional properties vary depending on the subunits' composition. The channel properties (trafficking, open probability, conductance, permeability, kinetics or sensitivity to blockade) also depend on the combination of GluN subunits. In this line, GluN1 isoforms affect the receptor activity. Indeed, GluN1b isoform (which contains the N1 cassette) show lower affinity for glutamate, faster deactivation than GluN1a isoform (without N1 cassette) and a reduced proton sensitivity (Regan MC. et al., 2018; Liu H. et al., 2019).

 The presence of the GluN3 subunit also affects NMDAR activity. Indeed, the expression of GluN3 in combination with GluN1 subunits *in vitro* form excitatory glycine receptors that do not respond to glutamate or NMDA and are Mg^{2+}-insensitive and less permeant to Ca^{2+} (Chatterton JE. Et al., 2002) although *in vivo* expression has not been confirmed, due to the fact that these receptors might be rapidly degraded or removed from the membrane (Henson M.A. et al., 2010; Pérez-Otaño I. et al., 2016). Thus, to form a functional NMDA receptor, this subunit must associate with GluN1 and GluN2 subunits, forming tri-heteromeric receptors. Nevertheless, these tri-heteromeric receptors have lower conductance than GluN1/GluN3 receptors (Chatterton JE. Et al., 2002). Concomitantly, the NMDARs containing GluN3 subunits are thought to have a role as guide for neuronal pruning and brake for synapse maturation (Pérez-Otaño I. et al., 2016).

The distinct GluN2 isoforms also differ regarding the channel properties. For instance, GluN2A- and GluN2B-subunit containing NMDARs exhibit higher conductance, Ca^{2+} permeability and sensitivity to Mg^{2+} blockade than GluN2C- and GluN2D-subunit containing NMDARs (Traynelis SF. et al., 2010). Furthermore, despite all NMDARs present slow activation and deactivation kinetics, the constant rates are GluN2 subunit-depending, being GluN2A the fastest and the one with the lowest glutamate affinity, followed by GluN2B and GluN2C, and finally, GluN2D as the slowest but the one with the highest glutamate affinity (Cull-Candy S. et al., 2001).

In relation with NMDAR open probability, GluN2A-containing receptors present the highest one, followed by GluN2B, then GluN2D and finally, GluN2C. In addition to the different affinities towards glutamate, GluN2 identity also determines the level of GluN1 affinity for the co-agonist, with the following order: GluN2C > GluN2B > GluN2D >> GluN2A (Yuan H. et al., 2009). Regarding desensitization, synaptic NMDARs (predominantly GluN2A) show less desensitization than extrasynaptic NMDARs (mostly GluN2B) due to NMDAR association with PSD in the synapse (Sornarajah L. et al., 2011). Moreover, this process is absent in GluN2C- and GluN2D-containing NMDARs (Traynelis SF. et al., 2010).

Besides the intrinsic regulation of NMDARs biophysical properties, GluN subunbits composition also dictates de subcellular localisation of the NMDARs. Specifically, GluN2B-containing NMDARs are thought to be preferentially localized at extrasynaptic sites and can, under certain pathophysiological scenarios, promote neurotoxicity and cell death (Hardingham GE. and Bading H. et al., 2010). In contrast, GluN2A-containing NMDARs are mostly synaptic and, in addition to participate in synaptic plasticity processes, have been proposed to potentiate neuronal survival (Zhang S. et al., 2007). Nevertheless, both subunits are located at both locations (Thomas C.G. et al., 2005), and the dynamics of NMDARs both in physiological and pathophysiological scenarios are the object of investigational efforts (Petit-Pedrol M. and Groc L., 2020). Interestingly, synaptic location might also be influenced by the GluN1 subunit. GluN1 C0 interacts with α-actinin (an actin-binding protein) to anchor NMDAR to cytoskeleton. However, this interaction might be antagonized by Ca^{2+}-calmodulin interaction with GluN1 C0 and C1 cassettes. Thus, Ca^{2+} entering via synaptic NMDARs might disassemble NMDAR from cytoskeleton, resulting in their redistribution to extrasynaptic sites, and some subunits might be more prone than other to be re-located (Arundine M. and Tymianski M., 2003).

Finally, GluN subunits composition also determines the differential pharmacological sensitivity to modulators and drugs that modify NMDAR channel gating (Traynelis SF. et al., 2010), as further presented in this Thesis.

2.7. NMDAR regulation by post-translational modifications

Multiple post-translational modifications (PTM) regulate both NMDAR surface expression (biogenesis) and channel gating. These modifications are dynamic, reversible and rely on synaptic activity, conferring to the NMDARs a wide and fast tuning range, adapting to neuronal inputs and homeostasis.

One of these modifications is phosphorylation which consists on the enzymatic (carried out by protein kinases) addition of a phosphate group to a serine, threonine, tyrosine residue in a protein. Phosphorylation results in a change of hydrophobicity and electric charge of the region where the phosphate group is added, and consequently, this process might affect protein conformation, interaction with other proteins, the channel properties and/or the receptor trafficking. For instance, some residues which are phosphorylated and promote surface trafficking and functioning of NMDARs are GluN1-1a-S896, S897, S917 and S918, GluN2A-S1048, S1291, S1312 and GluN2B-S1116, S1303, S1323, Y1336 and Y1474 whereas phosphorylation of GluN1-S890, GluN2A-S1459 and GluN2B-S1482 has the opposite effect (Tingley WG. et al., 1997; Scott DB. et al., 2001; Qiu S. et al., 2011; Lussier MP. et al., 2015; Yong XLH. et al., 2021) (see **figure 24**). Furthermore, phosphorylation of GluN2A (Y1292, Y1325, Y1387, S1048) potentiates NMDA currents (Yang M. and Leonard JP., 2001; Grau et al., 2014) and GluN2B-Y1472 phosphorylation is related with synaptic plasticity (Nakazawa T. et al., 2001) (see **figure 24**). Importantly, NMDARs phosphorylation is also associated with GluN2B-to-GluN2A developmental switch, in particular by the phosphorylation of GluN2B-S1480 (Sanz-Clemente A. et al., 2010) (see **figure 24**).

The enzymatic activity of protein kinases is counterbalanced by phosphatases actions. Concomitantly, phosphorylation events also play a role in NMDAR activity and surface expression. Protein phosphatase-1 (PP1), by a selective dephosphorylation of pGluN2B-S1303, promotes neuronal survival by reducing NMDAR open probability and activity (Farinelli M. et al., 2012) (see **figure 24**). In addition, GluN2A-Y842 and GluN2B-Y1472 dephosphorylation regulate the interaction of NMDA receptor with the AP-2 adaptor, a protein complex that is involved in clathrin-coated endocytic vesicle formation (Vissel B. et al., 2001, Lavezzari G. et al., 2003) (see **figure 24**). Moreover, dephosphorylation of GluN2A-S900 and S929 have a role in NMDAR desensitization (Krupp JJ. et al., 2002) (see **figure 24**). Another example is the dephosphorylation of GluN2A-S1459 that occurs at the cell surface and results in an increased MAGUK binding that stabilizes the receptor at the membrane (Mota Viera M. et al., 2020) (see **figure 24**).

NMDARs are also subject to glycosylation processes, mediating the incorporation of glycans modifying NMDARs folding, trafficking and biophysical properties. Examples of this modification are some residues located in the ligand-binding domain such as GluN1-N440 and GluN2B-N444, N491 and N688, that are related with the rearrangement of the ligand-binding domain and consequently, the ligand affinity (Sinitskiy AV. et al., 2017) (see **figure 24**).

NMDARs also undergo palmitoylation, consisting on palmitic acid addition (by the action of palmitoyltransferases) to a cysteine residue usually surrounded by basic and hydrophobic residues, frequently occurring in the transmembrane domain. This process increases hydrophobicity and regulates the receptor presence at the membrane. GluN1 subunit is not palmitoylated while in GluN2A and GluN2B subunits, there are two NMDAR domains regulated by this mechanism. One is located in the TM4 domain (including GluN2A-C848, C853, and C870; and GluN2B-C849, C854, and C871) and favors NMDAR surface expression, while the other one is located in the CTD (containing GluN2A-C1214, C1217, C1236, C1239; and GluN2B-C1215, C1218, C1239, C1242, C1245) and is related with NMDAR retention in the Golgi apparatus (Lussier MP. et al., 2015; Hayashi T., 2020) (see **figure 24**).

GluN1 and GluN2 subunits are also modulated by endogenous or exogenous *S*-nitrosylation on cysteine thiol groups based on the extracellular redox state. GluN1-C744 and C798, and GluN2A-C87, C320 and C399 participate in this modulation (Choi Y-B. et al., 2000) (see **figure 24**).

Ubiquitination is another process which can regulate NMDARs. This mechanism is based on the incorporation of an ubiquitin molecule to a lysine residue, labeling proteins for degradation. It is known that residues from 1170 to 1482 in GluN2B subunits interact with proteins that promote their ubiquitination and degradation (Qiu S. et al., 2011) (see **figure 24**).

There are also several proteases that might cleave NMDAR subunits and consequently, regulate the receptor's function. For instance, tissue plasminogen activator, plasmin, metalloproteinase-7 and thrombin cleave GluN1 at multiple sites, with different functional consequences. For instance, metalloproteinase-7 cleavages GluN1 P516-K517, impairing ligand binding (Szklarczyk A. et al., 2008). Plasmin and metalloproteinase-7 also cleaves GluN2A. Indeed, it is known that plasmin cleaves GluN2A-K317 causing NMDAR insensitivity to Zn^{2+} blockade (Yuan H. et al., 2009), while thrombin might cleave GluN2B. Both, GluN2A and GluN2B are also degraded by calpains (Traynelis SF. et al, 2010) (see **figure 24**).
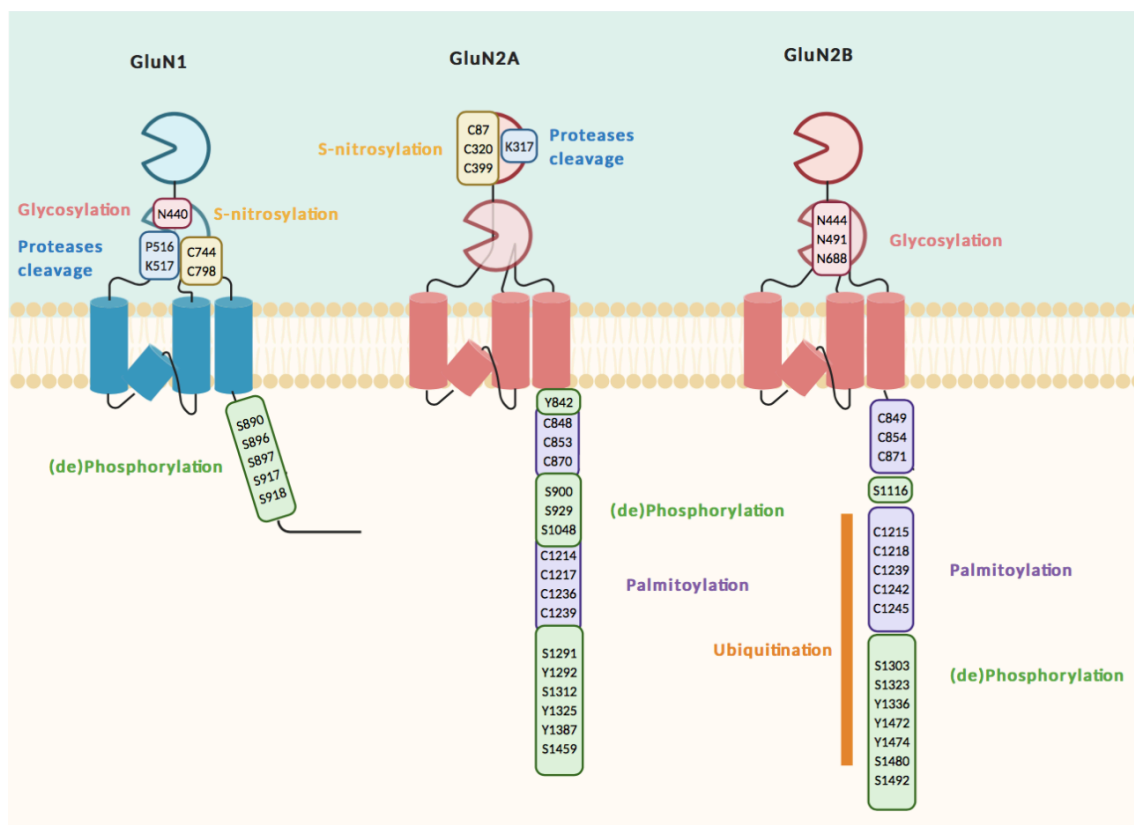
Figure 24. Scheme of GluN1, GluN2A, GluN2B subunits, showing the localization of residues where post-translational modifications occur: phosphorylation/dephosphorylation (green), glycosylation (pink), palmitoylation (purple), proteases-mediated cleavage (blue), S-nytrosylation (yellow) and ubiquitination (orange).

<u>**2.8. NMDAR physiological roles**</u>

2.8.1.   Neuronal NMDARs: Plasticity

NMDA receptors and their function as coincident detectors are crucial for the priming of potentiation events at neuronal level, which are the basis for learning and memory. These processes are determined by experiences that lead to changes in neural circuitries, via synaptic plasticity which is a modification of strength and/or efficacy of synaptic transmission. Based on the lasting effects, synaptic plasticity can be classified into short-term plasticity (transient or non-stabilized post-translational modifications) or long-term plasticity, when it provokes several changes lasting over long periods of time (Morgado-Bernal I. et al, 2011).

Moreover, plasticity processes might result in synaptic potentiation or depression, depending on how they are generated. Traditionally, when a synapse is repeatedly activated pre-synaptically at the same time as the postsynaptic neuron is strongly depolarized (large and quick increments of intracellular calcium) the synapse becomes stronger by potentiation. Conversely, if a synapse is repeatedly activated pre-synaptically while the postsynaptic neuron is weakly or not depolarized (small and slower amounts of calcium) synapse becomes weaker by a process known as depression (Traynelis SF. et al., 2010). Calmodulin protein sense those calcium differences and activates Ca^{2+}/calmodulin-dependent protein kinase (CAMKII) in the case of long-term potentiation and phosphatases (calcineurin and protein phosphatase 1, PP1) for long-term depression (DeMaria CD. et al., 2001; Sjöström PJ. et al., 2002; Lüscher C. and Malenka RC., 2012) (see **figure 25**).

In long-term potentiation, the downstream signaling cascade result in an increase of AMPAR-mediated transmission, by 1) a triggering of AMPAR synthesis and their insertion in the membrane (from recycled endosomes or lateral diffusion) supported by additional NMDAR trafficking to the cell surface, 2) an exchange of AMPAR types from GluA2-containing receptors to GluA2-lacking AMPARs of higher conductance or 3) a higher AMPAR conductance by means of phosphorylation via CaMKII activity (Morgado-Bernal I. et al., 2011; Lüscher C. and Malenka RC., 2012; Bu Y. et al., 2015). AMPARs synthesis is triggered by adenyl cyclase (AC) activation, which produces cAMP that activates protein kinase A (PKA) and phosphorylation of diverse transcription factors, such as cAMP response element binding protein (CREB). Moreover, long-term potentiation also modifies the neuronal cytoskeleton by inducing changes in actin dynamics. Spines morphological changes are due to the phosphorylation of kalirin-7, which activates that, in turn, activates PAK that controls actin polymerization. Moreover, Ca^{2+}-calmodulin activates myosin light-chain kinase (MLCK) that phosphorylates myosin IIb which is also critical in this process (Morgado-Bernal I. et al., 2011; Bu Y. et al., 2015) (see **figure 25**).

Opposing to long-term potentiation, during long-term depression, AMPARs are endocytosed and dendritic spines are contracted and/or reduced due to activity of phosphatases with an opposite effect on the abovementioned signaling cascades involved in long-term potentiation (Lüscher C. and Malenka RC., 2012) (see **figure 25**).
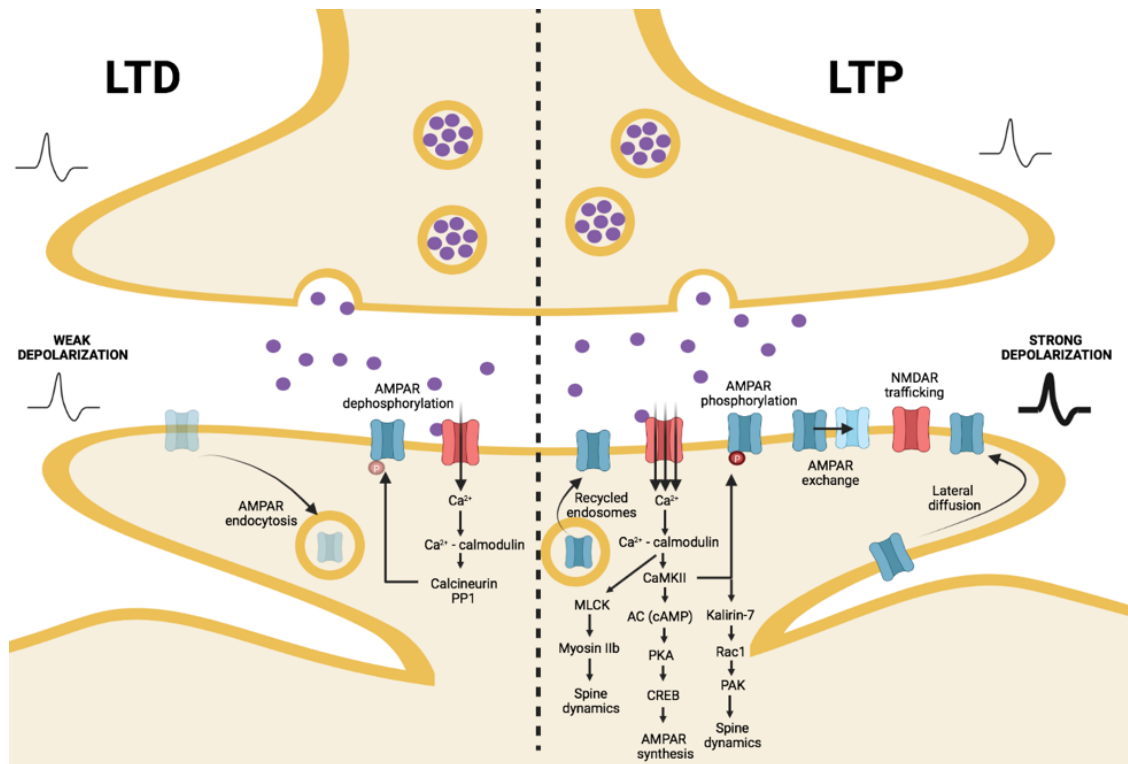
Figure 25. Model of synaptic LTD (left) and LTP (right) processes. Weak depolarization of the post-synaptic terminal lead to LTD where phosphatases (calcineurin and PP1) are activated and provoke AMPAR dephosphorylation, resulting in a decreased signaling and the receptor endocytosis. Strong depolarization trigger LTP where AMPAR signaling is increased (synthesis, trafficking by lateral diffusion or recycled endosomes, phosphorylation leading to higher conductance, exchange to more conducting AMPAR), and CaMKII is activated. This kinase phosphorylates MLCK (that activates myosin IIb with a role in spine dynamics), adenyl cyclase (that produces cAMP which activates PKA and consequently, CREB, for AMPAR synthesis) and kalirin-7 (which activates Rac1 and consequently, PAK, that also participates in spine dynamics). Purple dots represent glutamate, red receptors are NMDARs and blue receptors are AMPARs.

2.8.2.   Non-neuronal NMDARs

Since the identification of glutamate as neurotransmitter, literature has focused on glutamatergic receptors in the CNS. Nevertheless, there is great evidence of NMDARs expression in several cell types and tissues, exerting distinct physiological functions that has been under-explored for many years (Hogan-Cann AD. and Anderson CM., 2016). In the following table, there is a compilation of NMDAR roles in distinct non-neuronal cell types and tissues (see **table 3**).

Cell type/Tissue	Physiological function
Astrocytes	Neuron-astrocyte communication
Oligodendrocytes	Oligodendrocyte progenitor cell migration and differentiation, myelinization
Microglia	Proinflammatory cytokines release
Müller glia	Retinal progenitor proliferation, ganglion cell survival
Sensory system	Processing of afferent sensory information
Satellite glia	Sensitization of sensory neurons to nociceptive stimulation
Enteric glia	Pro-survival growth factor release
Schwann cells	Migration and survival, regulation of myelin morphology
Brain endothelial cells	Vasodilation, glucose uptake
Kidney	Vasodilation, proximal reabsorption and glomerular filtration, blood pressure regulation, reduction of vitamin D3 synthesis
Pancreas	β-cells function and survival, inhibition of insulin secretion
Skin	Inhibition of re-epithelization and epidermal development
Lung	Airway responsiveness, bronchiole smooth muscle contraction
Heart	Electrical and pacemaker activities
Osteoblasts	Differentiation and bone deposition
Osteoclasts	Differentiation and bone resorption
Platelets	Activation and aggregation
Parathyroid gland	Reduction of parathyroid hormone synthesis and secretion
Megakaryocytes	Differentiation and maturation, induction of platelet production and activation
Testis	Promotion of androgen receptor expression, induction of testosterone synthesis
Melanocytes	Regulation of cytoskeletal organization, morphology and survival
Lower urogenital tract	Modulation of male genital organ tone, sexual activity and bladder emptying reflexes
Stomach	Inhibition of histamine-induced acid secretion, regulation of gastric motility
Merkel cells	Mechano-sensation
Adrenal gland	Stress-induced release of adrenocorticotropic hormone (ACTH) and catecholamines, modulation of adrenal stress response
Ileum	Intestinal muscle contraction
Taste buds	Umami taste
Larynx and esophagus	Release of nitric oxide (NO) and vasoactive intestinal peptide (VIP), contraction of lower esophageal sphincter

Table 3. Table summarizing different cell types and tissues where NMDARs are expressed and the exerted functions in each of them (reviewed in Hogan-Cann AD. and Anderson CM., 2016).

Chapter 3.

NMDAR dysfunction and neurodevelopmental disorders

3.1. The dichotomic role of NMDARs

Activated NMDARs induce calcium influx in the postsynaptic neuron, participating in several critical neuronal processes such as changes in membrane excitability, exocytosis, synaptic transmission, or enzymes activation, among others. Thus, NMDAR activity and its derived calcium influx must be tightly regulated to maintain physiological functions.

When the NMDAR signaling is decreased and do not reach the optimal levels, several problems arise given that NMDAR-dependent functions are disturbed. In the opposite scenario, NMDARs overactivation can dysregulate Ca^{2+} signaling and might also be deleterious. Under physiological conditions, neurons regulate intracellular calcium concentration by exchanging Ca^{2+} with the extracellular fluid (influx/efflux regulation), intracellular storage (endoplasmic reticulum) and Ca^{2+} buffering molecules. Nevertheless, when these systems capacities are exceeded, there might be also pathological consequences, which are encompassed under the term 'excitotoxicity'. Non-physiological and excessive Ca^{2+} rise activates phospholipases, which release arachidonic acid that, and the oxidation of this acid, produces free radicals, resulting in lipid peroxidation. Moreover, there is an activation of distinct enzymes (calpains, DNAses, proteases, endonucleases) that can damage DNA and different cellular elements. Furthermore, there is an increase of nitric oxide (NO) via NMDAR-PSD95 interaction. Physiologically, NO regulates guanylate cyclase activity and participates in S-nitrosylation. However, under pathological conditions NO may react with superoxide and generate peroxynitrite, which might damage DNA or provoke irreversible protein modifications (tyrosine nitration or thiol oxidation). This peroxynitrite might also cause mitochondria dysfunction and deficits in energy production, that could promote apoptosis (Leist M. and Nicotera P., 1998; Arundine M. and Tymianski M., 2003) (see **figure 26**).
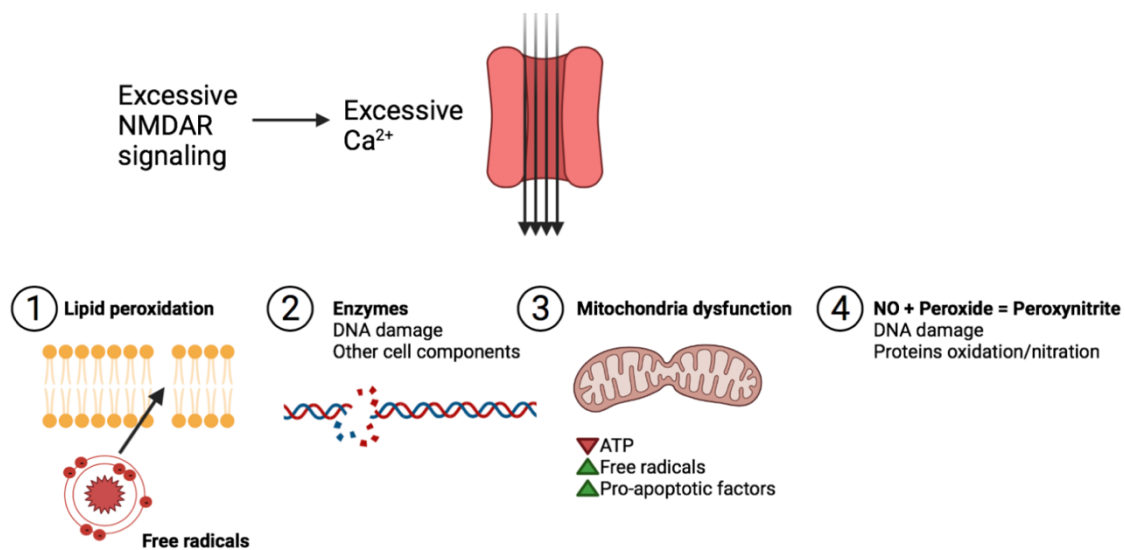
Figure 26. Scheme representing different excitatory processes due to excessive NMDAR signaling and consequently, dysregulation of calcium amounts: **1,** generation of free radicals that cause lipid peroxidation; **2,** enzymes activation which can damage DNA and other cell components; **3,** mitochondria dysfunction which reduces energy production and increases free radicals and the release of pro-apoptotic factors; **4,** nitric oxide production that reacts with peroxide to produce peroxynitrite which damages DNA and produces permanent changes in proteins.

It has been proposed that NMDAR subsynaptic location might influence the probability to trigger excitotoxicity, since some authors showed that synaptic NMDARs predominantly promote cell survival while extra-synaptic NMDARs are more related with excitotoxicity and neuronal death (Hardingham GE. and Bading H., 2010).

There is no consensus about the reason why synaptic and extrasynaptic receptors present different signaling pathways, but it might be due to: a) subsynaptic location, b) NMDAR subunit composition, c) interaction with other proteins (Hardingham GE. and Bading H., 2010).

Regardless of the reason, the fact is that activating both kinds of receptors results in the activation of different signaling cascades. When synaptic NMDARs are activated, calcium activates Ca^{2+}-calmodulin and CaMKII that via adenyl cyclase, cAMP and PKA activates CREB transcription factor which is related with neuronal survival, plasticity and synaptogenesis, generating neuroprotection against neuronal death and excitotoxicity through the induction of survival genes (Atf3, activating transcription factor 3; Btg2, B-cell translocation gene 2; Bcl6, B-cell lymphoma 6; GADD45, growth arrest and DNA damage induced gene 45; Inhba, Inhibin beta-A; Ifi202B, Interferon activated gene 202B; Npas4, neuronal PAS domain protein 4; Nr4a1, nerve growth factor IB; Serpinb2, serine protease inhibitor B2; and BDNF, brain-derived neurotrophic factor) and the suppression of pro-apoptotic transcription factors (FOXO, forkhead box O; p53) and consequently, several death genes (Puma; Bcl2l11, Bcl2-like protein 11; Noxa; Fas ligand; Txnip, thioredoxin-interacting protein; and Apaf-1, protease activating factor 1). Furthermore, synaptic NMDAR activation also generates antioxidant effects by promoting thioredoxin-peroxiredoxin activity through the activation of Srxn1 (sulfiredoxin) and Sesn2 (sestrin 2) genes (Hardingham GE. and Bading H., 2010) (see **figure 27**).

In the other hand, extrasynaptic NMDARs do not activate CREB-dependent gene expression and activates FOXO transcription factor. Moreover, it inactivates ERK1/2 (extracellular signal-regulated kinases 1/2) pathway, leading to a lack of inactivation of the pro-death protein Bcl-2-associated death promoter (BAD) and activates calpains (Hardingham GE. and Bading H., 2010) (see **figure 27**).
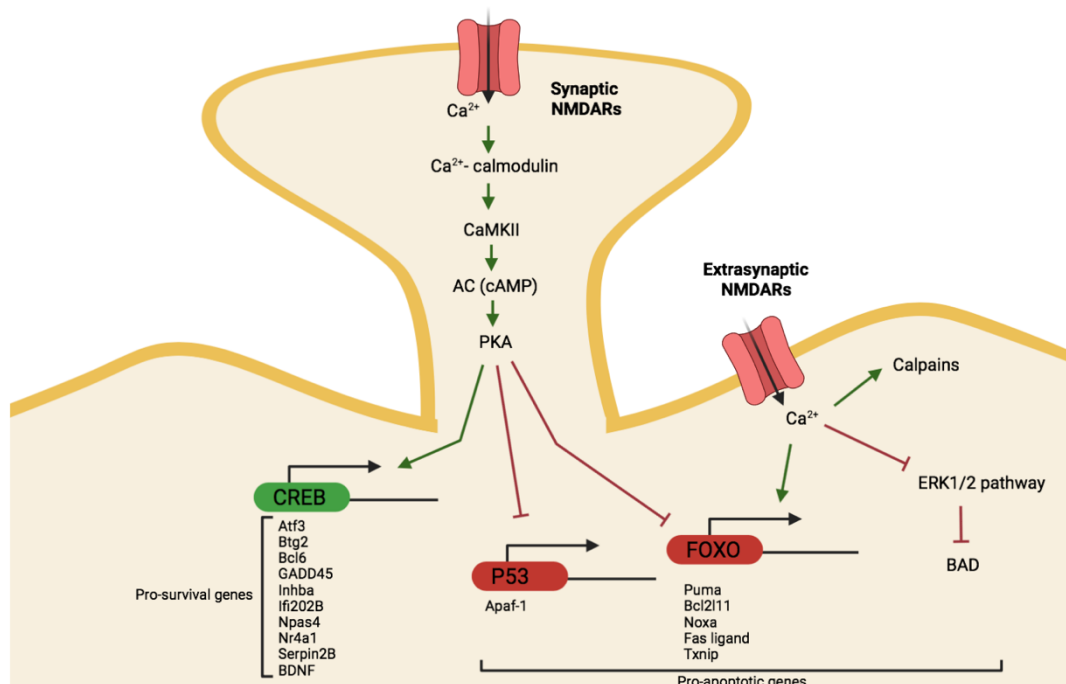
Figure 27. Scheme representing different NMDAR-mediated signaling cascades, depending on NMDAR subsynaptic location. Synaptic NMDARs activation promotes neuronal health and survival, via Ca^{2+}-calmodulin activation of CaMKII, adenyl cyclase (AC), PKA and activation of CREB transcription factor promoting different pro-survival genes expression (Atf3, Btg2, Bcl6, GADD45, Inhba, Ifi202B, Npas4, Nr4a1, Serpin2B and BDNF) and inactivation of P53 and FOXO transcription factors and consequently, different pro-apoptotic genes (Apaf-1, Puma, Bcl2l11, Noxa, fas ligand, Txnip). Alternatively, extrasynaptic NMDARs promote neuronal death by activating calpains and FOXO transcription factor while inactivating ERK1/2 pathway, not allowing the inhibition of the pro-apoptotic gene BAD.

3.2. NMDAR dysregulation in neurological disorders

Given that NMDARs play a pivotal role in excitatory neurotransmission and, consequently, in synaptic plasticity processes and other physiological roles in non-neuronal tissues (see **table 2**), NMDAR signaling disruption is implicated in a wide range of diseases.

3.2.1. Alzheimer's disease

Alzheimer's disease (AD) is a neurodegenerative disorder which is characterized by amyloid-beta plaques, neurofibrillary tangles, hyperphosphorylated tau, and neuronal loss, which affects distinct brain areas depending on the disease evolution. It is hypothesized that AD is derived from an overproduction of amyloid-beta peptide (Aβ) due to an altered proteolytic cleavage of its precursor, the amyloid precursor protein (APP). The symptoms of AD include cognitive deficits, memory loss and dementia (Wang R. and Reddy PH., 2017).

Aβ protein increases neuron vulnerability and triggers NMDAR-derived excitotoxicity due to direct modulation of NMDARs and an impairment in glutamate uptake by altering glutamate transporters (for instance, EAAT2 or VGLUT) (Wang R. and Reddy PH., 2017). This NMDAR-derived excitotoxicity might result in oxidative stress, that promotes amyloid-beta accumulation, tau hyperphosphorylation, neurofibrillary tangles production and synaptic dysfunction (Kamat PK. et al., 2016). It is believed that Aβ promotes excitotoxicity via extrasynaptic NMDARs while reducing synaptic NMDAR activity (Wang R. and Reddy PH., 2017).

3.2.2. Amyotrophic Lateral Sclerosis

Amyotrophic lateral sclerosis (ALS) is a disease affecting the cortico-motor system (specifically the neurons controlling voluntary movements), presenting muscle atrophy, weakness and fasciculations. This disease might be sporadic or familial (*e.g.* alteration of *SOD1* or other genes). ALS is a multifactorial disorder with, probably, multiple molecular etiologies including glutamate toxicity (Eisen A., 1995).

In regard of this hypothesis, an alteration of glutamate transporters (particularly, GLT1 transporters in astroglia and EAAC1 in neurons) has been detected in ALS, leading to glutamate accumulation and further NMDAR overactivation, which might cause Ca^{2+} overload altering mitochondrial function and ultimately causing motoneuron degeneration (Eisen A., 1995; Spalloni A. et al., 2012). Supporting this hypothesis, increased glutamate levels have been found in the cerebrospinal fluid and serum of ALS patients (Spalloni A. et al., 2012). Along disease progression, NMDAR-derived excitotoxicity might decline, and other pathophysiological mechanisms are more predominant (Eisen A., 1995).

3.2.3. Anxiety

Anxiety is a critical component of the stress response to threatening situations. Nevertheless, this situation might become pathological when anxiety turns to be persistent, even in the absence of dangerous / noxious situations. NMDAR dysregulation has been proposed to underlie this pathological mood disorder. Several brain areas (amygdala, medial prefrontal cortex, hippocampus) are involved in the evaluation of the threatening severity in a situation and the elaboration of an adapted defense response (conditioned fear) via synaptic changes and consequently, glutamatergic neurotransmission. Thus, the glutamatergic system is closely related with the fear-mediated learning and emotional processing of stressful events (Bermudo-Soriano CR. et al., 2012). Accordingly, NMDAR dysregulation might cause a misprocessing of the events (considering events as dangerous when they are non-noxious), triggering a defense response (when not needed) and contributing to anxiety.

3.2.4. Autism-spectrum disorders

Autism-spectrum disorders (ASDs) are a group of neurodevelopmental disorders characterized by stereotypies, social alterations and altered communication skills. Despite ASD is a multifactorial disorder, the alteration of glutamatergic neurotransmission (and NMDAR function) is a risk factor. Indeed, *GRIN* genes are considered high-susceptibility ASD genes (https://gene.sfari.org/database/human-gene). Experimental data showed increased glutamate levels in ASD patients' serum, an excitotoxic situation that might derive from oxidative stress, immune system dysfunction, overstimulation of glutamatergic receptors and inhibitory signaling dysregulation (Essa MM. et al., 2013). Alternatively, ASD might also be derived from NMDAR hypofunction, as supported by studies in anti-NMDAR autoimmune encephalitis (Tzang RF. et al., 2019) or in patients harboring *GRIN de novo* variants causing NMDAR loss of function (more detailed in the next sections).

3.2.5. Autoimmune encephalitis

NMDAR autoimmune encephalitis is associated with psychiatric symptoms (anxiety, insomnia, hallucinations, delusions, agitation, mania), personality changes, seizures, amnesia, stereotypical behaviors, language problems, autonomic dysregulation (arrythmias, blood pressure alterations, hypersalivation, hyperventilation) and movement disorders (Newman MP. et al., 2016), being all these features a direct consequence of NMDAR hypofunction.

Autoimmune encephalitis is caused by the presence of anti-GluN1 auto-antibodies, which are found in serum and cerebrospinal fluid of patients and are frequently associated with the presence of tumors (*e.g.*, ovarian teratomas) or viral infections (for instance, herpes or varicella zoster infections) (Lynch DR. et al., 2018). These autoantibodies interfere with NMDAR surface expression and channel activity, leading to NMDAR hypofunction, and consequently, defects in synaptic plasticity (Planagumà J. et al., 2016). Mechanistically, the hypofunction is due to NMDAR internalization/degradation or re-location to extra-synaptic sites (Miya K. et al., 2013; Lynch DR. et al., 2018). Nevertheless, prior to hypofunction, NMDAR autoantibodies can activate the receptors by prolonging open time (Lynch DR. et al., 2018).

3.2.6. Depression

Depression is a multifactorial psychiatric disorder that is associated with excitotoxic damage (oxidative stress and metabolic alterations) of brain areas closely associated with stress response and emotional processing. In fact, glutamate and its metabolites (glutamine and GABA) are increased in plasma and brain tissue of depression-suffering patients. Increase on glutamate levels might be associated with a loss of glial cellularity and, consequently, a reduction in the number of glutamate transporters (such as EAAT1 and EAAT2) which are critical for glutamate uptake (Sanacora G. et al., 2012; Marsden WM., 2013).

Moreover, dendritic spines loss in combination with a reduction in synaptic proteins and plasticity alterations, have been detected in depressive patients' hippocampus and prefrontal cortex areas while the amygdala undergoes hypertrophy, leading to deficits in emotional learning and processing (Marsden WM., 2013; Gerhard DM. et al., 2016).

3.2.7.   Epilepsy

It is well known that epilepsy and the generation of seizures is correlated with an excitatory/inhibitory disbalance, leading to brain hyperexcitability. Nevertheless, this hyperexcitability state might be due to overactivation of NMDA and AMPA receptors in glutamatergic pathways, inhibition of glutamatergic receptors in inhibitory pathways, ectopic release of glutamate and/or loss of glutamate uptake (reduction of EAAT1, GLT1 or GLAST) resulting in increased levels of glutamate in patients' CSF and brain tissue (Chapman AG., 2000; Hanada T., 2020). One of the causes of epilepsy is NMDAR dysregulation that might be caused by *GRIN* genetic variants (further discussed in topics below).

3.2.8.   Huntington's disease

Huntington's disease is a genetic disease caused by an expansion of a 'CAG' triplet in *HTT* gene encoding for the huntingtin protein. More precisely, the disease is clinically manifested when the expansion is above 35 CAG' repeats expansion, and the number of repetitions is inversely correlated with the age of onset. Patients present movement disorders (chorea and alterations in motor coordination), cognitive dysfunction and psychiatric traits (depression, anxiety, and/or psychosis) (Raymond LA., 2016).

It is believed that the physiological role of huntingtin protein is related with gene transcription, vesicular transport, endocytosis and mitochondrial function. Nevertheless, when mutated, huntingtin affects particular GABAergic neurons populations (medium spiny projection neurons) located in the caudate and putamen (Sepers MD. and Raymond LA., 2014; Raymond LA., 2016).

Mutant huntingtin is associated with an increase in extrasynaptic activity of GluN2B-containing NMDARs, and this might result in the triggering of excitotoxicity and cell death pathways. Interestingly, glutamate-derived excitotoxicity is more pronounced in neurons with longer CAG expansions (Raymond LA., 2016). Moreover, an increased glutamate release in combination with a reduced glutamate uptake (by astrocytes, via GLT1 transporter) are observed at initial stages whereas at later stages, neurodegeneration is accompanied by a loss of glutamatergic terminals (Sepers MD. and Raymond LA., 2014).

3.2.9.   Schizophrenia

Schizophrenia is a multifactorial psychiatric disorder that is characterized by positive symptoms (hallucinations, delusions, abnormal motor behavior), negative symptoms (emotional and social alterations) and cognitive deficits. While positive symptoms are proposed to be provoked by excessive dopamine signaling, negative and cognitive symptoms might be caused by NMDAR hypofunction. In fact, mutations affecting *GRIN2C* and *GRIN2D* genes have been recently associated with schizophrenia (Uno Y. and Coyle JT., 2019).

NMDAR hypofunction is correlated with reduced levels of GluN subunits and glutamate, in prefrontal cortex of schizophrenia patients (Balu DT., 2016), causing NMDAR hypofunctionality. Mechanistically, this association might result from a reduction of fast-spiking parvalbumin positive GABA inhibitory interneurons activity, disturbing antioxidant agents and altering excitatory/inhibitory balance (Hardingham GE. and Do. KQ, 2016).

3.2.10. Pain

Pain is an unpleasant sensation that acts as an alert mechanism to avoid tissue damage when painful (noxious) stimuli are acute. Several mechanisms, including peripheral nerve injury, diabetic neuropathy, postherpetic neuralgia, or chemotherapy can also lead to chronic neuropathic pain, implying spontaneous pain, hyperalgesia (increased pain sensation) and allodynia (pain sensation with non-noxious stimuli) (Deng M. et al., 2019).

Noxious stimuli activate nociceptive afferent fibers that release glutamate in the spinal dorsal horn. Neurons from spinal dorsal horn project to the thalamus-somatosensory cortex or cingulate and insular cortices. Chronic pain is associated with peripheral sensitization of nociceptors and long-term plasticity in different neuronal regions that are related with pain processing (anterior cingulate cortex, insular cortex, somatosensory cortex, or spinal cord). An up-regulation of glutamate release, overexpression of GluN2B-containing NMDARs and an altered phosphorylation pattern have been observed in chronic pain (Bliss TVP. et al., 2016; Deng M. et al., 2019; Li XH. et al., 2019).

3.2.11. Parkinson's disease

Parkinson's disease (PD) is a neurodegenerative disorder with distinct motor symptoms (bradykinesia, tremor, rigidity) that is caused by a loss of dopaminergic neurons in basal ganglia, specifically affecting the substantia nigra pars compacta (SNpc). PD is characterized by α-synuclein aggregates, forming 'Lewy bodies' histopathological hallmark (Blandini F. et al., 1996).

Dopaminergic loss in the SNpc reduces inhibition of striatal GABAergic projections to medial globus pallidus (MGP) and substantia nigra pars reticulata (SNr) (direct pathway) and consequently reducing thalamico-cortical glutamatergic projections. In parallel, via different dopaminergic receptors, striatal GABAergic neurons projecting to lateral globus pallidus (LGP) turn overactive (indirect pathway), inhibiting LGP GABAergic neurons in this region and disrupting the inhibition of sub-thalamic nucleus (STN) which becomes overactive, and overstimulates MGP and SNr (see **figure 28**). Reduced GABAergic inhibition and increased glutamatergic excitation pathways in striatum, lead to excitotoxicity, and consequently oxidative stress that also causes neuronal damage (Blandini F. et al., 1996).
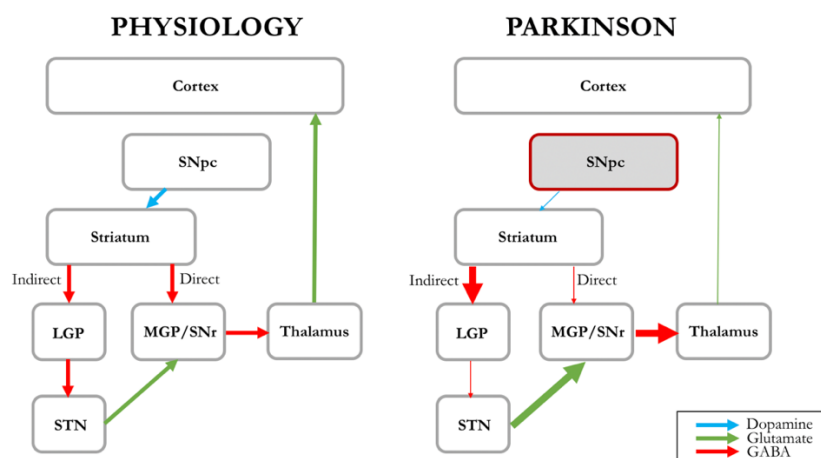
Figure 28. Basal ganglia circuits in physiological (left) and Parkinson's disease (right) scenarios. Dopaminergic loss in SNpc affects the direct pathway (reduced GABAergic inhibition of MGP/SNr and consequently, increased inhibition from MGP/SNr to thalamus, reducing glutamatergic projections to the cortex) and the indirect pathway (increased GABAergic inhibition of LGP, overactivates the STN, resulting in increased excitation of MGP/SNR nuclei); Abbreviations: SNpc, substantita nigra pars compacta; LGP, lateral globus pallidus; MGP, medial globus pallidus; SNR, substantia nigra pars reticulata; STN, sub-thalamic nucleus.

3.2.12. White matter damage: stroke, vascular dementia, spinal cord injury or multiple sclerosis

White matter is the neural tissue that consists largely of myelinated nerve fibers bundled into tracts, displaying a whitish color, where nerve fibers and the supported glial cells are contained. White-matter damage might be a consequence of stroke, vascular dementia, mechanical injury or multiple sclerosis. In all of them, there is an increase of calcium via glutamatergic signaling, resulting in excitotoxicity and consequently, oligodendrocyte damage and myelin loss (Matute C., 2011). Massive glutamate release might be due to an excessive neuronal activity, a higher release efficacy, or an impairment of glutamate uptake (Lai TW. et al., 2013). Following NMDAR overactivation, additional studies showed an NMDAR hypofunctionality phase, ascribed to NMDAR desensitization and/or NMDARs removal (Shohami E. and Biegon A., 2014).

3.3. *GRIN* mutations and the arise of *GRIN*-related disorders (GRDs)

As abovementioned, NMDARs activity is -and needs to be- tightly regulated. Concomitantly, secondary alterations of NMDAR-mediated neurotransmission contribute to the pathophysiology of multiple neurological conditions. Besides the secondary alteration of NMDAR-mediated neurotransmission, recently a primary alteration of the NMDAR has been identified, with the association between *GRIN* genetic variants and neurodevelopmental disorders. Mutations of *GRIN* genes (encoding for GluN subunits of the NMDAR) are mostly prevalently affecting *GRIN1*, *GRIN2A* and *GRIN2B* genes. These *GRIN* mutations are autosomic dominant genetic variants that mostly are generated *de novo*. Thus, the majority of patients with GRDs only present one affected allele (heterozygosis) but this is enough to develop the disease. The increasing number of reported *GRIN* variants in patients with neurodevelopmental disorders and the common genetic etiology (disease-associated variants of *GRIN* genes family) has resulted in the grouping of these neurodevelopmental disorders under the term '*GRIN*-related disorders' or -by analogy with other synaptopathies - also-called 'grinpathies'. In the following sections, GRD genetic studies, clinical symptoms and preclinical investigational background will be presented, to further delineate GRDs.

3.3.1. Clinical cases

3.3.1.1. *GRIN1* disease-associated variants

Since the first association of *GRIN1* genetic variants with neurodevelopmental disorders, several variants have been identified in patients with different clinical outputs (see **supplementary table 1**). Most of these variants are missense (a single aminoacid change) although indel (insertion/deletion of one or more aminoacids), nonsense (a premature stop codon, with or without an open reading frame frameshift) and splice-site variants (see **supplementary table 1**) have also been detected. The majority of *GRIN1* variants (see **supplementary table 1**) are located in the LBD and TMD (highly conserved regions) while very few appear in the ATD and CTD (less conserved) in agreement with the role of highly conserved regions in NMDAR crucial functions (Amin JB. et al., 2021). Indeed, *GRIN1* variants (see **supplementary table 1**) have been related with alterations on NMDAR-mediated current amplitude, the receptor assembly and surface trafficking, the receptor inhibition by Zn^{2+}, protons or Mg^{2+}, the channel Ca^{2+} permeability, the channel gating properties and agonists affinities (see **supplementary table 1**) (Hamdan FF. et al, 2011; Burnashev N. et al., 2015; Ohba C. et al., 2015; Lemke JR. et al., 2016; Chen W. et al., 2017; Odgen KK. Et al., 2017; Rossi M. et al., 2017; Xu XX. and Luo J-H, 2017; Zehavi Y. et al., 2017; Fry AE. et al., 2018; Yu Y. et al., 2018; Li J. et al., 2019; Skrenkova K. et al., 2020; Amin JB. et al., 2021).

Despite *GRIN1*-related disorders natural history is not yet completed (as for GRD ensemble), the growing number of reports showed the syndromic symptomatology of GRIN1-related disorders (Hamdan FF. et al, 2011; Burnashev N. et al., 2015; Ohba C. et al., 2015; Lemke JR. et al., 2016; Chen W. et al., 2017; Odgen KK. Et al., 2017; Rossi M. et al., 2017; Xu XX. and Luo J-H, 2017; Zehavi Y. et al., 2017; Fry AE. et al., 2018; Yu Y. et al., 2018; Li J. et al., 2019; Skrenkova K. et al., 2020; Amin JB. et al., 2021). Individuals harboring *GRIN1* pathogenic variants frequently exhibit the presence of movement alterations that include spasms/myoclonus (sudden muscular tightening, without control), hypotonia (muscle tone reduction), and chorea/dyskinesia (involuntary movements) or paralysis (50-60 %), intellectual disability (ID) (40-50 %, from mild to severe ID), and epilepsy or seizures (40-50 %). Occasionally, *GRIN1* variants are related with developmental delay (DD) (30 %), brain alterations like polymicrogyria (cortex malformation with excessive folds and ridges) (25 %) and visual alterations such as cortical visual impairment or oculogyric crises (involuntary movements of the eyeballs) (20-30 %). Finally, although very rarely, *GRIN1* patients might present stereotypies (repetitive movements) (15 %), language problems (10 %), sleep pattern disturbance (5 %), and gastrointestinal alterations such as feeding problems or constipation (5 %). There are isolated clinical cases with dysmorphism features and only 2 variants have been associated with an increased risk of schizophrenia (see **supplementary table 1**).

3.3.1.2. <u>*GRIN2A* disease-associated variants</u>

To date, up to 105 distinct *GRIN2A* variants have been reported (88 missense variants, 16 nonsense variants, 1 indel variant and sporadic translocations or splice-site variants which are not included in this compilation) (see **supplementary table 2**). Regarding domain affectation, *GRIN2A* reported variants are spread along the whole GluN2A subunit, although highly concentrated in conserved regions (25 % ATD, 50 % LBD, TMD and linker regions and 25 % CTD) (see **supplementary table 2**). Functional annotations of NMDAR containing *GRIN2A* variants revealed different molecular alterations. More precisely, *GRIN2A* pathogenic variants might alter NMDAR current amplitude, receptor assembly and surface trafficking, receptor inhibition by Zn^{2+}, protons or Mg^{2+}, channel Ca^{2+} permeability, channel gating properties and kinetics (rise time and deactivation), channel open probability, agonists affinities and some phosphorylation sites, affecting interaction with other synaptic proteins (see **supplementary table 2**) (Endele S. et al., 2010; Tarabeux J. et al, 2011; Lemke JR. et al., 2013; Lesca G. et al., 2013; Pierson TM. et al., 2014; Yuan H. et al., 2014; Burnashev N. et al, 2015; Serraz B. et al., 2016; Swanger SA. et al., 2016; Addis L. et al., 2017; Gao K. et al., 2017; Odgen KK. Et al., 2017; von Stülpnagel C. et al., 2017; Xu XX. et al., 2017; Xu XX. and Luo J-H, 2017; Yang X. et al., 2017; Fernández-Marmiesse A. et al., 2018; Strehlow V. et al., 2018; XiangWei W. et al., 2018; Yu Y. et al., 2018; Li J. et al., 2019; Marwick KFM. Et al., 2019; Nicotera A. et al., 2019; Amador A. et al., 2020Li X. et al., 2020; Mora Viera M. et al., 2020; Amin JB. et al., 2021).

Opposing to *GRIN1* variants, *GRIN2A* variants are frequently associated (60-70 % of *GRIN2A* patients) with heterogenic epilepsy episodes, such as partial epilepsy (only affecting a particular brain area), seizures (convulsions of unknown cause), rolandic epilepsy (RE) (seizures originated in the Rolandic area), continuous-spike and wave-during-sleep (CSWS) (a rare form of epilepsy with additional alterations), absence epilepsy (provokes a 'blank out' episode) or Landau-Kleffner syndrome (LKS) (commonly accompanied with language regression). In addition to epilepsy, *GRIN2A* individuals can also exhibit different clinical alterations, such as autism (5-10 %), schizophrenia (5-10 %), activity-deficit and hyperactivity disorder (ADHD) (< 5 %) or developmental delay with intellectual disability (30 %). Considering specific symptoms that might also overlap with these conditions, *GRIN2A* variants are very frequently associated with language alterations (20-25 %), including aphasia (affecting speaking, writing and comprehension), apraxia (normal comprehension but altered executive function), dysarthria (muscle weakness impairing speaking).

Moreover, *GRIN2A* dysfunction is also related with motor alterations such as spasms/myoclonus, hypotonia, dyskinesias, dystonia (involuntary muscle contractions) or ataxia (lack of motor coordination) (10-15 %), and very rarely with dysmorphism, feeding alterations, hormonal affectations (*e.g.* hypothyroidism), strabismus, sleep problems, gastrointestinal disturbances or brain alterations (< 5 %) (see **supplementary table 2**) (Endele S. et al., 2010; Tarabeux J. et al, 2011; Lemke JR. et al., 2013; Lesca G. et al., 2013; Pierson TM. et al., 2014; Yuan H. et al., 2014; Burnashev N. et al, 2015; Serraz B. et al., 2016; Swanger SA. et al., 2016; Addis L. et al., 2017; Gao K. et al., 2017; Odgen KK. Et al., 2017; von Stülpnagel C. et al., 2017; Xu XX. et al., 2017; Xu XX. and Luo J-H, 2017; Yang X. et al., 2017; Fernández-Marmiesse A. et al., 2018; Strehlow V. et al., 2018; XiangWei W. et al., 2018; Yu Y. et al., 2018; Li J. et al., 2019; Marwick KFM. Et al., 2019; Nicotera A. et al., 2019; Amador A. et al., 2020; Li X. et al., 2020; Mora Viera M. et al., 2020; Amin JB. et al., 2021).

3.3.1.3. *GRIN2B disease-associated variants*

Since the first and recent association studies between *GRIN2B* variants and neurodevelopmental disorders, up to 102 *GRIN2B* genetic variants have been reported (87 missense variants, 13 nonsense variants, 2 indel variant and sporadic translocations or splice-site variants) (see **supplementary table 3**). *GRIN2B* reported variants are highly concentrated in conserved LBD-TMD regions (15 % ATD, 65 % LBD, TMD and linker regions and 20 % CTD) (see **supplementary table 3**). Functional annotation of disease-associated *GRIN2B* variants showed that the mutant *GRIN2B*-containing NMDARs can have alterations of current density, agonist potency, desensitization rate, deactivation rate, open probability, open time, conductance, inhibition by Mg^{2+} or protons, surface trafficking or interaction with MAGUK proteins (see **supplementary table 3**) (Endele S. et al., 2010; Tarabeux J. et al, 2011; Lemke JR. et al., 2013; Burnashev N. et al, 2015; Hu C. et al., 2016; Swanger SA. et al., 2016; Liu S. et al., 2017; Mullier B. et al., 2017; Platzer K. et al., 2017; Xu XX. and Luo J-H, 2017; Fedele L. et al., 2018; Kyriakopoulos P. et al., 2018; Vyklicky V. et al., 2018; Wells G. et al., 2018; XiangWei W. et al., 2018; Li J. et al., 2019; Sceniak MP. et al., 2019; Bahry JA. et al., 2021; Kellner S. et al., 2021; Amin JB. et al., 2021).

GRIN2B variants are mainly associated with developmental delay and intellectual disability (75 %), autism spectrum disorders (40 %), Lennox-Gastaut or West epileptic syndromes (40 %) and, less prevalently, with attention-deficit and hyperactivity disorder (ADHD) (10 %) or schizophrenia (< 5 %). In combination with these clinical presentations, specific symptoms have been regularly reported such as motor alterations (hypotonia, hypertonia, myoclonus/spasms, dyskinesia) (15 %), brain alterations (20 %), visual impairments (CVI, strabismus) (15 %) or rarely detected, such as language deficits, behavioral alterations, dysmorphism, sleep pattern disturbance, stereotypies (~5 %) and gastrointestinal alterations (constipation, reflux) in several cases (see **supplementary table 3**) (Endele S. et al., 2010; Tarabeux J. et al, 2011; Lemke JR. et al., 2013; Burnashev N. et al, 2015; Hu C. et al., 2016; Swanger SA. et al., 2016; Liu S. et al., 2017; Mullier B. et al., 2017; Platzer K. et al., 2017; Xu XX. and Luo J-H, 2017; Fedele L. et al., 2018; Kyriakopoulos P. et al., 2018; Vyklicky V. et al., 2018; Wells G. et al., 2018; XiangWei W. et al., 2018; Li J. et al., 2019; Sceniak MP. et al., 2019; Bahry JA. et al., 2021; Kellner S. et al., 2021; Amin JB. et al., 2021).

3.3.1.4. GRD genotype-phenotype association studies

Despite recent investigational efforts, the overwhelming and fragmented information of *GRIN* variants hurdled the establishment of a robust genotype-phenotype correlation. In general, *GRIN2A* variants are mostly associated with epileptic syndromes, while *GRIN2B* pathogenic variants are frequently associated with intellectual disability and developmental delay. Regarding *GRIN1* disease-associated variants, genotype-phenotype studies do not allow to establish genotype-phenotype correlations yet (Xu XX. and Luo J-H, 2017) (see **supplementary tables 1-3**).

The heterogeneity between clinical symptomatology and the identity of the affected *GRIN* gene is accompanied by a lack of direct correlation between the affected GluN subunit domain and GRD clinical symptomatology. Despite disease-associated *GRIN* variants are scattered along *GRIN* open-reading frames, particular genetic hotspots are present in *GRIN* genes. These genetic vulnerability hotspots include nucleotide regions encoding for the ligand-binding and transmembrane domains of GluN1, GluN2A and GluN2B subunits, ultimately affecting agonists binding, Ca^{2+} permeability, channel gating, Mg^{2+} blockade, or allosteric modulation. On the contrary, with few exceptions *GRIN* variants affecting the ATD and CTD regions are generally devoid of pathogenicity (neutral changes). Indeed, these variants cause subtle alterations of NMDARs, affecting receptor assembly, surface trafficking and allosteric modulation by different compounds such Zn^{2+} or protons (ATD) or the regulation by phosphorylation and the receptor's interaction with MAGUKs (CTD) (Lemke JR. et al., 2016; Amin JB. et al., 2021). In spite of *GRIN* variants annotation studies efforts, still a large amount of *GRIN* variants remains non-annotated. Further characterization of the functional outcomes of "orphan" (non-annotated) *GRIN* variants will help to delineate genotype-phenotype correlation (Strehlow V. et al., 2018) (see **supplementary tables 1-3**).

Another difficulty to establish this genotype-phenotype correlation is that a particular genetic variant might be altering different parameters of the NMDAR physiology and these changes sometimes might be contradictory (*e.g.*, an increased glutamate potency in a receptor that is not trafficking to the cell surface). Therefore, a more comprehensive and consensual annotation of both functional and clinical data is required, in order to delineate genotype-phenotype relationship in GRD (Xu XX. and Luo J-H, 2017) (see **supplementary tables 1-3**).

Despite this coexistence of functional alterations, annotation distinguish *GRIN* variants into loss-of-function (whether NMDAR activity is reduced regardless of the underlying mechanism), gain-of-function (when NMDAR activity is increased) or complex variants (some altered parameters result in loss-of-function and the modification of other aspects by the same variant lead to gain-of-function). This information is crucial because, based on this stratification, the therapeutic approach should be different.

The abovementioned statements and *GRIN* variants summary lists (**supplementary tables 1-3**) have been retrieved from the scientific literature. Together with these publications, several *GRIN* variants databases (containing other reported *GRIN* variants and additional information) are publicly available. Recently, in collaboration with Dr. Olivella (University Vic, Spain), the fragmented GRIN variants-associated structural, genetic, functional and clinical data have been compiled in a single and publicly available database. Currently, *GRIN* variants database (https://alf06.uab.es/grindb/home), contains. 4513 *GRIN* variants (September 2021) and their relative functional and clinical annotations (García Recio A. et al., 2020).

3.3.2. GRD murine models

Animal models are valuable tools for the study of disease pathophysiological mechanisms and the evaluation of therapeutic strategies. Since GRD are a group of NDD with heterogeneous genetic etiology, several efforts have been recently focused in the generation and characterization of potential GRD-like phenotypic alterations in distinct GRD models and the exploration of therapeutic interventions. In this chapter, despite the existence of recently produced knock in mouse models (expressing *GRIN* missense mutations), most of the content will focus on Grin1, Grin2a and Grin2b haploinsufficient or knockout mouse models.

3.3.2.1. *Grin1* mouse models

Initially, the generation of a full *Grin1$^{-/-}$* knock-out (KO) mouse model was attempted. Nevertheless, KO-*Grin1$^{-/-}$* pups showed neonatal lethality, indicating that the GluN1 subunit is critical for early development (Forrest D. et al., 1994). In parallel to this pioneering study, a *Grin1* knock-down (KD) was created by conventional first-generation transgenesis method. By serendipity (original goal being the creation of a full knock-out *Grin1* model), the insertion of a neomycin cassette into an intronic region (intron 20) of the *Grin1* gene do not completely invalidated Grin1 expression, and GluN1 subunit levels were about 5-10 % of wildtype GluN1 expression levels (Mohn AR. et al., 1999). Phenotypically, *Grin1* KD mice are slightly smaller at early developmental stages, with further spontaneous normalization in adulthood. This mouse model is characterized by distinct phenotypical traits: hyperlocomotion, stereotypies, self-injury, decreased anxiety-like behavior (increased time in the open-field central zone and increased time in open arms in the elevated plus maze), reduced nest building, impaired social and sexual interactions (lack of preference for the novel mouse instead of the familiar mouse in the 3-chamber test, reduced investigation and increased escape behaviors in the resident-intruder test), affected spatial memory (increased perseverative errors in a radial arm maze), sensorimotor gating deficits (enhanced acoustic startle amplitude and a reduce pre-pulse inhibition), synaptic alterations (spines density reduction), altered metabolism in specific brain areas (reduced ^{14}C-2-deoxyglucose (2-DG) uptake) and fertility problems (Mohn AR. et al., 1999; Duncan GE. et al., 2002; Duncan GE. et al., 2004; Moy SS. et al., 2006; Dzirasa K. et al., 2009; Halene TB. et al., 2009; Ramsey A. et al., 2011).

In additional to the constitutive *Grin1* knockout and knock-down murine models, conditional *Grin1* knock-out models have been generated. Within this group, a *Grin1* model depleting *Grin1* expression in corticotropin releasing factor (CRF) neurons (expressed in fear- and anxiety-related brain areas, *e.g.* amygdala, hypothalamus, hippocampus and cortex) by cross-breeding a mouse with the Cre recombinase gene under the CRF promoter and another mouse with floxed *Grin1*. This model exhibits enhanced fear acquisition without changes in anxiety-like behaviors, memory, locomotion or pain sensitivity (Gafford G. et al. 2014). Conditional deletion of *Grin1* during early postnatal period has also been conducted in parvalbumin GABAergic neurons from cortex and hippocampus, using Ppp1r2 promoter and the Cre-loxP system. This model presents schizophrenia-like phenotypes that include hyperlocomotion, nest-building deficits, anhedonia, memory, pre-pulse inhibition and anxiety like phenotypes (Belforte JE. et al., 2010).

In the context of GRD, several knock-in mouse models have been recently generated and/or are currently under development. One of these models includes a particular non-synonymous mutation (GluN1-R844C) that causes an increased and prolonged calcium influx through the channel, indicative of a gain-of-function. This model show hyperactivity in the open-field test, impaired working memory in the radial arm maze, impaired fear memory and decreased startle response (Umemori J. et al., 2013).

3.3.2.2. *Grin2A* mouse models

A constitutive *Grin2a$^{-/-}$* knock-out mouse model was generated, resulting in a viable mouse model showing hyperlocomotion (increased horizontal activity in the open-field test), deficits in spatial and fear memory (working errors in T-maze rewarded alternation and win-shift radial maze and increased threshold in contextual-fear conditioning task), impaired discrimination learning (worse performance in pairwise visual discrimination task), attention defects (in attention set-shifting task), anxiety-like behaviors (increased time in open arms in elevated plus maze, in light compartment of light-dark chamber and the center of the open-field test), reduced depressive-like behaviors (less immobility in tail-suspension and forced swimming test), impaired vocalization communication, sleep-related discharges in electroencephalogram (EEG), impaired hippocampal long-term potentiation in hippocampal *ex vivo* slices (field-potential recordings), dendritic changes (reduced dendritic length and complexity, detected by Golgi's

impregnation), and increased dopaminergic and serotonergic tone (Ito I. et al., 1997; Kiyama Y. et al., 1998; Miyamoto Y. et al., 2001; Boyce-Rustay JM. and Holmes A., 2006; Brigman JL. et al., 2008; Bannerman DM., 2008; Masquardt K. et al. 2014; Kannangara TS. et al., 2014; Kannangara TS. et al., 2015; Salmi M. et al., 2019).

A model where GluN2A presents a homozygous truncation of the CTD was generated by a substitution of the CTD exon with a neomycin gene preceded by in-frame stop codons. This model shows impaired synaptic plasticity and defects in contextual memory (Sprengel R. et al., 1998).

Another *Grin2a* mouse model is a knock-in (KI) of GluN2A-S644G genetic variant, that shows altered hippocampal morphology (thinning of dentate gyrus and CA1 regions), seizures in homozygous mice and susceptibility to seizures in heterozygous mice, hyperactivity (increased ambulation in open-field test), repetitive behaviors, (jumping, backflips and self-grooming) reduced anxiety-like phenotype (increased time in open arms of the elevated plus maze), reduced startle response (Amador A. et al., 2020).

3.3.2.3. *Grin2B* mouse models

A constitutive full *Grin2b$^{-/-}$* knock-out mouse model was generated through the interruption of the translation initiation site exon. KO-*Grin2b$^{-/-}$* mouse model is perinatally lethal, due to the lack of postnatal suckling reflex (Kutsuwada T. et al., 1996). Nevertheless, heterozygous *Grin2b$^{+/-}$* mice are viable (Kutsuwada T. et al., 1996) and show diminished NMDAR excitatory postsynaptic currents (EPSCs) and LTP alterations, as shown in electrophysiological recordings of *Grin2b$^{+/-}$*-derived neuronal primary cultures or *Grin2b$^{+/-}$* hippocampal slices. Heterozygous mice also present enhanced pre-pulse inhibition and altered startle response, indicating sensorimotor gating alterations (Ito et al., 1997; Takeuchi T. et al., 2001). Interestingly, a mouse model with a homozygous truncation in the CTD of GluN2B subunits (generated by substitution with the neomycin gene preceded by stop codons) also die perinatally, as reported for total *Grin2b* KO (Sprengel R. et al., 1998).

Additional conditional knock-out *Grin2b* mouse models have been generated, towards the specific deletion of GluN2B subunit expression in certain brain regions. GluN2B deletion in forebrain neurons results in hyperactivity, depressive-like behaviours, impaired spatial and working memory (longer latencies to find the platform in the Morris water maze, worse performance in the elevated Y-maze and T-maze with spontaneous alternation approach), impaired visual discrimination (in T-maze test), impaired memory in novel object recognition test, reduced anxiety-like phenotypes in elevated plus-maze, and LTP alterations (von Engelhardt J. et al., 2008).

Conditional deletion of GluN2B subunit in hippocampal pyramidal cells showed spatial and working memory alterations as well as LTP dysfunction (von Engelhardt J. et al., 2008). Moreover, specific deletion in hippocampus and cortex of the GluN2B subunit, revealed deficits in attentional set formation, fear-conditioned memory formation, dendritic spines density and morphology, and plasticity processes (Brigman JL. et al., 2010; Thompson SM. et al., 2015).

Also, intrathecal injection of short-hairpin RNAs (shRNAs) to silence spinal GluN2B was performed in a formalin-induced mouse model of pain to demonstrate that GluN2B suppression has analgesic effects (Zhang RX. Et al., 2013).

Along the recent efforts to generate GRD "avatars" (mouse models harboring *GRIN* disease-associated variants), an heterozygous mouse model with a missense *Grin2b* mutation has been generated (GluN2B-C456Y). This model shows decreased hippocampal NMDAR-derived currents, LTD deficits, hypoactivity (open-field test), repetitive self-grooming, and anxiety-like phenotypes (elevated plus maze) (Shin W. et al., 2020).

Chapter 4.

GRIN-related disorders personalized medicine

4.1. Pharmacological modulation of NMDAR activity

GRDs are due to *GRIN* genetic variants which are classified into loss-of-function, gain-of-function or complex variants (where the predominant effect should be determined). This classification is critical because *GRIN* variants pharmacological modulation should be based on their functional deviation. Hence, *GRIN* loss-of-function variants should be potentiated to rescue deficits in NMDAR-mediated activity whereas the excessive NMDAR activity which is associated with *GRIN* gain-of-function variants should be attenuated. In the following sections, distinct compounds with pharmacological activity in NMDAR will be discussed.

4.1.1.   NMDAR activity potentiation

The NMDAR function might be potentiated with different pharmacological arms: using full orthosteric compounds (agonists and co-agonists that bind to the primary active site, also known as orthosteric site), partial orthosteric compounds, positive allosteric modulators (that modify NMDAR response to agonists and co-agonist via binding to a different site, also known as allosteric site) and/or compounds that block proteins/enzymes which degrade or uptake agonists (see **figure 30**).

NMDAR full agonists include compounds targeting GluN1 and GluN2 subunits. GluN1 full agonists include D-serine, glycine, and alanine (see **figure 30**). D-serine will be further discussed in following topics ('NMDAR current therapeutics for the potentiation of loss-of-function *GRIN* variants') while Glycine and D- and L- alanine therapeutic indications are summarized in **table 4**.

GluN1 full agonist	Therapeutic indications	References
Glycine	Gastrointestinal diseases, endotoxic shock, metabolic disorders, organ transplantation failure, arthritis, or wound healing	Wang W. et al., 2013; Razak MA. et al., 2017
D and L-Alanine	Schizophrenia	Karakawa S. et al., 2013; Peyrovian B. et al., 2018

Table 4. Summary of GluN1 full agonists with therapeutic indications.

GluN2 full agonists include the following compounds: D- and L-glutamate (see **note[4]**) and their analogs (*e.g.*, SYM2081 and cis-2,4-methanoglutamate) (see **note[3]**), D- and L- aspartate and their analogs (*e.g.* tetrazol-5-yl glycine), sulfur-containing aminoacids (SAAs) (aspartate analogs: L- and D- cysteine sulfinate, CSA and cysteate, CA; and glutamate analogs: homocysteate, HCA and homocysteine sulfinate, HCSA), cyclic agonists (aminocyclopentane-1,3-dicarboxylic acid, ACPD; 1-aminocyclobutane-1,3-dicarboxylic acid, ACBD; 2-carboxycyclopropylglycine, CGG; azetidine-2,4-dicarboxylic acid, ADA; and azetidine-2,3-dicarboxylic acid, ADC), quinolinate and homoquinolinate acids, ibotenate, and NMDA (see **figure 30**) (Krogsgaard-Larsen P. et al., 1984; Prado de Carvalho L. et al., 1996; Erreger K. et al., 2007; Traynelis SF. et al., 2010).   Regarding endogenous agonists, only glutamate and aspartate have been used with therapeutic goals (summarized in **table 5**) while the other abovementioned GluN2 agonists have not been used with therapeutic goals and they are most commonly related with excitotoxicity and extra-site effects (Allan RD. et al., 1990; Kawai M. et al., 1992; Johnson PI. et al., 1996; Madsen U. et al., 1998; Blaabjerg M. et al., 2001; McBean GJ., 2008; Lugo-Huitrón R. et al., 2013).

GluN2 full agonist	Therapeutic indications	References
D- and L-glutamate	Myocardial recovery and gastrointestinal alterations	Zai H. et al., 2009; Yamamoto S. et al., 2009; Vidlund M. et al., 2016
D and L-Aspartato	Schizophrenia	Errico F. et al., 2008

Table 5. Summary of GluN2 full agonists with therapeutic indications.

Note³: Stereoisomers are molecules with the same molecular formula and composition but different orientation. Enantiomers are stereoisomers that are 'mirror' images of each other and are distinguished by preceding the name with a D- or a L-, upon their optical properties, with different functional impact.

Note⁴: Cis-Trans isomers correspond to another type of isomerism which is very common in cyclic or alkene compounds. In this case, '*cis*' means that the functional groups are on the same side of the carbon chain while '*trans*' means that they are on opposite sides. To give additional information, it should be used the R/S configuration nomenclature, that indicates each functional group orientation.

<u>Partial NMDAR agonists</u> action mechanism depends on two intrinsic properties, namely the compound's dose administration (dictating bioavailability) and NMDAR affinity that will determine their overall pharmacological efficacy. Hence, at low doses these compounds act as agonists whereas at high doses, their behavior is antagonistic via competition with full agonists. Thus, partial agonists might also be used to potentiate an NMDAR loss-of-function although doses should be tightly regulated to achieve this effect.

GluN1 partial agonists include D-cycloserine (at low doses, behaving as GluN2C agonist; at high doses, exerting an antagonistic activity on GluN2A- and GluN2B-subunits containing NMDARs), HA-966 (3-amino-1-hydroxy-pyrrolidin-2-one), 1-aminocyclopropane-1-carboxylic acid (ACPC) (partial agonist of GluN site and antagonist of GluN2 site), 1-aminocyclobutane-1-carboxylic acid (ACBC), and Rapastinel (formerly Glyx-13) (see **figure 30**) (Traynelis SF. et al., 2010). Rapastinel will be further discussed in following topics ('NMDAR current therapeutics for the potentiation of loss-of-function *GRIN* variants') while the potential therapeutic applications of the other GluN1 partial agonists are summarized in **table 6**.

GluN1 partial agonist	Therapeutic indications	References
D-cycloserine	Schizophrenia, Alzheimer, depression and autism (inconclusive results and side effects)	Schade S. and Paulus W, 2016
HA-966 (antagonistic action)	Tremors, convulsions and Parkinson's disease	Singh L. et al., 1990; Goldstein LE. et al., 1994; Kanthasamy A. et al., 1997
ACPC	Agonist: Pro-cognitive Antagonist: Anti-convulsant, neuroprotective, anxiolytic, antidepressant, antioxidant, hypotensive and reduce noradrenaline release in mice (induces tolerance)	Fossom LH. et al., 1995; Clos MV. et al., 1996; Nahum-Levy R. et al., 1999; Gao M. et al., 2007; Popik P. et al., 2015
ACBC	ACBC is rapidly cleared, inactivated or removed after administration, limiting its therapeutic potential	Rao TS. et al., 1990

Table 6. Summary of GluN1 partial agonists with therapeutic indications.

These compounds include hydroxypyrazol glycine derivatives (NHP4G or N-hydroxypyrazol-4-yl glycine, a glutamate analogue and ethyl-, propyl-NHP5G aspartate analogues), Cis-2,3-piperidine dicarboxylic acid (PDA, a NMDA analog), and N-acetylaspartylglutamate (NAAG) which is a combination of N-acetylaspartate (NAA) and glutamate (Traynelis SF. et al., 2010) (see **figure 30**). Clinically, only the therapeutic potential of NAAG has been evaluated. NAAG might act as antagonist via a negative regulation of glycine binding and acting in pre-synaptic glutamatergic metabotropic receptors to reduce glutamate release. This antagonistic action results in a protective role for ischemia (Yourick DL. et al., 2003), although NAAG agonistic effect might can also provoke neurotoxicity (Thomas AG. et al., 2000).

Full and partial agonists present distinct affinities towards the different NMDARs depending on which GluN2 subunit is present in the receptor, indicated by the EC50 (Traynelis SF. et al., 2010) (see **figure 29**).
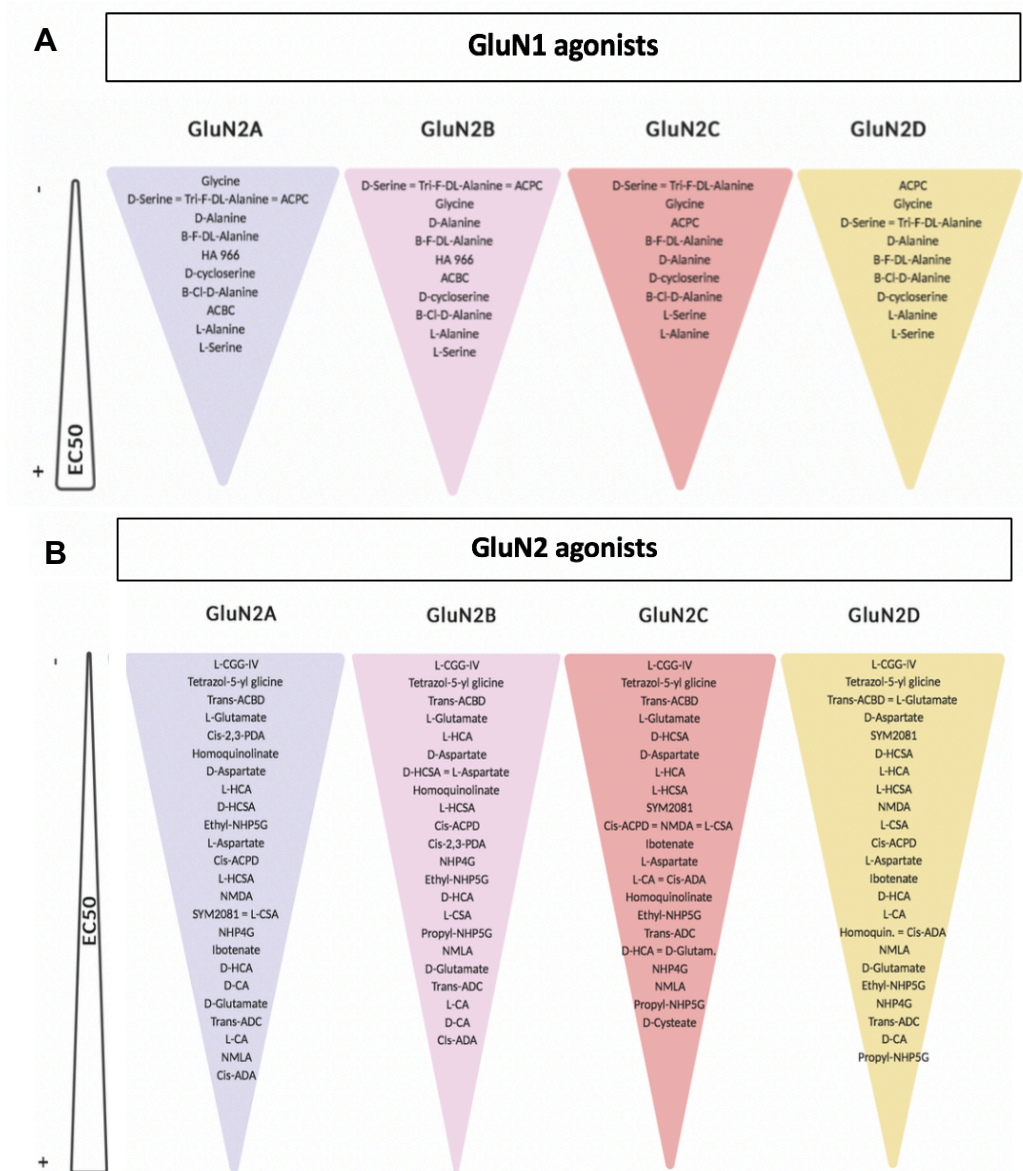
Figure 29. GluN1 (**panel A**) and GluN2 (**panel B**) full and partial agonists potencies, based on EC_{50} values for the different GluN subunits combinations of NMDAR populations (reviewed in Traynelis SF. et al., 2010). EC_{50} is the half maximal efficacy concentration, i.e. the compound concentration that elicits a 50 % response (halfway the baseline and the maximum).

Positive allosteric modulators (PAMs) bind to a secondary allosteric site and modify the conformation of the primary biological site, enhancing the binding affinity of orthosteric compounds. Some PAMs of the NMDAR are polyamines (spermidine and spermine), monovalent ions (Na^+), unsaturated sulfated neuroesteroids (pregnenolone sulfate), 24-S-hydroxycholesterol and derivatives (SGEs), unsaturated fatty acids, pituitary adenylate cyclase-activating polypeptide (PACAP), aminoglycoside antibiotics, quinolones (via Mg^{2+} blockade removal), histamine (increasing NMDAR-derived currents amplitude and decreasing the desensitization rate), ATP (promoting NMDAR-mediated long-term potentiation via activation of ectoprotein kinases and phosphorylation mechanisms), or GNE (GluN2A-containing NMDARs at saturating glutamate concentrations) (see **figure 30**) (Vorobjev VS. et al., 1993; Brown RE. et al., 1995;

Zwart R. et al., 1996; Stahlmann R. et al., 2002; Fujii S., 2004; Traynelis SF. et al., 2010; Hackos DH. et al., 2016; Villemure E. et al., 2016; Volgraf M. et al., 2016).

The effects of polyamines (spermidine and spermine), pregnenolone sulfate, 24-S-hydroxycholesterol and derivatives (SGE-301) and aminoglycoside antibiotics like Tobramycin will be further discussed in the next section ('NMDAR current therapeutics for the potentiation of loss-of-function *GRIN* variants') while the therapeutic potential of the other PAMs is summarized in **table 7**.

Positive allosteric modulators	Therapeutic indications	References
Monovalent ions (Na⁺, Cs⁺)	(These ions regulate the kinetics and affinities of NMDAR blockers)	Antonov SM. et al., 1998
Omega-3 polyunsaturated fatty acids (docosahexaenoic acid), omega-6 fatty acids (arachidonic acid) and omega-9 monounsaturated fatty acids (oleic acid)	Improved spatial memory deficits and neuroprotection against excitatory brain damage (ischemia); reversed ageing associated GluN2B and GluR2 reduction; attenuated pain sensitivity, microglial activation and oxidative stress	Miller B. et al., 1992; Nishikawa M. et al., 1994; Dyall SC. et al., 2006; Gódor-Kacsándi A. et al., 2012; Zhang E. et al., 2017
PACAP-27, PACAP-28 (two biologically active forms)	Neuroprotection in ischemia by decreasing oxidative stress, cytochrome C release and apoptosis, maintaining mitochondrial activity, promoting neurotrophic factors expression (BDNF), and regulating NMDAR subunits expression; protection against Aβ toxicity (Alzheimer disease); fear-related memory (side effect: NMDA-induced excitotoxicity in glaucoma)	Wu SY. and Dun NJ., 1997; Onoue S. et al., 2002; Macdonald DS. et al., 2005; Endo K. et al., 2011; Schmidt SD. et al., 2015; Kaneko Y. et al., 2018
Quinolones (antibiotic)	(Neurotoxic effects: seizures or anxiety; it is not clear whether these neurotoxic effects are due to NMDA positive modulation or GABA antagonism)	Zareifopoulos N. and Panayiotakopoulos G., 2017
GNE-0723	Reduction of epileptiform discharges (through a reduction of low frequency oscillations); improvement of cognitive functions in Alzheimer disease and Dravet syndrome mouse models	Hanson JE. et al., 2020

Table 7. Summary of positive allosteric modulators with therapeutic indications.

In order to potentiate NMDAR-derived responses, an alternative is drugs potentiating NMDARs agonists availability which maintain elevated agonists levels in the synaptic cleft. Within this category, some compounds are able to reduce / block agonists metabolization. In particular, D-aminoacid oxidase (DAO) and D-aspartate oxidase (DDO) blockade can reduce D-serine, glycine, alanine and D-aspartate degradation. Drugs targeting these enzymes include but are not limited to sodium benzoate or 5-chlorobenzo(d)isoxazol-3-ol (CBIO) for DAO, and thiolactomycin for DDO (see **figure 30**) (Katane M. et al., 2010; Traynelis SF. et al., 2010; Gong N. et al., 2011; Wang W. et al., 2013; Durrant AR. and Heresco-Levy U., 2014; Punzo D. et al., 2016; Razak MA. et al., 2017). Moreover, glycine and glutamate transporters might also be blocked, in order to reduce agonists uptake and thus increase the levels of NMDAR agonists in the synaptic cleft. Some blockers of the glycine transporters are sarcosine, or bitopertin and some glutamate transporters blockers include DL-threo-beta-benzyloxyaspartic acid (DL-TBOA), methylglutamate derivatives or some dicarboxylic acids (see **figure 30**) (Griffiths R. et al., 1993; Vanderberg RJ. et al., 1997; Tsai G. et al., 2004; Su LD. et al., 2009; Traynelis SF. et al., 2010; Armbruster A. et al., 2018).
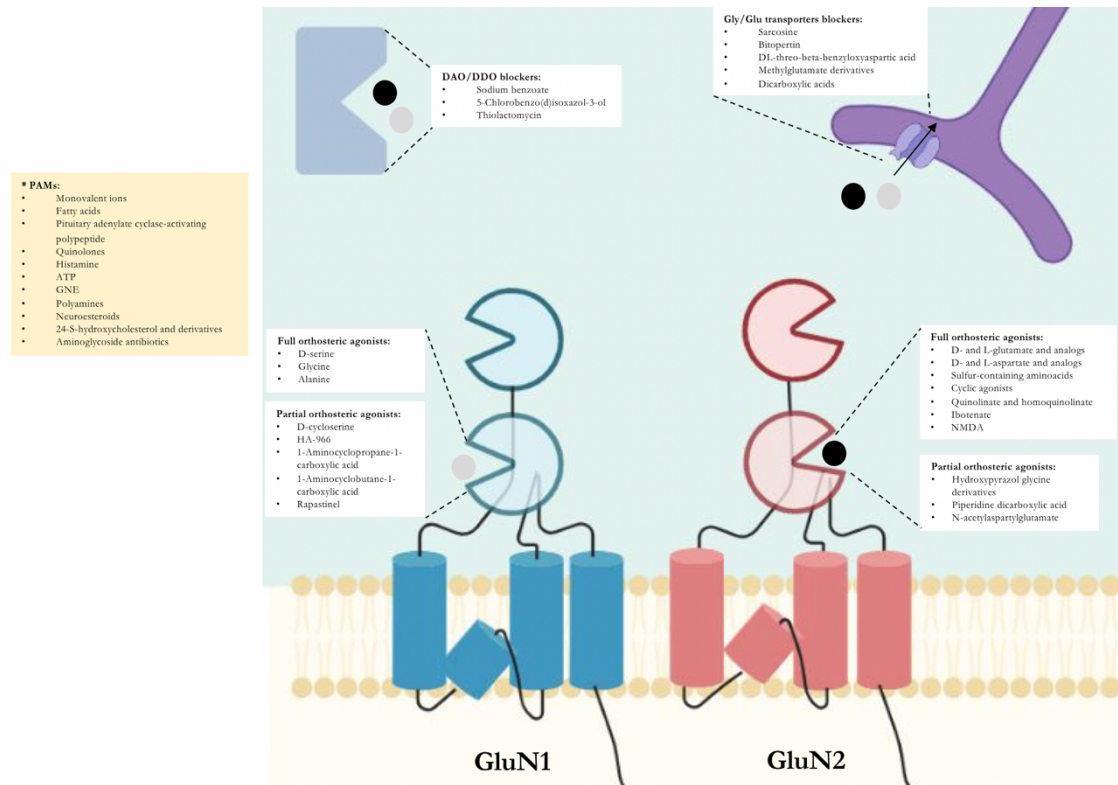
Figure 30. Graphic summary of NMDAR potentiating compounds: DAO/DDO blockers, Gly/Glu transporters blockers, full and partial orthosteric agonists and positive allosteric modulators of GluN1 and GluN2 subunits. Abbreviations: DAO, D-aminoacid oxidase; DDO, D-aspartate oxidase; PAMs, positive allosteric modulators; Gly, glycine; Glu, glutamate.

4.1.2. NMDAR activity attenuation/blockade

In biological scenarios where NMDAR function turns out to be pathologically excessive, NMDARs activity can be attenuated/blocked, using different pharmacological arms including, but not restricted to, the administration of competitive antagonists, non-competitive antagonists, open-channel blockers and compounds that reduce agonist release.

NMDAR competitive antagonists bind to the orthosteric site, resulting in the agonist blockade. This group include 7-chlorokynurenic acid (7-CK) and 5,7-dichlorokynurenic acid (5,7-dCK), indole-2-carboxylate, 2-carboxytetrahydroquinolines, 4-hydroxy-2-quinolones, Quinoxaline-2,3-diones, 3-Hydroxy-1H-1-benzazepine-2,5-diones, tricyclic compounds, CGP 37849, CGP 39551, CGP 40116, ACEA-1011, ACEA-1021, L-689,560, L-701,324, ZD9379, MDL105,519, cycloleucin, D-α-aminoadipic acids, 2-amino-5-phosphonopentanoate (AP5), 2-amino-7-phosphonopentanoate (AP7), 3-(2-carboxypiperazin-4-yl)propyl-1-phosphonic acid (CPP), phosphonomethylpentanedioic acid (PMPA), NVP-AAM077, 1-(phenanthren-2-carbonyl)piperazine-2,3-dicarboxylic acid (PPDA), α-aminoadipate, 1-(biphenyl-4-carbonyl)piperazine-2,3-dicarboxylic acid (PBPD), UBP141 (selective for GluN2C and GluN2D), CGS19175, conantokins (from marine cone snail venom), and EVT101 (Traynelis SF. Et al., 2010) (see **figure 33**). NMDAR competitive antagonists with potential therapeutic applications are summarized in **table 8**.

NMDAR competitive antagonists	Therapeutic indications	References
7-CK	Anti-convulsant (epilepsy) (side effects: ataxia, hypotonia, hypoactivity)	Namba T. et al., 1993
5,7-dCK	Peripherical injury, allodynia, inflammation and neuropathic pain, without sedation and ataxia side-effects (limited BBB permeability)	Christoph T. et al., 2005
Indole-2-carboxylate and derivatives (GV150526)	Protective in mouse models of brain ischemia and stroke via anticonvulsant effects	Hewkin CT. et al., 1999; Di Fabio R. et al., 1999
Tryciclic compounds (Mrz 2/576, SM-18400, SM-31900)	Reduced nociceptive responses; anti-convulsant (ischemic mouse model) (side effects: impaired motor coordination)	McClean M. et al., 1997; Katayama S. et al., 2003; Nagata R. et al., 2006
CGP 37849, CGP 39551, CGP 40116 (oral administration)	Reduced parkinsonian dyskinesias in combination with clonidine; anti-convulsant; neuroprotective (ischemia) (side effects: impaired cognitive and motor abilities)	Schmutz M. et al., 1990; Maj J. et al., 1993; Maier CM. et al., 1995; Hauben U. et al., 1998
ACEA-1011	Anticonvulsant and analgesic	Vaccarino AL. et al., 1993; Lutfy K. et al., 1994
ACEA-1021	Reduced pain-related responses and neuroprotection against ischemic insults	Lutfy K. and Weber E., 1996; Petty MA. et al., 2003
L701, 324	Reduced anxiety-like behaviors; anti-convulsant; improved rigidity in parkinsonian mouse model (no effect in dyskinesias) (side effects: motor abnormalities)	Kotlinska J. and Liljequist S., 1998; Konieczny J. et al., 1999; Wlaź P. and Poleszak E., 2011
ZD9379	Neuroprotective (ischemia)	Tatlisumak T. et al., 1998
AP5	Reduced anxiety and pain-related behaviors	Häckl LPN. and Carborez AP., 2007; Soleimannejad E. et al., 2007
AP7	Anxiolytic	Molchanov ML. and Guimãraes FS., 2001
CPP	Anti-convulsant in combination with valproate, carbamazepine, and phenobarbital (side effects: co-administration of CPP and valproic acid lead to moderate motor impairment)	Borowicz KK. Et al., 2000
Conantokins	Reduced pain-related behaviors (analgesic in distinct mouse models of pain); neuroprotective in ischemia (mouse models of stroke); anti-convulsant (mouse models of epilepsy)	Jimenez Ec. Et al., 2002; Hama A. and Sagen J., 2009; Balsara R. et al., 2015

Table 8. Summary of NMDAR competitive antagonists with therapeutic indications.

Non-competitive NMDAR antagonists (or negative allosteric modulators) bind to an allosteric site and prevent NMDA receptor activation. This group include dynorphins (acting as non-competitive antagonists but also, under some circumstances, as NMDAR potentiators), ifenprodil and analogues (Ro-63-1908, CI-1041, CP-101,606, Ro-256981; GluN2B subunit-selectivity), ethanol, felbamate, haloperidol, xenon, nitrous oxide, radiprodil, divalent ions (Pb^{2+}, Zn^{2+}, Mg^{2+}), monovalent ions (H^+), planar saturated neuroesteroids (pregnanolone sulfate, promoting NMDAR desensitization), sulfonamides (TCN201, selective antagonist of GluN2A subunit-containing NMDARs), lysophospholipids, DET, CP2323 (cyclic polyamine) (Kussius CL. Et al., 2009; Traynelis SF. Et al. 2010) (see **figure 33**). Non-competitive antagonists present distinct affinities towards the different NMDAR depending on which GluN2 subunit is present in the receptor, indicated by the IC50 (Traynelis SF. et al., 2010) (see **figure 31**).

Radiprodil will be further discussed in following topics ('NMDAR current therapeutics for the blockade of gain-of-function *GRIN* variants') while other NMDAR non-competitive antagonists with potential therapeutic applications are summarized in **table 9**.

Non-competitive NMDAR antagonists	Therapeutic indications	References
Dynorphins	At certain doses, moderate analgesia (side effects: excitotoxicity, hyperacusis, cognitive defects)	Kuzmin A. et al., 2006; Sahley TL. Et al., 2013; Ménard C. et al., 2014
Ifenprodil	Analgesic (allodynia and hyperalgesia murine models); anti-depressant (stress murine model); neuroprotective (traumatic brain injury murine models); anti-epileptic at high doses	Yourick DL. Et al., 1999; Dempsey RJ. et al., 2000; Zhang W. et al., 2009; Rondon ES. et al., 2010; Yao Y. et al., 2020
CI-1041	Neuroprotective (status epilepticus murine model)	Loss CM. et al., 2019
CP-101,606	Analgesic (pain mouse models); reduced levodopa-induced dyskinesias (clinical trial); attenuated cognitive defects after traumatic brain injury (mouse models); neuroprotection (neuronal primary cultures under excitotoxic insults) (side effects: cognitive impairments)	Menniti F. et al., 1997; Okiyama K. et al., 1997; Taniguchi K. et al., 1997; Nutt JG. et al., 2008
Felbamate	Anti-convulsant; reduced dyskinesias; neuroprotective (murine model of hypoxia/ischemia); anti-depressant (mouse models of depression)	Ktreschmer BD., 1994; Fraser CM. Et al., 1999; Germanò A. et al., 2007; Li X. et al., 2019
Zinc	Analgesic (pain evaluation in a mouse model with a GRIN2A variant that remove Zn^{2+} blockade); anti-depressant	Kroczka B et al., 2001; Nozaki C. et al., 2015
Magnesium	Analgesic (neuropathic pain, fibromyalgia, headaches, migraine); anti-depressant (murine models); neuroprotective (glaucoma murine model); pro-cognitive (traumatic brain injury murine model);	Smith DH. Et al., 1993; Pochwat B. et al., 2014; Lambuk L. et al., 2017; Shin HJ. Et al., 2020
Pregnanolone sulfate	Neuroprotective and moderate anxiolytic (murine model of excitotoxicity); anti-depressant	Holubova K. et al., 2014; Marketa C. et al., 2020
CP2323	Neuroprotective against excitotoxic insults (cell assays)	Masuko T. et al., 2008
Xenon	Anesthetic; neuroprotective via reduced glial proliferation (excitotoxicity, hipoxia, ischemia murine models); reduced dyskinesias (murine and primate Parkinson models); social improvement and anti-depressant (autism murine models); anti-depressant and anxiolytic (depression mouse models); anti-convulsant; analgesic	Dingley J. et al., 2006; Giacalone M. et al., 2013, Azzopardi D. et al., 2014; Lavaur J. et al., 2017; Baufreton J. et al., 2018; Dobrovolsky AP. Et al., 2019; Shao J. et al., 2020
Nitrous oxide	Anesthetic; anti-depressant (patients); persistent reduction in neuropathic pain (murine models); neuroprotective (ischemia murine models) (side-effects: abuse)	David HN. et al., 2003; Boujema MB. Et al., 2015; Zorumski CF. et al., 2015

Table 9. Summary of NMDAR non-competitive antagonists with therapeutic indications.
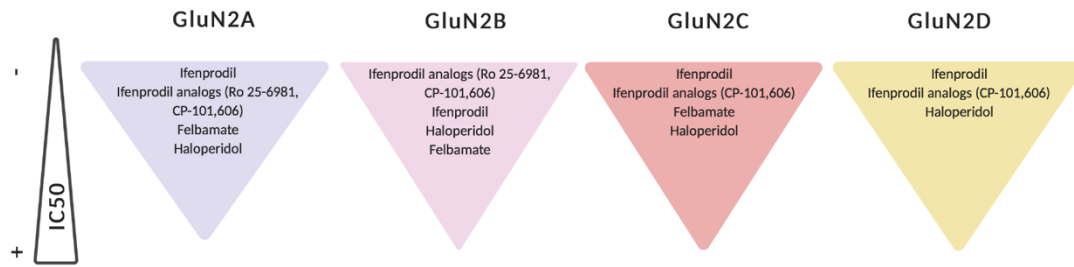
Figure 31. Subunit-dependent affinity of non-competitive antagonists of NMDARs based on IC_{50} (half maximal inhibitory concentration) values, reviewed in Traynelis SF. et al., 2010.

Open-channel blockers (also known as trapping blockers) are NMDAR antagonists that penetrate the NMDAR in the open channel configuration, binding and being trapped into the blocking site, located at the channel pore. As a consequence of their mechanistic action mode, the blockade is slow to reverse because it requires channel reactivation by agonists before the blocker can dissociate. This group includes phencyclidine (PCP) (PCP is used to generate animal models of schizophrenia, based on the glutamatergic hypothesis), MK-801 (dizocilpine maleate), MK-0657 (GluN2B-selective), ketamine, norketamine (ketamine metabolite), tiletamine, amantadine, pentamidine (antimicrobial compound from *Pneumocystis carinii* with voltage-dependent inhibition of NMDARs), remacemide, 9-tetrahydroaminoacridine (GluN2B-selective), dextromethorphan, levomethorphan, 1-phenylcyclohexylamine (PCA), CNS-1102 (Cerestat, Aptiganel), AZD6765 (Lanicemide) and DA10 (Traynelis SF. et al., 2010) (see **figure 33**). Likewise, other NMDAR modulating compounds, trapping blockers exhibit distinct affinities (indicated by the IC_{50} values) depending on GluN2 subunits composition of NMDARs (Traynelis SF. et al., 2010) (see **figure 32**). Memantine and dextromethorphan, two other important open-channel blockers, will be further discussed in following topics ('NMDAR current therapeutics for the blockade of gain-of-function *GRIN* variants') while other NMDAR trapping blockers with potential therapeutic applications are summarized in **table 10**.

Trapping blockers	Therapeutic indications	References
MK-801	Anti-depressant; rapid short-term analgesia (murine model of neuropathic pain); neuroprotective (reduced infarct size in ischemia mouse model); anticonvulsant but no anti-epileptogenic (kindling model), anti-dystonic (retarded progression); pro-cognitive (traumatic brain injury murine model) (side-effects: MK-801 is also used to generate animal models of schizophrenia, increasing locomotion and stereotypies)	Richter A. et al., 1991; Hamm RJ. et al., 1993; Gilbert ME., 1994; Ma J. et al., 1998: Wu J. et al., 2005; Yang B. et al., 2016; Wang J. et al., 2017
MK-0657	Anti-depressant (treatment-resistant patients with major depressive disorder)	Ibrahim L. et al., 2012
Ketamine	Anesthetic At sub-anesthetic doses: anti-depressant (rapid and persistent in treatment-resistant patients with major depressive disorder); analgesic (treatment-resistant neuropathic pain) (side-effects: abuse; it is used to generate animal models of schizophrenia; psychomimetic, sedative and motor alterations)	Covvey JR. et al., 2012; Niesters M. et al., 2013
Norketamine	At subanesthetic doses: Analgesic (neuropathic and inflammatory pain in murine models); anti-depressant (S isomer)	Holtman Jr. JR. et al., 2008; Salat K. et al., 2015; Yokoyama R. et al., 2020
Amantidine	Anxiolytic and anti-dyskinetic in murine models and L-DOPA treated Parkinson patients (side-effect: corneal edema, via K^+ channels but also neuropsychiatric symptoms, fatigue, hypotension, constipation or cardiovascular dysfunction)	Perez-Lloret S. and Rascol O., 2018; Dudley CE. et al., 2019; Walia V. et al., 2020
Pentamidine	Neuroprotective (cells under excitotoxic insults)	Reynolds IJ. and Aizenman E., 1992
Remacemide	Neuroprotective (ischemia murine models); prevented vasospasm in aneurysmal subarachnoid hemorrhage (rabbit model); reduced lesion after traumatic brain injury (although cognitive defects were detected in this murine model); anti-convulsant; anti-parkinsonian (mouse and primate models)	Greenamyre JT. et al., 1994; Zuccarello M. et al., 1994; Davies JA.,1997; Smith D.H. et al., 1997; Calabresi P. et al., 2003
PCA	Anti-convulsant without motor side effects (mouse model with seizures)	Blake PA. et al., 1992
CNS-1102 (Aptiganel)	Neuroprotective and reduced neuronal damage (ischemia, stroke) (side effects: at high doses, increased blood pressure, motor alterations, euphoria, hallucinations, paresthesia)	Muir KW. et al., 1997; Schäbitz WR. et al., 2000
AZD6765 (Lanicemide)	Anti-depressant with minimal psychomimetic side-effects in mouse models and treatment-resistant patients	Sanacora G. et al., 2014

Table 10. Summary of NMDAR trapping blockers with therapeutic indications.
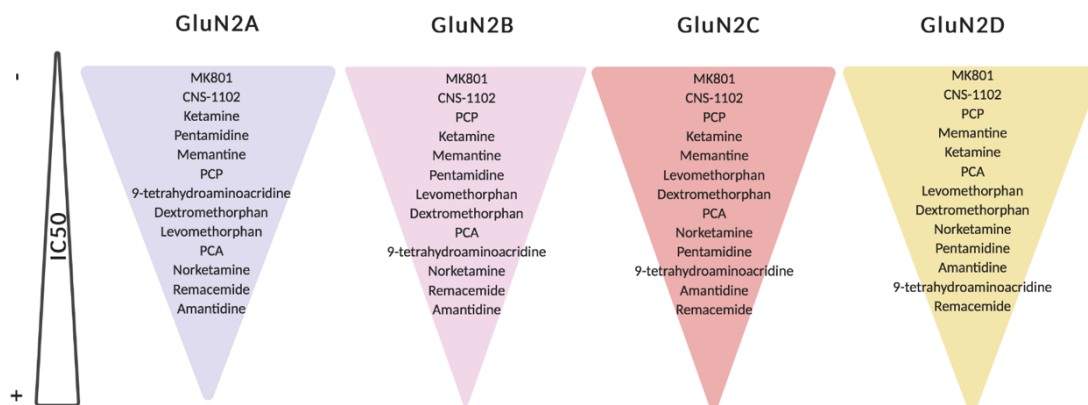
Figure 32. Subunit-dependent affinity of NMDARs trapping blockers based on IC$_{50}$ (half maximal inhibitory concentration) values, reviewed in Traynelis SF. et al., 2010.

There is increasing evidence that sub-threshold changes in the pre-synaptic membrane potential prior to spike-evoked glutamate release might have a role in the neurotransmitter release (Zbili M. et al., 2016). In fact, there are several drugs that can indirectly decreased glutamate release via blockade of pre-synaptic voltage-gated sodium channels. Some of these compounds are riluzole (also enhancing astroglia-mediated glutamate uptake), lamotrigine (also blocking voltage-gated calcium and potassium channels, inhibiting serotonin uptake and associated with NO reduction), phenytoin or carbamazepine (see **figure 33**) (Lizasoain I. et al., 1995; Lapidus KAB. et al., 2013; Traynelis SF. et al., 2010). The therapeutic potential of these compounds is summarized in **table 11**.

Compounds that reduce glutamate release (blocking voltage-gated sodium channels)	Therapeutic indications	References
Riluzole	FDA-approved drug for ALS; antidepressant; anxiolytic; effective for neuropathic pain; cognitive improvement and reduced Aβ deposition in mouse model of Alzheimer;	Mirza NR. et al., 2005; Lapidus KAB. et al., 2013; Moon ES. et al., 2014; Okamoto M. et al., 2018
Lamotrigine	Neuroprotective in ischemia; co-adjuvant therapy to manage schizophrenia cognitive and negative symptoms; effective for the treatment of seizures, bipolar disorder, post-traumatic stress disorder, mania and anxiety (It has been administered to a patient with a *GRIN2A* genetic variant (N447K) in combination with valproate to treat seizures)	Calabresi P. et al., 2003; Large CH. et al., 2005; Mirza NR. et al., 2005; Lapidus KAB. et al., 2013; Xu XX. et al., 2018
Phenytoin	Anti-convulsant; analgesic (neuropathic pain) (side effects: sedation and motor disturbances)	Dickenson AH. and Ghandehari J., 2006
Carbamazepine	Anxiolytic; anti-convulsant; effective in neuropathic pain	Mirza NR. et al., 2005; Dickenson AH. and Ghandehari J., 2006

Table 11. Summary of pharmacological compounds blocking voltage-gated sodium channels in the pre-synaptic glutamatergic synapse, with concomitant reduction of glutamate release and therapeutic potential.

Additionally, felbamate that is a non-competitive GluN2 antagonist have also been associated with reduced glutamate release. Nevertheless, felbamate-associated reduction is due to pre-synaptic NMDAR blockade without affecting voltage-gated sodium channels (Yang J. et al., 2007) (see **figure 33**).

Blockers of glutamate release:
- Riluzole
- Lamotrigine
- Phenytoin
- Carbamazepine
- DA10
- Felbamate

*Non-competitive antagonists:
- Dynorphins
- Ifenprodil and analogs (Ro-63-1908, CI-1041, CP-101,606, Ro-256981)
- Ethanol
- Felbamate
- Haloperidol
- Xenon
- Nitrous oxide
- Radiprodil
- Divalent ions (Pb^{2+}, Zn^{2+}, Mg^{2+})
- Monovalent ions (H^{+})
- Pregnanolone sulfate
- Sulfonamides (TCN201)
- Lysophospholipids
- DET
- CP2323

Trapping blockers:
- Phencyclidine
- MK-801
- MK-0657
- Ketamine
- Norketamine
- Tiletamine
- Amantadine
- Pentamidine
- Remacemide
- 9-tetrahydroaminoacridine
- Dextromethorphan,
- Levomethorphan
- 1-phenylcyclohexylamine
- CNS-1102
- AZD6765
- DA10

Competitive antagonists:
- 7-chlorokynurenic acid
- 5,7-dichlorokynurenic acid
- indole-2-carboxylate
- 2-carboxytetrahydroquinolines
- 4-hydroxy-2-quinolones
- Quinoxaline-2,3-diones
- 3-Hydroxy-1H-1-benzazepine-2,5-diones
- Tricyclic compounds
- CGP 37849
- CGP 39551
- CGP 40116
- ACEA-1011
- ACEA-1021
- L-689,560
- L-701,324
- ZD9379
- MDL105,519
- Cycloleucin
- D-α-aminoadipic acids
- 2-amino-5-phosphonopentanoate
- 2-amino-7-phosphonopentanoate
- 3-(2-carboxypiperazin-4-yl)propyl-1-phosphonic acid
- Phosphonomethylpentanedioic acid
- NVP-AAM077
- 1-(phenanthren-2-carbonyl)piperazine-2,3-dicarboxylic acid
- α-aminoadipate, 1-(biphenyl-4-carbonyl)piperazine-2,3-dicarboxylic acid
- UBP141
- CGS19175
- Conantokins
- EVT101

Figure 33. Graphic summary of the different NMDAR blocking compounds: competitive antagonists, non-competitive antagonists, trapping blockers of GluN1 and GluN2 subunits and blockers of glutamate release.

4.2. Current NMDAR pharmacotherapeutic approaches for the blockade of gain-of-function _GRIN_ variants

4.2.1. Memantine

In a pathological situation associated with an excessive activation of the NMDAR (_e.g._ gain-of-function _GRIN_ variants), a therapeutic approach might consist on the use of NMDAR antagonists. A tentative NMDAR antagonist is memantine, an EMA- and FDA-approved compound with antagonistic effects on the NMDAR. Memantine is a derivative of 1-aminoadamantane (see **figure 34**) which act as trapping blocker of NMDARs (Traynelis SF. et al., 2010).
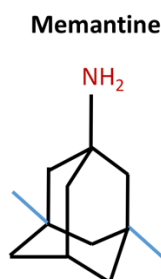
Memantine

Figure 34. Molecular model of memantine chemical structure containing an adamantane structure with methyl groups (blue), and an amino group (red). Adapted from PubChem database.

Memantine (Namenda) is a FDA-approved drug for the treatment of Alzheimer's disease and other neurodegenerative dementias. Indeed, preclinical studies showed that memantine administration reduced Aβ deposition, improved cognitive defects, reduced neurofibrillary tangles formation, increased BNDF release and reduced excitotoxicity (Folch J. et al., 2018). Nevertheless, in the clinical practice, Memantine alone has not achieved satisfactory results, and it is used in combination with other AD drugs, such as cholinesterase inhibitors (Folch J. et al., 2018).

Memantine has been also evaluated in mouse models of neuromyelitis optica, showing motor improvement and neuroprotection that could result from a reduction of inflammation, demyelination and axonal loss, while increasing neurotrophic factors release (Yick LG. et al., 2020). Furthermore, memantine might be used as adjuvant therapy in major depressive disorder (in combination with sertraline, memantine improves anti-depressant treatment efficacy) or schizophrenia (in combination with auditory targeted cognitive training) (Amidfar M. et al., 2017, Swerdlow NR. et al., 2020). Despite these successful indications, memantine-based treatment in other neurological disorders (i.e. multiple sclerosis) was not well-tolerated and do not ameliorated prognosis (Saint Paul LP. Et al., 2016).

In the context of GRD, memantine therapeutic potential has been evaluated both *in vitro* and in patients with GRDs. For instance, GluN2A-P552R variant, which is related with increased agonist potency and a prolonged time course, was identified in a patient with seizures, intellectual disability and brain alterations. Memantine application to neuronal primary cultures expressing GluN2A-P552R variant showed a normalization of NMDAR-mediated currents and neurotoxicity preventive effect (Odgen KK. et al., 2017). In line with this result, GluN1-M641I and GluN2A-L812M (associated with increased agonist potency and decreased Mg^{2+} blockade) also supported the use of memantine for *in vitro* rescue of gain-of-function *GRIN* variants. Importantly, memantine treatment of patients harboring GluN1-M641I and GluN2A-L812M variants resulted in a reduction of epileptic seizures pharmaco-resistant to conventional anti-epileptic drugs (Pierson TM. et al., 2014; Xu Y. et al., 2021). Despite the therapeutic benefit of memantine has been supported by additional studies (Papa FT. et al., 2018), other clinical studies showed the lack of efficacy (Ogden et al., 2017) and memantine use is under debate. Further, *GRIN* variants located within the NMDAR channel pore (frequently associated with gain-of-function outcomes, i.e. GluN2B-N615I and GluN2B-V618G that affect Mg^{2+} blockade) might affect memantine potency to block NMDAR-mediated currents (Mullier B. et al., 2017).

4.2.2. Radiprodil

Radiprodil (2-[4-[(4-fluorophenyl)methyl]piperidin-1-yl]-2-oxo-*N*-(2-oxo-3*H*-1,3-benzoxazol-6-yl)acetamide) is a selective GluN2B subunit-containing NMDAR non-competitive antagonist binding the same site as Ifenprodil (see **figure 35**) (Traynelis SF. et al. 2010).
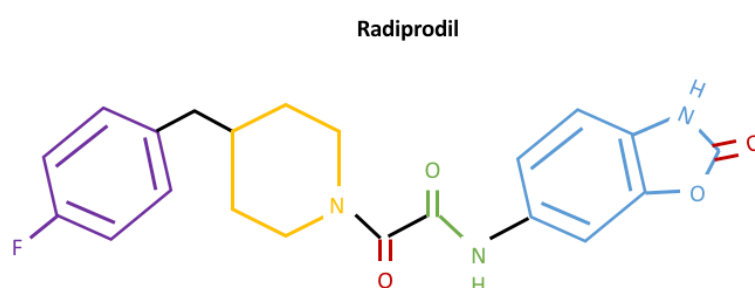
Radiprodil

Figure 35. Molecular model of radiprodil chemical structure containing a fluorophenyl group (purple), a piperidine group (yellow), carbonyl groups (red), acetamide group (green) and a benzoxazol group (blue). Adapted from PubChem database.

Regarding its therapeutic potential, radiprodil was evaluated in a clinical trial for diabetic neuropathic pain (Gilron I. and Coderre TJ., 2007). Nevertheless, this clinical trial was interrupted, since radiprodil was unable to reduce pain scores (RG8-MD-02; NCT00838799).

Besides this clinical trial, radiprodil has been also evaluated as a potential treatment in a murine model of Parkinson's disease (unilateral lesion with 6-dihidroxydopamine). In this model, co-administration of radiprodil and an adenosine receptors antagonist (at certain doses), improved motor defects and mimicked L-DOPA treatment, without dopaminergic side-effects (enhanced locomotion in open field test, restored position without bending, and lack of stereotyped rotations) (Michel A. et al., 2015).

Additionally, there are preliminary investigations revealing a plausible therapeutic potential of this compound in *GRIN*-related disorders. One of these studies evaluated radiprodil in oocytes expressing three *GRIN2B* gain-of-function variants (GluN2B-R540H, N615I and V618G). These variants were identified in patients with epilepsy and intellectual disability. GluN2B-R540H is associated with increased glutamate potency while N615I and V618G are related with a lack of Mg^{2+} blockade. In vitro, radiprodil administration reduced NMDAR-mediated currents in all three *GRIN2B* variants, even under acidic conditions (associated with post-seizures relapse) (Mullier B. et al., 2017). Beyond investigation using *in vitro* models, radiprodil was also administered to murine models of epilepsy, demonstrating a protective effect (Auvin S. et al., 2020). Importantly, radiprodil was translated to the clinical practice and was given to three patients with *GRIN*-related disorders (harboring *GRIN2B* gain-of-function variants) that presented spams and were not responding to conventional anti-epileptic drugs. The compound was proven well-tolerated, and the three patients experimented an improvement in spams although not at the same level (Auvin S. et al., 2020).

4.2.3.   Dextromethorphan

Another potential treatment for gain-of-function *GRIN* variants is dextromethorphan (see **figure 36**), traditionally used as an antitussive compound (Traynelis SF. et al., 2010).
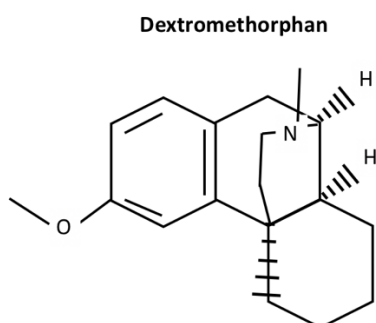
Dextromethorphan

Figure 36. Molecular model of dextromethorphan chemical structure. Adapted from PubChem database.

Dextromethorphan has been already evaluated in animal models of neurological diseases associated with NMDAR dysfunction, including a murine model of hypoxia. In this model, dextromethorphan administration after hypoxic insult reduced brain damage (Laroia N. et al., 1996). Moreover, dextromethorphan has been shown to reduce convulsions in a murine model of seizures (although at high doses, where motor impairments and stereotypies appear) (Löscher W. and Hönack D., 1993), to exert anti-depressant effects (Sakhaee E. et al., 2016) and to revert nociception in a mouse model of neuropathic pain (Morel V. et al., 2014).

Besides its antitussive effects, dextromethorphan use has been proposed for the treatment of neurological disorders. Indeed, dextromethorphan has been administered to patients with diabetic neuropathy to reduce pain due to its analgesic action (Carlsson KC. et al., 2004). In the GRD context, dextromethorphan was evaluated *in vitro* in oocytes expressing a gain-of-function variant (GluN1-M641I, causing increased agonist potency and decreased Mg^{2+} blockade), and demonstrated its ability to reduce increased NMDAR-derived currents (Xu Y. et al., 2021).

4.3. Current NMDAR pharmacotherapeutic approaches for the potentiation of loss-of-function *GRIN* variants

4.3.1.   D-serine

D--serine is a natural co-agonist of the NMDAR. Traditionally, glycine was thought as the unique co-agonist of NMDARs, but D-serine co-localization with NMDAR distribution in the brain and the lack of NMDAR-derived responses when D-serine is selectively degraded, identified D-serine as a NMDAR co-agonist (Mothet JP. et al., 2000). D-serine is formed from L-serine (coming from diet, intestinal bacteria, and glycine and/or glucose transformation) through serine-racemase (SR) activity, an enzyme located in pre-synaptic neurons and astrocytes (Wolosker H. et al., 2008). SR is activated by calcium, magnesium, manganese, ATP, ADP, and GTP whereas it is inhibited by gluthatione and cystamine through post-traslational modifications (Baumgart F. and Rodríguez-Crespo I., 2008). After synthesis, D-serine is released via Ca^{2+} dependent- or independent-mechanisms (Mothet JP. et al., 2005; Kartvelishvily E. et al., 2006; Pan HC. et al., 2015).

D-serine presents an amino group, a carboxyl group and a hydroxymethyl group (see **figure 37**). D-enantiomer act as NMDAR co-agonist (instead of L-serine enantiomer), since the hydroxymethyl group location of L-serine affects the co-agonist interaction with the binding pocket (see **figure 37**) (Wolosker H. et al., 2008).
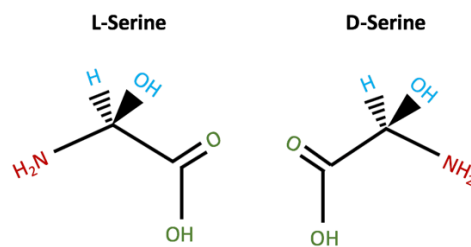
Figure 37. Molecular model of L- and D-Serine chemical structures containing an amino group (red), a carboxyl group (green) and a hydroxymethyl group (blue). Adapted from PubChem database.

D-serine has been widely studied for its potentiating effects in several diseases where NMDAR is dysregulated. For instance, D-serine has been used in schizophrenia (glutamatergic hypofunction theory of schizophrenia-associated negative and cognitive symptoms), in combination with non-clozapine antipsychotic drugs (clozapine promotes D-serine release) (Nunes EA. et al., 2012). Moreover, D-serine has been used for Alzheimer's disease treatment at early stages. In this precise time window, when NMDAR blockers (*i.e.* memantine) do not provide a therapeutic benefit, D-serine treatment could elicit neurogenesis and neuronal survival (Guercio GD. and Panizzutti R., 2018). Interestingly, co-administration of D-serine and L-DOPA revealed improvement of behavioral and motor symptoms (such as reduced dyskinesias) in Parkinson's disease (Gelfin E. et al., 2012). Furthermore, D-serine has been used as cognitive enhancer in healthy subjects reducing anxiety and depression feelings and increasing attention, vigilance, and information retaining (Durrant AR. and Heresco-Levy U., 2014; Levin R. et al., 2015; Guercio GD. and Panizzutti R., 2018).

Despite these promising results, D-serine administration is not devoid of side effects. Indeed, high doses of D-serine can trigger excitotoxic processes. Moreover, there is a concern regarding nephrotoxicity due to D-serine metabolism via DAO enzyme. Thus, a combination of D-serine with a DAO inhibitor could increase D-serine bioavailability and prevent undesired side effects (Guercio GD. and Panizzutti R., 2018). Furthermore, long-term D-serine supplementation might impair insulin secretion and glucose metabolism via sympathetic nervous system but an α2-adrenergic receptor antagonist might revert this situation (Suwandhi L. et al., 2018).

To circumvent this hurdle, different groups evaluated the therapeutic benefit of L-serine enantiomer. Originally, L-serine dietary supplementation has been used in paediatric neurology, administering high doses of L-serine (dietary supplement) for the treatment of neurometabolic conditions with a serine synthesis deficiency. These treatments were devoid of side-effects and improved both epileptic and psychomotor symptoms (De Koning TJ. And Klomp LWJ., 2004).

According to its tolerability and precursor role for D-serine synthesis, L-serine is presented as a good candidate molecule for potentiating *GRIN* loss-of-function variants in patients with GRD paediatric encephalopathies. Indeed, L-serine was evaluated in a patient with a severe encephalopathy that present a GluN2B loss-of-function variant (P553T). This genetic variant is associated with a pore reduction of the channel, and consequently, reduced NMDAR-derived currents and synaptic morphological alterations (spines density reduction). Firstly, L-serine was evaluated *in vitro* to demonstrate that the compound is able to rescue reduced NMDAR-derived currents and spines deficit in cells expressing that particular genetic variant. Then, the patient started receiving L-serine supplementation. After several months of dietary L-serine, the patient experienced improvement of intellectual, behavioural, communication and motor symptoms (Soto D. et al., 2019).

4.3.2. Polyamines: Spermidine and Spermine

Polyamines like Spermidine and Spermine are aliphatic compounds which are polybasic and positive at physiological pH. Spermidine is the metabolic precursor of spermine, and both come from putrescine and S-adenosylmethionine (Williams K. et al.,1997) (see **figure 38**). These compounds are released via Ca^{2+}-dependent mechanisms from neurons and glial cells (Pegg AE. et al., 2016).
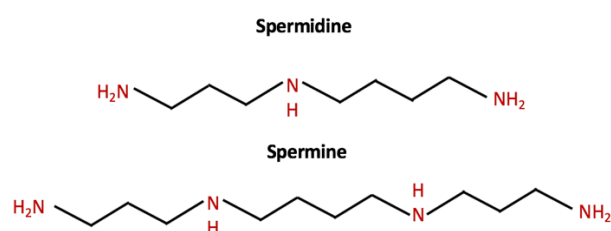
Figure 38. Molecular model of spermidine and spermine chemical structures containing amino groups (red). Adapted from PubChem database.

Polyamines binding-site is located in a dimer interface formed by GluN1 and GluN2 ATD (Mony L. et al., 2011) and play essential roles in cell proliferation, migration and viability (Pegg AE. et al., 2016).

Spermine might impact NMDAR function in different modes, based on its location (intracellular *vs.* extracellular), dose and GluN composition of the NMDAR. For instance, at high doses, spermine blocks GluN2A- and GluN2B-containing NMDARs in a voltage-dependent manner (similar to Mg^{2+} blockade). On the contrary, at low doses, spermine might activate GluN2A and GluN2B-containing NMDARs by decreasing the rate of glycine dissociation or exclusively GluN2B-containing receptors via glycine and voltage-independent mechanisms. Glycine and voltage-independent potentiation is mediated by favoring the channel open state configuration, regulating desensitization and releasing tonic proton inhibition. This potentiation mechanism is specific for GluN2B-containing NMDARs and is more pronounced in NMDARs containing GluN1α isoforms (lacking exon 5 / N1 cassette) that modifies proton sensitivity (Lerma J., 1992; Gallagher MJ. et al., 1997; Mony L. et al., 2011). Moreover, there are specific residues like GluN2B-G689 that also have a role in proton sensing and might fail to respond to spermine potentiation when mutated (Kellner S. et al., 2021).

Despite both polyamines can potentiate NMDAR-mediated currents, spermine EC_{50} on NMDARs activity is more reduced, indicating a higher potency. Therefore, likewise L-serine administration (precursor of NMDAR agonist D-serine), spermidine supplementation could theoretically increase spermine levels towards NMDARs potentiation. Regarding spermidine supplementation, several studies pointed out a therapeutic benefit, in particular the attenuation of memory impairments (via activation of Trkβ receptor and PI3K/Akt pathway) (Fabbrin SB. et al., 2020), the reduction of blood pressure, the prevention of cardiac disease, and the promotion of gut maturation (Gréco S. et al., 2001; Velloso NA. et al., 2008; Eisenberg T. et al., 2016; Wirth M. et al., 2018; Kiechl S. et al., 2018). Despite these promising studies, polyamines supplement dose still represents an important issue, as indicated by reports describing pain-related behaviours and toxicity due to overexcitation of NMDA and non-NMDA receptors, and the increase of hydrogen peroxide or reactive aldehydes metabolites (Otsuki M. et al., 1995; Tan-No K. et al., 2000).

4.3.3. Rapastinel

Rapastinel (formerly known as Glyx-13) is an amidated tetrapeptide di-pyrrolidine which is derived from a monoclonal antibody (B6B21) (see **figure 39**) (Moskal JR. et al., 2014). This compound binds to an NMDAR allosteric site that regulates the co-agonist site in the GluN1 subunit, while acting as a partial agonist (Donello JE. et al., 2019).
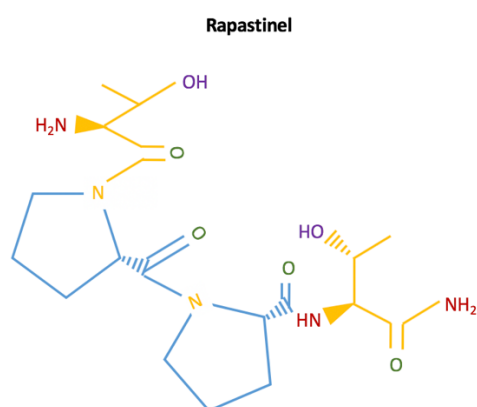
Figure 39. Molecular model of rapastinel chemical structure containing amino groups (red), hydroxyl groups (purple), pyrrolidine groups (yellow) and carboxyl groups (green). Lines are blue when the structure comes from prolines and yellow when it comes from threonine. Adapted from PubChem database.

Based on NMDAR agonist properties, rapastinel has been evaluated as a potential antidepressant drug. Molecular studies showed that rapastinel action via BDNF release, TrkB signaling and orexin-hypocretin-induced EPSCs have an antidepressant effect devoid of psychomimetic secondary effects (lack of rapastinel effects on the serotoninergic system) (Liu RJ. et al., 2017; Kato T. et al., 2018). Besides this indication, rapastinel induces anxiolytic effects (reducing corticosterone and adrenocorticotropic hormone (ACTH), and increasing the glucocorticoid receptor) (Jin Z. et al., 2016) and promotes a cognitive benefit (promoting LTP through extrasynaptic NMDARs and reducing LTD through synaptic NMDARs) (Zhang XL. et al., 2008). In autism spectrum disorders, rapastinel administration rescued social/emotional communication deficits in murine models that show low rate of pro-social ultrasonic vocalizations (Moskal RJ. et al., 2011).

Rapastinel is considered a partial agonist. Thus, this compound might occupy a large number of NMDARs without eliciting a response and consequently blocking the effects of the agonists. This 'antagonistic' effect could occur at the same concentrations than the agonistic effect, depending on the full agonist concentration (Neubig RR. et al., 2003). This 'antagonistic' action of rapastinel is neuroprotective and reduce ischemia injury in mice models, promoting phosphorylation of synaptic GluN2A-containing NMDARs and decreasing phosphorylation of extra-synaptic GluN2B-containing receptors (Zheng C. et al., 2017). Rapastinel 'antagonistic' actions also include its anti-nociceptive effects without ataxic secondary effects in several mouse models of pain (Wood PL. et al., 2008).

Regardless of acting as an agonist or an antagonist, no safety concerns have been described for rapastinel therapeutic use, and its effects are relatively quick and long-lasting (Moskal RJ. et al., 2014).

4.3.4. Pregnenolone sulfate

Unsaturated sulfated neuroesteroids like pregnenolone sulfate (20-oxo-5- pregnen-3β-yl sulfate) act predominantly as positive allosteric modulators of NMDARs. In particular, pregnenolone sulfate acts as a PAM of GluN2A- and GluN2B subunits-containing NMDARs while interestingly acting as a negative allosteric modulator of GluN2C and GluN2D-containing NMDARs, preferentially at resting state (Burnell ES. et al., 2019). Pregnenolone is obtained from cholesterol through cytochrome P450 CYP46A1 enzymatic activity and it is further sulfated by SULT2B1a (see **figure 40**) (Ratner MH. et al., 2019).
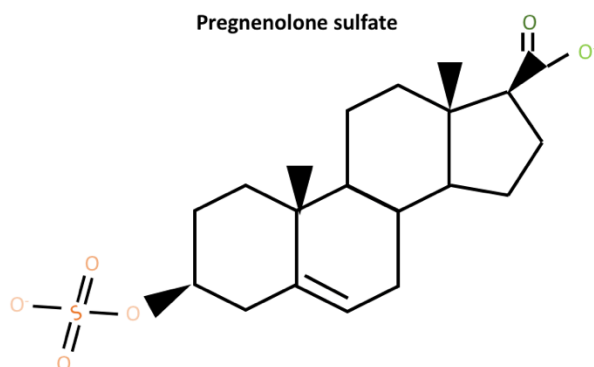
Figure 40. Molecular model of pregnenolone sulfate chemical structure containing carboxyl group (green) and sulfate group (orange). Adapted from PubChem database.

Pregnenolone sulfate potentiating role occurs via binding to TMD at W559, M562, Y823 and M824 residues in GluN2B M1 and M4 transmembrane domains and G638 and I642 residues in GluN1 transmembrane M3 domain (Krausova BH. et al., 2020). The potentiation conducted by pregnenolone is based on deactivation and desensitization slow-down and increased open probability of NMDARs (Burnell ES. et al., 2019).

Pregnenolone sulfate has been associated with memory improvement, particularly concerning spatial orientation and object discrimination (Plescia F. et al., 2014). Moreover, its potential therapeutic action has been evaluated in schizophrenia, as an adjuvant of standard antipsychotic drugs, and have revealed that pregnenolone is able to mitigate schizophrenia-associated negative symptoms, without reporting significant side effects (Marx CE. et al., 2009). Regarding *GRIN*-related disorders, preliminary studies indicate that pregnenolone sulfate is able to potentiate NMDAR-derived currents when certain loss-of-function *GRIN* variants are expressed, such GluN2A-D731N and GluN2B-E413G (Tang W. et al. 2020).

4.3.5. 24-S-Hydroxycholesterol

24-S-hydroxycholesterol is a metabolic derivative of cholesterol, via cytochrome P450 CYP46A1 enzymatic activity. This compound is similar to pregnenolone sulfate (see **figure 41**), but its binding to a distinct allosteric site results on a higher NMDAR potentiation effect mediated by the increase of NMDAR open probability (Burnell ES. et al., 2019). Chemical modification of particular 24-S-hydroxycholesterol functional groups (*e.g.* SGE-301) have shown to increase the potency (see **figure 41**).

24-S-Hydroxycholesterol
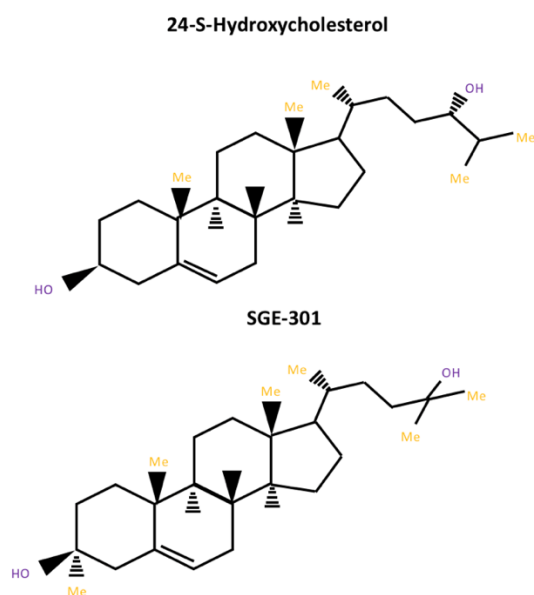
SGE-301

Figure 41. Molecular model of 24-S-hydroxycholesterol and SGE-301 chemical structures containing hydroxyl groups (purple), and methyl groups (yellow). Adapted from La DS. et al., 2019.

In Alzheimer's disease, 24-S-hydroxycholesterol has been related with protective effects (suppressing Aβ production) and pathological effects (promoting Aβ aggregation and neurotoxic effects), depending on the context and the compound levels (Sun MY. et al. 2016). Moreover, 24-S-hydroxycholesterol might have a protective role in glaucoma by reducing pressure-induced injury (Ishikawa M. et al, 2018). 24-S-hydroxycholesterol and derivatives (*i.e.* SGE-301) have been evaluated in anti-NMDAR encephalitis revealing that these PAMs are able to persistently potentiate NMDAR-mediated responses, by prolonging open time and reducing NMDARs internalization (Warikoo N. et al., 2018; Mannara F. et al., 2020). In the context of GRD, preliminary studies show that 24-S-Hydroxycholesterol is able to potentiate NMDAR-derived currents and to slow the deactivation rate of NMDARs expressing GluN2A-D731N and GluN2B-E413G loss-of-function *GRIN* variants (Tang W. et al. 2020).

4.3.6.   Tobramycin

Tobramycin is an aminoglycoside antibiotic (see **figure 42**) that also acts as a GluN2B-selective positive allosteric modulator, via binding to the polyamines binding site (Segal JA. and Skolnick P., 1998).

Tobramycin

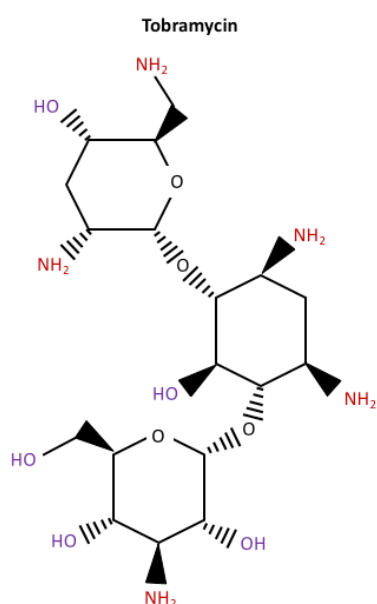**Figure 42.** Molecular model of tobramycin chemical structure containing hydroxyl groups (purple), and amino groups (red). Adapted from PubChem database.

Traditionally, these antibiotics have been used for the treatment of Gram(-) bacterial infections and resistant tuberculosis. However, recent studies showed the capacity of this compound for the potentiation of NMDAR-mediated current amplitudes of certain loss-of-function *GRIN* variants, particularly GluN2A-D731N and GluN2B-E413G (Tang W. et al. 2020). Nevertheless, since tobramycin administration exhibits significant side effects (ototoxicity and hearing loss, via excessive excitation of cochlear NMDA receptors) (Segal JA. et al., 1999), the translation to the clinical practice is compromised.

4.4. Novel therapeutic approaches for GRIN-related disorders

In addition to current investigation of pharmacological and nutraceutical approaches for GRD treatment, novel therapeutic strategies (based on gene therapy approaches and microbiota manipulation) are under investigational research.

4.4.1.   Gene therapy strategies

GRIN-related disorders (GRDs) are caused by the presence of *GRIN* genes variants that alter NMDAR activity. Likewise, other rare genetic neurodevelopmental diseases, GRDs are currently symptomatically treated, since no cure (correcting the primary genetic etiology of GRD) is available yet. In this line, gene therapy is envisioned as the ideal therapeutic management of GRD, allowing to silence and/or repair the mutant *GRIN* allele.   Gene therapy approaches for neurological diseases treatments are classified according to the following strategies: 1) down-regulation of aberrant gene (via RNA interference, RNA$_i$ or antisense oligonucleotides, ASOs); 2) replacement with non-aberrant transgene (can be used in combination with down-regulation approach); 3) protective approach by infusion of neurotrophic factors; and 4) gene editing, using CRISPR-Cas9 technology that allows gene silencing or correction in target cells (Benger M. et al., 2018).

Despite the physical difficulties intrinsic to CNS viral transduction, gene therapy of neurological disorders has been explored along clinical trials. In Parkinson's disease, gene therapy has been designed to introduce different transgenes encoding for enzymes (glutamic acid decarboxylase, aromatic L-aminoacid decarboxylase) or neurotrophic factors, in order to synthetize GABA from glutamate, to transform levodopa into dopamine, or to release the glial-derived neurotrophic factor, respectively (Sudhakar V. and Richardson RM., 2019). In Huntington's disease, gene therapy has been directed towards RNA$_i$ delivery to knock-down mutant huntingtin (Sudhakar V. and Richardson RM., 2019).

Despite potentially being an optimal approach, gene therapy for GRD harbors multiple hurdles. One of the difficulties in the gene strategy treatment of *GRIN*-related disorders is related to the massive *GRIN* transgene size. Using adenoviruses (instead of lentivirus or AAVs, with reduced packaging capacity) Yamada and colleagues were able to express NMDA receptors in PC12 cells bypassing packaging limitation (Yamada N. et al., 1999; Choudhury S. et al., 2017). Nevertheless, adenoviral transgenes are not integrative and are highly immunogenic, causing inflammation and cytotoxicity (Choudhury S. et al., 2017). Later, Holehonnur and colleagues modified lentiviral vectors and succeeded to express GluN subunits in neurons by means of viral transduction (Holehonnur R. et al., 2015).

Regarding the knock-down strategy to correct particular *GRIN* variants, without the necessity to express a massive transgene, AAVs and lentiviral vectors containing RNAi against were injected in the spinal cord of murine models and resulted on efficient GluN subunits knock-down for several weeks or months without causing toxicity and improving pain-related behaviors (Garraway SM. et al., 2007; Wu F. et al., 2014).

4.4.2.   Microbiota manipulation

The gastrointestinal tract contains trillions of microorganisms (microbiota) whose composition depends on the host genome, diet, and/or health conditions. Between the gastrointestinal tract and the central nervous system (brain-gut axis), a bidirectional neuroendocrine communication exists. This brain-gut axis has a role in intestinal permeability and motility, immune function, enteric nervous system (ENS) activity, stress response, emotional behavior, and brain biochemistry (Mayer EA. et al., 2015; Li Q. and Zhou M., 2016). The CNS influences the gut via the sympathetic/parasympathetic autonomic system (inhibition and activation, respectively) and the hypothalamus-pituitary-adrenal axis (HPA) through cytokines and the endocrine system. In parallel, the gut impacts the neuronal system via neuronal pathways (*e.g.* vagus nerve) and microbial-associated metabolites (MAMs) such as tryptophan, short-chain fatty acids (SCFAs: acetate, butyrate propionate), glutamate, GABA, noradrenaline, dopamine, serotonin, or BDNF (see **figure 43**) (Maqsood R. and Stone TW., 2016).

Under pathological conditions, it has been shown that the autonomic sympathetic system and HPA axis are overactivated, and hormones release became dysregulated, resulting in changes in microbiota composition and function (dysbiosis). Further, microbiota changes result in a dysregulation of the associated MAMs (increased release of lipopolysaccharides and pro-inflammatory cytokines) and altered feedback neuronal pathways, with an impact on normal brain functioning by increasing immune response and triggering inflammation. Microbiota dysbiosis has been recently associated with several neurological conditions, such as Parkinson's disease, chronic pain, depression, anxiety, autism spectrum disorders, ADHD, intellectual disability and inflammatory intestinal diseases (see **figure 43**) (Maqsood R. and Stone TW., 2016). For instance, the increased production of p-cresol metabolite (from tyrosine degradation by certain bacteria populations) might be related with the appearance of ASD symptoms (social deficits, stereotypies, decreased dopaminergic activity in the ventral tegmental area which is related with reward circuits) (Bermudez-Martin P. et al., 2020).
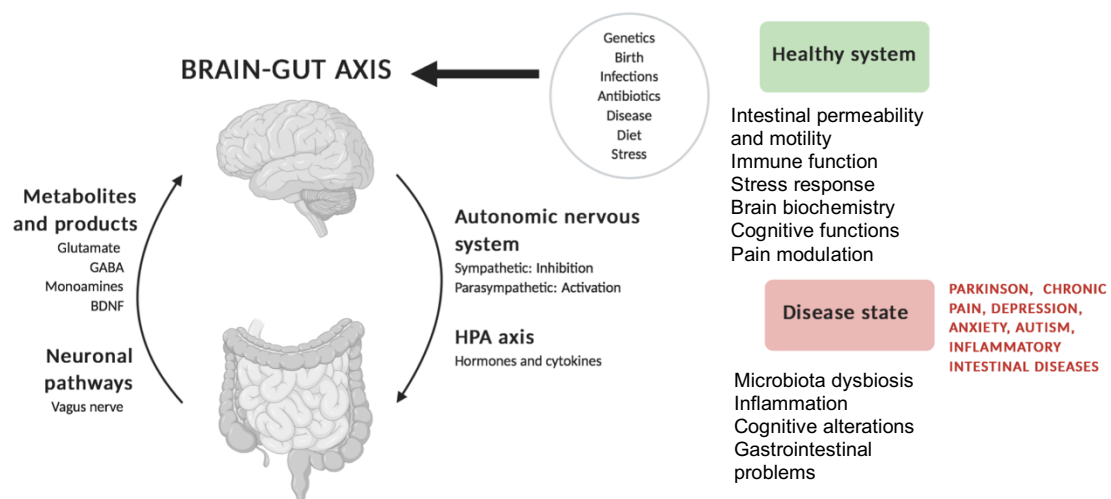
Figure 43. Brain-gut axis functioning is influenced by genetics, environmental and health conditions. The central nervous system is influencing the gastrointestinal system via the autonomic nervous system and the HPA axis while the gastrointestinal system is releasing metabolites and sending neuronal feedback projections to the brain. Normal functioning of the brain-gut axis is related with intestinal and cognitive functions but a pathological brain-gut axis functioning results in microbiota dysbiosis and several diseases.

Therapeutic approaches that promote microbiota changes may include the use of probiotics, prebiotics, fecal microbiota transplantation (FMT), helminths or certain diets such as the Mediterranean diet. Prebiotics are non-digested and fermented ingredients (fructo-oligosaccharides, inulin, resistant starch, pectic oligosaccharides, galacto-oligosaccharides and flavanols) that modify microbiota composition and activity. Prebiotics naturally exist in some foods (asparagus, beet, artichoke, garlic, onion, wheat, honey, banana, tomato, milk, beans, peas…) at low concentration. Prebiotics fermentation increases short fatty acids levels that improve cognitive functions, mood, immune response, metabolism processes, stress response, or reduce the risk of cardiovascular diseases (Davani-Davari D. et al., 2019). Probiotics consist on living bacteria that are able to colonize the gut of the host and to reestablish the microbiota by competing with harmful bacterial. Probiotics include *Lactobacillus, Bifidobacterium, Escherichia coli, Enterococcus* and *Saccharomyces* phyla / species, and have been associated with beneficial effects in distinct diseases like inflammatory bowel disease, Crohn's disease and colorectal cancer (Kim SK. et al., 2019).

Fecal microbiota transplantation (FMT) consists on the transfer of stool (microbiota) from a donor to an acceptor. FMT evaluation in murine models indicate that this therapeutic approach might be useful in the treatment of neurobiological diseases where microbiota dysbiosis is related with physiopathology. For instance, FMT transplantation in mouse models of Alzheimer's disease have been associated with cognitive improvement, reduction of Aβ deposition, decrease of Tau hyperphosphorylation, reduction of glial reactivity and recovery of normal microbiota composition (Kim MS. et al., 2019; Sun J. et al., 2019). In a mouse model of multiple sclerosis, FMT has been associated with dysbiosis correction, BBB integrity, increased normal myelin sheaths, decreased axonal damage, and reduced microglial activation (Li K. et al., 2020). FMT application in a traumatic brain injury model in rats also rescues microbiota changes, improves learning and spatial memory, and reduced oxidative stress (Du D. et al., 2021). Another model that supports therapeutic benefit of FMT is an autism mouse model, where FMT ameliorates inflammation and improves memory and social deficits but not anxiety-like or locomotor phenotypes (Goo N. et al., 2020). In humans, FMT has already been applied in patients with recurrent *Clostridium Difficile* infection, inflammatory bowel diseases, autoimmune diseases, metabolic diseases (for instance, diabetes), multiple sclerosis, or autism improving some of the diseases' symptoms (Vindigni SM. and Surawicz CM., 2017).

The presence and contribution of brain-gut axis dysfunction and microbiota dysbiosis in *GRIN*-related disorders has not been addressed yet. Nevertheless, there are several parental reports of gastrointestinal dysfunction (abdominal pain, constipation, flatulence…) in GRD patients. Thus, there might be a potential GI dysfunction contribution to GRD pathophysiology, and in that case, microbiota manipulation could represent a potential therapeutic option.

Hypothesis and Objectives

1. Hypothesis

This project is based on the hypothesis that *GRIN de novo* mutations can alter the functionality of NMDAR, affecting different physiological processes such as the receptor stability/oligomerization, the surface trafficking, the receptor docking to the cell membrane, the biophysical properties and functionality of the channel and consequently, neuronal function and morphology. Single or combined alterations of any of these processes will affect glutamatergic neurotransmission, leading to severe neurodevelopmental conditions.

We hypothesize that disease-associated *GRIN de novo* mutations are pathogenic and can be roughly stratified, based on their biological impact into a continuum functional outcome, ranging from gain-of-function to loss-of-function or complex outcomes. This stratification might allow the evaluation of personalized therapies, in particular by potentiating NMDARs activity in *GRIN* loss-of-function scenario.

2. Objectives

The overarching goal of this Thesis is to functionally stratify disease-associated *GRIN* variants for further evaluation of precision therapies, both in cellular and animal models. In order to achieve this main goal, the following specific objectives have been defined:

1. Recruitment of patients with *GRIN*-related disorders and multidisciplinary functional annotation studies (biochemistry, cell biology, electrophysiology) of respective *GRIN* variants.
2. Development of cell-based assays and phenotypic assessment of *Grin2b*$^{+/-}$ haploinsufficient mouse model for the study of *GRIN*-related disorders pathophysiology.
3. Assessment of potential therapeutic strategies for the rescue of *Grin2b* loss-of-function using *in vitro* and *in vivo* models.

Together, the achievement of these objectives will allow the development of experimental models to stratify *GRIN de novo* mutations and to evaluate personalized therapies in preclinical models, for further translation to the clinical practice.

Materials and Methods
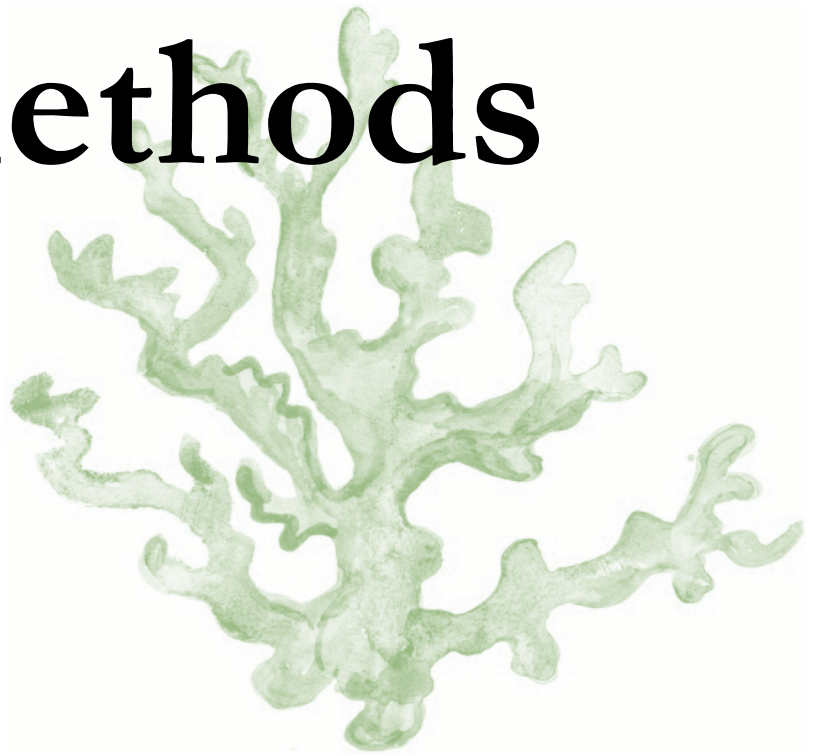
Cell lines

HEK-293T and COS-7 cell lines (see **figure 44**) were obtained from the American Type Culture Collection and maintained at 37ºC, 5% CO_2 and 90% relative humidity, in Dulbecco's modified Eagle's medium (DMEM, Gibco, Cat#41965-062), supplemented with 10% heat-inactivated fetal bovine serum (FBS$_i$) (Gibco, Cat#10270106), antibiotics (100 units/ml penicillin and 100 µg/ml streptomycin, Gibco, Cat#15140-122) for biochemistry, immunofluorescence and electrophysiological approaches.
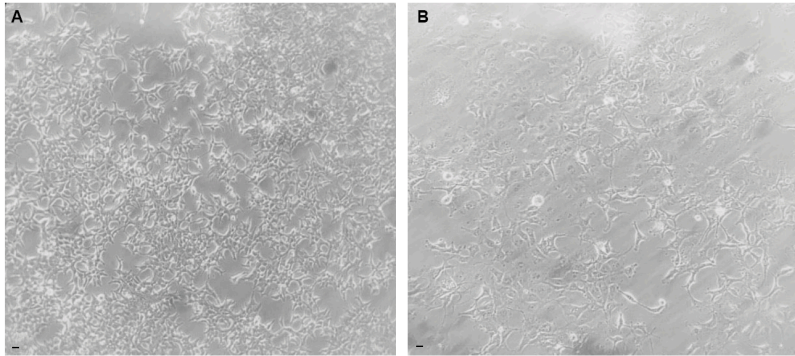
Figure 44. Representative images of HEK293T (~80 % confluency) (**panel A**) and COS-7 (~60 % confluency) (**panel B**) cell lines in DMEM supplemented with 10% fetal bovine serum and antibiotics (100 units/ml penicillin and 100 µg/ml streptomycin). Olympus CK30 10X magnification. Scale: 10 µm

Furthermore, D-2-amino-5-phosphonsopentanoic acid (D-AP5, HelloBio, Cat#HB0225) (500 µM for HEK-293T, 1 mM for COS-7) was added to the medium to avoid excitotoxicity in cells co-transfected with GluN1 and GluN2A or GluN2B (1:1 ratio).

Mice

CD1 mice

Mice with CD1 background were purchased from Charles River. The mice were housed under a 12 h dark/light cycle in controlled environmental conditions of humidity (60%) and temperature (22 °C ± 2 °C) with food and water *ad libitum.*

All the experimental procedures were carried out according to European Union guidelines (Directive 2010/63/EU) and following protocols that were approved by the Ethics Committee of the Bellvitge Biomedical Research Institute (IDIBELL).

Grin2B $^{+/-}$ mice

Wild-type and Grin2b heterozygous (Grin2b$^{+/-}$) mice with a C57BL/6 background, as characterized previously (Kutsuwada et al., 1996) were kindly provided by Dr. A.L. Carvalho (CNC, Coimbra, Portugal). We use heterozygous animals instead of knock-out (KO) mice because KO animals showed no suckling response and died shortly after birth (Kutsuwada et al., 1996). The mice were housed under a 12 h dark/light cycle in controlled environmental conditions of humidity (60%) and temperature (22 °C ± 2 °C) with food and water *ad libitum.*

Mice were genotyped by PCR (Truett et al., 2000). Genomic DNA was extracted from ear snips punch. Briefly, the biopsies were incubated with 100 µl NaOH solution (25 mM NaOH, 0.2 mM EDTA, pH 12) for 30 minutes at 95ºC. Then, the mixture was neutralized with 100 µl 40 mM Tris-HCl pH 5 solution. Genomic DNA (500 ng) was combined with 2.5 U supreme NZYTaq 2X Green Master Mix (0.2 U/µl)(NZYtech, Cat#MB05402) and different primers (0.16 µM Grin2B primer 1 (WT-specific), 0.4 µM Grin2B primer 3 (KO-specific) and 0.44 µM Grin2B primer 4 (common) (see **table 15**) following the conditions specified in **table 12**.

Cycles	Temperature (°C)	Time
1	95	4'
35	94	30"
	67	40"
	72	50'
1	72	7'
1	4	∞

Table 12. PCR conditions for Grin2b wild-type and heterozygous mice genotyping.

Both genotypes are differentiated because by running the PCR product in a 1 % agarose gel in combination with Sybr Safe Gel Stain (Invitrogen, Cat#S33102), wildtype band is 422 bp and knockout band is 793 bp, so wild type present only one and heterozygous mice present two different bands (see **figure 45**).
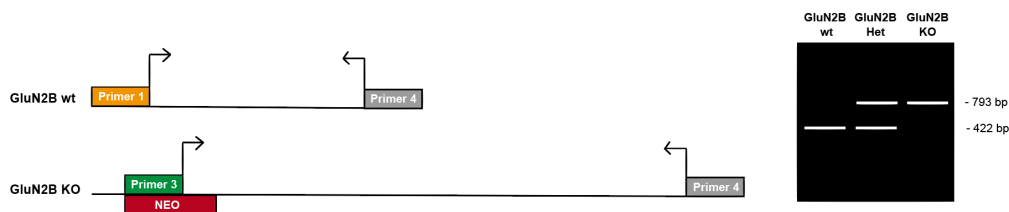
Figure 45. Primers annealing in the GluN2B genotyping PCR reaction and the expected PCR product band in the agarose gel (422 bp for wild-type, 793 bp for KO and both bands in the case of heterozygous mice).

All the experimental procedures were carried out according to European Union guidelines (Directive 2010/63/EU) and following protocols that were approved by the Ethics Committee of the Bellvitge Biomedical Research Institute (IDIBELL).

Embryonic mouse hippocampal primary neuronal cultures

CD1 pregnant female mice were sacrificed in a CO_2-chamber. To prepare dissociated hippocampal neuron cultures, embryonic day (E18) mouse embryos were obtained from pregnant females (CD1 mouse strain). Thanks to a posterior cut and anterior pressure, the brain is removed from the skull. Then, both hemispheres were separated, and meninges were carefully removed. The dissection of the hippocampus was performed with scalpel and tweezers under visual control through a binocular surgical microscope (Leica EZ4). When both hemispheres were separated, hippocampus was automatically exposed and by introducing the tweezers below the hippocampus was lifted out. Isolated hippocampi were maintained in cold Hank's Balanced Salt Solution (HBSS, Gibco, Cat#14175-129) supplemented with 0.45% glucose (Sigma-Aldrich, Cat#G8769) (HBSS-Glucose) (see **figure 46**).
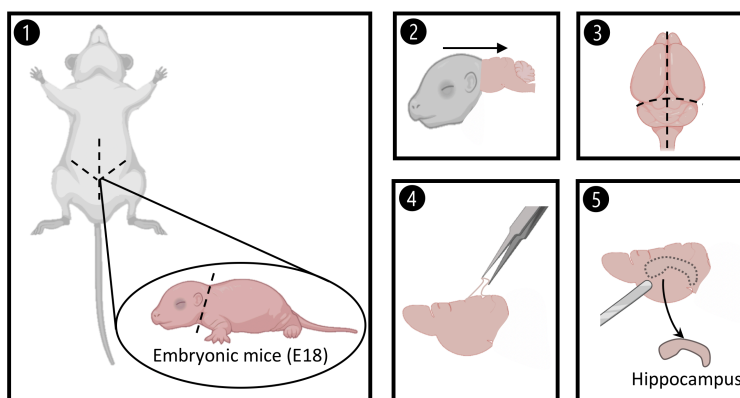
Figure 46. Hippocampus dissection from embryonic (E18) mice; **1,** Pregnant female sacrifice and embryos obtention; **2,** Brain extraction by a posterior cut and anterior pressure; **3,** Hemispheres separation; **4,** Meninges and blood vessels removal by clamping; **5,** Hippocampus dissection introducing the tweezers below the structure.

Then, tissue was digested mildly with 0.05 % trypsin (Gibco, Cat#25300-062) for 17 min at 37°C and mechanically dissociated. The cells were washed three times in HBSS, resuspended in Neurobasal medium (Gibco, Cat#21103049) supplemented with 2 mM Glutamax (Gibco, cat#35050-061) and filtered with 70 µm mesh filters (BD Falcon, Cat#352356). The cells were then plated onto glass coverslips (7.5×10^4 cells/coverslip) previously coated with 0.1 mg/ml poly-L-lysine (Sigma-Aldrich, Cat#P6282) and two hours after seeding, the plating medium was substituted by complete growth medium which is Neurobasal medium supplemented with 2% B27 (Invitrogen, Cat#17504-044) and 2 mM Glutamax (700 µl/well). Cells were incubated at 37°C in a humidified 5% CO_2 atmosphere. Every 3–4 days, half of the conditioned medium was removed and replaced by fresh growth medium (see **figure 47**).

Figure 47. Representative image of neuronal hippocampal primary culture (E18) at 7 days *in vitro* (DIV7) in neurobasal medium supplemented with 2% B27 and 2 mM Glutamax. Olympus CK30 10X. Scale: 10 µm

Plasmids and Site-directed Mutagenesis

The expression plasmids for rat GluN1, GFP-GluN2A and GFP-GluN2B were kindly provided by Dr. Vicini (Georgetown University Medical Center, Washington, USA; Vicini S. et al., 1998). The plasmids to express HA-tagged rat GluN1 and HA-tagged rat GluN2A were kindly provided by Dr. Nakanishi (Institute of Medical Science, University of Tokyo, Japan; Tezuka T. et al., 1999; Taniguchi S. et al., 2009). The plasmid to express rat GFP-GluN1 was kindly provided by Dr. Barria (Cold Spring Harbor, New York, USA; Barria A. et al, 2002). The plasmid to express Flag-tagged rat GluN2B was kindly provided by Dr. Sanz-Clemente (National Institute of Neurological Disorders and Stroke, Bethesda, USA). Myc-tagged HOMER2 plasmid was kindly provided by Dr. Smith (Molecular Otolaryngology and Renal Research Laboratories, Iowa Institute of Human Genetics; Azaiez H. et al. 2015).

Nucleotide changes of interest were introduced in the respective plasmid backbones, by oligonucleotide-directed mutagenesis, using the QuikChange site-directed mutagenesis kit (Agilent, Cat#200524) according to the manufacturer's instructions and GeneAmp PCR System 9700 (Applied Biosystems) thermocycler. 100 ng of template DNA (HA-GluN1wt, GFP-GluN2Awt or GFP-GluN2Bwt) was combined with 125 ng of forward and reverse primers containing the genetic variant of interest (designed with Agilent software, https://www.agilent.com/store/primerDesignProgram.jsp) (see **table 15**), dNTPmix (composition is Agilent's proprietary), 10X reaction buffer, a 'Quiksolution' provided by the kit (composition is Agilent's proprietary) and 2.5 U of *PfuUltra* High-Fidelity DNA polymerase (2.5 U/µl). This combination underwent a PCR protocol, described in **table 13**.

Cycles	Temperature (°C)	Time
1	95	1'
18	95	50"
	60	50"
	68	10'
1	68	7'
1	4	∞

Table 13. PCR conditions for site-directed mutagenesis.

The PCR product was digested with 10 U of DpnI restriction enzyme (10 U/µl). DpnI is a methylation-sensitive enzyme which allows template DNA degradation while preserving the PCR product. DpnI-resistant PCR product was transformed into 45 µl of XL-10 Gold Ultracompetent bacteria by heat shock (water bath at 42 ℃ for 45 seconds, followed by ice). Transformed bacteria were re-suspended in Luria Broth media (LB) (10 g/L NaCl, 10 g/L tryptone and 5 g/L yeast extract) and plated in LB agar plates (15 g agar per 1 L LB media) supplemented with antibiotic: 1 µg/ml ampicillin (Sigma-Aldrich, Cat#A9518, 50 mg/ml) for GluN1, GluN2A and GluN2B plasmids and 1 µg/ml kanamycin (Roche Diagnostics, Cat#1278700, 50 mg/ml) for HOMER2 plasmid. Agar plates were incubated O/N at 37 ℃. 24 hours later, 1-2 colonies were picked, and grown in LB media supplemented with antibiotic (1 µg/ml ampicillin for GluN1, GluN2A and GluN2B plasmids; 1 µg/ml kanamycin for HOMER2 plasmid) O/N at 220 rpm and 37 ℃. Finally, amplified DNA was extracted by NucleoSpin Plasmid (NoLid) Mini kit for plasmid DNA purification (Macherey-Nagel, Cat#740499.50) according to the manufacturer's instructions (see **figure 48**).
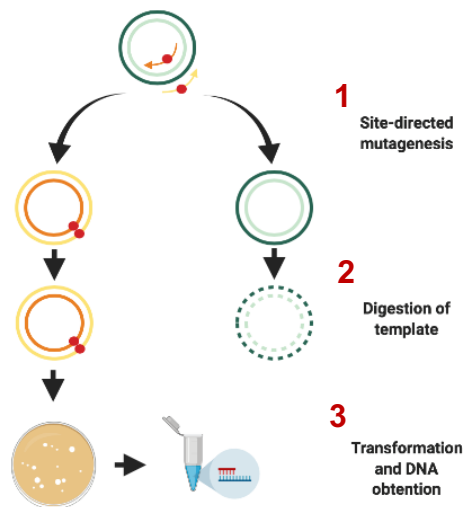
Figure 48. Site-directed mutagenesis protocol: **1,** Site-directed mutagenesis to introduce genetic variants of interest in the corresponding backbone plasmid (HA-Grin1, GFP-Grin2a, GFP-Grin2b) via designed forward and reverse primers containing the mutation; **2,** DpnI-mediated digestion of template DNA; **3,** DpnI-resistant PCR product transformation in XL-10 Gold Ultracompetent bacteria and DNA purification.

Purified DNA from site-directed mutagenesis was verified by DNA sequencing using a combination of 265 ng DNA, 3.2 µM sequencing primers (see **table 15**), BigDye (Life Technologies, Cat#4458687), BigDye Terminator v.1.1 v3.1 5X sequencing buffer (Life Technologies, Cat#1802293)and 5 % DMSO (Sigma-Aldrich, Cat#D2650) (according to UPF-CRG's instructions) and following the conditions specified in **table 14**.

Cycles	Temperature (°C)	Time
1	94	3'
40	96	15"
	Tm primers – 5 °C	15"
	60	4'
1	4	∞

Table 14. PCR conditions for DNA sequencing.

Results were analysed using Basic Local Alignment Search Tool (BLAST) from National Center of Biotechnology Information (NCBI) (https://blast.ncbi.nlm.nih.gov/Blast.cgi) to make a local alignment of the purified DNA and the template DNA to check the introduction of the modification of interest without provoking additional modifications, 4peaks 1.7.2 (http://nucleobytes.com/index.php/4peaks) to visualize chromatograms from DNA sequencing, EnzymeX 3.3.3 (https://nucleobytes.com/enzymex/index.html) to visualize DNA sequences, and ExPASy from SIB Bioinformatics Resource Portal (https://www.expasy.org) to translate the DNA sequences into protein sequences for checking the aminoacid change.

Oligonucleotide Primers

The oligonucleotide primers (Biomers, https://www.biomers.net) used in this work are describe in **table 15**.

Name	Sequence (5' → 3')
Sequencing oligonucleotide primers	
GluN1 rat seq1 for	CCACATCATCCTGCTGGTCA
GluN2A rat seq1 for	GAGAGAGGCTGCGAGCCCTGCT
GluN2A rat seq2 for	GAGGCTGTGGCCCAGATGCTGGA
GluN2A rat seq3 for	AGCCTGGAGGCAAGAGTGAGAGA
GluN2A rat seq4 for	GTCCAGAACTGTGAAGTTCACCT
GluN2A rat seq5 for	CCAACCTGGCTGCCTTCATGATCCA
GluN2A rat seq5.1 for	CTTGAACTACAAGGCCGGGA
GluN2A rat seq6 for	CAGCCATGGCCCTCAGCCTC
GluN2A rat seq7 for	AACTCCCGACCCCGGCAGCT
GluN2A rat seq8 for	ACACAGTGAGGGCAGTGATCGA
GluN2A rat seq9 for	GGTCTGGAGGACAGCAAGAGGA
GluN2B rat seq1 for	GCATCGGCATCGCTGTCATCCT
GluN2B rat seq2 for	TAACTCAGTTGGGCTGACTGGCT
GluN2B rat seq2.1 for	AGGGTGGGGAAATGGAAGGA
GluN2B rat seq3 for	AAATGCTGCAAGGGGTTCTG
GluN2B rat seq3.1 for	TGTGGGCCTTCTTTGCTGTC
GluN2B rat seq4 for	TGACAAGAAGTTCCAGAGACCT
GluN2B rat seq5 for	TGAACTCCCCCACTGCCACCA
GluN2B rat seq6 for	CAGCAGTATAAGGACAGTCT
GluN2B rat seq7 for	ACGACACCTTCGTGGACCTGCA
HOMER2 human seq1 for	GCTGAAGATTGCCTTGACGC
Genotyping oligonucleotide primers	
Grin2B primer 1	ATGAAGCCCAGCGCAGAGTG
Grin2B primer 3	GGCTACCTGCCCATTCGACCACCAAGCGAAAC
Grin2B primer 4	AGGACTCATCCTTATCTGCCATTATCATAG
Site-directed mutagenesis oligonucleotide primers	
GluN1 R217W for	GGGAACTGGAGGCCTGGGTCATCATCCTT
GluN1 R217W rev	AAGGATGATGACCCAGGCCTCCAGTTCCC
GluN1 D227H for	GCAAGCGAGGACCACGCTGCCACAG
GluN1 D227H rev	CTGTGGCAGCGTGGTCCTCGCTTGC
GluN1 W247* for	TCTGGGTACGTGTAGCTGGTCGGGGAA
GluN1 W247* rev	TTCCCCGACCAGCTACACGTACCCAGA
GluN1 P305Rfs*21 for	AATATCACTGACCCACGCGGGGTTGCG
GluN1 P305Rfs*21 rev	CGCAACCCCGCGTGGGTCAGTGATATT
GluN1 R306Q for	CTGACCCACCGCAGGGTTGCGTGGG
GluN1 R306Q rev	CCCACGCAACCCTGCGGTGGGTCAG
GluN1 R548W for	CAAGAAGGAGATTCCCTGGAGCACACTGGACTC
GluN1 R548W rev	GAGTCCAGTGTGCTCCAGGGAATCTCCTTCTTG
GluN1 Q556* for	ACACTGGACTCATTTATGTAGCCTTTTCAGAGCACAC
GluN1 Q556* rev	GTGTGCTCTGAAAAGGCTACATAAATGAGTCCAGTGT
GluN1 E597L for	GAACAGTGAGGAGGAGCTGGAAGATGCACTGAC
GluN1 E597L rev	GTCAGTGCATCTTCCAGCTCCTCCTCACTGTTC
GluN1 S617C for	GGGCGTCCTGCTCAACTGCGGCATCGG
GluN1 S617C rev	CCGATGCCGCAGTTGAGCAGGACGCCC

GluN1 I619G620dup for (Liu H. et al., 2018)	CTCAACTCCGGCATTGGCATTGGGGAAGTTGCCCCCCGGAGT
GluN1 I619G620dup rev (Liu H. et al., 2018)	CCAATGGCTAACGGTCCCAACTCGTCCTGCGGGGTCCTTTT
GluN1 G620R for	CCTGCTCAACTCCGGCATTAGGGAAGGTGC
GluN1 G620R rev	GCACCTTCCCTAATGCCGGAGTTGAGCAGG
GluN1 M641V for	GTGGGCTGGTTTCGCCGTGATCATAGTGGCTTC
GluN1 M641V rev	GAAGCCACTATGATCACGGCGAAACCAGCCCAC
GluN1 V656M for	CTTGGCAGCTTTCCTGATGCTGGATCGGCCTG
GluN1 V656M rev	CAGGCCGATCCAGCATCAGGAAAGCTGCCAAG
GluN1 D732E for	CACGCCTTTATCTGGGAGTCGGCCGTG
GluN1 D732E rev	CACGGCCGACTCCCAGATAAAGGCGTG
GluN1 P805L for	CCCGCAGCAATGCTCTTGCAACCCTCACTTT
GluN1 P805L rev	AAAGTGAGGGTTGCAAGAGCATTGCTGCGGG
GluN1 P805S for	CGACTCCCGCAGCAATGCTAGTGCAACCCTC
GluN1 P805S rev	GAGGGTTGCACTAGCATTGCTGCGGGAGTCG
GluN1 M813T for	CAACCCTCACTTTTGAGAACACGGCAGGGGTCT
GluN1 M813T rev	AGACCCCTGCCGTGTTCTCAAAAGTGAGGGTTG
GluN1 A814D for	CTTTTGAGAACATGGACGGGGTCTTCATGCTGG
GluN1 A814D rev	CCAGCATGAAGACCCCGTCCATGTTCTCAAAAG
GluN1 G815V for	TTTTGAGAACATGGCAGTGGTCTTCATGCTGGTGG
GluN1 G815V rev	CCACCAGCATGAAGACCACTGCCATGTTCTCAAAA
GluN1 M818V for	GGCAGGGGTCTTCGTGCTGGTGGCTGG
GluN1 M818V rev	CCAGCCACCAGCACGAAGACCCCTGCC
GluN1 G827R for	GGCTGGAGGCATCGTAGCTAGGATTTTCCTCAT
GluN1 G827R rev	ATGAGGAAAATCCTAGCTACGATGCCTCCAGCC
GluN1 E834Q for	AGCTGGGATTTTCCTCATTTTCATTCAGATCGCCTACAA
GluN1 E834Q rev	TTGTAGGCGATCTGAATGAAAATGAGGAAAATCCCAGCT
GluN1 R844P for	GACACAAGGATGCCCCTAGGAAGCAGATGCA
GluN1 R844P rev	TGCATCTGCTTCCTAGGGGCATCCTTGTGTC
GluN2A E58* for	AATCTGTGGGGCCCATAGCAGGCAACCG
GluN2A E58* rev	CGGTTGCCTGCTATGGGCCCCACAGATT
GluN2A E182Nfs*23 for	CTTCCCTGGCTACCGAAATTCATCAGCTTTATC
GluN2A E182Nfs*23 rev	GATAAAGCTGATGAATTTCGGTAGCCAGGGAAG
GluN2A V452Cfs*11 for	CAACGAAGGGATGAATTGTGAAGAAATGCTGC
GluN2A V452Cfs*11 rev	GCAGCATTTCTTCACAATTCATCCCTTCGTTG
GluN2A G458R for	TGAAGAAATGCTGCAAGAGGTTCTGCATCGACATC
GluN2A G458R rev	GATGTCGATGCAGAACCTCTTGCAGCATTTCTTCA
GluN2A G483D for	CCTCTACCTGGTGACCAATGATAAGCATGGGAAAAAGGTTAA
GluN2A G483D rev	TTAACCTTTTTCCCATGCTTATCATTGGTCACCAGGTAGAGG
GluN2A N490H for	GGAAGCATGGGAAAAAGGTTCACAATGTGTGGAATGG
GluN2A N490H rev	CCATTCCACACATTGTGAACCTTTTTCCCATGCTTCC
GluN2A T531A for	TGCCCTTCGTGGAGGCAGGAATCAGCGTC
GluN2A T531A rev	GACGCTGATTCCTGCCTCCACGAAGGGCA
GluN2A G542R for	ATGGTCTCCAGGAGTAATCGCACTGTCTCCC
GluN2A G542R rev	GGGAGACAGTGCGATTACTCCTGGAGACCAT
GluN2A V563L for	CCTCCGTCTGGGTGATGATGTTTTTGATGCTGCTCA
GluN2A V563L rev	TGAGCAGCATCAAAAACATCATCACCCAGACGGAGG
GluN2A H595Rfs*28 for	GGGAAAGCTCCCCGGGCCTTCTTTTAC
GluN2A H595Rfs*28 rev	GTAAAAGAAGGCCCGGGGAGCTTTCCC
GluN2A H595Lfs*60 for	CAAAGGGAAAGCTCCCCTTACGGGCCTTCTTTTAC
GluN2A H595Lfs*60 rev	GTAAAAGAAGGCCCGTAAGGGGAGCTTTCCCTTTG
GluN2A V639I for	TGTGGGCCTTCTTTGCTATCATCTTCCTGGCC
GluN2A V639I rev	GGCCAGGAAGATGATAGCAAAGAAGGCCCACA
GluN2A T646A for	CCTGGCCAGTTACGCAGCCAACCTGGC
GluN2A T646A rev	GCCAGGTTGGCTGCGTAACTGGCCAGG
GluN2A G664S for	GAGTTTGTGGACCAAGTGACTAGCCTCAGTGAC
GluN2A G664S rev	GTCACTGAGGCTAGTCACTTGGTCCACAAACTC
GluN2A G688S for	CGATTTGGGACGGTACCCAATAGCAGTACAGAGAGGAATA
GluN2A G688S rev	TATTCCTCTCTGTACTGCTATTGGGTACCGTCCCAAATCG
GluN2A R692G for	TACCCAATGGAAGTACAGAGGGGAATATTCGTAACAACTAC
GluN2A R692G rev	GTAGTTGTTACGAATATTCCCCTCTGTACTTCCATTGGGTA
GluN2A G819A for	ATCGATAACATGGCGGCCGTGTTCTACATGCTG
GluN2A G819A rev	CAGCATGTAGAACACGGCCGCCATGTTATCGAT
GluN2A G819E for	CATCGATAACATGGCGGAGGTGTTCTACATGCTGGC
GluN2A G819E rev	GCCAGCATGTAGAACACCTCCGCCATGTTATCGATG

GluN2A V820I for	CGATAACATGGCGGGCATATTCTACATGCTGGCTGC
GluN2A V820I rev	GCAGCCAGCATGTAGAATATGCCCGCCATGTTATCG
GluN2A M823V for	GGGCGTGTTCTACGTGCTGGCTGCAGC
GluN2A M823V rev	GCTGCAGCCAGCACGTAGAACACGCCC
GluN2A T888R for	AAAGAAGAAATCTCCAGATTTCAATCTGAGGGGATCACAGAGCAAC
GluN2A T888R rev	GTTGCTCTGTGATCCCCTCAGATTGAAATCTGGAGATTTCTTCTTT
GluN2A T1150A for	GTGGGCTTCCCAGATGCCTACCAAGATCAC
GluN2A T1150A rev	GTGATCTTGGTAGGCATCTGGGAAGCCCAC
GluN2A W1271* for	GTCTACCAGCAGGACTAGTCACAGAACAACGCC
GluN2A W1271* rev	GGCGTTGTTCTGTGACTAGTCCTGCTGGTAGAC
GluN2A E1301* for	TAACATTCTGGACAAACCCAGATAGATAGACCTTAGCAG
GluN2A E1301* rev	CTGCTAAGGTCTATCTATCTGGGTTTGTCCAGAATGTTA
GluN2A E1321Q for	AGGGAACGGCTACTGCAGGGCAACTTGTATG
GluN2A E1321Q rev	CATACAAGTTGCCCTGCAGTAGCCGTTCCCT
GluN2A C1448F for	CCCAGGGGTTTTAAATTCCTTCAGCAATAGACGAGTGTAC
GluN2A C1448F rev	GTACACTCGTCTATTGCTGAAGGAATTTAAAACCCTGGG
GluN2B S34Qfs*25 for	CGATGCCGATGCTGGGGGGGGGCTCTTT
GluN2B S34Qfs*25 rev	AAAGAGCCCCCCCCAGCATCGGCATCG
GluN2B L229Yfs*2 for	CCAAAGCCCCATCATTTACCTTTAATGCACGAAGG
GluN2B L229Yfs*2 rev	CCTTCGTGCATTAAAGGTAAATGATGGGGCTTTGG
GluN2B Q331Sfs*5 for	GTAAAAGAAGGCCCGTAAGGGGAGCTTTCCCTTTG
GluN2B Q331Sfs*5 rev	CAACATGTTAGACTGTAGATCCTCTTCTC
GluN2B C457Y for	GAACCAGGCTACATCAAAAAATGCTATAAGGGGTTCTGTATTGACATC
GluN2B C457Y rev	GATGTCAATACAGAACCCCTTATAGCATTTTTTGATGTAGCCTGGTTC
GluN2B G459R for	CATCAAAAAATGCTGCAAGAGGTTCTGTATTGACATCC
GluN2B G459R rev	GGATGTCAATACAGAACCTCTTGCAGCATTTTTTGATG
GluN2B G484D for	CCTGGTGACCAATGACAAGCACGGGAAG
GluN2B G484D rev	CTTCCCGTGCTTGTCATTGGTCACCAGG
GluN2B T514A for	TGGCAGTGGGATCACTAGCTATCAATGAAGAACGG
GluN2B T514A rev	CCGTTCTTCATTGATAGCTAGTGATCCCACTGCCA
GluN2B R519Q for	CTAACTATCAATGAAGAACAGTCAGAGGTGGTTGACTTC
GluN2B R519Q rev	GAAGTCAACCACCTCTGACTGTTCTTCATTGATAGTTAG
GluN2B R519* for	CTAACTATCAATGAAGAATGATCAGAGGTGGTTGAC
GluN2B R519* rev	GTCAACCACCTCTGATCATTCTTCATTGATAGTTAG
GluN2B T532A for	GTACCCTTCATAGAAGCTGGCATCAGTGTC
GluN2B T532A rev	GACACTGATGCCAGCTTCTATGAAGGGTAC
GluN2B G543R for	CATGGTATCTCGCAGCAATAGGACTGTGTCACCTT
GluN2B G543R rev	AAGGTGACACAGTCCTATTGCTGCGAGATACCATG
GluN2B A549V for	GACTGTGTCACCTTCTGTCTTCTTAGAGCCATTCA
GluN2B A549V rev	TGAATGGCTCTAAGAAGACAGAAGGTGACACAGTC
GluN2B S555N for	CTGCCTTCTTAGAGCCATTCAACGCTGACGTGT
GluN2B S555N rev	ACACGTCAGCGTTGAATGGCTCTAAGAAGGCAG
GluN2B A556D557dup for (Liu H. et al., 2018)	GAGCCATTCAGTGCTGACGCTGACGTGTGGGTGATGATGTTT
GluN2B A556D557dup rev (Liu H. et al., 2018)	GTCAGCGTCAGCACTGAATGGCTCTAAGAAGGCAGAAGGTGA
GluN2B W559R for	CATTCAGCGCTGACGTGAGGGTGATGATGTTTGTG
GluN2B W559R rev	CACAAACATCATCACCCTCACGTCAGCGCTGAATG
GluN2B N616K for	CTGGGGTCTGGTGTTTAACAAGTCCGTACCTGT
GluN2B N616K rev	ACAGGTACGGACTTGTTAAACACCAGACCCCAG
GluN2B S628C for	CAAAGGGGACCACCTGCAAGATCATGGTGTCA
GluN2B S628C rev	TGACACCATGATCTTGCAGGTGGTCCCCTTTG
GluN2B L650-F653del for	CCAGCTACACTGCCAACATGATCCAAGAGGAGTA
GluN2B L650-F653del rev	TACTCCTCTTGGATCATGTTGGCAGTGTAGCTGG
GluN2B K670Vfs*5 for	GCCTGAGTGACAAGAAAGTTCCAGAGACCTAATG
GluN2B K670Vfs*5 rev	CATTAGGTCTCTGGAACTTTCTTGTCACTCAGGC
GluN2B G689S for	TTTGGGACTGTGCCCAATAGCAGCACAGAGAG
GluN2B G689S rev	CTCTCTGTGCTGCTATTGGGCACAGTCCCAAA
GluN2B R693G for	CAATGGCAGCACAGAGGGGAATATCCGTAATAAC
GluN2B R693G rev	GTTATTACGGATATTCCCCTCTGTGCTGCCATTG
GluN2B R696H for	CAGCACAGAGAGGAATATCCATAATAACTATGCAGAAATGC
GluN2B R696H rev	GCATTTCTGCATAGTTATTATGGATATTCCTCTCTGTGCTG
GluN2B A733E for	GATGCATTCATCTATGATGAAGCTGTGCTCAACTACATG

GluN2B A733E rev	CATGTAGTTGAGCACAGCTTCATCATAGATGAATGCATC
GluN2B C746Y for	GCCAATGGTCACCAGTTTATAGCCTTCGTCCCTTCCAG
GluN2B C746Y rev	CTGGAAGGGACGAAGGCTATAAACTGGTGACCATTGGC
GluN2B I751T for	CAAACTGGTGACCACTGGCAGTGGCAAG
GluN2B I751T rev	CTTGCCACTGCCAGTGGTCACCAGTTTG
GluN2B D786Mfs*23 for	GCAGCTGTTTGGGATGGGGAGATGG
GluN2B D786Mfs*23 rev	CCATCTCCCCATCCCAAACAGCTGC
GluN2B M818L for	CTGGACATCGACAATTTGGCAGGTGTCTTC
GluN2B M818L rev	GAAGACACCTGCCAAATTGTCGATGTCCAG
GluN2B G820A for	CATCGACAATATGGCAGCTGTCTTCTATATGTTG
GluN2B G820A rev	CAACATATAGAAGACAGCTGCCATATTGTCGATG
GluN2B G820E for	CATCGACAATATGGCAGAAGTCTTCTATATGTTGGGG
GluN2B G820E rev	CCCCAACATATAGAAGACTTCTGCCATATTGTCGATG
GluN2B G820V for	GACATCGACAATATGGCAGTTGTCTTCTATATGTTGGGG
GluN2B G820V rev	CCCCAACATATAGAAGACAACTGCCATATTGTCGATGTC
GluN2B V821F for	CGACAATATGGCAGGTTTCTTCTATATGTTGGG
GluN2B V821F rev	CCCAACATATAGAAGAAACCTGCCATATTGTCG
GluN2B M824V for	ACAATATGGCAGGTGTCTTCTATGTGTTGGGGGGCAG
GluN2B M824V rev	CTGCCCCCAACACATAGAAGACACCTGCCATATTGT
GluN2B G826W for	GTGTCTTCTATATGTTGTGGGCAGCCATGGCCCTC
GluN2B G826W rev	GAGGGCCATGGCTGCCCACAACATATAGAAGACAC
GluN2B E839* for	CATCACCTTCATCTGTTAGCATCTGTTCTATTGG
GluN2B E839* rev	CCAATAGAACAGATGCTAACAGATGAAGGTGATG
GluN2B R847* for	GACACCCATGAAGCAATGCTAGAACTGCCAATAGAACAGA
GluN2B R847* rev	TCTGTTCTATTGGCAGTTCTAGCATTGCTTCATGGGTGTC
GluN2B S993C for	CACCGGCCACACTGCATCGGCAGCA
GluN2B S993C rev	TGCTGCCGATGCAGTGTGGCCGGTG
GluN2B G1026R for	CCCTGGACATCCGCCTGCCCTCC
GluN2B G1026R rev	GGAGGGCAGGCGGATGTCCAGGG
GluN2B I1056Mfs*7 for	GACGACTTGATGTCGATCGGATGTCTCTGAC
GluN2B I1056Mfs*7 rev	GTCAGAGACATCCGATCGACATCAAGTCGTC
GluN2B R1081H for	AGGGCAACGCAGCCAAGAGGCATAAACAGCAGTATAAGGACAG
GluN2B R1081H rev	CTGTCCTTATACTGCTGTTTATGCCTCTTGGCTGCGTTGCCCT
GluN2B K1090R for	AGCAGTATAAGGACAGTCTAAGGAAGCGGCCAGC
GluN2B K1090R rev	GCTGGCCGCTTCCTTAGACTGTCCTTATACTGCT
GluN2B K1293del for	CCAAGGCTCAGAAGAATCGGAACAAACTG
GluN2B K1293del rev	CAGTTTGTTCCGATTCTTCTGAGCCTTGG
GluN2B T1390Ffs*4 for	CCTTTCATCCCCTTTTGGGGATGAC
GluN2B T1390Ffs*4 rev	GTCATCCCCAAAAGGGGATGAAAGG
GluN2B Q1408L for	CTGCCACCGTGGGCAGCCTGAAGAAGTAG
GluN2B Q1408L rev	CTACTTCTTCAGGCTGCCCACGGTGGCAG
HOMER2 E221K for	GAGCCGGTCATTCTTATCACGGCAGATGGAGAA
HOMER2 E221K rev	TTCTCCATCTGCCGTGATAAGAATGACCGGCTC

Table 15. Oligonucleotide primers used in this work.

Antibodies

The antibodies used in this work are described in **table 16.**

Primary antibodies					
Antibodies	Dilution	Provider	N. Catalog	Host	Use
Anti-beta actin	1:10000	Cell Signalling	4970T	Rabbit	WB/IF
Anti-GFP	1:1000	Clontech	632381	Mouse	WB
Anti-GFP	1:500	Life technologies	A11122	Rabbit	IF
Anti-GFP conjugated Ab	1:500	Life technologies	A31851	-	WB
Anti-GluA1	1:2000	NeuroMab	75-327	Mouse	WB
Anti-GluN1	1:500	Millipore	AB9864R	Rabbit	WB
Anti-GluN2A	1:500	Frontier Institute	AB2571605	Rabbit	WB
Anti-GluN2B	1:500	Frontier Institute	AB2571762	Rabbit	WB
Anti-HA	1:1000	Covance	MMS-101R	Mouse	WB/IF
Anti-HOMER2	1:500/1:200	BioNova	BS-4632R	Rabbit	WB/IF
Anti-PSD95	1:10000	NeuroMab	75-028	Mouse	WB
Anti-Synaptophysin	1:5000	Sigma-Aldrich	S5768	Mouse	WB
Anti-VGLUT	1:5000	Millipore	AB5905	Guinea Pig	WB

Secondary antibodies				
Antibodies	Dilution	Provider	N. Catalog	Use
Anti-Guinea Pig IgG-HRP	1:2000	Pierce Bio	AB2535546	WB
Anti-Mouse IgG-HRP	1:2000	Dako	P0447	WB
Anti-Rabbit IgG-HRP	1:2000	Dako	P0448	WB
Alexa 488 Anti-Rabbit	1:1000	Life technologies	A11034	IF
Alexa 555 Anti-Mouse	1:1000	Life technologies	A21424	IF
Alexa 555 Anti-Rabbit	1:1000	Life technologies	A21429	IF
Alexa 647 Anti-Rabbit	1:1000	Life technologies	A21245	IF

Table 16. Primary and secondary antibodies used in this work.

Transfection of GluN subunits

HEK293T cells were used for electrophysiological recordings for protein stability determination whereas COS-7 cells and hippocampal primary cultures were used for immunofluorescence analysis.

For the protein stability determination, HEK293T cells were plated in 6-well plates and transfected at 70-80 % confluency with equimolar quantities of Grin1 and Grin2A/Grin2B plasmids (1 µg of each plasmid) by the calcium phosphate method (CalPhos™ Mammalian Transfection Kit, Clontech, Cat#631312) following manufacturer's instructions. Before transfection, DMEM media was supplemented with 0.5 mM D-AP5 (D(−)-2-Amino-5-phosphonopentanoic acid, NMDA receptor antagonist) to avoid excitotoxicity. DNA plasmids were combined with calcium solution and phosphate buffer and the mix was incubated for 15 minutes to form complexes. Then, the mixture was added drop by drop and cells were placed in the incubator at 37ºC for 16 hours. After this time, cells were washed with PBS 1X (Gibco, Cat#14190-169) and the media was replaced with fresh media supplemented with D-AP5 0.5 mM. Cells were incubated O/N at 37ºC and analyzed 48 h after transfection.

For electrophysiological recordings, HEK293T cells were plated in 4-well plates and transfected at 70-80 % confluency with a 1:2 ratio of Grin1 and Grin2 subunits (0.4 µg Grin1 and 0.8 µg Grin2) in combination with 0.2 µg GFP plasmid, using polyethylenimine (PEI) (Polysciences, Cat#23966-2, 1 mg/ml) (ratio 1:3, 1,4 µg DNA: 4,2 µg PEI). Before transfection, cells media was replaced by DMEM without antibiotics and serum to avoid toxic antibiotic uptake. Plasmids and PEI were mixed and incubated for 20 minutes at RT to allow the formation of the complexes. After that, the mixture was added drop by drop and cells were placed in the incubator at 37ºC. Three hours later, the medium was replaced with fresh DMEM medium supplemented with antibiotics and serum, 1 mM D-AP5 and 0.1 mM 7-CK (7-chlorokynurenic acid) (Tocris, Cat#0237) to avoid excitotoxicity. Finally, cells were treated with 50 U accutase (Sigma-Aldrich, Cat#A6964, 400-600 units/ml) for one minute, plated onto previously poly-D-lysinated (Sigma-Aldrich, Cat#A-003-E, 1 mg/ml)) coverslips (dilution 1:10 or 1:20), and placed in the incubator at 37ºC and recorded 24 h after transfection.

For immunofluorescence, COS-7 cells were plated in 4-well plates with poly-L-lysinated (Sigma-Aldrich, Cat#P6282) coverslips. Cells were transiently transfected at 70-80 % confluency using Lipofectamine 2000 reagent (Life Technologies, Cat#11668019), according to the manufacturer's recommendations. Lipofectamine allows the formation of liposomes containing the DNA of interest and these liposomes might be transported through the cell membrane. Before transfection, cells media was replaced by DMEM without antibiotics and serum to avoid toxic antibiotic uptake by the liposomes. Plasmids and Lipofectamine 2000 reagent were mixed and incubated for 20 minutes at RT to allow the formation of complexes. Then, the mixture was added drop by drop and cells were placed in the incubator at 37°C for four hours. Subsequently, medium was replaced with fresh DMEM supplemented with antibiotics, serum, 1 mM D-AP5 and 20 mM $MgCl_2$ (VWR, Cat#1058330250) to avoid excitotoxicity. Finally, cells were placed in the incubator at 37°C and fixed 24 h after transfection. COS-7 cells were used to study the biallelic and monoallelic expression of the variants of interest. To analyse biallelic expression, cells were transfected with equimolar quantities of HA-Grin1 and GFP-Grin2A/Grin2B subunits (0.4 µg of each plasmid). However, to evaluate their monoallelic expression in combination with a wild type subunit we combined different tagged subunits (see **table 17**).

	Approach	
GRIN gene	**Detection of the total density of NMDARs**	**Detection of the wild-type or mutated subunit**
GRIN1	HA-GluN1 wt (0.2 µg) + HA-GluN1 mut (0.2 µg) + GFP-GluN2B wt (0.4 µg)	GFP-GluN1 wt (0.2 µg) + HA-GluN1 mut (0.2 µg) + Flag-GluN2B wt (0.4 µg)
GRIN2A	HA-GluN1 wt (0.4 µg) + GFP-GluN2A wt (0.2 µg) + GFP-GluN2A mut (0.2 µg)	Untag-GluN1 wt (0.4 µg) + HA-GluN2A wt (0.2 µg) + GFP-GluN2A mut (0.2 µg)
GRIN2B	HA-GluN1 wt (0.4 µg) + GFP-GluN2B wt (0.2 µg) + GFP-GluN2B mut (0.2 µg)	HA-GluN1 wt (0.4 µg) + Flag-GluN2B wt (0.2 µg) + GFP-GluN2B mut (0.2 µg)

Table 17. Summary of the different conditions of transfection in COS-7 cells based on the affected subunit and the used approach, in monoallelic conditions.

Primary cultures were transfected with Lipofectamine 2000 on day 11 *in vitro* (div11), according to the manufacturer's, instructions. Primary cultures were transfected with 0.6 µg Grin2A/Grin2B and 0.2 µg GFP (ratio 3:1) for dendritic spines analysis and with equimolar quantities of Grin1 and Grin2A/Grin2B (0.4 µg of each plasmid) for surface trafficking analysis. Before transfection, half of conditioned media was collected, mixed with same amount of fresh complete growth medium (to a total volume of 700 µl) and kept at 37°C. Neurons were incubated with DNA-Lipofectamine 2000 complexes for four hours. Then, medium was removed. After a quick wash, the previously collected conditioned medium was supplemented with 100 µM D-AP5 and added to transfected neurons. 72 hours after transfection, neurons underwent chemical-LTP if needed and were fixed for further immunofluorescence analysis.

All the experimental procedures were carried out according to European Union guidelines (Directive 2010/63/EU) and following protocols that were approved by the Ethics Committee of the Bellvitge Biomedical Research Institute (IDIBELL).

Protein extraction from transiently transfected HEK293T cells

For protein extraction, cells were scraped off the plate in 400 µl of PBS 1X, pelleted at 600×g, and then re-suspended in 300 µl of lysis buffer (50 mM HEPES [pH 7.4], 1% SDS (BioRad, Cat#1610301) and 1X Halt TM Proteases and Phosphatase Inhibitor cocktail (Cultek, Cat#78440)). After 15 min incubation at 4 degrees, the cell debris was pelleted at 15,000×*g*, the solubilized proteins were collected and sonicated. Protein concentration was determined using the bicinchoninic acid (BCA) assay (Pierce™ BCA Protein Assay Kit, Thermo Scientific, Cat#4823228) following the manufacturer's instructions. Based on samples of known BSA standards (0.15, 0.25, 0.5, 0.75, 1, 1.5 and 2 mg/ml), we determined the concentration of unknown protein samples in a 96-well plate, considering the solvent background. Protein concentration was determined by measurement of the absorbance at 495 nm using a Victor X5 plate reader (Perkin Elmer). Protein extracts from transiently transfected HEK293T cells (in SDS 1% buffer, 4 ug) were prepared in 1X sample buffer with 5 % β-mercaptoethanol and denatured (15 minutes at 37 °C) to perform western blot analysis.

Western blot

Proteins were separated by electrophoresis using a 8% SDS-PAGE resolving gel (Tris-HCl 0.4 M pH 8.8, Acrylamide 8 %, SDS 0.1 %, APS 0.1 %, TEMED 0.1 %) and 4 % stacking gel (Tris-HCl 0.125 M pH 6.8, Acrylamide 4 %, SDS 0.1 %, APS 0.1 %, TEMED 0.1 %) at 40 mA per gel for nearly an hour. After gels equilibration in ethanol 20 % (10 min), protein cues were transferred to nitrocellulose membranes (Amersham, Life Technologies, Cat#IB301031) using a semi-dry blotting system (iBlot, Life technologies). After transient staining of transferred proteins by Ponceau S staining, the membranes were blocked with 10% skimmed milk in 10 mM Tris-HCl (pH 7.5)/100 mM NaCl (TBS) plus 0.1% Tween 20 (TBS-T). The membranes were incubated overnight at 4°C with the primary antibody (Ab) of interest (diluted in TBS-T + 5% skimmed milk) (see **table 16**). After washing the membranes, incubation for 1 h at room temperature (RT) with a secondary antibody coupled to horseradish peroxidase (see **table 16**) was performed. The immunocomplexes were visualized by chemiluminescence (Amersham, ECL detection system, GE Healthcare, Cat#12316992), following the manufacturer's instructions. The immunoreactive bands were visualized using ChemiDoc MP device (BioRad) and the immunoreactive signals were analyzed with Image Lab Biorad software.

Immunofluorescence analysis

Transiently transfected COS-7 cells were briefly washed with PBS before they were fixed with 4% paraformaldehyde (PFA) (10 minutes, under agitation, RT). Then, fixated cells were washed with PBS.

<u>Cell lines</u>

Non-permeabilized COS-7 cells were blocked with FBS$_i$ 10 % for one hour at RT. Then, cells were incubated for one hour with an antibody against GFP (see **table 16**) recognizing the GFP extracellular epitope of expressed receptors containing GluN2 subunits (GFP-GluN2A or GFP-GluN2B) (diluted in FBS$_i$ 1 %, under agitation, RT). After washing with PBS, cells were incubated with Alexa 555-conjugated goat anti-rabbit Ab (see **table 16**) (diluted in FBS$_i$ 1 %, under agitation, RT). The total pool of receptors was detected by the fluorescent signal emitted by the GFP-GluN2A/GluN2B plasmid.

A similar approach was used to evaluate monoallelic conditions (co-expression of wild-type and mutant plasmids in heterozygosity) but using different antibodies depending on the transfected plasmids (See **table 16** and **figure 49**).
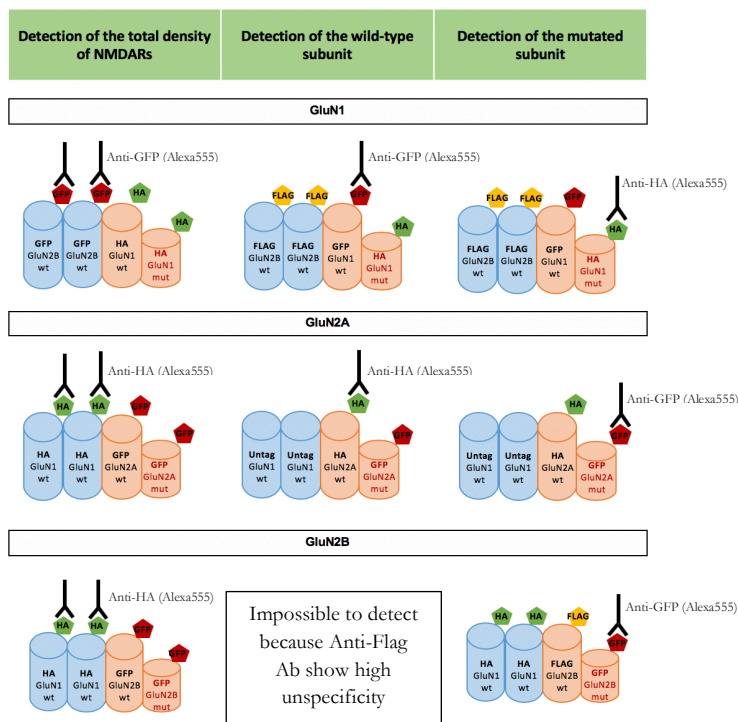

Figure 49. Graphic summary of the different conditions of transfection and immunofluorescence in transiently transfected COS-7 cells based on the affected subunit and the used approach in monoallelic conditions.

Fluorescence samples were mounted in microscopes slides using ProLong Gold Antifade Mountant with DAPI (Thermo Fisher Scientific, Cat#P36931) and were visualized with a Nikon Eclipse 80i microscope with 63× objective/1 N.A. immersion oil objective and Leica microsystems immersion oil (Thermo Fischer Scientific, Cat#11944399). Alexa555 fluorophore and GFP intrinsic fluorescent signal were excited with excitation laser beams at 546 nm and 488 nm wavelengths, respectively. Fluorescence intensity was measured in 5-15 COS-7 cells per condition, in at least 3 independent experiments.

Fluorescence of COS-7 was quantified using Adobe Photoshop CS5 software (Adobe Systems Inc.) by delimiting the cells with the 'magnetic lasso tool' and noting average number of the corresponding channel (red) in histogram (see **figure 50**). Background signal was subtracted. Results were represented as the mean ± standard errors of the means (SEM) of surface immunofluorescent signal.

<u>Neuronal primary cultures</u>

To analyze the surface expression or morphological traits of the transfected primary pyramidal neuronal cultures, expressing NMDARs, neurons were washed briefly with PBS and fixed with 4% PFA in PBS containing 4% sucrose (10 minutes, under agitation, RT).

The surface expression of GFP-GluN2A and GFP-GluN2B subunits was detected by incubating with anti-GFP (see **table 16**) for one hour (diluted in FBS_i 1 %, under agitation, RT). Antibody binding was detected with an Alexa 488-conjugated goat anti-rabbit Ab (against the GFP) (see **table 16**) (diluted in FBS_i 1 %, under agitation, RT). Further, the intracellular pool of receptors was identified by permeabilizing cells with 0.1% Triton X-100 (15 minutes, under agitation, RT) and labeling with either a rabbit anti-GFP (GluN2 detection) (see **table 16**) or a mouse anti-HA (GluN1 detection) (see **table 16**) for one hour (diluted in FBS_i 1 %, under agitation, RT). Antibody binding was detected by incubating with an Alexa 647-conjugated goat anti-rabbit Ab (against the GFP) and an Alexa 555-conjugated goat anti-mouse Ab (against the HA) (see **table 16**) for one hour (diluted in FBS_i 1 %, under agitation, RT).

To analyze morphological parameters (number and type of spines at basal/stimulated state) of neurons-expressing mutant NMDARs, after conducting chemical-LTP inducting protocol (see next paragraph), cells were fixed with 4% PFA in PBS containing 4% sucrose at 4ºC (10 minutes, under agitation, RT). Then, cells were permeabilized with 0.1% Triton X-100 (15 minutes, under agitation, RT) and labelled with anti-GFP (see **table 16**) for one hour (diluted in FBSi 1 %, under agitation, RT). After washing, antibody binding was detected by incubating with Alexa 488-conjugated goat anti-rabbit secondary antibody (see **table 16**) for one hour.

Fluorescence samples were mounted in microscopes slides using ProLong Gold Antifade Mountant with DAPI. Fluorescence of neuronal primary pyramidal cultures was visualized with a Leica TCS-SL spectral confocal microscope (Leica Microsystems, Wetzlar, Germany) using a Plan-Apochromat 63×/1.4 N.A. immersion oil objective (Leica Microsystems), a pinhole aperture of 114.54 μm and Leica microsystems immersion oil. Alexa555, Alexa488 and Alexa647 were excited with excitation laser beams at 546 nm, 488 nm and 650 nm wavelengths, respectively. Fluorescence intensity was measured in 1-15 dendrites from at least 1- 3 pyramidal neurons per condition in at least 3 independent experiments.

Surface trafficking of NMDARs in neuronal primary cultures was quantified using Adobe Photoshop CS5 software (Adobe Systems Inc.) by delimiting the cells with the 'magnetic lasso tool' and noting average number of the corresponding channel (green) in histogram (see **figure 50**). Background signal was subtracted. Results were represented as the mean ± standard errors of the means (SEM) of surface immunofluorescent signal.
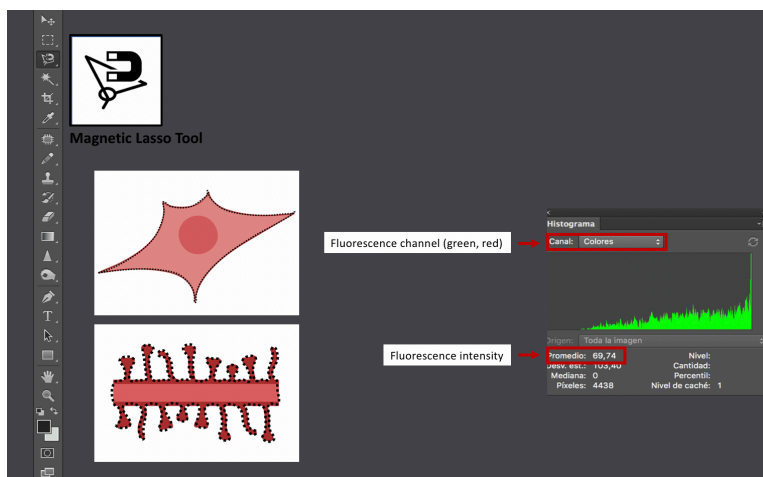

Figure 50. COS-7 or neuronal dendrites were delimited using the 'magnetic lasso tool'. In the histogram, channel color was selected, and average number corresponds to the average fluorescence intensity of the delimited area.

Chemical-LTP inducting protocol

Neurons were transiently transfected with GFP-Grin2A or GFP-Grin2B plus GFP (0.6 μg : 0.2 μg) constructs at DIV11 with lipofectamine 2000 for four hours. Before transfection, half of conditioned media was collected, mixed with same amount of fresh complete growth medium (to a total volume of 700 μl, and supplemented with 100 μM D-AP5) and kept at 37ºC.

At DIV14, glycine-mediated chemical long-term potentiation assay (cLTP) was performed (adapted from Tao-Cheng et al., 2011). It is well reported that synaptic activity rapidly changes spine number, shape and subcellular composition of dendritic spines (Morgado-Bernal I. et al., 2011) which is critical for synaptic plasticity and it is also known that altered spine morphology and plasticity are common hallmarks of several neurodevelopmental disorders (Knobloch M. et al., 2008; Penzes P. et al., 2011).

This protocol resulting in the induction of synaptic activity *in vitro,* allowed the evaluation of dendritic spines density and morphology under basal or activated states, to check whether there was any disruption of this mechanism associated with different *GRIN* variants. Under basal conditions, nonstimulated neurons were incubated with Krebs-Ringer solution (124 mM NaCl, 2 mM KCl, 1.24 mM KH_2PO_4, 1.3 mM $MgCl_2$, 2.5 mM $CaCl_2$, and 30 mM glucose in 25 mM HEPES at pH 7.4) supplemented with 1 mM $MgCl_2$ and 1 µM tetrodotoxin (TTX) (Abcam, Cat#AB120055) to avoid action potential generation and neuronal firing. The induction of cLTP was achieved by a pulse administration of the NMDAR coagonist glycine (Lu H. et al., 2001). Briefly, neurons were washed in 20 µM bicuculline (Bic) (Tocris Bioscience, Cat#2503) to selectively block inhibitory $GABA_A$ receptors and 20 µM strychnine (Sigma-Aldrich, Cat#S0532) to block inhibitory glycine receptors. Then, we incubated for 5 min in Krebs-Ringer solution (with 20 µM bicuculline and 20 µM strychnine) supplemented with 200 µM glycine (Sigma-Aldrich, Cat#G8790).

In addition to the previous stimulated condition, we tested the combination of glycine together with different potentiators to evaluate whether a possible hypofunction that might result in disturbed plasticity and dendritic morphological changes could be rescued (100 µM D-serine supplement, Sigma-Aldrich, Cat#S4250; 200 µM Spermine supplement, Sigma-Aldrich, Cat#S2826; and 5 µM Rapastinel, Tocris Bioscience, Cat#3406). After stimulation with glycine (with or without potentiators), the solutions were replaced by Krebs-Ringer supplemented with 20 µM Bic, 20 µM strychnine, and 1 mM $MgCl_2$ to block receptors again and limit the stimulation period, and after 35 min of incubation at 37°C (elicitation of LTP, signalling cascades and morphological changes), cells were fixed with ice-cold 4% PFA in PBS containing 4% sucrose (10 min, under agitation at 4 °C).

Immunofluorescence analysis of dendritic spines morphology and density

Cells were washed once with PBS and fixed with 4% PFA in cold PBS containing 4% sucrose (10 min, under agitation, at 4 °C). Transfected neurons were immunolabeled, after permeabilizing with 0.1% Triton X-100 (15 min, under agitation, RT), with anti-GFP for one hour (see **table 16**) (diluted in FBS_i 1 %, at RT) and visualized by incubating for one hour with an Alexa 488-conjugated goat anti-rabbit Ab (see **table 16**) (diluted in FBS_i 1 %, at RT). Fluorescence samples were mounted in microscopes slides using ProLong Gold Antifade Mountant with DAPI. Fluorescence of neuronal primary pyramidal cultures was visualized with a Leica TCS-SL spectral confocal microscope (Leica Microsystems, Wetzlar, Germany) using a Plan-Apochromat 63×/1.4 N.A. immersion oil objective (Leica Microsystems), a pinhole aperture of 114.54 µm and Leica microsystems immersion oil to visualize neuron morphology. A 4X zoom was used to evaluate tertiary dendrites.

Between 1-3 pyramidal neurons (1-15 tertiary dendrites) were evaluated and approximately 9-14 Z-stack images (0.3 µm per stack) were acquired per dendrite. Dendrites were manually traced with Neuron Studio software (http://research.mssm.edu/cnic/tools-ns.html). Dendritic spines from tertiary neurites were counted and classified into morphological categories (thin, consisting on a long thin neck and a round head; mushroom, consisting on a large head and a short narrow neck; and stubby, consisting on a large head and a short wide neck) (see **figure 51**), using Neuron Studio software automatic analysis, based on aspect (the extent of shape elongation), head-to-neck diameters ratio and spine head diameter. This automatic classification was followed by manual revision to discard artifacts and/or spines counts redundancy.
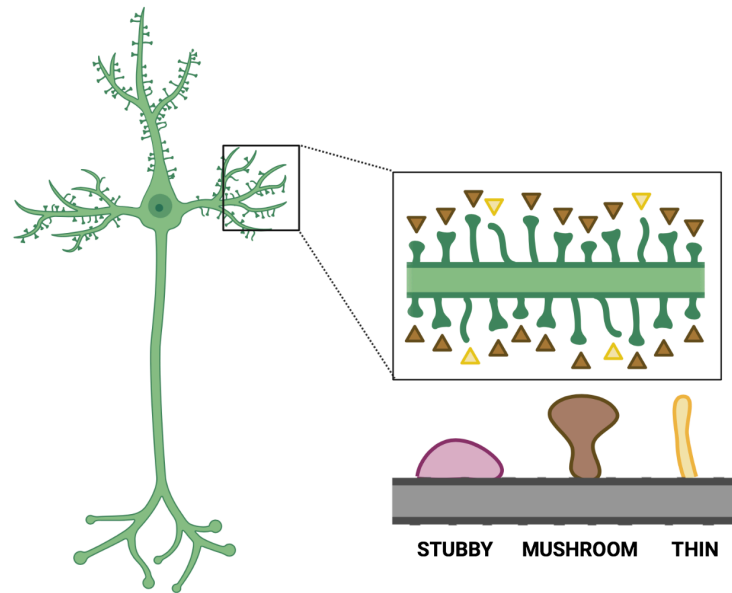
Figure 51. Tertiary dendrites from pyramidal neurons were selected to evaluate dendritic spines density and morphology. Dendritic spines were classified in different morphological categories depending on size and shape: thin (yellow), mushroom (brown), and stubby (pink) spines.

Electrophysiological recordings of whole-cell NMDAR currents in HEK293T cells

Electrophysiological recordings were obtained 24 h after transfection of HEK293T cells with PEI method, perfusing the cells continuously at room temperature with extracellular physiological bath solution: 140 mM NaCl, 5 mM KCl, 1 mM $CaCl_2$, 10 mM glucose, and 10 mM HEPES, adjusted to pH 7.42 with NaOH.

Voltage-clamp recordings in whole-cell configuration were acquired. Membrane potential was held at a set level (-60 mV). Glutamate (1 mM, Tocris, Cat#0218), in the presence of glycine (100 µM, Sigma-Aldrich, Cat#G8790) was applied for 5 sec by piezoelectric translation (P-601.30; Physik Instrument) of a theta-barrel application tool made from borosilicate glass (1.2 mm O.D., 0.69 mm I.D., with filament, Sutter Instruments, Cat#30-0044) (known as 'fast application tool') (see **figure 52**).
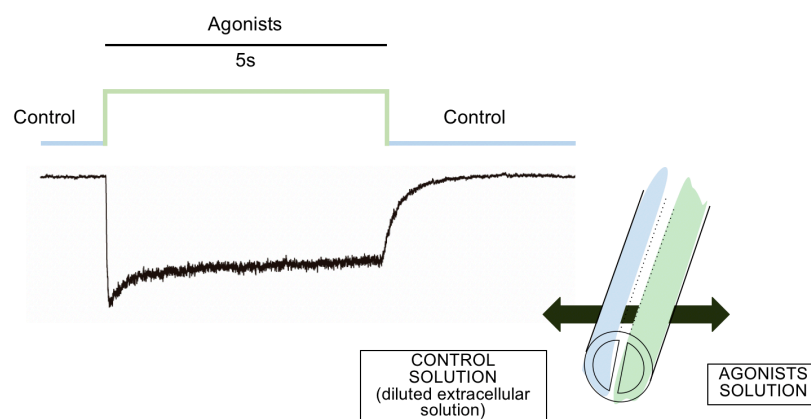

Figure 52. Scheme of agonists application for 5 seconds using the fast application tool that allows to applicate control solution (in blue) and agonists solution (in green) controlling the application time-course and consequently, the NMDAR current.

Pipettes with open-tip resistances of 2-4 MΩ were made from borosilicate glass (1.5 mm O.D., 1.16 mm I.D., no filament, Harvard Apparatus, Cat#HA30-0094), pulled with a P-97 horizontal puller (Sutter Instruments) and tip polished with a MF-830 forge (Narishige). Whole-cell patch-clamp allowed electrical access to inside of the cell, so these pipettes (recording electrodes) were filled with intracellular pipette solution containing: 140 mM CsCl, 5 mM EGTA, 4 mM Na_2ATP, 0.1 mM Na_3GTP and 10 mM HEPES, adjusted to pH 7.25 with CsOH (see **figure 53**).
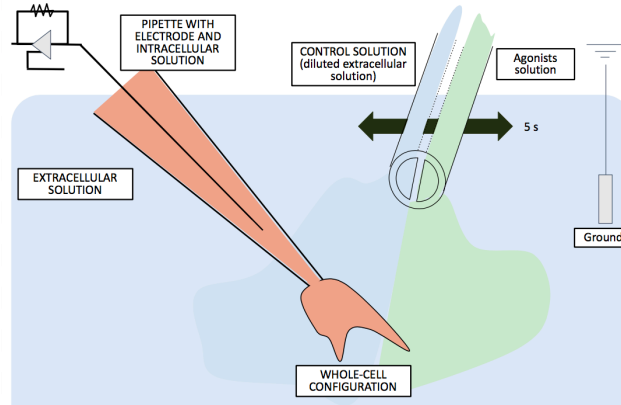

Figure 53. Scheme of whole-cell patch-clamp recording technique for the recording of fast excitatory NMDAR-mediated currents in HEK293T cells, using a fast application tool (in blue, control solution; and in green, agonists solution) and the glass pipette, containing intracellular solution and attached to the cell membrane (in orange). Currents went into the pipette and were recorded by an electrode which was connected to an amplifier.

The activated currents were acquired at 5 kHz and filtered at 2 kHz by means of Axopatch 200B amplifier, Digidata 1440A interface and pClamp10 software (Molecular Devices Corporation). Glutamate and glycine-evoked currents were expressed as current density (-pA/pF; maximum current divided by input capacitance as measured from the amplifier settings) to avoid differences due to variations in the surface area present in the recorded cells. The kinetics of deactivation and desensitization of the NMDAR responses were determined by fitting the glutamate/glycine-evoked responses at Vm –60 mV to a double-exponential function in order to determine the weighted time constant:

$$\tau_{weighted} = \tau_f \left(\frac{A_f}{A_f + A_s} \right) + \tau_s \left(\frac{A_s}{A_f + A_s} \right)$$

where A_f and τ_f are the amplitude and time constant of the fast component of recovery and A_s and τ_s are the amplitude and time constant of the slow component of the fitting. Desensitization was measured in the presence of agonists (blue fitting from the example in **figure 54**), while deactivation kinetics where measured from the inactivation of the current upon agonists removal (yellow fitting from **figure 54**).

Thus, peak amplitude, steady-state, desensitization and deactivation rates were measured for each current (see **figure 54**).
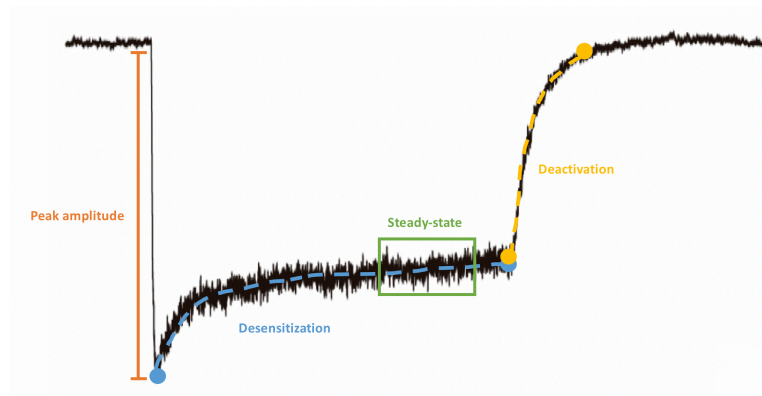
Figure 54. A representative NMDAR trace with the measured parameters: peak amplitude (minimum of the trace) (in orange), steady-state (average of a selected area) (in green), desensitization kinetics (weighted time constant) (in blue) and deactivation kinetics (weighted time constant) (in yellow).

NMDAR electrophysiological responses were analyzed using IGOR Pro 6.06 (wavemetrics) program and NeuroMatic 2.03 (Rothman JS. and Silver R.A., 2018) (https://www.wavemetrics.net/updaters60.html; http://www.neuromatic.thinkrandom.com).

Phenotypic assessment of Grin2b$^{+/-}$ mouse model

Phenotypic assessment of Grin2$^{+/-}$ mouse model included a behavioral evaluation to investigate whether this model recapitulates the alterations in learning, memory, motor function, social behaviours and GI function which are present in patients but also a biochemical and electrophysiological characterization to analyze different glutamatergic synaptic proteins levels and the ability to form long-term potentiation in the Schaffer collateral pathway of hippocampus.

<u>Subsynaptic fractionation of Grin2b $^{+/-}$ mice cortex</u>

Subsynaptic fractionation protocol was adapted from Morató X. et al., 2017. This protocol allowed the obtaining of the extrasynaptic (Extra), postsynaptic (Post) and presynaptic (Pre) enriched fractions from brain regions of 7-months-old mice. Frozen cortex fractions were thawed in 1 ml cold isolating buffer (IB) (0.32 M sucrose, 0.1 mM $CaCl_2$, 1 mM $MgCl_2$, PPIC) and mechanically homogenized (10 strokes at 700-900 rotations per min). Then, 6 ml of 2M sucrose solution (2M sucrose, DTT, 0.1 mM $CaCl_2$, PPIC) and 2.5 ml of 0.1 mM $CaCl_2$ were added and mixed by inverting the tube. After that, 2.5 ml of 1M sucrose solution (1M sucrose, DTT, 0.1 mM $CaCl_2$, PPIC) was added on top to form the sucrose gradient. Samples were centrifuged for 3 h at 100000xg and 4 °C using a swinging bucket rotor centrifuge (SW41Ti, Optima™ L-90K, Beckman coulter). After centrifugation, the top layer composed by myelin was discarded and a white ring between the 1.25M and 1M sucrose interphase corresponding to the synaptosome fraction was collected (see **figure 55**).

Then, synaptosomes were diluted with 9X their volume of IB and centrifuged for 30 min at 15000xg and 4 °C using a swinging bucket rotor centrifuge. After discarding the supernatant, the pellet was resuspended with 1.1 ml of IB solution. Part of this synaptosomal solution (100 µl) was collected to be pelleted by centrifugation for 5 min at 11000xg and 4 ºC. Supernatant was discarded and pellet was resuspended in 200 µl 5% sodium dodecyl sulfate (SDS) (this synaptosomal fraction will be known as P2) (see **figure 55**).

The rest of the synaptosomal solution (the volume that was not pelleted), was diluted with 5 ml of 0.1 mM CaCl$_2$ and 5 ml of 2X solubilization buffer, pH 6 (40 mM Trizma Base, triton X-100 2 %) and incubated for 60 minutes on ice under agitation. After this incubation, sample was centrifuged for 30 min at 40000xg and 4 °C using a swinging bucket rotor centrifuge. The resulting supernatant represents the extrasynaptic fraction, and the pellet corresponds to the synaptic junctions (pre- and postsynaptic fractions). The extrasynaptic fraction was concentrated to a final volume of 200 µl using Amicon Ultra-15 units (Millipore, Cat#UFC901008) and centrifugation at 4000xg and 4 degrees, for 30-60 minutes. After that, the concentrated extrasynaptic fraction was precipitated with 1 ml pre-chilled acetone overnight (O/N) at -20 degrees. 24 hours later, the extrasynaptic fraction was centrifuged for 30 min at 18,000xg and 4 degrees. The dry pellet containing the extrasynaptic proteins was resuspended with 200 µl 5% SDS (this extrasynaptic fraction will be known as Extra) (see **figure 55**). In parallel, the pellet containing the pre- and postsynaptic fractions was washed with 2 ml of 1X solubilization buffer, pH 6.0 (20 mM Trizma Base, triton X-100 1 %) and re-suspended with 10 ml of 1X solubilization buffer, pH 8.0 (20 mM Trizma Base, triton X-100 1 %). This sample was incubated for 60 minutes on ice under agitation, and then, centrifuged for 30 min at 40000xg and 4 °C using a swinging bucket rotor centrifuge. The resulting supernatant corresponded to the presynaptic fraction (Pre) and the pellet to the postsynaptic fraction (Post). Both fractions were concentrated following the same protocol than the extrasynaptic fraction and re-suspended in 200 µl of 5 % SDS (presynaptic fraction will be known as Pre and postsynaptic fraction will be known as Post) (see **figure 55**).
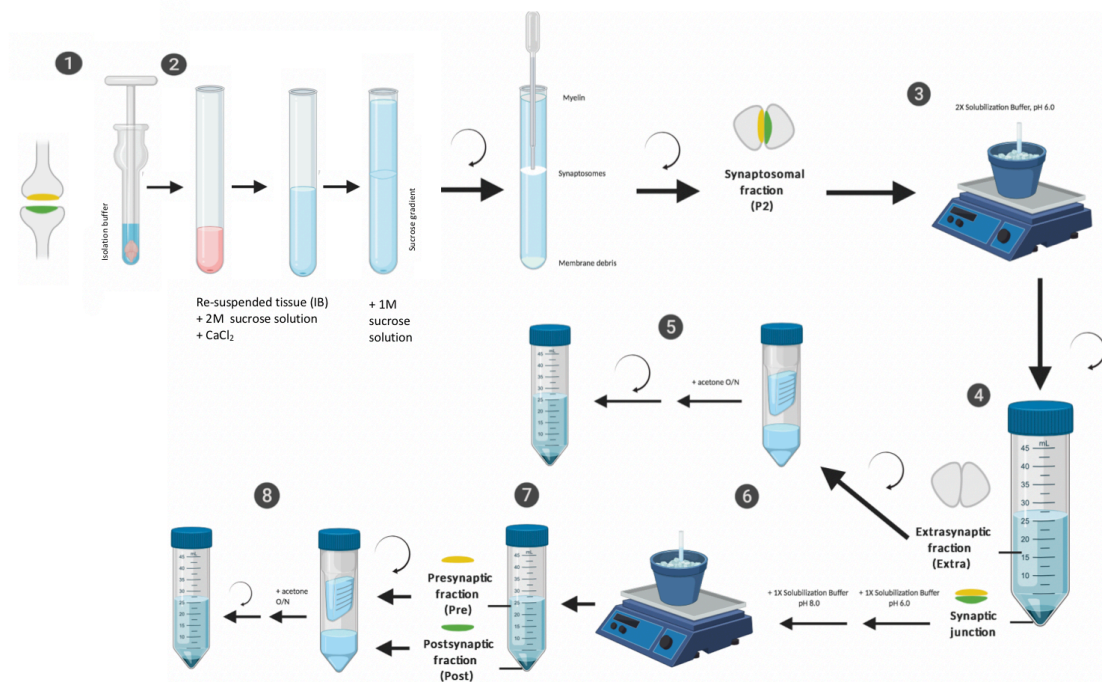

Figure 55. Scheme of subsynaptic fractionation protocol from murine cortex; **1,** Tissue homogenization; **2,** Sucrose gradient formation and synaptosomes obtaining; **3,** 1st solubilization step; **4,** Extrasynaptic fraction obtaining; **5,** Extrasynaptic fraction concentration; **6,** 2nd solubilization step; **7,** Synaptic junction separation in pre- and postsynaptic fractions; **8,** Pre- and postsynaptic fractions concentration.

All the subsynaptic fractions were sonicated and prepared in 1.5X sample buffer with 5 % β-mercaptoethanol and denatured for 30 minutes at 60 ºC. Then, proteins were separated according to western blot protocol described in **page 101.**

Field-potential recordings and long-term potentiation experiments in hippocampal slices

Adult mice (3-5 months old), were deeply anaesthetized, decapitated, and the brain was removed in ice-cold protective cutting artificial cerebrospinal fluid (CSF) aCSF1 (sucrose 206 mM; KCl 1.3 mM; $CaCl_2$-$2H_2O$ 1 mM; $MgSO_4$-$7H_2O$ 10 mM; $NaHCO_3$ 26 mM; Glucose 11 mM; NaH_2PO_4 1.25 mM), incubated with 95% O_2/5% CO_2. The brain was then subdivided into hemispheres and coronal hippocampal slices (380 mm-thick) were prepared on a vibratome (Leica VT1200 S; speed: level 2; vibration intensity: level 7). Coronal hippocampal slices were transferred into an incubation chamber with aCSF2 (NaCl 1.19 M; KCl 25 mM; $CaCl_2$-$2H_2O$ 25 mM; $MgSO_4$-$7H_2O$ 15 mM; $NaHCO_3$ 25 mM; Glucose 11 mM; NaH_2PO_4 12.5 mM), incubated with 95% O_2/5% CO_2. Slices were kept at 33 ^{o}C for 60 min and subsequently at room temperature for at least 60 additional minutes. Slices were then transferred into a measurement chamber perfused with aCSF2 at 26 ^{o}C.

A bipolar stimulation electrode (Platinum-Iridium stereotrode, Science Products, Microprobes, cat#P125T30.1A5) was placed in the Schaffer collateral pathway (Planagumà J. et al., 2016). Recording electrodes were made from borosilicate glass (1.5 mm O.D., 0.86 mm I.D., 10 cm, with filament, Sutter Instruments, Cat#BF150-86- 10). The recording electrode filled with aCSF2 was placed in the dendritic branching of the CA1 region for local field potential measurement (field excitatory postsynaptic potential, fEPSP) (see **figure 56**). Signals were amplified and stored using AxoClamp 2B (Molecular Devices). A stimulus isolation unit A385 (World Precision Instruments) was used to elicit stimulation currents.

Before recordings, input-output curves were determined for each slice with stimulation currents ranging from 25 to 200 mA at 0.03 Hz. The stimulation current was adjusted for each recording to evoke fEPSP, which was at half of its maximal evoked amplitude. After baseline recordings for 30 min with 0.03 Hz to determine the slice health, long term potentiation (LTP) was induced by theta-burst stimulation (10 theta bursts of four pulses at 100 Hz with an interstimulus interval of 200 ms, repeated seven times at 0.03 Hz). After LTP induction, fEPSPs were recorded for additional 60 min at 0.03 Hz (see **figure 56**). Recordings with unstable baseline measurements (variations higher than 20% in baseline fEPSPs) were discarded. The recordings were analyzed using Axon pCLAMP Software (Molecular Devices, version 10.6). Slopes of all recordings were measured within 0.7–1 ms of the linear part of the rising fEPSP (see **figure 56**) and compared between genotypes.
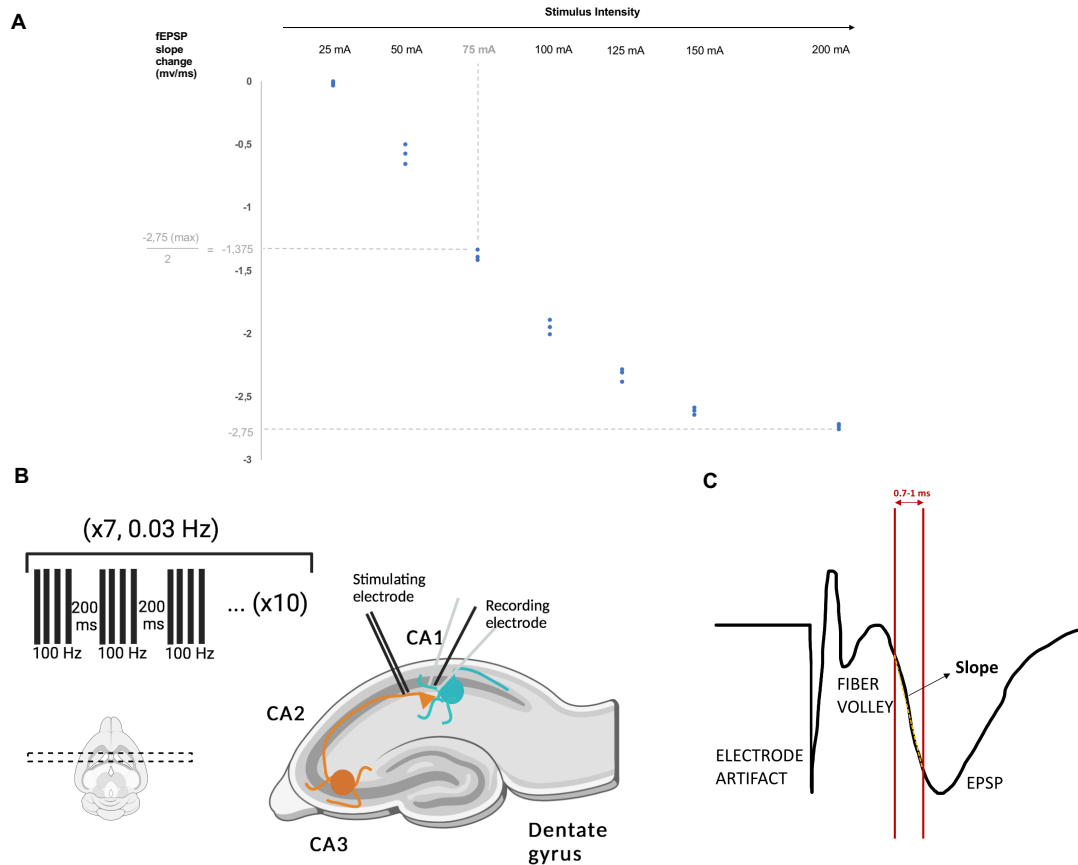
Figure 56. A, An example of an input-ouput curve with stimulus intensities ranging from 25 to 200 mA (3 stimulations of each point) and the corresponding voltage change in the slope of the fEPSP (mV/ms). The maximum voltage change is found and the half of this value and the corresponding stimulus intensity should be the selected one for the whole stimulation protocol (in gray); **B**, Schematic representation of field potential recording in Schaffer collateral connections, after theta-burst stimulation (10 theta bursts of four pulses of 100 Hz with an interstimulus interval of 200 ms, repeated seven times at 0.03 Hz) in a coronal hippocampal slice; **C,** Representative signal of a field-potential recording in hippocampal slices and delimited region (red lines) where slope (yellow dashed line) was measured; see **Note3** for further information about the field potential signal.

Note3: Firstly, an artifact from electrode is observed due to the insertion of the electrode in a conductive medium and the application of an electric field to that medium that creates a voltage change. Then, another wave which is known as 'fiber volley' appeared. The size of the fiber volley reflects the number of axons that are activated to give rise to a synaptic response. Thus, stimulation intensity is correlated with the size of the fiber volley. Ideally, fiber volley should be smaller relative to the synaptic response because slices that show a large fiber volley are usually unhealthy. Finally, the fEPSP is the last observed wave (Sweatt JD., 2007)

<u>Behavioral assessment of Grin2b$^{+/-}$ mouse model</u>

Behavioural tests were conducted from 9:00 to 14:00, in 2-months old mice. In order to characterize the motor, cognitive, anxiety, sociability and gastrointestinal phenotypes of young-adult Grin2b$^{+/-}$ mouse model, a comprehensive behavioral phenotyping battery was implemented, according to the timeline depicted below. Animals were weaned, separated by gender and genotyped on day 21 after birth. Nearly a month later, behavioral assessment was performed. Tests were ordered considering the level of stress that each of the tests causes to the animal (1, Open field; 2, Novel-object recognition test; 3, T-maze; 4, Marble bury test; 5, Rotarod; 6, Wire-hanging test; 7, Three-chamber; 8, Elevated plus maze; 9, Stool water content determination; 10, Intestinal transit time evaluation). After this behavioral battery, field-potential recordings were done to evaluate the ability of long-term potentiation formation (see **figure 57**).
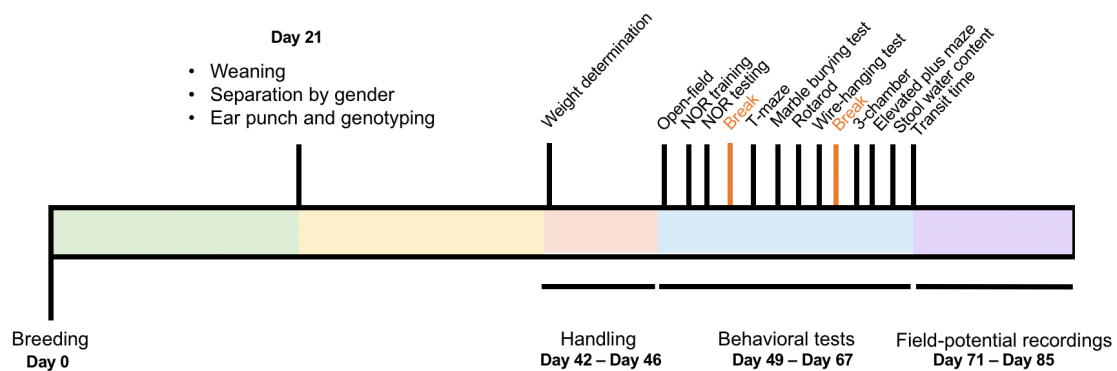

Figure 57. Timeline indicating behavioral assessment of Grin2b$^{+/-}$ mouse model. At Day 0, breedings (in green) were placed and 21 days after, mice were weaned, separated by gender and genotyped via ear punch. Three weeks later, one week of handling (in orange) was performed where mice were weighted. Then, three weeks of behavioral tests (in blue) (1, Open field; 2, Novel-object recognition test; 3, T-maze; 4, Marble bury test; 5, Rotarod; 6, Wire-hanging test; 7, Three-chamber; 8, Elevated plus maze; 9, Stool water content determination; 10, Intestinal transit time evaluation). Finally, field-potential recordings were performed for two weeks (in purple).

Handling, and body weight measurement

Handling was carried out for five to seven consecutive days (5 minutes/mouse/day). Mice were also weighted at this point to evaluate whether there was any different between genotypes.

Locomotor activity: Open field

The open-field test was adapted from Seibenhener ML. and Wooten MC., 2015. This test gives information about spontaneous locomotor activity under dim light conditions (15-20 lux) at 21.4-24 ºC and 24-35 % humidity. The open-field apparatus was a wall-enclosed gray squared area (PVC, 50x50x38 cm) (see **figure 58**).

Mice were habituated to the experimental anteroom for 60 minutes. After this period, the mice were individually placed in the center of the open-field apparatus. The mice were allowed to freely explore the area for 10 minutes and the trajectory was video-recorded with a digital camera on top which was connected to the video-tracking software SMART v3.0 (Panlab, https://www.panlab.com/en/products/smart-video-tracking-software-panlab). Thus, the experimenter was unobserved during the whole procedure. Between trials, the system was cleaned with ethanol 5 % to remove odor cues.

Total travelled distance, zone transitions (between the center and the periphery) and time spent in each zone were evaluated (see **figure 58**).
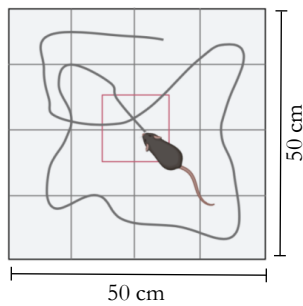

Figure 58. An open field system (50x50x38 cm). Mouse was tracked while exploring the open field area (gray line). Central (delimited with a red square) and peripherical areas were distinguished.

Long-term memory: Novel-object recognition test

The novel object recognition test (NOR) was adapted from Leger M. et al., 2013 and Lueptow LM., 2017. This test represents a gold-standard behavioral paradigm to evaluate learning and memory. The paradigm was based on mice innate preference for novelty. The test was conducted in the open-field system (gray PVC, 50x50x38 cm) under dim light conditions (15-20 lux) at 21.4-24 ºC and 24-35 % humidity. Two different objects, with identical exploratory preference, were selected to conduct the experiment. These objects were easily discriminated but with a similar degree of complexity and mouse sized. Objects were located and fastened to the floor (to avoid displacement) 15 cm from the walls in alternate opposite quadrants (see **figure 59**).

Mice were placed equidistantly from the objects and facing the wall which is the nearest to the experimenter. Object's interaction was considered when the mouse's nose pointed the object within 2-3 cm, with active vibrissae sweeping or sniffing. When mice climbed and sat on top of the object during a period of time, no interaction event was annotated.

Prior to the experimental groups, a pilot study was conducted in order to validate the experimental conditions and the appropriateness of the selected objects (discarding potential preferences). To test this, non-related mice were habituated to the arena for 5 minutes. Then, animals were allowed to freely explore the arena containing two different objects in opposite quadrants (alternated between animals) for 10 minutes. The number of events and time exploring the different objects (vs. total exploration) were calculated revealing no preferences for either object. The object location within the four quadrants was also randomized.

Upon validation of the objects, the experimental groups started the NOR test. Subject mice were habituated to the experimental anteroom for 60 minutes. On day 1, habituation to the experimental set-up was conducted (open-field test). On day 2, mice were trained with two identical objects that were placed on opposite quadrants. During training, mice were allowed to freely explore for 10 minutes, while measuring both the exploratory events and time for each object. On day 3, mice were tested for object novelty. One of the identical objects was replaced by a novel one and mice were allowed to freely explore for 10 minutes. Each object was randomly selected as familiar or novel, and the location of the novel object was also counterbalanced (see **figure 59**). Again, number of events and interaction time with each object were measured. Mice with a total exploration time of both objects inferior to 20 seconds were discarded. Discrimination index was calculated, following this equation:

$$\text{Discrimination index} = \frac{\text{Exploration }_{\text{Familiar}} - \text{Exploration }_{\text{Novel}}}{\text{Exploration }_{\text{Total}}}$$
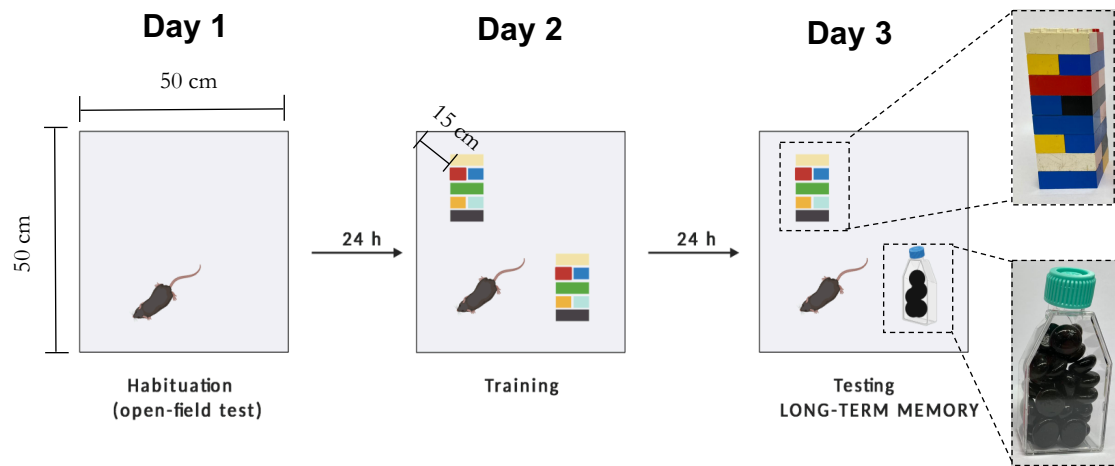
Figure 59. Graphic representation of the novel object recognition test performed in the open field arena (50x50x38 cm). On day 1, habituation to the experimental set-up. On day 2, training with two identical objects. On day 3, test for object novelty. Objects were placed 15 cm from the walls at opposite quadrants. In this particular scheme, a tower made from plastic construction blocks (Lego Systems A/S; Billund, Denmark) was selected as trained object while flask with black stones (no odor) as the novel one, but this was randomly modified between mice.

After each trial, the mouse was placed in a new holding cage to avoid contact with its littermates. Furthermore, between trials, the system was cleaned with ethanol 5% to remove odor cues. The experimenter was unobserved during the whole procedure. The presence of a camera on top allowed the recording for posterior analysis.

Spontaneous alternation paradigm: T-maze

The T-maze test (PVC, gray, 3 arms of 30x10 cm and a central region of 10x10 cm) in the 'spontaneous alternation' configuration was adapted from Chang YC. et al., 2017. This test is used to evaluate spatial working memory (see **figure 60**). The test was conducted under dim light conditions (15-20 lux) at 21.4-24 ºC and 24-35 % humidity.

Mice were habituated to the experimental anteroom for 60 minutes. Then, they were placed in the distal part of the base arm and were allowed to freely explore the maze. When mice chose an arm, door closing trapped the mouse in the selected arm for 30 seconds. Then, the mouse was placed again in the starting place, and the test was repeated. The spontaneous behavior of a wild-type mouse is to choose the opposite arm in the following trial ('alternation') but it might also choose the same arm ('repetition') (see **figure 60**).

An entry was considered when all four limbs of the mice enter in the arm. The number of alternations and repetitions were recorded for 16 trials. The lack of choice for 2 minutes in two consecutive trials or more than three trials without choice, discarded the animal. Alternation over a 50 % was considered choice by chance. The presence of a camera on top allowed the recording for posterior analysis. Between trials, the system was cleaned with ethanol 5 % to remove odor cues.
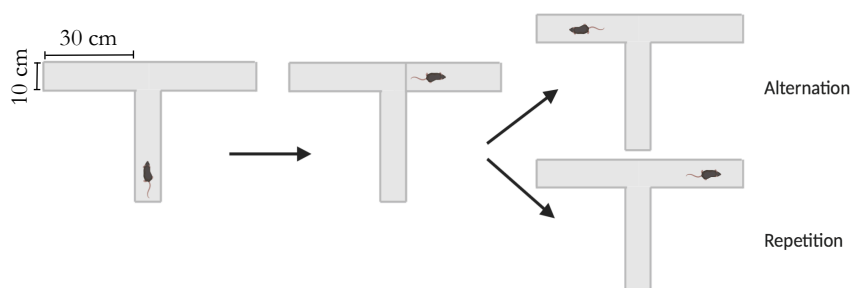

Figure 60. Graphic representation of the T-maze outputs: alternation (the mouse chooses the opposite arm) and repetition (the mouse chooses the same arm in which it has been trapped during the previous trial).

Repetitive behaviors: Marble bury test

The marble bury test, adapted from Angoa-Pérez M. et al., 2013, was performed to evaluate the presence of meaningless repetitive behaviors, based on the tendency of mice to dig in natural environments, under bright light conditions (80 lux) at 21.4-24 ºC and 24-35 % humidity.

In large housing cages (25x50 cm) with familiar bedding 5 cm height), 20 glass marbles of assorted styles and colors (1 mm diameter, 5,2 g) were arrayed (4 columns, 5 arrows) (see **figure 61**).
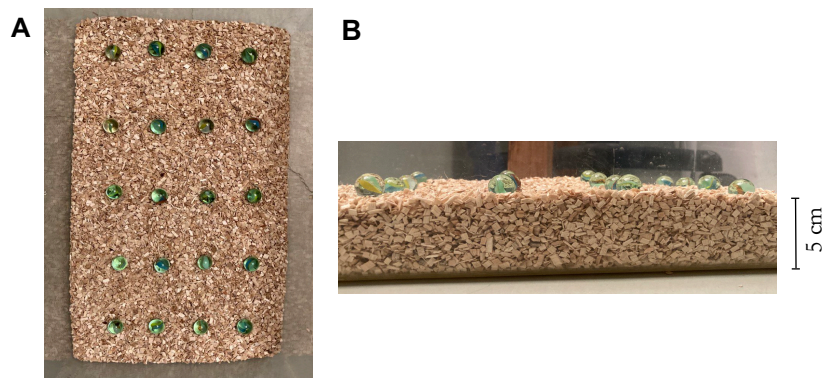

Figure 61. A marble bury arena seen from two different perspectives: **A**, Top view of the cage with natural bedding and 20 marbles equidistantly placed forming 4 columns and 5 rows; **B**, Lateral view showing the amount of bedding (5 cm).

The experiment took place in a familiar environment and since the marbles did not produce fear or anxiety, habituation to the experimental set-up was not required. Mice were habituated to the experimental anteroom for 60 minutes. Then, mice were individually placed into a corner and were allowed to explore and bury for 30 minutes. The number of buried marbles after the session was counted. A marble was considered buried when two thirds of its surface were covered by bedding. During the whole evaluation, experimenter was unobserved. Between trials, the marbles were cleaned with ethanol 5 % and the bedding was changed, to remove odor cues.

Motor coordination: Rotarod

The rotarod test, evaluating motor coordination, consists of a horizontal rotating rod (ø = 3 cm) with parallel ridges to allow grasping, placed at 30-50 cm over a soft surface in the base. The test was conducted under dim light conditions (40 lux) at 21.4-24 ºC and 24-35 % humidity (see **figure 62**). This test was adapted from Deacon RMJ., 2013.

Mice were habituated to the experimental anteroom for 60 minutes, and then, placed on the horizontal rotating rod at 4 rpm. The speed was accelerated from 4 rpm to 40 rpm at 8 rpm/min rate (~ 5 min). The speed and time when the mouse fell were annotated. Mice were tested in 3 consecutive trials to demonstrate a consistent performance (despite this, best mark was selected as representative of the mouse). Mice falling before 10 seconds repeated the trial and mice holding onto the rod without walking, were noted as fallen. Between subjects, the system was cleaned with ethanol 5 %.
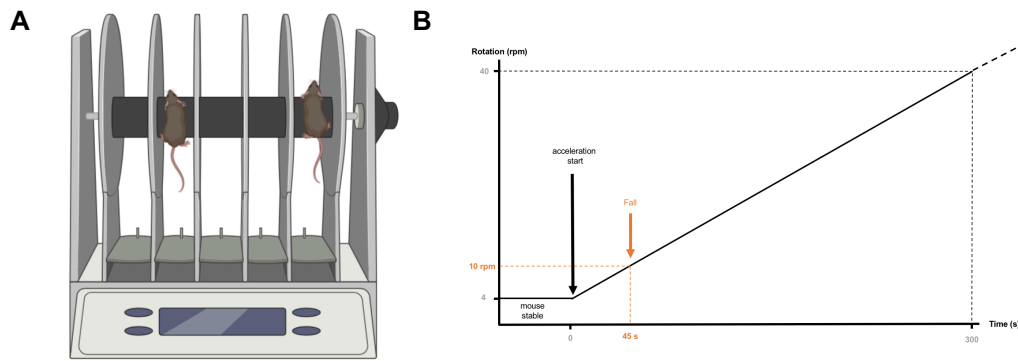
Figure 62. A, A rotarod system with 2 mice simultaneously performing the test; **B**, A schematic graph representing rotarod acceleration from 4 to 40 rpm at 8 rpm/min. Acceleration started (black arrow) when mouse was stable at the rotating rod and time started to count at this point. In the example, the mouse fell (in orange), 45 seconds later at 10 rpm.

Motor strength and coordination: Wire hanging test ('Falls and reaches')

The wire hanging test allows motor function assessment, based on the latency of a mouse to fall due to defects on muscle tone, strength, coordination and/or fatigue. The test was adapted from Klein SM. et al., 2012 and consists of a triangular wire at 35 cm height, with soft bedding underneath (see **figure 63**). The test was carried out under dim light conditions (40 lux) at 21.4-24 ºC and 24-35 % humidity.

Subject mice were habituated to the experimental anteroom for 60 minutes. No acclimatization to the experimental set-up was needed. The wire hanging test was used in a 'fall and reaches' configuration. The test lasted 180 sec and different scores were noted: A) Falls score: from 10, a unit was subtracted each time that the mouse fell; B) Reaches score: from 0, a unit was added each time that the mouse reached one of the sides of the wire. Each time that the mouse fell and/or reached the wire extreme, it was placed in the middle of the wire again until the 180 sec ending. Mice were placed in the system with fore limbs hanging the wire. Between subjects, the system was cleaned with ethanol 5 %.
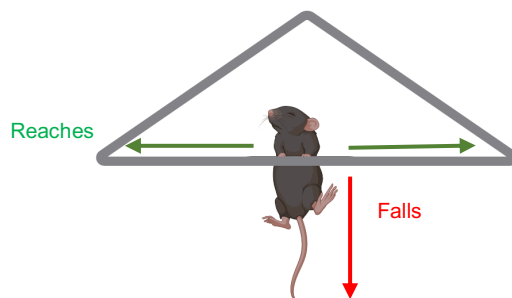

Figure 63. Wire hanging test simulation: Falls (in red) and reaches (in green).

Social interaction: Three-chamber test

A three-chamber box was used to evaluate mice social interaction abilities. The test was adapted from Kaidanovich-Beilin O. et al., 2011 and was performed on a rectangular Plexiglass three-chamber box (19x45 cm each chamber) with dividing walls containing an open middle section, allowing the mouse subject to explore any of the compartments. In the lateral compartments, wire cup-like containers were placed (see **figure 64**). The test was conducted under dim light conditions (15-20 lux) at 21.4-24 ºC and 24-35 % humidity.

Before starting, mice were habituated to the experimental anteroom for 60 minutes. Then, the animals were acclimatized to the set-up by allowing free exploration for 10 minutes of the middle chamber (with closed doors to prevent exploration of the lateral chambers). After that, empty wire cup-like containers were placed in the lateral chambers and doors were opened allowing mice to freely explore for 10 minutes the three compartments (see **figure 64)**.

In a first session, sociability was tested, and a control mouse (without prior contact but similar background, age, gender and weight) was placed into one of the containers while an object (a paper mouse) was placed in the other container. Control mouse location alternately changed between subjects. The subject mouse was placed in the middle chamber and it was allowed to freely explore and interact for 10 minutes (see **figure 64**). Immediately after that, in a second session of 10 minutes, the object was replaced by a second control mouse. Here, the preference for novelty was evaluated (see **figure 64**).
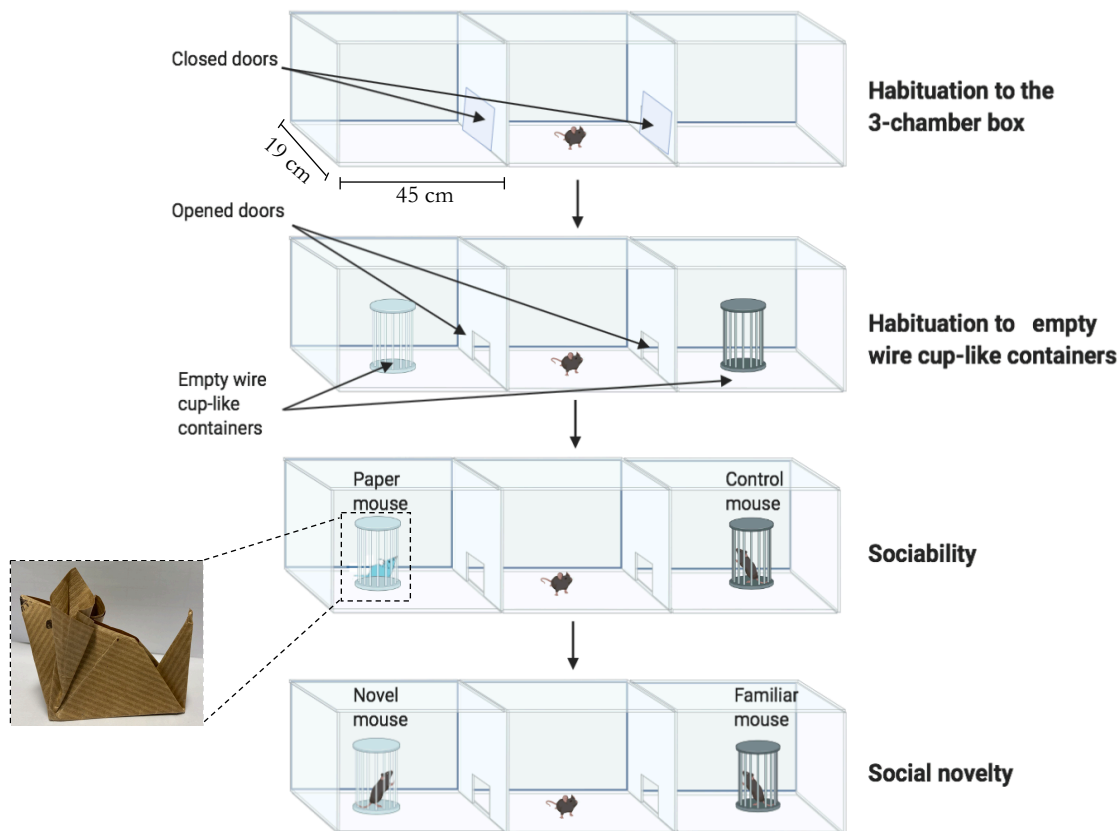

Figure 64. Graphic representation of the three-chamber test. Firstly, mice were habituated to the experimental set-up by placing them in the middle chamber with closed doors. Then, they were habituated to empty wire cup-like containers (doors were opened). After that, sociability was tested by exposing the subject mouse to a paper mouse and a control mouse. Finally, social novelty was tested by substituting the paper mouse with a novel mouse.

The number and duration of active contacts with both containers were measured. A contact was considered 'active' when the mouse was exploring within 3-5 cm around the container, with the nose pointing the container content. Mice climbing on top of the container, was not considered an active contact. During the whole evaluation, experimenter was unobserved. The presence of a camera on top allowed the recording for posterior analysis. Between trials, the system was cleaned with ethanol 5 % to remove odor cues.

Anxiety-related behavior: Elevated plus maze (adapted from Komada M. et al., 2008)

The elevated plus maze is used to measure anxiety-like behavior, based on the mice innate aversion to open, elevated and unknown environments. The test was adapted from Komada M. et al., 2008 and consists of a X-shaped maze (50 cm height) with two open and two enclosed arms (PVC, open arms – 25x5x0,5 cm; closed arms – 25x5x16 cm; center – 5x5x0,5 cm). The platform of the maze was white, and the walls were gray (see **figure 65**). The maze was located in a bright room (enclosed arms: 40 lux; open arms: 100 lux) at 21.4-24 °C and 24-35 % humidity.
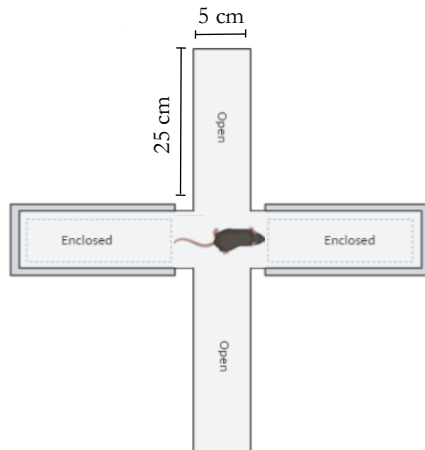

Figure 65. An elevated plus maze with two open and two enclosed arms. Mice were placed in the center region, pointing and enclosed arm.

Mice were habituated to the experimental anteroom for 60 minutes. Then, mice were placed on the center of the maze with the head pointing towards an enclosed arm. The mice were allowed to freely explore the maze for 10 minutes. The number and time of entries, in each type of arm were measured. An entry was considered when the center of the mouse's body entered the arm. Mice performed individually the test, in the absence of the experimenter, while being recorded by a camera on top. Between trials, the system was cleaned with ethanol 5 % to remove odor cues.

Evaluation of gastrointestinal function

To evaluate gastrointestinal function, feces water content was determined. Mice were housed individually in a clean cage without bedding for 1 hour with food and water *ad libitum* After this period of time, the number of fecal pellets were collected, counted and weighted to note the wet weight of the feces. Then, the pellets were left to dry at 65 °C for 24 hours to measure the stools dry weight. The stool water content percentage was calculated following this equation and compared between genotypes:

$$100 - \left[\frac{(\text{Wet weight - Dry weight})}{\text{Wet weight}} \times 100 \right]$$

To measure gastrointestinal motility, carmine red (not absorbed dye) oral gavage test was performed to evaluate total GI transit time (adapted from Kimball ES. et al., 2005). Animals were housed individually in a clean cage without bedding with food and water *ad libitum*.

A 6 % (w/v) carmine red solution (Sigma-Aldrich, Cat#C1022) was prepared in water. This solution was administered by oral gavage with a round-tip canula (single use feeding needles, Fine Science Tools, 20x1,75mm, Cat#18061-20) and the time 't$_0$' was annotated. Mice were monitored during the whole test lasting until the first carmine red-containing stoll (dark red colored) was excreted at 't$_r$' (time of release). GI transit time was considered as the interval between the initial time and the time of the first observance of carmine red in stool. Average GI transit times were compared between groups.

Grin2b$^{+/-}$ mice therapeutic interventions

Chronic spermidine supplementation

Spermidine, a polyamine that can be metabolized into spermine, is a positive allosteric modulator of the NMDA receptor (Rock DM. and Macdonald RL., 1992). Spermidine (Sigma-Aldrich, Cat#S0266) supplementation was administered orally by dissolving in drinking water (3 mM final concentration) (Chrisam M. et al., 2015; Eisenberg T. et al., 2016; Wirth A. et al., 2021) from P21 to the end of experiments (3 months) (see **figure 66**). Supplemented water was replaced every 2-3 days to avoid the compound deamination (Chrisam M. et al., 2015). Water consumption was measured along the experiment.

The treatment started at P21, and one month later, different behavioral tests were performed: 1, Open field; 2, Novel-object recognition test; 3, T-maze; 4, Marble bury test; 5, Rotarod; 6, Wire-hanging test; 7, Three-chamber; 8, Elevated plus maze; 9, Stool water content determination; 10, Intestinal transit time evaluation. Finally, field-potential recordings were carried out (see **figure 66**).
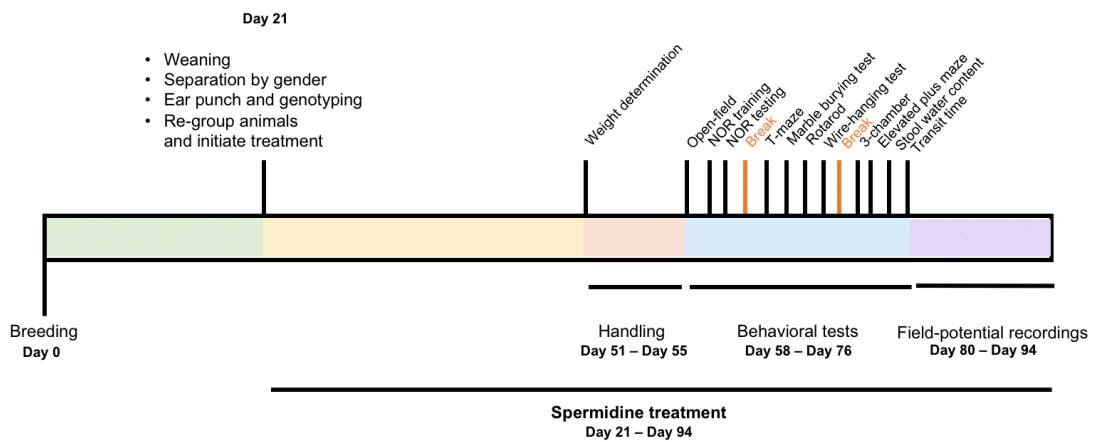

Figure 66. Timeline indicating behavioral assessment of Grin2b$^{+/-}$ mouse model. At Day 0, breedings (in green) were placed and 21 days after, mice were weaned, separated by gender, genotyped via ear punch, and re-grouped for initiating spermidine treatment. One month later, one week of handling (in orange) was performed where mice were weighted. Then, three weeks of behavioral tests (in blue) (1, Open field; 2, Novel-object recognition test; 3, T-maze; 4, Marble bury test; 5, Rotarod; 6, Wire-hanging test; 7, Three-chamber; 8, Elevated plus maze; 9, Stool water content determination; 10, Intestinal transit time evaluation). Finally, field-potential recordings were performed for two weeks (in purple).

Fecal microbiome transplantation (FMT)

Preparation of donor feces

In order to manipulate the mouse microbiota in a relatively homogenous microbiota/genotype background, after weaning and genotyping, mice were housed by genotype (wild-type cages and heterozygous cages).

Two weeks later, mice were handled. In the process of handling, stools were collected with tweezers and rapidly snap-frozen (liquid nitrogen), for future fecal microbiota transplantation (FMT) experiments. Feces from mice donors (same genotype) were homogenized in ice-cold distilled water (weight : volume, 1:50) by vortex (see **figures 67-68**).

Preparation of acceptor mice and microbiota transfer

Fecal microbiota transplantation protocol has been adapted from Bermudez-Martin P. et al., 2021. Firstly, acceptor mice were treated with orally gavaged omeprazole (200 µl/mouse, 100 mM, tris pH 8, Kern Pharma) for three consecutive days, to lower acidity and avoid damage to the microbiota transplant. Then, animals were food-deprived until the end of the treatment. The following day, a laxative solution (Moviprep, Norgine, 200 µl, 5 times) was administered by oral gavage. After 24 hours, mice were weighted and received orally gavaged omeprazole again. Three hours later, they received fecal supernatant by oral gavage (200 µl) twice with an interval of four hours between administrations. Then, food is added. 2-3 days later, mice were weighted again to supervise weight recovery after starvation. Finally, animals were returned to their cages for three weeks to allow the GI colonization with the transferred microbiota (see **figures 67-68**).
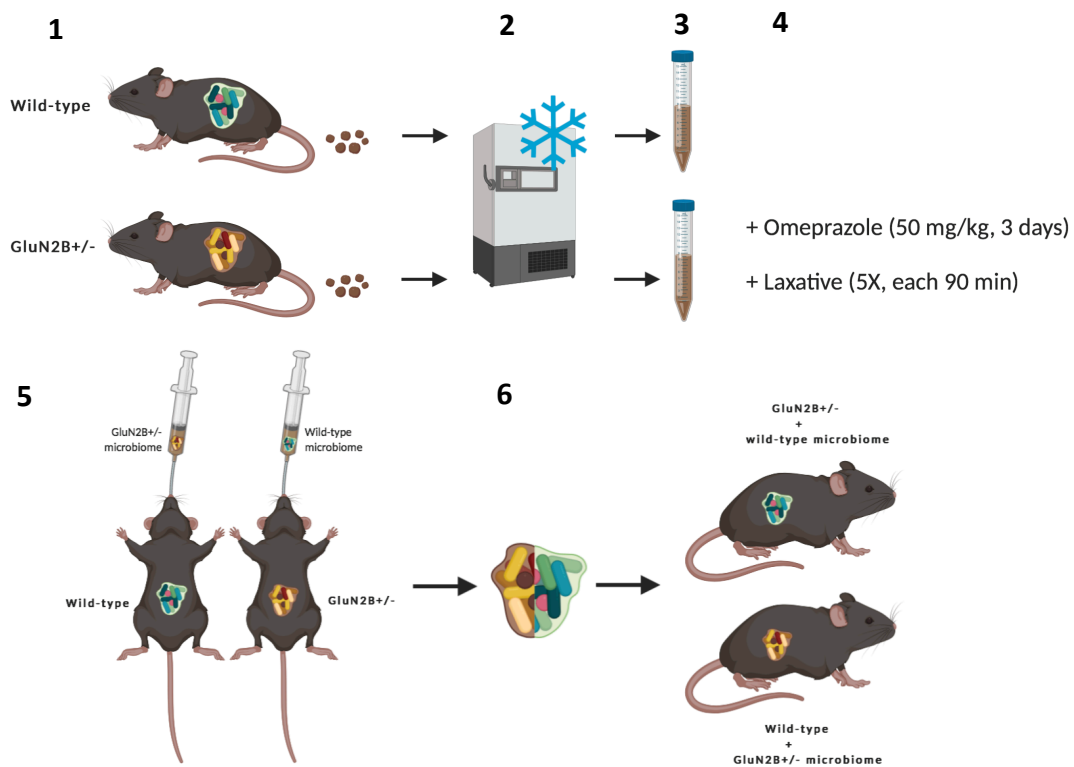

Figure 67. Schematic representation of fecal microbiota transplantation; **1,** Feces collection; **2,** Feces storage at -80 ºC; **3,** Fees processing; **4,** Omeprazole and laxative administration to acceptor mice; **5,** Fecal microbiota transplantation by oral gavage; **6,** GI tract microbiota colonization.

After colonization, some behavioral tests were performed: 1, Open field; 2, Novel-object recognition test; 3, Marble bury test; 4, Rotarod; 5, Wire-hanging test; 6, Elevated plus maze; 7, Stool water content determination; 8, Intestinal transit time evaluation. Finally, field-potential recordings were carried out (see **figure 68**).
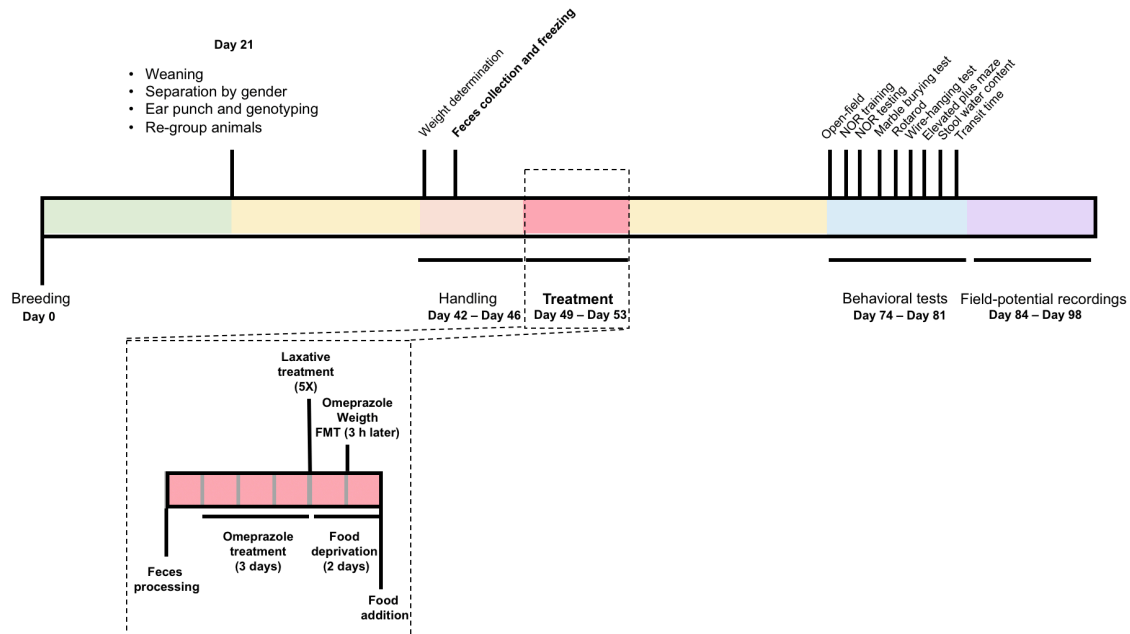

Figure 68. Timeline indicating FMT intervention in Grin2b$^{+/-}$ mouse model. At Day 0, breedings (in green) were placed and 21 days after, mice were weaned, separated by gender and genotyped via ear punch. Three weeks later, one week of handling (in orange) was performed where mice were weighted, and stools were collected and frozen. The following, week, FMT treatment took place (zoom out: 1, stools processing; 2, omeprazole treatment (for three days); 3, laxative treatment (5 times, same day) and from this point, animals were deprived of food until the end of the intervention; 4, omeprazole treatment, weight and three hours later, FMT). Then, three weeks later, one week of behavioral tests (in blue) (1, Open field; 2, Novel-object recognition test; 3, Marble bury test; 4, Rotarod; 5, Wire-hanging test; 6, Elevated plus maze; 7, Stool water content determination; 8, Intestinal transit time evaluation). Finally, field-potential recordings were performed for two weeks (in purple).

Statistical analysis

Comparison between experimental groups was evaluated using InStat software (GraphPad Software Inc.), applying a One-way Analysis of Variance (ANOVA), followed by a Bonferroni post hoc test for multiple comparisons. For single comparisons, either Student's t test (for parametric data) or Mann-Whitney U test (for nonparametric data) was used. Data are presented as means ± SEM from at least three independent experiments (cell-based experiments).

Results
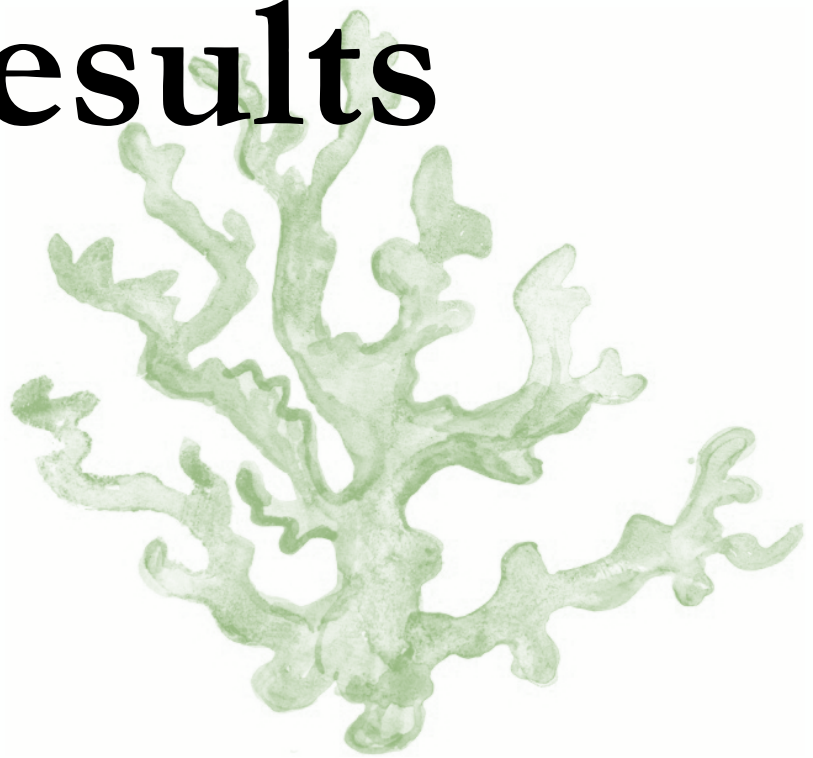
Chapter 1.

Recruitment of patients with *GRIN*-related disorders and *GRIN* variants annotation

1.1. Recruitment of patients with *GRIN*-related disorders

Recent advances in Next-Generation sequencing have allowed to identify several mutations affecting the genes that encode for NMDAR subunits (*GRIN* genes), with high prevalence in the *GRIN1*, *GRIN2A* and *GRIN2B* genes, present in patients with neurodevelopmental conditions. Based on a common etiology, the neurodevelopmental disorders (NDDs) are encompassed under the term *GRIN*-related disorders *(*GRDs*)*. In fact, 4513 *GRIN* variants have been reported, and of these, 437 are likely associated with the disease (according to GRINdb server, https://alf06.uab.es/grindb/home) (García-Recio A. et al., 2021).

Given the disease's prevalence, it was very important to select an appropriate cohort of *GRIN* variants to perform the different studies. Along this Thesis, via direct contact with families and clinicians, 107 GRD patients have been recruited from different locations (Spain, Belgium, Denmark, Norway, Italy, United Kingdom, Netherlands, India, Poland, Sweden, Germany, France, Greece, Israel, USA, China, Austria, etc.). Nevertheless, some of the variants are coincident, leading to 72 different genetic variants from patients. These variants occur in *GRIN1*, *GRIN2A* and *GRIN2B* genes, which are the most predominantly affected genes in GRD conditions. Additionally, 9 *GRIN* variants have been artificially generated and 14 *GRIN* variants have been selected from databases in order to cover the vulnerable GluN domains from the different subunits, resulting in the evaluation of 95 different *GRIN* variants (see **figures 70-71**).

According the <u>inheritance of the recruited variants</u>, most of the selected *GRIN* variants are 'de novo' (90 %) as a result of a modification in a germ cell of one of the parents or during embryogenesis. Nevertheless, 10 % of recruited patients have inherited the *GRIN* variant from one of their parents (see **figure 69, panel A**).

Regarding the <u>type of genetic variant</u>, the most predominant variants are '*missense*' (70 %) where a single aminoacid is substituted by a different one. Slightly less common, the variants which are '*frameshift/nonsense*' (25 %) that incorporate a premature 'stop' codon, which truncates the protein, with or without previous alteration of the nucleotide sequence reading frame. Finally, some '*indel*' variants (5 %) that introduce or delete some aminoacids of the sequence, have also been selected. Noteworthy, these are the percentages that are found within the total group of reported *GRIN* disease-associated variants (according to GRINdb server, 314/437 are missense, 105/437 are frameshift/nonsense and 18/437 are indels). Thus, the selected cohort is representative of the original population (see **figure 69, panel A**).

In the recruited cohort, the most <u>affected subunit</u> is GluN2B (50 %) followed by GluN1 (30 %) and GluN2A (20 %). In each of these subunits there is a wide distribution of the recruited variants along the different domains (GluN1: 20 % ATD, 5 % LBD, 20 % LBD-TMD linker regions, 50 % TMD and 5 % CTD; GluN2A: 10 % ATD, 20 % LBD, 10 % LBD-TMD linker regions, 25 % TMD and 35 % CTD; GluN2B: 5 % ATD, 35 % LBD, 15 % LBD-TMD, 25 % TMD and 20 % CTD). Despite this, it is very clear that most of the GRIN variants are located in the LBD and the TMD, which are the most conserved regions among subunits (see **figure 69, panel B**).

It is necessary to stratify the *GRIN* variants due to an unclear genotype-phenotype correlation in the disease. Indeed, there is a highly heterogenous <u>clinical spectrum</u> associated with the different subunits and this can be observed in the recruited cohort. GluN1 variants are commonly related with moderate-severe intellectual disability (ID) (100 %) and motor disorders (65%) but these variants might also be associated, in some particular cases, with autism (40 %), epilepsy (30 %), visual impairments (30 %), brain abnormalities (20 %) and in a very few cases, with sleep disturbances (5 %). GluN2A is frequently related with epilepsy (65 %) and a milder ID than GluN1 variants (73 %) but GluN2A can also be associated with motor problems (30 %) and brain abnormalities (15 %) in some cases, and autism (8 %), visual impairments (8 %) and behavior problems (8 %) in a very few cases.

GluN2B patients present mild-to-severe ID (85 %), motor problems (60 %), epilepsy (45 %), autism (30 %), sleep disturbance (17 %), GI tract alterations (15 %), behavior problems (10 %), stereotypies (6 %), brain abnormalities (4 %), dysmorphic traits (8 %), and visual impairments (2 %) (see **figure 69, panel C**).

GluN1		
Symptoms		**%**
	Mild	0
ID	Moderate	40
	Severe	60
Abnormal EEG / Epilepsy		30
Motor and movement disorders		65
Autism		40
Visual impairments		30
Sleep pattern disturbance		5
GI tract problems		0
Brain abnormalities (MRI)		20
Behavior alterations		0
Dysmorphic traits		0
Stereotypias		0

GluN2A		
Symptoms		**%**
	Mild	40
ID	Moderate	25
	Severe	8
Abnormal EEG / Epilepsy		65
Motor and movement disorders		30
Autism		8
Visual impairments		8
Sleep pattern disturbance		0
GI tract problems		0
Brain abnormalities (MRI)		15
Behavior alterations		8
Dysmorphic traits		0
Stereotypias		0

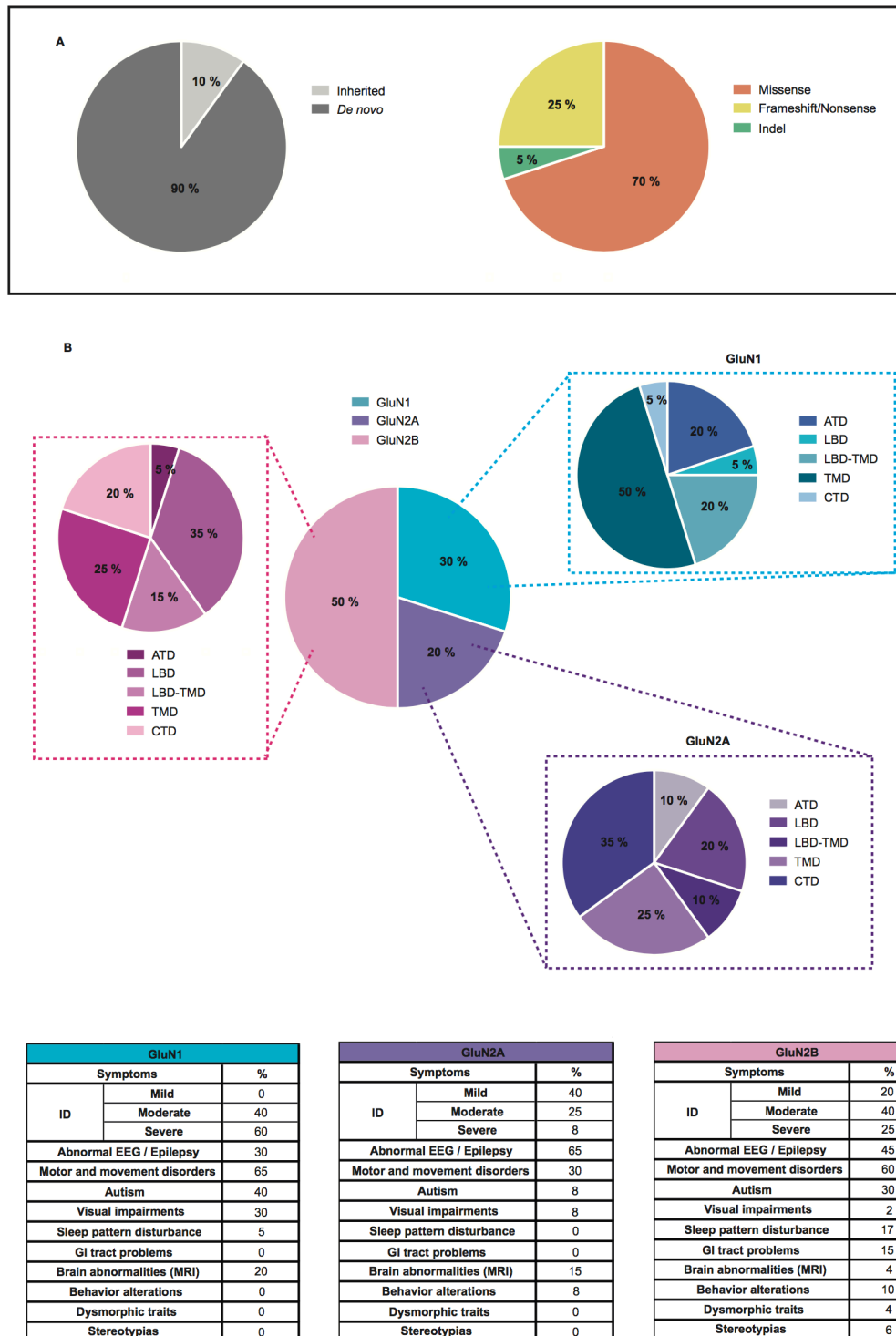| GluN2B		
Symptoms		**%**
	Mild	20
ID	Moderate	40
	Severe	25
Abnormal EEG / Epilepsy		45
Motor and movement disorders		60
Autism		30
Visual impairments		2
Sleep pattern disturbance		17
GI tract problems		15
Brain abnormalities (MRI)		4
Behavior alterations		10
Dysmorphic traits		4
Stereotypias		6

Figure 69. A-B, GRIN recruited variants classification in terms of inheritance (inherited, *de novo*) (**A, left panel**), type of variant (missense, frameshift/nonsense and/or indels) (**A, right panel**), affected GluN subunit (GluN1, GluN2A or GluN2B) (**B**) and altered domain (ATD: amino-terminal domain; LBD: ligand-binding domain; LBD-TMD: linker regions between the ligand-binding domain and the transmembrane domain; TMD: transmembrane domain; CTD: carboxyterminal domain). **C,** Summary of the different symptoms which have been reported for the GluN1, GluN2A and GluN2B variants.

Despite this great variability in relation to the different *GRIN* variants, we hypothesize that there might be a subunit and/or a domain effect on the variants functional impact and consequences which could help to stratify the variants into groups to determine personalized therapies. Thus, the selected cohort might look a bit heterogenous but, indeed, it is very representative of the whole spectrum of *GRIN* variants, which will allow us to understand the *GRIN* mutations pathophysiology in order to find the most suitable therapeutic option for each case.

As mentioned before, this cohort is formed by 95 different genetic variants. Selected GRIN variants were generated using rat *GRIN* cDNA as template, providing a perfect match for all the variants except some *GRIN2A* variants (E182Nfs*22, H595Wfs*20, H595Sfs*60, P1150A) and a particular *GRIN2B* variant (L229Yfs*9) that showed mild changes in the corresponding constructs generated from rat Grin2a (E182Nfs*23, H595Rfs*28, H595Lfs*60, T1150A) and Grin2b (L229Yfs*2) cDNA templates.

In **figure 70**, there is a schematic representation of the 95 *GRIN* recruited variants and how these variants are distributed along the different *GRIN* genes codifying for the GluN1, GluN2A and GluN2B subunits. In the scheme, the source, the inheritance pattern and the type of variant are indicated (see legend, **figure 70**).
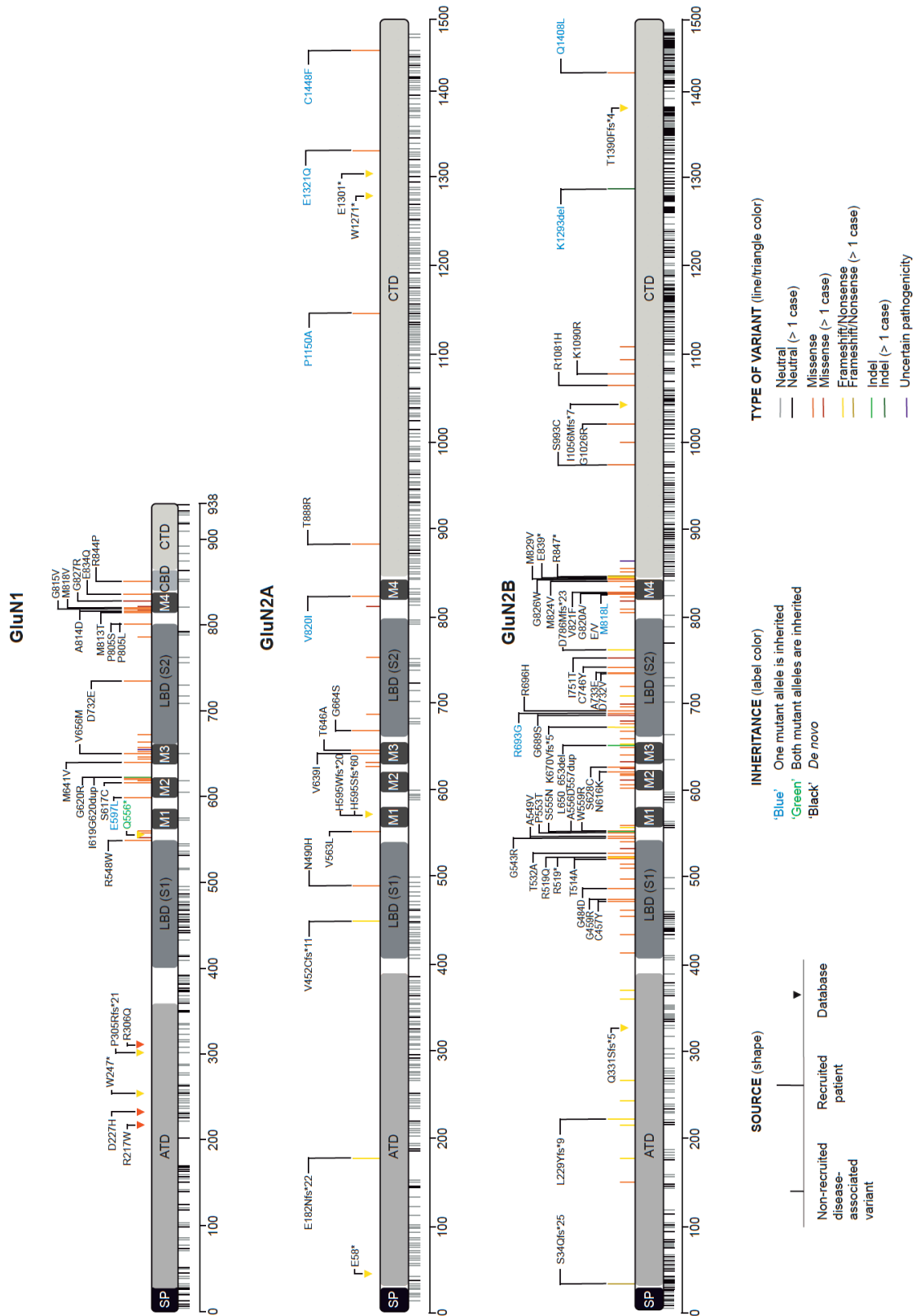
Figure 70. Scheme of *GRIN1*, *GRIN2A*, *GRIN2B* genes, showing the localization of *GRIN* variants coming from recruited patients (long lines) or databases (triangles) which might be de novo ('name in black') or inherited ('name in blue or green' depending on the number of copies which have been inherited, one or two respectively). Variants can be missense (orange), frameshift/nonsense (yellow), or indel (green). Neutral variants are in grey and variants with uncertain pathogenicity are in purple. Dark colors represent higher prevalence.

Additionally, in **figure 71**, there is another schematic representation of the 95 *GRIN* recruited variants. Nevertheless, this time, the figure shows the distribution of the variants within the protein structure of each of the subunits (GluN1, GluN2A and GluN2B).
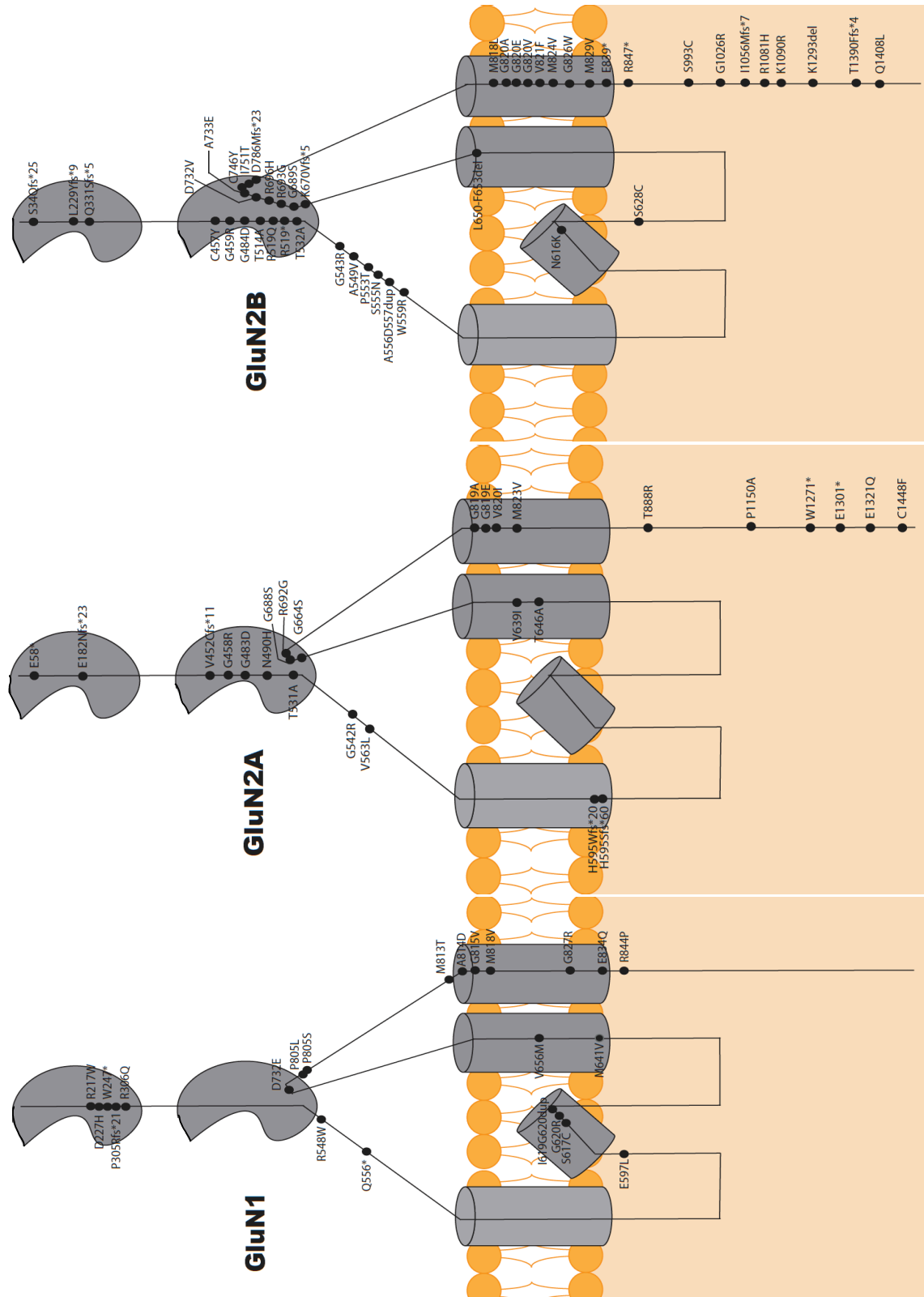
Figure 71. Scheme of GluN1, GluN2A, GluN2B subunits, showing the localization of *GRIN* variants into the different domains.

1.2.   *GRIN* variants annotation

GRIN variants might be affecting different processes of the NMDAR physiology. These changes might alter the NMDAR protein stability and/or oligomerization (leading to the receptor degradation) (1), the receptor trafficking to the cell surface (2), as well as its docking and stabilization at the surface (3), the correct function of the receptor (4), and consequently, the activity of the neurons where this kind of receptors are expressed (5) (see **figure 72**). Each of these processes will be discussed in detail in the next paragraphs.
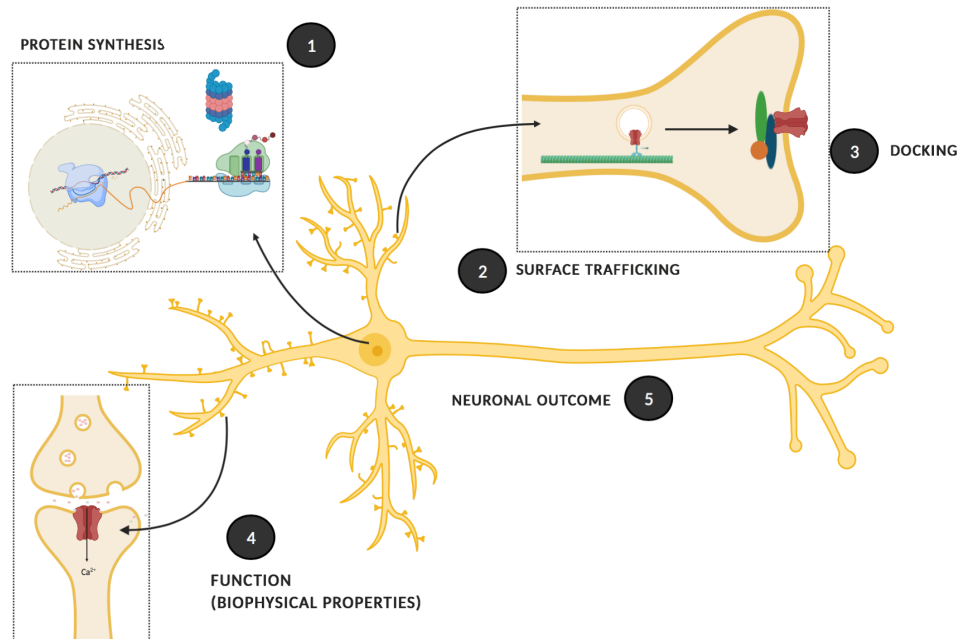
Figure 72. Schematic representation of the different processes which might be affected with the presence of *GRIN* variants: **1**, protein synthesis and receptor stability; **2**, surface trafficking; **3**, docking; **4**, the receptor function and its biophysical properties; **5**, neuronal activity.

1.2.1.   Impact of *GRIN* variants on NMDAR synthesis, oligomerization and the receptor stability

NMDAR physiological levels are determined by synthesis and degradation rates. Specifically, NMDARs, when needed, are degraded by the ubiquitin-proteasome pathway. Thus, ubiquitin molecules bind to particular regions of the NMDAR and this ubiquitinated protein is recognized and degraded by the proteasome (Qiu S. et al., 2011). Degradation of NMDARs can occur after neuronal activity and it might reflect the need of neuronal cells to control synaptic density to avoid excitotoxicity (Kato A. et al., 2005) or due to protein misfolding (Amm I. et al., 2014). There might be critical residues into the protein, that when affected, may result in the generation of protein instability and/or misfolding, leading to the degradation of the NMDARs, and consequently, a NMDAR loss-of-function.

Transient expression of the different *GRIN* variants in HEK293T cells and western blot analyses allow to specifically detect GluN subunits in a pool of proteins which have been extracted from cells, separating them based on molecular weight and using a specific antibody that recognizes the protein of interest. The detection of the GluN subunits containing the recruited *GRIN* variants gives information regarding protein stability given that instability results in protein degradation and consequently, a lack of protein detection using this technique (lack of bands of the corresponding molecular weight of each tagged subunit: 110 kDa for HA-GluN1, 178 kDa for GFP-GluN2A and 184 kDa for GFP-GluN2B).

This approach has revealed that most of the missense variants do not affect protein stability, regardless of the affected subunit (GluN1, GluN2A or GluN2B) and/or the inheritance pattern (*de novo* or inherited variants; inherited variants are indicated with '*' in **figure 73**, **panels A-C**). Only, 3 out of 62 missense variants (specifically, GluN1-R217W, GluN2B-S555N, and GluN2B-D732V) and a particular case (where GluN2B-D732V segregates with GluN2B-M829V in the same individual) might be related with the NMDAR degradation when these genetic variants are present in the corresponding subunit (see **figure 73, panels A-C,** red labels and red boxes indicating the lack of band detection), although the underlying reason for this instability is still unknown. Indel and nonsense variants are neither affecting the NMDAR stability (see **figure 73, panels A-C**).
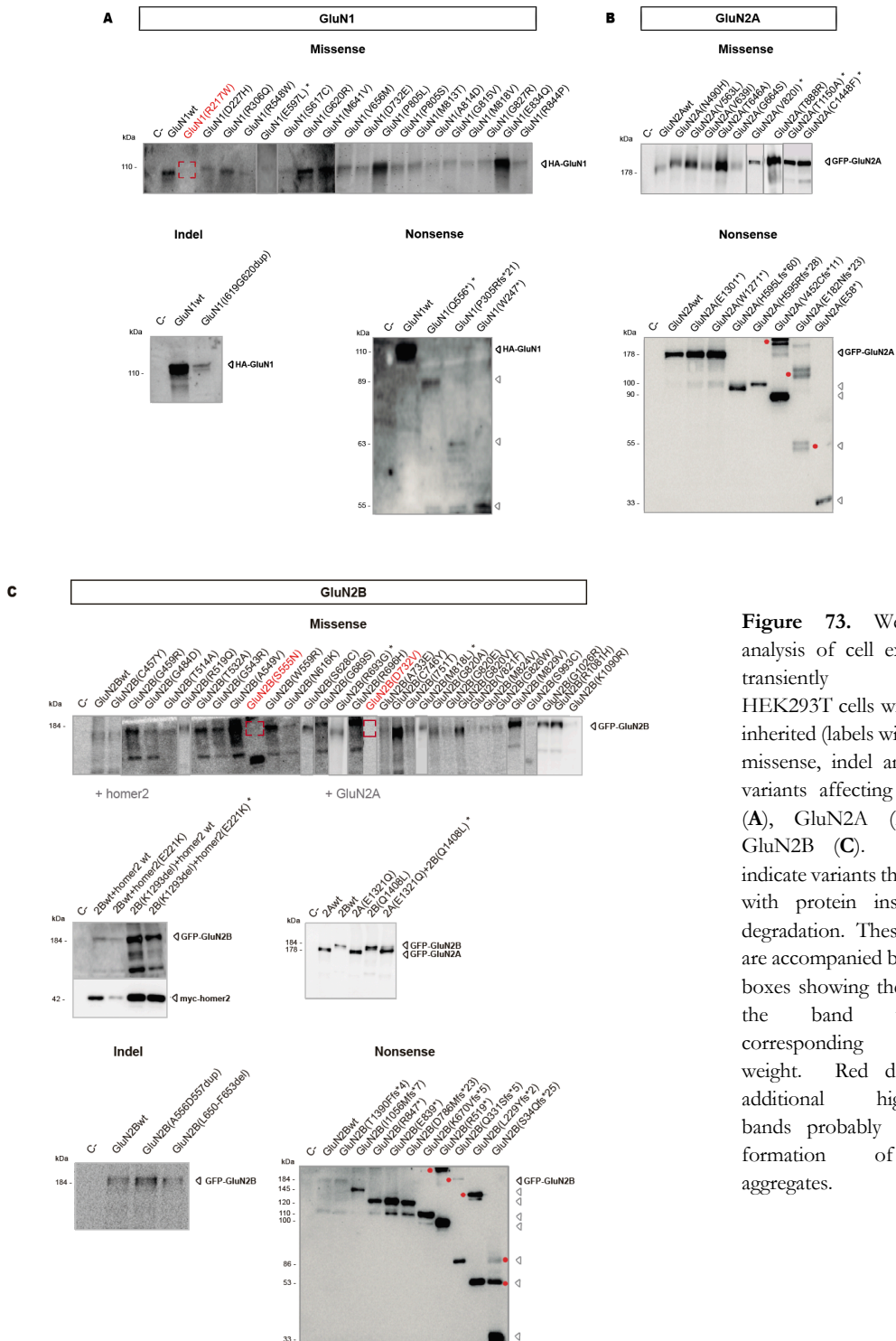
Figure 73. Western Blot analysis of cell extracts from transiently transfected HEK293T cells with *de novo* or inherited (labels with '*') *GRIN* missense, indel and nonsense variants affecting the GluN1 (**A**), GluN2A (**B**) or the GluN2B (**C**). Red labels indicate variants that are related with protein instability and degradation. These red labels are accompanied by red dashed boxes showing the absence of the band with the corresponding molecular weight. Red dots indicate additional high-molecular bands probably due to the formation of protein aggregates.

In addition to being degraded, misfolded proteins might form aggregates. Indeed, western blot approach also showed that some particular frameshift/nonsense variants (specifically, those affecting the ATD and the first segment of the LBD of the GluN2A and GluN2B subunits) formed high-molecular immunoreactive bands, suggestive of the presence of intermolecular aggregates (see **figure 73**, **panels B-C**, red dots).

To check the composition of those aggregates, a similar western blot approach was used. Nevertheless, for these experiments, HEK293T cells transiently expressed a combination of wild-type and truncated GluN subunits with different tags and distinct antibodies were used against the same protein extract to detect different GluN populations. This approach allowed us to identify that these aggregates were only composed by the mutant GluN2 subunit, with the absence of the wild-type allele product (**figure 74, panel B,** *light orange*) and/or the complementary GluN1 subunit (see **figure 74, panel A,** *blue*).
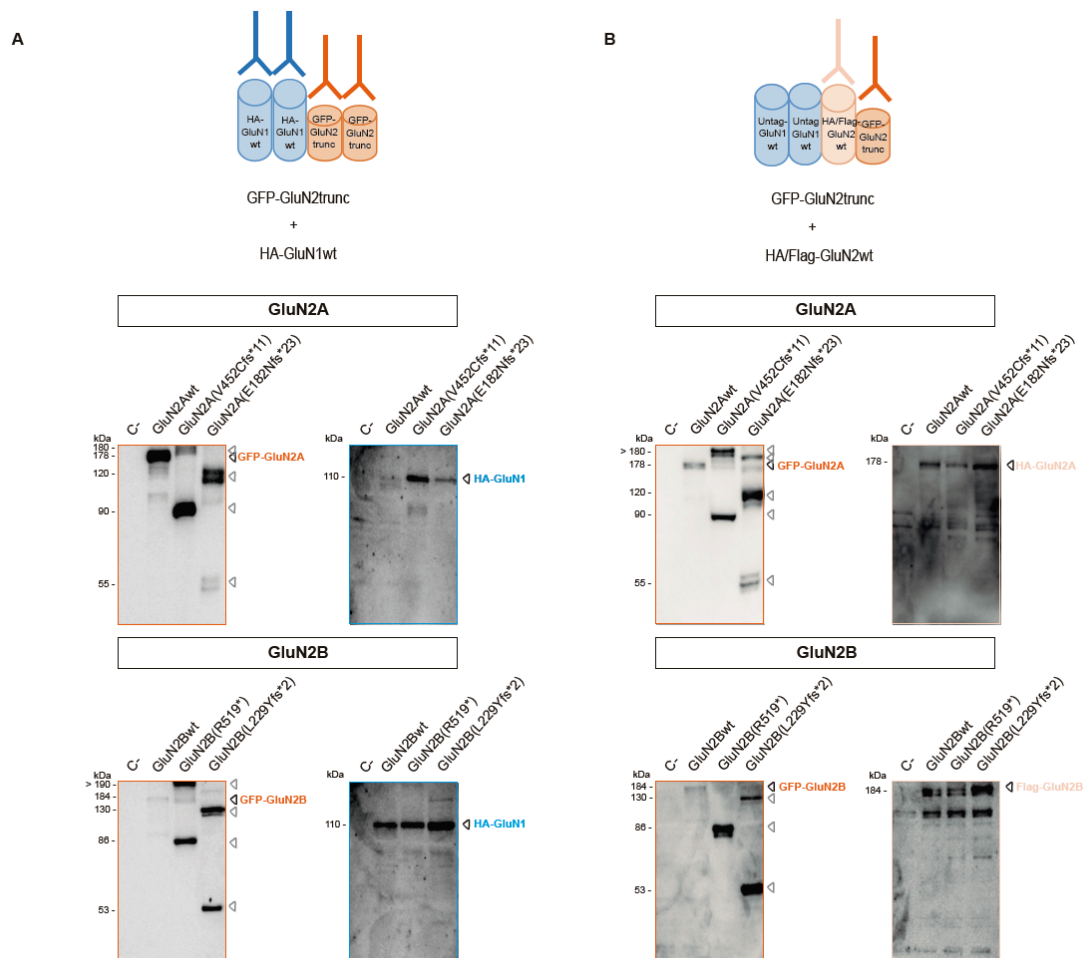
Figure 74. Western Blot analysis of cell extracts from transiently transfected HEK293T cells with *GRIN* nonsense variants. **A,** Co-expression of a wild-type complementary GluN1 subunit and a wild-type or a truncated GluN2A and/or GluN2B subunits. The presence of distinct tags and the use of different antibodies have allowed the detection of the GluN2B subunits in the left panels (dark orange) and the identification of the GluN1 subunits in the right panels (blue). **B,** Co-expression of a wild-type GluN2 subunit and a truncated GluN2 subunit, with different tags. Distinct antibodies have allowed the detection of the truncated GluN2 subunits in the left panels (dark orange) and the identification of the wild-type GluN2 subunits in the right panels (light orange).

1.2.2.   Impact of *GRIN* variants on NMDAR surface trafficking and docking

After the synthesis, if protein stability is not affected, the NMDAR must travel through different mechanisms to the cell surface where these receptors exert their function. This process is tightly regulated via distinct checkpoints: appropriate assembly, masking of retention signals, release from the reticulum-Golgi apparatus, stabilization at the membrane, internalization, etc. Consequently, changes in an aminoacid with a crucial role in one of these processes might be potentially affecting how the NMDAR is transported and/or stabilized at the cell surface.

Transient expression of the tagged GluN subunits in COS-7 cells together with the application of an immunofluorescence approach, without permeabilizing the cells and using specific antibodies against the tags, allowed to particularly detect the surface population of NMDARs.

This approach has showed that the vast majority of *GRIN* missense variants do not affect the ability of GluN subunits to reach the cell surface, independently of the affected subunit (GluN1, GluN2A or GluN2B) and/or the inheritance pattern (*de novo* or inherited variants; inherited variants are indicated with "*" in **figure 75**, **panels A-C**). Nevertheless, the alteration of some particular residues (GluN1-R217W and GluN2B- S555N, D732V) and a particular case (where GluN2B-D732V and GluN2B-M829V segregates in the same individual), almost completely abolish surface trafficking of the mutated receptors (see **figure 75, panels A-C**) due to receptor instability and degradation (revealed by western blot, **figure 73**). Additionally, GluN1-D227H, G827R and E834Q, GluN2A-T646A; and GluN2B-C457Y, G459R and R519Q genetic variants resulted in a lack of surface trafficking of the mutated receptors, although protein stability is not affected. Thus, D227, G827 and E834 residues in the GluN1 subunit, T646A residue in the GluN2A subunit and C457, G459 and R519 residues in the GluN2B subunit might have a critical role in the unmasking of retention signals, the release from the reticulum/Golgi system, the trafficking itself, the complex stabilization at the cell surface or NMDAR internalization. Further investigations are required to elucidate the underlying mechanism for this lack of surface expression.

This immunofluorescence approach also revealed that indel variants affecting the transmembrane domain but not other regions (such as GluN1-I619G620dup and GluN2B-L650-F653del) also affect the NMDAR membrane insertion in cell lines (see **figure 75, panels A,C**), probably due to the disturbance of the conserved TMD and consequently, the alteration of some of the four hydrophobic helixes which are located within the lipid bilayer.

Regarding nonsense variants, immunofluorescence data indicated that the truncation of the NMDAR protein in proximal regions (ATD, LBD, and TMD) also abolish the insertion of mutated receptors at the cell surface of cell lines (see **figure 75, panels A-C**), probably due to unproper oligomerization/assembly and/or lacking of export signals which are critical to unmask retention signals that are blocking the release from the reticulum-golgi system. Some nonsense variants with unproper surface expression are GluN1-W247*, P305Rfs*21, and Q556*; GluN2A-E58*, E182Nfs*23, V452Cfs*11, H595Rfs*28, and H595Lfs*60; and GluN2B-S34Qfs*25, Q331Sfs*5, R519*, K670Vfs*5, D786Mfs*23 and E839* (see **figure 75, panels A-C**). Noteworthy, with GluN2B-E839*, there is a lacking of only 2 aminoacids of the transmembrane region, and even with this short deletion, the mutated receptor is not able to insert in the cell surface.

Overall, these data indicate that several *GRIN* variants have a dramatic effect on NMDAR surface expression, and the decrease of cell surface expression might be related with a NMDAR loss-of-function.
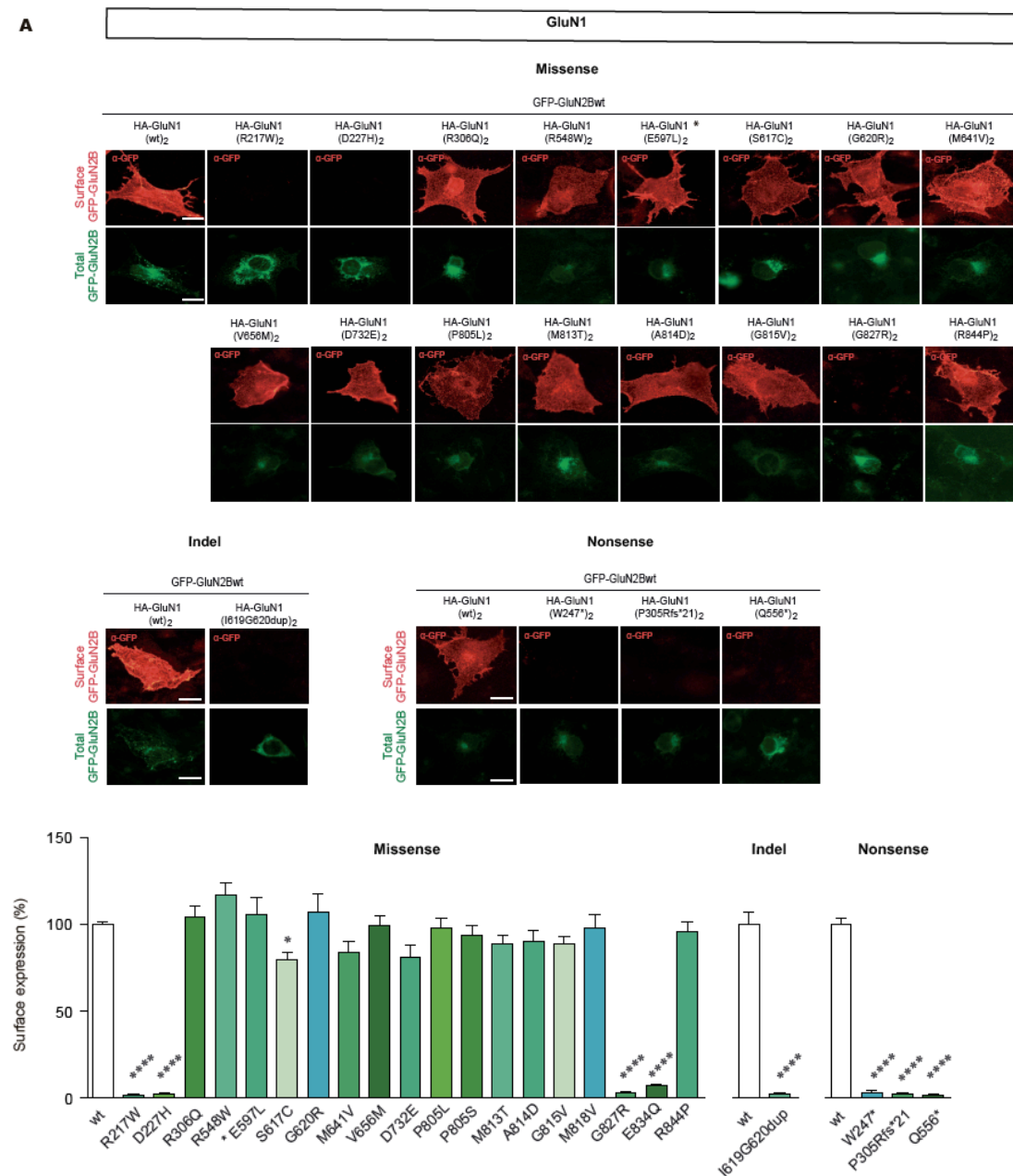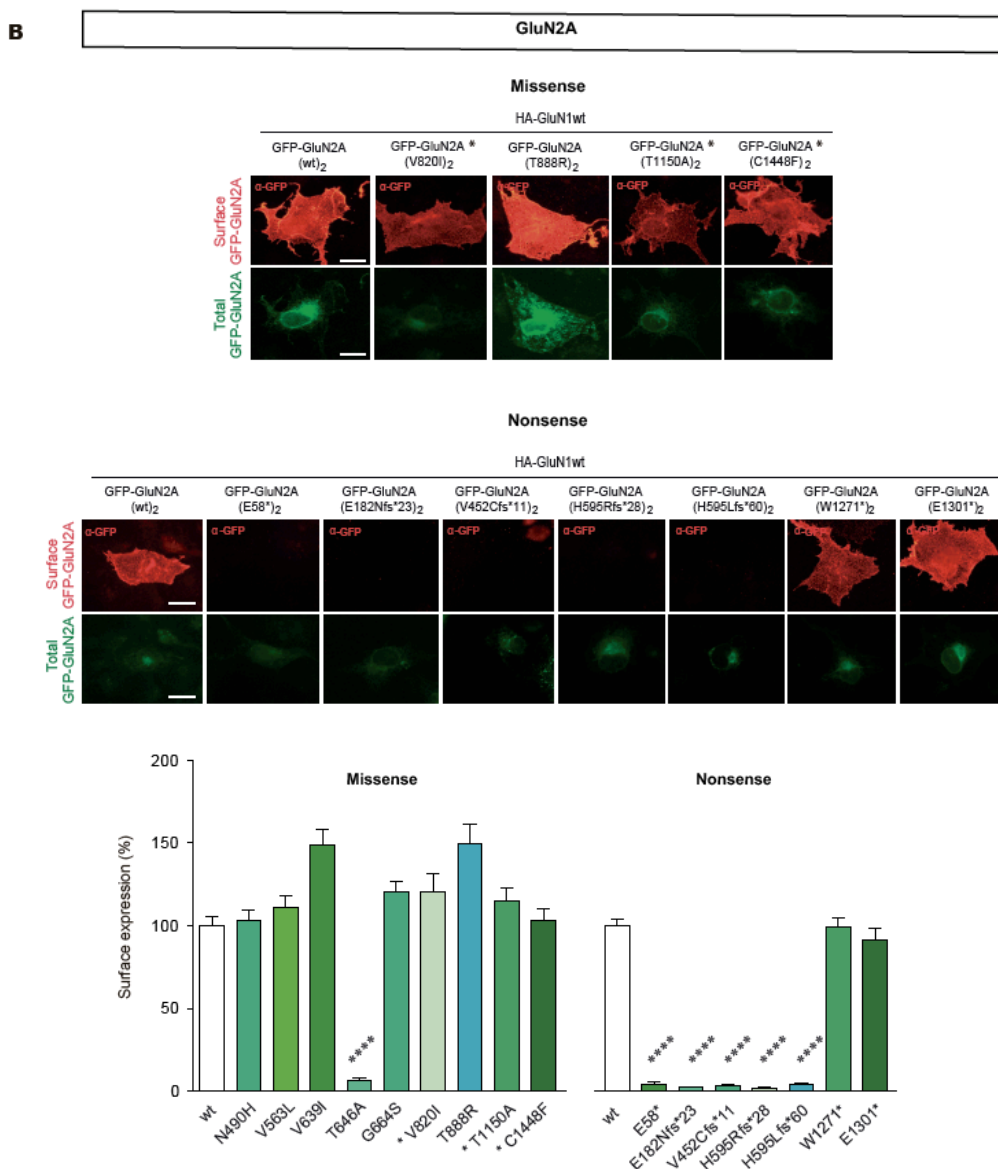
Figure 75. Immunofluorescence analysis of COS-7 cells transiently co-transfected with HA-GluN1 (wt/mutated) and GFP-GluN2Bwt plasmids (**A**), HA-GluN1wt and GFP-GluN2A(wt/mutated) plasmids (**B**), HA-GluN1wt and GFP-GluN2B(wt/mutated) plasmids (**C**), alone or in combination with myc-homer2(wt/mutated) or GFP-GluN2A(wt/mutated) (in gray) (missense, indel or nonsense variants). Surface NMDAR receptors were detected by GFP immunostaining (red channel) against the plasmid tag, total homer2 proteins were also detected by homer2 immunostaining (blue channel) while green channel is endogenous GFP signal without amplification as transfection control. Scale bar = 10 µm; Bar graphs representing the normalized surface expression of *GRIN* variants affecting GluN1, GluN2A, GluN2B and homer2 proteins, compared to wild-type (3 independent experiments, > 20 cells per condition; ns, P-value > 0.05; *, P-value < 0.05; **, P-value > 0.01; ***, P-value > 0.001; ****, P-value < 0.0001; ANOVA + Bonferroni post hoc test).
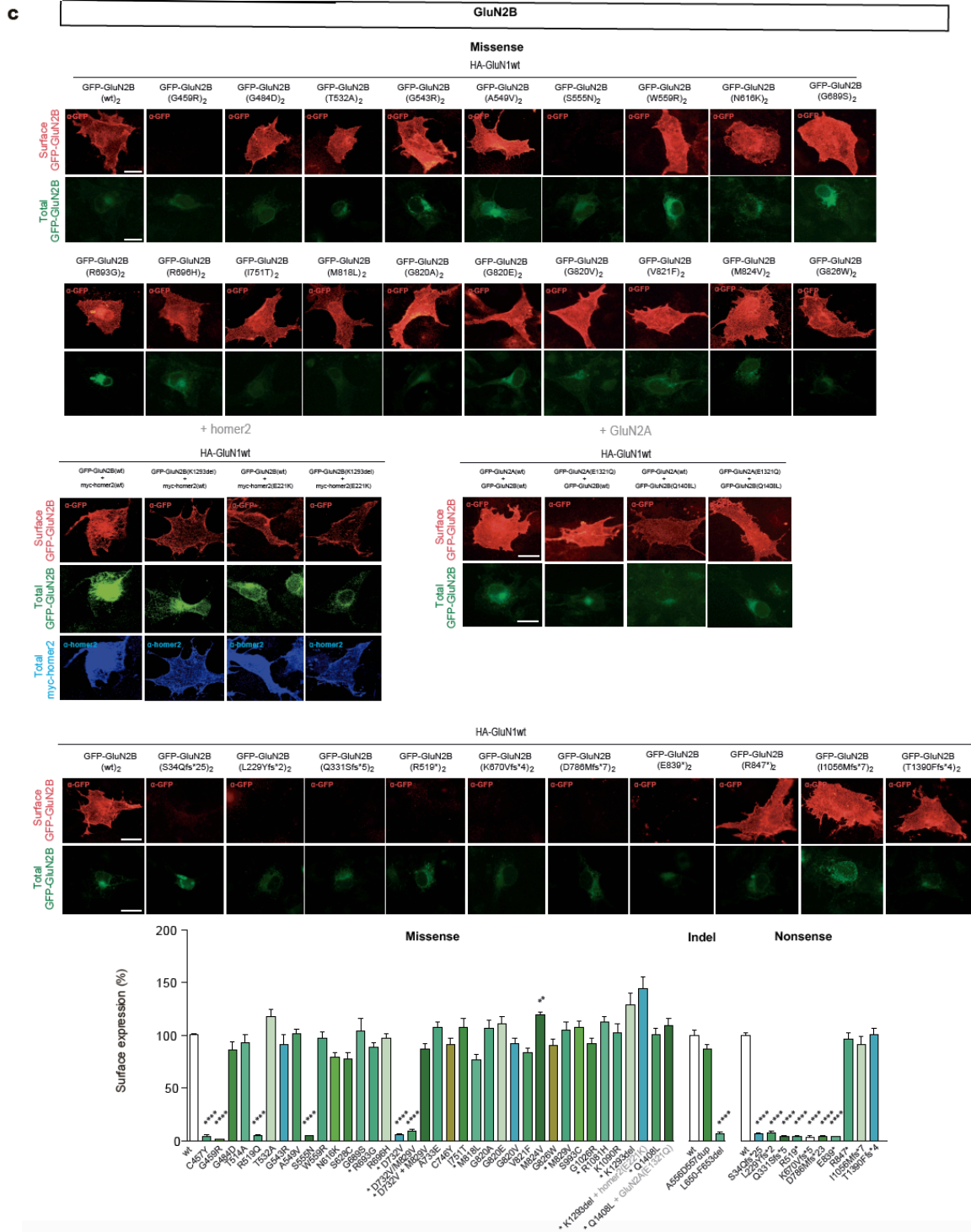
Figure 75: continued. Immunofluorescence analysis of COS-7 cells transiently co-transfected with HA-GluN1 (wt/mutated) and GFP-GluN2Bwt plasmids (**A**), HA-GluN1wt and GFP-GluN2A(wt/mutated) plasmids (**B**), HA-GluN1wt and GFP-GluN2B(wt/mutated) plasmids (**C**), alone or in combination with myc-homer2(wt/mutated) or GFP-GluN2A(wt/mutated) (in gray) (missense, indel or nonsense variants). Surface NMDAR receptors were detected by GFP immunostaining (red channel) against the plasmid tag, total homer2 proteins were also detected by homer2 immunostaining (blue channel) while green channel is endogenous GFP signal without amplification as transfection control. Scale bar = 10 μm; Bar graphs representing the normalized surface expression of _GRIN_ variants affecting GluN1, GluN2A, GluN2B and homer2 proteins, compared to wild-type (3 independent experiments, > 20 cells per condition; ns, P-value > 0.05; *, P-value < 0.05; **, P-value > 0.01; ***, P-value > 0.001; ****, P-value < 0.0001; ANOVA + Bonferroni post hoc test).

Figure 75: continued. Immunofluorescence analysis of COS-7 cells transiently co-transfected with HA-GluN1 (wt/mutated) and GFP-GluN2Bwt plasmids (**A**), HA-GluN1wt and GFP-GluN2A(wt/mutated) plasmids (**B**), HA-GluN1wt and GFP-GluN2B(wt/mutated) plasmids (**C**), alone or in combination with myc-homer2(wt/mutated) or GFP-GluN2A(wt/mutated) (in gray) (missense, indel or nonsense variants). Surface NMDAR receptors were detected by GFP immunostaining (red channel) against the plasmid tag, total homer2 proteins were also detected by homer2 immunostaining (blue channel) while green channel is endogenous GFP signal without amplification as transfection control. Scale bar = 10 µm; Bar graphs representing the normalized surface expression of *GRIN* variants affecting GluN1, GluN2A, GluN2B and homer2 proteins, compared to wild-type (3 independent experiments, > 20 cells per condition; ns, P-value > 0.05; *, P-value < 0.05; **, P-value > 0.01; ***, P-value > 0.001; ****, P-value < 0.0001; ANOVA + Bonferroni post hoc test).

Additionally, given that cell lines do not fully represent what is occurring *in vivo* due to a lack of endogenous expression of NMDARs or the required machinery for the regulation of these receptors, cell lines might be used as a screening method but data should be validated in a more complex and tightly regulated system, like neuronal primary cultures which are isolated directly from brain tissue and retain the morphological and functional traits of the original tissue.

An immunofluorescence approach in hippocampal primary cultures from embryonic mice, using specific antibodies against the subunits' tags, without permeabilizing the cells, revealed that there are difficulties to detect *GRIN1* variants in this neuronal system given that cultured neurons endogenously express NMDARs and the intrinsic GluN1 expression displace the oligomerization of exogenous tagged-GluN1 subunits, leading to a lack of tagged-GluN1 expression (even for the wild-type GluN1 subunit) at the neuronal surface (see **figure 76, panel A**).

Conversely, GluN2 subunits' endogenous expression do not overcome tagged-subunits' expression. Thus, some particular missense and nonsense variants have been selected and immunofluorescence results from cell lines were confirmed (see **figure 76, panel B**). Interestingly, while most nonsense variants affecting the CTD did not show significant changes comparing with the wild-type in cell lines, GluN2B-R847* showed a significant 20 % reduction of NMDAR surface density, when expressed in neuronal primary cultures (see **figure 76, panel B**). This reduction might result from an altered docking to the cell membrane, due to a lack of the PDZ-binding motif which is responsible of the NMDAR interaction with post-synaptic proteins to stabilize the receptors at the surface.
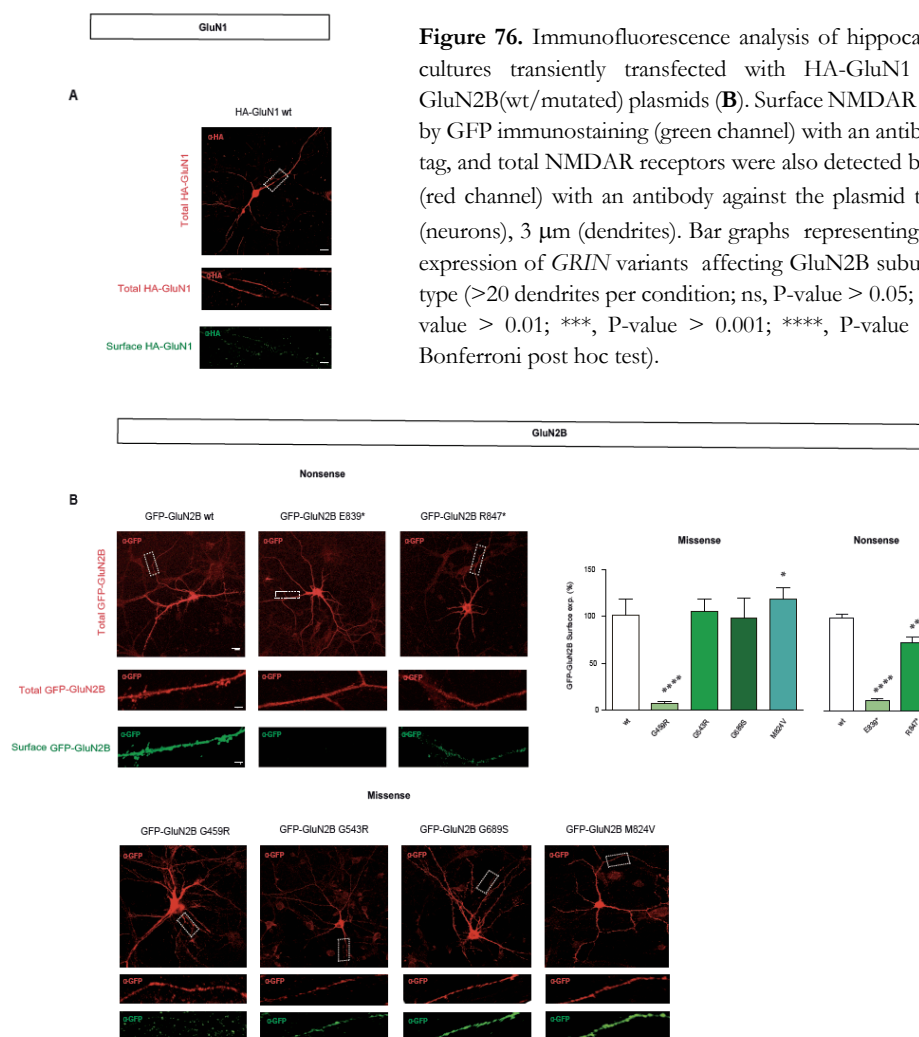

Figure 76. Immunofluorescence analysis of hippocampal neuronal primary cultures transiently transfected with HA-GluN1 (wt) (**A**) and GFP-GluN2B(wt/mutated) plasmids (**B**). Surface NMDAR receptors were detected by GFP immunostaining (green channel) with an antibody against the plasmid tag, and total NMDAR receptors were also detected by GFP immunostaining (red channel) with an antibody against the plasmid tag. Scale bar = 40 μm (neurons), 3 μm (dendrites). Bar graphs representing the normalized surface expression of *GRIN* variants affecting GluN2B subunits, compared to wild-type (>20 dendrites per condition; ns, P-value > 0.05; *, P-value < 0.05; **, P-value > 0.01; ***, P-value > 0.001; ****, P-value < 0.0001; ANOVA + Bonferroni post hoc test).

1.2.3. Functional impact of *GRIN* variants on NMDAR-mediated currents

NMDAR physiological correct function depends on several critical residues which determine the different biophysical properties and gating of the channel: opening, ion permeability, conductance, desensitization rate, deactivation rate, etc.

Patch-clamp experiments in whole-cell configuration allowed us to evaluate different biophysical properties of transiently transfected HEK293T cells. Cells expressing NMDARs containing some of the recruited genetic variants were exposed to a fast glutamate (1 mM) and glycine (50 μM) application (0,5 s) by means of a piezo-electric translator and NMDARs-mediated currents were recorded. This approach allowed to identify whether GluN genetic variants might result in a gain-of-function, a loss-of-function or a complex phenotype (some parameters are modified resulting in a loss-of-function while others are affected leading to a gain-of-function), evaluating the peak current amplitude, the steady-state, the desensitization rate and the deactivation rate of NMDAR currents.

These parameters have been studied in several missense GluN genetic variants (GluN1-R548W, V656M, P805S, M813T; GluN2A-N490H, V563L, V639I, G664S; GluN2B-W559R, S628C, C746Y, M818L, M829V and the co-expression of two GluN2B variants D732V and M829V) (see **table 18**).

GluN variant	Normalized current density (% vs. wild-typ)	S-S (%)	Desensitization rate (msec)	Deactivation rate (msec)	Functional stratification
GluN1 wt	100 ± 29.34 (N=17)	58.45 ± 2.805 (N=17)	1.539 ± 0.3317 (N=9)	0.3660 ± 0.031 (N=10)	
GluN1-R548W	72.22 ± 9.307 (N=5) ns	**75.5 ± 6.057 (N=4) ***	1.91 ± 0.6351 (N=3) ns	**4.983 ± 2.896 (N=4) ****	GOF
GluN1-V656M	59.72 ± 20.11 (N=7) ns	**72.10 ± 3.257 (N=6) ****	**4.165 ± 1.154 (N=4) ***	0.294 ± 0.023 (N=5) ns	GOF
GluN1-P805S	61.41 ± 21.6 (N=12) ns	66.61 ± 6.435 (N=8) ns	**3.908 ± 0.9675 (N=5) ***	0.5414 ± 0.034 (N=7) ns	GOF
GluN1-M813T	**15.41 ± 4.569 (N=6) ****	58.53 ± 8.625 (N=3) ns	ND	ND	LOF
GluN2A wt	100 ± 30.76 (N=7)	42.24 ± 2.334 (N=7)	0.8267 ± 0.1091 (N=6)	0.2101 ± 0.032 (N=7)	
GluN2A-N490H	106.4 ± 35.38 (N=9) ns	47.7 ± 4.468 (N=8) ns	1.201 ± 0.2081 (N=7) ns	0.3086 ± 0.066 (N=7) ns	Uncertain
GluN2A-V563L	**22.12 ± 4.4 (N=9) ***	52.71 ± 8.272 (N=8) ns	0.4425 ± 0.082 (N=4) ns	0.2767 ± 0.074(N=6) ns	LOF
GluN2A-V639I	51.51 ± 15.49 (N=5) ns	**80.3 ± 7.838 (N=5) ****	0.255 ± 0.185 (N=2) ns	**0.4267 ± 0.095 (N=3) ***	GOF
GluN2A-G664S	146 ± 51.42 (N=8) ns	42.423 ± 4.768 (N=8) ns	0.6583 ± 0.079 (N=6) ns	0.23 ± 0.02 (N=6) ns	Uncertain
GluN2B wt	100 ± 28.36 (N=17)	58.87 ± 2.678 (N=18)	1.616 ± 0.3065 (N=9)	0.3656 ± 0.028 (N=11)	
GluN2B-W559R	ND	ND	ND	ND	LOF
GluN2B-S628C	50.85 ± 17.45 (N=5)	**77.39 ± 5.889 (N=7) ***	2.765 ± 1.043 (N=4) ns	**0.833 ± 0.1584 (N=6) *****	GOF
GluN2B-C746Y	**24.95 ± 8.814 (N=6) ***	**39.72 ± 4.832 (N=5) ***	1.243 ± 0.4686 (N=4) ns	**0.195 ± 0.023 (N=4) ****	LOF
GluN2B-M818L	45.07 ± 19.37 (N=5) ns	67.96 ± 0.8511 (N=5) ns	**3.995 ± 0.8974 (N=4) ***	**1.373 ± 0.267 (N=3) ****	GOF
GluN2B-M829V	68.84 ± 29.67 (N=6) ns	59.88 ± 8.615 (N=10) ns	4.518 ± 2.1 (N=4) ns	0.5143 ± 0.1226 (N=7) ns	Uncertain
GluN2B-D732V+M829V	159.3 ± 50.99 (N=10) ns	50.84 ± 13.7 (N=5) ns	3.334 ± 1.495 (N=5) ns	0.335 ± 0.047 (N=6) ns	Uncertain

Table 18. Biophysical characterization of GRIN missense variants associated NMDAR-mediated currents in cell lines. Biophysical parameters have been statistically evaluated in HEK293T cells transiently co-transfected with GluN1-GluN2 subunits (GOF: gain-of-function; LOF: loss-of-function; ND: Not detectable). Non-parametric Mann-Whitney test for non-normal distribution and unpaired t-test with Welch's correction for normal distribution; ns (not significant), P-value > 0.05; *, P-value < 0.05; **, P-value > 0.01; ***, P-value > 0.001; ****, P-value < 0.0001.

NMDAR-mediated current amplitudes are completely abolished in GluN2B-W559R (loss-of-function) and significantly reduced in GluN1-M813T, GluN2A-V563L and GluN2B-C746Y (loss-of-function). Steady-state is increased in GluN1-R548W, V656M, GluN2A-V639I, and GluN2B-S628C (gain-of-function) whereas it is decreased in GluN2B-C746Y (loss-of-function). Slower desensitization rates are observed in GluN1-V656M, P805S and GluN2B-M818L (gain-of-function) and slower deactivation rates are detected in GluN1-R548W, GluN2A-V639I, GluN2B-S628C and GluN2B-M818L (gain-of-function). A faster deactivation rate is observed in GluN2B-C746Y (loss-of-function). GluN2A-N490H, G664S and GluN2B-M829V, D732V+M829V did not present significant changes, presenting uncertain pathogenicity (see **figure 77** and **table 18**).
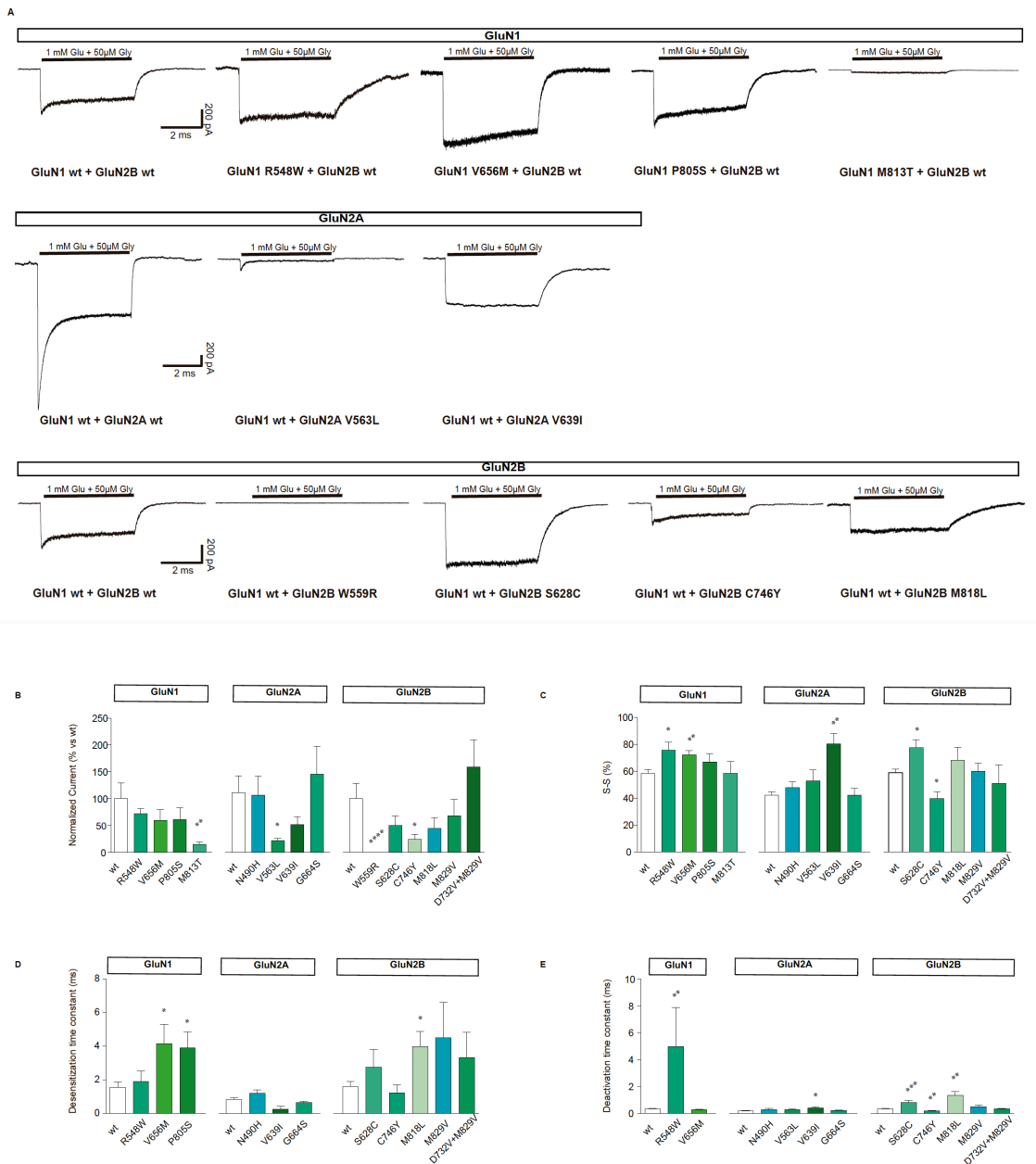
Figure 77. Functional annotation of GRIN variants. **A**, Representative whole-cell currents evoked by rapid application of 1 mM glutamate plus 50 μM glycine (0.5 second duration; -60 mV) in HEK293T cells expressing GluN1, GluN2A or GluN2B wt/mutated. **B-E**, Bar graph representing normalized peak currents ± SEM of cells transfected with the genetic variants vs wild-type (**B**), S-S % (**C**), desensitization time constant (**D**) and deactivation time constant (**E**) (N = 3-17 cells per condition; ns, P-value > 0.05; *, P-value < 0.05; **, P-value > 0.01; ***, P-value > 0.001; ****, P-value < 0.0001; non-parametric Mann-Whitney test).

1.2.4. Analysis of *GRIN* variants heterozygous expression

GRIN-related disorders have an autosomal dominant pattern, with the presence of *GRIN* mutations in heterozygosity. Accordingly, the previously used immunofluorescence and electrophysiological approaches were adapted to evaluate the co-expression of a wild-type subunit together with a mutated allele for a given subunit in order to study the impact of this co-expression in the NMDAR surface trafficking and the receptor functional aspects.

Thus, this approach was aimed to determine whether the lack of surface expression and/or the reduction in NMDAR currents in some particular variants might be rescued by the presence of a wild-type subunit or, in the contrary, NMDAR mutated alleles might have a detrimental impact on the non-mutated subunit.

To determine *GRIN* variants heterozygosity effect on NMDARs surface trafficking, *GRIN* missense and indel variants that were not reaching the cell surface when expressed in homozygosis, and nonsense variants affecting all GluN domains, were selected. These variants were expressed in COS-7 cells in combination with wild-type plasmids and the corresponding complementary subunit (GluN1 for GluN2 variants and GluN2 for GluN1 variants). An immunofluorescence approach, using a specific antibody against the tag of the complementary subunit was used in order to detect the total amount of NMDARs that were trafficking to the cell surface. This experimental approach revealed that missense and indel variants with a lack of surface expression when expressed in homozygosis, do not exert a dominant negative effect on the wild-type subunit, showing no significant changes in the total density of NMDARs in the surface (see **figure 78**). Nevertheless, the surface density of NMDARs was reduced in nearly a 50 % in most of the nonsense variants which are affecting the ATD, the LBD and the TMD of GluN2A and GluN2B subunits, but not the GluN1 subunit, suggesting a dominant negative effect of *GRIN2* nonsense variants on NMDAR biogenesis (see **figure 78**). There were some specific exceptions such as GluN2A-E58*, GluN2A-H595Rfs*28, GluN2A-H595Lfs*60 and GluN2B-S34Qfs*25 (see **figure 78**, **panels B, C**, red arrows), probably due to limitations in the sensitivity of the immunofluorescence approach, given that, performing electrophysiological recordings of these variants demonstrated that these mutations behave equally than the rest of nonsense variants (Santos-Gómez A. et al., 2020, data not shown, experiments performed by F. Miguez).
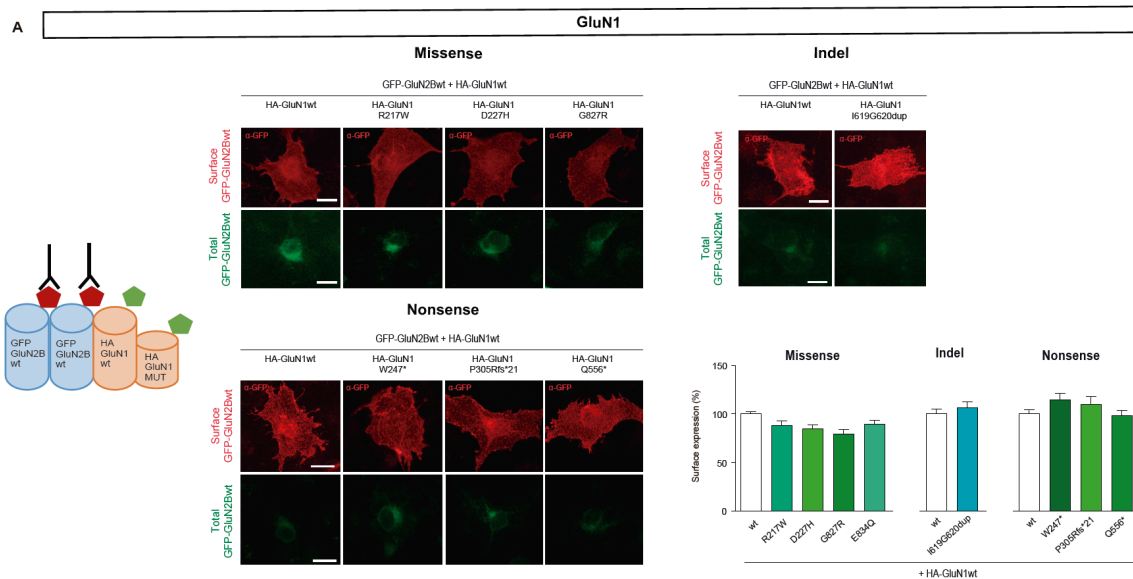

Figure 78. Immunofluorescence analysis of COS-7 cells transiently co-transfected with HA-GluN1wt + HA-GluN1 mutated accompanied by a GFP-GluN2Bwt plasmid (**A**), GFP-GluN2A wt + GFP-GluN2A mutated accompanied by an HA-GluN1wt plasmid (**B**) or GFP-GluN2B wt + GFP-GluN2B mutated accompanied by an HA-GluN1wt plasmid. Surface NMDAR receptors, using an antibody against the tag of the complementary subunit, were detected by GFP (**A**) or HA (**B, C**) immunostaining (red channel), while green channel is endogenous GFP signal without amplification as transfection control. Scale bar = 10 μm; Bar graphs representing the normalized surface expression of the corresponding complementary GluN subunit in each case, compared to wild-type (3 independent experiments, > 20 cells per condition; ns, P-value > 0.05; *, P-value < 0.05; **, P-value > 0.01; ***, P-value > 0.001; ****, P-value < 0.0001; ANOVA + Bonferroni post hoc test). Red arrows represent *GRIN* variants discrepancies.
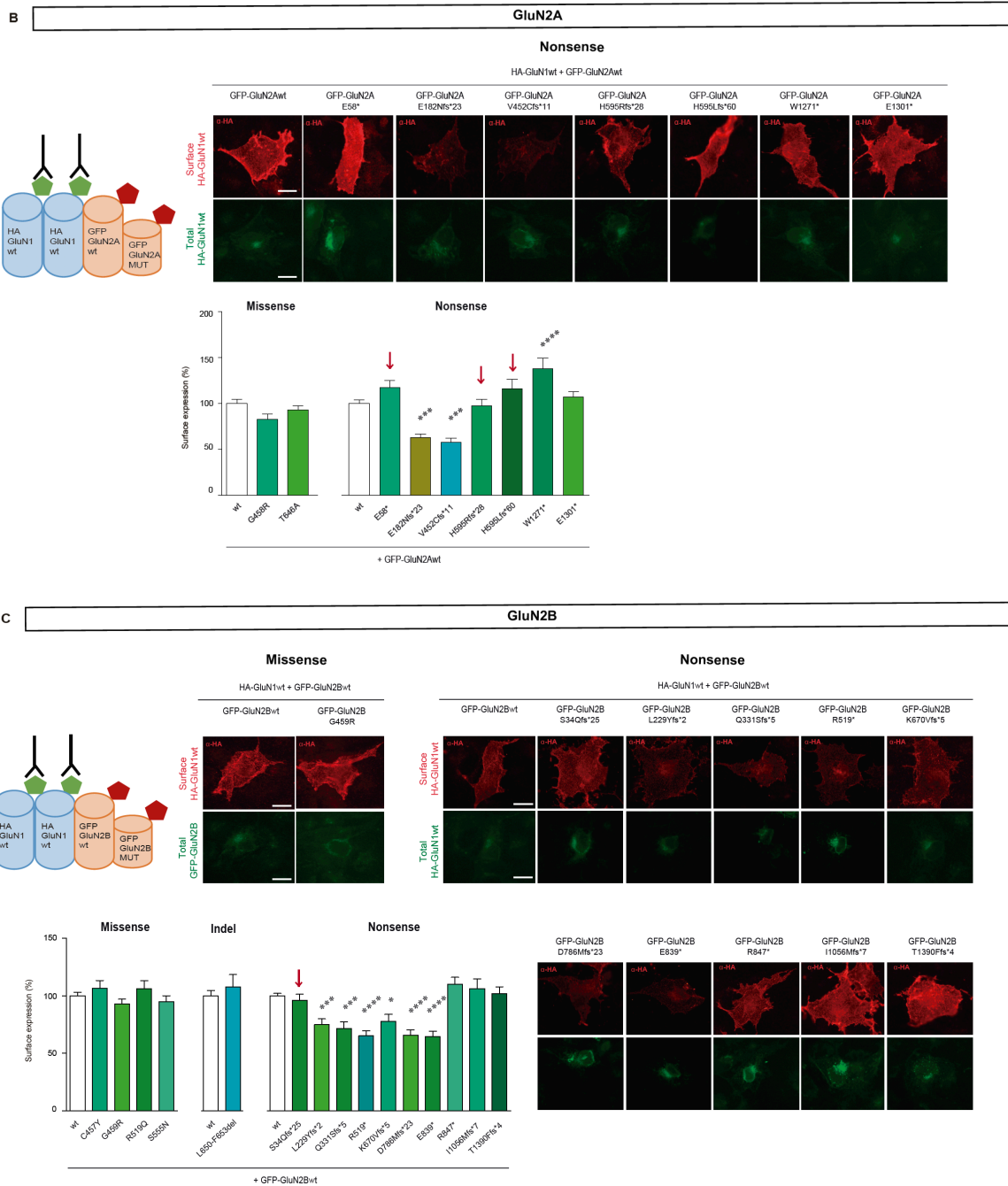
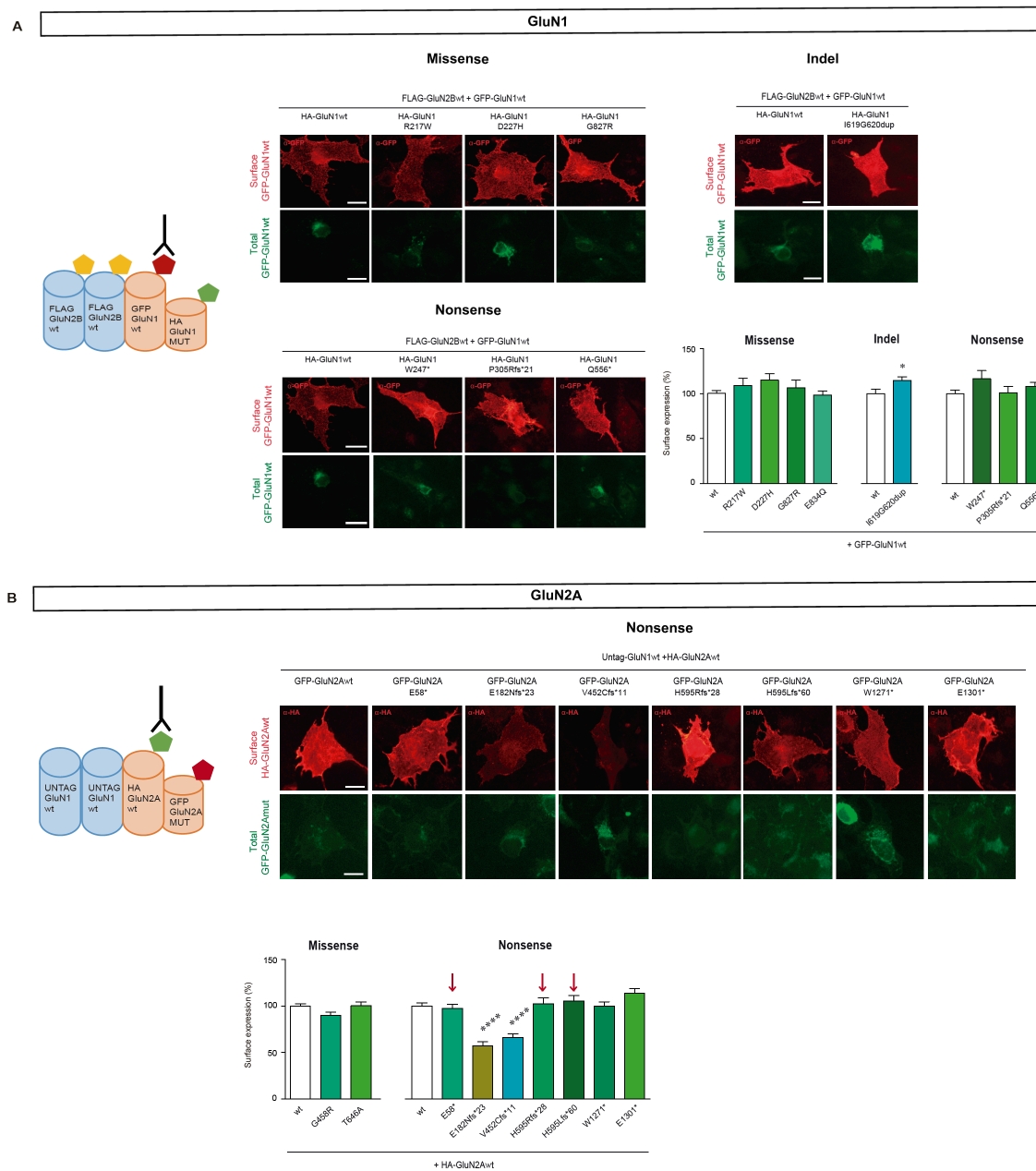**Figure 78: continued.** Immunofluorescence analysis of COS-7 cells transiently co-transfected with HA-GluN1wt + HA-GluN1 mutated accompanied by a GFP-GluN2Bwt plasmid (**A**), GFP-GluN2A wt + GFP-GluN2A mutated accompanied by an HA-GluN1wt plasmid (**B**) or GFP-GluN2B wt + GFP-GluN2B mutated accompanied by an HA-GluN1wt plasmid. Surface NMDAR receptors, using an antibody against the tag of the complementary subunit, were detected by GFP (**A**) or HA (**B, C**) immunostaining (red channel), while green channel is endogenous GFP signal without amplification as transfection control. Scale bar = 10 μm; Bar graphs representing the normalized surface expression of the corresponding complementary GluN subunit in each case, compared to wild-type (3 independent experiments, > 20 cells per condition; ns, P-value > 0.05; *, P-value < 0.05; **, P-value > 0.01; ***, P-value > 0.001; ****, P-value < 0.0001; ANOVA + Bonferroni post hoc test). Red arrows represent *GRIN* variants discrepancies.

These findings were also confirmed with a similar immunofluorescence approach, using differently tagged plasmids in order to detect the specific sub-population of NMDARs containing wild-type subunits (see **figure 79**).

This approach revealed that *GRIN1* variants do not exert a dominant negative effect on the wild-type subunit, independently of the type of variant. Moreover, *GRIN2A* missense variants do not exert this effect while nonsense variants reduce the wild-type-containing receptors surface expression (see **figure 79**). Same *GRIN2A* exceptions were observed with this modified approach (GluN2A-E58*, H595Rfs*28, H595Lfs*60) (see **figure 79,** red arrows). *GRIN2B* variants were not evaluated due to limitations in tagged-GluN2B plasmids availability, given that we only had GFP- and Flag-tagged *GRIN2B* plasmids and there was 'Flag' unespecifity with available antibodies.
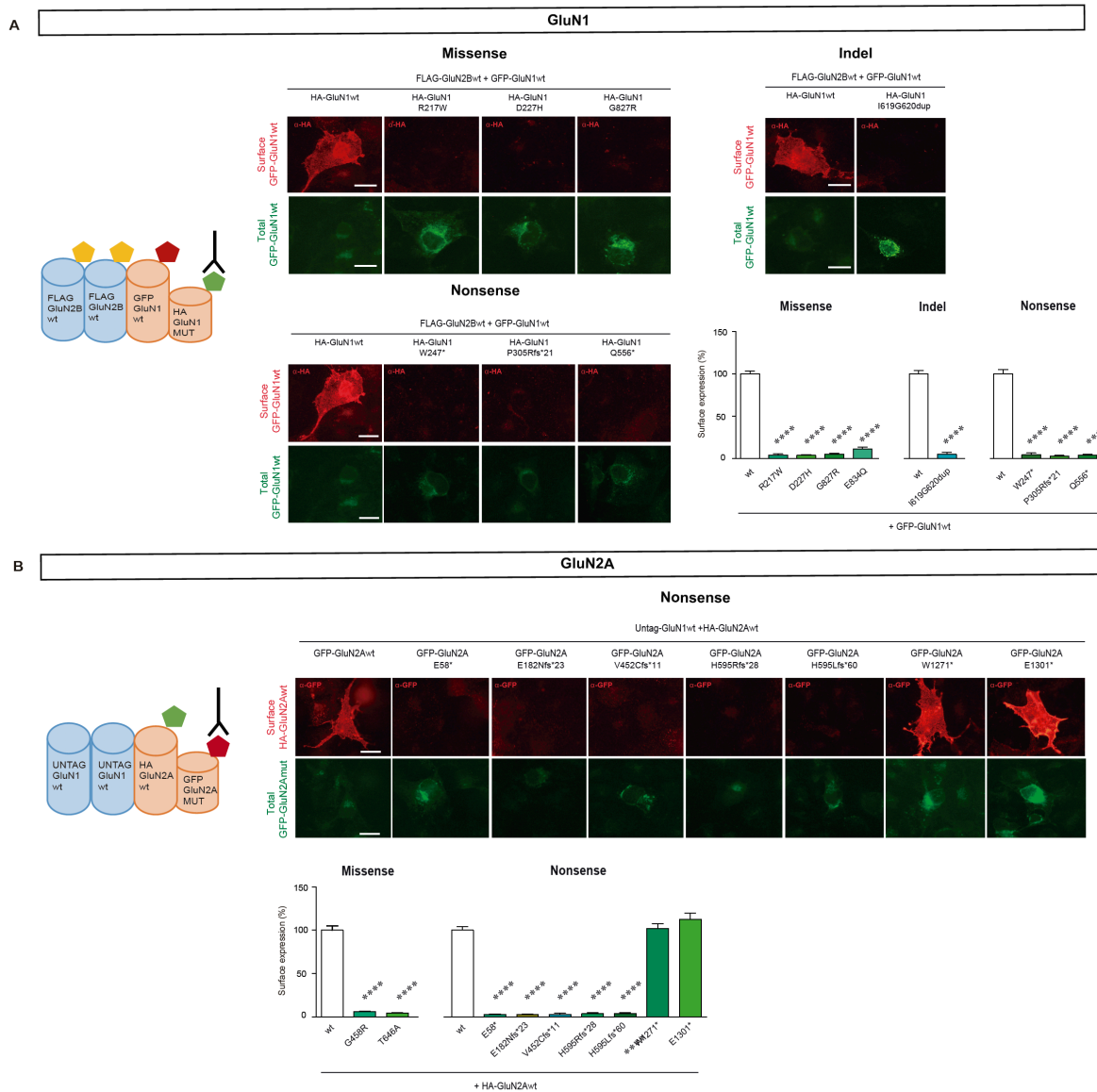
Figure 79. Immunofluorescence analysis of COS-7 cells transiently co-transfected with GFP-GluN1wt + HA-GluN1 mutated accompanied by a Flag-GluN2Bwt plasmid (**A**), or HA-GluN2A wt + GFP-GluN2A mutated accompanied by an Untag-GluN1wt plasmid (**B**). Surface wild-type-containing NMDAR receptors, using an antibody against the tag of the wild-type subunit, were detected by GFP (**A**) or HA (**B**) immunostaining (red channel) against the plasmid tag, while green channel is endogenous GFP signal without amplification as transfection control. Scale bar = 10 μm; Bar graphs representing the normalized surface expression of the wild-type GluN subunit in each case, compared to wild-type (3 independent experiments, > 20 cells per condition; ns, P-value > 0.05; *, P-value < 0.05; **, P-value > 0.01; ***, P-value > 0.001; ****, P-value < 0.0001; ANOVA + Bonferroni post hoc test). Red arrows represent *GRIN* variants discrepancies.
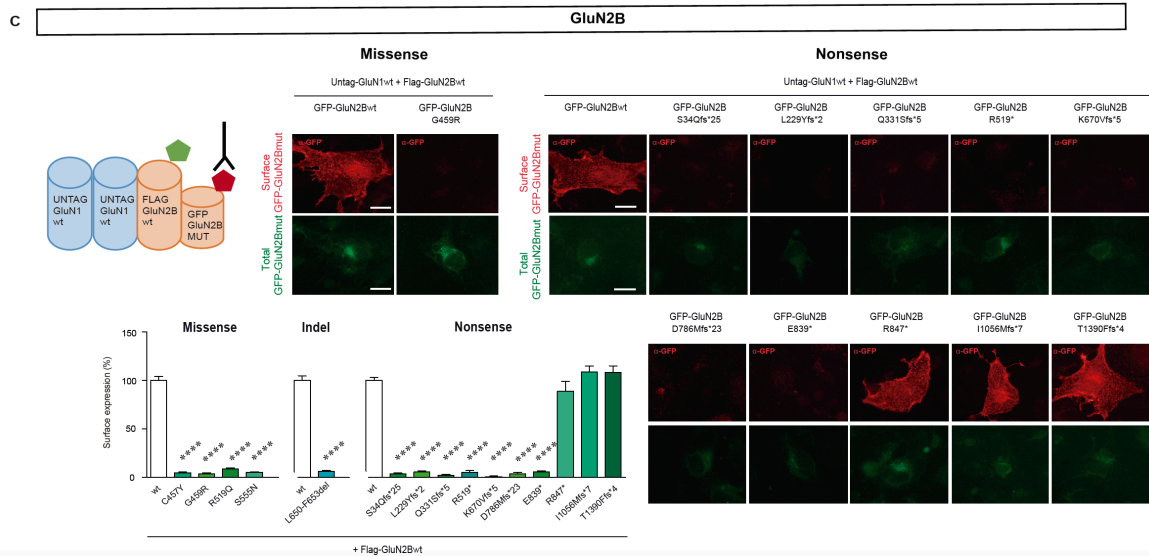
Moreover, this approach was also adapted to specifically detect the sub-population which contains the mutated allele in order to demonstrate that the mutated alleles of *GRIN* variants which never reach the cell surface when expressed in homozygosis, independently whether they exert a dominant negative effect over the wild-type subunit or not, are not rescued by the wild-type subunit. Thus, NMDARs which are able to traffic normally to the cell surface do not contain those mutated alleles (see **figure 80**).

Figure 80. Immunofluorescence analysis of COS-7 cells transiently co-transfected with GFP-GluN1wt + HA-GluN1 mutated accompanied by a Flag-GluN2Bwt plasmid (**A**), HA-GluN2A wt + GFP-GluN2A mutated accompanied by an Untag-GluN1 wt plasmid (**B**), and Flag-GluN2B wt + GFP-GluN2B mutated accompanied by an Untag-GluN1 wt plasmid (**C**). Surface NMDAR receptors, using an antibody against the tag of the mutated subunit, were detected by GFP (**B, C**) or HA (**A**) immunostaining (red channel) against the plasmid tag, while green channel is endogenous GFP signal without amplification as transfection control. Scale bar = 10 μm; Bar graphs representing the normalized surface expression of the mutated GluN subunit in each case, compared to wild-type (3 independent experiments, > 20 cells per condition; ns, P-value > 0.05; *, P-value < 0.05; **, P-value > 0.01; ***, P-value > 0.001; ****, P-value < 0.0001; ANOVA + Bonferroni post hoc test).

Figure 80: continued. Immunofluorescence analysis of COS-7 cells transiently co-transfected with GFP-GluN1wt + HA-GluN1 mutated accompanied by a Flag-GluN2Bwt plasmid (**A**), HA-GluN2A wt + GFP-GluN2A mutated accompanied by an Untag-GluN1 wt plasmid (**B**), and Flag-GluN2B wt + GFP-GluN2B mutated accompanied by an Untag-GluN1 wt plasmid (**C**). Surface NMDAR receptors, using an antibody against the tag of the mutated subunit, were detected by GFP (**B, C**) or HA (**A**) immunostaining (red channel) against the plasmid tag, while green channel is endogenous GFP signal without amplification as transfection control. Scale bar = 10 μm; Bar graphs representing the normalized surface expression of the mutated GluN subunit in each case, compared to wild-type (3 independent experiments, > 20 cells per condition; ns, P-value > 0.05; *, P-value < 0.05; **, P-value > 0.01; ***, P-value > 0.001; ****, P-value < 0.0001; ANOVA + Bonferroni post hoc test).

Next, electrophysiological recordings were performed in HEK293T cell lines, transiently expressing this combination of wild-type and mutated alleles of some of the selected *GRIN* variants affecting surface trafficking to confirm results from immunofluorescence approaches. Patch-clamp experiments in whole-cell configuration allowed to evaluate the peak current amplitude of transiently transfected HEK293T cells, after a fast glutamate (1 mM) and glycine (50 μM) application (0,5 s).

Previously, the group demonstrated that *GRIN2*A and *GRIN2*B nonsense variants affecting the ATD, LBD, and TMD were reducing almost to a 50 % the peak current amplitude while *GRIN1* nonsense variants were not affecting the peak current amplitude, independently of the domain which was affected (Santos-Gómez A. et al., 2020, data not shown, experiments performed by F. Miguez). These results confirmed the data from immunofluorescence analysis of *GRIN* nonsense variants.

In this Thesis, similar approach was performed to analyze missense and indel variants affecting *GRIN1*, *GRIN2A* and *GRIN2B* genes. These experiments revealed that missense and indel variants which were affecting surface trafficking (GluN1-R217W, G827R, I619G620dup; GluN2A G458R; and GluN2B-G459R, S555N), when expressed in heterozygosis, do not have a detrimental effect on the wild-type subunit because peak current amplitude is not reduced, confirming immunofluorescence results and a distinct behavior between indel/missense (no detrimental effect) and nonsense (dominant negative effect) GluN2 variants (see **figure 81** and **table 19**).
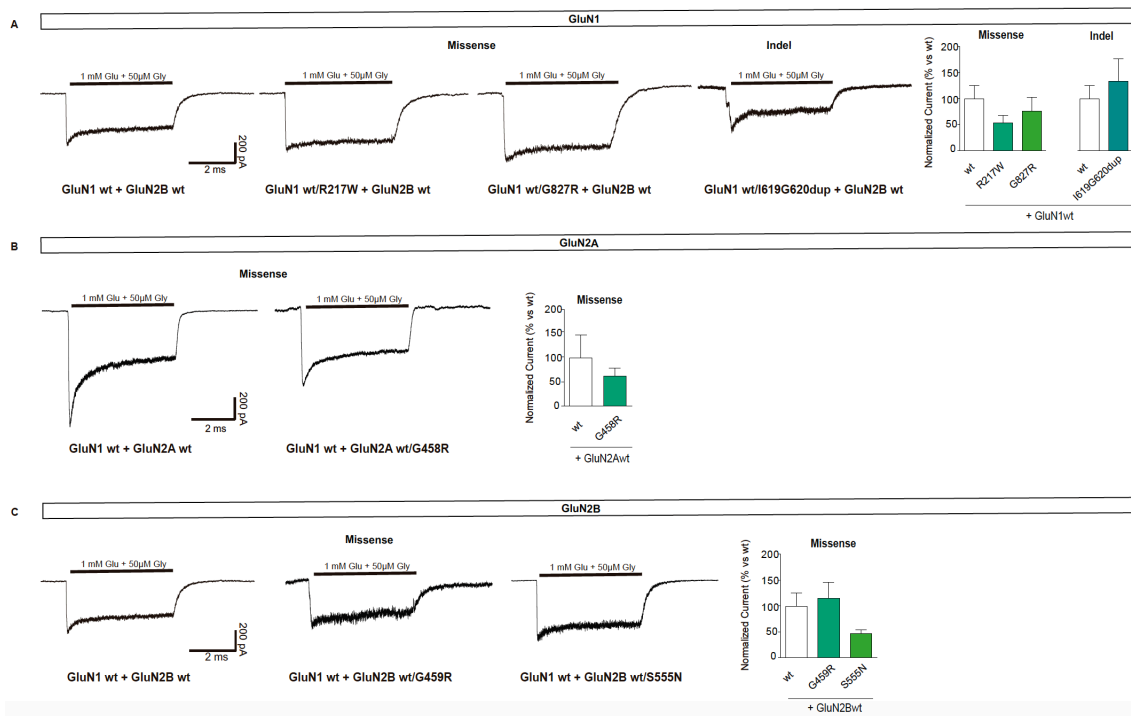
Figure 81. Functional annotation of GRIN heterozygous variants. **A-C**, Representative whole-cell currents evoked by rapid application of 1 mM glutamate plus 50 µM glycine (0.5 second duration; -60 mV) in HEK293T cells expressing GluN1 wt + GluN1 wt/mutated accompanied by GluN2B wt (**A**); GluN2A wt + GluN2A wt/mutated accompanied by GluN1 wt (**B**); and GluN2B wt + GluN2B wt/mutated accompanied by GluN1 wt (**C**); Bar graphs representing average normalized peak currents comparing with wild-type ± SEM of cells transfected with the heterozygous conditions (N = 4-18 cells per condition; ns, P-value > 0.05; *, P-value < 0.05; **, P-value > 0.01; ***, P-value > 0.001; ****, P-value < 0.0001; non-parametric Mann-Whitney test).

GluN variant	Normalized current density (% vs. wild-type)
GluN1 wt/wt	100 ± 25.65 (N=16)
GluN1 wt/R217W	53.64 ± 13.63 (N=18) ns
GluN1 wt/G827R	76.05 ± 26.95 (N=7) ns
GluN1 wt/I619G620dup	133.6 ± 43.14 (N=9) ns
GluN2A wt/wt	100 ± 47.4 (N=4)
GluN2A wt/G458R	62.47 ± 16.75 (N=5) ns
GluN2B wt/wt	100 ± 25.65 (N=14)
GluN2B wt/G459R	115 ± 31.22 (N=8) ns
GluN2B wt/S555N	46.56 ± 7.65 (N=15) ns

Table 19. Table summarizing sample size and average normalized peak currents comparing with wild-type ± SEM of cells transfected with the heterozygous conditions (N = 4-18 cells per condition; ns, P-value > 0.05; *, P-value < 0.05; **, P-value > 0.01; ***, P-value > 0.001; ****, P-value < 0.0001; non-parametric Mann-Whitney test).

Additionally, two missense variants affecting the GluN1 and the GluN2B subunits, that were previously annotated as loss-of-function regarding peak current amplitude, have been expressed in heterozygosity to evaluate, using the same electrophysiological approach, whether there is a detrimental effect on the wild-type subunit or a rescue of the mutated subunit in terms of the receptor function. This approach revealed that *GRIN2B* missense variants (*e.g.* GluN2B-I751T) exert a dominant negative effect in terms of NMDAR function by reducing the peak current amplitude of the heterozygous condition comparing with the wild-type while *GRIN1* variants (*e.g.* GluN1-G620R) do not exert this effect (see **figure 82** and **table 20**).
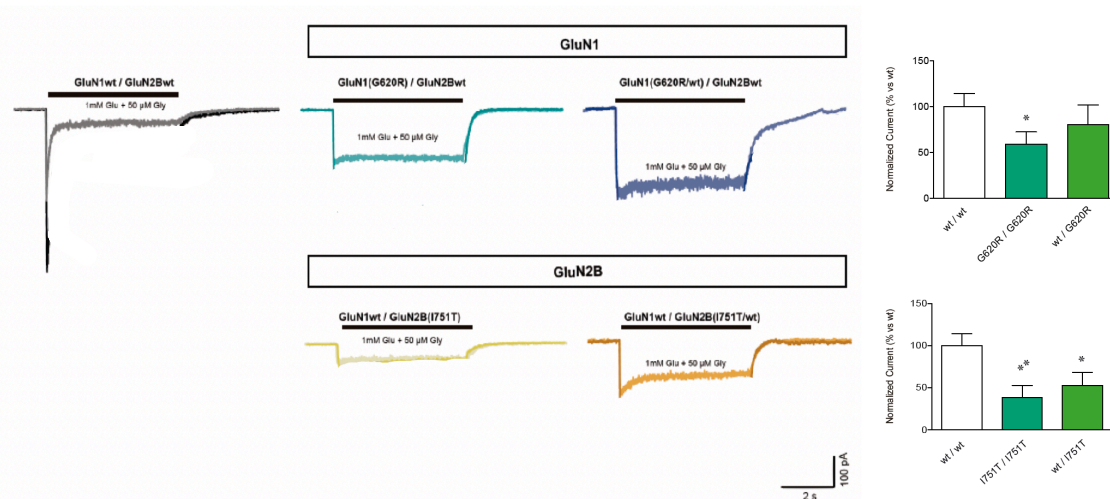
Figure 82. Functional annotation of GRIN heterozygous variants. Representative whole-cell currents evoked by rapid application of 1 mM glutamate plus 50 µM glycine (0.5 second duration; -60 mV) in HEK293T cells expressing GluN1 wt + GluN1 wt/mutated accompanied by GluN2B wt (**A**); and GluN2B wt + GluN2B wt/mutated accompanied by GluN1 wt (**B**); Bar graphs representing average normalized peak currents comparing with wild-type ± SEM of cells transfected with the heterozygous conditions (N = 7-17 cells per condition; ns, P-value > 0.05; *, P-value < 0.05; **, P-value > 0.01; ***, P-value > 0.001; ****, P-value < 0.0001; unpaired t-test with Welch's correction for normal distribution and non-parametric Mann-Whitney test for non-normal distribution).

GluN variant	Normalized current density (% vs. wild-type)
GluN1 wt/wt	100 ± 14.45 (N=17)
GluN1 G620R/G620R	59.04 ± 13.29 (N=7) *
GluN1 wt/G620R	80.08 ± 21.50 (N=7) ns
GluN2B wt/wt	100 ± 14.45 (N=17)
GluN2B I751T/I751T	38.35 ± 14.51 (N=10) **
GluN2B wt/I751T	52.56 ± 15.83 (N=8) *

Table 20. Table summarizing sample size and average normalized peak currents comparing with wild-type ± SEM of cells transfected with the heterozygous conditions (N = 7-17 cells per condition; ns, P-value > 0.05; *, P-value < 0.05; **, P-value > 0.01; ***, P-value > 0.001; ****, P-value < 0.0001; unpaired t-test with Welch's correction for normal distribution and non-parametric Mann-Whitney test for non-normal distribution).

1.2.5.   Impact of *GRIN* variants on neuronal morphology

Dendritic spines are crucial for neuronal function because they represent the central structure where synaptic communication occurs (Morgado-Bernal I. et al., 2011). Furthermore, it is well known that several brain disorders are associated with abnormal dendritic spines (Knobloch M. et al., 2008; Penzes P. et al., 2011), because their formation and maintenance rely on the correct synaptic activity. Thus, given the importance of NMDARs on excitatory synapses, we hypothesized that GluN genetic variants, might be affecting dendritic spines development in patients with *GRIN*-related disorders.

The overexpression of GluN variants in primary hippocampal neurons and an adapted immunofluorescence approach allowed to measure neuronal morphological parameters as well as synaptic plasticity processes. After transient transfection at DIV11 of selected recruited *GRIN* variants, neurons were treated with D-AP5 (100 µM) to block NMDAR-activity. At DIV15, D-AP5 was removed, but Krebs Ringer solution (124 mM NaCl, 2 mM KCl, 1.24 mM KH$_2$PO$_4$, 1.3 mM MgCl$_2$, 2.5 mM CaCl$_2$, and 30 mM glucose in 25 mM HEPES at pH 7.4) supplemented with 1 mM MgCl$_2$ and 1 µM TTX to avoid neuronal depolarization, was added. This D-AP5 removal plus the addition of supplemented Krebs Ringer solution allowed NMDAR-activity in a simulated basal condition, without neuronal stimulation.

Subsequently, neurons were fixed at 4 ºC to maintain neuronal morphology, permeabilized and stained with a specific antibody against the *GRIN* variants plasmids' tag to highlight the entire neuronal shape and perform dendritic spines quantification and morphology classification.

This approach revealed that spine density was significantly reduced in neurons expressing GluN2A and GluN2B nonsense variants, affecting distinct NMDAR domains, such as E182Nfs*23 (ATD) and V452Cfs*11 (LBD) in the GluN2A subunit, and R519* (LBD), E839* (TMD) and R847* (CTD) in the GluN2B subunit (see **figure 83**). These variants were known to be associated with a NMDAR loss-of-function by affecting surface trafficking when occurring in the ATD, LBD or TMD (GluN2A-E182Nfs*23, V452Cfs*11; GluN2B-R519*, E839*) or membrane docking when altering the CTD (GluN2B-R847*). This reduction is due to a decrease in the different spine subtypes, but specifically, in 'stubby' spines (see **figure 83**) which are the predominant ones when neuronal cultures are at DIV14-15.

Moreover, neurons overexpressing some GluN2B missense variants, alone or in combination with other mutations (GluN2B-P553T, GluN2B-K1293del and GluN2B-K1293del+Homer2-E221K) also experienced a deficient spines development (see **figure 83**). Nevertheless, a particular missense variant affecting the C-terminal domain of the GluN2A subunit (GluN2A-T888R) seem to increase spines density although there is not statistical significance (see **figure 83**).
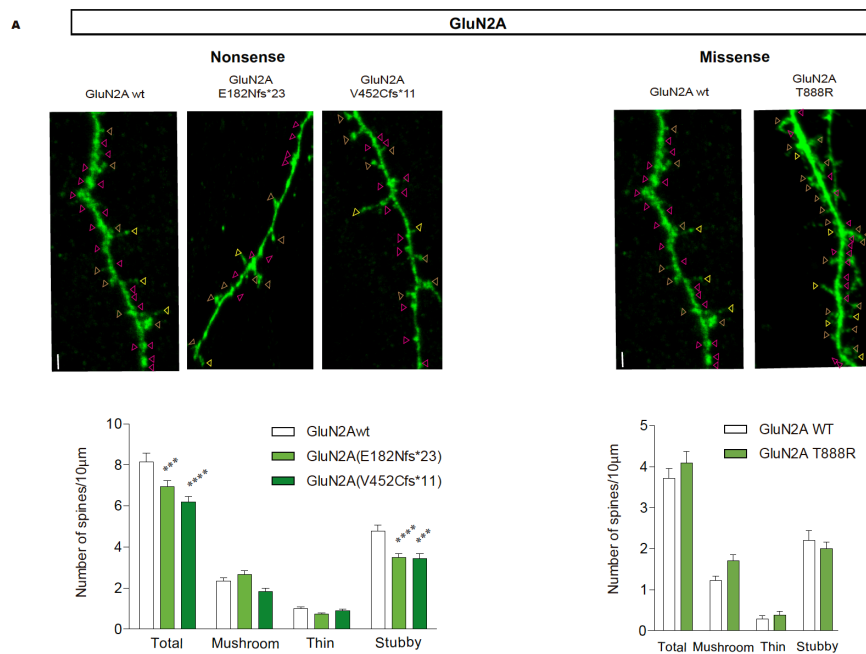

Figure 83. **A, B,** Representative images of murine primary hippocampal neurons transfected with GFP-GluN2A wt/mutated (**A**) or GFP-GluN2B wt/mutated (**B**). Triangles are indicating dendritic spines: stubby (pink), mushroom (brown) and thin (yellow). Scale bar = 3 μm. Bar graphs representing the quantification of spine density and morphology in neurons at basal conditions (>20 dendrites per condition; ns, P-value > 0.05; *, P-value < 0.05; **, P-value > 0.01; ***, P-value > 0.001; ****, P-value < 0.0001; two-way ANOVA + Bonferroni post hoc test).
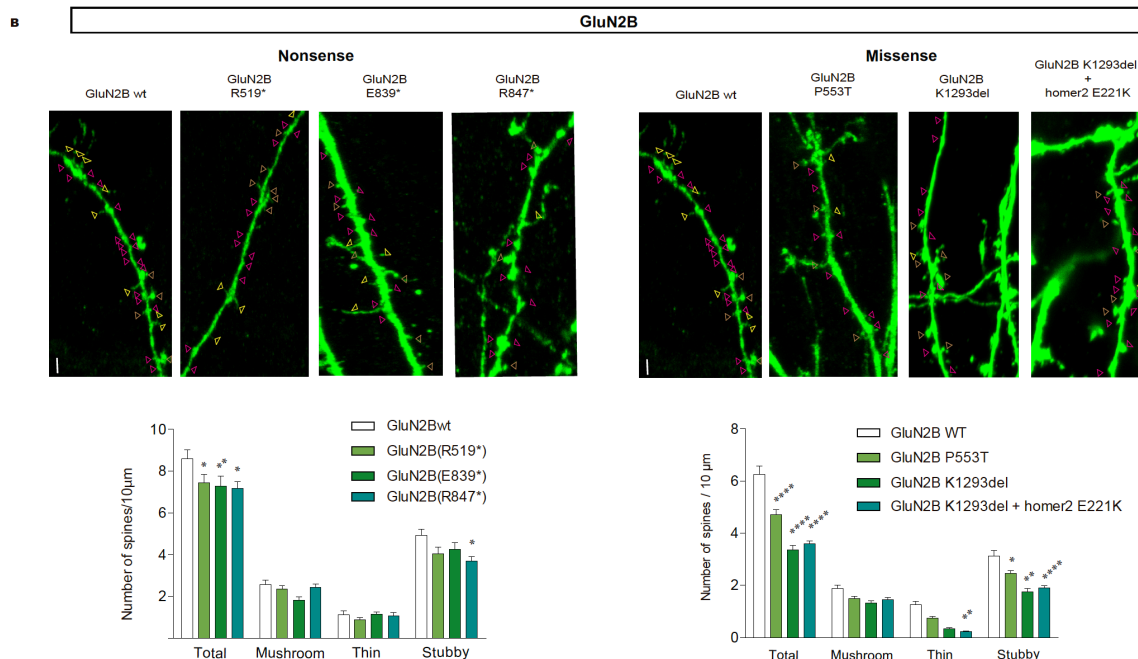
Figure 83: continued. **A, B,** Representative images of murine primary hippocampal neurons transfected with GFP-GluN2A wt/mutated (**A**) or GFP-GluN2B wt/mutated (**B**). Triangles are indicating dendritic spines: stubby (pink), mushroom (brown) and thin (yellow). Scale bar = 3 μm. Bar graphs representing the quantification of spine density and morphology in neurons at basal conditions (>20 dendrites per condition; ns, P-value > 0.05; *, P-value < 0.05; **, P-value > 0.01; ***, P-value > 0.001; ****, P-value < 0.0001; two-way ANOVA + Bonferroni post hoc test).

1.2.6. Acceleration of functional annotation: GluN structural superimposition model validation

Despite the experimental pipeline is well-established, the biophysical characterization of the growing number of *GRIN* variants constitutes a bottleneck limiting the functional annotation, needed to determine the most suitable treatment. In order to accelerate the annotation and drug screening of *GRIN* variants, a GluN subunits structural superimposition model has been developed by our collaborator, Dra. Mireia Olivella (Universitat Vic). This model suggests that in terms of structural domains, GluN subunits are strongly overlapping. Thus, information from an annotated variant in one of the subunits might be used to infer the functional output of equivalent positions in the other GluN subunits (Santos-Gómez A. et al., 2021, *submitted*).

To validate this model, several artificial variants in the GluN2A subunit, based on equivalent mutations in the GluN2B subunit, were generated. Additionally, one GluN1 variant reported in a patient which is equivalent to a GluN2B variant from another patient was selected for this analysis. The surface expression and the functional aspects of these GluN variants were evaluated in order to demonstrate whether GluN2A and GluN1 variants present a similar behavior than GluN2B mutations whose impact was already known (see **figure 84** and **table 21**).
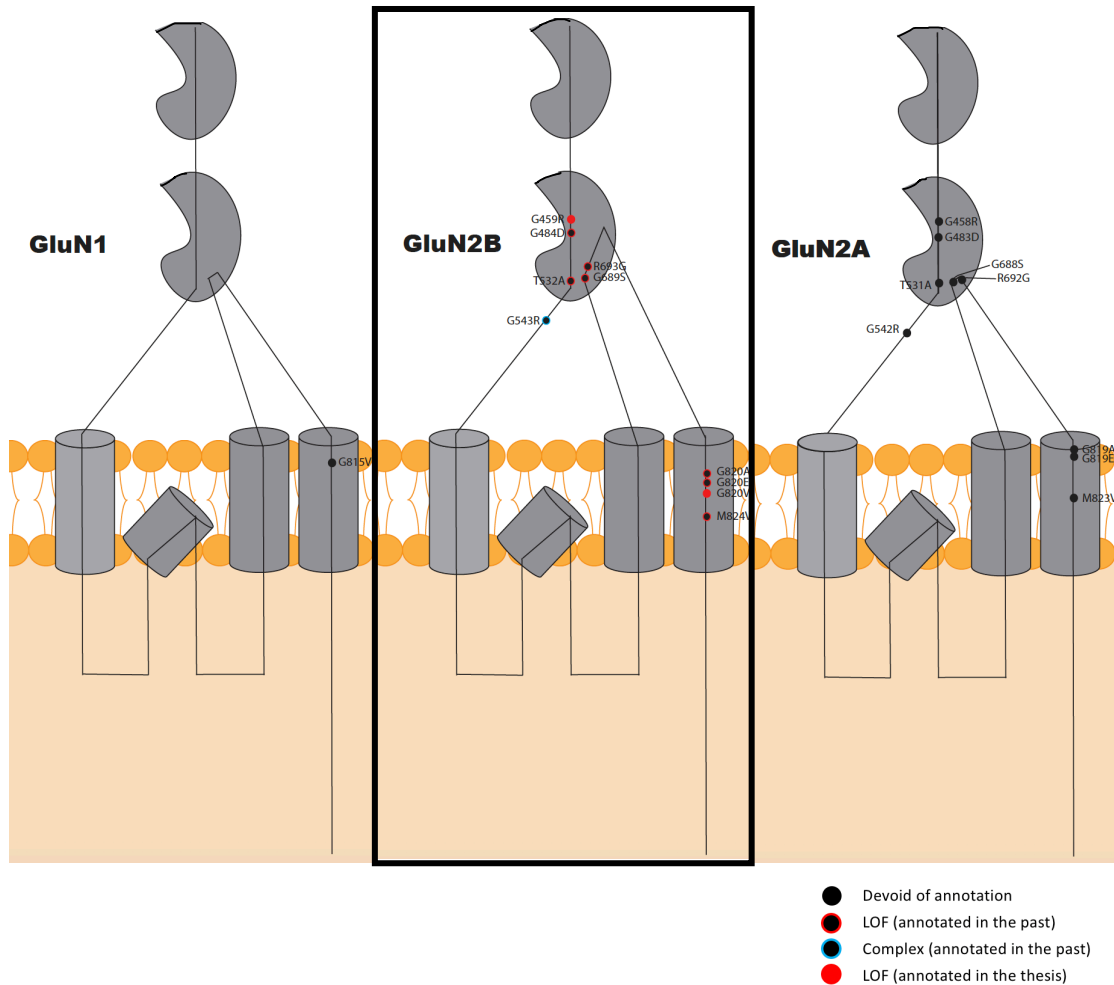
Figure 84. GluN2B variants from patients (previously annotated, a GluN1 equivalent variant from a patient (devoid of annotation) and GluN2A artificial equivalent genetic variants (devoid of annotation). Legend: Black, variant devoid of annotation; red circumference, variant annotated as LOF in the past; blue circumference, variant annotated as complex in the past; red dot, variant annotated as LOF in this Thesis; Abbreviations: LOF, loss-of-function.

A	GluN2B (patient)	GluN1 (patient)
	G820V	G815V

B	GluN2B (patients)	GluN2A (artificial)
	G459R	G458R
	G484D	G483D
	T532A	T531A
	G543R	G542R
	G689S	G688S
	R693G	R692G
	G820A	G819A
	G820E	G819E
	M824V	M823V

Table 21. A, A GluN2B variant from a patient (previously annotated) and a GluN1 equivalent variant from a patient (devoid of annotation); **B,** GluN2B variants from patients (previously annotated) and GluN2A artificial equivalent genetic variants (devoid of annotation).

Immunofluorescence and electrophysiological results that allowed the functional annotation of *GRIN2B* variants are available in this Thesis or in unpublished data from previous experiments carried out by the group (Thesis F. Miguez). In this section, immunofluorescence and electrophysiological results for equivalent *GRIN1* and *GRIN2A* genetic variants (devoid of annotation) will be presented to evaluate the potential validity of the GluN structural superimposition model.

Surface trafficking analysis to validate the GluN structural superimposition model

GRIN2B variants from patients were previously analyzed by an immunofluorescence approach in non-permeabilized transiently transfected COS-7 cells, using a specific antibody against the plasmid tag. This approach allowed to evaluate surface trafficking and revealed that only GluN2B-G459R from the selected variants was affecting the NMDAR surface expression while there were not significant changes in the other GluN2B variants comparing with the wild-type receptors.

COS-7 cells were also used to express *GRIN* equivalent variants (see **table 21** and **figure 84**). Immunofluorescence analyses of these cells revealed that among the selected GluN1 and GluN2A variants, only GluN2A(G458R) alters the ability of GluN subunits to reach the cell surface, replicating data from GluN2B variants (see **figure 85**). GluN2B-M824V and its equivalent position in the GluN2A subunit seemed to cause an increase in the NMDA receptors surface density (like GluN2A-R692G and GluN2A-G819A but not their equivalents in the GluN2B subunit) (see **figure 85**). Nevertheless, this increment might be due to the GluN overexpression in cell lines without necessarily being a gain-of-function.
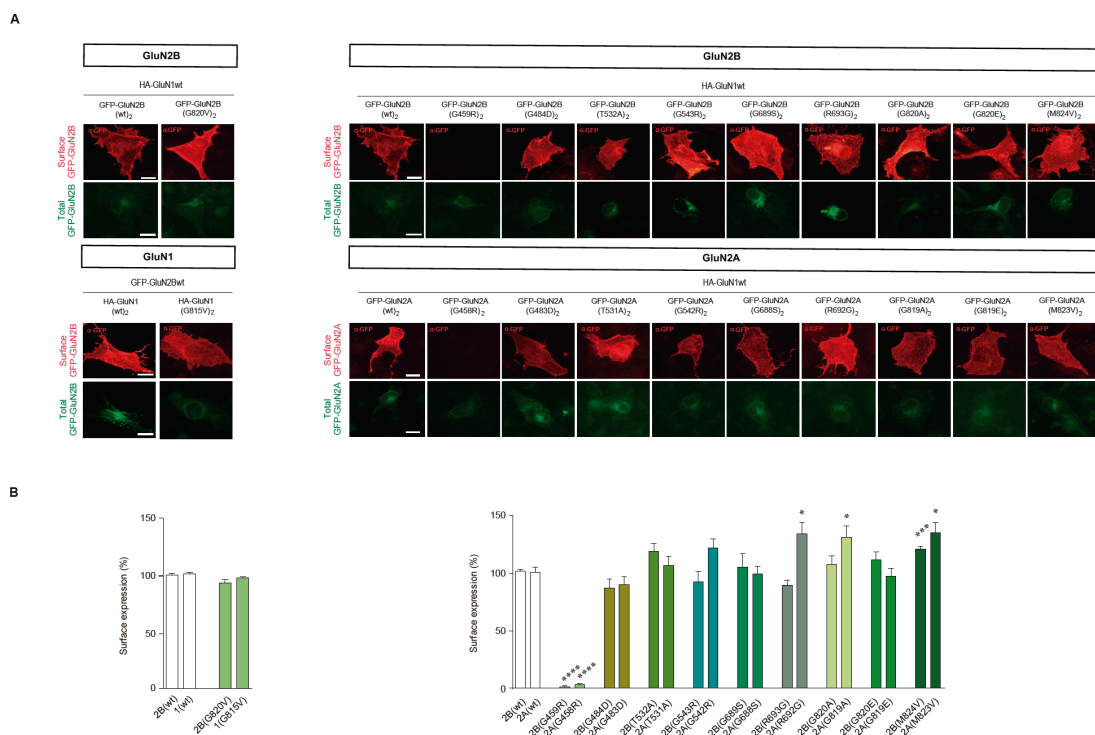

Figure 85. A, Immunofluorescence analysis of COS-7 cells transiently co-transfected with HA-GluN1wt+GFP-GluN2B wt or mutated (**A, upper panel**), GFP-GluN2Bwt+HA-GluN1 wt or mutated (**A, lower panel, left**) or HA-GluN1wt+GFP-GluN2A wt or mutated plasmids (**A, lower panel, right**). Surface NMDAR receptors were detected by GFP immunostaining (red channel) against the plasmid tag while green channel is endogenous GFP signal without amplification as transfection control. Scale bar = 10 μm. **B,** Bar graphs representing the normalized surface expression of *GRIN* variants affecting GluN1 or GluN2A vs. GluN2B proteins, compared to wild-type (3 independent experiments, > 20 cells per condition; ns, P-value > 0.05; *, P-value < 0.05; **, P-value > 0.01; ***, P-value > 0.001; ****, P-value < 0.0001; ANOVA + Bonferroni post hoc test).

Electrophysiological recordings to validate the GluN structural superimposition model

Patch-clamp recordings of transiently transfected HEK293T cells, after a fast glutamate (1 mM) and glycine (50 µM) application (0,5 s) were also used to validate the GluN structural superimposition model in terms of determining the functional impact of the different genetic variants. 7 out of 10 GluN2B selected variants from patients were annotated as loss-of-function (GluN2B-G459R, G484D, T532A, R693G, G820A, G820E, G820V) and the other 3 variants presented a complex phenotype (GluN2B-G543R, G689S and M824V) (see **figure 84**). GluN2A and GluN1 equivalent mutations were evaluated to determine whether these variants show a homologous behavior.

The functional classification of these pairs of variants are coincident in almost all cases. GluN2B-G820A, G820E, G820V and their equivalent variants (GluN2A-G819E, G819E and GluN1-G815V, respectively) show almost negligible currents. GluN2B(T532A)-GluN2A(T531A) present a significant reduced normalized current, GluN2B(M824V)-GluN2A(M823V) show a significant reduced steady-state and a faster desensitization rate, GluN2B(G543R)-GluN2A(G542R) reveal a significant reduced normalized peak current amplitude and a slower deactivation rate, and GluN2B(G689S)-GluN2A(G688S) present a reduced normalized peak current amplitude and an increased steady-state (see **figure 86** and **table 22**). However, despite being mainly coincident, there are some small discrepancies. For instance, GluN2A-G543R and GluN2A-G542R present some differences in terms of steady-state and the pair GluN2B-G689S/GluN2A-G688S show divergence regarding their deactivation rate (see **figure 86** and **table 22**).

Nevertheless, there are two pairs of variants that were not coincident. GluN2A-G483D was not clearly classified as a loss-of-function due to a lack of significant changes in any of the evaluated biophysical parameters while GluNB-G484D present a reduced normalized peak current amplitude and a faster deactivation rate. Moreover, GluN2A-R692G do not present significant alterations while GluN2B-R693G showed a significant reduction in normalized peak current amplitude (see **figure 86** and **table 22**).
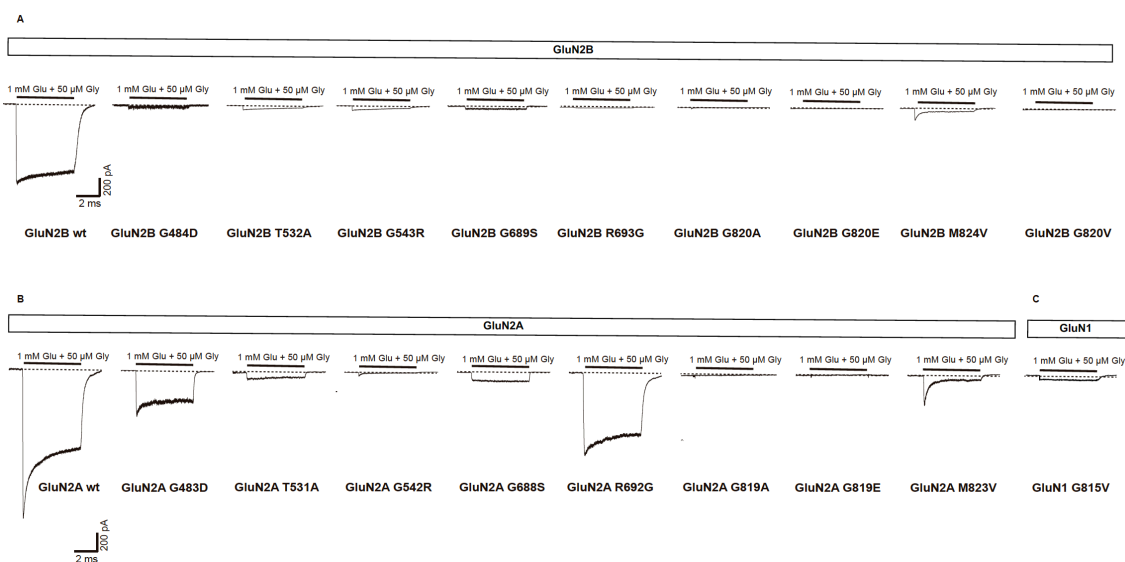

Figure 86. Functional annotation of GluN2B selected variants and their equivalent GluN2A and GluN1 variants. **A-B**, Representative whole-cell currents evoked by rapid application of 1 mM glutamate plus 50 µM glycine (0.5 second duration; -60 mV) in HEK293T cells expressing GluN1 wt + GluN2B wt/mutated variants (**A**), GluN1 wt + GluN2A wt/mutated variants (**B**) and GluN2B wt + GluN1 wt/mutated variants (**C**). **D-G,** Bar graphs representing average normalized peak currents ± SEM (**D**), steady-state (**E**), desensitization rate (**F**) and deactivation rate (**G**) of cells transfected with the GRIN variants (N = 2-91 cells per condition; ns, P-value > 0.05; *, P-value < 0.05; **, P-value > 0.01; ***, P-value > 0.001; ****, P-value < 0.0001; non-parametric Mann-Whitney test).
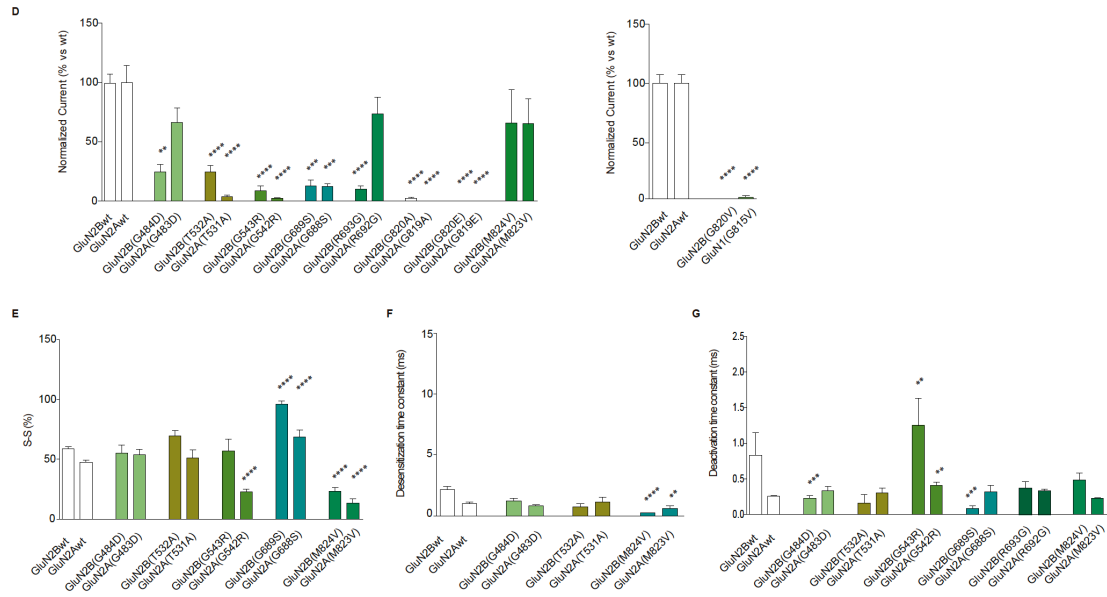
Figure 86: continued. Functional annotation of GluN2B selected variants and their equivalent GluN2A and GluN1 variants. **A-B**, Representative whole-cell currents evoked by rapid application of 1 mM glutamate plus 50 µM glycine (0.5 second duration; -60 mV) in HEK293T cells expressing GluN1 wt + GluN2B wt/mutated variants (**A**), GluN1 wt + GluN2A wt/mutated variants (**B**) and GluN2B wt + GluN1 wt/mutated variants (**C**). **D-G,** Bar graphs representing average normalized peak currents ± SEM (**D**), steady-state (**E**), desensitization rate (**F**) and deactivation rate (**G**) of cells transfected with the GRIN variants (N = 2-91 cells per condition; ns, P-value > 0.05; *, P-value < 0.05; **, P-value > 0.01; ***, P-value > 0.001; ****, P-value < 0.0001; non-parametric Mann-Whitney test).

GluN variant	Topological Domain	Surface expression (%)	Normalised current density (% vs. wild-type)	S-S (%)	Desensitization rate (msec)	Deactivation rate (msec)	Functional stratification
GluN2B-WT		100 ± 1.488 (N=290)	100 ± 7.992 (N=91)	58.83 ± 1.853 (N=82)	2.125 ± 0.2517 (N=36)	0.8098 ± 0.3057 (N=49)	
GluN2A-WT		100 ± 3.909 (N=42)	100 ± 15.89 (N=36)	47.48 ± 1.719 (N=37)	0.9948 ± 0.094 (N=23)	0.2692 ± 0.020 (N=25)	
GluN2B-G459R	LBD	1.088 ± 0.592 (N=28) ****	NA	NA	NA	NA	LOF
* GluN2A-G458R		3.019 ± 0.8275 (N=26) ****	NA	NA	NA	NA	LOF
GluN2B-G484D	LBD	85.94 ± 7.834 (N=24) ns	25.66 ± 6.705 (N=6) **	53.73 ± 7.407 (N=7) ns	1.233 ± 0.2321 (N=6) ns	0.2313 ± 0.036 (N=8) ***	LOF
* GluN2A-G483D		89.18 ± 6.723(N=20) ns	65.76 ± 13.11 (N=12) ns	54.03 ± 4.036 (N=11) ns	0.7488 ± 0.073 (N=8) ns	0.29 ± 0.045 (N=10) ns	Uncertain
GluN2B-T532A	LBD	117.6 ± 7.035 (N=26) ns	23.71 ± 4.987 (N=11) ****	69.46 ± 4.461 (N=9) ns	0.86 ± 0.36 (N=2) ns	0.22 ± 0.18 (N=2) ns	LOF
* GluN2A-T531A		105.7 ± 7.581 (N=20) ns	4.611 ± 1.358 (N=6) ****	51.13 ± 6.921 (N=7) ns	1.153 ± 0.3752 (N=4) ns	0.3067 ± 0.063 (N=6) ns	LOF
GluN2B-G543R	LBD	91.62 ± 8.789 (N=35) ns	9.385 ± 1.408 (N=10) ****	60.12 ± 7.36 (N=11) ns	ND	1.3 ± 0.43261 (N=7) **	CompleX: LOF > GOF
* GluN2A-G542R		120.6 ± 7.679 (N=23) ns	2.706 ± 0.3890 (N=8) ****	22.71 ± 2.444 (N=8) ***	ND	0.4057 ± 0.050 (N=7) ns	CompleX: LOF > GOF
GluN2B-G689S	LBD	103.9 ± 12.04 (N=27) ns	17.02 ± 4.242 (N=5) ***	96 ± 2.777 (N=5) ****	ND	0.082 ± 0.044 (N=5) ***	CompleX: LOF > GOF
* GluN2A-G688S		98.16 ± 6.542 (N=21) ns	16.47 ± 1.989 (N=10) ***	69.76 ± 5.063 (N=7) ****	ND	0.334 ± 0.071 (N=5) ns	CompleX: LOF > GOF
GluN2B-R693G	LBD	88.82 ± 4.339 (N=20) ns	9.802 ± 2.737 (N=8) ****	ND	ND	0.3467 ± 0.088 (N=3) ns	LOF
* GluN2A-R692G		128.2 ± 9.712 (N=23) ns	79.11 ± 15.85 (N=13) ns	ND	ND	0.3031 ± 0.021 (N=13) ns	Uncertain
GluN2B-G820A	M4	106.7 ± 7.374 (N=27) ns	1.997 ± 0.9347 (N=5) ****	ND	ND	ND	LOF
* GluN2A-G819A		126.1 ± 9.431 (N=27) ns	ND	ND	ND	ND	LOF
GluN2B-G820E	M4	110.7 ± 6.739 (N=23) ns	ND	ND	ND	ND	LOF
* GluN2A-G819E		96.57 ± 6.592 (N=20) ns	ND	ND	ND	ND	LOF
GluN2B-M824V	M4	119.6 ± 2.616 (N=66) ***	67.59 ± 27.10 (N=7) ns	23.17 ± 3.017 (N=6) ****	0.2383 ± 0.028 (N=6) ****	0.4814 ± 0.099 (N=7) ns	CompleX: LOF > GOF
* GluN2A-M823V		133.7 ± 9.151 (N=23) *	67.45 ± 24.38 (N=7) ns	13.6 ± 2.425 (N=7) **	0.5483 ± 0.1387 (N=6) **	0.2183 ± 0.019 (N=6) ns	CompleX: LOF > GOF
GluN variant	Topological Domain	Surface expression (%)	Normalised current density (% vs. wild-type)	S-S (%)	Desensitization rate (msec)	Deactivation rate (msec)	Functional stratification
GluN1-WT+GluN2B-WT		100 ± 1.488 (N=290)	100 ± 7.992 (N=91)	58.83 ± 1.853 (N=82)	2.125 ± 0.2517 (N=36)	0.8098 ± 0.3057 (N=49)	
GluN2B-G820V	M4		ND	ND	ND	ND	LOF
* GluN1-G815V			1.685 ± 0.9577 (N=9) ****	ND	ND	ND	LOF

Table 22. Surface and biophysical characterization of GluN2B selected variants and their equivalent GluN2A and GluN1 variants, associated NMDAR-mediated currents in cell lines. Sample size is indicated and biophysical parameters (normalized peak current vs. wild-type; steady-state, desensitization rate, deactivation rate) have been statistically evaluated (ns, P-value > 0.05; *, P-value < 0.05; **, P-value > 0.01; ***, P-value > 0.001; ****, P-value < 0.0001; non-parametric Mann-Whitney test).

1.3. Summary and conclusions: Chapter 1

In this Thesis, 95 genetic _GRIN_ variants affecting _GRIN1, GRIN2A_ and _GRIN2B_ genes have been recruited. These _de novo_ or inherited variants are missense, frameshift/nonsense or indel variants and they are spread along the whole gene, affecting the different GluN domains (ATD, LBD, TMD, CTD). Out of 95 recruited variants, 57 _GRIN_ variants have been annotated along this Thesis (42 loss-of-function variants, 7 gain-of-function variants, 3 complex variant and 5 likely non-pathogenic). 14 loss-of-function variants, 1 gain-of-function variant, 6 complex variants, and 4 likely non-pathogenic were previously characterized by the group. 11 variants are still devoid of functional annotation (see **figure 87**).
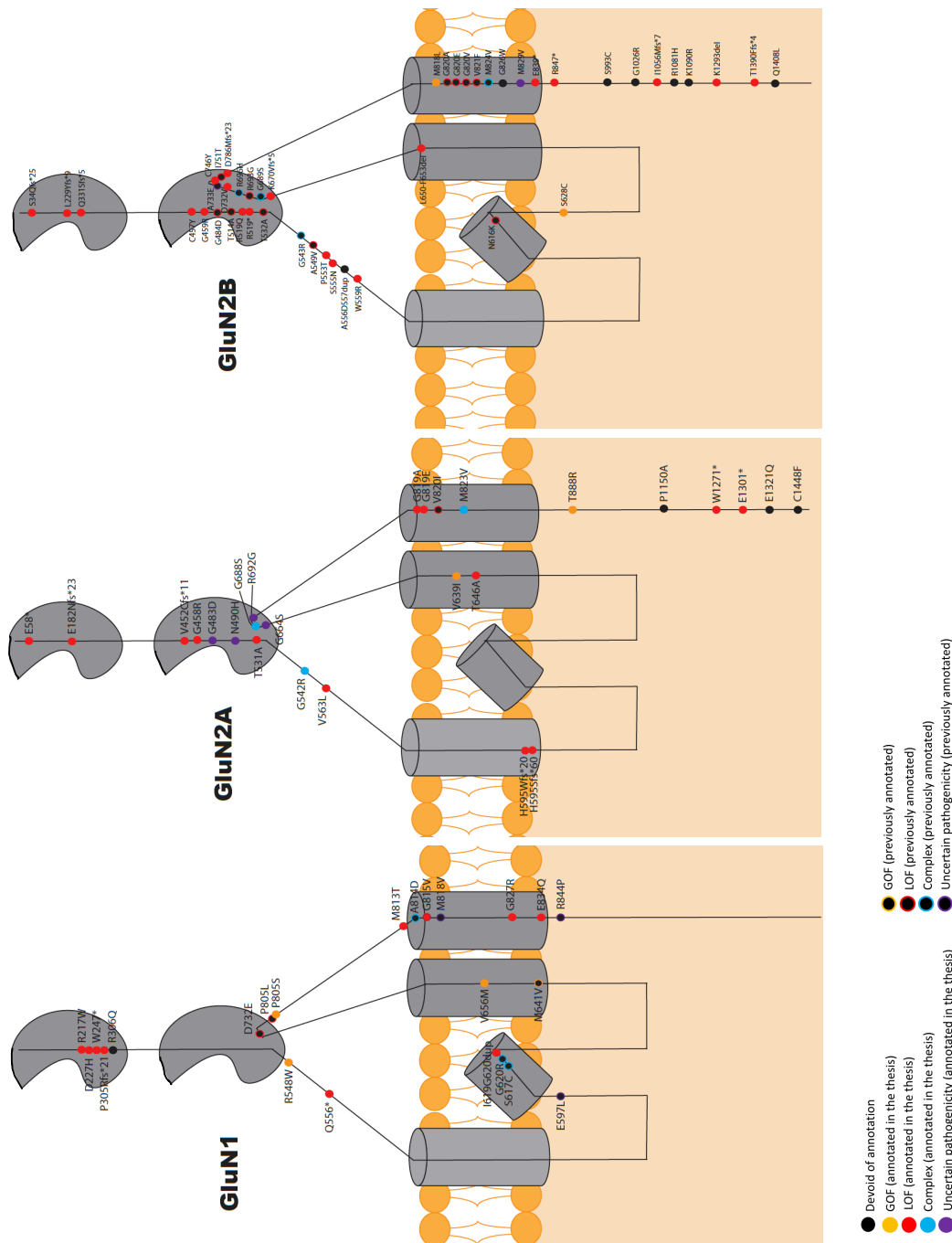
Figure 87. Scheme of GluN1, GluN2A, GluN2B subunits, showing the localization of _GRIN_ variants in the different domains. Color pattern indicates the functional annotation. Legend: Red, loss-of-function; Yellow, gain-of-function; Blue, complex; Purple, uncertain pathogenicity; Black, devoid of annotation; Filling dot, annotated during the Thesis; Colored circumference, previously annotated by the group. Abbreviations: GOF, gain-of-function; LOF, loss-of-function.

From the 57 annotated variants, 52 *GRIN* variants are likely pathogenic, when expressed in homozygosity, due to different functional impacts (see **figure 87**):

- 3 missense variants affecting GluN1 and GluN2B subunits cause a loss-of-function due to protein instability (GluN1-R217W, and GluN2B-S555N, D732V).
- 7 nonsense variants affecting the ATD and LBD (GluN2A-E58*, E182Nfs*23, V452Cfs*11; GluN2B-S34Qfs*25, L229Yfs*9, Q331Sfs*5, R519*) form aggregates composed exclusively by the mutated subunit.
- 8 missense variants affecting GluN1, GluN2A and GluN2B subunits reduce surface trafficking, causing a loss-of-function (GluN1-D227H, G827R, E834Q; GluN2A-G458R, T646A; GluN2B-C457Y, G459R, R519Q) while 2 missense variants in GluN2A and GluN2B subunits (GluN2A-M823V and GluN2B-M824V) increase surface trafficking.
- 2 indel variants affecting the TMD (GluN1-I619G620dup and GluN2B-L650-F653del) alter surface trafficking.
- 15 nonsense variants affecting the ATD, LBD, TMD alter surface trafficking (GluN1-W247*, P305Rfs*21, Q556*; GluN2A-E58*, E182Nfs*23, V452Cfs*11, H595Rfs*20, H595Lfs*60; GluN2B-S34Qfs*25, L229Yfs*9, Q331Sfs*5, R519*, K670Vfs*5, D786Mfs*23 and E839*).
- 5 nonsense variants affecting the CTD alter NMDARs docking (GluN2A-W1271*, E1301*; GluN2B-R847*, I1056Mfs*7, T1390Ffs*4).
- 5 missense variants have been annotated as gain-of-function by electrophysiological recordings, via increasing steady-state and/or slowing deactivation and desensitization rates (GluN1-R548W, V656M, P805S; GluN2B-S628C, M818L) while 4 missense variants have been annotated as loss-of-function via reducing the normalized peak current with or without affecting other kinetic parameters (GluN1-M813T; GluN2A-V563L, V639I; GluN2B-W559R, C746Y). Moreover, 3 missense variants in the GluN2A subunit (G542R, G688S and M823V) have been classified as complex.
- 2 missense variants affecting the GluN2B subunit are associated with spines density reduction (GluN2B-P553T, K1293del) while 1 missense variant seems related with increased spines density (GluN2A-T888R).
- Nonsense variants (for instance, GluN2A-E182Nfs*23, V452Cfs*11 and GluN2B-R519*, E839* and R847*) are related with a reduced spines density.
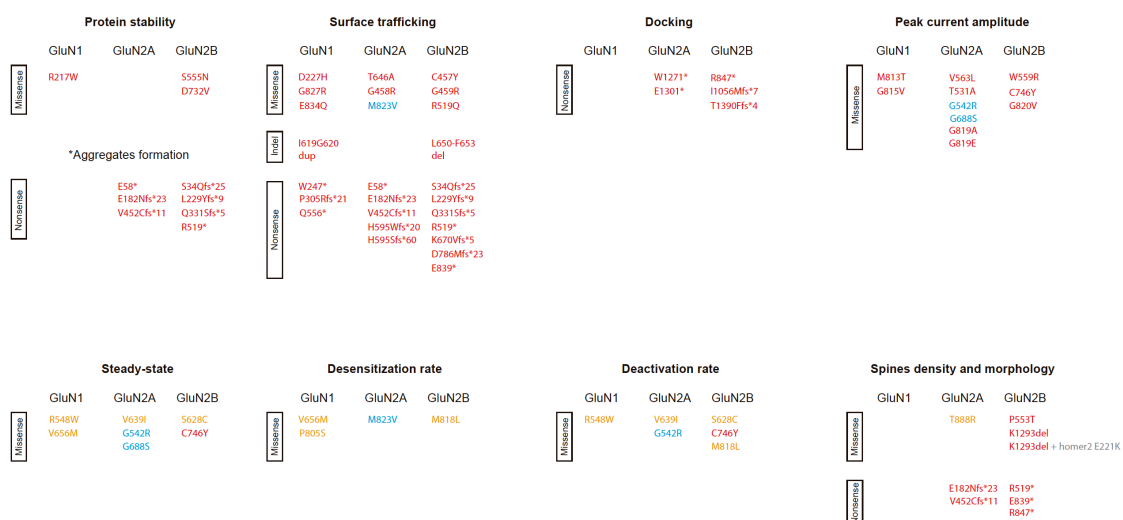

Figure 88. List of annotated *GRIN* variants during the Thesis. These variants might result in a loss-of-function (red label), a gain-of-function (yellow label) or a complex phenotype (blue label) by affecting critical processes in the biogenesis and functioning of the NMDAR: protein stability (degradation or aggregates formation), surface trafficking, the receptor docking to the cell surface, electrophysiological parameters (peak current amplitude, steady-state, desensitization and deactivation rates) and spines density and morphology.

Additionally, some of these variants have been evaluated, when expressed in heterozygosity. Immunofluorescence studies revealed that GluN1 frameshift/nonsense variants (affecting the ATD, LBD and TMD), that alter NMDAR surface trafficking in homozygosis do not exert a dominant negative effect in the wild-type subunit. Thus, *GRIN1* frameshift/nonsense variants are likely non-associated with disease (see **figure 89**). Alternatively, *GRIN2* frameshift/nonsense variants affecting those domains are likely disease-associated because these genetic variants are exerting a dominant negative effect in the wild-type allele, reducing the total density of surface NMDARs (see **figure 89**). These results were further confirmed by electrophysiological recordings (Santos-Gómez A. et al., 2020, data not shown, experiments performed by F. Miguez).
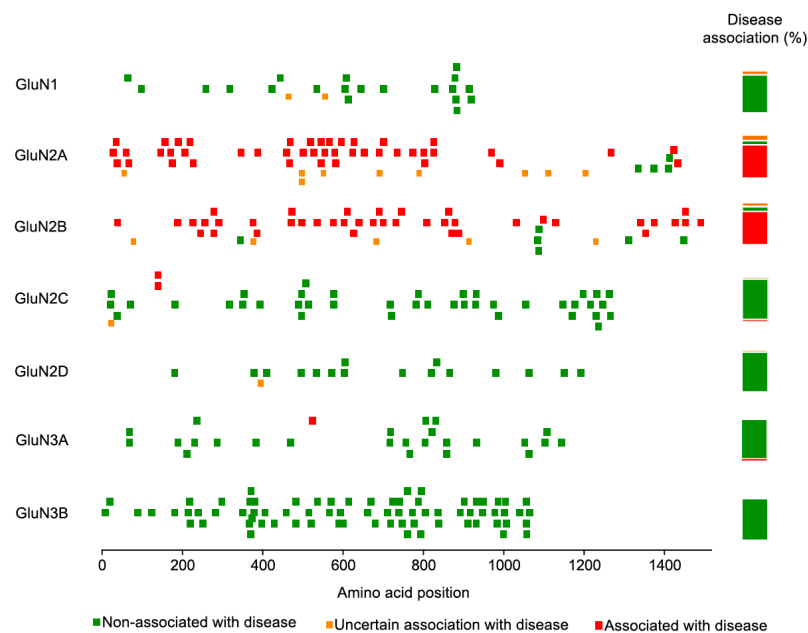
Figure 89. Scatter plot of *GRIN* frameshift/nonsense variants and their distribution along the aminoacid sequence. Right, Stacked bars representing the percentage of genetic variants (association, non-association, uncertain association with disease). Legend: Green squares, *GRIN* variants non-associated with disease; red squares, disease-associated *GRIN* variants; orange squares, uncertain genetic association and/or functional annotation. Adapted from Santos-Gómez A. et al., 2020.

Furthermore, this association was also found when evaluating *GRIN1* and *GRIN2B* variants which alter some functional aspects of the receptor, without affecting the NMDARs surface trafficking. In this case, *GRIN2B* variants are exerting a dominant negative effect, by reducing the peak current amplitude in the heterozygous condition comparing with the wild-type receptor.

The only exception to this *GRIN* heterozygous behavior was detected when analyzing *GRIN* missense/indel variants that alter the NMDAR surface trafficking in homozygosis, given that neither *GRIN1* nor *GRIN2* variants exerted a dominant negative effect.

Finally, in order to accelerate this functional annotation given the increasing number of *GRIN* patients, a structure-based superimposition model (developed by M.Olivella, Universitat Vic), was experimentally validated in terms of surface trafficking and electrophysiological parameters. This validation revealed that the model presents a predictive power in terms of functional annotation (gain-of-function, loss-of-function or complex) although some discrepancies have been found, mostly regarding specific kinetic parameters.

Chapter 2.

Phenotypic assessment of haploinsufficient $Grin2b^{+/-}$ mouse model

2. Phenotypic assessment of haploinsufficient
***Grin2b*^{+/-} mouse model**
Results

Animal models represent a valuable tool to evaluate protein function and pathology *in vivo*. Among the 95 genetic *GRIN* recruited variants, 84 have been already annotated based on their functional impact and almost a 70 % of these variants are annotated as loss-of-function. Moreover, 50 % are *GRIN2B*, 30 % *GRIN1* and 20 % *GRIN2A* variants. Thus, we decided to focus in *Grin2b* heterozygous (+/-) mouse model to determine the function of this particular GluN subunit, assuming a loss-of-function in this model. Other reasons to choose the heterozygous mouse model is that *Grin2b* knock-out (KO) mice showed no suckling response and died shortly after birth (Kutsuwada et al., 1996) and also most GRD patients present heterozygous *GRIN* variants due to an autosomal dominant inheritance pattern.

2.1. Behavioral assessment

This mouse model was generated some time ago (Kutsuwada et al., 1996) but little is known about its behavioural phenotype. Therefore, a global phenotypic behavioural assessment was performed in 2-months old mice, in order to identify potential GRD-like phenotypes of this model: weight, short-term and long-term memory, stereotypies, sociability, motor activity/coordination, anxiety-like behaviours, and GI tract function. In order to characterize these phenotypes of young-adult *Grin2b*^{+/-} mouse model, a comprehensive behavioral phenotyping battery was implemented: 1, Open field; 2, Novel-object recognition test; 3, T-maze; 4, Marble bury test; 5, Rotarod; 6, Wire-hanging test; 7, Three-chamber; 8, Elevated plus maze; 9, Stool water content determination; 10, Intestinal transit time evaluation.

2.1.1. Weight

A characteristic trait of GRD patients is a slim constitution. Thus, *Grin2b* wild-type and heterozygous mice were weighted and the results showed no significant differences in weight (g) in female mice whereas a slight reduction was observed in male mice (see **figure 90**). Nevertheless, this weight decrease does not seem as a common feature of the *Grin2b* loss-of-function model.
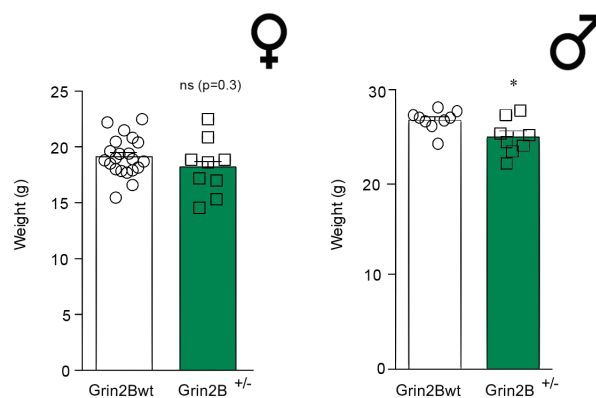
Figure 90. Bar graphs representing average weight (g) ± SEM of female (**left panel**) and male mice (**right panel**) of both genotypes (white, wild-type and green, heterozygous *Grin2b*^{+/-}) (N = 8-21 animals per condition; ns, P-value > 0.05; *, P-value < 0.05; **, P-value > 0.01; ***, P-value > 0.001; ****, P-value < 0.0001; unpaired t-test with Welch's correction).

2.1.2. Learning and memory paradigms

The vast majority of patients with *GRIN*-related disorders present learning and memory deficits. Hence, different forms of memory were evaluated in the *Grin2b*^{+/-} mouse model.

T-maze test: Short-term memory paradigm

Short-term memory is responsible of storing a limited amount of information which is available for a short period of time. This kind of memory might be studied using the T-maze alternation test.
The T-maze alternation test consists of a T-shaped maze which allows to evaluate cognitive defects based on the mice's innate exploratory behavior and the assumption that mice are able to remember previous chosen arms and alternate in subsequent trials. Our results showed that, by chance, wild-type animals chose the alternated arm over a 50 % of the trials and *Grin2b* heterozygous mice did not show significant changes in the tendency to repeat or alternate, in comparison with control animals (see **figure 91**). Thus, short-term memory does not seem to be affected in *Grin2b+/-* mice.
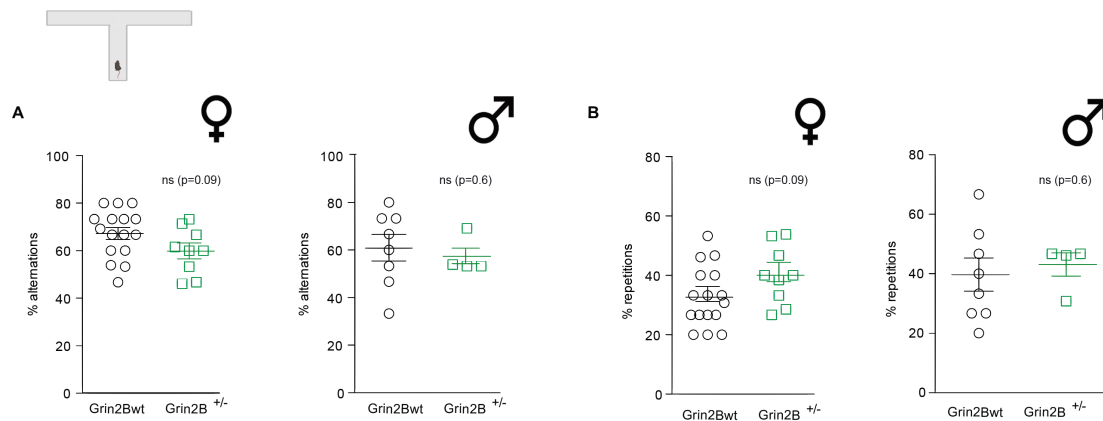
Figure 91. Scatter plots representing average % of alternations (**A**) and % of repetitions (**B**) ± SEM of female (**left panels**) and male mice (**right panels**), of both genotypes (black, wild-type and green, heterozygous *Grin2b+/-*)(N = 4-16 animals per condition; mice were discarded with two consecutive trials without making a choice in 120 sec or more than three trials without making a choice in 120 sec, without needing to be consecutive; ns, P-value > 0.05; *, P-value < 0.05; **, P-value > 0.01; ***, P-value > 0.001; ****, P-value < 0.0001; unpaired t-test with Welch's correction).

Novel-object recognition test: Long-term memory paradigm

Long-term memory stores information for longer periods of time and might be evoked consciously or not. To evaluate this kind of memory, a novel object recognition test was performed, based on the assumption that mice are able to recapitulate previously exposed objects. Mice are trained with one of the objects and 24 hours later, one of the objects is substituted by a new one and time exploring both objects (familiar vs. novel) is recorded.

This test revealed that, certainly, both wild-type and heterozygous *Grin2b* mice naturally preferred novel objects to familiar ones and there were no differences between genotypes regarding exploration times or discrimination index. Moreover, there were no gender differences, showing no changes regarding long-term memory processes in male or female mice (see **figure 92**).
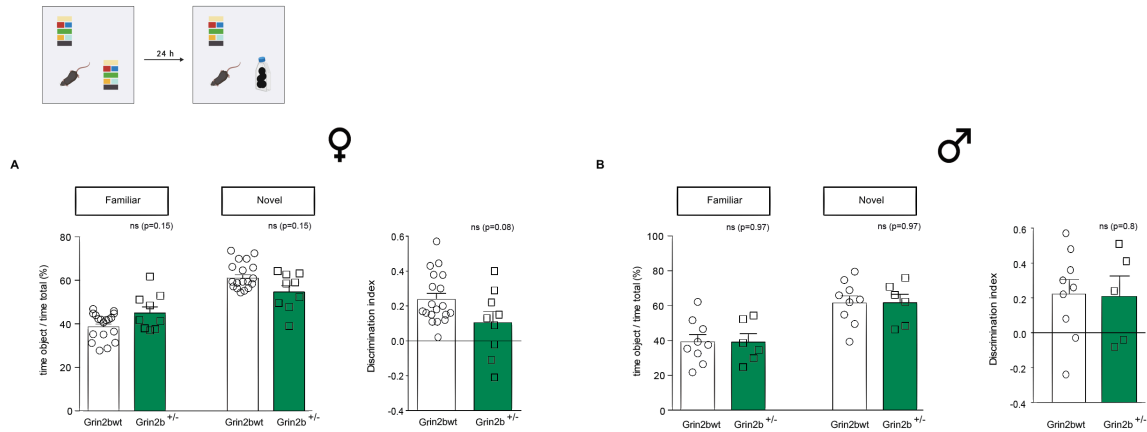
Figure 92. Bar graphs representing % average time of active contacts with each object (familiar vs novel) with regard to the total exploration time ± SEM (**left panel**) and discrimination index (**right panel**) of female (**A**) and male mice (**B**) of both genotypes (white, wild-type and green, heterozygous *Grin2b^{+/-}*) (N = 6-20 animals per condition; mice with total exploration time inferior to 20 sec were discarded; ns, P-value > 0.05; *, P-value < 0.05; **, P-value > 0.01; ***, P-value > 0.001; ****, P-value < 0.0001; nonparametric Mann-Whitney test).

2.1.3. Repetitive behaviours: Stereotypies

Another common symptom of GRD patients are stereotypies. Stereotypies are repetitive behaviours, like hand flapping or head nodding, which are rhythmic and repetitive. To measure this repetitive and compulsive-like behaviours in mice, we performed the so-called marble burying test that is based on the natural mice behavior of digging and burying. In a rat cage, 20 marbles are arrayed, and, the number of buried marbles in a 30 min session is compared between genotypes.

The marble burying test showed that there were no significant changes in the level of stereotypies in the *Grin2b^{+/-}* heterozygous mice comparing with the wild-type mice (see **figure 93**).
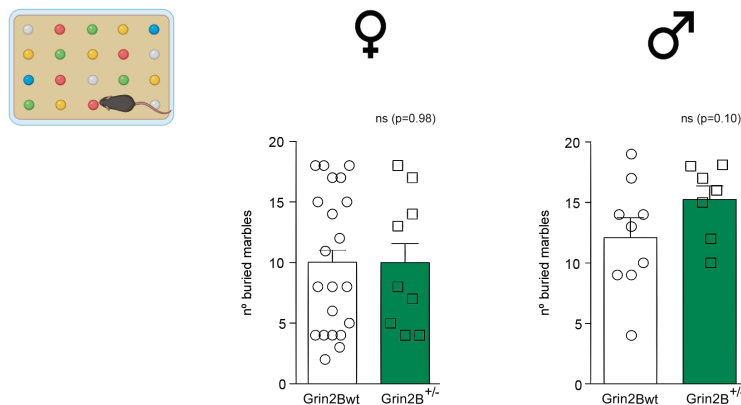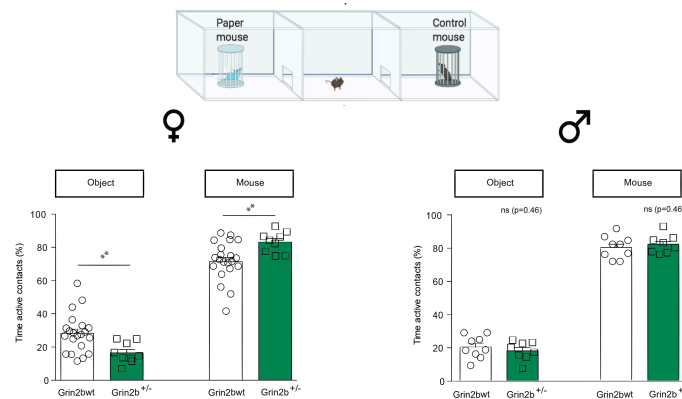

Figure 93. Bar graphs representing average number of buried marbles after a 30 min session ± SEM of female (**left panel**) and male mice (**right panel**) of both genotypes (white, wild-type and green, heterozygous *Grin2b^{+/-}*) (N = 7-21 animals per condition; ns, P-value > 0.05; *, P-value < 0.05; **, P-value > 0.01; ***, P-value > 0.001; ****, P-value < 0.0001; unpaired t-test with Welch's correction).

2.1.4.   Social behavior

GRIN-related disorders are associated with an autistic phenotype, and consequently, social dysfunction. This phenotype can be evaluated in mice by the three-chamber test. In the first session of the test, sociability is evaluated by exposing the subject mouse to a never-met-before mouse and a toy, to evaluate whether the subject mouse prefer the mouse or the toy, based on the premise that mice preferentially interact with other rodents. This test revealed that both wild-type and heterozygous *Grin2b+/-* mice always deeply preferred the mouse intruder instead of a toy mouse made of paper (female heterozygous mice even explore the mouse significantly more than their wild-type counterparts). Thus, there were no differences between genotypes regarding exploration times, and consequently, the *Grin2b+/-* model does not show social deficits (neither in female nor male mice) (see **figure 94**).

Figure 94. Bar graphs representing % average time of active contacts with the object and the mouse with regard to the total exploration time ± SEM of female (**left panel**) and male mice (**right panel**) of both genotypes (white, wild-type and green, heterozygous *Grin2b+/-*) (N = 7-21 animals per condition; ns, P-value > 0.05; *, P-value < 0.05; **, P-value > 0.01; ***, P-value > 0.001; ****, P-value < 0.0001; unpaired t-test with Welch's correction).

In the second session of this test, social novelty was also analyzed to confirm the previously observed lack of short-term memory deficits. This approach showed that *Grin2b* heterozygous mice showed preference to investigate a novel mouse instead of a familiar one to whom they have been recently exposed and there are not differences regarding times of exploration. Thus, it is confirmed that *Grin2b+/-* mouse model do not present short-term memory alterations (see **figure 95**).
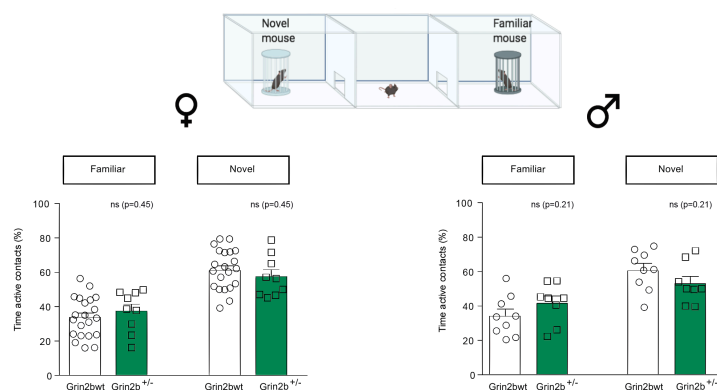

Figure 95. Bar graphs representing % average time of active contacts ± SEM with familiar and novel mice of female (**left panel**) and male mice (**right panel**) of both genotypes (white, wild-type and green, heterozygous *Grin2b+/-*) (N = 8-21 animals per condition; ns, P-value > 0.05; *, P-value < 0.05; **, P-value > 0.01; ***, P-value > 0.001; ****, P-value < 0.0001; unpaired t-test with Welch's correction).

2.1.5.   Motor activity and coordination

Patients with *GRIN* mutations usually present important delayed development of motor skills, presenting hypotonia (low muscle tone) or spasticity. Thus, motor activity and coordination should be evaluated in this mouse model by means of different behavioural tests.

By means of the open field test we explored general locomotor activity by analyzing patterns of ambulation. This approach showed that *Grin2b*+/- female heterozygous mice travelled significant less distance and performed fewer transitions between the central and the peripheral regions of the system than wild-type mice. Nevertheless, despite this reduction, time spent in each of these zones with regard to the total exploration time did not differ between genotypes. In the male group, we did not observe significant differences, but tendencies were detected (see **figure 96**).
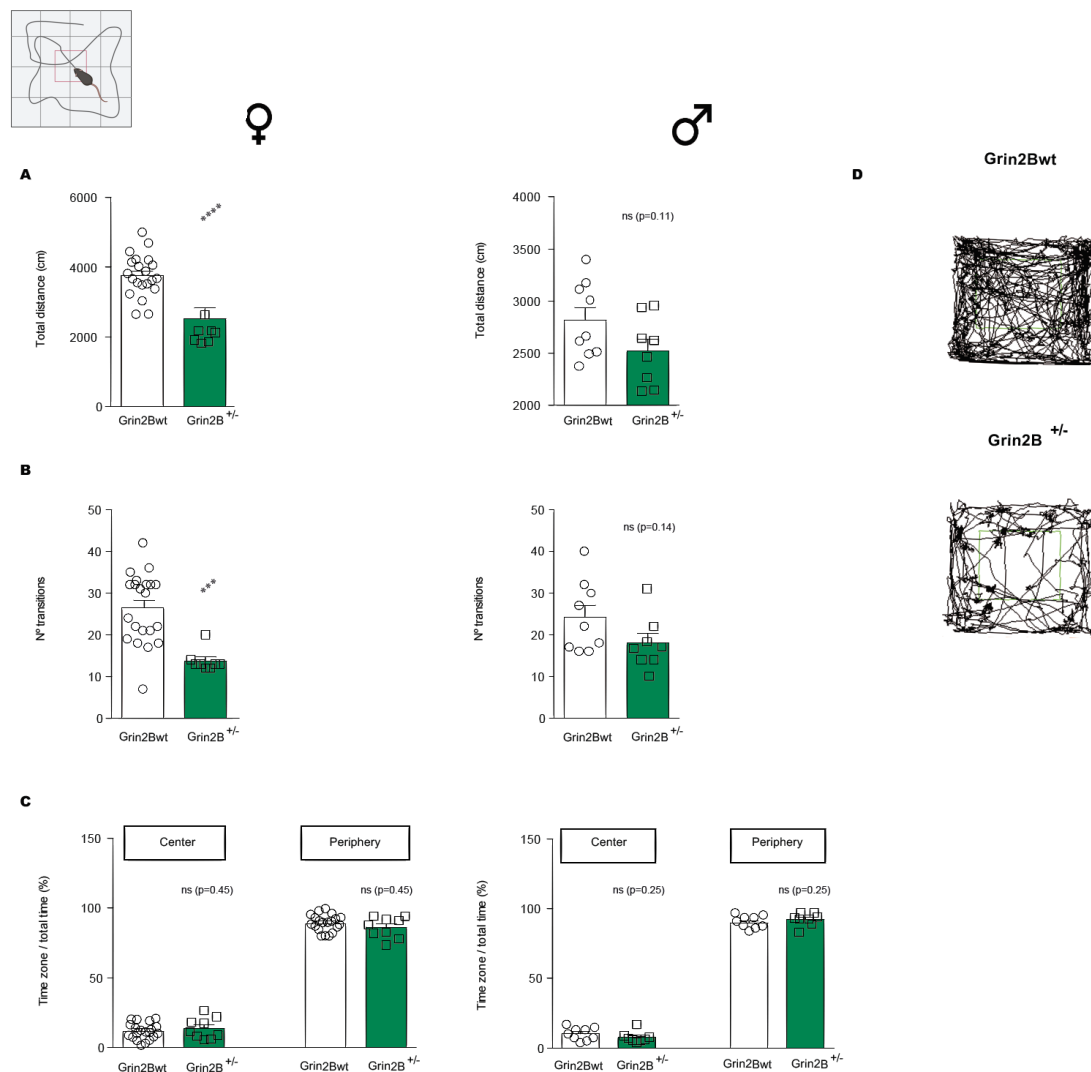
Figure 96. A-C, Bar graphs representing total distance (cm) ± SEM (**A**), number of transitions ± SEM (**B**) and % of time spent in each zone with regard to total exploration time ± SEM (**C**) of female (**left panel**) and male mice (**right panel**) of both genotypes (white, wild-type and green, heterozygous *Grin2b*+/-) (N = 8-21 animals per condition; ns, P-value > 0.05; *, P-value < 0.05; **, P-value > 0.01; ***, P-value > 0.001; ****, P-value < 0.0001; unpaired t-test with Welch's correction for normal distribution and nonparametric Mann-Whitney test for non-normal distribution). **D,** Example traces of wild-type and heterozygous *Grin2b*+/- mice performance in the open field test.

Additionally, the rotarod test was performed, which is commonly used to analyze motor coordination, balance and/or fatigue in mice. This evaluation revealed a significant worse performance in *Grin2b+/-* heterozygous female mice which fell at lower revolutions-per-minute (RPM). In male mice, results were more disperse but this might be due to a small sample size (see **figure 97**).
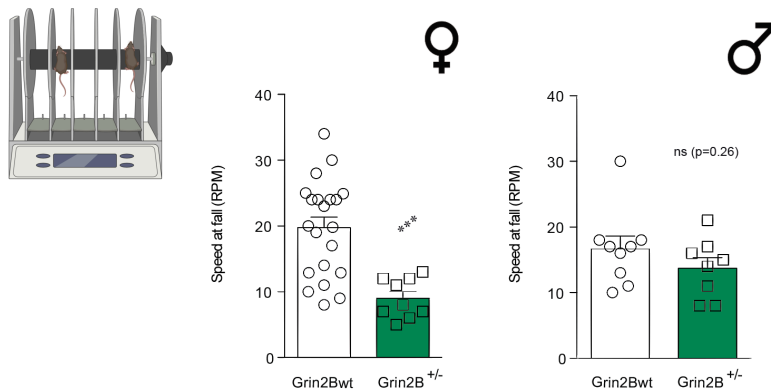

Figure 97. Bar graphs representing RPM ± SEM of female (**left panel**) and male mice (**right panel**) of both genotypes (white, wild-type and green, heterozygous *Grin2b+/-*) (N = 8-21 animals per condition; ns, P-value > 0.05; *, P-value < 0.05; **, P-value > 0.01; ***, P-value > 0.001; ****, P-value < 0.0001; unpaired t-test with Welch's correction).

Furthermore, to complement the motor evaluation, a wire-hanging test was also performed. Number of falls and reaches were counted. Each time that the mouse fell, a unit was subtracted from the 'falls' score and when the mouse reached the wire extreme, a unit was summed up to the 'reaches' score. *Grin2b+/-* heterozygous mice did not show changes in the number of falls, indicating no alterations in muscle tone. Nevertheless, the heterozygous group demonstrate a significant worse performance in reaching the wire extremes, which might be indicative of alterations in motor coordination. Thus, this test supports the motor deficits which have been observed in previous motor tests (see **figure 98**).
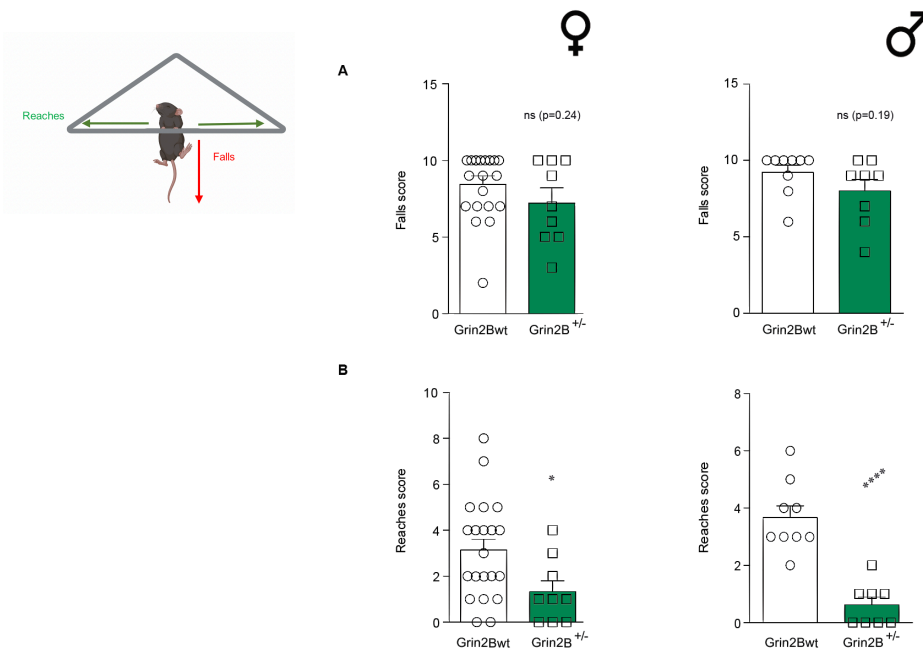

Figure 98. Bar graphs representing falls score ± SEM (**A**) and reaches score ± SEM (**B**) of female (**left panel**) and male mice (**right panel**) of both genotypes (white, wild-type and green, heterozygous *Grin2b+/-*) (N = 8-21 animals per condition; ns, P-value > 0.05; *, P-value < 0.05; **, P-value > 0.01; ***, P-value > 0.001; ****, P-value < 0.0001; unpaired t-test with Welch's correction).

2.1.6. Anxiety-like behaviours

Anxiety might also be present in patients with *GRIN* related disorders. One of the most widely used behavioural test to measure anxiety-like phenotypes is the elevated plus maze which is based on the natural aversion of mice to open and elevated spaces. This test consists of a X-shaped maze with open and enclosed arms. The time that mice spent in each type of arm was measured.

This test revealed that both genotypes preferentially entered in enclosed arms. Moreover, it also showed that *Grin2b*+/- female heterozygous mice spent significant less time in open arms than wild-type mice, showing an anxiety-like behavior. Although there was a tendency in male, we did not observe statistical significance between genotypes (see **figure 99**).
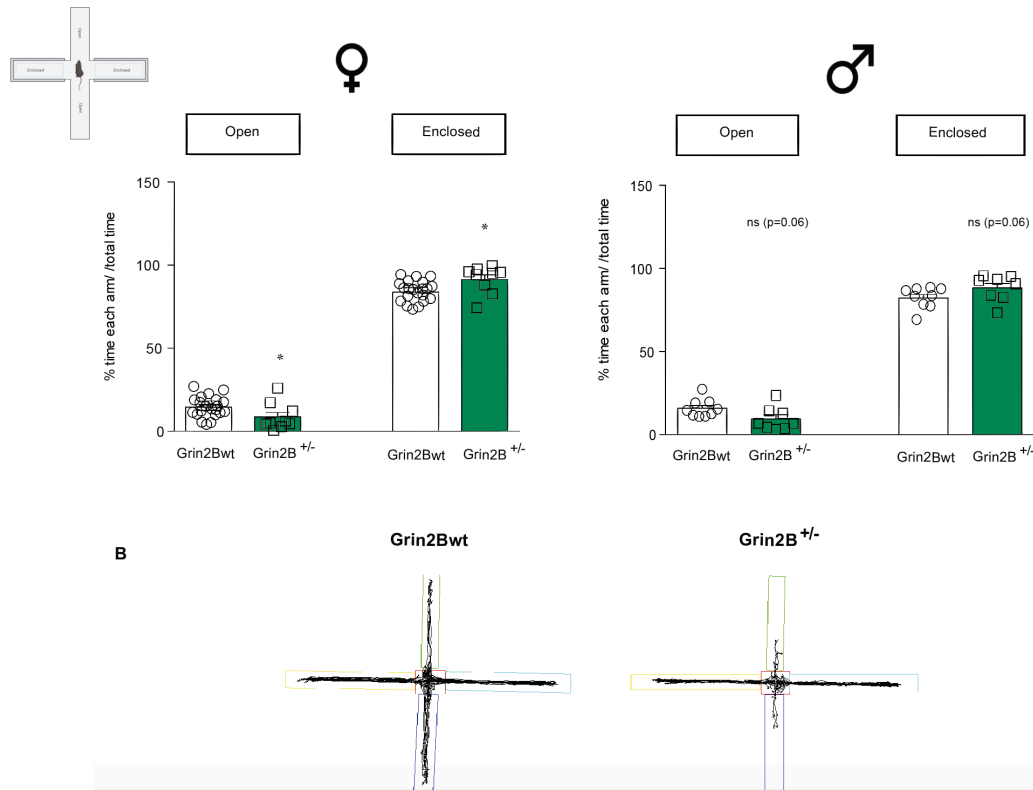

Figure 99. A, Bar graphs representing % time spent in each kind of arm in regard with total exploration time ± SEM of female (**left panel**) and male mice (**right panel**) of both genotypes (white, wild-type and green, heterozygous *Grin2b*+/-) (N = 8-21 animals per condition; ns, P-value > 0.05; *, P-value < 0.05; **, P-value > 0.01; ***, P-value > 0.001; ****, P-value < 0.0001; unpaired t-test with Welch's correction). **B,** Example traces of wild-type and heterozygous *Grin2b*+/- mice performance in the elevated plus maze.

2.1.7. Gastrointestinal function

Recently questionnaires from 34 families of GRD patients indicated that patients suffer from gastrointestinal (GI) dysfunction possibly reflecting changes in microbiota composition that lead to different symptoms such as constipation, flatulence, gastro-esophageal reflux or abdominal pain.

To establish whether *Grin2b*+/- model recapitulates this GI dysfunction, the number of stools after a particular period of time, the stool water content and the transit time were evaluated. A slight increase was observed regarding the stool water content in heterozygous female mice, but no other significant differences were observed in any of these gastrointestinal phenotypes (see **figure 100**). Thus, GI dysfunction was not highly reproduced in the *Grin2b*+/- mouse model.
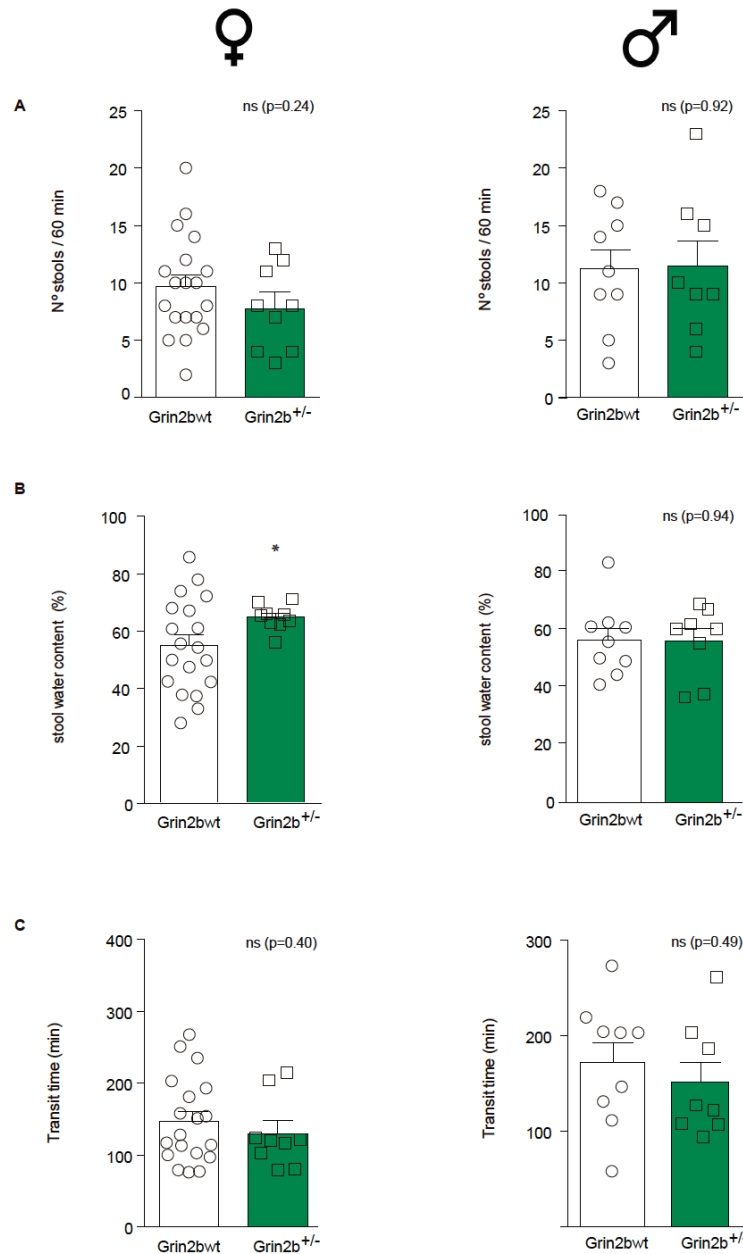
Figure 100. A-C, Bar graphs representing number stools ± SEM (**A**), stool water content per pellet ± SEM (**B**) and transit time (min) ± SEM (**C**) of female (**left panel**) and male mice (**right panel**) of both genotypes (white, wild-type and green, heterozygous _Grin2b+/-_) (N = 8-21 animals per condition; ns, P-value > 0.05; *, P-value < 0.05; **, P-value > 0.01; ***, P-value > 0.001; ****, P-value < 0.0001; unpaired t-test with Welch's correction).

2.2. Biochemical assessment

Grin2b heterozygous mouse model is representative of a constitutive loss-of-function of the GluN2B subunit of the NMDAR, due to a reduced amount of the GluN2B subunit. To demonstrate this GluN2B reduction, a subsynaptic fractionation protocol was conducted. This protocol allows to enrich the distinct synaptic compartments (pre-synaptic, post-synaptic, extra-synaptic) to evaluate isolated proteins and observe subtle changes. Synaptic fractions of wild-type and heterozygous mice were separated by this protocol and western blot, using antibodies against distinct proteins allowed to evaluate different NMDAR and AMPAR subunits and other synaptic proteins that are enriched in the different subsynaptic fractions, such as VGLUT (pre-synaptic), synaptophysin (extra-synaptic) and PSD95 (post-synaptic).

Preliminary results revealed a reduction of GluN2B subunit without affecting other GluN subunits or related proteins (such GluA1 AMPAR subunit, VGLUT transporter, PSD95, and/or synaptophysin) (see **figure 101**). Further experiments are needed to confirm this GluN2B reduction in the heterozygous mouse model and determine the amount of subunit which is present in the model.
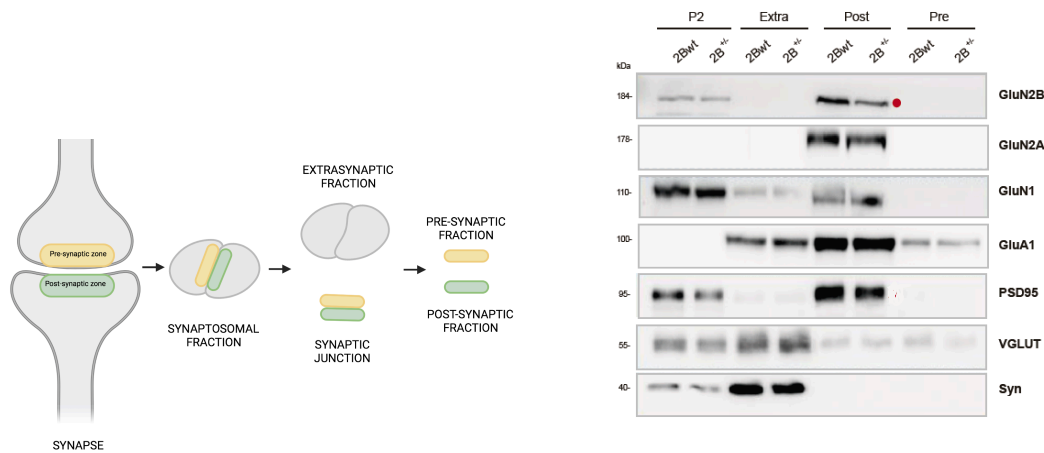

Figure 101. Left, Scheme of the synaptic fractions' separation by subsynaptic fractionation protocol. **Right,** Western Blot analysis of different subsynaptic fractions (P2: synaptosomes; Extra: extra-synaptic fraction; Post: post-synaptic fraction; Pre: pre-synaptic fraction) from wild-type and *Grin2b+/-* mice. GluN2B, GluN2A, GluN1, GluA1, PSD95, VGLUT and synaptophysin were detected. Red dot and arrow indicate proteins which were reduced in the heterozygous mice comparing with the wild type.

2.3. Electrophysiological assessment

In the previously explored memory paradigms, *Grin2b+/-* heterozygous mice did not show short-term (T-maze) or long-term (novel-object recognition test) memory deficits. Nevertheless, several brain areas are implicated in learning and memory processes. Moreover, memory tasks might be not very sensitive to slight/mild changes. Thus, the fact that behavioural alterations were not observed, in terms of memory and learning tasks, did not necessarily mean the lack of synaptic plasticity alterations in certain brain regions.

Synaptic plasticity is widely recognized as the cellular base from learning and memory processes. Thus, taking advantage of hippocampal Schaffer collateral-CA1 pathway which is widely used as a model for the study of synaptic plasticity, we decided to study long-term plasticity processes in this pathway that is initiated in axons from the CA3 region of the hippocampus and goes to dendrites of pyramidal neurons in the CA1 region, releasing glutamate and evoking an excitatory postsynaptic potential (EPSP).

Using acute hippocampal slices *ex vivo* model, EPSPs from a population of neurons (field EPSP) might be recorded. Moreover, a tetanic stimulation protocol which provokes a larger release of glutamate, might elicit long-term potentiation which can be measured in terms of changes in the EPSP slope.

Field potential recordings of Schaffer collateral connections in hippocampal slices from wild-type and heterozygous mice revealed that *Grin2b+/-* mice presented alterations in terms of long-term potentiation formation, provoking EPSPs with a lower slope (see **figure 102**). This might be explained by the fact that these mice contain less GluN2B-containing receptors and LTP formation is highly dependent on NMDAR activation.
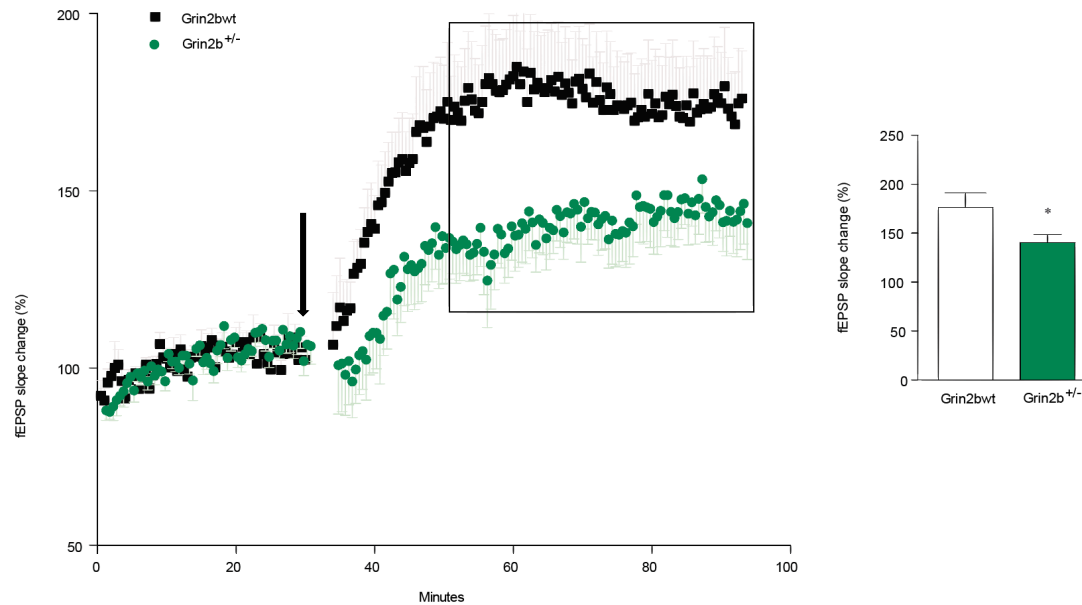
Figure 102. Time course of LTP after theta-burst stimulation demonstrating the changes on fEPSP slope values in slices of different types of mice (3-5 months age): wild-type (black) and *Grin2b*⁺/⁻ (green); 6 animals per condition, 6-9 LTP recordings. Black arrow is showing when theta-burst stimulus is applied. Bar graphs comparing the average change on fEPSP slope values in the stable phase (last 40 minutes) (white, wild-type mice; green, *Grin2b*⁺/⁻ mice) (ns, P-value > 0.05; *, P-value < 0.05; **, P-value > 0.01; ***, P-value > 0.001; ****, P-value < 0.0001; unpaired t-test with Welch's correction).

2.4. Chapter 2: Summary and conclusions

After functionally annotated several *GRIN* variants in Chapter 1, it was revealed that *GRIN* recruited variants (in this Thesis) mostly affect *GRIN2B* gene and result in the NMDAR loss-of-function. Thus, there was an urgent need to characterize a *Grin2b* loss-of-function mouse model to investigate the role of this particular subunit in *vivo*. This chapter focused in the characterization of a *Grin2b* heterozygous mouse model (haploinsufficiency) in terms of behavior, biochemistry and electrophysiology.

- Behavioral assessment showed no differences in mice weight, short-term and long-term learning and memory capacities, repetitive behaviors, social behavior and gastrointestinal function.
- *Grin2b*⁺/⁻ mouse model presents motor deficits that might be indicative of hypoactivity and alterations in motor coordination (confirmed by several motor tests: open-field, rotarod, wire-hanging test) and an anxiety-like behavior, by spending less time in open arms comparing with the wild-type.
- The biochemical characterization of *Grin2b*⁺/⁻ mouse model confirmed that the model is characterized by a GluN2B reduction.
- The electrophysiological characterization revealed that the *Grin2b*⁺/⁻ mouse model is able to develop long-term potentiation but EPSPs are reduced comparing with the wild-type, despite the lack of changes in memory behavioral assessment.

Chapter 3.

Evaluation of therapeutic strategies for the rescue of *GRIN* variants loss-of-function

GRIN-related disorders are complex diseases to treat, given that they are due to a NMDAR dysfunction and NMDARs are located in the whole CNS and other non-neuronal locations with very distinct roles. Moreover, NMDARs behave in different ways depending on its composition and the specific genetic variant. Thus, *GRIN* specific variants should be annotated prior to the decision of the most suitable therapeutic intervention.

As explained earlier, NMDAR dysfunction might result in a gain- or a loss-of-function (although occasionally, both functional impacts might be present in a complex phenotype) and this determines how the condition should be treated (blockade in the case of gain-of-function situations and potentiation for the loss-of-function variants). From the 95 recruited variants in this Thesis, almost a 70 % were annotated as loss-of-function. Thus, this chapter will focus on the evaluation of therapeutic strategies for this specific condition (NMDAR loss-of-function).

From all the available possibilities, given the extensive NMDAR pharmacology, three different approaches were selected and evaluated in cell lines, neuronal primary cultures and the previously described *Grin2b*$^{+/-}$ mouse model, to test whether they are effective and without side-effects in *GRIN*-related disorders. These approaches are genetic, nutraceutical/pharmacological (D -Serine, rapastinel, spermidine) and a microbiota manipulation.

3.1. Genetic strategy

In chapter 1, immunofluorescence approaches revealed that certain *GRIN* missense variants and nonsense variants affecting the ATD, LBD and TMD affect the NMDAR surface trafficking, when expressed in homozygosis. Then, these variants were evaluated to analyze whether they exert a dominant negative effect on the wild-type allele, when expressed in heterozygosis. While missense variants did not exert a dominant negative effect over the wild-type subunit or the total population of NMDARs in heterozygous situations, nonsense variants affecting ATD, LTD or TMD were reducing the total amount of surface receptors in those conditions by a competition or a retention effect over the wild-type subunit. Thus, a gene therapy approach is proposed, based on the premise that overexpressing a wild-type allele or a subunit with a nonsense variant affecting the CTD that is able to traffic, might be able to displace the dominant truncated subunit and rescue the reduced surface expression, given that neither the wild-type nor the CTD truncated subunit affect NMDAR trafficking and/or exert a dominant negative effect on the wild-type subunit.

To evaluate this strategy, an ATD-truncated and a CTD-truncated GluN2B variants were selected (GluN2B-L229Yfs*2 and R847*, respectively) and distinct combinations of plasmids were used to transiently transfect COS-7 cells (see **table 23**).

		Conditions			
				wt/ATD(t)	wt/ATD(t)
		wt	wt/ATD(t)	wt	CTD(t)
GRIN1 wt (complementary)		++	++	++	++
GRIN2B wt		++	+	+	+
GRIN2B ATD(t)			+	+	+
	additional *GRIN2B* wt			+	
Interventions	additional *GRIN2B* CTD(t)				+

Table 23. Table that summarizes the different plasmids combinations in each condition of the genetic rescue strategy evaluation: wt (*GRIN1*wt+*GRIN2B*wt); wt/ATD(t) (*GRIN1*wt+*GRIN2B*wt+*GRIN2B*-ATD(t)); wt/ATD(t) + additional wt (*GRIN1*wt+*GRIN2B*wt+*GRIN2B*-ATD(t) + additional *GRIN2B*wt); wt/ATD(t) + additional CTD(t) (*GRIN1*wt+*GRIN2B*wt+*GRIN2B*-ATD(t) + additional *GRIN2B*-CTD(t)). Abbreviations: ATD(t), ATD-truncated; CTD(t), CTD-truncated; wt, wild-type.

Preliminary results from an immunofluorescence approach, using an antibody against the complementary subunit tag, have confirmed that a nonsense variant affecting the ATD of the GluN2B subunit in heterozygosis reduces the total amount of NMDARs in the cell surface. Moreover, this approach revealed that these plasmids encoding for a wild-type allele and a CTD-truncated subunit (GluN2B-R847*) compete with the ATD-truncated subunit (GluN2B-L229Yfs*2) in the receptor assembly and they are able to displace it, increasing the NMDARs surface density that was reduced at first when the mutant subunit was expressed in heterozygosis without additional plasmids (see **figure 103**).
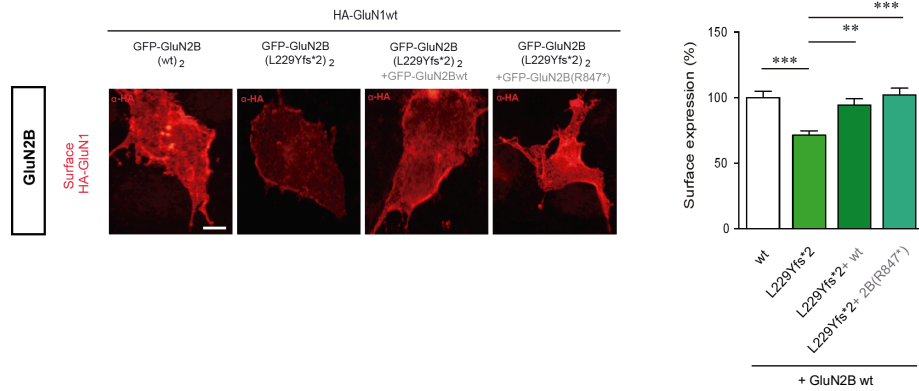

Figure 103. A, Immunofluorescence analysis of COS-7 cells transiently co-transfected with HA-GluN1wt and GFP-GluN2B wt/L229Yfs*2 accompanied by a GFP-GluN2Bwt or GFP-GluN2B(R847*) plasmid. Surface NMDAR receptors were detected by HA immunostaining (red channel) against the plasmid tag. Scale bar = 10 µm; **B,** Bar graphs representing the normalized surface expression of the genetic variant GFP-GluN2B(L229Yfs*2) alone or in combination with the wild-type or the GFP-GluN2B(R847*) plasmid, compared to wild-type (3 independent experiments, > 20 cells per condition; ns, P-value > 0.05; *, P-value < 0.05; **, P-value > 0.01; ***, P-value > 0.001; ****, P-value < 0.0001; ANOVA + Bonferroni post hoc test).

3.2.   Nutraceutical and pharmacological strategies

3.2.1.   D-Serine

D-Serine is a natural co-agonist of the NMDA receptor (Johnson and Ascher, 1987; Mothet JP. et al., 2000). Thus, it is a perfect candidate to potentiate loss-of-function variants.

It has been demonstrated that sustained activation of synaptic NMDARs modifies post-synaptic biochemistry and induces morphological changes in neurons, resulting in long-term potentiation. Moreover, it is also known that NMDAR dysfunction might be associated with morphological alterations that affect neuronal activity. Indeed, in chapter 1 of this Thesis, it was revealed that particular missense and nonsense variants affecting GluN subunits (for instance, GluN2B-P553T causing a pore reduction and GluN2B-R519* that affects NMDAR surface trafficking) are related with a NMDAR loss-of-function, showing a reduction in neuronal spines density.

Besides, our group has demonstrated that D-serine is able to potentiate reduced NMDAR-derived currents in cells expressing GluN2B-P553T missense variant of the GluN2B subunit (Soto D. et al., 2019).

In this chapter, D-serine is evaluated to test whether this compound also potentially rescues morphological alterations associated with loss-of-function variants in neuronal primary cultures.

Hippocampal neurons were transfected to express previously characterized NMDAR loss-of-function missense and nonsense variants (GluN2B-P553T and R519*) and then, treated with 200 μM glycine (*in vitro*, this glycine concentration simulates and maintains NMDAR activation, inducing a chemical-LTP) alone or in combination with 100 μM D-Serine. Then, an immunofluorescence approach allowed dendritic spines quantification.

This approach revealed that D-Serine application in neuronal cultures expressing loss-of-function variants is able to potentiate the formation of dendritic spines (see **figure 104**).
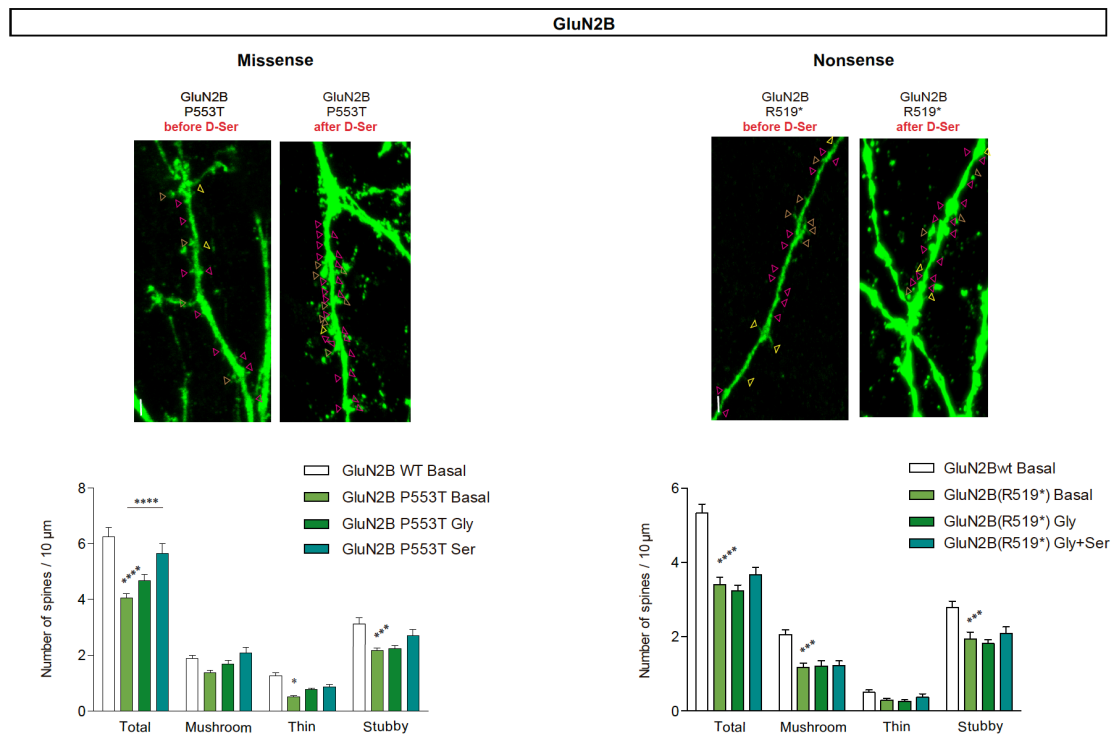
Figure 104. Representative images of murine primary hippocampal neurons transfected with GFP-GluN2B wt/mutated (**left,** missense P553T**; right,** nonsense R519*). Triangles are indicating dendritic spines: stubby (pink), mushroom (brown) and thin (yellow). Scale bar = 3 μm. Bar graphs representing the quantification of spine density and morphology in neurons at basal conditions and after 100 μM D-Serine (green tones) comparing with the wild-type (white) (>20 dendrites per condition; ns, P-value > 0.05; *, P-value < 0.05; **, P-value > 0.01; ***, P-value > 0.001; ****, P-value < 0.0001; two-way ANOVA + Bonferroni post hoc test).

3.2.2. Rapastinel

Another promising compound to potentiate NMDAR loss-of-function is Rapastinel which acts as partial agonist at the glycine-site (Moskal JR. et al., 2017).

The potentiating effect of Rapastinel was evaluated in hippocampal primary cultures. Neurons were transfected to transiently express NMDAR loss-of-function missense and nonsense variants (GluN2B-P553T and R519*). To evaluate the potential rescue of spines reduction, observed in neurons expressing these *GRIN* variants, neurons were treated with 200 μM glycine (chemical-LTP) alone or in combination with 5 μM D-Rapastinel. Then, an immunofluorescence approach allowed dendritic spines quantification.

This approach showed that Rapastinel might be effective in rescuing the spine deficit observed in neurons expressing GluN2B-P553T and GluN2B-R519* genetic variants (see **figure 105**).
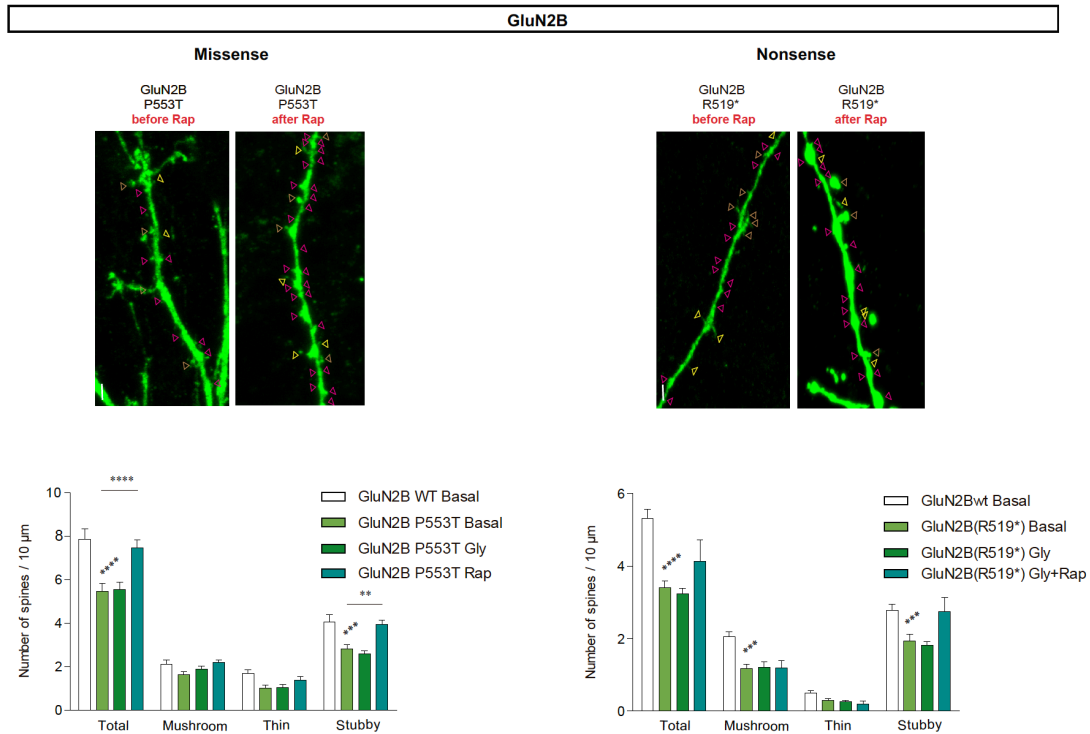
Figure 105. Representative images of murine primary hippocampal neurons transfected with GFP-GluN2B wt/mutated (**left,** missense P553T; **right,** nonsense R519*). Triangles are indicating dendritic spines: stubby (pink), mushroom (brown) and thin (yellow). Scale bar = 3 μm. Bar graphs representing the quantification of spine density and morphology in neurons at basal conditions and after 5 μM Rapastinel (green tones) comparing with the wild-type (white) (>20 dendrites per condition; ns, P-value > 0.05; *, P-value < 0.05; **, P-value > 0.01; ***, P-value > 0.001; ****, P-value < 0.0001; two-way ANOVA + Bonferroni post hoc test).

3.2.3.   Polyamines-based treatment

Spermine and its precursor, spermidine, are polyamines which act as positive allosteric modulators of GluN2B-containing NMDA receptors (William K. et al., 1991).

In order to determine whether spermine potentiates NMDAR loss-of-function, HEK293T cells were transfected with certain *GRIN* variants. Cells expressing missense variants with a functional loss-of-function without affecting surface trafficking (GluN1-G620R and GluN2B-I751T) (homozygosis and heterozygosis) and cells expressing missense and nonsense variants which affect NMDAR surface trafficking (GluN1-R217W, G827R and GluN2B-G459R, S555N and R519*) (heterozygosis) were evaluated to determine whether spermine potentiates distinct kinds of *GRIN* variants and the level of potentiation in each type.

Transiently transfected cells were recorded in the whole-cell configuration of the patch clamp technique and treated with 200 μM spermine. This approach revealed that spermine is able to potentiate wild-type currents as well as these variants' reduced currents (1.5-fold) (see **figure 106**).
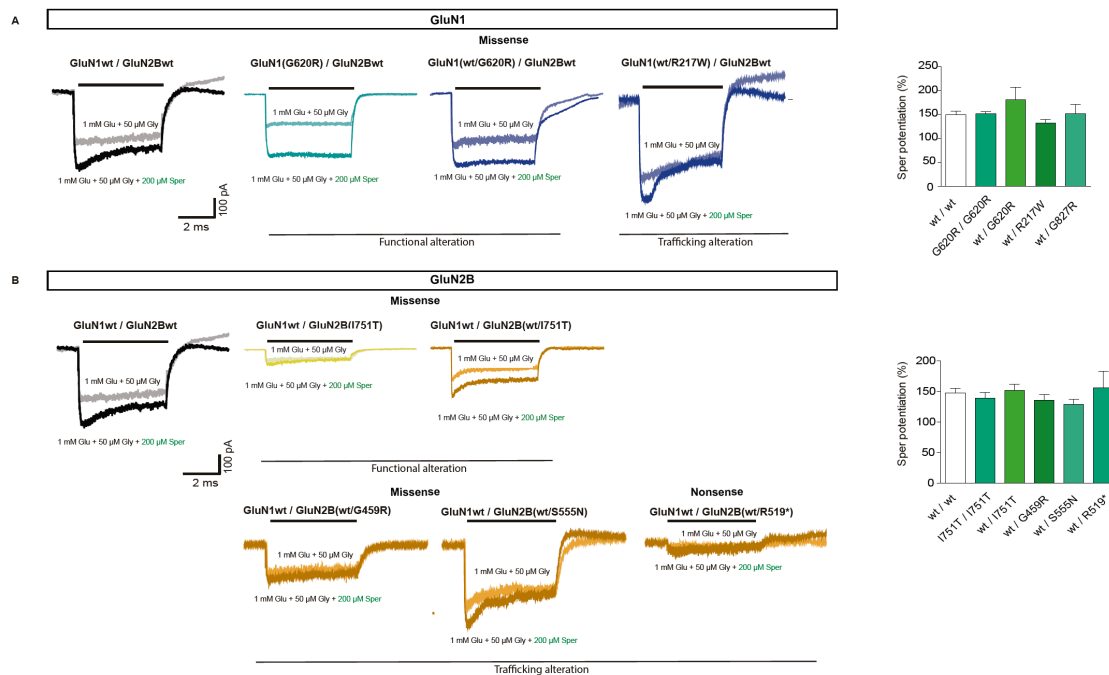
Figure 106. Functional characterization of spermine potentiation of selected variants. Representative whole-cell currents evoked by rapid application (0.5 second duration; -60 mV) of 1 mM glutamate plus 50 μM glycine ± 200 μM spermine (light colors for traces with agonists only and dark colors for traces with agonists + spermine) in HEK293T cells expressing missense GluN1 variants (**A**, blue in homozygosis and purple in heterozygosis) and missense GluN2B selected variants (**B,** yellow in homozygosis and orange in heterozygosis) comparing with the wild-type (grey/black). Bar graphs representing spermine potentiation (%) ± SEM of transfected cells (N = 7-23 cells per condition; ns, P-value > 0.05; *, P-value < 0.05; **, P-value > 0.01; ***, P-value > 0.001; ****, P-value < 0.0001; one-way ANOVA + Bonferroni post hoc test).

Despite demonstrating that spermine is able to potentiate NMDAR currents to a 150 % in cell lines expressing wild-type or mutated GluN1 or GluN2B subunits, it is different to potentiate a wild-type or a mutated receptor given that biophysical performance is not equal before the treatment. Thus, for instance, a wild-type receptor can be potentiated until it reaches a 150 % whereas a mutation reducing NMDAR current to a 50 % (like GluN2B wt/R519*), will be potentiated only to a 75 % (see **figure 107**). Thus, dosage probably might be adjusted depending on each case. Moreover, there will be cases (for instance, wt/I751T or I751T/I751T, see **figure 107** and **figure 107**) with which achieving a 100 % (complete rescue) will be impossible.
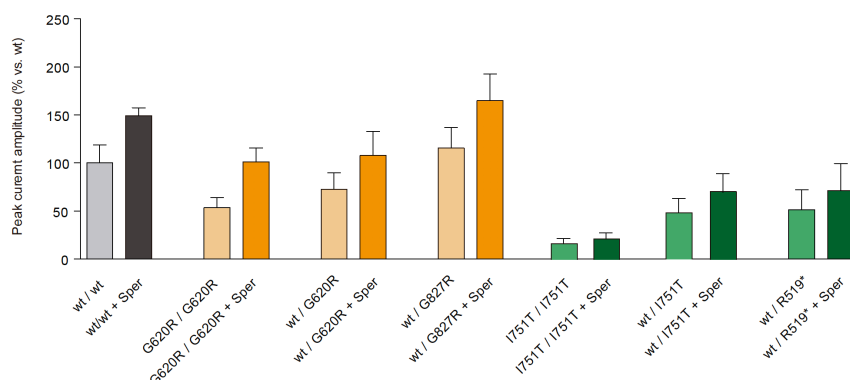

Figure 107. Experimental validation of predicted values before and after Spermine potentiation of selected variants: wt/wt; G620R/G620R, wt/G620R, wt/G827R, I751T/I7521T, wt/I751T, wt/R519* (gray, wild-type; yellow, GluN1 variants; green, GluN2B variants; light color, before spermine; dark color, after spermine).

After demonstrating that spermine is able to potentiate NMDAR reduced currents in cell lines, this compound was evaluated to investigate whether it was able to rescue spine deficit observed in neurons expressing *GRIN2B* loss-of-function genetic variants (GluN2B-P553T, GluN2B-K1293del, GluN2B-K1293del+Homer2-E221K and GluN2B-R519*). Hippocampal primary cultures transiently expressing these variants were stimulated (chemical-LTP), via 200 μM glycine alone or in combination with 200 μM spermine. Then, an immunofluorescence approach was used to count dendritic spines. This experiment revealed that spermine is able to potentiate the number of dendritic spines in those GluN mutations (see **figure 108**).
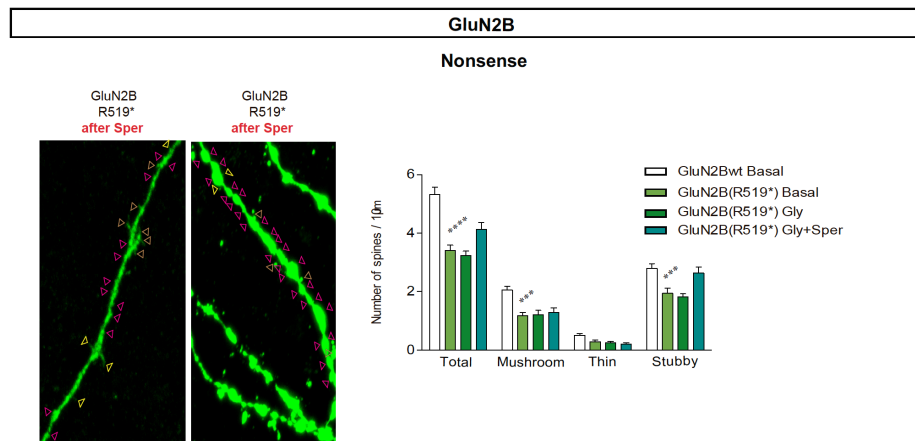

Figure 108. Representative images of murine primary hippocampal neurons transfected with GFP-GluN2B wt/mutated (missense: P553T, K1293del, K1293del (+homer2 E221K); nonsense R519*). Triangles are indicating dendritic spines: stubby (pink), mushroom (brown) and thin (yellow). Scale bar = 3 μm. Bar graphs representing the quantification of spine density and morphology in neurons at basal conditions and after 200 μM spermine (green tones) comparing with the wild-type (white) (>20 dendrites per condition; ns, P-value > 0.05; *, P-value < 0.05; **, P-value > 0.01; ***, P-value > 0.001; ****, P-value < 0.0001; two-way ANOVA + Bonferroni post hoc test).
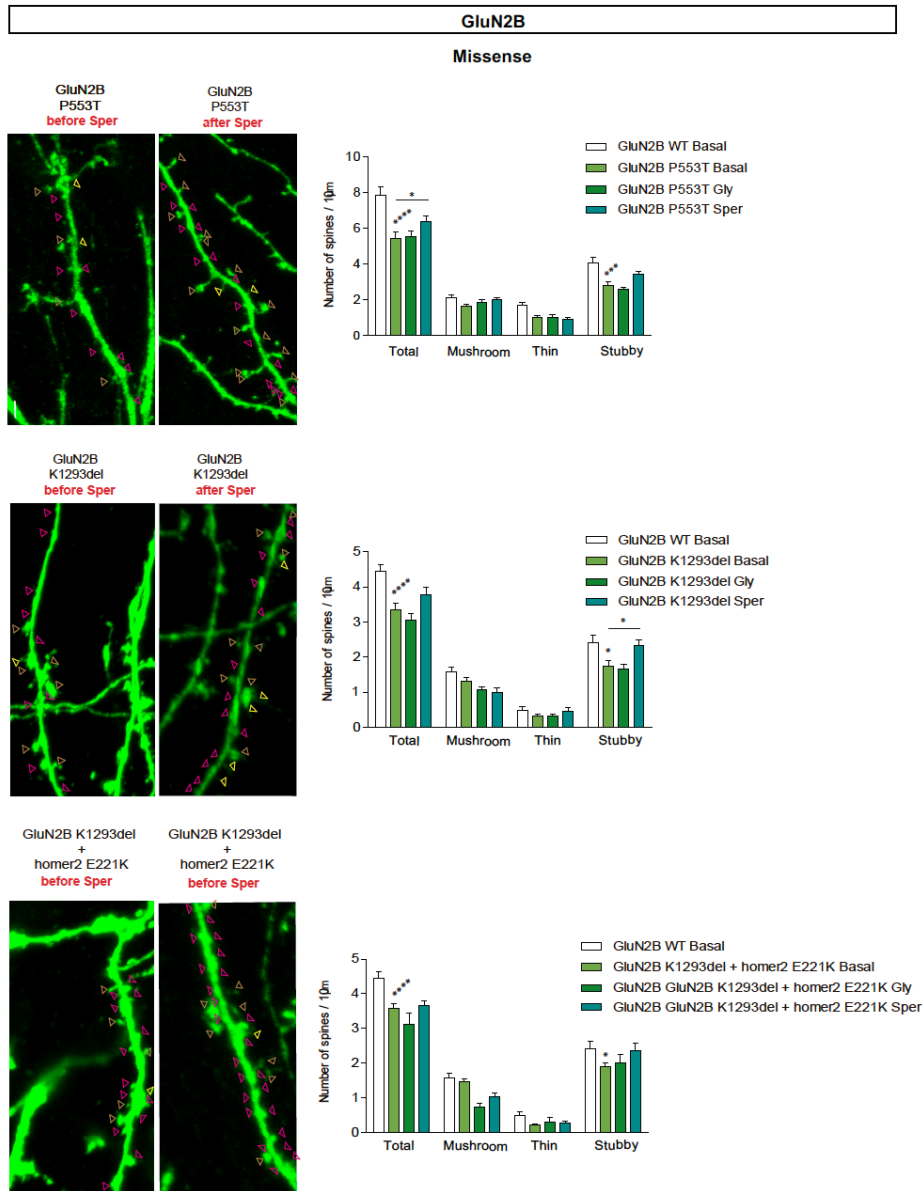
Figure 108: continued. Representative images of murine primary hippocampal neurons transfected with GFP-GluN2B wt/mutated (missense: P553T, K1293del, K1293del (+homer2 E221K); nonsense R519*). Triangles are indicating dendritic spines: stubby (pink), mushroom (brown) and thin (yellow). Scale bar = 3 μm. Bar graphs representing the quantification of spine density and morphology in neurons at basal conditions and after 200 μM spermine (green tones) comparing with the wild-type (white) (>20 dendrites per condition; ns, P-value > 0.05; *, P-value < 0.05; **, P-value > 0.01; ***, P-value > 0.001; ****, P-value < 0.0001; two-way ANOVA + Bonferroni post hoc test).

Thus, spermine is able to potentiate NMDARs *in vitro* by potentiating NMDAR-derived currents in cell lines and rescuing spines deficits in neuronal primary cultures.

To investigate this NMDAR potentiation by polyamines *in vivo*, female *Grin2b* wild-type and heterozygous mice received 3 mM spermidine (which is the spermine precursor, based on available drugs for patients) in drunk water (Chrisam M. et al., 2015; Eisenberg T. et al., 2016; Wirth A. et al., 2021) for 1,5 months before the behavioural assessment, until the end of experiments. Supplemented water was renewed each 2 days to avoid excessive deamination of the compound (Chrisam M. et al., 2015). Consumed water (supplemented with spermidine or not) was controlled along the whole administration to demonstrate that there were no differences in the ingested volume of water due to spermidine addition (see **figure 109**).
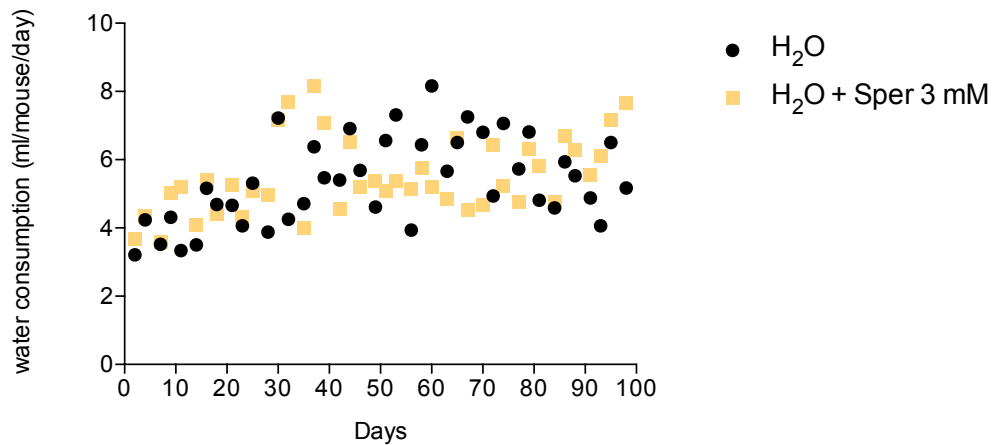

Figure 109. Scatter plot representing water consumption (ml/mouse/day) ± spermidine 3 mM (control, black; + 3mM spermidine, yellow) for 3 months.

After 1.5 months of supplementation, behavioral assessment was conducted to evaluate whether spermidine administration was able to rescue altered phenotypes in the *Grin2b*^{+/-} mouse model (motor and anxiety) and/or modify unaltered phenotypes (weight, short-term and long-term memory, stereotypies, social behavior and gastrointestinal function). Behavioral assessment was executed following the same protocols and analyzing the same parameters than in Chapter 2 of this Thesis.

Most unaltered phenotypes in *Grin2b*^{+/-} mouse model were not modified by spermidine supplementation, neither in wild-type nor heterozygous mice. These phenotypes include mice weight (see **figure 110, panel A**), short-term memory (percentage of alternations over 50 % and percentage of repetitions under 50 %, in T-maze test) (see **figure 110, panel B**), long-term memory (similar times of interaction with familiar and novel objects, being longer the exploration time for novel object) (see **figure 110, panel C**), some GI tract functions (number stools in 60 min and transit time) (see **figure 110, panel B**), and social behavior (similar times of interaction with paper and alive mouse in sociability phase, similar times of interaction with familiar and novel mice in social novelty phase, being longer the exploration time for alive mouse in sociability phase and novel mouse in social novelty phase) (see **figure 110, panel E**).
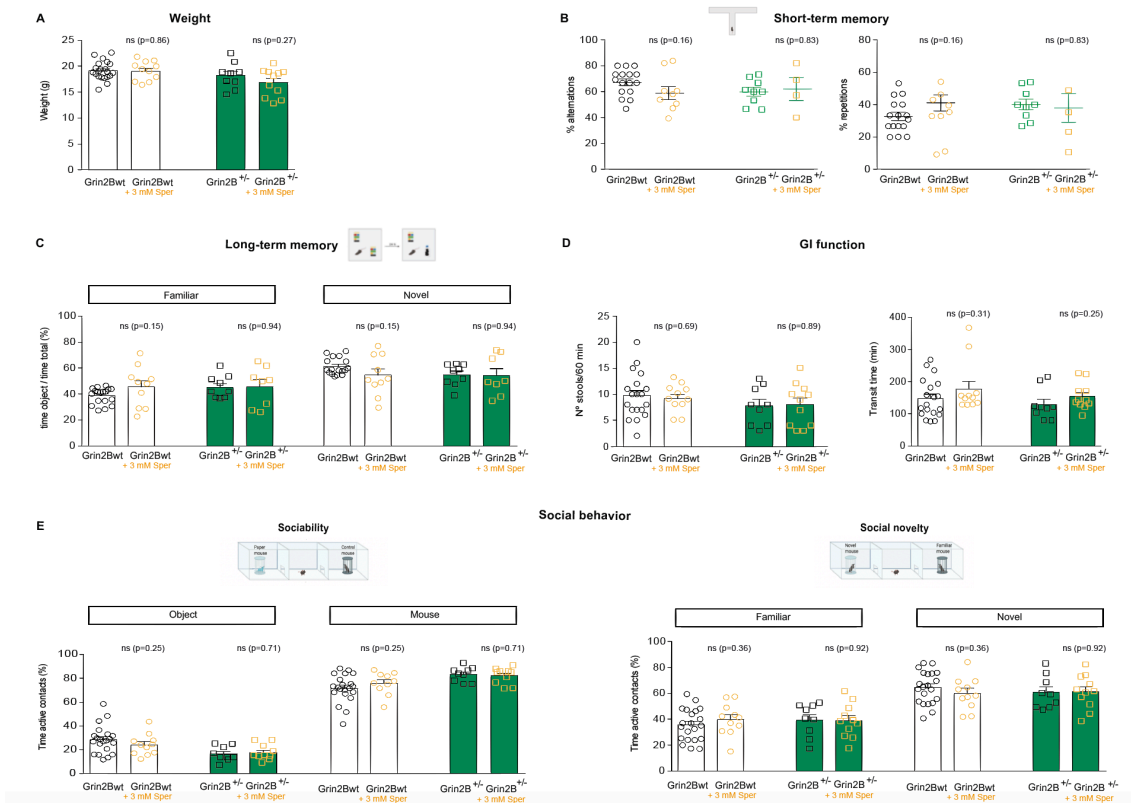
3. Evaluation of therapeutic strategies
for the rescue of *GRIN* variants loss-of-function
Results

Figure 110. A-E, Bar graphs and scatter plots representing average weight (g) ± SEM (**A**), average % of alternations (**B, left panel**) and % of repetitions (**B, right panel**) ± SEM, % average time of active contacts with each object (familiar vs novel) with regard to the total exploration time ± SEM in novel-object test (**C**), number stools ± SEM (**D, left panel**) and transit time (min) ± SEM (**D, right panel**), % average time of active contacts with the object and the mouse with regard to the total exploration time ± SEM in sociability phase of 3-chamber test (**E, left panel**) and % average time of active contacts ± SEM with familiar and novel mice in social novelty phase of 3-chamber test (**E, right panel**) of female mice of both genotypes (white, wild-type and green, heterozygous *Grin2b*^{+/-}) with 3 mM spermidine supplementation (yellow circles and boxes) or control water (black circles and boxes)(N = 4-21 animals per condition; ns, P-value > 0.05; *, P-value < 0.05; **, P-value > 0.01; ***, P-value > 0.001; ****, P-value < 0.0001; unpaired t-test with Welch's correction for normal distribution and nonparametric Mann-Whitney test for non-normal data). In T-maze test, mice were discarded with two consecutive trials without making a choice in 120 sec or more than three trials without making a choice in 120 sec, without needing to be consecutive. In NOR test, mice were discarded if total exploration time was inferior to 20 sec.

Nevertheless, there are some unaltered phenotypes in the *Grin2b*^{+/-} mouse model, that are modified after spermidine supplementation. For instance, stool water content is significantly reduced in both genotypes, wild-type and heterozygous mice, after supplementation (see **figure 111, panel A**). Moreover, the number of buried marbles in a 30 min session (indicative of stereotypies) is significantly increased in *Grin2b*^{+/-} heterozygous mice but not wild-type mice (see **figure 111, panel B**).
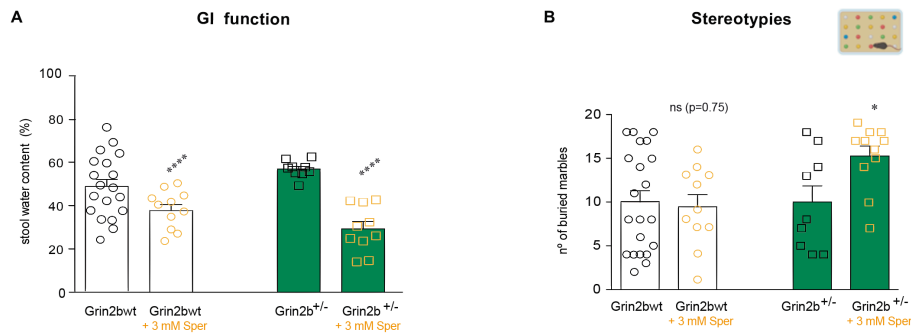
Figure 111. A-B, Bar graphs representing stool water content per pellet (g) ± SEM (**A**) and average number of buried marbles after a 30 min session ± SEM (**B**) of female mice of both genotypes (white, wild-type and green, heterozygous *Grin2b*^{+/-}) with 3 mM spermidine supplementation (yellow circles and boxes) or control water (black circles and boxes) (N = 10-21 animals per condition; ns, P-value > 0.05; *, P-value < 0.05; **, P-value > 0.01; ***, P-value > 0.001; ****, P-value < 0.0001; unpaired t-test with Welch's correction).

Regarding phenotypes that were altered in *Grin2b*^{+/-} mice (motor deficits and anxiety-like phenotypes), spermidine supplementation partially rescued defects in general locomotion (by increasing total distance and transitions of heterozygous mice in open-field test) (see **figure 112, panel A**) and alterations in motor coordination (by improving rotarod performance of heterozygous mice) (see **figure 112, panel B**). Nevertheless, there is no significant spermidine effect neither in the wire-hanging test performance (only a slight tendency in heterozygous mice to fall less) (see **figure 112, panel C**) nor in anxiety like-behaviors, given that spermidine do not modify the time spent in each type of arm in the elevated plus maze test (see **figure 112, panel D**).
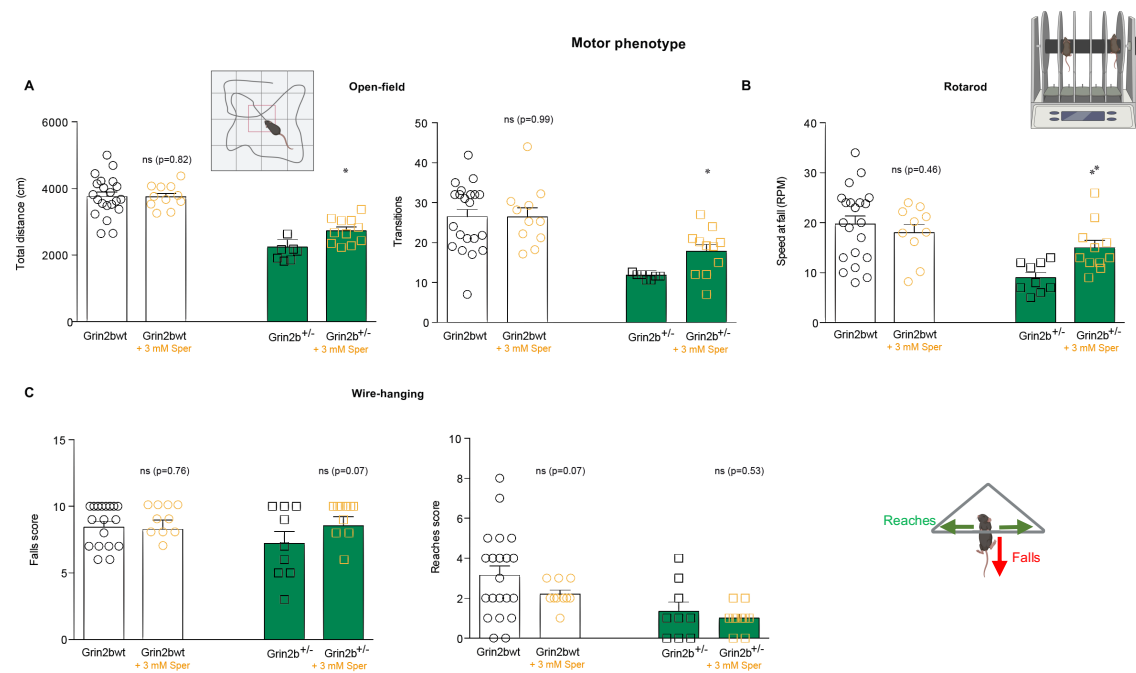

Figure 112. A-D, Bar graphs representing total distance (cm) ± SEM (**A, left panel**), and number of transitions ± SEM (**A, right panel**) in open-field test, RPM ± SEM in rotarod test (**B**), falls score ± SEM (**C, left panel**) and reaches score ± SEM (**C, right panel**), and % time spent in each kind of arm in regard with total exploration time ± SEM in elevated-plus maze (**D**) of female mice of both genotypes (white, wild-type and green, heterozygous *Grin2b*^{+/-}) with 3 mM spermidine supplementation (yellow circles and boxes) or control water (black circles and boxes) (N = 8-21 animals per condition; ns, P-value > 0.05; *, P-value < 0.05; **, P-value > 0.01; ***, P-value > 0.001; ****, P-value < 0.0001; unpaired t-test with Welch's correction for normal distribution and non-parametric Mann-Whitney test for non-normal distribution).
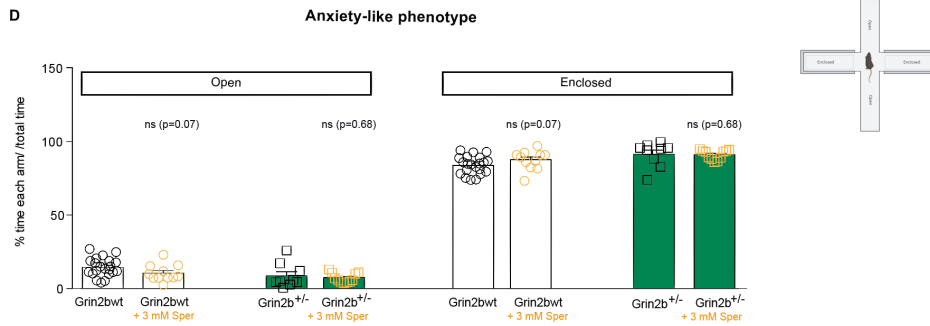
Figure 112: continued. A-D, Bar graphs representing total distance (cm) ± SEM (**A, left panel**), and number of transitions ± SEM (**A, right panel**) in open-field test, RPM ± SEM in rotarod test (**B**), falls score ± SEM (**C, left panel**) and reaches score ± SEM (**C, right panel**), and % time spent in each kind of arm in regard with total exploration time ± SEM in elevated-plus maze (**D**) of female mice of both genotypes (white, wild-type and green, heterozygous *Grin2b*+/-) with 3 mM spermidine supplementation (yellow circles and boxes) or control water (black circles and boxes) (N = 8-21 animals per condition; ns, P-value > 0.05; *, P-value < 0.05; **, P-value > 0.01; ***, P-value > 0.001; ****, P-value < 0.0001; unpaired t-test with Welch's correction for normal distribution and non-parametric Mann-Whitney test for non-normal distribution).

After behavioural assessment, mice were sacrificed to obtain hippocampal *ex vivo* slices. Field potential recording of Schaffer collateral connections in the hippocampus of wild-type and heterozygous mice showed that spermidine supplementation to *Grin2b*+/- mice provokes a partial rescue of the reduced EPSPs slope (see **figure 113**).
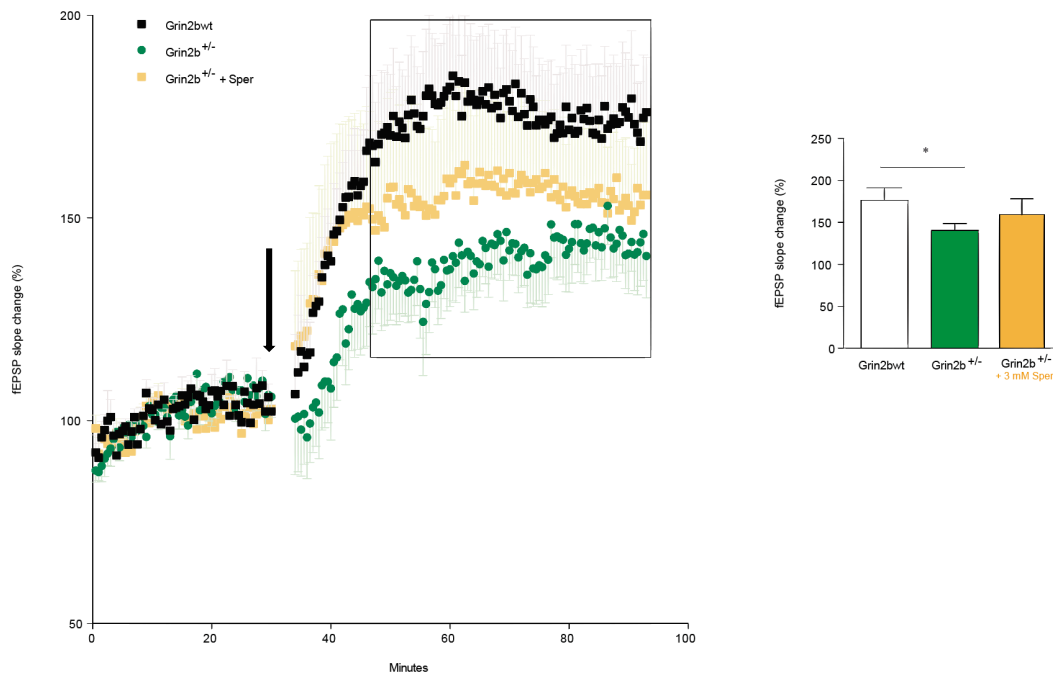

Figure 113. Time course of LTP after theta-burst stimulation demonstrating the changes on fEPSP slope values in slices of different types of mice (3-5 months age): wild-type (black); *Grin2b*+/- (green); and *Grin2b*+/- + 3mM spermidine (yellow); 6 animals per condition, 6-9 LTP recordings. Black arrow is showing when theta-burst stimulus is applied. Bar graphs comparing the average change on fEPSP slope values in the stable phase (last 40 minutes, indicated with the black box) (white, wild-type; green, *Grin2b*+/-; yellow, *Grin2b*+/- + 3mM spermidine); (ns, P-value > 0.05; *, P-value < 0.05; **, P-value > 0.01; ***, P-value > 0.001; ****, P-value < 0.0001; unpaired t-test with Welch's correction).

3.3.   Fecal Microbiota Transplantation (FMT)

Recently, the brain-gut axis is receiving considerable attention. The brain-gut axis is a neurohumoral bidirectional axis that communicates the central nervous system and the gut microbiota, via metabolic precursors, neurotransmitters and other molecules. This communication is crucial for brain development and synaptogenesis and consequently, microbiota alterations might be related with central nervous disorders (Schächtle MA. et al., 2021).

Moreover, in *GRIN*-related disorders, patients present gastrointestinal alterations like constipation, flatulence, reflux or abdominal pain (reported in questionnaires answered by the families) although *Grin2b*$^{+/-}$ mouse model behavioral characterization did not reveal severe alterations in terms of gastrointestinal phenotypes (number of stools in 60 min, stool water content and transit time).

Despite these findings in the *Grin2b*$^{+/-}$ mouse model, microbiota manipulation might be a therapeutic option for GRDs. Thus, fecal microbiota transplantation was evaluated to assess whether heterozygous microbiota transference provokes behavioural and plasticity alterations (motor deficits, anxiety-like behaviors and plasticity alterations) and/or wild-type microbiota is able to rescue those phenotypic alterations of the *Grin2b*$^{+/-}$ mouse model.

Wild-type and heterozygous *Grin2b* mice were house separately to form a relatively homogenous microbiota based on genotype. Then, feces were collected and processed while receptor mice were prepared via omeprazole and laxative administration (oral gavage). Wild-type mice received microbiota from heterozygous mice while heterozygous mice received microbiota from wild-type mice. After allowing transferred microbiota re-colonization of the receptor mice, behavioral assessment was conducted to evaluate long-term memory, stereotypies, gastrointestinal function, motor phenotype and anxiety-like behavior.

Regarding phenotypes that were not affected in *Grin2b*$^{+/-}$ mice, there were not significant changes in wild-type receiving heterozygous microbiota except for novel-object recognition test, in which wild-type mice improved their performance (spending more time with novel object than with the familiar one) (see **figure 114, panel A**). Thus, heterozygous microbiota transplantation does not worsen long-term memory, stereotypies or gastrointestinal functions.

In contrast, heterozygous mice receiving wild-type microbiota show increased stereotypies (burying significantly more marbles) (see **figure 114, panel B**), an increased number of stools and a reduced stool water content (see **figure 114, panel C**) while there are not changes in long-term memory (there are no modification of times spent interacting neither with familiar nor novel object) (see **figure 114, panel A**) or in transit time (see **figure 114, panel C**). Hence, wild-type microbiota transplantation in heterozygous mice produces changes in some gastrointestinal functions and repetitive behaviors.
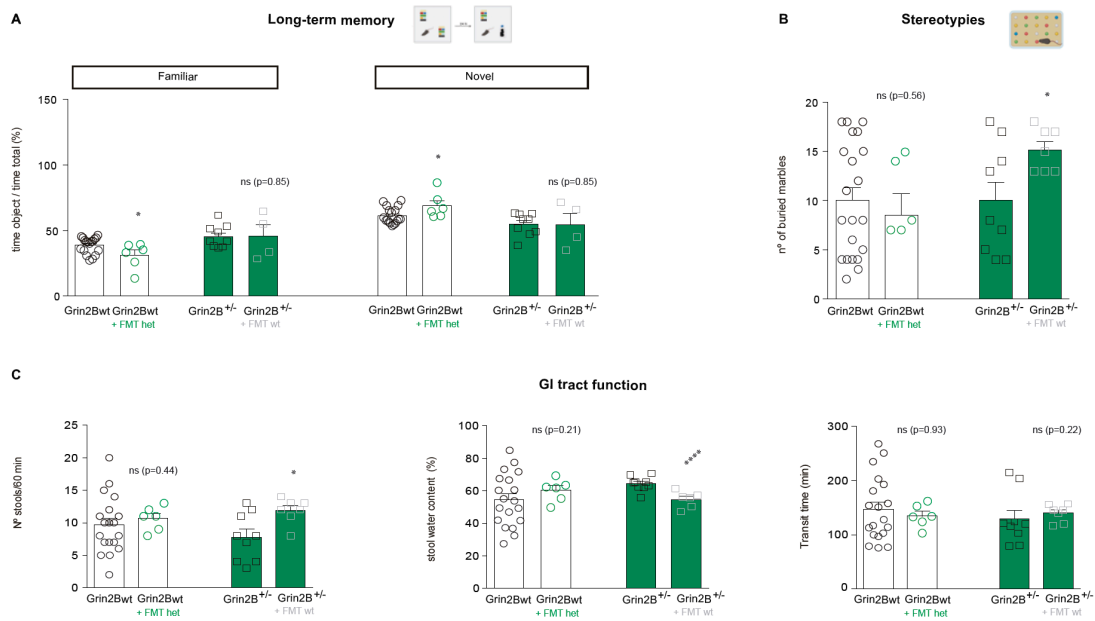
Figure 114. A-C, Bar graphs representing % average time of active contacts with each object (familiar vs novel) with regard to the total exploration time ± SEM in novel-object test (**A**), average number of buried marbles after a 30 min session ± SEM (**B**), number stools ± SEM (**C, left panel**), stool water content per pellet (g) ± SEM (**C, middle panel**) and transit time (min) ± SEM (**C, right panel**) of female mice of both genotypes (white, wild-type; green, heterozygous *Grin2b*+/-) ± FMT (black circles and boxes, no FMT; green circles and boxes, *Grin2b*+/- microbiota is transferred; gray circles and boxes, wild-type microbiota is transferred) (N = 4-21 animals per condition, in NOR test, mice were discarded if total exploration time was inferior to 20 sec); ns, P-value > 0.05; *, P-value < 0.05; **, P-value > 0.01; ***, P-value > 0.001; ****, P-value < 0.0001; unpaired t-test with Welch's correction for normal distribution and nonparametric Mann-Whitney test for non-normal distribution).

Behavioural assessment also showed a lack of changes in either of the treated groups (wild-type mice receiving heterozygous microbiota or heterozygous mice with transferred wild-type microbiota) regarding number of transitions center-periphery in open-field test (see **figure 115, panel A**), falls and reaches scores in wire-hanging test (see **figure 115, panel C**) or anxiety-like behavior given that there are no changes in the times spent in open and/or enclosed arms in the elevated plus-maze (see **figure 115, panel D**).

Nevertheless, wild-type animals receiving *Grin2b*+/- heterozygous microbiota worsened their rotarod performance while *Grin2b*+/- mice receiving wild-type microbiota were not rescued (see **figure 115, panel B**). Thus, alterations in motor coordination that were observed in *Grin2b*+/- mouse model in rotarod test are transferred to wild-type mice with heterozygous microbiota transplantation whereas wild-type microbiota is not able to rescue those alterations in the heterozygous mice.

In parallel, heterozygous mice receiving wild-type microbiota travelled more distance in the open-field test whereas wild-type mice receiving *Grin2b*+/- microbiota did not reduce the travelled distance (see **figure 115, panel A**). Hence, alterations in general locomotion that were observed in the *Grin2b*+/- mouse model in open-field test are not transferred to wild-type mice with heterozygous microbiota transplantation while heterozygous mice receiving wild-type microbiota experiment an improvement in their hypoactivity.
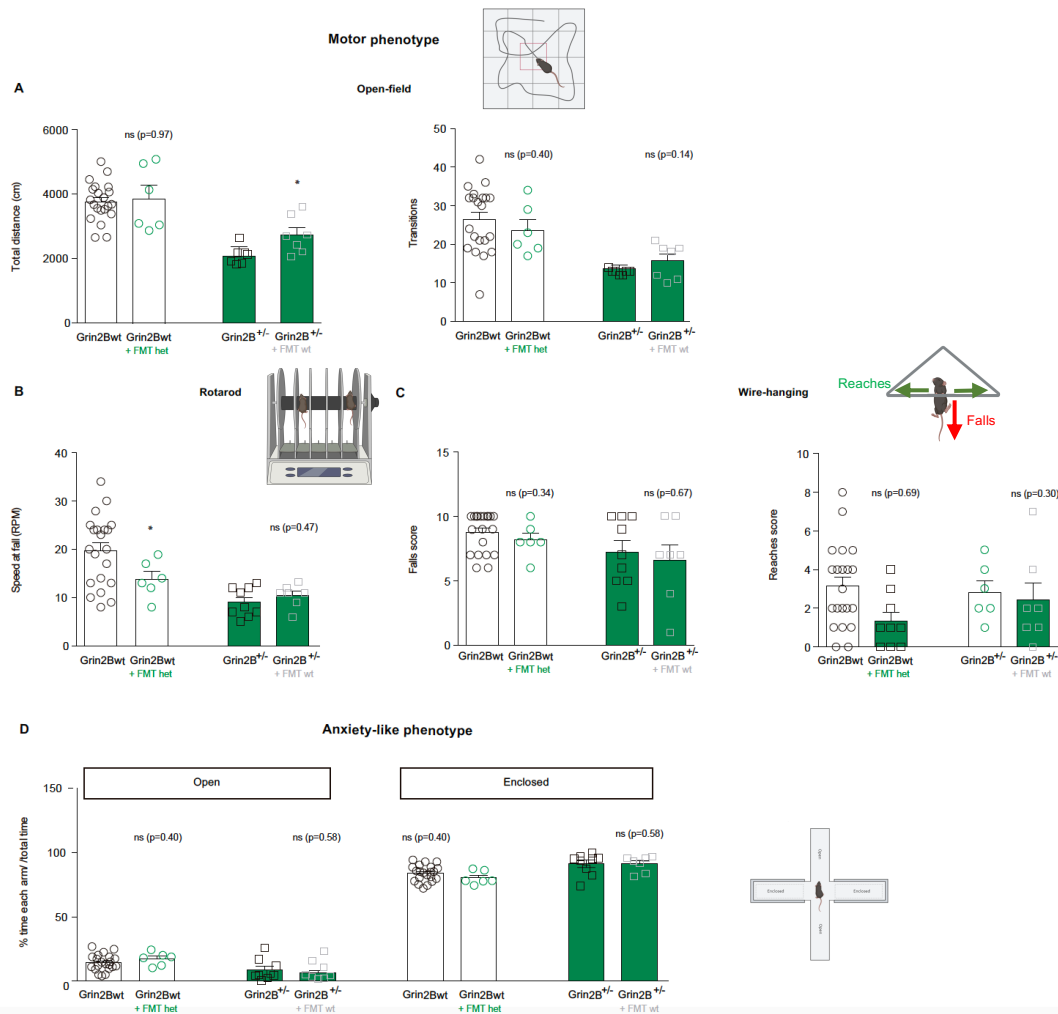
Figure 115. A-D, Bar graphs representing total distance (cm) ± SEM (**A, left panel**), and number of transitions ± SEM (**A, right panel**) in open-field test, RPM ± SEM in rotarod test (**B**), falls score ± SEM (**C, left panel**) and reaches score ± SEM (**C, right panel**), and % time spent in each kind of arm in regard with total exploration time ± SEM in elevated-plus maze (**D**) of female mice of both genotypes (white, wild-type; green, heterozygous *Grin2b$^{+/-}$*) ± FMT (black circles and boxes, no FMT; green circles and boxes, *Grin2b$^{+/-}$* microbiota is transferred; gray circles and boxes, wild-type microbiota is transferred) (N = 6-21 animals per condition; ns, P-value > 0.05; *, P-value < 0.05; **, P-value > 0.01; ***, P-value > 0.001; ****, P-value < 0.0001; unpaired t-test with Welch's correction for normal distribution and nonparametric Mann-Whitney test for non-normal data).

After behavioural assessment, mice were sacrificed to obtain hippocampal *ex vivo* slices. Field potential recordings of Schaffer collateral-CA1 pathway in the hippocampus of wild-type mice receiving *Grin2b$^{+/-}$* microbiota and heterozygous mice receiving wild-type microbiota show a slight bidirectional transference, given that wild-type microbiota transplantation to *Grin2b$^{+/-}$* mice provokes a partial increase of the reduced EPSPs slope without achieving wild-type levels (see **figure 116**) whereas heterozygous microbiota transference to wild-type mice slightly reduce EPSPs slope without reaching *Grin2b$^{+/-}$* heterozygous levels (see **figure 117**).

Figure 116. Time course of LTP after theta-burst stimulation demonstrating the changes on fEPSP slope values in slices of different types of mice (3-5 months age): wild-type (black); *Grin2b*+/- (green); and *Grin2b*+/- + wild-type FMT (gray); 6 animals per condition, 6-9 LTP recordings. Black arrow is showing when theta-burst stimulus is applied. Bar graphs comparing the average change on fEPSP slope values in the stable phase (last 40 minutes, indicated with black box)(ns, P-value > 0.05; *, P-value < 0.05; **, P-value > 0.01; ***, P-value > 0.001; ****, P-value < 0.0001; unpaired t-test with Welch's correction).
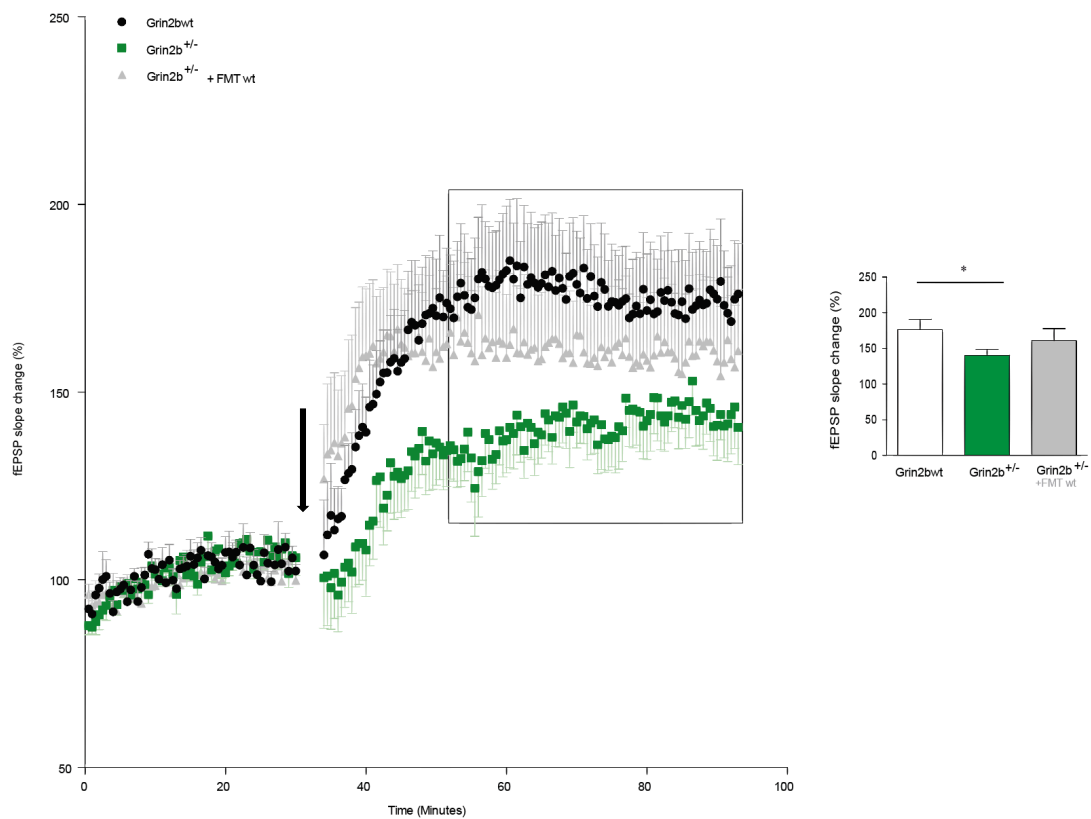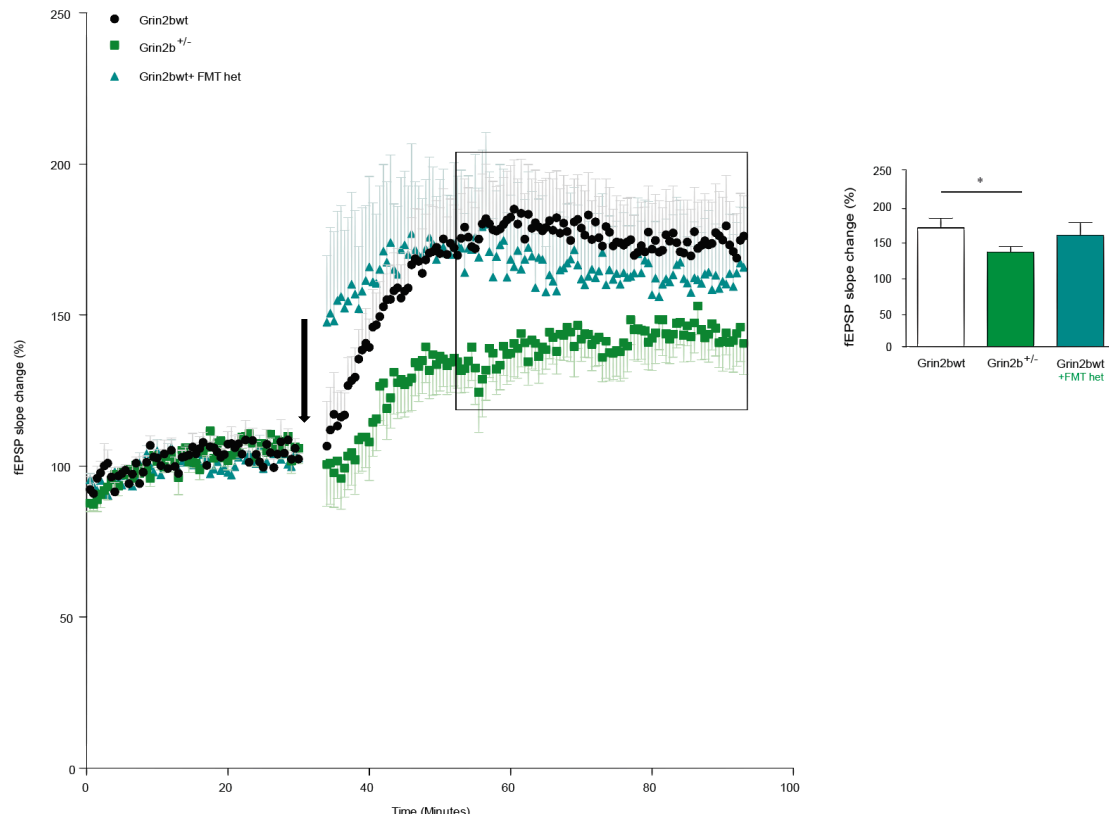
Figure 117. Time course of LTP after theta-burst stimulation demonstrating the changes on fEPSP slope values in slices of different types of mice (3-5 months age): wild-type (black); *Grin2b*$^{+/-}$ (green); and *Grin2b*$^{+/-}$ + wild-type FMT (blue); 6 animals per condition, 6-9 LTP recordings. Black arrow is showing when theta-burst stimulus is applied. Bar graphs comparing the average change on fEPSP slope values in the stable phase (last 40 minutes, indicated with black box)((ns, P-value > 0.05; *, P-value < 0.05; **, P-value > 0.01; ***, P-value > 0.001; ****, P-value < 0.0001; unpaired t-test with Welch's correction).

3.6.   Chapter 3: Summary and Conclusions

In this chapter, several therapeutic strategies to rescue loss-of-function variants were evaluated:

- A genetic strategy to overexpress a wild-type plasmid or a CTD-truncated plasmid (which are able to reach the cell surface) in combination with an ATD, LBD or TMD-truncated genetic variant, because these variants in heterozygosity were exerting a dominant negative effect in the wild-type subunit.
- D-serine, which is one of the natural co-agonists for NMDARs.
- Rapastinel, which acts as partial agonist of the NMDAR.
- Polyamines (specifically, spermine and its precursor, spermidine) which act as positive allosteric modulators for GluN2B-containing NMDARs.
- A fecal microbiota transplantation protocol in both directions:
  - The transference of wild-type microbiota to a loss-of-function mouse model (for the GluN2B subunit, *Grin2b*$^{+/-}$) to investigate whether wild-type microbiota is able to rescue previously observed alterations in this model (see Chapter 2).
  - The transference of heterozygous microbiota (from *Grin2b*$^{+/-}$ mice) to wild-type mice to investigate whether previously observed alterations in this model (see Chapter 2) are transferred to the wild-type mice.
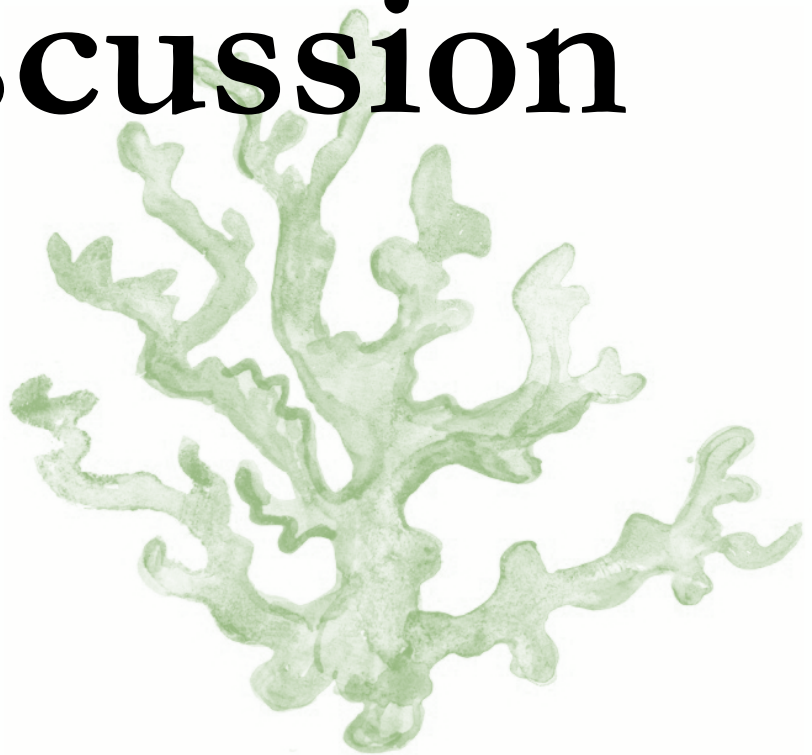
These strategies were evaluated in different systems (cell lines, neuronal primary cultures, a mouse model and *ex vivo* hippocampal slices) with different impacts that are summarized in the following table (**table 24**).

Table 24. Table summarizing the different therapeutic strategies evaluated in the chapter 3 (genetic, D-serine, Rapastinel, polyamines (spermine/spermidine), FMT with wild-type or heterozygous microbiota) and their effects on different systems and approaches (surface trafficking in cell lines, NMDAR-currents in cell lines, spines density in neuronal primary cultures, different behavioral tasks (memory, repetitive behaviors, short-term and long-term memory, social behavior, motor behavior, anxiety-like behavior and GI function) in a mouse model and LTP in hippocampal slices); Legend: white, ND; green, improvement/increase; red, worsening/reduction; gray, no effect. Abbreviations: IF, immunofluorescence; LTP, long-term potentiation; cLTP, chemical LTP; NOR, novel object recognition; GI, gastrointestinal; EPSPs, excitatory post-synaptic potential.

Strategy	Surface trafficking (IF cell lines)	NMDAR-derived currents (Patch-clamp in cell lines)	Dendritic spines density (cLTP and IF hippocampal cultures)	Behavior — Weight	Short-term memory (T-maze)	Long-term memory (NOR)	Stereotypies (marble-bury)	General activity (open-field)	Motor (rotarod)	Social behavior (3-chamber)	Motor (wire-hanging)	Anxiety-like behavior (EPM)	GI (n° stools)	GI (stool water content)	GI (transit time)	LTP — EPSPs slope (Ex vivo hippocampal slices and field-recording)
Genetic strategy	green															
D-serine			green													
Rapastinel																
Polyamines					gray								red	red		green
FMT: wild-type microbiota to Grin2b+/-				gray	gray	gray		green	gray				green			gray
FMT: Grin2b+/- microbiota to wild-type				gray		green	green		red				gray	gray	gray	red

Legend:
- white — ND
- green — Improvement/increase
- red — Worsening/reduction
- gray — No effect

Discussion

The glutamatergic system is the main excitatory pathway in the human body, and it is related with innumerable body functions. Due to its critical role in the normal physiology, in the glutamatergic synapse there are several elements that, when affected, can be related with severe neurodevelopmental disorders. One of these crucial elements is the NMDAR. Thus, NMDAR dysfunction has been related with distinct diseases such as Alzheimer disease, amyotrophic lateral sclerosis, autism, autoimmune encephalitis, depression, epilepsy, Huntington disease, schizophrenia, or Parkinson disease (Eisen A., 1995; Blandini F. et al., 1996; Chapman AG., 2000; Essa MM. et al., 2013; Marsden WM., 2013; Kamat PK. et al., 2016; Raymond LA., 2016; Lynch DR. et al., 2018; Tzang RF. et al., 2019; Uno Y. and Coyle JT., 2019).

Until very recently, there were a group of neurodevelopmental disorders that were diagnosed as autism spectrum disorders. Nevertheless, the implementation of Next-Generation Sequencing as diagnostic method revealed that this group of disorders was an entity in its own due to the presence of genetic variants in the same subset of genes (*GRIN* genes, which encode for the NMDAR subunits), receiving the name of *GRIN*-related disorders (GRDs).

It is difficult to conclude that *GRIN* variants are the definitive determinant of GRDs pathology because the functional understanding of these variants is scarce. Nevertheless, the increasing number of reported diseases-associated *GRIN* variants (437 according to GRINdb server, https://alf06.uab.es/grindb/home) (García-Recio A. et al., 2021) prove that the further delineation of the disease spectrum (to establish a genotype-phenotype correlation) and the evaluation of potential therapeutic options for GRDs, will contribute to the establishment of a personalized medicine for these neurodevelopmental disorders.

Unmet genotype-phenotype correlation in GRDs

GluN subunit impact in the pathogenicity and clinical aspects of GRDs

In this Thesis, 95 genetic variants in *GRIN1*, *GRIN2A* and *GRIN2B* genes have been recruited, which represent the most commonly affected genes in GRDs.

GRIN2C, *GRIN2D*, *GRIN3A* and *GRIN3B* are not considered in this Thesis because the majority of variants in these genes are identified as neutral variants (according to GRINdb server, https://alf06.uab.es/grindb/home) (García-Recio A. et al., 2021). Only discrete variants have been associated with autism, schizophrenia, or epileptic encephalopathy (Makino C. et al., 2005; Shen YC. Et al., 2009; Yu Y. et al., 2018; XiangWei W. et al., 2019). This might be indicating that *GRIN2C, GRIN2D, GRIN3A,* and *GRIN3B* subunits are more tolerant to variation than *GRIN1*, *GRIN2A* or *GRIN2B* subunits which are more prone to cause neurological diseases (see **figure 118**) (see **note[5]** for further information regarding genic variation tolerance).

Note[5]: Traditionally, variation tolerance was estimated based on how conserved a sequence is. If a sequence is highly conserved it is because it has a crucial role and variations on that sequence are more probably related with pathology. Then, several algorithms were developed. One of the most widely used is Residual Variation Intolerance Score (RVIS) which is based on available information regarding gene polymorphisms (Gussov AB. et al., 2016). The idea relies on the hypothesis that the more polymorphisms are found in a gene or a domain, the most tolerant this domain is to variation and less probability of pathogenicity. A negative RVIS represents less functional variation and less tolerance to variation. This approach (http://genic-intolerance.org), scores *GRIN1* with a RVIS = -1,11; *GRIN2A* RVIS = -1,46: *GRIN2B* RVIS = -2,41; *GRIN3A* RVIS = 0,21 while *GRIN2C*, *GRIN2D* and *GRIN3B* are not scored due to lack of information. These values support the hypothesis that *GRIN1*, *GRIN2A* and *GRIN2B* are less tolerant than *GRIN3A*, explaining why genetic variants in those subunits are more probably disease-associated.
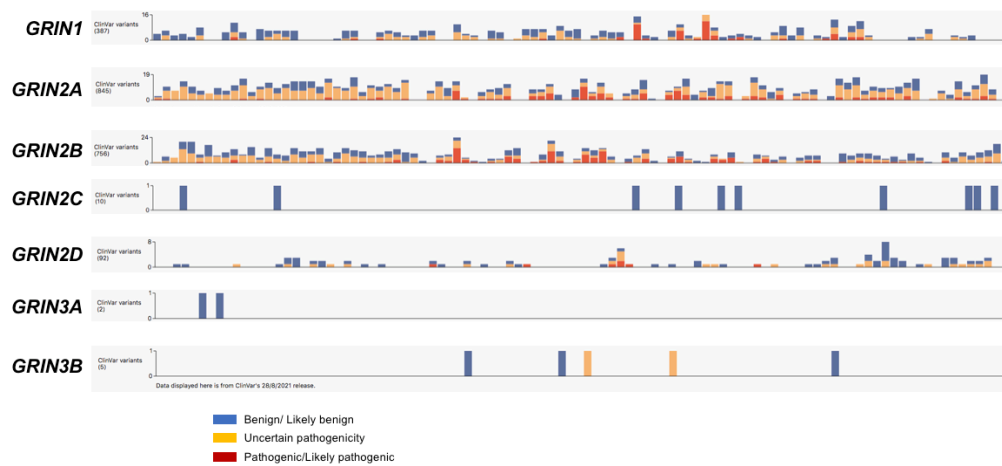
Figure 118. Graphs extracted from GnomAD (https://gnomad.broadinstitute.org) genome sequencing web server. The graphs show information of genomic variation and its association with health/disease, extracted from ClinVar database (NCBI, https://www.ncbi.nlm.nih.gov/clinvar/) of *GRIN1*, *GRIN2A*, *GRIN2B*, *GRIN2C*, *GRIN2D*, *GRIN3A* and *GRIN3B* genes. Legend: Blue, benign/likely benign; yellow, uncertain pathogenicity; red, pathogenic/likely pathogenic.

Considering those RVIS scores, *GRIN2B* seems the most intolerant gene, followed by *GRIN2A* and GRIN*1*. Nevertheless, reported variants and available functional annotations suggest that *GRIN1* variants are less abundant but highly associated with disease whereas many *GRIN2A* have been reported but there is less association with disease (García-Recio A. et al., 2021) (see **figure 118**). This might be explained by the different temporal expression pattern of each GluN subunit. *GRIN1* is the obligatory subunit, which is expressed from embryonic stages to the adulthood, *GRIN2B* is very abundant at neonatal stages and later, *GRIN2B* is substituted by *GRIN2A* in adulthood (Paoletti P. et al., 2013). Given that *GRIN1* is so critical, it is possible that genetic variants are less tolerated and consequently, very pathological but less detected. Indeed, it is demonstrated that mouse models completely lacking the GluN1 subunit result in lethality (Forrest D. et al., 1994). Regarding GluN2 subunits, early insults when development is still ongoing might be more determinant in pathology that late insults when most neuronal connections are already formed, explaining why *GRIN2B* variants are likely more pathogenic than *GRIN2A* variants. This is also supported by *GRIN2* mouse models given that *Grin2a* KO mice is viable while *Grin2b* complete KO is also lethal (Kutsuwada T. et al., 1996; Ito I. et al., 1997). In our cohort, these proportions are very similar, except for the fact that the most represented subunit is *GRIN2B* instead of *GRIN2A*. However, this slight variation is due to the fact that recruitment has been conducted via direct contact with GRDs families and clinicians, and at the beginning of the project, the association of families mainly was constituted by relatives of patients suffering from *GRIN2B* variants.

GRIN-related disorders are characterized by a wide spectrum of symptoms (developmental delay, intellectual disability, movement and motor alterations, epilepsy, brain abnormalities, stereotypies, language affectations, sleep disturbance, gastrointestinal alterations…) and this might be explained by the broad NMDAR distribution in the CNS and non-neuronal tissues (neurons, kidney, pancreas, skin, lung, heart, bone cells, blood cells, genital system, or GI tract) (Hogan-Cann AD. and Anderson CM., 2016).

Nevertheless, there is variability in the clinical presentation based on the affected subunit. *GRIN1* variants are very variable in their presentation: movement alterations, intellectual disability and epilepsy (> 50 %), brain abnormalities (20-30 %), stereotypies (15 %) and other manifestations in less than the 10 % of patients (language alterations, sleep disturbance and gastrointestinal alterations). *GRIN2A* most common clinical presentation is epilepsy (70 %) that might be frequently accompanied of intellectual disability and/or language alterations (30 %), and rarely accompanied of motor alterations (10 %). *GRIN2B* variants are mostly related with intellectual disability (70 %) although epilepsy and/or autism might also be present (40 %) (see **supplementary tables 1-3**).

In our cohort, *GRIN1* variants are also frequently related with intellectual disability (100 %) and motor alterations (65 %) although epilepsy (30 %) and brain abnormalities (30 %) are also reported while *GRIN2A* variants are mostly related with epilepsy (65 %) and *GRIN2B* variants are generally associated with intellectual disability (85 %). Thus, no clear correlation has been established that might explain the variable clinical presentation in *GRIN1* variants and the association between *GRIN2A* and epilepsy or *GRIN2B* and intellectual disability. Nevertheless, the comparison of clinical data extracted from our cohort and general reported data points toward a subunit effect in the clinical presentation.

GluN domains impact in the pathogenicity and functional alterations of *GRIN* variants

Regarding the location of the along the NMDAR subunit, *GRIN* variants are scattered along GluN subunit domains. Despite this, disease-associated *GRIN* variants, regardless of the affected subunit, are highly concentrated in the ligand-binding and the transmembrane domains (Amin et al., 2020; XiangWei et al., 2018; García-Recio A. et al., 2021) (see **figure 118**). These domains have also been evaluated in terms of genic variation tolerance. Nevertheless, these scores have been modified to improve the interpretation of the genic intolerance. Firstly, the missense tolerance ratio (MTR) was developed. This score compares the observed missense variants in a region with the predicted number of missense variants based on the region sequence context (Traynelis J. et al., 2017). This MTR approach applied to *GRIN1*, *GRIN2A* and *GRIN2B* genes has revealed that LBD, TMD and their linker regions are more intolerant than the ATD or CTD (lower score). Thus, this intolerance might explain why most disease-associated variants clearly cluster in these regions. Moreover, further analysis using algorithms that implement tridimensional structure (that consider nonadjacent residues that might interact or be close in the tridimensional structure) will tightly indicate what are the most susceptible regions to be affected by pathogenic variants (Perszyk RE. et al., 2021). In our cohort, this clustering of genetic variants in the LBD and TMD is also present. Nevertheless, we have generated additional artificial variants aimed to cover the whole GluN subunits.

These domains are less tolerant to genetic variation due to their critical role in NMDAR function (agonist binding and receptor gating) (Traynelis SF. et al., 2010). The importance of these domains explains why genetic variants are more prone to be pathogenic when affecting LBD and TMD of NMDARs. In fact, variants affecting each domain are commonly associated (although not exclusively) with alterations in the activities in which that domain is involved. For instance, *GRIN* variants which are located in the ATD are commonly associated with alterations in Zn^{2+} inhibition (Zn^{2+} allosteric site is located in this domain). Moreover, *GRIN* variants in the LBD and TMD domains are frequently related with agonists potencies, channel opening and permeability, or Mg^{2+} blockade while *GRIN* variants in the CTD have been associated with alterations in the receptor post-translational modification (there are several phosphorylation sites in this region) or in the receptor-MAGUKs interaction that determines the receptor docking at the cell surface (see **supplementary tables 1-3**).

Despite of these relative associations, *GRIN* variant associated-alteration and the functional impact (gain- or loss-of function) cannot be linearly correlated, except for variants which are located near the Mg^{2+} blocking site that are most commonly related with gain-of-function via reduction of the blockade by this ion (García-Recio A. et al., 2021).

Moreover, it is not enough to determine that a *GRIN* variant is affecting a particular aspect of NMDARs because it is very frequent that these kinds of variants alter more than one parameter of the NMDAR physiology. Furthermore, alterations might be even contradictory, and the lack of a complete evaluation might result in a misclassification of the variant (Xu XX. and Luo J-H, 2017). For instance, a particular variant might be annotated only in terms of agonist potency and it can be concluded that this hypothetical variant is related with increased glutamate potency. However, if surface expression is not evaluated in this variant, there is a possibility that the alteration in that particular residue might be also related to a lack of

surface trafficking. Hence, in this case, that variant that has been classified as gain-of-function due to increased glutamate potency is wrongly classified because the receptor is actually not reaching the cell surface and causing a loss-of-function. Thus, an evaluation as much complete as possible is needed to functionally annotate *GRIN* variants and this is currently not implemented in routine diagnosis. In this Thesis, to overcome this challenge, an experimental pipeline that evaluates distinct aspects of the NMDAR physiology has been implemented.

Experimental pipeline established for variants annotation

Along this Thesis, *GRIN* variants annotation has been performed based on the hypothesis that every critical step in the NMDAR physiology might be affected with *GRIN* variants: 1, synthesis and oligomerization; 2, release from the endoplasmic reticulum; 3, surface trafficking; 4, docking; 5, NMDAR opening and signaling. Thus, we have designed different approaches that might reveal the impact of *GRIN* variants in each of these processes.

Firstly, upon GRIN variant annotation inquiry, bioinformatic search has been performed in databases. Particularly, we search the variant in the GRINdb web server (https://alf06.uab.es/grindb/home) (García-Recio A. et al., 2021), which is continuously updated and reunites information from ClinVar (pathogenicity), LOVD (gene variation), Uniprot (protein), GnomAD (genome), GRIN-Leipzig (Lemke JR. group), CFERV (Traynelis SF. group), BCN-GRIN (own database) and previously published data (see **figure 119**). For reported variants already annotated, we investigated whether all critical parameters have been evaluated. If some parameters are lacking or there is no available information regarding the functional annotation, our experimental pipeline is implemented (see **figure 119**).

This pipeline initially determines whether the *GRIN* variant impairs the protein stability, because a protein misfolding results in the receptor degradation and consequently, a loss-of-function, regardless of other receptor properties. Then, if the NMDAR is not degraded due to the genetic variant, surface expression is evaluated given that a lack of surface expression is definitely related with a loss-of-function, despite other modifications. Finally, if the NMDARs are stable and able to reach the cell surface, NMDAR-mediated currents and distinct kinetic parameters are investigated. From these studies, variants might be annotated as loss-of-function, gain-of-function or complex variants (see **figure 119**).

The classification of a *GRIN* variant as complex results from the presence of a an altered parameter leading to gain-of-function but also another modified parameter that causes a loss-of-function. In these particular cases, an additional evaluation is conducted to determine what alteration predominates. With this aim, Traynelis SF. and colleagues have developed a formula ('charge transfer') that considers current amplitude, deactivation time, open probability, surface protein levels, an relative response to a given agonist concentration (for synaptic and non-synaptic responses) (Swanger SA. et al., 2016).
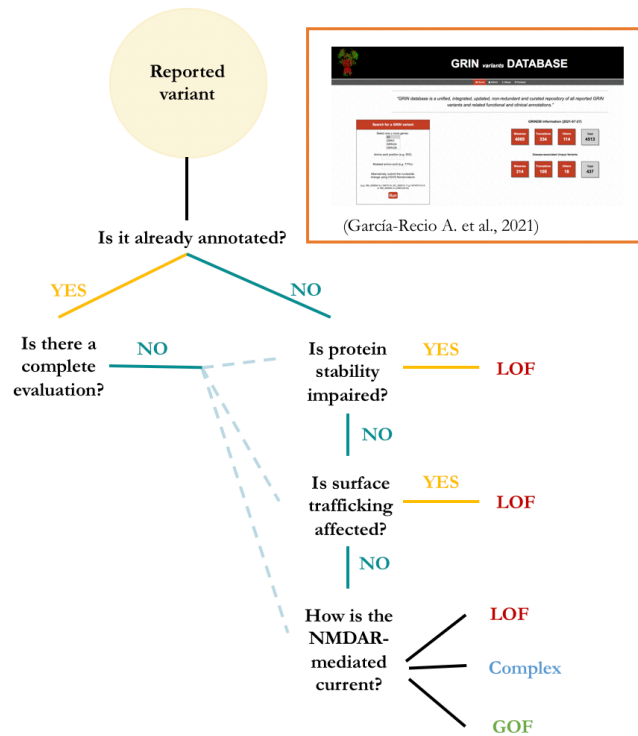
Figure 119. Decision tree that determines the experimental pipeline conducted in the lab for *GRIN* variants annotation.

Nonsense variants and NMDAR loss-of-function

Nonsense variants via a premature stop codon alter NMDAR protein length. The implementation of the abovementioned experimental pipeline has allowed us to determine the behavior of nonsense variants affecting ATD, LBD, TMD and CTD of *GRIN1*, *GRIN2A* and *GRIN2B*.

Our experimental pipeline has revealed that *GRIN* nonsense variants do not result in the degradation of the NMDAR, although *GRIN* nonsense variants affecting the ATD and LBD-S1 of NMDARs result in the formation of intermolecular aggregates, exclusively composed by the mutated subunit. Additionally, this experimental pipeline has also showed that nonsense variants affecting the ATD, LBD and TMD of NMDARs, reduce surface expression (Santos-Gómez A. et al., 2020). This lack of surface trafficking as well as the formation of aggregates might be explained by the absence of certain required sequences, resulting in the aggregation and retention of these truncated subunits in the ER-Golgi system. The oligomerization and release from ER-Golgi system is a tightly regulated process. For a correct interaction between GluN1 and GluN2 subunits, there are several critical residues (GluN1-I519, A524, K531, P532, Y535, R755, L777; GluN2A-I514, F524, V526, P527, E530, L777, L780 and their equivalent positions in GluN2B). When the NMDAR is truncated at the ATD, LBD or TMD (M1, M2, M3), these residues are lost, and proper oligomerization does not occur. Moreover, if this oligomerization does not occur, there is not masking of retention signals and NMDARs are not released from the ER-Golgi system. When the NMDAR is truncated at the last portions of the TMD, these residues are not absent but the truncated protein is lacking sequences that are necessary for masking retention signals (at the proximal CTD, the C0 cassette in GluN1, or EHL residues in GluN2 but also particular residues in the M3 helix (GluN1-W636, Y647 and T648; GluN2A-S644 and Y645; GluN2B-W635, S645, Y646, and T647). If masking of retention signals is not produced, NMDARs are not able to be released neither. Further experiments, to detect co-localization of this mutated NMDARs with distinct markers of specific intracellular compartments are needed to confirm the hypothesis of truncated NMDARs being retained in the ER-Golgi system (Singh R. et al., 2017).

Additionally, *GRIN* nonsense variants affecting the CTD (for instance, GluN2B-R847*) experiment a slight reduction (~20 %) of the surface NMDAR density, probably due to a lack of the PDZ-binding motif, which is responsible of the interaction with MAGUKs and the receptor docking to the cell surface (Santos-Gómez A. et al., 2020). The fact that this reduction was not observed in cell lines might be explained by the limitations of using cell lines as system. Cell lines are suitable as overexpression system for screening methods, but their machinery is not fully representative of the physiological machinery in neurons.

Partial stratification of *GRIN* missense and indel variants

To evaluate missense and indel variants, we have implemented the same experimental pipeline. This evaluation has resulted in the characterization of certain *GRIN* variants, but a global pattern of behavior has not been found.

<u>Biogenesis and surface expression of *GRIN* missense and indel variants</u>

Particular missense residues result in the degradation of the channel (particularly, GluN1-R217W, GluN2B-S555N and GluN2B-D732V). The reason why these particular residues are associated with protein instability is unknown, but we hypothesize that the aminoacid change could affect quaternary structure, leading to protein misfolding and consequently, degradation. Previously published data determined that GluN1-R217W was associated with increased Zn^{2+} inhibition and consequently a mild loss-of-function (Lemke JR. et al., 2016) and GluN2B-S555N was associated with an increased glutamate and glycine potency and consequently it is associated with a gain-of-function (CFERV data, http://functionalvariants.emory.edu/database/index.html) whereas there was no available information regarding GluN2B-D732V. Nevertheless, protein stability and/or surface trafficking were not evaluated in those investigations, and these variants are degrading the receptor and consequently, they are associated with a severe loss-of-function, regardless of agonists or Zn^{2+} potencies.

Additionally, we have demonstrated that indel variants that were affecting the TMD result in a lack of surface expression (GluN1-I619G620dup and GluN2B-L650F653del). The TMD is a very conserved region, in terms of sequence and polarity because it is the region of the receptor which is inserted in the lipid bilayer. Thus, we hypothesize that any modification of the sequences that are located inside the membrane might be affecting the receptor insertion in the cell surface via hydrophobic changes.

Moreover, other particular *GRIN* missense variants also affect surface expression (GluN1-D227H, G827R, E834Q; GluN2A-T646A; GluN2B-C457Y, G459R, R519Q). The reason why these residues affect surface expression is unknown and it has not been investigated during this Thesis, but those residues might be critical in any of the processes which are needed for the NMDAR to reach the cell surface or to be stabilized at the membrane (avoiding endocytosis) or alternatively, the aminoacid change affects the interaction and/or position of one of the critical residues. Further investigations are needed to fully elucidate why *GRIN* variants affect surface trafficking without degrading the receptor. There were not previous functional data regarding GluN1-E834Q, GluN2B-C457Y, G459R and R519Q that are characterized in this Thesis as loss-of-function due to a lack of surface expression. Moreover, we have also confirmed GluN1-G827R that was already considered a loss-of-function due to NMDAR-mediated currents reduction (CFERV data, http://functionalvariants.emory.edu/database/index.html) (although currently we also know that this reduction is due to reduced surface trafficking). GluN1-D227H was considered neutral and GluN2A-T646A, a gain-of-function (CFERV data, http://functionalvariants.emory.edu/database/index.html) because only pharmacological parameters were evaluated, but neither of these variants is able to reach the cell surface, so they are leading to a NMDAR loss-of-function.

Functional impact of *GRIN* missense and indel variants

Nevertheless, only certain missense variants are associated with protein instability and/or surface trafficking alterations. Thus, the majority of *GRIN* variants will be associated with functional modifications. The functional evaluation via electrophysiological recordings is very time-consuming due to the complexity of the technique and consequently, it was not possible to functionally annotate all the recruited variants. From the 95 recruited variants, 29 *GRIN* variants were already annotated by previous work conducted in the lab (D. Soto and F. Miguez), 33 *GRIN* variants were annotated in terms regarding their effects in protein stability and/or surface trafficking, 22 *GRIN* variants have been annotated in this Thesis (of these, 10 *GRIN* variants are annotated to validate the structure based-superimposition model and they will be further discussed in the following section) and 11 *GRIN* variants are still devoid of functional annotation.

Thus, out of the 12 *GRIN* variants that have been functional evaluated along this Thesis, 4 GRIN variants are classified as loss-of-function (GluN1-M813T; GluN2A-V563L; GluN2B-W559R, C746Y), 6 GRIN variants result in gain-of-function (GluN1-R548W, V656M, P805S; GluN2A-V639I; GluN2B-S628C, M818L) and in 2 of the variants, we were not able to detect any modification (although some parameters have not been evaluated like agonists potencies, rise-time or Mg^{2+} blockade, since the location of the variant is highly improbable to modify these parameters). From the loss-of-function variants, there was available data only for GluN1-M813T which was already classified as loss-of-function (reduced glutamate and glycine potency, CFERV data, http://functionalvariants.emory.edu/database/index.html). There was no available information regarding GluN2A-N490H and GluN2B-M829V, and we were not able to detect any alteration (uncertain pathogenicity). Concerning the variants that are classified as gain-of-function, there was not available information of GluN1-R548W and V656M. GluN1-P805S, GluN2A-V639I and GluN2B-S628C, and M818L were already classified as gain-of-function due to increased glutamate and glycine potencies (CFERV data, http://functionalvariants.emory.edu/database/index.html) and we have confirmed these annotations with additional data. Despite the annotation of several *GRIN* variants, no linear correlation has been found between the affected subunit and/or altered GluN domain and the *GRIN* variant functional impact. Further annotations are needed to elucidate a potential correlation.

Structure-based superimposition model as an acceleration tool is limited

The experimental pipeline we have been applying during the Thesis is effective, but the majority of variants need to be functionally evaluated by means of electrophysiological recordings and this approach is very laborious, delaying the diagnose and consequently, the therapeutic intervention. In order to overcome this issue, Dra. M. Olivella and colleagues (Vic) have developed a superimposition model of GluN1, GluN2A and GluN2B subunits based on their crystallographic structures and topological domains conservation, under the hypothesis that functional annotations of specific *GRIN* missense variants could predict the functional changes in equivalent structural positions in other GluN subunits (see **figure 120**).
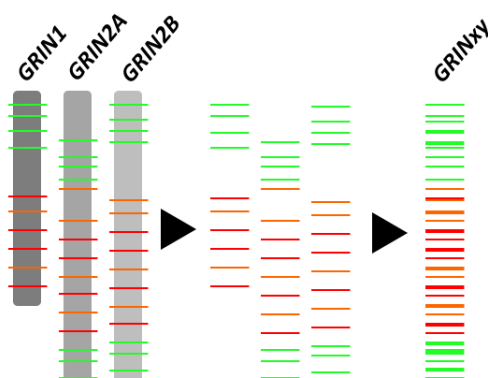

Figure 120. Schematic representation of the hypothesis that functional annotations of specific *GRIN* missense variants could predict the functional changes in equivalent structural positions in other GluN subunits based on the statement that *GRIN1*, *GRIN2A*, *GRIN2B* are equivalent.

This structure model has been already validated *in silico,* revealing a potential predictive power of the algorithm regarding pathogenicity and functional impact. Along this Thesis, we have experimentally investigated this predictive power. To do that, we have selected 10 *GRIN* variants affecting the GluN1 subunit and the GluN2A subunit that are equivalent to already annotated GluN2B variants from patients. Then, mutant NMDAR surface expression was assessed, revealing surface patterns conservation between the different subunits (Santos-Gómez A. et al., 2021, *submitted*). Additionally, biophysical characterization was performed. Similarly, to surface trafficking pattern effect, whole-cell patch clamp experiments displayed an overall conserved electrophysiological impact between GluN1 and GluN2B and mostly of the GluN2A-GluN2B pairs except for GluN2A-G483D/GluNB-G484D and GluN2A/GluN2B-R693G pairs where the GluN2B showed a significant reduction in normalized peak current amplitude and the GluN2A phenotype was not so clear. Additionally, there were some discrepancies in terms of kinetics parameters in the GluN2A-G543R/GluN2A-G542R and the GluN2A-G688S/GluN2B-G689S pairs (Santos-Gómez A. et al., 2021, *submitted*). Currently, the reason why these inconsistencies have been found is unknown. However, it is possible that certain residues in one of the subunits present certain roles or interactions that are not present in other subunits and these slight differences result in exceptions that cannot be extrapolated from one subunit to another different subunit. Thus, the structure-based superimposition model will need to incorporate additional information in order to determine what these exceptions are and still maintain its predictive power.

Homozygosis *vs*. Heterozygosis: What is really happening in patients?

In order to determine the functional impact of the different *GRIN* variants, the experimental pipeline has been applied in cells lines transiently expressing the distinct mutations without the presence of wild-type subunits. This has allowed us to determine the direct effect of the mutation in that specific subunit. Nevertheless, most of the variants reported in patients are in heterozygosity. Thus, immunofluorescence and electrophysiological approaches have been adapted to evaluate a modified situation where both kinds of subunits (wild-type and mutated) are expressed in equimolar quantities. Thus, these adapted protocols allow to investigate different kind of variants in 'heterozygosity', a more realistic situation.

These modified approaches revealed that GluN2 nonsense variants exert a dominant negative effect on the wild-type subunit by reducing NMDAR total surface density and also the wild-type containing receptors (except for certain exceptions that were confirmed by electrophysiological recordings), whereas GluN1 nonsense variants do not present this behavior (Santos-Gómez A. et al., 2020). The discordances of certain *GRIN* variants outcomes between immunofluorescence and electrophysiological approaches might be explained because we are using a cell system overexpressing the different variants and an antibody concentration that amplifies the detection of those overexpressed proteins. Moreover, we are actually not controlling the different receptor populations because wild-type and mutated plasmids are combined with a complementary plasmid (GluN1 for GluN2 variants and vice versa) but different populations are formed with this combination (receptors that only contain mutated subunits, receptors that only contain wild-type subunits and receptor that contain both types of subunits). In order to express only combined receptors (with wild-type and mutated subunits), engineered plasmids might be use, using different tags with retention signals for the different types of subunits which guarantee that only receptors containing both type of subunits are able to mask those retention signals by a coiled-coil formation between the two tags (Yi F. et al., 2017). All these factors can contribute to the lack of detection of subtle changes in some conditions by immunofluorescence and consequently, the disclosure of certain discrepancies between both techniques. The different behavior between GluN1 and GluN2 nonsense variant is due to the fact that GluN1 expression is not limiting (see **figure 121**).
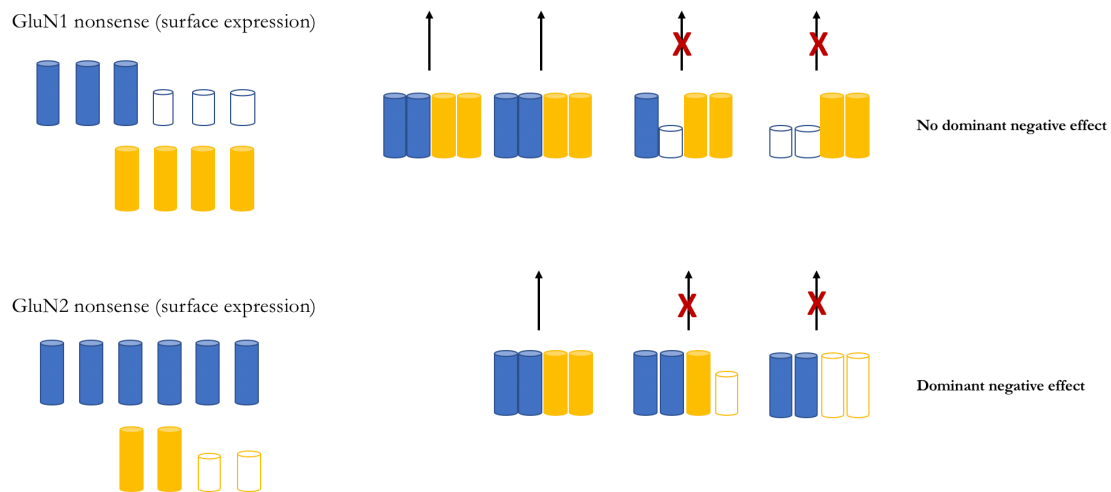
Figure 121. Working model for GluN1 and GluN2 nonsense variants biallelic expression behavior: GluN2 exert a dominant negative effect while GluN1 do not, because GluN1 expression is not limiting. Empty and short shapes represent truncated GluN subunits while colored and completed shapes represent wild-type subunits (blue, GluN1 subunits; yellow, GluN2 subunits).

Contrasting with nonsense variants, GluN1 and GluN2 missense and indel variants dominant negative effect is based on the underlying alteration. If GluN variants cause a functional alteration without affecting surface expression are also exerting a dominant negative effect, while GluN variants that affect surface expression do not present this behavior.

GRIN variants affecting the NMDAR function do not affect oligomerization, so they form 'functional' complexes but all the complexes that contain a mutated subunit present the corresponding functional alteration (completely altered when both alleles are mutated and an intermediate phenotype when one allele is wild-type and another allele is mutated) (see **figure 122**).
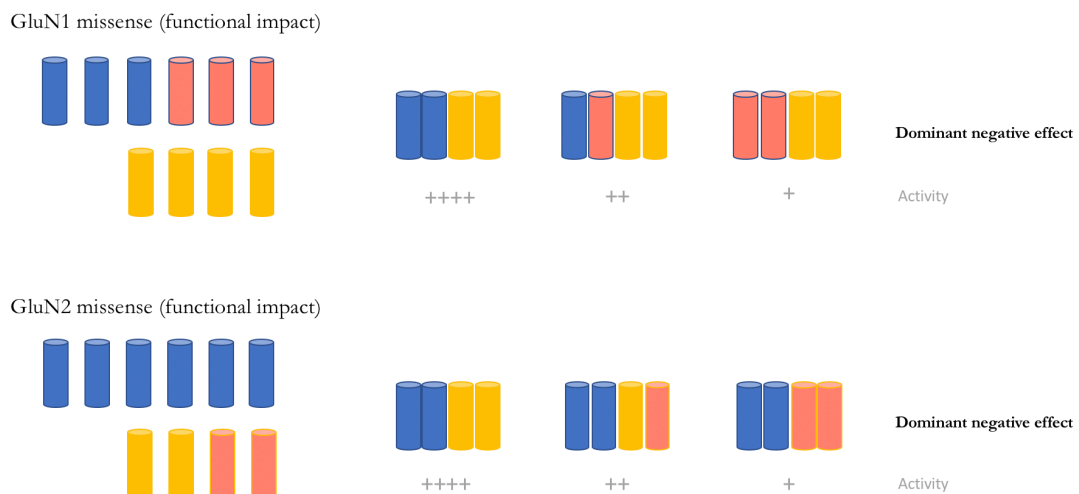

Figure 122. Working model for GluN1 and GluN2 missense variants affecting the NMDAR function and consequently, exerting a dominant negative effect because oligomerization and/or surface expression are not altered, and 'combined' receptors are formed although do not function properly. Pink shapes represent mutated GluN subunits while wild-type subunits are painted in blue (GluN1) or yellow (GluN2).

Alternatively, *GRIN* variants that affect surface expression do not exert a dominant negative effect, regardless of the affected subunit. GluN1 behavior might also be explained but the fact that it is not a limiting subunit, but this explanation does not apply for GluN2 variants. GluN2 lack of dominant negative effect might be explained by the subunit degradation in certain GluN2 missense variants but for GluN2 variants that affect surface trafficking without being degraded (for instance, GluN2B-G459R) the underlying mechanism explaining the lack of dominant negative effect is unknown given that we still do not fully understand why this kind of variants affect surface expression (see **figure 123**).
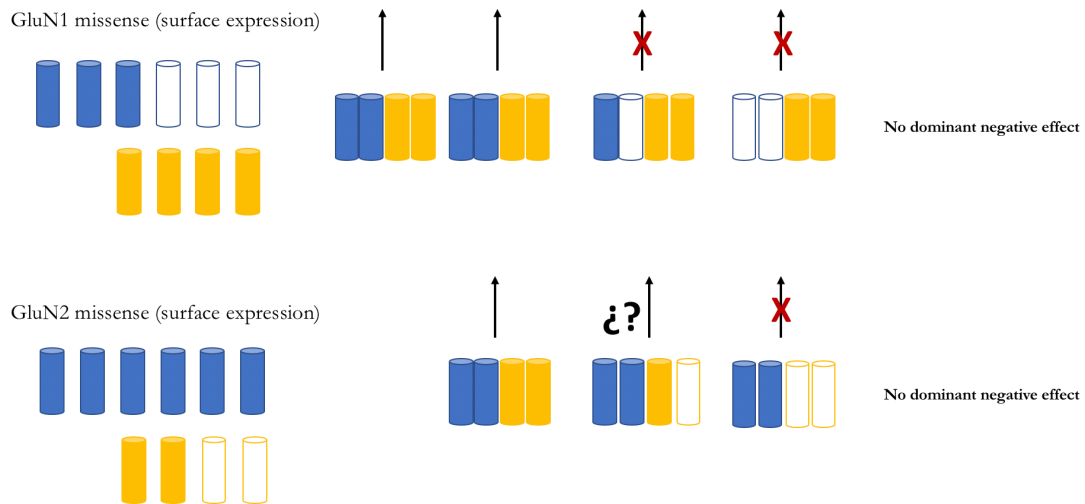

Figure 123. Working model for GluN missense variants that affect surface trafficking. GluN1 variants do not exert a dominant negative effect because its expression is not limiting whereas the reason why GluN2 variants do not exert this dominant negative effect is unknown. Empty shapes represent GluN missense variants while colored shapes represent wild-type constructs (blue, GluN1 subunits; yellow, GluN2 subunits).

The evaluation of *GRIN1* variants is limited in neuronal primary cultures with conventional approaches

The functional annotation of *GRIN* variants (via our experimental pipeline) and the evaluation of their effect in heterozygosity (simulating what is happening in patients) were conducted in cell lines because this system is manageable and has been proven effective as screening method. Nevertheless, we have seen that some incongruencies can be detected due to limitations in the techniques' sensitivity to detect subtle changes. This limitation might be explained because of the technique itself but also because cell lines due to their characteristics express high levels of proteins, and this overexpression might be masking slight modifications. Thus, additional experiments have been conducted in hippocampal neuronal primary cultures which are isolated directly from the brain tissue, retaining some morphological and functional traits. Neuronal primary cultures have been used to confirm findings from surface trafficking evaluation and to investigate the impact of *GRIN* variants in neuronal morphology in basal and stimulated conditions.

Unfortunately, this system also revealed some limitations. After transfecting GluN1, GluN2A and GluN2B wild-type and mutated plasmids with fluorescent tags, we noticed that the tagged-GluN1 subunit (regardless of being wild-type or mutated) was not detected in the neuronal surface while wild-type GluN2A and GluN2B were detected. This might be explained by the fact that neurons endogenously express NMDAR subunits and the intrinsic GluN1 which is overexpressed displace the oligomerization of exogenous tagged-GluN1 subunits, leading to a lack of tagged-GluN1 expression (Prybylowski K. et al., 2002).

Thus, it is not possible to study GluN1 variants in neuronal primary cultures with conventional approaches. In order to evaluate *GRIN1* variants impact in neuronal morphology and activity, firstly, a knock-down of the endogenous GluN1 subunit mediated by shRNA might be conducted prior to the expression of the mutated GluN1 subunits (Lichnerova K. et al., 2015).

Loss-of-function variants are associated with dendritic spines reduction

GRIN variants evaluation in cell lines is suitable as screening method of the functional impact. In fact, immunofluorescence analysis of certain variants in neuronal primary cultures have confirmed the findings from surface trafficking analysis in cell lines. Nevertheless, neuronal primary cultures allow for further investigations regarding *GRIN* variants impact in the neuron physiology. In this Thesis, the analysis of dendritic spines density and morphology has been applied to further characterize several loss-of-function variants. Particularly, some *GRIN* nonsense variants affecting surface trafficking or docking (GluN2A-E182Nfs*23, V452CFs*11; and GluN2B-R519*, E839*, and R847*), a missense GluN2B variant that causes a pore reduction (P553T), and an indel variant devoid of functional annotation (GluN2B-K1293del ± homer2-E221K). Despite of being devoid of functional annotation, we hypothesize that the indel variant is also related with loss-of-function because the variant is located in a region where interaction with post-synaptic proteins like homer2 is very frequent (homer2 is also mutated in the same patient).

This approach revealed that all the evaluated loss-of-function variants were related with a reduction in the number of dendritic spines. This might be explained by the reduction of NMDAR activity, regardless of the affected process. Variants that are affecting NMDAR trafficking to the cell surface reduce the total density of receptor that might be activated with LTP induction, and GluN2B-P553T present a normal density but the channel pore is reduced. Thus, in both situations, there is a reduction of the Ca^{2+} signaling that is responsible of spines dynamics. The fact that spines are also being reduced in GluN2B-K1293del ± homer2-E221K, supports the hypothesis that this is variant is possibly associated with a. loss-of-function, although the underlying mechanism is not known. The reduction of spine density in variants that affect surface trafficking have been previously reported (Mota-Vieira M. et al., 2020).

In addition of evaluating dendritic spines density, types of spines are also distinguished, using this approach (from most immature to most mature formation: thin, stubby and mushroom), despite it is demonstrated that spines are not static and a snapshot from the microscope represents spines in morphological transition (Hering H. and Sheng M., 2014). Nevertheless, despite this dynamic behavior, the evaluation of spines morphology might reveal modifications in neuronal maturation. Particularly, these variants are associated with a reduction in the number of stubby spines, because neuronal primary cultures are transfected at DIV11, and neurons are fixed for immunofluorescence analysis at DIV14, when cells are not completely mature. In this period, stubby spines are the predominant type at that maturation state, so changes will be more evident in this type of spines than the others. Despite being immature (synaptic contact zone is still small, and number of vesicles reduced), we are conducting the experiments in that particular moment, because after DIV14, a reduction in synaptic density has been observed in neuronal cultures from embryonic rat (Ichikawa M. et al., 1993).

Does *Grin2b*$^{+/-}$ mouse model recapitulates symptoms associated with *GRIN* loss-of-function variants?

In vitro assessment has revealed that the majority of *GRIN* variants are related with NMDAR loss-of-function. In order to evaluate *GRIN* loss-of-function *in vivo*, there are distinct available mouse models of reduced GluN1, GluN2A and GluN2B subunits, as well as, some particular models with specific *GRIN* variants. Given that, in our cohort of 95 *GRIN* variants, the most represented subunit is the GluN2B subunit, we decided to focus on a *Grin2b* heterozygous mouse, assuming a loss-of-function in this model.

This mouse model is the only option to have reduced GluN2B subunit because *Grin2b* KO mice are lethal due to a lack in the suckling response (Kutsuwada et al., 1996). Nevertheless, it resembles what is happening in patients, because most patients with GRDs present *GRIN* variants in heterozygosis. Based on GRD symptoms (slim constitution, intellectual disability, developmental delay, stereotypies, autism, motor alterations, anxiety, gastrointestinal alterations, epilepsy, brain alterations, language alterations, sleep disturbance, altered pain responses) we have generated a battery of behavioral tests to conduct a full characterization of the *Grin2b*$^{+/-}$ mouse model because very few studies are available regarding this mouse model phenotype. Due to technical limitations, there are several phenotypes which we were not able to measure such as epilepsy, brain alterations, language alterations, sleep disturbance or pain response. Thus, we still do not know whether this model reproduce those GRD-associated alterations or not.

Concerning the evaluated phenotypes, the mouse model reproduces the motor deficits and the anxiety-like phenotype observed in GRD patients, while no significant changes were detected in the rest of phenotypes. Some of these phenotypes are seen in male mice only as tendencies but this might be explained by the reduced sample size because apparently there are not differences regarding gender. There are no available information conducting a complete phenotypic assessment of the *Grin2b*$^{+/-}$ mouse model. Nevertheless, the hypoactivity and the anxiety-like phenotypes were also observed in a heterozygous mouse model with a point mutation in the GluN2B subunit (GluN2B-C456Y) (Shin W. et al., 2020).

After the behavioral assessment, mice were sacrificed, and *ex vivo* hippocampal slices were obtained to perform field potential recordings of EPSPs in Schaffer collateral-CA1 pathway. This electrophysiological approach revealed a slight reduction in the slope of EPSPs from heterozygous mice while there were not significant changes in memory tasks during behavioral assessment. Nevertheless, although EPSPs slope is reduced, heterozygous mice are still able to develop long-term potentiation and this result is in agreement with behavioral tasks where heterozygous mice presented a slightly reduced discrimination index in novel object recognition test and less tendency to alternate in the T-maze spontaneous alternation paradigm, but they still prefer novel object instead of the familiar one and they alternate more than repeat the previously chosen arm.

Grin2b$^{+/-}$ is likely mimicking *GRIN2B* pathogenic nonsense variants. Thus, it is a good model to evaluate potential therapeutic options for patients with this kind of variants, even though some phenotypes are not fully represented. Furthermore, these therapeutic interventions might be effective with other kind of variants (for instance, those leading to functional modifications) despite the fact that this mouse model is not fully representative of all the loss-of-function *GRIN* variants. To fully represent all the spectrum of loss-of-function variants, knock-in mice of representative *GRIN* variants should be developed but this specific approach is expensive and time-consuming. However, the study of KI mice harboring highly representative mutations (in a great number of patients) might be a valid strategy in the future.

Therapeutic strategies towards *in vitro* rescue of *GRIN* variants functional outcomes

Based on *in vitro* evaluation of functionally annotated *GRIN* variants, we can adapt distinct protocols to check whether the different therapeutic interventions are able to rescue those reported modifications. Almost the 70 % of the 95 recruited *GRIN* variants have been annotated as loss-of-function variants. Thus, this Thesis mainly focused on defining these variants behavior *in vitro* and *in vivo* (*Grin2b*$^{+/-}$ mouse model) to further evaluate potential therapeutic interventions.

In vitro analysis of loss-of-function *GRIN* variants demonstrated the existence of two main LOF (loss-of-function) categories. One of these groups is affecting surface trafficking and/or docking, leading to reduced NMDAR surface density while the other group does not reduce the total pool of receptors, but they do not properly function (reduced peak current amplitudes, faster kinetics, reduced agonists potencies...).

Several approaches have been evaluated to investigate a potential rescue of these variants: genetic strategy, dietary/pharmacological strategy (D-serine, rapastinel, polyamines) or microbiota manipulation.

<u>Genetic strategy towards nonsense variants rescue</u>

During this Thesis, we have extensively characterized nonsense variants behavior demonstrating that nonsense variants affecting ATD, LBD, TMD impair surface trafficking and exert a dominant negative effect when expressed in 'heterozygosis' (monoallelic expression). For this kind of variants, several strategies might be used, including those that are going to be discussed in the following sections. In addition to those strategies, for this kind of variants, we have evaluated the potential rescue of a genetic strategy. This genetic strategy is based on the dominant negative effect that might be indicative of a competition or a retention effect between the different subunits. Thus, we hypothesize that increasing the amount of wild-type subunit, the mutated subunit that it is not able to reach the cell surface might be displaced. Preliminary results confirmed this displacement when a wild-type plasmid or even a CTD-truncated plasmid (that it is able to traffic, and it is smaller to be packaged in viral vectors) are overexpressed. Thus, gene therapy might be a potential therapeutic option for GRDs after defining some aspects of the protocol (further discussed in following sections: 'Finding a cure: Is gene therapy possible for GRDs?').

<u>D-serine, rapastinel and spermine rescue spines deficits</u>

D-serine (a natural co-agonist of the NMDARs) and rapastinel (a partial agonist) have been evaluated to check whether these compounds are able to rescue spines deficit associated with loss-of-function variants in basal and under stimulating conditions in hippocampal primary cultures. In order to study long-term potentiation (LTP) *in vitro*, there is a well-established protocol where LTP is promoted by glycine application in neuronal primary cultures (Lu WY. et al., 2001) and it is demonstrated that there is an actin-mediated change in spines morphology during long-term potentiation (LTP) due a calcium increase via NMDAR activity and/or NMDAR-mediated AMPAR insertion (Fortin DA. et al., 2010). This approach revealed that after LTP, spines density is increased in wild-type conditions whereas in neurons expressing the variants that were associated with reduced spines density in basal conditions, there is not such increase. Additionally, D-serine, spermine and rapastinel have been added in combination with glycine, showing that these compounds are able to rescue the observed spines deficits, via NMDAR potentiation that result in an increased Ca^{2+} signaling and consequently, a recovery of spines dynamics. Again, greater changes are observed regarding stubby spines that are the predominant ones between DIV11-DIV14.

<u>Spermine rescue of NMDAR-currents and spines deficits</u>

Moreover, spermine has also been proved to be effective in the potentiation of NMDAR-mediated currents in wild-type and several genetic variants affecting GluN1 and GluN2B subunits, without changes in potency (1.5-fold increase). Nevertheless, depending on the variant, the achieved rescue will be different. Based on actual recordings from some *GRIN* variants, we have predicted the level of rescue that it might be achieved with spermine addition in different conditions, and there are certain genetic variants in which spermine is not able to potentiate or its effect is almost null (*e.g.* biallelic expression of *GRIN* variants affecting surface NMDAR density, completely abolish NMDAR insertion at the cell surface and consequently there are no available surface NMDARs to be potentiated). Thus, spermine dosage should be adjusted because there are several conditions that do not need a saturating dose (as the one which has been used in these experiments) and other conditions, that despite using the highest dose, will not achieve wild-type levels.

Evaluation of novel therapeutic strategies in *Grin2b*+/- mouse model of GRD

Two therapeutic options have also been evaluated *in vivo* for the rescue of *Grin2b*+/- mouse model associated phenotypes: a polyamines-based treatment and microbiota manipulation.

Spermidine chronic supplementation

From all the dietary and pharmacological compounds, spermine was selected for further evaluation *in vivo* in *Grin2b*+/- mouse model, because previous studies conducted by the group revealed that spermine is more potent than D-serine (data not shown) and it is available in the market as dietary supplement in its precursor form (spermidine capsules). Spermidine was chronically administered to mice (3 mM in drinking water) based on other studies evaluating orally administered spermidine in mouse models (Chrisam M. et al., 2015; Eisenberg T. et al., 2016; Wirth A. et al., 2021).

Spermidine chronic supplementation partially rescued hypoactivity and motor coordination but there were not effects in anxiety-like phenotypes. The partial rescue might be due to short supplementation prior to behavioral assessment (other studies are supplementing for 6 months while we supplemented for 1.5 month), mice age because it is not demonstrated whether spermidine is able to cross the blood brain barrier in young mice, or mice gender given that other groups also had trouble in identifying improvements in female mice but not in male mice (Schroeder S. et al., 2021).

Despite the low dose and the lack of rescue of anxiety-like phenotypes, spermidine supplementation resulted in additional modifications in parameters that were not affected initially in the *Grin2b*+/- mice. These modifications were a reduced stool water content in both genotypes and an increased number of buried marbles in the heterozygous group. The increased number of buried marbles is usually associated with repetitive behaviors that might be related with anxiety-like behaviors (Angoa-Pérez M. et al., 2013). Interestingly, the increased number of buried marbles has also been observed in a mouse model lacking spermidine/spermine N-acetyltransferase (SSAT) that inactivates polyamines via acetylation (Sandusky-Beltran LA. et al., 2019). Moreover, several polymorphisms in SSAT and other polyaminergic enzymes (like spermine synthase or spermine oxidase) have been associated with an increased risk for anxiety, mood disorders and attempt suicide (Fiori LM. et al., 2010). Thus, polyamines and their metabolism seem to be related with this particular behavior, and this might also explain the lack of rescue of *Grin2b*+/- anxiety-like behaviors and the fact that we only observe this increased compulsive behavior in *Grin2b*+/- mice and not wild-type mice that are less prompted to develop anxiety-like phenotypes. Moreover, the reduced stool water content which is observed in both genotypes might be due to an enhancement of intestinal absorption by spermidine or its metabolite, spermine via loosening of the epithelium tight junctions (Gao Y. et al., 2007).

Additionally, field potential recording of the Schaffer collateral-CA1 pathway in *ex vivo* hippocampal slices revealed a slight increase in the EPSP slope of *Grin2b*+/- mice, without reaching statistical significance nor the wild-type levels. This increase is not observed in the performed memory tasks because mice that did not receive spermidine already prefer the novel object rather than the familiar one in the novel object recognition test and preferentially alternate in the T-maze paradigm.

Fecal microbiota transplantation

The presence of gastrointestinal alterations in GRDs patients prompted us to believe that microbiota manipulation might be potentially recommended to improve GRD symptomatology, despite the fact that *Grin2b*+/- mouse model do not reproduce those alterations.

Thus, fecal microbiota transplantation was evaluated to assess whether heterozygous microbiota transference provokes motor deficits, anxiety-like behaviors and plasticity alterations in the wild-type mice and/or wild-type microbiota transference is able to rescue those phenotypic alterations of the *Grin2b*$^{+/-}$ mouse model. The only transferred phenotype from *Grin2b*$^{+/-}$ to wild-type mice is a worse performance in the rotarod test, indicating that motor coordination of wild-type animals could be affected due to the transplant of heterozygous microbiota. Nevertheless, other motor deficits (reduced locomotion in open field test or reduced reaches score in the wire-hanging test) are not transferred with FMT. Alternatively, *Grin2b*$^{+/-}$ mice receiving wild-type microbiota increased locomotion in the open field test but there was not rescue of anxiety-like phenotypes (reduced time in open arms) or motor discoordination (worse performance in rotarod and worse reaches score in wire-hanging test).

The fact that only few phenotypes have been transferred from one genotype to the other and vice versa might indicate that there are several aspects determining their presence or the lack of proper bacterial engraftment. To improve this engraftment, several modifications might be implemented in our protocol.

One possibility is the modification of the pre-treatment regimen, using antibiotics instead of laxatives. However, there is a debate regarding the use of antibiotics or laxatives as pre-treatment due to the fact that antibiotics might result in additional alterations or residual antibiotics which could affect the engraftment whereas laxative cannot guarantee a total depletion of the host microbiota. Studies comparing both pre-treatments, revealed that antibiotics might affect or delay the engraftment ability of certain bacterial populations (Le Roy T. et al., 2019). Thus, the use of antibiotics instead of laxatives does not seem to be a good option to improve the transplant engraftment.

In order to facilitate engraftment, in addition to the treatment regimen modification, germ-free mice might be used. However, there is also a debate regarding the use of germ-free or conventional mice with this type of approaches, because germ-free mice are devoid of endogenous microbiota, and facilitate colonization. Nevertheless, the lack of endogenous microbiota also causes metabolic dysfunction, an altered immune system and an immature gastrointestinal tract. Moreover, some studies have revealed that the engraftment depends on the bacterial richness prior to the intervention and germ-free mice seems to delay the engraftment due to low bacterial richness and to be at higher risk of colonization by exogenous bacterial populations coming from the environment instead of the transplant (Le Roy T. et al., 2019). Consequently, the use of germ-mice instead of conventional mice does not seem advantageous.

Another possibility is to increase the amount of fecal microbiota transplant. Some groups have demonstrated a good engraftment after 5 administrations of fecal microbiota transplant (Gopalakrishnan V. et al., 2021) while we only performed 2 administrations. Another option is an earlier intervention (shortly after weaning because few days later the immune system is further developed) and a longer period for colonization (9 weeks) (Le Roy T. et al., 2019) instead of performing the intervention two weeks post-weaning and the behavioral assessment 3 weeks after the FMT. In fact, Le Roy T. and colleagues demonstrated that bacterial replacement is more effective if it is conducted shortly after weaning (Le Roy T. et al., 2019). Thus, these regimen modifications might be beneficial and improve our results.

Although there is a possibility that complete engraftment has not occurred, the transference of wild-type microbiota to *Grin2b*$^{+/-}$ mice resulted in increased number of stools with reduced water content and increased buried marbles, as it was happening with spermidine supplementation. This might be explained by the modification of microbiota itself, that might result in an increase of different compounds including spermidine (Bruno G. et al., 2019).

Perspectives of therapeutic interventions in GRDs

Until very recently, therapeutic interventions in patients with GRDs were aimed to mitigate symptomatology (for instance, using melatonin for sleep disturbances, prebiotics/probiotics for gastrointestinal alterations, therapies for environmental enrichment or anti-epileptic drugs if needed, among other compounds). Nevertheless, great efforts are being made to evaluate distinct therapeutic interventions directly targeted against loss- and gain-of-function *GRIN* variants to improve the quality of life of these patients and their families. In the following sections, therapeutic interventions for loss-of-function variants which have been investigated during this Thesis, will be discussed to evaluate how plausible is its application in the treatment of pediatric patients suffering from GRDs.

L-Serine ongoing clinical trial

L-serine has been translated to the clinical practice in a patient with severe encephalopathy, harboring a loss-of-function GluN2B variant. This variant was characterized *in vitro* in our laboratory and it was associated with reduced pore size, reduced glutamate potency, together with reduced spines density and the addition of D-serine *in vitro* was able to rescue those alterations. L-serine is considered a safe food additive by the FDA and L-serine is transformed in the human body into D-serine that it is able to potentiate NMDARs. Thus, the patient with the loss-of-function variant started an L-serine supplementation (which is converted in D-serine after administration) resulting in the improvement of motor, cognitive and communication deficits after several months of supplementation (Soto D. et al., 2019).

This proof-of-concept study has resulted in the establishment of a clinical trial in *GRIN*-related disorders (https://clinicaltrials.gov/ct2/show/NCT04646447?cond=GRIN&draw=2&rank=1). From November 2020, there is an ongoing clinical trial that consists of L-serine orally supplementation (3 administrations per day) to 20 patients from 2 to 18 years old, starting with 250 mg/kg/day for 2 weeks, and 500 mg/kg/day from week 3 to week 52. The aim of this initial clinical trial is to elucidate possible side effects (although L-serine is considered a safe compound), and the therapeutic potential of this compound via conducting distinct questionnaires and assessments based on scales (measuring adaptative, cognitive, learning, behavioral, emotional, motor, and social skills) as well as an evaluation of sleep pattern disturbances and microbiota dysbiosis.

Moreover, this Thesis has demonstrated that D-serine (L-serine metabolite) is able to rescue spines deficits in distinct types of loss-of-function variants. Thus, L-serine seems a very promising compound for the treatment of GRDs that are associated with loss-of-function variants, regardless of the functional impact, and with less reported side effects than D-serine (Guercio GD. and Panizzutti R., 2018; Suwandhi L. et al., 2018). Consequently, if this clinical trial results in an improvement of the symptomatology of recruited patients without significant side effects, a generalized therapy with L-serine supplementation might be close to be implemented for patients with loss-of-function variants.

Spermidine, a promising nutraceutical therapy for the treatment of loss-of-function GRDs

There are several studies claiming the potential therapeutic effect of spermidine oral supplementation given its antioxidant and anti-inflammatory effects and its role in promoting autophagy activation. In fact, it has been demonstrated that oral spermidine supplementation to mice extends lifespan and exert cardioprotection (Eisenberg T. et al., 2016) and improve spatial learning in male aged mice (Schroeder S. et al., 2021).

During this Thesis, we have demonstrated that spermine (spermidine metabolite) is able to rescue NMDAR-mediated reduced currents and spines deficits associated with distinct *GRIN* loss-of function variants. Moreover, we have also evaluated the potential therapeutic effect of spermidine oral supplementation in *Grin2b*$^{+/-}$ mouse model (GRDs model), revealing a partial rescue of motor deficits. Despite being a preliminary result, which might be improved via increasing time of supplementation, this behavioral study in combination with our in vitro results and other studies in different mouse models, support the benefits of this compound.

Furthermore, the fact that spermidine is already present in diet (nuts, mushroom, soybean…) prompted to its use in humans as cognitive enhancer and for cardioprotection in distinct clinical trials, revealing that elevated levels of spermidine (from diet) correlate with reduced risk of cardiovascular disease (Eisenberg T. et al., 2016, https://clinicaltrials.gov/ct2/show/NCT04405388?term=spermidine&draw=2&rank=2) and a 3-months spermidine supplementation (750 mg of spermidine-rich plant extract with a daily spermidine dose of 1.2 mg, dispersed in three doses, SpermidineLIFE® from Longevity Labs+, https://www.spermidinelife.com/en/)) is associated with prevention of cognitive decline in older adults (Wirth M. et al., 2018; https://clinicaltrials.gov/ct2/show/NCT02755246). Both clinical studies also demonstrated that spermidine supplements, which are already available (Primeadine® from Oxford Healthspan, https://oxfordhealthspan.com; and SpermidineLIFE® from Longevity Labs+, https://www.spermidinelife.com/en/) are safe and well-tolerated, except for diseases where polyamines levels are increased (renal failure, certain tumors, stroke, or cardiac infarction) where spermidine supplementation is still not recommended. Further studies are needed to determine if these increased polyamines are a compensatory mechanism to avoid damage or contribute to the disease (Madeo F. et al., 2018).

Although there is not an ongoing clinical trial, spermidine has also been associated with increased longevity (Madeo F. et al., 2018) because it is a caloric restriction mimetic (CRM) that simulates intermittent fasting and/or caloric restriction effects, that impact longevity. The relationship between fasting or caloric restriction and longevity is mediated via a reduction of circulating insulin-like growth factor-1 (IGF-1) and insulin pathways, because of the decreased aminoacids and glucose. This pathway reduction results in the expression of certain transcription factors that activate autophagy, stress response, and antioxidative responses (Longo VD. et al., 2021).

Despite being a safe compound and the association with distinct therapeutic effects, polyamines doses should be tightly regulated because spermidine and spermine at high doses might act as blockers (Lerma J., 1992; Gallagher MJ. et al., 1997; Mony L. et al., 2011). In fact, a 6 mM supplementation in mice do not show significant improvement in memory tasks and 30 mM supplementation for one month resulted in muscle strength alteration due to excessive autophagy processes (Chrisam M. et al., 2015). Furthermore, spermidines might be also associated with pain-related behaviors and toxicity due to overexcitation of NMDA and non-NMDA receptors, and metabolism products like hydrogen peroxide or reactive aldehydes (Otsuki M. et al., 1995; Tan-No K. et al., 2000).

Thus, spermidine is a potential therapeutic option for GRDs. Nevertheless, further studies are needed to fully determine the therapeutic window and the safety/tolerability in pediatric patients. Despite this, spermidine is already commercialized, and it has been proven effective in humans for distinct applications, and this will ease the path for GRDs treatment.

Rapastinel is still not ready to be implemented in GRDs treatment

Currently, there are not available studies evaluating Rapastinel in GRDs. Nevertheless, in this Thesis, we have demonstrated that rapastinel is able to rescue spines deficits in neuronal primary cultures transiently expressing *GRIN* loss-of-function variants.

There were not studies regarding the potential benefit of rapastinel in GRDs but there were several studies claiming its potential as antidepressant agent without ketamine-like side effects using 10– 30 mg/kg doses in murine models (Liu RJ. et al., 2017; Kato T. et al., 2018; Donello JE. et al., 2019). In fact, the compound seemed very promising and several clinical trials started investigating its role as antidepressant. Some of these studies even reported antidepressant effects two hours post-intravenous injection (5 mg-10 mg/kg) that lasted for 7 days without significant side effects (Preskorn S. et al., 2015). Nevertheless, these studies also showed response in the placebo group. Thus, despite being safe and well tolerated, there were not differences between the compound and the placebo, leading to the termination of the distinct trials (failed trials) (Neurex, Allergan, https://clinicaltrials.gov). These failed trials evaluating rapastinel as antidepressant agent do not mean that rapastinel could not be effective in other diseases, such as GRDs. However, further investigations are needed in order to determine: 1, the potential therapeutic role in GRDs *in vivo* (experiments conducted during the Thesis only assess its potential rescue *in vitro*); 2, the exact effective dose window to potentiate loss-of-function *GRIN* variants (due to its partial agonism); and 3, the safety and tolerability of the compound in pediatric patients. Thus, currently, the application of rapastinel in GRDs is far from being a therapeutic option for patients.

FMT for the treatment of GRDs: so far, so close

There is an increasing interest in the brain-gut axis and its role in neurologic diseases (such as Parkinson, chronic pain, depression, anxiety or autism) (Maqsood R. and Stone TW., 2016; Bermudez-Martin P. et al., 2020). Thus, many efforts have been oriented to demonstrate the pathological role of microbiota alterations (dysbiosis) in these neurological diseases and how therapeutic interventions targeting these microbiota modifications could benefit patients suffering from those disorders.

Several families have reported that GRD patients suffer from distinct gastrointestinal alterations (constipation, abdominal pain and/or flatulence) that might due to microbiota alterations. Despite this, to-date, there is no demonstration of such dysbiosis in GRD patients. Nevertheless, this evaluation has been included in the L-serine clinical trial. During this Thesis, when characterizing the *Grin2b$^{+/-}$* mouse model (GRD 'loss-of-function' model), several gastrointestinal parameters were evaluated (number of stools in 60 minutes, stool water content and transit time), without revealing significant changes. However, this heterozygous mouse model only reproduces certain phenotypes and the absence of gastrointestinal alterations does not mean that dysbiosis is not present in GRD patients.

Thus, a potential GI dysfunction contributing to GRD pathophysiology still cannot be discarded, and in that case, microbiota manipulation could be a potential therapeutic option. Thus, during this Thesis, we have also conducted a preliminary evaluation of fecal microbiota transference from wild-type mice to *Grin2b$^{+/-}$* mice and vice versa, revealing that only alterations in motor coordination (rotarod test) can be transferred to wild-type animals with heterozygous microbiota transplant but there is no transference of other motor deficits or anxiety-like phenotypes. Moreover, wild-type microbiota transplant is only able to increase locomotion (open field test) without changes in alterations of motor coordination (rotarod and wire-hanging test) or anxiety-like phenotypes. Thus, it seems that microbiota dysbiosis could have a pathological role in GRDs and that microbiota manipulation could benefit those patients. However, our preliminary study has certain limitations (discussed in the previous sections) and consequently, further studies are needed in order to confirm this.

If microbiota dysbiosis in GRD patients and microbiota manipulation potential benefit for GRDs are confirmed with further evaluations (L-serine clinical trial and redefined FMT protocols, respectively), it will be very easy to apply this therapeutic option in GRD patients because several ongoing clinical trials are evaluating the application of FMT in distinct diseases (for instance, autism) affecting pediatric patients (https://clinicaltrials.gov/ct2/home).

Finding a cure: Is gene therapy possible for GRDs?

All the discussed therapeutic options, although targeting the NMDAR loss-of-function, do not correct the gene defect. Thus, rather than a cure for GRDs, it is mitigating the effects of the NMDAR dysfunction. To actually cure the disease, the genetic defect ought to be removed and replaced by a correct gene, what is known as gene therapy.

In order to achieve this, traditionally, viral vectors have been used, and depending on the approach, some viral vectors might be better than others. The most widely used are the adeno-associated viruses (AAVs) because they are less immunogenic, less oncogenic and there are several classes with specific tropism (for instance, AAV2 and AAV9 present neuronal tropism) (Choudhury S. et al., 2017). Nevertheless, the encapsulated gene length is limited (~5 kB) and this might be insufficient for *GRIN2* genes. Alternatively, lentivirus (higher capacity but more immunogenic and oncogenic) or a combination of various AAVs might be used (Choudhury S. et al., 2017). Still, there is the limitation that viral vectors should be prepared to down-regulate first and then, replace with the correct gene, and this should be specific for each *GRIN* variant. During this Thesis, we have investigated the potential benefit of a gene therapy without the necessity of the prior down-regulation, which might be useful for certain *GRIN* nonsense variants that exert a dominant negative effect in heterozygosity (monoallelic expression), by expressing additional wild-type receptors or even CTD-truncated receptors that are able to displace the mutated subunits via a competition effect. Thus, a potential therapeutic option for patients expressing this type of variants is gene therapy with wild-type or CTD-truncated *GRIN* subunits, without the need of down-regulation prior to the expression. However, this approach is only suitable for that particular kind of variants and not for every *GRIN* variant. A potential option that might target all kind of variants is CRISPR-Cas9 technology which allows gene silencing or the variant correction in target cells (Benger M. et al., 2018). Regardless of the selected method, further studies are needed to evaluate specific CRISPR strategies for *GRIN* genes or the optimal viral vector approach to efficiently express *GRIN* genes *in vitro* (cell lines, neuronal primary cultures, stereotaxic injection in mouse models).

In addition to select the proper gene therapy approach, additional aspects should be considered to make gene therapy achievable in the treatment of GRDs. One of these aspects is the gene therapy target given that NMDARs are widely expressed in the whole body, determining some of the GRDs symptoms. There are several delivery pathways (intraparenchymal, intrathecal or intravenous) and the choice is based on the selected target, although each of them present advantages/disadvantages regarding immunogenicity and leaking to other locations (Benger M. et al., 2018). For GRDs, the main target is the CNS, despite the NMDAR expression in the whole body (additional treatments should be administered to treat residual symptomatology). Thus, any of the pathways is suitable (although with intravenous administration, a viral vector which can cross the BBB like AAV9 should be selected). Nevertheless, the advantage of having NMDAR expression in the whole body is that gene therapy could be targeted to a specific location where NMDARs are expressed to evaluate whether it is effective, prior to target the CNS.

Another aspect is: in which specific moment the gene therapy should be performed? As GRDs are neurodevelopmental disorders, it is believed that 'the sooner, the better'. This is the reason why we have evaluated all the therapeutic interventions in mice as soon as possible, when the development is still taking place. Nevertheless, it has been revealed very recently that a correction in adult brain might also be possible. This investigation aimed to rescue a GluN1 KD in adult mice (P70) by a Cre-LoxP system showed that GluN1 expression is recovered in brain tissue, NMDAR-mediated currents were restored to wild-type levels and the mouse model defects were improved (cognitive, social, and sensory skills, and anxiety-like phenotypes), despite the late intervention. Consequently, genetic strategies might also be effective at later stages.

Thus, although gene therapy is still far from being applied in the treatment of GRDs because several parameters need to be evaluated, preliminary studies indicate that it is a therapeutic possibility for GRDs treatment.

Concluding remarks

The initial goal of this Thesis was to establish a genotype-phenotype correlation that allows to stratify the distinct *GRIN* variants for further design of personalized therapies. This goal has not been achieved completely, because we still do not know how to explain the divergent symptomatology or functional impact of the variants. Nevertheless, the development of an experimental pipeline that has been implemented in the characterization of several *GRIN* variants and the validation of a structure-based superimposition model, will help in the establishment of that correlation in the future and accelerate the functional annotation of a great number of *GRIN* variants. Despite this, we have been able to stratify certain types of GRIN variants and this will allow a quick diagnose and consequently, a sooner treatment onset.

Additionally, a GRD loss-of-function model has been almost fully characterized, revealing certain phenotypes that are representative of the patients' symptomatology, and several therapeutic approaches have been investigated in the rescue of those phenotypes, revealing that there are distinct interventions that could be effective in the treatment of certain GRDs.

Conclusions
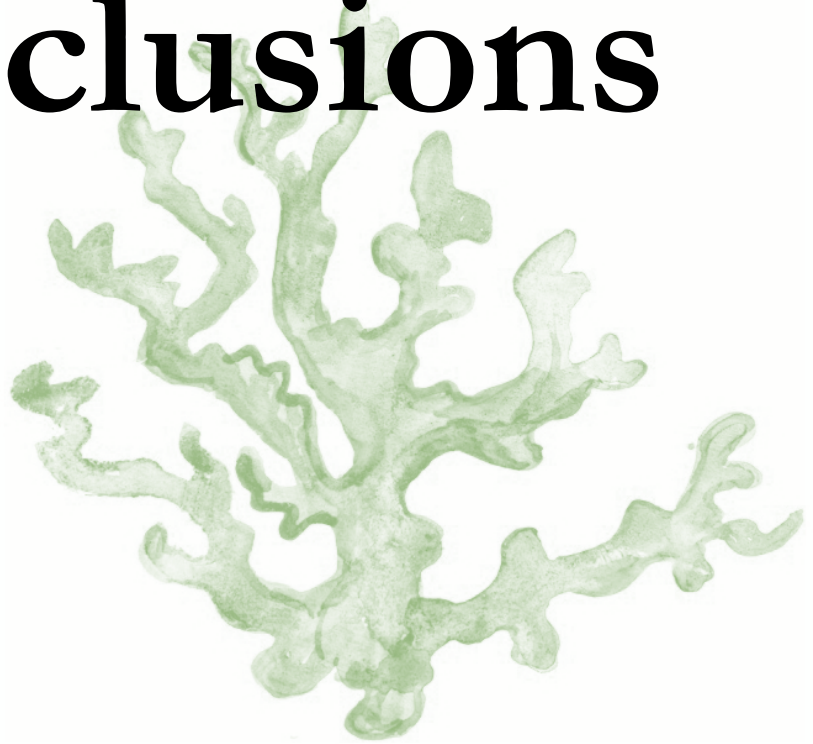
1. Along this Thesis, a cohort of 95 *GRIN*-related disorders individuals have been recruited. The patients display *GRIN1* (24), *GRIN2A* (26) or *GRIN2B* (25) likely pathogenic *GRIN* variants, and 57 (out of 95) *GRIN* variants have been annotated: 42 variants cause a loss-of-function, 7 variants lead to gain-of-function, 3 variants present a complex phenotype and 5 variants are likely non-disease causing.

2. NMDA receptors surface density is decreased in heterologous cell systems expressing *GRIN* biallelic indel variants located within the TMD, biallelic *GRIN* nonsense variants truncating the ATD, LBD or TMD and discrete biallelic missense variants.

3. In monoallelic conditions, heterologous expression of nonsense variants affecting *GRIN2A* or *GRIN2B* ATD, LBD or TMD result in loss-of-function, while *GRIN1* protein truncating variants are non-pathogenic.

4. In neuronal primary cultures, disease-associated *GRIN* loss-of-function variants (nonsense and discrete missense variants) trigger a reduction in spines density. These synaptic alterations can be rescued by the administration of the NMDAR co-agonist D-serine or by the partial agonist rapastinel.

5. Phenotypic assessment of the *Grin2b*$^{+/-}$ mice showed that this haploinsufficient model recapitulates *GRIN*-related disorders-associated phenotypes, consisting on hypoactivity and motor alterations, anxiety-like behaviours, and impaired long-term potentiation.

6. Spermine potentiates NMDAR-mediated currents in in cells expressing *GRIN* loss-of-function variants. *In vivo*, spermidine (spermine precursor) chronic dietary supplementation rescues the motor deficits and partially recover impaired long-term processes of *Grin2b*$^{+/-}$ mice.

7. Fecal microbiota transfer (FMT) preliminary studies showed that wild-type mice microbiota transfer to *Grin2b*$^{+/-}$ mice partially rescues GRD-like phenotypic alterations (hypoactivity and long-term potentiation). Concomitantly, FMT from donor *Grin2b*$^{+/-}$ mice to wild-type mice induces an impairment of motor coordination and partially affects long-term potentiation.

References
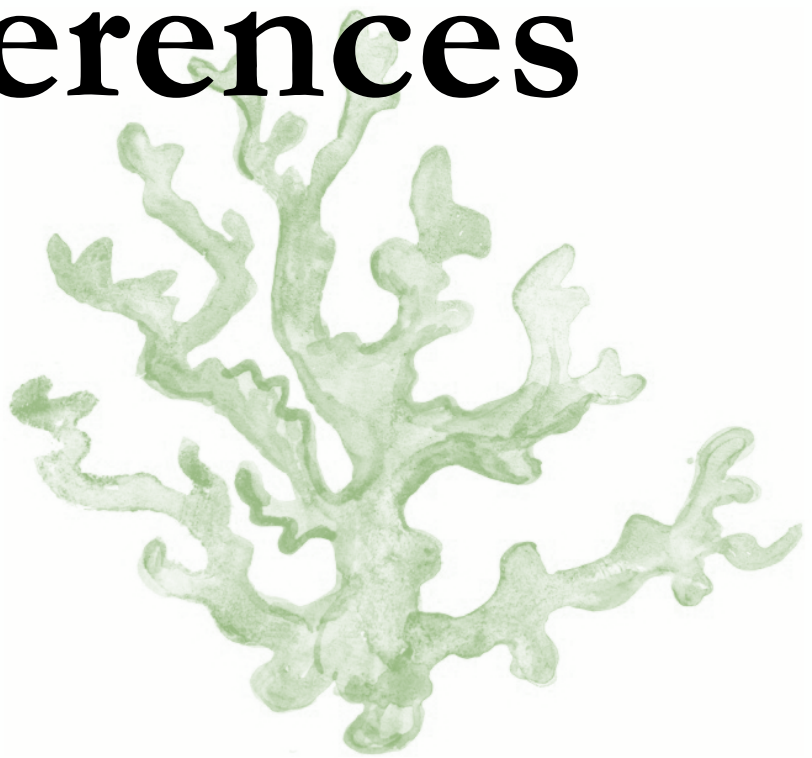
Publications

Abbaszadeh S, Javidmehr A, Askari B, Janssen PML, Soraya H. Memantine, an NMDA receptor antagonist, attenuates cardiac remodeling, lipid peroxidation and neutrophil recruitment in heart failure: A cardioprotective agent? Biomed Pharmacother. 2018;108(July):1237–43.

Addis L, Virdee JK, Vidler LR, Collier DA, Pal DK, Ursu D. Epilepsy-associated GRIN2A mutations reduce NMDA receptor trafficking and agonist potency – molecular profiling and functional rescue. Sci Rep. 2017 Dec 27;7(1):66.

Akram M, Szent-gyo A. Citric Acid Cycle and Role of its Intermediates in Metabolism. Cell Biochem Biophys. 2014;68:475–8.

Allan RD, Hanrahan JR, Hambley TW, Johnston GAR, Mewett KN, Mitrovic AD. Synthesis and Activity of a Potent N-Methyl-D-aspartic Acid Agonist, trans-1-Aminocyclobutane-1,3-dicarboxylic Acid and Related Phosphonic and Carboxylic Acids. J Med Chem. 1990;33:2905–15.

Amador A, Bostick CD, Olson H, Peters J, Camp CR, Krizay D, et al. Modelling and treating GRIN2A developmental and epileptic encephalopathy in mice. Brain. 2020;143(7):2039–57.

Amidfar M, Khiabany M, Kohi A, Salardini E, Arbabi M, Roohi Azizi M, et al. Effect of memantine combination therapy on symptoms in patients with moderate-to-severe depressive disorder: randomized, double-blind, placebo-controlled study. J Clin Pharm Ther. 2017;42(1):44–50.

Amin JB, Moody GR, Wollmuth LP. From bedside-to-bench: What disease-associated variants are teaching us about the NMDA receptor. J Physiol. 2021;599(2):397–416.

Amm I, Sommer T, Wolf DH. Protein quality control and elimination of protein waste: The role of the ubiquitin-proteasome system. Biochim Biophys Acta - Mol Cell Res. 2014;1843(1):182–96.

Anaparti V, Ilarraza R, Orihara K, Stelmack GL, Ojo OO, Mahood TH, et al. NMDA receptors mediate contractile responses in human airway smooth muscle cells. Am J Physiol Cell Mol Physiol. 2015 Jun 15;308(12):L1253–64.

Angoa-Pérez M, Kane MJ, Briggs DI, Francescutti DM, Kuhn DM. Marble burying and nestlet shredding as tests of repetitive, compulsive-like behaviors in mice. J Vis Exp. 2013;(82):50978.

Antonov SM, Gmiro VE, Johnson JW. Binding sites for permeant ions in the channel of NMDA receptors and their effects on channel block. Nat Neurosci. 1998;1(6):451–61.

Armbruster A, Neumann E, Kötter V, Hermanns H, Werdehausen R, Eulenburg V. The GlyT1 inhibitor bitopertin ameliorates allodynia and hyperalgesia in animal models of neuropathic and inflammatory pain. Front Mol Neurosci. 2018;10(January):1–12.

Arroyo-López C. Helminth therapy for autism under gut-brain axis- hypothesis. Med Hypotheses. 2019;125(February):110–8.

Arundine M, Tymianski M. Molecular mechanisms of glutamate-dependent neurodegeneration in ischemia and traumatic brain injury. Cell Mol Life Sci. 2004;61(6):657–68.

Atlason PT, Garside ML, Meddows E, Whiting P, McIlhinney RAJ. N-methyl-D-aspartate (NMDA) receptor subunit NR1 forms the substrate for oligomeric assembly of the NMDA receptor. J Biol Chem. 2007 Aug 31;282(35):25299–307.

Auvin S, Dozières-Puyravel B, Avbersek A, Sciberras D, Collier J, Leclercq K, et al. Radiprodil, a NR2B negative allosteric modulator, from bench to bedside in infantile spasm syndrome. Ann Clin Transl Neurol. 2020;7(3):343–52.

Azaiez H, Decker AR, Booth KT, Simpson AC, Shearer AE, Huygen PLM, et al. HOMER2, a Stereociliary Scaffolding Protein, Is Essential for Normal Hearing in Humans and Mice. PLoS Genet. 2015 Mar 27;11(3).

Azzopardi D, Robertson NJ, Kapetanakis A, Griffiths J, Rennie JM, Mathieson SR, et al. Anticonvulsant effect of xenon on neonatal asphyxial seizures. Arch Dis Child Fetal Neonatal Ed. 2013;98(5):437–40.

Balu DT. The NMDA Receptor and Schizophrenia: From Pathophysiology to Treatment. Adv Pharmacol. 2016;76:351–82.

Bahry JA, Fedder-Semmes KN, Sceniak MP, Sabo SL. An Autism-Associated de novo Mutation in GluN2B Destabilizes Growing Dendrites by Promoting Retraction and Pruning. Front Cell Neurosci. 2021;15(July):1–11.

Balsara R, Dang A, Donahue DL, Snow T, Castellino FJ. Conantokin-G attenuates detrimental effects of NMDAR hyperactivity in an ischemic rat model of stroke. PLoS One. 2015;10(3):1–21.

Bannerman, D.M., Niewoehner, B., Lyon, L., Romberg, C., Schmitt, W.B., Taylor, A., Sanderson, D.J., Cottam, J., Sprengel, R., Seeburg, P.H. et al. (2008) NMDA receptor subunit NR2A is required for rapidly acquired spatial working memory but not incremental spatial reference memory. J. Neurosci. 28, 3623–3630

Barria A, Malinow R. Subunit-specific NMDA receptor trafficking to synapses. Neuron. 2002 Jul 18;35(2):345–53.

Bar-Shira O, Maor R, Chechik G. Gene Expression Switching of Receptor Subunits in Human Brain Development. PLoS Comput Biol. 2015;11(12):1–21.

Baufreton J, Milekovic T, Li Q, McGuire S, Moraud EM, Porras G, et al. Inhaling xenon ameliorates l-dopa-induced dyskinesia in experimental parkinsonism. Mov Disord. 2018;33(10):1632–42.

Baumgart F, Rodríguez-Crespo I. D -Amino acids in the brain : the biochemistry of brain serine racemase. FEBS J. 2008;275:3538–45.

Belforte JE, Zsiros V, Sklar ER, Jiang Z, Yu G, Li Y, et al. Postnatal NMDA receptor ablation in corticolimbic interneurons confers schizophrenia-like phenotypes. Nat Neurosci. 2010;13(1):76–83.

Benger M, Kinali M, Mazarakis ND. Autism spectrum disorder: Prospects for treatment using gene therapy. Mol Autism. 2018;9(1):1–10.

Bermudez-Martin P, Becker JAJ, Fernandez SP, Costa-Campos R, Barbosa S, Martinez-Gili L, et al. The microbial metabolite p-Cresol induces autistic-like behaviors in mice by remodeling the gut microbiota. bioRxiv. 2020;33(0):1–33.

Bermudo-Soriano CR, Perez-Rodriguez MM, Vaquero-Lorenzo C, Baca-Garcia E. New perspectives in glutamate and anxiety. Pharmacol Biochem Behav. 2012;100(4):752–74.

Blaabjerg M, Kristensen BW, Bonde C, Zimmer J. The metabotropic glutamate receptor agonist 1S,3R-ACPD stimulates and modulates NMDA receptor mediated excitotoxicity in organotypic hippocampal slice cultures. Brain Res. 2001;898(1):91–104.

Blake PA, Yamaguchi S, Thurkauf A, Rogawski MA. Anticonvulsant 1-Phenylcycloalkylamines: Two Analogues with Low Motor Toxicity When Orally Administered. Epilepsia. 1992;33(1):188–94.

Blandini F, Porter RHP, Greenamyre JT. Glutamate and Parkinson's disease. Mol Neurobiol. 1996;12(1):73–94.

Blanke ML, VanDongen AMJ. Activation mechanisms of the NMDA receptor. Biol NMDA Recept. 2008;283–312.

Bliss TVP, Collingridge GL, Kaang BK, Zhuo M. Synaptic plasticity in the anterior cingulate cortex in acute and chronic pain. Nat Rev Neurosci. 2016;17(8):485–96.

Borowicz KK, Kleinrok Z, Czuczwar SJ. Influence of D(-)CPP and (+/-)CPP upon the protective action of conventional antiepileptic drugs against electroconvulsions in mice. Pol J Pharmacol. 2000;52(6):431-9.

Boujema M Ben, Laboureyras E, Pype J, Bessière B, Simonnet G. Nitrous oxide persistently alleviates pain hypersensitivity in neuropathic rats: A dose-dependent effect. Pain Res Manag. 2015;20(6):309–15.

Boyce-Rustay JM, Holmes A. Genetic inactivation of the NMDA receptor NR2A subunit has anxiolytic- and antidepressant-like effects in mice. Neuropsychopharmacology. 2006;31(11):2405–14.

Brigman JL, Feyder M, Saksida LM, Bussey TJ, Mishina M, Holmes A. Impaired discrimination learning in mice lacking the NMDA receptor NR2A subunit. Learn Mem. 2008;15(2):50–4.

Brigman JL, Wright T, Talani G, Prasad-Mulcare S, Jinde S, Seabold GK, et al. Loss of GluN2B-containing NMD A receptors in CA1 hippocampus and cortex impairs long-term depression, reduces dendritic spine density, and disrupts learning. J Neurosci. 2010;30(13):4590–600.

Brown RE, Fedorov NB, Haas HI, Reyman KG. Histaminergic modulation of synaptic plasticity in area CA1 of rat hippocampal slices. Neuropharmacology. 1995;34(2):181–90.

Bruno G, Gagliardi A, Oliva A, Trancassini M, Macone A, Cicerone C, et al. Fecal Microbial Transplantation impact on gut microbiota composition and metabolome, microbial translocation and T-lymphocyte immune activation in recurrent Clostridium difficile infection patients. New Microbiol. 2019;42(4):221–4.

Bu Y, Wang N, Wang S, Sheng T, Tian T, Chen L, et al. Myosin IIb-dependent regulation of actin dynamics is required for N-Methyl-D-aspartate receptor trafficking during synaptic plasticity. J Biol Chem. 2015;290(42):25395–410.

Burnashev N, Szepetowski P. NMDA receptor subunit mutations in neurodevelopmental disorders. Curr Opin Pharmacol. 2015;20:73–82.

Burnell ES, Irvine M, Fang G, Sapkota K, Jane DE, Monaghan DT. Positive and Negative Allosteric Modulators of N-Methyl-D- Aspartate (NMDA) Receptors; Structure-Activity Relationships and Mechanisms of Action. J Med Chem. 2019;62(1):3–23.

Calabresi P, Marti M, Picconi B, Saulle E, Costa C, Centonze D, et al. Lamotrigine and remacemide protect striatal neurons against in vitro ischemia: An electrophysiological study. Exp Neurol. 2003;182(2):461–9.

Cani PD, Bibiloni R, Knauf C, Waget A, Neyrinck AM, Delzenne NM, et al. Changes in gut microbiota control metabolic endotoxemia-induced inflammation in high-fat diet-induced obesity and diabetes in mice. Diabetes. 2008 Jun 1;57(6):1470–81.

Carlsson KC, Hoem NO, Moberg ER, Mathisen LC. Analgesic effect of dextromethorphan in neuropathic pain. Acta Anaesthesiol Scand. 2004;48(3):328–36.

Černý J, Božíková P, Balík A, Marques SM, Vyklický L. NMDA receptor opening and closing-Transitions of a molecular machine revealed by molecular dynamics. Biomolecules. 2019;9(10):1–17.

Chang YC, Cole TB, Costa LG. Behavioral phenotyping for autism spectrum disorders in mice. Curr Protoc Toxicol. 2017;2017(May):1–21.

Chapman AG. Glutamate and Glutamine in the Brain: Glutamate and Epilepsy. Am Soc Nutr Sci. 2000;1043–5.

Chatterton JE, Awobuluyi M, Premkumar LS, Takahashi H, Talantova M, Shin Y, et al. Excitatory glycine receptors containing the NR3 family of NMDA receptor subunits. Nature. 2002;415(6873):793–8.

Chaudhry FA, Reimer RJ, Edwards RH. The glutamine commute: Take the N line and transfer to the A. Vol. 157, Journal of Cell Biology. The Rockefeller University Press; 2002. p. 349–55.

Chen N, Li B, Murphy TH, Raymond LA. Site within N-Methyl-D-aspartate Receptor Pore Modulates Channel Gating. Mol Pharmacol. 2004;65(1):157–64.

Chen W, Shieh C, Swanger SA, Tankovic A, Au M, McGuire M, et al. GRIN1 mutation associated with intellectual disability alters NMDA receptor trafficking and function. J Hum Genet. 2017;62(6):589–97.

Chenu C, Serre CM, Raynal C, Burt-Pichat B, Delmas PD. Glutamate receptors are expressed by bone cells and are involved in bone resorption. Bone. 1998 Apr;22(4):295–9.

Choi YB, Tenneti L, Le DA, Ortiz J, Bai G, Chen HSV, et al. Molecular basis of NMDA receptor-coupled ion channel modulation by S-nitrosylation. Nat Neurosci. 2000;3(1):15–21.

Choudhury SR, Hudry E, Maguire CA, Sena-Esteves M, Breakefield XO, Grandi P. Viral vectors for therapy of neurologic diseases. Neuropharmacology. 2017;120:63–80.

Chrisam M, Pirozzi M, Castagnaro S, Blaauw B, Polishchuck R, Cecconi F, et al. Reactivation of autophagy by spermidine ameliorates the myopathic defects of collagen VI-null mice. Autophagy. 2015;11(12):2142–52.

Christoph T, Reißmüller E, Schiene K, Englberger W, Chizh BA. Antiallodynic effects of NMDA glycineB antagonists in neuropathic pain: Possible peripheral mechanisms. Brain Res. 2005;1048(1–2):218–27.

Clos M, García Sanz A, Trullas R, Badia A. Effect of 1-aminocyclopropanecarboxylic acid on N-methyl-D-aspartate-stimulated [3H]-noradrenaline release in rat hippocampal synaptosomes. Br J Pharmacol. 1996;118:901–4.

Collingridge GL, Olsen RW, Peters J, Spedding M. A nomenclature for ligand-gated ion channels. Neuropharmacology. 2009;56(1):2–5.

Covvey JR, Crawford AN, Lowe DK. Intravenous Ketamine for Treatment-Resistant Major Depressive Disorder. Ann Pharmacother. 2012;46(1):117–23.

Cubelos B, Giménez C, Zafra F. Localization of the GLYT1 glycine transporter at glutamatergic synapses in the rat brain. Cerebral Cortex. 2005. p. 448–59.

Cull-Candy S, Brickley S, Farrant M. NMDA receptor subunits: diversity, development and disease. Curr Opin Neurobiol. 2001;11:327–35.

Curtis D, Phillis J, Watkins J. Chemical Excitation of Spinal Neurones. Nature. 1959;183(February 28).

Dai J, Zhou HX. Semiclosed Conformations of the Ligand-Binding Domains of NMDA Receptors during Stationary Gating. Biophys J. 2016;111(7):1418–28.

Davani-Davari D, Negahdaripour M, Karimzadeh I, Seifan M, Mohkam M, Masoumi SJ, et al. Prebiotics: Definition, types, sources, mechanisms, and clinical applications. Foods. 2019;8(3):1–27.

David HN, Leveille F, Chazalviel L, MacKenzie ET, Buisson A, Lemaire M, et al. Reduction of ischemic brain damage by nitrous oxide and xenon. J Cereb Blood Flow Metab. 2003;23(10):1168–73.

Davies JA. Remacemide Hydrochloride: A Novel Antiepileptic Agent. Gen Pharmac. 1997;28(4):499–502.

Deacon RMJ. Measuring motor coordination in mice. J Vis Exp. 2013;(75):2609.

De Koning TJ, Klomp LWJ. Serine-deficiency syndromes. Curr Opin Neurol. 2004;17(2):197–204.

DeMaria CD, Soong TW, Alseikhan BA, Alvania RS, Yue DT. Calmodulin bifurcates the local Ca2+ signal that modulates P/Q-type Ca2+ channels. Nature 2001, 411:484-489.

Dempsey RJ, Bakaya MK, Doǧan A. Attenuation of brain edema, blood-brain barrier breakdown, and injury volume by ifenprodil, a polyamine-site N-methyl-D-aspartate receptor antagonist, after experimental traumatic brain injury in rats. Neurosurgery. 2000;47(2):399–406.

Deng M, Chen S-R, Pan H-L. Presynaptic NMDA receptors control nociceptive transmission at the spinal cord level in neuropathic pain. Cell Mol Life Sci. 2019;176(10):1889–99.

Dickenson AH, Ghandehari J. Anti-convulsants and Anti-depressants. In: HEP. 2006. p. 147:145–77.

Di Fabio R, Conti N, De Magistris E, Feriani A, Provera S, Sabbatini FM, et al. Substituted analogues of GV150526 as potent glycine binding site antagonists in animal models of cerebral ischemia. J Med Chem. 1999;42(18):3486–93.

Dingley J, Tooley J, Porter H, Thoresen M. Xenon provides short-term neuroprotection in neonatal rats when administered after hypoxia-ischemia. Stroke. 2006;37(2):501–6.

Dobrovolsky AP, Gedzun VR, Bogin VI, Ma D, Ichim TE, Sukhanova IA, et al. Beneficial effects of xenon inhalation on behavioral changes in a valproic acid-induced model of autism in rats. J Transl Med. 2019;17(1):1–15.

Dolino DM, Adariani SR, Shaikh SA, Jayaraman V, Sanabria H. Conformational selection and submillisecond dynamics of the ligand-binding domain of the N-methyl-D-aspartate receptor. J Biol Chem. 2016;291(31):16175–85.

Donello JE, Banerjee P, Li YX, Guo YX, Yoshitake T, Zhang XL, et al. Positive N-Methyl-D-Aspartate Receptor Modulation by Rapastinel Promotes Rapid and Sustained Antidepressant-Like Effects. Int J Neuropsychopharmacol. 2019;22(3):247–59.

Du D, Tang W, Zhou C, Sun X, Wei Z, Zhong J, et al. Fecal Microbiota Transplantation Is a Promising Method to Restore Gut Microbiota Dysbiosis and Relieve Neurological Deficits after Traumatic Brain Injury. Oxid Med Cell Longev. 2021;2021.

Du J, Li XH, Li YJ. Glutamate in peripheral organs: Biology and pharmacology. Vol. 784, European Journal of Pharmacology. Elsevier B.V.; 2016. p. 42–8.

Dudley CE, Morell AJ, Duffey ME, Patel SP. Effects of amantadine on corneal endothelium. Exp Eye Res. 2019;181:208–12.

Duncan GE, Miyamoto S, Gu H, Lieberman JA, Koller BH, Snouwaert JN. Alterations in regional brain metabolism in genetic and pharmacological models of reduced NMDA receptor function. Brain Res. 2002;951(2):166–76.

Duncan GE, Moy SS, Perez A, Eddy DM, Zinzow WM, Lieberman JA, et al. Deficits in sensorimotor gating and tests of social behavior in a genetic model of reduced NMDA receptor function. Behav Brain Res. 2004;153(2):507–19.

Durrant AR, Heresco-levy U. D-Serine in Neuropsychiatric Disorders: New Advances. Adv Psychiatry. 2014(7):1-16

Dyall SC, Michael GJ, Whelpton R, Scott AG, Michael-Titus AT. Dietary enrichment with omega-3 polyunsaturated fatty acids reverses age-related decreases in the GluR2 and NR2B glutamate receptor subunits in rat forebrain. Neurobiol Aging. 2007;28(3):424–39.

Dzirasa K, Ramsey AJ, Takahashi DY, Stapleton J, Potes JM, Williams JK, et al. Hyperdopaminergia and NMDA receptor hypofunction disrupt neural phase signaling. J Neurosci. 2009;29(25):8215–24.

Eisen A. Amyotrophic lateral sclerosis is a multifactorial disease. Muscle Nerve. 1995;18(7):741–52.

Eisenberg T, Abdellatif M, Schroeder S, Primessnig U, Stekovic S, Pendl T, et al. Cardioprotection and lifespan extension by the natural polyamine spermidine. Nat Med. 2016;22(12):1428–38.

Endele S, Rosenberger G, Geider K, Popp B, Tamer C, Stefanova I, et al. Mutations in GRIN2A and GRIN2B encoding regulatory subunits of NMDA receptors cause variable neurodevelopmental phenotypes. Nat Genet. 2010;42(11):1021–6.

Endo K, Nakamachi T, Seki T, Kagami N, Wada Y, Nakamura K, et al. Neuroprotective effect of PACAP against NMDA-induced retinal damage in the mouse. J Mol Neurosci. 2011;43(1):22–9.

Erdem FA, Ilic M, Koppensteiner P, Golacki J, Lubec G, Freissmuth M, et al. A comparison of the transport kinetics of glycine transporter 1 and glycine transporter 2. J Gen Physiol. 2019 Aug 5;151(8):1035–50.

Erreger K, Traynelis SF. Allosteric interaction between zinc and glutamate binding domains on NR2A causes desensitization of NMDA receptors. J Physiol. 2005;569(2):381–93.

Erreger K, Geballe MT, Kristensen A, Chen PE, Hansen KB, Lee CJ, et al. Subunit-specific agonist activity at NR2A-, NR2B-, NR2C-, and NR2D-containing N-methyl-D-aspartate glutamate receptors. Mol Pharmacol. 2007;72(4):907–20.

Errico F, Rossi S, Napolitano F, Catuogno V, Topo E, Fisone G, et al. D-aspartate prevents corticostriatal long-term depression and attenuates schizophrenia-like symptoms induced by amphetamine and MK-801. J Neurosci. 2008;28(41):10404–14.

Essa MM, Braidy N, Vijayan KR, Subash S, Guillemin GJ. Excitotoxicity in the pathogenesis of autism. Neurotox Res. 2013;23(4):393–400.

Fabbrin SB, Girardi BA, de Lorena Wendel A, Coelho Ilha Valin C, Pillat MM, Viero FT, et al. Spermidine-induced improvement of memory consolidation involves PI3K/Akt signaling pathway. Brain Res Bull. 2020;164(March):208–13.

Farinelli M, Heitz FD, Grewe BF, Tyagarajan SK, Helmchen F, Mansuy IM. Selective regulation of NR2B by protein phosphatase-1 for the control of the NMDA receptor in neuroprotection. PLoS One. 2012;7(3).

Fedele L, Newcombe J, Topf M, Gibb A, Harvey RJ, Smart TG. Disease-associated missense mutations in GluN2B subunit alter NMDA receptor ligand binding and ion channel properties. Nat Commun. 2018;9(1).

Fernández-Marmiesse A, Kusumoto H, Rekarte S, Roca I, Zhang J, Myers SJ, et al. A novel missense mutation in GRIN2A causes a nonepileptic neurodevelopmental disorder. Mov Disord. 2018;33(6):992–9.

Fiori LM, Wanner B, Jomphe V, Croteau J, Vitaro F, Tremblay RE, et al. Association of Polyaminergic Loci With Anxiety, Mood Disorders, and Attempted Suicide. PLoS One. 2010;5(11):1–9.

Folch J, Busquets O, Ettcheto M, Sánchez-López E, Castro-Torres RD, Verdaguer E, et al. Memantine for the treatment of dementia: A review on its current and future applications. J Alzheimer's Dis. 2018;62(3):1223–40.

Forrest D, Yuzaki M, Soares HD, Ng L, Luk DC, Sheng M, et al. Targeted disruption of NMDA receptor 1 gene abolishes NMDA response and results in neonatal death. Neuron. 1994;13(2):325–38.

Fortin DA, Davare MA, Srivastava T, Brady JD, Nygaard S, Derkach VA, et al. Long-term potentiation-dependent spine enlargement requires synaptic Ca2+-permeable AMPA receptors recruited by CaM-kinase I. J Neurosci. 2010;30(35):11565–75.

Fossom LH, Basile AS, Skolnick P. Sustained exposure to 1-aminocyclopropanecarboxylic acid, a glycine partial agonist, alters N-methyl-D-aspartate receptor function and subunit composition. Mol Pharmacol. 1995;48(6):981–7.

Fraser CM, Sills GJ, Forrest G, Thompson GG, Brodie MJ. Neurochemical studies with the anticonvulsant felbamate in mouse brain. Pharmacol Res. 1999;40(3):257–61.

Fry AE, Fawcett KA, Zelnik N, Yuan H, Thompson BAN, Shemer-Meiri L, et al. De novo mutations in GRIN1 cause extensive bilateral polymicrogyria. Brain. 2018;141(3):698–712.

Fujii S. ATP- and Adenosine-Mediated Signaling in the Central Nervous System: The Role of Extracellular ATP in Hippocampal Long-Term Potentiation. J Pharmacol Sci. 2004;94(2):103–6.

Furukawa H, Singh SK, Mancusso R, Gouaux E. Subunit arrangement and function in NMDA receptors. Nature. 2005;438(7065):185–92.

Gafford G, Jasnow AM, Ressler KJ. Grin1 receptor deletion within CRF neurons enhances fear memory. PLoS One. 2014;9(10).

Gallagher MJ, Huang H, Grant ER, Lynch DR. The NR2B-specific interactions of polyamines and protons with the N- methyl-D-aspartate receptor. J Biol Chem. 1997;272(40):24971–9.

Gao M, Kondo F, Murakami T, Xu JW, Ma N, Zhu X, et al. 1-Aminocyclopropanecarboxylic acid, an antagonist of N-methyl-D-aspartate receptors causes hypotensive and antioxidant effects with upregulation of heme oxygenase-1 in stroke-prone spontaneously hypertensive rats. Hypertens Res. 2007;30(3):249–57.

Gao K, Tankovic A, Zhang Y, Kusumoto H, Zhang J, Chen W, et al. A de novo loss-of-function GRIN2A mutation associated with childhood focal epilepsy and acquired epileptic aphasia. PLoS One. 2017;12(2):1–20.

Gao Y, He L, Katsumi H, Sakane T, Fujita T, Yamamoto A. Improvement of intestinal absorption of water-soluble macromolecules by various polyamines : Intestinal mucosal toxicity and absorption-enhancing mechanism of spermine. Int J Pharm. 2008;354:126–34.

García-Recio A, Santos-Gómez A, Soto D, Julia-Palacios N, García-Cazorla À, Altafaj X, et al. GRIN database: A unified and manually curated repertoire of GRIN variants. Hum Mutat. 2021;42(1):8–18.

Garraway SM, Xu Q, Inturrisi CE. Design and evaluation of small interfering RNAs that target expression of the N-methyl-D-aspartate receptor NR1 subunit gene in the spinal cord dorsal horn. J Pharmacol Exp Ther. 2007;322(3):982–8.

Gelfin E, Kaufman Y, Korn-Lubetzki I, Bloch B, Kremer I, Javitt DC, et al. D-serine adjuvant treatment alleviates behavioural and motor symptoms in Parkinson's disease. Int J Neuropsychopharmacol. 2012;15(4):543–9.

Genever PG, Maxfield SJ, Kennovin GD, Maltman J, Bowgen CJ, Raxworthy MJ, et al. Evidence for a novel glutamate-mediated signaling pathway in keratinocytes. J Invest Dermatol. 1999;112(3):337–42.

Gerhard DM, Wohleb ES, Duman RS. Emergin Treatmen Mechanisms for Depression: Focus on Glutamate and Synaptic Plasticity. Drug Discov Today. 2016;21(3):454–64.

Germanò A, Caffo M, Angileri FF, Arcadi F, Newcomb-Fernandez J, Caruso G, et al. NMDA receptor antagonist felbamate reduces behavioral deficits and blood-brain barrier permeability changes after experimental subarachnoid hemorrhage in the rat. J Neurotrauma. 2007;24(4):732–44.

Gielen M, Retchless BS, Mony L, Johnson JW, Paoletti P. Mechanism of differential control of NMDA receptor activity by NR2 subunits. Nature. 2009 Jun 4;459(7247):703–7.

Gilbert ME. The NMDA antagonist MK-801 suppresses behavioral seizures, augments afterdischarges, but does not block development of perforant path kindling. Epilepsy Res. 1994;17(2):145–56.

Gill S, Pulido O. Glutamate Receptors in Peripheral Tissues: Current Knowledge, Future Research, and Implications for Toxicology. Toxicol Pathol. 2001;29(2):208–23.

Gill S, Veinot J, Kavanagh M, Pulido O. Human Heart Glutamate Receptors—Implications for Toxicology, Food Safety, and Drug Discovery. Toxicol Pathol. 2007 Apr 25;35(3):411–7.

Gilron I, Coderre TJ. Emerging drugs in neuropathic pain. Expert Opin Emerg Drugs. 2007;12(1):113–26.

Gódor-Kacsándi A, Felszeghy K, Ranky M, Luiten P, Nyakas C. Developmental docosahexaenoic and arachidonic acid supplementation improves adult learning and increases resistance against excitotoxicity in the brain. Acta Physiol Hung. 2013;100(2):186–96.

Goldstein LE, Rasmusson AM, Bunney BS, Roth RH. The NMDA glycine site antagonist (+)-HA-966 selectively regulates conditioned stress-induced metabolic activation of the mesoprefrontal cortical dopamine but not serotonin systems: A behavioral, neuroendocrine, and neurochemical study in the rat. J Neurosci. 1994;14(8):4937–50.

Gong N, Gao ZY, Wang YC, Li XY, Huang JL, Hashimoto K, et al. A series of d-amino acid oxidase inhibitors specifically prevents and reverses formalin-induced tonic pain in rats. J Pharmacol Exp Ther. 2011;336(1):282–93.

Goo N, Bae HJ, Park K, Kim J, Jeong Y, Cai M, et al. The effect of fecal microbiota transplantation on autistic-like behaviors in Fmr1 KO mice. Life Sci. 2020;262(May):118497.

Gopalakrishnan V, Dozier EA, Glover MS, Novick S, Ford M, Morehouse C, et al. Engraftment of Bacteria after Fecal Microbiota Transplantation Is Dependent on Both Frequency of Dosing and Duration of Preparative Antibiotic Regimen. Microorganisms. 2021;9(1399).

Gréco S, Niepceron E, Hugueny I, George P, Louisot P, Biol M-C. Dietary Spermidine and Spermine Participate in the Maturation of Galactosyltransferase Activity and Glycoprotein Galactosylation in Rat Small Intestine. J Nutr. 2001;131(7):1890–7.

Greenamyre JT, Eller R V., Zhang Z, Ovadia A, Kurlan R, Gash DM. Antiparkinsonian effects of remacemide hydrochloride, a glutamate antagonist, in rodent and primate models of Parkinson's disease. Ann Neurol. 1994;35(6):655–61.

Griffiths R, Dunlop J, Gorman A, Senior J, Grieve A. L-TRANs-Pyrrolidine-2,4-dicarboxylate and cis-1-aminocyclobutane-1, 3-dicarboxylate behave as transportable, competitive inhibitors of the high-affinity glutamate transporters. Biochem Pharmacol. 1994;47(2):267–74.

Guercio GD, Panizzutti R. Potential and challenges for the clinical use of D-Serine as a cognitive enhancer. Front Psychiatry. 2018;9(FEB):1–10.

Gussow AB, Petrovski S, Wang Q, Allen AS, Goldstein DB. The intolerance to functional genetic variation of protein domains predicts the localization of pathogenic mutations within genes. Genome Biol. 2016;17(1):1–11.

Häckl LPN, Carobrez AP. Distinct ventral and dorsal hippocampus AP5 anxiolytic effects revealed in the elevated plus-maze task in rats. Neurobiol Learn Mem. 2007;88(2):177–85.

Hackos DH, Lupardus PJ, Grand T, Chen Y, Wang TM, Reynen P, et al. Positive Allosteric Modulators of GluN2A-Containing NMDARs with Distinct Modes of Action and Impacts on Circuit Function. Neuron. 2016;89(5):983–99.

Halene TB, Ehrlichman RS, Liang Y, Christian EP, Jonak GJ, Gur TL, et al. Assessment of NMDA receptor NR1 subunit hypofunction in mice as a model for schizophrenia. Genes, Brain Behav. 2009 Oct;8(7):661–75.

Hama A, Sagen J. Antinociceptive effects of the marine snail peptides conantokin-G and conotoxin MVIIA alone and in combination in rat models of pain. Neuropharmacology. 2009;56(2):556–63.

Hamdan FF, Gauthier J, Araki Y, Lin DT, Yoshizawa Y, Higashi K, et al. Excess of de novo deleterious mutations in genes associated with glutamatergic systems in nonsyndromic intellectual disability. Am J Hum Genet. 2011;88(3):306–16.

Hamdani EH, Gudbrandsen M, Bjørkmo M, Chaudhry FA. The system N transporter SN2 doubles as a transmitter precursor furnisher and a potential regulator of NMDA receptors. Glia. 2012 Nov;60(11):1671–83.

Hamm RJ, O'Dell DM, Pike BR, Lyeth BG. Cognitive impairment following traumatic brain injury: the effect of pre- and post-injury administration of scopolamine and MK-801. Cogn Brain Res. 1993;1(4):223–6.

Hanada T. Ionotropic glutamate receptors in epilepsy: A review focusing on ampa and nmda receptors. Biomolecules. 2020;10(3).

Hansen KB, Furukawa H, Traynelis SF. Control of assembly and function of glutamate receptors by the amino-terminal domain. Vol. 78, Molecular Pharmacology. American Society for Pharmacology and Experimental Therapy; 2010. p. 535–49.

Hanson JE, Ma K, Elstrott J, Weber M, Khan AS, Simms J, et al. GluN2A NMDA Receptor Enhancement Improves Brain Oscillations, Synchrony, and Cognitive Functions in Dravet Syndrome and Alzheimer's Disease Models. Cell Rep. 2020;30(2):381–96.

Hardingham GE, Bading H. Synaptic versus extrasynaptic NMDA receptor signalling: Implications for neurodegenerative disorders. Nat Rev Neurosci. 2010;11(10):682–96.

Hardingham GE, Do KQ. Linking early-life NMDAR hypofunction and oxidative stress in schizophrenia pathogenesis. Nat Rev Neurosci. 2016;17(2):125–34.

Hauben U, D'Hooge R, Soetens E, De Deyn PP. Effects of oral administration of the competitive N-methyl-D-aspartate antagonist, CGP 40116, on passive avoidance, spatial learning, and neuromotor abilities in mice. Brain Res Bull. 1999;48(3):333–41.

Hawkins LM, Prybylowski K, Chang K, Moussan C, Stephenson FA, Wenthold RJ. Export from the endoplasmic reticulum of assembled N-methyl-D-aspartic acid receptors is controlled by a motif in the C terminus of the NR2 subunit. J Biol Chem. 2004 Jul 9;279(28):28903–10.

Hayashi T. Post-translational palmitoylation of ionotropic glutamate receptors in excitatory synaptic functions. Br J Pharmacol. 2020;178(4):784–97.

Henson MA, Roberts AC, Pérez-Otaño I, Philpot BD. Influence of the NR3A subunit on NMDA receptor functions. Prog Neurobiol. 2010;91(1):23–37.

Hering H, Sheng M. Dentritic spines: structure, dynamics and regulation. Nat Rev Neurosci. 2001;2(12):880–8.

Hewkin CT, Di Fabio R, Conti N, Cugola A, Gastaldi P, Micheli F, et al. New synthesis of substituted 2-carboxyindole derivatives: Versatile introduction of a carbamoylethynyl moiety at the C-3 position. Arch Pharm (Weinheim). 1999;332(2):55–8.

Hogan-Cann AD, Anderson CM. Physiological Roles of Non-Neuronal NMDA Receptors. Trends Pharmacol Sci. 2016;37(9):750–67.

Holehonnur R, Lella SK, Ho A, Luong JA, Ploski JE. The production of viral vectors designed to express large and difficult to express transgenes within neurons. Mol Brain. 2015 Feb 24;8(1):12.

Holtman JR, Crooks PA, Johnson-Hardy JK, Hojomat M, Kleven M, Wala EP. Effects of norketamine enantiomers in rodent models of persistent pain. Pharmacol Biochem Behav. 2008;90(4):676–85.

Holubova K, Nekovarova T, Pistovcakova J, Sulcova A, Stuchlík A, Vales K. Pregnanolone glutamate, a novel use-dependent NMDA receptor inhibitor, exerts antidepressant-like properties in animal models. Front Behav Neurosci. 2014;8(APR):1–10.

Horak M, Chang K, Wenthold RJ. Masking of the endoplasmic reticulum retention signals during assembly of the NMDA receptor. J Neurosci. 2008 Mar 26;28(13):3500–9.

Horak M, Wenthold RJ. Different roles of C-terminal cassettes in the trafficking of full-length NR1 subunits to the cell surface. J Biol Chem. 2009 Apr 10;284(15):9683–91.

Hornig T, Grüning B, Kundu K, Houwaart T, Backofen R, Biber K, et al. GRIN3B missense mutation as an inherited risk factor for schizophrenia: Whole-exome sequencing in a family with a familiar history of psychotic disorders. Genet Res (Camb). 2017;99.

Hu C, Chen W, Myers SJ, Yuan H, Traynelis SF. Human GRIN2B variants in neurodevelopmental disorders. J Pharmacol Sci. 2016;132(2):115–21.

Ibrahim L, Diazgranados N, Jolkovsky L, Brutsche N, Luckenbaugh DA, Joseph Herring W, et al. A randomized, placebo-controlled, crossover pilot trial of the oral selective NR2B antagonist MK-0657 in patients with treatment-resistant major depressive disorder. J Clin Psychopharmacol. 2012;32(4):551–7.

Ichikawa M, Muramoto K, Kobayashi K, Kawahara M, Kuroda Y. Formation and maturation of synapses in primary cultures of rat cerebral cortical cells: an electron microscopic study. Neurosci Res. 1993;16(2):95–103.

Ishikawa M, Yoshitomi T, Covey DF, Zorumski CF, Izumi Y. Additive neuroprotective effects of 24(S)-hydroxycholesterol and allopregnanolone in an ex vivo rat glaucoma model. Sci Rep. 2018;8(1):1–15.

Ito I, Futai K, Katagiri H, Watanabe M, Sakimura K, Mishina M, et al. Synapse-selective impairment of NMDA receptor functions in mice lacking NMDA receptor epsilon 1 or epsilon 2 subunit. J Physiol. 1997 Apr 15;500(2):401–8.

Jimenez EC, Donevan S, Walker C, Zhou LM, Nielsen J, Cruz LJ, et al. Conantokin-L, a new NMDA receptor antagonist: Determinants for anticonvulsant potency. Epilepsy Res. 2002;51(1–2):73–80.

Jin ZL, Liu JX, Liu X, Zhang LM, Ran YH, Zheng YY, et al. Anxiolytic effects of GLYX-13 in animal models of posttraumatic stress disorder-like behavior. J Psychopharmacol. 2016;30(9):913–21.

Johnson JW, Ascher P. Glycine potentiates the NMDA response in cultured mouse brain neurons. Nature. 1987;325(5):529–31.

Johnson PI, Parente MA, Stellar JR. NMDA-induced lesions of the nucleus accumbens or the ventral pallidum increase the rewarding efficacy of food to deprived rats. Brain Res. 1996;722(1–2):109–17.

Kaidanovich-Beilin O, Lipina T, Vukobradovic I, Roder J, Woodgett JR. Assessment of social interaction behaviors. Journal of Visualized Experiments. 2011; p. 2473.

Kalbaugh TL, VanDongen HMA, VanDongen AMJ. Ligand-binding residues integrate affinity and efficacy in the NMDA receptor. Mol Pharmacol. 2004;66(2):209–19.

Kamat PK, Kalani A, Rai S, Swarnkar S, Tota S, Nath C, et al. Mechanism of Oxidative Stress and Synapse Dysfunction in the Pathogenesis of Alzheimer's Disease: Understanding the Therapeutics Strategies. Mol Neurobiol. 2016;53(1):648–61.

Kaneko Y, Tuazon JP, Ji X, Borlongan C V. Pituitary adenylate cyclase activating polypeptide elicits neuroprotection against acute ischemic neuronal cell death associated with NMDA receptors. Cell Physiol Biochem. 2018;51(4):1982–95.

Kaniakova M, Krausova B, Vyklicky V, Korinek M, Lichnerova K, Vyklicky L, et al. Key amino acid residues within the third membrane domains of NR1 and NR2 subunits contribute to the regulation of the surface delivery of N-methyl-D-aspartate receptors. J Biol Chem. 2012 Jul 27;287(31):26423–34.

Kannangara TS, Bostrom CA, Ratzlaff A, Thompson L, Cater RM, Gil-Mohapel J, et al. Deletion of the NMDA receptor GluN2A subunit significantly decreases dendritic growth in maturing dentate granule neurons. PLoS One. 2014;9(8).

Kannangara TS, Eadie BD, Bostrom CA, Morch K, Brocardo PS, Christie BR. GluN2A-/- Mice Lack Bidirectional Synaptic Plasticity in the Dentate Gyrus and Perform Poorly on Spatial Pattern Separation Tasks. Cereb Cortex. 2015;25(8):2102–13.

Kanthasamy AG, Kanthasamy A, Matsumoto RR, Vu TQ, Truong DD. Neuroprotective effects of the strychnine-insensitive glycine site NMDA antagonist (R)-HA-966 in an experimental model of Parkinson's disease. Brain Res. 1997;759(1):1–8.

Karakas E, Simorowski N, Furukawa H. Structure of the zinc-bound amino-terminal domain of the NMDA receptor NR2B subunit. EMBO J. 2009 Dec 16; 28(24):3910-20.

Karakawa S, Miyoshi Y, Konno R, Koyanagi S, Mita M, Ohdo S, et al. Two-dimensional high-performance liquid chromatographic determination of day-night variation of d-alanine in mammals and factors controlling the circadian changes Amino Acid Analysis. Anal Bioanal Chem. 2013;405(25):8083–91.

Kartvelishvily E, Shleper M, Balan L, Dumin E, Wolosker H. Neuron-derived D-serine release provides a novel means to activate N-methyl-D-aspartate receptors. J Biol Chem. 2006 May 19;281(20):14151–62.

Katane M, Saitoh Y, Hanai T, Sekine M, Furuchi T, Koyama N, et al. Thiolactomycin inhibits d-aspartate oxidase: A novel approach to probing the active site environment. Biochimie. 2010;92(10):1371–8.

Katayama S, Ae N, Kodo T, Masumoto S, Hourai S, Tamamura C, et al. Tricyclic indole-2-carboxylic acids: Highly in vivo active and selective antagonists for the glycine binding site of the NMDA receptor. J Med Chem. 2003;46(5):691–701.

Kato A, Rouach N, Nicoll RA, Bredt DS. Activity-dependent NMDA receptor degradation mediated by retrotranslocation and ubiquitination. Proc Natl Acad Sci U S A. 2005;102(15):5600–5.

Kato T, Fogaça M V, Deyama S, Li X-Y, Fukumoto K, Duman RS. BDNF Release and Signaling are Required for the Antidepressant Actions of GLYX-13. Mol Psychiatry. 2018;23(10):2007–17.

Kawai M, Horikawa Y, Ishihara T, Shimamoto K, Ohfune Y. 2-(carboxycyclopropyl)glycines: binding, neurotoxicity and induction of intracellular free Ca2+ increase. Eur J Pharmacol. 1992;211(2):195–202.

Kazi R, Dai J, Sweeney C, Zhou H-X, Wollmuth LP. Mechanical coupling maintains the fidelity of NMDA receptor-mediated currents. Nat Neurosci. 2014;17(7):914–22.

Kellner S, Abbasi A, Carmi I, Heinrich R, Garin-Shkolnik T, Hershkovitz T, et al. Two de novo GluN2B mutations affect multiple NMDAR-functions and instigate severe pediatric encephalopathy. Elife. 2021;10.

Kennedy MB. The Protein Biochemistry of the Postsynaptic Density in Glutamatergic Synapses Mediates Learning in Neural Networks. Biochemistry. 2018 Jul 10;57(27):4005–9.

Kenny AV, Cousins SH, Pinho L, Stephenson A. The Integrity of the Glycine Co-agonist Binding Site of *N*-Methyl-d-aspartate Receptors Is a Functional Quality Control Checkpoint for Cell Surface Delivery. J Biol Chem. 2009 Jan 2;284(1):324-333.

Khakpai F, Zarrindast MR, Nasehi M, Haeri-Rohani A, Eidi A. The role of glutamatergic pathway between septum and hippocampus in the memory formation. EXCLI J. 2013 Jan 21;12:41–51.

Kiechl S, Pechlaner R, Willeit P, Notdurfter M, Paulweber B, Willeit K, et al. Higher spermidine intake is linked to lower mortality: A prospective population-based study. Am J Clin Nutr. 2018;108(2):371–80.

Kim MS, Kim Y, Choi H, Kim W, Park S, Lee D, et al. Transfer of a healthy microbiota reduces amyloid and tau pathology in an Alzheimer's disease animal model. Gut. 2020;69(2):283–94.

Kim SK, Guevarra RB, Kim YT, Kwon J, Kim H, Cho JH, et al. Role of probiotics in human gut microbiome-associated diseases. J Microbiol Biotechnol. 2019;29(9):1335–40.

Kimball ES, Palmer JM, D'Andrea MR, Hornby PJ, Wade PR. Acute colitis induction by oil of mustard results in later development of an IBS-like accelerated upper GI transit in mice. Am J Physiol - Gastrointest Liver Physiol. 2005 Jun;288(6 51-6).

Kiyama Y, Manabe T, Sakimura K, Kawakami F, Mori H, Mishina M. Increased thresholds for long-term potentiation and contextual learning in mice lacking the NMDA-type glutamate receptor ε1 subunit. J Neurosci. 1998;18(17):6704–12.

Klein S.M., et al., Noninvasive in vivo assessment of muscle impairment in the mdx mouse model-a comparison of two common wire hanging methods with two different results. J Neurosci Methods. 2012 Jan 30;203(2):292-7.

Knobloch M, Mansuy IM. Dendritic spine loss and synaptic alterations in Alzheimer's disease. Mol Neurobiol. 2008;37(1):73–82.

Komada M, Takao K, Miyakawa T. Elevated plus maze for mice. J Vis Exp. 2008 ;(22):1088.

Konieczny J, Ossowska K, Schulze G, Coper H, Wolfarth S. L-701,324, a selective antagonist at the glycine site of the NMDA receptor, counteracts haloperidol-induced muscle rigidity in rats. Psychopharmacology (Berl). 1999;143(3):235–43.

Kotlinska J, Liljequist S. A characterization of anxiolytic-like actions induced by the novel NMDA/glycine site antagonist, L-701,324. Psychopharmacology (Berl). 1998;135(2):175–81.

Krausova BH, Kysilov B, Cerny J, Vyklicky V, Smejkalova T, Ladislav M, et al. Site of action of brain neurosteroid pregnenolone sulfate at the N-methyl-D-aspartate receptor. J Neurosci. 2020;40(31):5922–36.

Kretschmer BD. Felbamate, an anti-convulsive drug, has anti-parkinsonian potential in rats. 1994;179:115–8.

Kroczka B, Branski P, Palucha A, Pilc A, Nowak G. Antidepressant-like properties of zinc in rodent forced swim test. Brain Res Bull. 2001;55(2):297–300.

Krogsgaard-Larsen P, Nielsen E, Curtis DR. Ibotenic acid analogues. synthesis and biological and in vitro activity of conformationally restricted agonists at central excitatory amino acid receptors. J Med Chem. 1984;27(5):585–91.

Krupp JJ, Vissel B, Thomas CG, Heinemann SF, Westbrook GL. Interactions of calmodulin and α-actinin with the NR1 subunit modulate Ca^{2+}-dependent inactivation of NMDA receptors. J Neurosci. 1999;19(4):1165–78.

Krupp JJ, Vissel B, Thomas CG, Heinemann SF, Westbrook GL. Calcineurin acts via the C-terminus of NR2A to modulate desensitization of NMDA receptors. Neuropharmacology. 2002;42(5):593–602.

Kussius CL, Kaur N, Popescu GK. Pregnanolone sulfate promotes desensitization of activated NMDA receptors. J Neurosci. 2009;29(21):6819–27.

Kutsuwada T, Sakimura K, Manabe T, Takayama C, Katakura N, Kushiya E, et al. Impairment of suckling response, trigeminal neuronal pattern formation, and hippocampal LTD in NMDA receptor epsilon 2 subunit mutant mice. Neuron. 1996 Feb; 16(2):333–44.

Kuzmin A, Madjid N, Terenius L, Ogren SO, Bakalkin G. Big dynorphin, a prodynorphin-derived peptide produces NMDA receptor-mediated effects on memory, anxiolytic-like and locomotor behavior in mice. Neuropsychopharmacology. 2006;31(9):1928–37.

Kyriakopoulos P, Mcniven V, Carter MT, Frcp C, Humphreys P, Frcp C, et al. Atypical Rett Syndrome and Intractable Epilepsy With Novel GRIN2B Mutation. Neuropharmacology. 2018;5:1–2.

La DS, Salituro FG, Martinez Botella G, Griffin AM, Bai Z, Ackley MA, et al. Neuroactive Steroid N-Methyl- d -aspartate Receptor Positive Allosteric Modulators: Synthesis, SAR, and Pharmacological Activity. J Med Chem. 2019;62(16):7526–42.

Ladislav M, Cerny J, Krusek J, Horak M, Balik A, Vyklicky L. The LILI motif of M3-S2 linkers is a component of the NMDA receptor channel gate. Front Mol Neurosci. 2018;11(113):1–16.

Lai TW, Zhang S, Wang YT. Excitotoxicity and stroke: Identifying novel targets for neuroprotection. Prog Neurobiol. 2014;115(C):157–88.

Lambuk L, Jafri AJA, Arfuzir NNN, Iezhitsa I, Agarwal R, Rozali KN Bin, et al. Neuroprotective Effect of Magnesium Acetyltaurate Against NMDA-Induced Excitotoxicity in Rat Retina. Neurotox Res. 2017;31(1):31–45.

Lapidus KAB, Soleimani L, Murrough JW. Novel glutamatergic drugs for the treatment of mood disorders. Neuropsychiatr Dis Treat. 2013;9:1101–12.

Large CH, Webster EL, Goff DC. The potential role of lamotrigine in schizophrenia. Psychopharmacology (Berl). 2005;181(3):415–36.

Laroia N, McBride L, Baggs R, Guillet R. Dextromethorphan ameliorates effects of neonatal hypoxia on brain morphology and seizure threshold in rats. Dev Brain Res. 1997;100(1):29–34.

Lavaur J, Le Nogue D, Lemaire M, Pype J, Farjot G, Hirsch EC, et al. The noble gas xenon provides protection and trophic stimulation to midbrain dopamine neurons. J Neurochem. 2017;142(1):14–28.

Lavezzari G, McCallum J, Lee R, Roche KW. Differential binding of the AP-2 adaptor complex and PSD-95 to the C-terminus of the NMDA receptor subunit NR2B regulates surface expression. Neuropharmacology. 2003;45(6):729–37.

Le Roy T, Debédat J, Marquet F, Da-cunha C, Ichou F, Guerre-millo M, et al. Comparative Evaluation of Microbiota Engraftment Following Fecal Microbiota Transfer in Mice Models : Age , Kinetic and Microbial Status Matter. Front Microbiol. 2019;9(January):1–16.

Leger M, Quiedeville A, Bouet V, Haelewyn B, Boulouard M, Schumann-Bard P, et al. Object recognition test in mice. Nat Protoc. 2013;8(12):2531–7.

Leist M, Nicotera P. Apoptosis, Excitotoxicity, and Neuropathology. Exp Cell Res. 1998;239:183–201.

Lemke JR, Lal D, Reinthaler EM, Steiner I, Nothnagel M, Alber M, et al. Mutations in GRIN2A cause idiopathic focal epilepsy with rolandic spikes. Nat Genet. 2013;45(9):1067–72.

Lemke JR, Hendrickx R, Geider K, Laube B, Schwake M, Harvey RJ, et al. GRIN2B mutations in west syndrome and intellectual disability with focal epilepsy. Ann Neurol. 2014;75(1):147–54.

Lemke JR, Geider K, Helbig KL, Heyne HO, Schütz H, Hentschel J, et al. Delineating the GRIN1 phenotypic spectrum A distinct genetic NMDA receptor encephalopathy. Am Acad Neurol. 2016;86(June 7).

Lerma J. Spermine regulates N-methyl-d-aspartate receptor desensitization. Neuron. 1992;8(2):343–52.

Lesca G, Rudolf G, Bruneau N, Lozovaya N, Labalme A, Boutry-Kryza N, et al. GRIN2A mutations in acquired epileptic aphasia and related childhood focal epilepsies and encephalopathies with speech and language dysfunction. Nat Genet. 2013;45(9):1061–6.

Levin R, Dor-abarbanel AE, Edelman S, Durrant AR, Hashimoto K, Javitt DC, et al. Behavioral and cognitive effects of the N-methyl- D -aspartate receptor co-agonist D -serine in healthy humans : Initial fi ndings. J Psychiatr Res. 2015;61:188–95.

Li J, Zhang J, Tang W, Mizu RK, Kusumoto H, XiangWei W, et al. De Novo GRIN Variants in NMDA Receptor M2 Channel Pore-Forming Loop Are Associated with Neurological Diseases. Hum Mutat. 2019;40(12):2393–413.

Li K, Wei S, Hu L, Yin X, Mai Y, Jiang C, et al. Protection of Fecal Microbiota Transplantation in a Mouse Model of Multiple Sclerosis. Mediators Inflamm. 2020;2020.

Li Q, Zhou JM. The microbiota-gut-brain axis and its potential therapeutic role in autism spectrum disorder. Neuroscience. 2016;324:131–9.

Li X, Wang H, Chen Q, Li Z, Liu C, Yin S, et al. Felbamate produces antidepressant-like actions in the chronic unpredictable mild stress and chronic social defeat stress models of depression. Fundam Clin Pharmacol. 2019;33(6):621–33.

Li X, Xie LL, Han W, Hong SQ, Ma JN, Wang J, et al. Clinical Forms and GRIN2A Genotype of Severe End of Epileptic-Aphasia Spectrum Disorder. Front Pediatr. 2020;8.

Li XH, Miao HH, Zhuo M. NMDA Receptor Dependent Long-term Potentiation in Chronic Pain. Neurochem Res. 2019;44(3):531–8.

Lichnerova K, Kaniakova M, Park SP, Skrenkova K, Wang YX, Petralia RS, et al. Two N-glycosylation sites in the GluN1 subunit are essential for releasing N-methyl-D-aspartate (NMDA) receptors from the endoplasmic reticulum. J Biol Chem. 2015 Jul 24;290(30):18379–90.

Liu H, Naismith JH. An efficient one-step site-directed deletion, insertion, single and multiple-site plasmid mutagenesis protocol. BMC Biotechnol. 2008; 8(1):91.

Liu H, Wang H, Peterson M, Zhang W, Hou G, Zhang Z wei. N-terminal alternative splicing of GluN1 regulates the maturation of excitatory synapses and seizure susceptibility. Proc Natl Acad Sci U S A. 2019;116(42):21207–12.

Liu RJ, Duman C, Kato T, Hare B, Lopresto D, Bang E, et al. GLYX-13 Produces Rapid Antidepressant Responses with Key Synaptic and Behavioral Effects Distinct from Ketamine. Neuropsychopharmacology. 2017;42(6):1231–42.

Liu S, Zhou L, Yuan H, Vieira M, Sanz-Clemente A, Badger JD, et al. A rare variant identified within the GluN2B C-terminus in a patient with autism affects NMDA receptor surface expression and spine density. J Neurosci. 2017;37(15):4093–102.

Lizasoain I, Knowles RG, Moncada S. Inhibition by Lamotrigine of the Generation of Nitric Oxide in Rat Forebrain Slices. J Neurochem. 1995;64(2):636–42.

Lodish H, Berk A, Zipursky SL et al. Neurotransmitters, Synapses, and Impulse Transmission. In: Molecular Cell Biology. 4th ed. New York: W.H. Freeman; 2000.

Longo VD, Di Tano M, Mattson MP, Guidi N. Intermittent and periodic fasting, longevity and disease. Nat Aging. 2021;1(1):47–59.

Löscher W, Hönack D. Differences in anticonvulsant potency and adverse effects between dextromethorphan and dextrorphan in amygdala-kindled and non-kindled rats. Eur J Pharmacol. 1993;238(2–3):191–200.

Loss CM, da Rosa NS, Mestriner RG, Xavier LL, Oliveira DL. Blockade of GluN2B-containing NMDA receptors reduces short-term brain damage induced by early-life status epilepticus. Neurotoxicology. 2019;71:138–49.

Lu WY, Man HY, Ju W, Trimble WS, MacDonald JF, Wang YT. Activation of synaptic NMDA receptors induces membrane insertion of new AMPA receptors and LTP in cultured hippocampal neurons. Neuron. 2001 Jan 1;29(1):243–54.

Lueptow LM. Novel object recognition test for the investigation of learning and memory in mice. J Vis Exp. 2017 Aug 1;2017(126):55718.

Lutfy K, Woodward RM, Keana JFW, Weber E. Inhibition of clonic seizure-like excitatory effects induced by intrathecal morphine using two NMDA receptor antagonists: MK-801 and ACEA-1011. Eur J Pharmacol. 1994;252(3):261–6.

Lutfy K, Weber E. Attenutation of nociceptive responses by ACEA-1021, a competitive NMDA receptor/glycine site antagonist, in the mice. Brain Res. 1996;743(1–2):17–23.

Lugo-Huitrón R, Ugalde Muñiz P, Pineda B, Pedraza-Chaverrí J, Ríos C, Pérez-De La Cruz V. Quinolinic acid: An endogenous neurotoxin with multiple targets. Oxid Med Cell Longev. 2013;2013.

Lüscher C, Malenka RC. NMDA Receptor-Dependent Long-Term Potentiation and Long-Term Depression (LTP/LTD). Cold Spring Harb Perspect om Biol. 2012;4:1–15.

Lussier MP, Sanz-Clemente A, Roche KW. Dynamic regulation of N-methyl-D-aspartate (NMDA) and α-amino-3-hydroxy-5-methyl-4-isoxazolepropionic acid (AMPA) receptors by posttranslational modifications. J Biol Chem. 2015;290(48):28596–603.

Lynch DR, Rattelle A, Dong YN, Roslin K, Gleichman AJ, Panzer JA. Anti-NMDA Receptor Encephalitis: Clinical Features and Basic Mechanisms. 1st ed. Vol. 82, Advances in Pharmacology. Elsevier Inc.; 2018. 235–260 p.

Ma J, Endres M, Moskowitz MA. Synergistic effects of caspase inhibitors and MK-801 in brain injury after transient focal cerebral ischaemia in mice. Br J Pharmacol. 1998;124(4):756–62.

Macdonald DS, Weerapura M, Beazely MA, Martin L, Czerwinski W, Roder JC, et al. Modulation of NMDA receptors by pituitary adenylate cyclase activating peptide in CA1 neurons requires Gαq, protein kinase C, and activation of Src. J Neurosci. 2005;25(49):11374–84.

Madeo F, Eisenberg T, Pietrocola F, Kroemer G. Spermidine in health and disease. Science. 2018;359(410).

Madsen U, Dumpis MA, Bräuner-Osborne H, Piotrovskyl LB. Synthesis and Pharmacology of N-alkylated Derivatives of the Excitotoxin Ibotenic Acid. Bioorganic Med Chem Lett. 1998;8:1563–8.

Maier CM, Sun GH, Kunis DM, Giffard RG, Steinberg GK. Neuroprotection by the N-Methyl-d-Aspartate Receptor Antagonist CGP 40116: In Vivo and In Vitro Studies. J Neurochem. 1995;65(2):652–9.

Maj J, Skuza G, Rogóz Z. Some central effects of CGP 37849 and CGP 39551, the competitive NMDA receptor antagonists: potential antiparkinsonian activity. J Neural Transm. 1993;6:53–62.

Maki BA, Aman TK, Amico-Ruvio SA, Kussius CL, Popescu GK. C-terminal domains of N-methyl-D-aspartic acid receptor modulate unitary channel conductance and gating. J Biol Chem. 2012;287(43):36071–80.

Makino C, Shibata H, Ninomiya H, Tashiro N, Fukumaki Y. Identification of single-nucleotide polymorphisms in the human N-methyl-D-aspartate receptor subunit NR2D gene, GRIN2D, and association study with schizophrenia. Psychiatr Genet. 2005;15(3):215–21.

Mannara F, Radosevic M, Planagumà J, Soto D, Aguilar E, García-Serra A, et al. Allosteric modulation of NMDA receptors prevents the antibody effects of patients with anti-NMDAR encephalitis. Brain. 2020;143(9):2709–20.

Maqsood R, Stone TW. The Gut-Brain Axis, BDNF, NMDA and CNS Disorders. Neurochem Res. 2016;41(11):2819–35.

Marketa C, Lukas R, Hana C, Eva K, Karel V. Synthetic structural modifications of neurosteroids pregnanolone sulfate: Assessment of neuroprotective effects *in vivo*. Eur J Pharmacol. 2020.

Marquardt K, Saha M, Mishina M, Young JW, Brigman JL. Loss of GluN2A-containing NMDA Receptors Impairs Extra-dimensional Set-Shifting. Genes Brain Behav. 2014;23(7):611–7.

Marsden WN. Synaptic plasticity in depression: Molecular, cellular and functional correlates. Prog Neuro-Psychopharmacology Biol Psychiatry. 2013;43:168–84.

Martineau M, Guzman RE, Fahlke C, Klingauf J. VGLUT1 functions as a glutamate/proton exchanger with chloride channel activity in hippocampal glutamatergic synapses. Nat Commun. 2017 Dec 1;8(1):1–13.

Marwick KFM, Hansen KB, Skehel PA, Hardingham GE, Wyllie DJA. Functional assessment of triheteromeric NMDA receptors containing a human variant associated with epilepsy. J Physiol. 2019;597(6):1691–704.

Marx CE, Keefe RSE, Buchanan RW, Hamer RM, Kilts D, Bradford DW, et al. Targeting Cognitive and Negative Symptoms in Schizophrenia. Neuropsychopharmacology. 2009;34(8):1885–903.

Masuko T, Miyake M, Kusama-Eguchi K, Koike T, Kimura E, Kizawa Y, et al. Differential effects of linear and cyclic polyamines on NMDA receptor activities. Neurochem Int. 2008;53(1–2):38–44.

Matsui T-A, Sekiguchi M, Hashimoto A, Tomita U, Nishikawa T, Wada K. Functional Comparison of d-Serine and Glycine in Rodents: The Effect on Cloned NMDA Receptors and the Extracellular Concentration. J Neurochem. 1995;65(1):454–8.

Mattson MP. Glutamate and neurotrophic factors in neuronal plasticity and disease. Annals of the New York Academy of Sciences. Blackwell Publishing Inc.; 2008. p. 97–112.

Matute C. Glutamate and ATP signalling in white matter pathology. J Anat. 2011;219(1):53–64.

Mayer E a, Tillisch K, Gupta A, Mondello P, Mian M, Aloisi C, et al. Gut/brain axis and the microbiota. Emeran. Nutr Cancer. 2015;125(4):463–79.

McBean GJ. Sulfur-Containing Amino Acids. 3rd Editio. Lajtha A, Oja SS, Saransaari P, Schousboe A, editors. Handbook of Neurochemistry and Molecular Neurobiology. Springer; 2008.

McClean M, Chizh B, Headley P. Effects of NMDA receptor antagonists on nociceptive responses in vivo: comparison of antagonists acting at the glycine site with uncompetitive antagonists. Amino Acids. 1998;14:217–21.

Mckenna MC. The Glutamate-Glutamine Cycle Is Not Stoichiometric : Fates of Glutamate in Brain. J Neurosci. 2007;85:3347–58.

Mei Y, Wu DC, Zhou N. Astrocytic Regulation of Glutamate Transmission in Schizophrenia. Front Psychiatry. 2018;9:1–10.

Ménard C, Herzog H, Schwarzer C, Quirion R. Possible role of dynorphins in alzheimer's disease and age-related cognitive deficits. Neurodegener Dis. 2014;13(2–3):82–5.

Menniti F, Chenard B, Collins M, Ducat M, Shalaby I, White F. CP-101,606, a potent neuroprotectant selective for forebrain neurons. Eur J Pharmacol. 1997;331(2–3):117–26.

Michel A, Downey P, Van Damme X, De Wolf C, Schwarting R, Scheller D. Behavioural assessment of the A2α/NR2B combination in the unilateral 6-OHDA-lesioned rat model: A new method to examine the therapeutic potential of non-dopaminergic drugs. PLoS One. 2015;10(8):1–15.

Mielnik CA, Binko MA, Chen Y, Funk AJ, Johansson EM, Intson K, et al. Consequences of NMDA receptor deficiency can be rescued in the adult brain. Mol Psychiatry. 2020.

Miller B, Sarantis M, Traynelis SF, Attwell D. Potentiation of NMDA receptor currents by arachidonic acid. Lett to Nat. 1992;355:722–5.

Mirza NR, Bright JL, Stanhope KJ, Wyatt A, Harrington NR. Lamotrigine has an anxiolytic-like profile in the rat conditioned emotional response test of anxiety: A potential role for sodium channels? Psychopharmacology (Berl). 2005;180(1):159–68.

Miya K, Takahashi Y, Mori H. Anti-NMDAR autoimmune encephalitis. Brain Dev. 2014;36(8):645–52.

Miyamoto Y, Yamada K, Noda Y, Mori H, Mishina M, Nabeshima T. Hyperfunction of dopaminergic and serotonergic neuronal systems in mice lacking the NMDA receptor ε1 subunit. J Neurosci. 2001;21(2):750–7.

Mohn AR, Gainetdinov RR, Caron MG, Koller BH. Mice with reduced NMDA receptor expression display behaviors related to schizophrenia. Cell. 1999;98(4):427–36.

Molchanov ML, Guimarães FS. Anxiolytic-like effects of AP7 injected into the dorsolateral or ventrolateral columns of the periaqueductal gray of rats. Psychopharmacology (Berl). 2002;160(1):30–8.

Mony L, Zhu S, Carvalho S, Paoletti P. Molecular basis of positive allosteric modulation of GluN2B NMDA receptors by polyamines. EMBO J. 2011;30(15):3134–46.

Moon ES, Karadimas SK, Yu WR, Austin JW, Fehlings MG. Riluzole attenuates neuropathic pain and enhances functional recovery in a rodent model of cervical spondylotic myelopathy. Neurobiol Dis. 2014;62:394–406.

Morató X, López-Cano M, Canas PM, Cunha RA, Ciruela F. Brain Membrane Fractionation: An Ex Vivo Approach to Assess Subsynaptic Protein Localization. J Vis Exp. 2017;(123):e55661–e55661.

Morel V, Pickering G, Etienne M, Dupuis A, Privat AM, Chalus M, et al. Low doses of dextromethorphan have a beneficial effect in the treatment of neuropathic pain. Fundam Clin Pharmacol. 2014;28(6):671–80.

Morgado-Bernal I. Learning and memory consolidation : linking molecular and behavioral data. Neuroscience. 2011;176:12–9.

Mori H, Masaki H, Yamakura T, Mishina M. Identification by mutagenesis of a Mg2+-block site of the NMDA receptor channel. Lett to Nat. 1992;359:673–5.

Moskal JR, Burgdorf J, Kroes RA, Brudzynski SM, Panksepp J. A novel NMDA receptor glycine-site partial agonist, GLYX-13, has therapeutic potential for the treatment of autism. Neurosci Biobehav Rev. 2011;35(9):1982–8.

Moskal JR, Burch R, Burgdorf JS, Kroes RA, Stanton PK, Disterhoft JF, et al. GLYX-13, an NMDA receptor glycine site functional partial agonist enhances cognition and produces antidepressant effects without the psychotomimetic side effects of NMDA receptor antagonists. Expert Opin Investig Drugs. 2014;23(2):243–54.

Moskal JR, Burgdorf JS, Stanton PK, Kroes RA, Disterhoft JF, Burch RM, et al. The Development of Rapastinel (Formerly GLYX-13); A Rapid Acting and Long Lasting Antidepressant. Curr Neuropharmacol. 2017;15(847):47–56.

Mota Vieira M, Nguyen TA, Wu K, Badger JD, Collins BM, Anggono V, et al. An Epilepsy-Associated GRIN2A Rare Variant Disrupts CaMKIIα Phosphorylation of GluN2A and NMDA Receptor Trafficking. Cell Rep. 2020;32(9):108104.

Mothet J, Parent AT, Wolosker H, Brady RO, Linden DJ, Ferris CD, et al. D -Serine is an endogenous ligand for the glycine site of the N-methyl- D -aspartate receptor. PNAS. 2000;97(9):4926–4931.

Mothet JP, Pollegioni L, Ouanounou G, Martineau M, Fossier P, Baux G. Glutamate receptor activation triggers a calcium-dependent and SNARE protein-dependent release of the gliotransmitter D-serine. Proc Natl Acad Sci U S A. 2005 Apr 12;102(15):5606–11.

Moy SS, Perez A, Koller BH, Duncan GE. Amphetamine-induced disruption of prepulse inhibition in mice with reduced NMDA receptor function. Brain Res. 2006;1089(1):186–94.

Muir KW, Grosset DG, Lees KR. Effects of prolonged infusions of the NMDA antagonist aptiganel hydrochloride (CNS 1102) in normal volunteers. Vol. 20, Clinical Neuropharmacology. 1997. p. 311–21.

Mullier B, Wolff C, Sands ZA, Ghisdal P, Muglia P, Kaminski RM. Neuropharmacology GRIN2B gain of function mutations are sensitive to radiprodil, a negative allosteric modulator of GluN2B-containing NMDA receptors. Neuropharmacology. 2017;123:322–31.

Musleh W, Bi X, Tocco G, Yaghoubi S, Baudry M. Glycine-induced long-term potentiation is associated with structural and functional modifications of α-amino-3-hydroxyl-5-methyl-4-isoxazolepropionic acid receptors. Proc Natl Acad Sci USA. 1997 Aug 19;94(17):9451–6.

Nagata R, Katayama S, Ohtani K, Tanaka H, Shimago K. Tricyclic Quinoxalinediones, Aza-kynurenic Acids, and Indole-2- Carboxylic Acids as In Vivo Active NMDA-Glycine Antagonists. Curr Top Med Chem. 2006;6(7):733–45.

Nahum-Levy R, Fossom LH, Skolnick P, Benveniste M. Putative partial agonist 1-aminocyclopropanecarboxylic acid acts concurrently as a glycine-site agonist and a glutamate-site antagonist at N- methyl-D-aspartate receptors. Mol Pharmacol. 1999;56(6):1207–18.

Nahum-Levy R, Lipinski D, Shavit S, Benveniste M. Desensitization of NMDA receptor channels is modulated by glutamate agonists. Biophys J. 2001;80(5):2152–66.

Nakazawa T, Komai S, Tezuka T, Hisatsune C, Umemori H, Semba K, et al. Characterization of Fyn-mediated tyrosine phosphorylation sites on GluRε2 (NR2B) subunit of the N-methyl-D-aspartate receptor. J Biol Chem. 2001;276(1):693–9.

Namba T, Morimoto K, Yamada N, Otsuki S. Antiepileptogenic action of 7-chlorokynurenic acid on amygdala kindling of rats. Pharmacol Biochem Behav. 1993;46(2):275–81.

Nedergaard M, Takano T, Hansen AJ. Beyond the role of glutamate as a neurotransmitter. Nat Rev. 2002;3:748–55.

Neubig RR, Spedding M, Kenakin T, Christopoulos A. International Union of Pharmacology Committee on Receptor Nomenclature and Drug Classification. XXXVIII. Update on Terms and Symbols in Quantitative Pharmacology. Pharmacol Rev. 2003;55(4):597–606.

Newman MP, Blum S, Wong RCW, Scott JG, Prain K, Wilson RJ, et al. Autoimmune encephalitis. Intern Med J. 2016;46(2):148–57.

Nicoletti F, Bockaert J, Collingridge GL, Conn PJ, Ferraguti F, Schoepp DD, et al. Metabotropic glutamate receptors: From the workbench to the bedside. Vol. 60, Neuropharmacology. Elsevier Ltd; 2011. p. 1017–41.

Nicotera AG, Calì F, Vinci M, Musumeci SA. GRIN2A: involvement in movement disorders and intellectual disability without seizures. Neurol Sci. 2019;40(11):2405–6.

Niesters M, Martini C, Dahan A. Ketamine for chronic pain: Risks and benefits. Br J Clin Pharmacol. 2013;77(2):357–67.

Nishikawa M, Kimura S, Akaike N. Facilitatory effect of docosahexaenoic acid on N-methyl-D-aspartate response in pyramidal neurones of rat cerebral cortex. J Physiol. 1994;475(1):83–93.

Nong Y, Huang YQ, Ju W, Kalia L V., Ahmadian G, Wang YT, et al. Glycine binding primes NMDA receptor internalization. Nature. 2003;422(6929):302–7.

Nowak L, Bregestovski P, Ascher P, Herbet A, Prochiantz A. Magnesium gates glutamate-activated channels in mouse central neurones. Nature. 1984;307(5950):462–5.

Nozaki C, Vergnano AM, Filliol D, Ouagazzal AM, Le Goff A, Carvalho S, et al. Zinc alleviates pain through high-affinity binding to the NMDA receptor NR2A subunit. Nat Neurosci. 2011;14(8):1017–22.

Nunes EA, MacKenzie EM, Rossolatos D, Perez-Parada J, Baker GB, Dursun SM. D-serine and schizophrenia: An update. Expert Rev Neurother. 2012;12(7):801–12.

Nutt JG, Gunzler SA, Kirchhoff T, Hogarth P, Weaver JL, Krams M, et al. Effects of a NR2B selective NMDA glutamate antagonist, CP-101,606, on dyskinesia and parkinsonism. Mov Disord. 2008;23(13):1860–6.

Ogden KK, Chen W, Swanger SA, McDaniel MJ, Fan LZ, Hu C, et al. Molecular Mechanism of Disease-Associated Mutations in the Pre-M1 Helix of NMDA Receptors and Potential Rescue Pharmacology. Vol. 13, PLoS Genetics. 2017. 1–35 p.

Ohba C, Shiina M, Tohyama J, Haginoya K, Lerman-Sagie T, Okamoto N, et al. GRIN1 mutations cause encephalopathy with infantile-onset epilepsy, and hyperkinetic and stereotyped movement disorders. Epilepsia. 2015;56(6):841–8.

Okamoto M, Gray JD, Larson CS, Kazim SF, Soya H, McEwen BS, et al. Riluzole reduces amyloid beta pathology, improves memory, and restores gene expression changes in a transgenic mouse model of early-onset Alzheimer's disease. Transl Psychiatry. 2018;8(1).

Okiyama K, Smith DH, White WF, Richter K, McIntosh TK. Effects of the Novel NMDA Antagonists CP-98,113, CP-101,581 and CP-101,606 on Cognitive Function and Regional Cerebral Edema Following Experimental Brain Injury in the Rat. J Neurotrauma. 1997;14(4):211–22.

Onoue S, Endo K, Ohshima K, Yajima T, Kashimoto K. The neuropeptide PACAP attenuates β-amyloid (1-42)-induced toxicity in PC12 cells. Peptides. 2002;23(8):1471–8.

Otsuki M, Davidson M, Goodenough S, Wilce PA, Tase C, Matsumoto I. In vivo pharmacological study of spermine-induced neurotoxicity. Neurosci Lett. 1995;196:81–4.

Pan HC, Chou YC, Sun SH. P2X7R-mediated Ca2+-independent d-serine release via pannexin-1 of the P2X7R-pannexin-1 complex in astrocytes. Glia. 2015 May 1;63(5):877–93.

Paoletti P, Perin-Dureau F, Fayyazuddin A, Le Goff A, Callebaut I, Neyton J. Molecular organization of a zinc binding N-terminal modulatory domain in a NMDA receptor subunit. Neuron. 2000;28(3):911–25.

Paoletti P, Bellone C, Zhou Q. NMDA receptor subunit diversity: Impact on receptor properties, synaptic plasticity and disease. Vol. 14, Nature Reviews Neuroscience. Nature Publishing Group; 2013. p. 383–400.

Papa FT, Mancardi MM, Frullanti E, Fallerini C, Della Chiara V, Zalba-Jadraque L, et al. Personalized therapy in a GRIN1 mutated girl with intellectual disability and epilepsy. Clin Dysmorphol. 2018;27(1):18–20.

Papadakis M, Hawkins LM, Stephenson FA. Appropriate NR1-NR1 Disulfide-linked Homodimer Formation Is Requisite for Efficient Expression of Functional, Cell Surface N-Methyl-D-aspartate NR1/NR2 Receptors. J Biol Chem. 2004 Apr 9;279(15):14703–12.

Papouin T, Ladépêche L, Ruel J, Sacchi S, Labasque M, Hanini M, et al. Synaptic and extrasynaptic NMDA receptors are gated by different endogenous coagonists. Cell. 2012;150(3):633–46.

Pegg AE. Functions of polyamines in mammals. J Biol Chem. 2016;291(29):14904–12.

Penzes P, Cahill ME, Jones KA, VanLeeuwen J-E, Woolfrey KM. Dendritic spine pathology in neuropsychiatric disorders : Nature Neuroscience : Nature Publishing Group. Nat Neurosci. 2011;14(3):285–93.

Perea G, Navarrete M, Araque A. Tripartite synapses: astrocytes process and control synaptic information. Trends Neurosci. 2009;32(8):421–31.

Perez-Lloret S, Rascol O. Efficacy and safety of amantadine for the treatment of l-DOPA-induced dyskinesia. J Neural Transm. 2018;125(8):1237–50.

Pérez-Otaño I, Larsen RS, Wesseling JF. Emerging roles of GluN3-containing NMDA receptors in the CNS. Vol. 17, Nature Reviews Neuroscience. Nature Publishing Group; 2016. p. 623–35.

Perszyk RE, Kristensen AS, Lyuboslavsky P, Traynelis SF. Three-dimensional missense tolerance ratio analysis. Genome Res. 2021;31(8):1447–61.

Petit-Pedrol M, Groc L. Regulation of membrane NMDA receptors by dynamics and protein interactions. J Cell Biol. 2020;220(1):1–15.

Petty MA, Neumann-Haefelin C, Kalisch J, Sarhan S, Wettstein JG, Juretschke HP. In vivo neuroprotective effects of ACEA 1021 confirmed by magnetic resonance imaging in ischemic stroke. Eur J Pharmacol. 2003;474(1):53–62.

Peyrovian B, Rosenblat JD, Pan Z, Iacobucci M, Brietzke E, McIntyre RS. The glycine site of NMDA receptors: A target for cognitive enhancement in psychiatric disorders. Prog Neuro-Psychopharmacology Biol Psychiatry. 2019;92(January):387–404.

Pierson TM, Yuan H, Marsh ED, Fuentes-Fajardo K, Adams DR, Markello T, et al. GRIN2A mutation and early-onset epileptic encephalopathy: personalized therapy with memantine. Ann Clin Transl Neurol. 2014;1(3):190–8.

Pinheiro PS, Mulle C. Presynaptic glutamate receptors: physiological functions and mechanisms of action. Vol. 9, Nature reviews. Neuroscience. 2008. p. 423–36.

Planagumà Jesús, Haselmann H, Mannara F, Petit-Pedrol M, Grünewald B, Aguilar E, et al. Ephrin-B2 Prevents N-Methyl-D-Aspartate Receptor Antibody Effects on Memory and Neuroplasticity. Ann Neurol. 2016;80(3):388–400.

Platzer K, Yuan H, Schütz H, Winschel A, Chen W, Hu C, et al. GRIN2B encephalopathy: novel findings on phenotype, variant clustering, functional consequences and treatment aspects. J Med Genet. 2017;54(7):460–70.

Plescia F, Sardo P, Rizzo V, Cacace S, Marino RAM, Brancato A, et al. Pregnenolone sulphate enhances spatial orientation and object discrimination in adult male rats: Evidence from a behavioural and electrophysiological study. Behav Brain Res. 2014;258:193–201.

Pochwat B, Szewczyk B, Sowa-Kucma M, Siwek A, Doboszewska U, Piekoszewski W, et al. Antidepressant-like activity of magnesium in the chronic mild stress model in rats: Alterations in the NMDA receptor subunits. Int J Neuropsychopharmacol. 2014;17(3):393–405.

Popik P, Holuj M, Nikiforuk A, Kos T, Trullas R, Skolnick P. 1-Aminocyclopropanecarboxylic acid (ACPC) produces procognitive but not antipsychotic-like effects in rats. Psychopharmacology (Berl). 2015;232(6):1025–38.

Prado De Carvalho L, Bochet P, Rossier J. The endogenous agonist quinolinic acid and the non endogenous homoquinolinic acid discriminate between NMDAR2 receptor subunits. Neurochem Int. 1996;28(4):445–52.

Preskorn S, Macaluso M, Mehra V, Zammit G, Moskal JR, Burch RM. Randomized Proof of Concept Trial of GLYX-13, an N-Methyl-D-Aspartate Receptor Glycine Site Partial Agonist, in Major Depressive Disorder Nonresponsive to a Previous Antidepressant Agent. J Psychiatr Pract. 2015;21(2):140–9.

Prybylowski K, Fu Z, Losi G, Hawkins LM, Luo J, Chang K, et al. Relationship between Availability of NMDA Receptor Subunits and Their Expression at the Synapse. J Neurosci. 2002;22(20):8902–10.

Punzo D, Errico F, Cristino L, Sacchi S, Keller S, Belardo C, et al. Age-related changes in D-aspartate oxidase promoter methylation control extracellular D-aspartate levels and prevent precocious cell death during brain aging. J Neurosci. 2016;36(10):3064–78.

Qiu S, Hua YL, Yang F, Chen YZ, Luo JH. Subunit assembly of N-methyl-D-aspartate receptors analyzed by fluorescence resonance energy transfer. J Biol Chem. 2005 Jul 1;280(26):24923–30.

Qiu S, Zhang XM, Cao JY, Yang W, Yan YG, Shan L, et al. An endoplasmic reticulum retention signal located in the extracellular amino-terminal domain of the NR2A subunit of N-methyl-D-aspartate receptors. J Biol Chem. 2009 Jul 24;284(30):20285–98.

Qiu S, Li XY, Zhuo M. Post-translational modification of NMDA receptor GluN2B subunit and its roles in chronic pain and memory. Semin Cell Dev Biol. 2011;22(5):521–9.

Ramsey AJ, Milenkovic M, Oliveira AF, Escobedo-Lozoya Y, Seshadri S, Salahpour A, et al. Impaired NMDA receptor transmission alters striatal synapses and DISC1 protein in an age-dependent manner. Proc Natl Acad Sci U S A. 2011;108(14):5795–800.

Rao TS, Cler JA, Compton RP, Emmett MR, Mick S, Sun ET, et al. Neuropharmacological characterization of 1-Aminocyclopropane-1-carboxylate and 1-Aminocyclobutane-1-carboxylate, Ligands of the N-Methyl-D-Aspartate-associated Glycine Receptor. Neuropharmacology. 1990;29(3):305–9.

Ratner MH, Kumaresan V, Farb DH. Neurosteroid actions in memory and neurologic/neuropsychiatric disorders. Front Endocrinol (Lausanne). 2019;10(APR):1–37.

Raymond LA. Striatal synaptic dysfunction and altered calcium regulation in Huntington disease. Biochem Biophys Res Commun. 2017;483(4):1051–62.

Razak MA, Begum PS, Viswanath B, Rajagopal S. Multifarious Beneficial Effect of Nonessential Amino Acid, Glycine: A Review. Oxid Med Cell Longev. 2017;2017.

Regan MC, Grant T, McDaniel MJ, Karakas E, Zhang J, Traynelis SF, et al. Structural Mechanism of Functional Modulation by Gene Splicing in NMDA Receptors. Neuron. 2018;98(3):521-529.e3.

Reynolds IJ, Aizenman E. Pentamidine is an N-methyl-D-aspartate receptor antagonist and is neuroprotective in vitro. J Neurosci. 1992;12(3):970–5.

Richter A, Fredow G, Löscher W. Antidystonic effects of the NMDA receptor antagonists memantine, MK-801 and CGP 37849 in a mutant hamster model of paroxysmal dystonia. Neurosci Lett. 1991;133(1):57–60.

Roche KW, Standley S, McCallum J, Dune Ly C, Ehlers MD, Wenthold RJ. Molecular determinants of NMDA receptor internalization. Nat Neurosci. 2001;4(8):794–802.

Rock DM, Macdonald RL. Spermine and related polyamines produce a voltage-dependent reduction of N-methyl-D-aspartate receptor single-channel conductance. Mol Pharmacol. 1992;42:157.

Rondon ES, Vieira AS, Valadão CAA, Parada CA. The improvement of the anti-hyperalgesic effect of ketamine and of its isomers by the administration of ifenprodil. Eur J Pharmacol. 2010;647(1–3):84–9.

Rossi M, Chatron N, Labalme A, Ville D, Carneiro M, Edery P, et al. Novel homozygous missense variant of GRIN1 in two sibs with intellectual disability and autistic features without epilepsy. Eur J Hum Genet. 2017;25(3):376–80.

Rothman JS, Silver RA. Neuromatic: An integrated open-source software toolkit for acquisition, analysis and simulation of electrophysiological data. Front Neuroinform. 2018;12(April):1–21.

Rubio-Aliaga I, Wagner CA. Regulation and function of the SLC38A3/SNAT3 glutamine transporter. Vol. 10, Channels. Taylor and Francis Inc.; 2016. p. 440–52.

Sahley TL, Hammonds MD, Musiek FE. Endogenous dynorphins, glutamate and N-methyl-d-aspartate (NMDA) receptors may participate in a stress-mediated Type-I auditory neural exacerbation of tinnitus. Brain Res. 2013;1499:80–108.

Saint Paul LP, Creveuil C, Heinzlef O, De Seze J, Vermersch P, Castelnovo G, et al. Efficacy and safety profile of memantine in patients with cognitive impairment in multiple sclerosis: A randomized, placebo-controlled study. J Neurol Sci. 2016;363:69–76.

Sakhaee E, Ostadhadi S, Khan MI, Yousefi F, Norouzi-Javidan A, Akbarian R, et al. The role of NMDA receptor and nitric oxide/cyclic guanosine monophosphate pathway in the antidepressant-like effect of dextromethorphan in mice forced swimming test and tail suspension test. Biomed Pharmacother. 2017;85:627–34.

Sakimura K, Kutsuwada T, Ito I, Manabe T, Takayama C, Kushiya E, et al. Reduced hippocampal LTP and spatial learning in mice lacking NMDA receptor ε1 subunit. Vol. 373, Nature. 1995. p. 151–5.

Salat K, Siwek A, Starowicz G, Librowski T, Nowak G, Drabik U, et al. Antidepressant-like effects of ketamine, norketamine and dehydronorketamine in forced swim test: Role of activity at NMDA receptor. Neuropharmacology. 2015;99:301–7.

Salmi M, Del Gallo F, Minlebaev M, Zakharov A, Pauly V, Perron P, et al. Impaired vocal communication, sleep-related discharges, and transient alteration of slow-wave sleep in developing mice lacking the GluN2A subunit of N-methyl-d-aspartate receptors. Epilepsia. 2019;60(7):1424–37.

Sanacora G, Trecanni G, Popoli M. Towards a glutamate hypothesis of depression: An emerging frontier of neuropsychopharmacology for mood disorders. Neuropharmacology. 2012;62(1):63–77.

Sanacora G, Smith MA, Pathak S, Su HL, Boeijinga PH, McCarthy DJ, et al. Lanicemine: A low-trapping NMDA channel blocker produces sustained antidepressant efficacy with minimal psychotomimetic adverse effects. Mol Psychiatry. 2014;19(9):978–85.

Sandhu K V., Sherwin E, Schellekens H, Stanton C, Dinan TG, Cryan JF. Feeding the microbiota-gut-brain axis: diet, microbiome, and neuropsychiatry. Transl Res. 2017;179:223–44.

Sandusky-Beltran LA, Kovalenko A, Ma C, Calahatian JIT, Placides DS, Watler MD, et al. Spermidine/spermine-N 1-acetyltransferase ablation impacts tauopathy-induced polyamine stress response. Alzheimer's Res Ther. 2019;11(1):1–24.

Sans N, Prybylowski K, Petralia RS, Chang K, Wang YX, Racca C, et al. NMDA receptor trafficking through an interaction between PDZ proteins and the exocyst complex. Vol. 5, Nature Cell Biology. 2003. p. 520–30.

Sans N, Wang PY, Du Q, Petralia RS, Wang YX, Nakka S, et al. mPins modulates PSD-95 and SAP102 trafficking and influences NMDA receptor surface expression. Nat Cell Biol. 2005 Dec;7(12):1079–90.

Santos-Gómez A, Miguez-Cabello F, García-Recio A, Locubiche S, García-Díaz R, Soto V, et al. Disease-associated GRIN protein truncating variants trigger NMDA receptor loss-of-function. Hum Mol Genet. 2020 Oct 10.

Sanz-Clemente A, Matta JA, Isaac JTR, Roche KW. Casein Kinase 2 Regulates the NR2 Subunit Composition of Synaptic NMDA Receptors. Neuron. 2010;67(6):984–96.

Sceniak MP, Fedder KN, Wang Q, Droubi S, Babcock K, Patwardhan S, et al. An autism-associated mutation in GluN2B prevents NMDA receptor trafficking and interferes with dendrite growth. J Cell Sci. 2019;132(20):1–14.

Schäbitz W, Li F, Fisher M. Cerebral Gray and White Matter From Ischemic Injury. Stroke. 2000;31:1709–14.

Schade S, Paulus W. D-Cycloserine in Neuropsychiatric Diseases: A Systematic Review. Int J Neuropsychopharmacol. 2016;19(4):1–7.

Schmutz M, Portet C, Jeker A, Klebs K, Vassout A, Allgeier H, et al. The competitive NMDA receptor antagonists CGP 37849 and CGP 39551 are potent, orally-active anticonvulsants in rodents. Naunyn Schmiedebergs Arch Pharmacol. 1990;342(1):61–6.

Schüler T, Mesic I, Madry C, Bartholoma I, Laube B. Formation of NR1/NR2 and NR1/NR3 heterodimers constitutes the initial step in N-methyl-D-aspartate receptor assembly. J Biol Chem. 2008 Jan 4;283(1):37–46.

Schwartz TL, Sachdeva S, Stahl SM. Glutamate Neurocircuitry : Theoretical Underpinnings in Schizophrenia. Front Pharmacol. 2012;3.

Scott DB, Blanpied TA, Swanson GT, Zhang C, Ehlers MD. An NMDA receptor ER retention signal regulated by phosphorylation and alternative splicing. J Neurosci. 2001 May 1;21(9):3063–72.

Scott DB, Michailidis I, Mu Y, Logothetis D, Ehlers MD. Endocytosis and Degradative Sorting of NMDA Receptors by Conserved Membrane-Proximal Signals. J Neurosci. 2004;24(32):7096–109.

Segal JA, Skolnick P. Polyamine-like actions of aminoglycosides and aminoglycoside derivatives at NMDA receptors. Eur J Pharmacol. 1998;347(2–3):311–7.

Segal JA, Harris BD, Kustova Y, Basile A, Skolnick P. Aminoglycoside neurotoxicity involves NMDA receptor activation. Brain Res. 1999;815(2):270–7.

Seibenhener ML, Wooten MC. Use of the open field maze to measure locomotor and anxiety-like behavior in mice. J Vis Exp. 2015 Feb 6;(96):52434.

Sepers MD, Raymond LA. Mechanisms of synaptic dysfunction and excitotoxicity in Huntington's disease. Drug Discov Today. 2014;19(7):990–6.

Serraz B, Grand T, Paoletti P. Altered zinc sensitivity of NMDA receptors harboring clinically-relevant mutations. Neuropharmacology. 2016;109:196–204.

Setou M, Nakagawa T, Seog DH, Hirokawa N. Kinesin superfamily motor protein KIF17 and mLin-10 in NMDA receptor- containing vesicle transport. Science. 2000 Jun 9;288(5472):1796–802.

Sheng M, Hoogenraad CC. The Postsynaptic Architecture of Excitatory Synapses: A More Quantitative View. Annu Rev Biochem. 2007 Jun 7;76(1):823–47.

Shibasaki K, Hosoi N, Kaneko R, Tominaga M, Yamada K. Glycine release from astrocytes via functional reversal of GlyT1. J Neurochem. 2017 Feb 1;140(3):395–403.

Shin HJ, Na HS, Do SH. Magnesium and pain. Nutrients. 2020;12(8):1–13.

Shin W, Kim K, Serraz B, Cho YS, Kim D, Kang M, et al. Early correction of synaptic long-term depression improves abnormal anxiety-like behavior in adult GluN2B-C456Y-mutant mice. PLoS Biol. 2020;18(4):1–28.

Shohami E, Biegon A. Novel Approach to the Role of NMDA Receptors in Traumatic Brain Injury. CNS Neurol Disord - Drug Targets. 2014;13(4):567–73.

Singh L, Donald AE, Foster AC, Hutson PH, Iversen LL, Iversen SD, et al. Enantiomers of HA-966 (3-amino-1-hydroxypyrrolid-2-one) exhibit distinct central nervous system effects: (+)-HA-966 is a selective glycine/N-methyl-D-aspartate receptor antagonist, but (-)-HA-966 is a potent γ-butyrolactone-like sedative. Proc Natl Acad Sci U S A. 1990;87(1):347–51.

Sinitskiy A V., Stanley NH, Hackos DH, Hanson JE, Sellers BD, Pande VS. Computationally Discovered Potentiating Role of Glycans on NMDA Receptors. Sci Rep. 2017;7:1–10.

Sjöström PJ, Nelson SB. Spike timing, calcium signals and synaptic plasticity. Curr Opin Neurobiol. 2002;12(3):305–14.

Skrenkova K, Song J man, Kortus S, Kolcheva M, Netolicky J, Hemelikova K, et al. The pathogenic S688Y mutation in the ligand-binding domain of the GluN1 subunit regulates the properties of NMDA receptors. Sci Rep. 2020;10(1):1–15.

Schmidt SD, Myskiw JC, Furini CRG, Schmidt BE, Cavalcante LE, Izquierdo I. PACAP modulates the consolidation and extinction of the contextual fear conditioning through NMDA receptors. Neurobiol Learn Mem. 2015;118:120–4.

Schroeder S, Hofer SJ, Zimmermann A, Kiechl S, Eisenberg T, Madeo F, et al. Dietary spermidine improves cognitive function. Cell Rep. 2021;35(April 13).

Shao J, Meng L, Yang Z, Yu P, Song L, Gao Y, et al. Xenon produces rapid antidepressant- And anxiolytic-like effects in lipopolysaccharide-induced depression mice model. Neuroreport. 2020;387–93.

Shen YC, Liao DL, Chen JY, Wang YC, Lai IC, Liou YJ, et al. Exomic sequencing of the glutamate receptor, ionotropic, N-methyl-d-aspartate 3A gene (GRIN3A) reveals no association with schizophrenia. Schizophr Res. 2009;114(1–3):25–32.

Singh R, Kursan S, Almiahoub MY, Almutairi MM, Garzón-Muvdi T, Alvarez-Leefmans FJ, et al. Plasma membrane targeting of endogenous NKCC2 in COS7 cells bypasses functional golgi cisternae and complex N-glycosylation. Front Cell Dev Biol. 2017;4(JAN):1–17.

Smith DH, Okiyama K, Gennarelli TA, McIntosh TK. Magnesium and ketamine attenuate cognitive dysfunction following experimental brain injury. Neurosci Lett. 1993;157(2):211–4.

Smith DH, Perri BR, Raghupathi R, Saatman KE, McIntosh TK. Remacemide hydrochloride reduces cortical lesion volume following brain trauma in the rat. Neurosci Lett. 1997;231(3):135–8.

Soleimannejad E, Naghdi N, Semnanian S, Fathollahi Y, Kazemnejad A. Antinociceptive effect of intra-hippocampal CA1 and dentate gyrus injection of MK801 and AP5 in the formalin test in adult male rats. Eur J Pharmacol. 2007;562(1–2):39–46.

Sornarajah L, Cristina Vasuta O, Zhang L, Sutton C, Li B, El-Husseini A, et al. NMDA receptor desensitization regulated by direct binding to PDZ1-2 domains of PSD-95. J Neurophysiol. 2008;99(6):3052–62.

Soto D, Olivella M, Grau C, Armstrong J, Alcon C, Gasull X, et al. l-Serine dietary supplementation is associated with clinical improvement of loss-of-function GRIN2B-related pediatric encephalopathy. Sci Signal. 2019 Jun 18;12(586):eaaw0936.

Spalloni A, Nutini M, Longone P. Role of the N-methyl-d-aspartate receptors complex in amyotrophic lateral sclerosis. Biochim Biophys Acta - Mol Basis Dis. 2013;1832(2):312–22.

Sprengel R, Suchanek B, Amico C, Brusa R, Burnashev N, Rozov A, et al. Importance of the intracellular domain of NR2 subunits for NMDA receptor function in vivo. Cell. 1998;92(2):279–89.

Stahlmann R. Clinical toxicological aspects of fluoroquinolones. Toxicol Lett. 2002;127(1–3):269–77.

Standley S, Baudry M. The role of glycosylation in ionotropic glutamate receptor ligand binding, function, and trafficking. Vol. 57, Cellular and Molecular Life Sciences. Birkhauser Verlag Basel; 2000. p. 1508–16.

Standley S, Roche KW, McCallum J, Sans N, Wenthold RJ. PDZ domain suppression of an ER retention signal in NMDA receptor NR1 splice variants. Neuron. 2000;28(3):887–98.

Strehlow V, Heyne HO, Vlaskamp DRM, Marwick KFM, Rudolf G, De Bellescize J, et al. GRIN2A -related disorders: Genotype and functional consequence predict phenotype. Brain. 2018;142(1):80–92.

Su LD, Shen Y. Blockade of glutamate transporters facilitates cerebellar synaptic long-term depression. Neuroreport. 2009;20(5):502–7.

Sudhakar V, Richardson RM. Gene Therapy for Neurodegenerative Diseases. Neurotherapeutics. 2019;16(1):166–75.

Sun J, Xu J, Ling Y, Wang F, Gong T, Yang C, et al. Fecal microbiota transplantation alleviated Alzheimer's disease-like pathogenesis in APP/PS1 transgenic mice. Transl Psychiatry. 2019;9(1).

Sun MY, Linsenbardt AJ, Emnett CM, Eisenman LN, Izumi Y, Zorumski CF, et al. 24(S)-Hydroxycholesterol as a Modulator of Neuronal Signaling and Survival. Neuroscientist. 2016;22(2):132–44.

Suwandhi L, Hausmann S, Braun A, Gruber T, Heinzmann SS, Gálvez EJC, et al. Chronic D-serine supplementation impairs insulin secretion. Mol Metab. 2018;16(July):191–202.

Swanger SA, Chen W, Wells G, Burger PB, Tankovic A, Bhattacharya S, et al. Mechanistic Insight into NMDA Receptor Dysregulation by Rare Variants in the GluN2A and GluN2B Agonist Binding Domains. Am J Hum Genet. 2016;99(6):1261–80.

Sweatt JD. Long-term potentiation: A candidate cellular mechanism for information storage in the CNS. In: Learning and Memory: A Comprehensive Reference. 2007. p. 295–326.

Swerdlow NR, Bhakta SG, Talledo J, Kotz J, Roberts BZ, Clifford RE, et al. Memantine effects on auditory discrimination and training in schizophrenia patients. Neuropsychopharmacology. 2020;45(13):2180–8.

Szklarczyk A, Ewaleifoh O, Beique J, Wang Y, Knorr D, Haughey N, et al. MMP‑7 cleaves the NR1 NMDA receptor subunit and modifies NMDA receptor function. FASEB J. 2008;22(11):3757–67.

Takahashi H, Yokoi N, Seino S. Glutamate as intracellular and extracellular signals in pancreatic islet functions. Vol. 95, Proceedings of the Japan Academy Series B: Physical and Biological Sciences. Japan Academy; 2019. p. 246–60.

Takeuchi T, Kiyama Y, Nakamura K, Tsujita M, Matsuda I, Mori H, et al. Roles of the glutamate receptor ε2 and δ2 subunits in the potentiation and prepulse inhibition of the acoustic startle reflex. Eur J Neurosci. 2001;14(1):153–60.

Tang W, Liu D, Traynelis SF, Yuan H. Positive allosteric modulators that target NMDA receptors rectify loss-of-function GRIN variants associated with neurological and neuropsychiatric disorders. Neuropharmacology. 2020;177:108247.

Taniguchi S, Nakazawa T, Tanimura A, Kiyama Y, Tezuka T, Watabe AM, et al. Involvement of NMDAR2A tyrosine phosphorylation in depression-related behaviour. EMBO J. 2009;28(23):3717–29.

Taniguchi K, Shinjo K, Mizutani M, Shimada K, Ishikawa T, Menniti FS, et al. Antinociceptive activity of CP-101,606, an NMDA receptor NR2B subunit antagonist. Br J Pharmacol. 1997;122(5):809–12.

Tan-No K, Taira A, Wako K, Niijima F, Nakagawasai O, Tadano T, et al. Intrathecally administered spermine produces the scratching, biting and licking behaviour in mice. Pain. 2000;86(1–2):55–61.

Tao-Cheng JH, Crocker VT, Winters CA, Azzam R, Chludzinski J, Reese TS. Trafficking of AMPA receptors at plasma membranes of hippocampal neurons. J Neurosci. 2011 Mar 30;31(13):4834

Tarabeux J, Kebir O, Gauthier J, Hamdan FF, Xiong L, Piton A, et al. Rare mutations in N-methyl-D-aspartate glutamate receptors in autism spectrum disorders and schizophrenia. Transl Psychiatry. 2011 Nov 15;1(11):e55.

Tatlisumak T, Takano K, Meiler MR, Fisher M. A glycine site antagonist ZD9379 reduces number of spreading depressions and infarct size in rats with permanent middle cerebral artery occlusion. Stroke. 1998;29:190–5.

Tezuka T, Umemori H, Akiyama T, Nakanishi S, Yamamoto T. PSD-95 promotes Fyn-mediated tyrosine phosphorylation of the N-methyl-D-aspartate receptor subunit NR2A. Proc Natl Acad Sci U S A. 1999;96(2):435–40.

Thomas AG, Vornov JJ, Olkowski JL, Merion AT, Slusher BS. N-Acetylated alpha-linked acidic dipeptidase converts N-acetylaspartylglutamate from a neuroprotectant to a neurotoxin. J Pharmacol Exp Ther. 2000 Oct; 295(1):16-22.

Thomas CG, Miller AJ, Westbrook GL. Synaptic and extrasynaptic NMDA receptor NR2 subunits in cultured hippocampal neurons. J Neurophysiol. 2006;95(3):1727–34.

Thompson SM, Josey M, Holmes A, Brigman JL. Conditional loss of GluN2B in cortex and hippocampus impairs attentional set formation. Behav Neurosci. 2015;129(2):105–12.

Tingley WG, Ehlers MD, Kameyama K, Doherty C, Ptak JB, Riley CT, et al. Characterization of protein kinase A and protein kinase C phosphorylation of the N-methyl-D-aspartate receptor NR1 subunit using phosphorylation site-specific antibodies. J Biol Chem. 1997;272(8):5157–66.

Tomé D. The Roles of Dietary Glutamate in the Intestine. Ann Nutr Metab. 2018 Dec 1;73(Suppl. 5):15–20.

Traynelis SF, Wollmuth LP, McBain CJ, Menniti FS, Vance KM, Ogden KK, et al. Glutamate receptor ion channels: Structure, regulation, and function. Vol. 62, Pharmacological Reviews. 2010. p. 405–96.

Traynelis J, Silk M, Wang Q, Berkovic SF, Liu L, Ascher DB, et al. Optimizing genomic medicine in epilepsy through a gene-customized approach to missense variant interpretation. Genome Res. 2017;27(10):1715–29.

Truett GE, Heeger P, Mynatt RL, Truett AA, Walker JA, Warman ML. Preparation of PCR-quality mouse genomic dna with hot sodium hydroxide and tris (HotSHOT). Biotechniques. 2000;29(1):52–4.

Tsai G, Ralph-Williams RJ, Martina M, Bergeron R, Berger-Sweeney J, Dunham KS, et al. Gene knockout of glycine transporter 1: Characterization of the behavioral phenotype. Proc Natl Acad Sci U S A. 2004 Jun 1;101(22):8485–90.

Tsai G, Lane HY, Yang P, Chong MY, Lange N. Glycine transporter I inhibitor, N-Methylglycine (sarcosine), added to antipsychotics for the treatment of schizophrenia. Biol Psychiatry. 2004;55(5):452–6.

Tzang RF, Chang CH, Chang YC, Lane HY. Autism associated with anti-NMDAR encephalitis: Glutamate-related therapy. Front Psychiatry. 2019;10(JUN):4–9.

Umemori J, Takao K, Koshimizu H, Hattori S, Furuse T, Wakana S, et al. ENU-mutagenesis mice with a non-synonymous mutation in Grin1 exhibit abnormal anxiety-like behaviors, impaired fear memory, and decreased acoustic startle response. BMC Res Notes. 2013;6(1).

Vaccarino AL, Marek P, Kest B, Weber E, Keana JFW, Liebeskind JC. NMDA receptor antagonists, MK-801 and ACEA-1011, prevent the development of tonic pain following subcutaneous formalin. Brain Res. 1993;615(2):331–4.

Valbuena S, Lerma J. Kainate Receptors, Homeostatic Gatekeepers of Synaptic Plasticity. Neuroscience. Elsevier Ltd; 2020.

Vandenberg RJ, Mitrovic AD, Chebib M, Balcar VJ, Johnston GAR. Contrasting modes of action of methylglutamate derivatives on the excitatory amino acid transporters, EAAT1 and EAAT2. Mol Pharmacol. 1997;51(5):809–15.

Velloso NA, Dalmolin GD, Gomes GM, Rubin MA, Canas PM, Cunha RA, et al. Spermine improves recognition memory deficit in a rodent model of Huntington's disease. Neurobiol Learn Mem. 2009;92(4):574–80.

Vicini S, Wang JF, Li JH, Zhu WJ, Wang YH, Luo JH, et al. Functional and pharmacological differences between recombinant N- methyl-D-aspartate receptors. J Neurophysiol. 1998;79(2):555–66.

Vidlund M, Tajik B, Håkanson E, Friberg Ö, Holm J, Vanky F, et al. Post hoc analysis of the glutamics-trial: Intravenous glutamate infusion and use of inotropic drugs after cabg. BMC Anesthesiol. 2016;16(1):1–9.

Villemure E, Volgraf M, Jiang Y, Wu G, Ly CQ, Yuen PW, et al. GluN2A-selective pyridopyrimidinone series of nmdar positive allosteric modulators with an improved in vivo profile. ACS Med Chem Lett. 2016;8(1):84–9.

Vindigni SM, Surawicz CM. Fecal Microbiota Transplantation. Gastroenterol Clin North Am . 2017;46(1):171–85.

Vissel B, Krupp JJ, Heinemann SF, Westbrook GL. A use-dependent tyrosine dephosphorylation of NMDA receptors is independent of ion flux. Nat Neurosci. 2001;4(6):587–96.

Volgraf M, Sellers BD, Jiang Y, Wu G, Ly CQ, Villemure E, et al. Discovery of GluN2A-Selective NMDA Receptor Positive Allosteric Modulators (PAMs): Tuning Deactivation Kinetics via Structure-Based Design. J Med Chem. 2016;59(6):2760–79.

von Engelhardt J, Doganci B, Jensen V, Hvalby Ø, Göngrich C, Taylor A, et al. Contribution of Hippocampal and Extra-Hippocampal NR2B-Containing NMDA Receptors to Performance on Spatial Learning Tasks. Neuron. 2008;60(5):846–60.

von Stülpnagel C, Ensslen M, Møller RS, Pal DK, Masnada S, Veggiotti P, et al. Epilepsy in patients with GRIN2A alterations: Genetics, neurodevelopment, epileptic phenotype and response to anticonvulsive drugs. Eur J Paediatr Neurol. 2017;21(3):530–41.

Vorobjev VS, Sharonova IN, Walsh IB, Haas HL. Histamine potentiates N-methyl-d-aspartate responses in acutely isolated hippocampal neurons. Neuron. 1993;11(5):837–44.

Vyklicky V, Krausova B, Cerny J, Ladislav M. Surface Expression, Function, and Pharmacology of Disease-Associated Mutations in the Membrane Domain of the Human GluN2B Subunit. Front Mol Neurosci. 2018;11(110):1–20.

Wadiche JI, Amara SG, Kavanaugh MP. Ion fluxes associated with excitatory amino acid transport. Neuron. 1995;15(3):721–8.

Walia V, Garg C, Garg M. Amantadine exerts anxiolytic like effect in mice: Evidences for the involvement of nitrergic and GABAergic signaling pathways. Behav Brain Res. 2020;380:112432.

Wang J, Qiao Y, Yang RS, Zhang CK, Wu HH, Lin JJ, et al. The synergistic effect of treatment with triptolide and MK-801 in the rat neuropathic pain model. Mol Pain. 2017;13:1–14.

Wang R, Reddy PH. Role of Glutamate and NMDA Receptors in Alzheimer's Disease. J Alzheimer's Dis. 2017;57(4):1041–8.

Wang W, Wu Z, Dai Z, Yang Y, Wang J, Wu G. Glycine metabolism in animals and humans: Implications for nutrition and health. Amino Acids. 2013;45(3):463–77.

Warikoo N, Brunwasser SJ, Benz A, Shu HJ, Paul SM, Lewis M, et al. Positive allosteric modulation as a potential therapeutic strategy in anti-NMDA receptor encephalitis. J Neurosci. 2018;38(13):3218–29.

Wells G, Yuan H, McDaniel MJ, Kusumoto H, Snyder JP, Liotta DC, et al. The GluN2B-Glu413Gly NMDA receptor variant arising from a de novo GRIN2B mutation promotes ligand-unbinding and domain opening. Proteins Struct Funct Bioinforma. 2018;86(12):1265–76.

Williams K. Interactions of polyamines with ion channels. Biochem J. 1997;325:289–97.

Wirth A, Wolf B, Huang CK, Glage S, Hofer SJ, Bankstahl M, et al. Novel aspects of age-protection by spermidine supplementation are associated with preserved telomere length. GeroScience. 2021;43(2):673–90.

Wirth M, Benson G, Schwarz C, Köbe T, Grittner U, Schmitz D, et al. The effect of spermidine on memory performance in older adults at risk for dementia: A randomized controlled trial. Cortex. 2018;109:181–8.

Wlaź P, Poleszak E. Differential effects of glycine on the anticonvulsant activity of D-cycloserine and L-701,324 in mice. Pharmacol Reports. 2011;63(5):1231–4.

Wolosker H, Dumin E, Balan L, Foltyn VN. D-Amino acids in the brain : D-serine in neurotransmission and neurodegeneration. FEBS J. 2008;275:3514–26.

Wood PL, Mahmood SA, Moskal JR. Antinociceptive action of GLYX-13: An N-methyl-D-aspartate receptor glycine site partial agonist. Neuroreport. 2008;19(10):1061–3.

Wu F, Pan R, Chen J, Sugita M, Chen C, Tao Y, et al. Lentivirus Mediated siRNA against GluN2B Subunit of NMDA Receptor Reduces Nociception in a Rat Model of Neuropathic Pain. Biomed Res Int. 2014;2014.

Wu J, Zou H, Strong JA, Yu J, Zhou X, Xie Q, et al. Bimodal effects of MK-801 on locomotion and stereotypy in C57BL/6 mice. Psychopharmacology (Berl). 2005;177(3):256–63.

Wu SY, Dun NJ. Potentiation of NMDA currents by pituitary adenylate cyclase activating polypeptide in neonatal rat sympathetic preganglionic neurons. J Neurophysiol. 1997;78(2):1175–9.

Yang M, Leonard JP. Identification of mouse NMDA receptor subunit NR2A C-terminal tyrosine sites phosphorylated by coexpression with v-Src. J Neurochem. 2001;77(2):580–8.

Yang X, Qian P, Xu X, Liu X, Wu X, Zhang Y, et al. GRIN2A mutations in epilepsy-aphasia spectrum disorders. Brain Dev. 2018;40(3):205–10.

Yang J, Wetterstrand C, Jones RSG. Felbamate but not phenytoin or gabapentin reduces glutamate release by blocking presynaptic NMDA receptors in the entorhinal cortex. Epilepsy Res. 2007;77(2–3):157–64.

Yano S, Tokumitsu H, Soderling TR. Calcium promotes cell survival through CaM-K kinase activation of the protein-kinase-B pathway. Nature. 1998 Dec 10;396(6711):584–7.

Yao Y, Ju P, Liu H, Wu X, Niu Z, Zhu Y, et al. Ifenprodil rapidly ameliorates depressive-like behaviors, activates mTOR signaling and modulates proinflammatory cytokines in the hippocampus of CUMS rats. Psychopharmacology (Berl). 2020;237(5):1421–33.

Yi F, Traynelis SF, Hansen KB. Selective cell-surface expression of triheteromeric NMDA receptors. Methods Mol Biol. 2017;1677:145–62.

Yick LW, Tang CH, Ma OKF, Kwan JSC, Chan KH. Memantine ameliorates motor impairments and pathologies in a mouse model of neuromyelitis optica spectrum disorders. J Neuroinflammation. 2020;17(1):1–16.

Yokoyama R, Higuchi M, Tanabe W, Tsukada S, Naito M, Yamaguchi T, et al. (S)-norketamine and (2S,6S)-hydroxynorketamine exert potent antidepressant-like effects in a chronic corticosterone-induced mouse model of depression. Pharmacol Biochem Behav. 2020;191:172876.

Yong XLH, Zhang L, Yang L, Chen X, Yu X, et al. Regulation of NMDA receptor trafficking and gating by activity-dependent CaMKIIα phosphorylation of the GluN2A subunit. bioRxiv 2021.

Yuan H, Hansen KB, Zhang J, Pierson TM, Markello TC, Fuentes-Fajardo K V., et al. Functional Analysis of a De Novo GRIN2A Missense Mutation Associated with Early-onset Epileptic Encephalopathy Hongjie. Nat Commun. 2014;5:3251.

Uno Y, Coyle JT. Glutamate hypothesis in schizophrenia. Psychiatry Clin Neurosci. 2019;73(5):204–15.

Xiangwei W, Jiang Y, Yuan H. De Novo Mutations and Rare Variants Occurring in NMDA Receptors. Curr Opin Physiol. 2018;2:27–35.

XiangWei W, Kannan V, Xu Y, Kosobucki GJ, Schulien AJ, Kusumoto H, et al. Heterogeneous clinical and functional features of GRIN2D-related developmental and epileptic encephalopathy. Brain. 2019;142(10):3009–27.

Xu XX, Liu XR, Fan CY, Lai JX, Shi YW, Yang W, et al. Functional Investigation of a GRIN2A Variant Associated with Rolandic Epilepsy. Neurosci Bull. 2018;34(2):237–46.

Xu X-X, Jian-hong L. Mutations of N -Methyl-D-Aspartate Receptor Subunits in Epilepsy. Neurosci Bull. 2018;34(3):549–65.

Yamada N, Sudo M, Okado H, Iino M, Tsuzuki K, Miwa A, et al. Expression of recombinant NMDA receptors in hippocampal neurons by adenoviral-mediated gene transfer. Mol Brain Res. 1999;68(1–2):169–80.

Yamamoto S, Tomoe M, Toyama K, Kawai M, Uneyama H. Can dietary supplementation of monosodium glutamate improve the health of the elderly? Am J Clin Nutr. 2009;90(3):844–9.

Yang B, Ren Q, Ma M, Chen QX, Hashimoto K. Antidepressant effects of (+)-MK-801 and (-)-MK-801 in the social defeat stress model. Int J Neuropsychopharmacol. 2016;19(12):1–5.

Yourick DL, Repasi RT, Rittase WB, Staten LD, Meyerhoff JL. Ifenprodil and arcaine alter amygdala-kindling development. Eur J Pharmacol. 1999;371(2–3):147–52.

Yourick DL, Koenig ML, Durden A V., Long JB. N-acetylaspartylglutamate and β-NAAG protect against injury induced by NMDA and hypoxia in primary spinal cord cultures. Brain Res. 2003;991(1–2):56–64.

Yu A, Lau AY. Glutamate and glycine binding to the NMDA receptor. Structure. 2018;26(7):1035–43.

Xu Y, Song R, Chen W, Strong K, Shrey D, Gedela S, et al. Recurrent seizure-related GRIN1 variant: Molecular mechanism and targeted therapy. Ann Clin Transl Neurol. 2021;8(7):1480–94.

Yu Y, Lin Y, Takasaki Y, Wang C, Kimura H, Xing J, et al. Rare loss of function mutations in N-methyl-d-aspartate glutamate receptors and their contributions to schizophrenia susceptibility. Transl Psychiatry. 2018;8(1).

Yuan H, Hansen KB, Vance KM, Ogden KK, Traynelis SF. Control of NMDA receptor function by the NR2 subunit amino-terminal domain. J Neurosci. 2009 Sep 30;29(39):12045–58.

Yuan H, Vance KM, Junge CE, Geballe MT, Snyder JP, Hepler JR, et al. The serine protease plasmin cleaves the amino-terminal domain of the NR2A subunit to relieve zinc inhibition of the N-methyl-D-aspartate receptors. J Biol Chem. 2009;284(19):12862–73.

Zai H, Kusano M, Hosaka H, Shimoyama Y, Nagoshi A, Maeda M. Monosodium L -glutamate added to a high-energy , high-protein liquid diet promotes gastric emptying. Am J Clin Nutr. 2009;89(3):431–5.

Zareifopoulos N, Panayiotakopoulos G. Neuropsychiatric Effects of Antimicrobial Agents. Clin Drug Investig. 2017;37(5):423–37.

Zbili M, Rama S, Debanne D. Dynamic control of neurotransmitter release by presynaptic potential. Front Cell Neurosci. 2016;10(DEC2016):1–6.

Zehavi Y, Mandel H, Zehavi A, Rashid MA, Straussberg R, Jabur B, et al. De novo GRIN1 mutations: An emerging cause of severe early infantile encephalopathy. Eur J Med Genet. 2017;60(6):317–20.

Zhang E, Kim JJ, Shin N, Yin Y, Nan Y, Xu Y, et al. High Omega-3 Polyunsaturated Fatty Acids in fat-1 Mice Reduce Inflammatory Pain. J Med Food. 2017;20(6):535–41.

Zhang RX, Yan X Bin, Gu YH, Huang D, Gan L, Han R, et al. Gene silencing of NR2B-containing NMDA receptor by intrathecal injection of short hairpin RNA reduces formalin-induced nociception in C57BL/6 mouse. Int J Neurosci. 2013;123(9):650–6.

Zhang SJ, Steijaert MN, Lau D, Schütz G, Delucinge-Vivier C, Descombes P, et al. Decoding NMDA Receptor Signaling: Identification of Genomic Programs Specifying Neuronal Survival and Death. Neuron. 2007;53(4):549–62.

Zhang W, Shi CX, Gu XP, Ma ZL, Zhu W. Ifenprodil induced antinociception and decreased the expression of nr2b subunits in the dorsal horn after chronic dorsal root ganglia compression in rats. Anesth Analg. 2009;108(3):1015–20.

Zhang XL, Sullivan JA, Moskal JR, Stanton PK. A NMDA receptor glycine site partial agonist, GLYX-13, that simultaneously enhances LTP and reduces LTD at Schaffer collateral-CA1 synapses in hippocampus. Neuropharmacology. 2008;55(7):1238–50.

Zheng C, Qiao ZH, Hou MZ, Liu NN, Fu B, Ding R, et al. GLYX-13, a NMDA receptor glycine-site functional partial agonist, attenuates cerebral ischemia injury in vivo and vitro by differential modulations of NMDA receptors subunit components at different post-ischemia stage in mice. Front Aging Neurosci. 2017;9(JUN):1–12.

Zhou Y, Danbolt NC. Glutamate as a neurotransmitter in the healthy brain. Vol. 121, Journal of Neural Transmission. 2014. p. 799–817.

Zorumski CF, Nagele P, Mennerick S, Conway CR. Treatment-resistant major depression: Rationale for NMDA receptors as targets and nitrous oxide as therapy. Front Psychiatry. 2015;6(DEC):1–14.

Zuccarello M, Lewis AI, Upputuri S, Farmer JB, Anderson DK. Effect of Remacemide Hydrochloride on Subarachnoid Hemorrhage-Induced Vasospasm in Rabbits. J Neurotrauma. 1994;11(6):691–8.

Zwart R, Blank T, Spiess J. Histamine slows the onset of desensitization of rat cortical NMDA receptors. Neuroreport. 1996;7(13):2206–10.

Databases

Pubchem database: Chemical information of distinct compounds

https://pubchem.ncbi.nlm.nih.gov

GnomAD: Exome and genome sequencing data

https://gnomad.broadinstitute.org

ClinVar: Information about genomic variation and its association with health or disease

https://www.ncbi.nlm.nih.gov/clinvar/

Grindb: Database developed by Olivella M. and colleagues (García-Recio A. et al., 2020), compiling information from distinct databases, about reported GRIN variants, the presence or the absence of pathogenicity and associated symptomatology

https://alf06.uab.es/grindb/home

CFERV: Information about distinct *GRIN* variants and pharmacological evaluation conducted by Traynelis SF. and colleagues via electrophysiology in oocytes

http://functionalvariants.emory.edu/database/

GRIN Leipzig: Information about distinct *GRIN* variants and the presence/absence of epilepsy, reunited by Lemke JR. and colleagues

http://grin-database.de/gen_table

Clinicaltrials: Information about registered clinical trials

https://clinicaltrials.gov/ct2/home

Annex
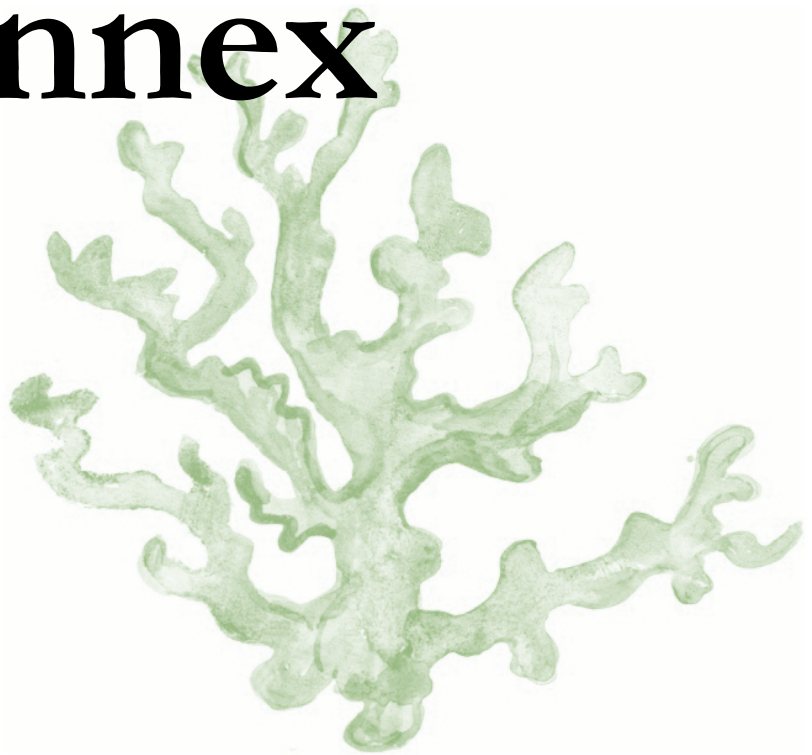
1.

Journal Publications

NEURODEVELOPMENT

L-Serine dietary supplementation is associated with clinical improvement of loss-of-function *GRIN2B*-related pediatric encephalopathy

David Soto[1,2,3]*, Mireia Olivella[4]*, Cristina Grau[5]*, Judith Armstrong[6], Clara Alcon[1,7],
Xavier Gasull[1,2,3], Ana Santos-Gómez[5], Sílvia Locubiche[5], Macarena Gómez de Salazar[5],
Roberto García-Díaz[1,2,3,8], Esther Gratacòs-Batlle[1,2,3], David Ramos-Vicente[9,10],
Emeline Chu-Van[11], Benoit Colsch[11], Víctor Fernández-Dueñas[5], Francisco Ciruela[5], Àlex Bayés[9,10],
Carlos Sindreu[1,7], Anna López-Sala[12], Àngels García-Cazorla[6,12]†, Xavier Altafaj[5]†

Autosomal dominant mutations in *GRIN2B* are associated with severe encephalopathy, but little is known about the pathophysiological outcomes and any potential therapeutic interventions. Genetic studies have described the association between de novo mutations of genes encoding the subunits of the *N*-methyl-D-aspartate receptor (NMDAR) and severe neurological conditions. Here, we evaluated a missense mutation in *GRIN2B*, causing a proline-to-threonine switch (P553T) in the GluN2B subunit of NMDAR, which was found in a 5-year-old patient with Rett-like syndrome with severe encephalopathy. Structural molecular modeling predicted a reduced pore size of the mutant GluN2B-containing NMDARs. Electrophysiological recordings in a HEK-293T cell line expressing the mutated subunit confirmed this prediction and showed an associated reduced glutamate affinity. Moreover, GluN2B(P553T)-expressing primary murine hippocampal neurons showed decreased spine density, concomitant with reduced NMDA-evoked currents and impaired NMDAR-dependent insertion of the AMPA receptor subunit GluA1 at stimulated synapses. Furthermore, the naturally occurring coagonist D-serine restored function to GluN2B(P553T)-containing NMDARs. L-Serine dietary supplementation of the patient was hence initiated, resulting in the increased abundance of D-serine in the plasma and brain. The patient has shown notable improvements in motor and cognitive performance and communication after 11 and 17 months of L-serine dietary supplementation. Our data suggest that L-serine supplementation might ameliorate *GRIN2B*-related severe encephalopathy and other neurological conditions caused by glutamatergic signaling deficiency.

INTRODUCTION

Rett syndrome (RTT; Online Mendelian Inheritance in Man, OMIM: 312750) is a neurodevelopmental disorder affecting 1 in 10,000 live female births (*1, 2*). Clinical manifestations include microcephaly, loss of achieved psychomotor abilities, intellectual disability (ID), and autistic behaviors (*3*). Whereas most cases of typical RTT harbor loss-of-function mutations in the X-linked gene encoding methyl-CpG–binding protein 2 (*MECP2*) (*4*), mutations in genes encoding cyclin-dependent kinase–like 5 (*CDKL5*) and Forkhead box G1 (*FOXG1*) have also been identified (*5*). Rett-like syndrome mostly affects patients exhibiting symptoms that are similar to those seen in patients with RTT; however, the genetic

and molecular etiologies of this rare disease are different from those associated with RTT.

A growing number of genetic and functional studies are unraveling the complex scenario and molecular players involved in neurodevelopmental disorders and, in particular, in Rett-like syndrome. It has been shown that the dysregulation of synaptic proteins can lead to neurodevelopmental disorder (*6–8*). Genes encoding for the *N*-methyl-D-aspartate receptor (NMDAR) could play critical roles in the dysfunction of glutamatergic transmission associated with RTT. Functionally, NMDARs play critical roles in neurogenesis, synaptogenesis, and synaptic plasticity processes. Early in development, NMDAR subunit GluN2B expression is particularly high (*9*). Accordingly, it has been proposed that *GRIN2B* gene disturbance might markedly compromise critical steps of neuronal, synaptic, and brain circuitry development (*10*). Moreover, discrete de novo mutations of *GRIN2B* gene have been associated with neurodevelopmental disorders (*11–13*) such as early infantile epileptic encephalopathy-27 (EIEE27; OMIM: 616139) (*14*) and autosomal dominant mental retardation (MRD6; OMIM: 613970) (*15–17*).

In this study, we investigated the effects of a de novo missense mutation in the *GRIN2B* gene in a patient with Rett-like syndrome and severe encephalopathy. Functional studies showed that channel gating is altered in mutant NMDARs markedly reducing NMDAR-mediated currents. Dietary supplementation with L-serine—the precursor of D-serine, an endogenous NMDAR coagonist (*18, 19*)—during 17 months was associated with ameliorated intellectual, communication, and motor deficits in the patient. These results support the pathogenicity of *GRIN2B* mutation and suggest that enhancing NMDAR

[1]Institute of Neurosciences, University of Barcelona, Barcelona 08036, Spain. [2]Department of Biomedicine, University of Barcelona, Barcelona 08036, Spain. [3]August Pi i Sunyer Biomedical Research Institute (IDIBAPS), Barcelona 08036, Spain. [4]Bioinformatics and Medical Statistics Group, University of Vic–Central University of Catalonia, Vic 08500, Spain. [5]Bellvitge Biomedical Research Institute (IDIBELL)–Unit of Neuropharmacology and Pain, University of Barcelona, Barcelona 08908, Spain. [6]Genetics and Molecular Medicine Service, Hospital Sant Joan de Déu and CIBERER, Barcelona 08950, Spain. [7]Department of Clinical Foundations, University of Barcelona, Barcelona 08036, Spain. [8]Grupo de Investigación en Química y Biotecnología (QUIBIO), Universidad de Santiago de Cali, Santiago de Cali 760035, Colombia. [9]Molecular Physiology of the Synapse Laboratory, Biomedical Research Institute Sant Pau (IIB Sant Pau), Barcelona 08026, Spain. [10]Autonomous University of Barcelona, Bellaterra 08193, Spain. [11]Service de Pharmacologie et d'Immunoanalyse (SPI), Laboratoire d'Etude du Métabolisme des Médicaments, CEA, INRA, Université Paris Saclay, MetaboHUB, F-91191 Gif-sur-Yvette, France. [12]Department of Neurology, Neurometabolic Unit, Hospital Sant Joan de Déu and CIBERER, Barcelona 08950, Spain.
*These authors contributed equally to this work.
†Corresponding author. Email: xaltafaj@idibell.cat (X.A.); agarcia@sjdhospitalbarcelona.org (À.G.-C.).

activity using L-serine dietary supplementation can have therapeutic benefits in certain neurodevelopmental disorders associated with NMDAR hypofunctionality.

RESULTS

Patient clinical symptomatology and genetic studies

The patient was a girl born after an uneventful pregnancy and with no family history of neurodevelopmental disorders. She was referred to our clinic at 1 year old, and the primary clinical examination showed a psychomotor delay with severe hypotonia (with the presence of osteotendinous reflexes and devoid of pyramidal signs) and an inability to hold up her head and to sit upright. Behaviorally, she had an overall "absence," as manifested by a poor visual contact, an impairment in social interaction, and no interest in the environment. Along with these alterations, the patient showed high irritability with sleep disturbances. Considering these symptoms, together with the presence of "hand-washing" stereotypies, the girl was tentatively diagnosed with RTT rather than Rett-like phenotype. Cytogenetic analysis, brain magnetic resonance imaging, and neurometabolic analysis did not show abnormalities. At 2.5 years old, she was less irritable and had developed the capacity to hold up her head. Behaviorally, she had slightly improved social interaction, and 1 year later, her sleeping pattern was ameliorated. At that age (3.5 years old), an electroencephalogram (EEG) indicated the presence of epileptiform alterations of brain activity, she was treated with valproic acid, and later, the treatment was changed to levetiracetam to prevent changes in irritability. At 5 years and 10 months old, the patient's adaptive behavior was assessed by the Vineland test, with scores indicative of a mental age below 1 year old (Fig. 5C).

As noted, the patient was tentatively diagnosed with RTT-like phenotype. Because no mutations of RTT candidate genes (*MECP2*, *CDKL5*, and *FOXG1*) were detected, whole-exome sequencing was performed (*20*). After genetic data filtering against parental variants and then against a pool of controls, we identified a de novo heterozygous missense mutation in *GRIN2B* gene coding for the GluN2B subunit of NMDARs, resulting in an amino acid substitution of a proline (Pro) residue by a threonine (Thr) at GluN2B subunit residue 553 (Fig. 1A).
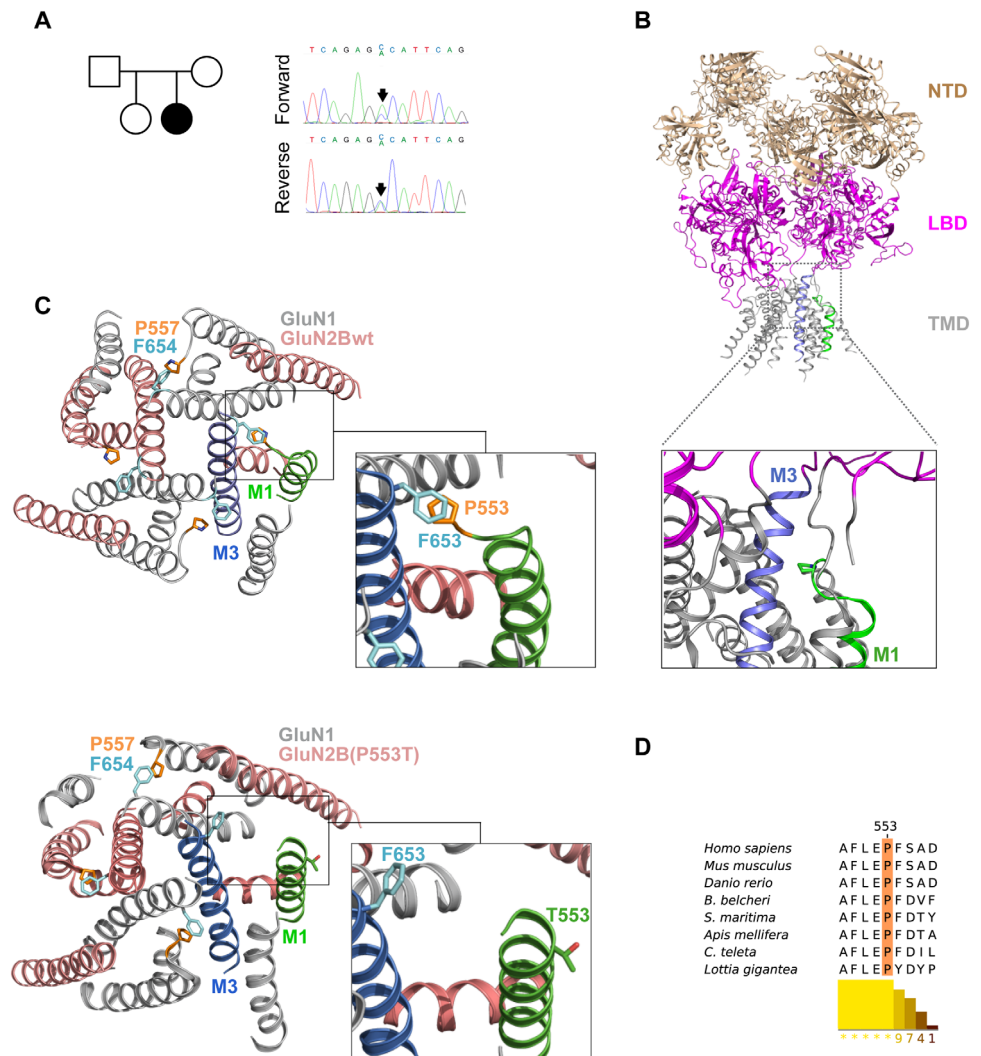
Fig. 1. Identification of GRIN2B(P553T) mutation associated with the case study and predicted structural consequences. (**A**) Left: Familial pedigree of the GRIN2B(P553T) case study. Right: Chromatograms of *GRIN2B* (c.1657C > A) mutated nucleotide (indicated by an arrow) using forward and reverse oligonucleotides. (**B**) Structure of heterotetrameric (GluN1)$_2$-(GluN2B)$_2$ NMDAR [Protein Data Bank (PDB) ID: 4PE5], according to Karakas and Furukawa (*61*), showing the N-terminal domain (NTD), the ligand-binding domain (LBD), and the transmembrane domain (TMD; containing the mutated amino acid P553T). Bottom: Magnification of the transmembrane domain, showing the topological position of Pro^{553} residue at the beginning of the M1 (P553; green) of the transmembrane domain, facing Phe^{653} residue (F653; light blue) at M3 (blue). (**C**) Top: Transmembrane domain structural molecular model of wild-type (GluN1)$_2$-(GluN2B)$_2$ receptor (from the extracellular domain). Inset: Magnification of residues Pro553(M1)-F653(M3) proximity. Bottom: Transmembrane domain structural molecular model of mutant (GluN1)$_2$-[GluN2B(P553T)]$_2$ receptor (from the extracellular domain). Inset: Magnification of residues Pro553(M1)-F653(M3) distance. (**D**) GluN2B protein sequence alignment around residue Pro^{553}. Representative sequences from a larger alignment containing 147 proteins from 12 metazoan species spanning seven phyla are shown. Displayed protein sequences are from the following species: *Homo sapiens* GluN2B (UniProt ref. Q13224), *Mus musculus* GluN2B (UniProt ref. Q01097), *Danio rerio* GluN2Bb (Ensembl ref. ENSDARG00000030376), *Branchiostoma belcheri* 254360R.t1 (from the database B.belcheri_v18h27.r3_ref_protein included in LanceletDB Genome browser; Sun Yat-sen University), *Saccoglossus kowalevskii* Sakowv30010297m (Metazome database), and *Strigamia maritima* SmarNMDAR2b, *Apis melifera* GB48097, *Capitela teleta* CapteT179505, and *Lottia gigantea* LotgiT137890 (all from Ensembl Metazoa).

Molecular modeling of mutant (GluN1)$_2$-[GluN2B(P553T)]$_2$ receptor

To identify the structural changes induced by GluN2B(P553T) mutation, molecular models of wild-type and mutant receptors were

generated by homology modeling (using crystal structures of NMDAR at closed state) and molecular dynamics simulation. The Pro[553] residue in GluN2B is located at the beginning of the transmembrane helix 1 (M1; Fig. 1B). This model suggested a role for Pro[553] in breaking M1 and bending it toward M3 (Fig. 1C, top), thereby enabling the interaction of Pro[553] with Phe[653] (M3) of the GluN2B subunits. In addition, according to this model, the residue Pro[557] (M1) is also bending M1 to M3 through its Pro kink, allowing the interaction with Phe[654] (M3) of the GluN1 subunit. This model predicted that the P553T mutation would prevent M1 bending, disrupting M1-M3 interaction (Fig. 1C, bottom), which in turn would bring M3 closer to the center of the pore and consequently induce a more closed channel conformation, altering the gating properties of the mutant receptor.

On the basis of this structural model, we investigated the evolutionary conservation of the GluN2B Pro[553] residue and its predicted interacting residue Phe[653]. We found that the Pro[553] motif was highly conserved across species (Fig. 1D). The GluN2B Phe[653] and GluN1 Phe[654] residues are within the SYTANLAAF motif (fig. S4), the most highly conserved motif among mammalian ionotropic glutamate receptors (iGluRs) (21, 22). Multiple sequence alignments of 147 metazoan iGluRs showed a high conservation of these residues (the Pro[553] and Phe[653] residues were detected in 144 and 131 iGluR protein–encoding gene sequences, respectively; fig. S4), supporting a potentially critical role of the Pro[553] residue in GluN2B in NMDAR channel activity.

Heteromerization and trafficking of GluN1-GluN2B(P553T) receptors

To assess the effects of GluN2B(P553T) on the oligomerization and trafficking of NMDARs, we cotransfected human embryonic kidney (HEK) 293T cells with GluN1 and hemagglutinin (HA)–tagged GluN2A, together with either green fluorescent protein (GFP)–tagged wild-type GluN2B (GFP-GluN2Bwt) or the P553T mutant [GFP-GluN2B(P553T)]. Biochemical analysis showed that the protein abundance of GluN2B(P553T) was similar to that of GluN2Bwt in these cells (fig. S1A). Further, coimmunoprecipitation experiments showed the presence of GluN1 and HA-GluN2A subunits in anti-GFP pulldown complexes, indicating that the mutant GluN2B(P553T) subunit interacted—in similar abundance as GluN2Bwt—with GluN1 and/or GluN2A subunits (fig. S1B). Immunofluorescence analysis showed that the missense mutation on Pro[553] does not abolish the trafficking of GluN1-GluN2B(P553T) to the surface of COS-7–transfected cells (fig. S1C), as previously reported for another GRIN2B missense variant affecting the same amino acid position, GluN2B(P553L) (23). In primary cortical murine neurons, the dendritic surface: intracellular abundance ratio of transfected GluN2B(P553T) was normal at days in vitro 7 (DIV7) and DIV11, with a slight decrease in DIV16 (fig. S1D).

Biophysical assessment of GluN2B(P553T) subunit–containing NMDARs

We performed patch-clamp experiments to evaluate the biophysical properties of GluN2B(P553T)-containing NMDARs in transfected HEK-293T cells. After a fast glutamate (1 mM) and glycine (50 µM) application, NMDAR-mediated current amplitudes were significantly reduced in HEK-293T cells expressing GluN1-GluN2B(P553T) receptors Fig. 2, A to C), whereas voltage-dependent channel blockade by extracellular Mg^{2+} was spared (Fig. 2, D to F). Because the P553T mutation is located in the vicinity of the agonist binding site and the chan-

nel pore in GluN2B, we explored the possible effects of the mutation on channel kinetics. Electrophysiological recordings showed a significantly faster deactivation rate in mutant receptors (Fig. 2, G and H) and a faster desensitization thereof, quantified upon 5-s duration jumps (Fig. 2, I and J). Moreover, in agreement with aforementioned modeling predictions, nonstationary fluctuation analysis (NSFA) (24) showed a reduction of the single-channel conductance in mutant receptors (Fig. 2, K to M) and a reduced open probability (Fig. 2N). Together with the biochemical data indicating normal expression and oligomerization, we concluded that GluN1-GluN2B(P553T) receptors are intrinsically hypofunctional.

Because GluN2B subunits can assemble into both (GluN1)$_2$-(GluN2B)$_2$ heterodimers and (GluN1)$_2$-GluN2A-GluN2B heterotrimers (25), we explored whether the GluN2B(P553T) mutation may also impair heterotrimeric receptors in HEK-293T cells (26). NMDA current amplitudes were not significantly reduced in GluN2B(P553T)-containing heterotrimers, although their deactivation and desensitization rates were increased similar to those of GluN1-GluN2B(P553T) heterodimers (fig. S2, A and B). However, administration of 100 µM D-serine potentiated GluN1-GluN2A-GluN2B(P553T) heterotrimers more strongly than wild-type heterotrimers (fig. S2, A to C). Likewise, the desensitization and deactivation kinetics of triheteromeric mutants were increased compared with controls (fig. S2, D to H), recapitulating some of the effects observed in the mutant (GluN1)$_2$-[GluN2B(P553T)]$_2$ diheterodimers.

Evaluation of D-serine effect in GluN1-GluN2B(P553T) receptors

Next, we sought to enhance the activity of mutant NMDARs using D-serine, an endogenous NMDAR coagonist. In agreement with a previous report (19), D-serine administration dose-dependently increased NMDAR-mediated currents in HEK-293T cells (Fig. 3, A and B). The relative increase mediated by D-serine was stronger in HEK-293T cells expressing GluN1-GluN2B(P553T) than in cells expressing GluN1-GluN2Bwt (Fig. 3, A and B). Although not reaching GluN1-GluN2Bwt–mediated current density, hypofunctional GluN1-GluN2B(P553T) receptor–mediated currents were significantly increased in D-serine coapplication (Fig. 3C). Further, a similar increase was observed in the presence of a high dose of glycine (100 µM), as well as with a stronger potentiation in GluN1-GluN2B(P553T)–expressing cells compared with GluN1-GluN2Bwt–expressing HEK-293T cells (Fig. 3, D to E). The differential potency of D-serine and glycine might result from a reduced affinity for GluN1-GluN2B(P553T), leading to the enhanced potentiation and faster deactivation/desensitization rates at higher concentrations. Alternatively, because glutamate binding increases the dissociation rate of glycine/D-serine coagonist with NMDARs (27), these changes in D-serine potency might be explained by altered glutamate affinity. Concentration-response experiments showed no changes in D-serine median effective concentration (EC$_{50}$; Fig. 3F), whereas glutamate EC$_{50}$ increased by sevenfold in GluN1-GluN2B(P553T) receptors (Fig. 3G).

Evaluation of GluN2B(P553T) variant neuronal outcomes

To evaluate the neuronal impact of GluN2B(P553T), we overexpressed GluN2B(P553T) in primary hippocampal neurons and measured morphological parameters, synaptic plasticity processes, and NMDAR-mediated synaptic currents. Sholl analysis of dendrites labeled with GFP-GluN2B(P553T) or GFP-GluN2Bwt indicated similar distributions of the subunit across the dendritic arbor (Fig. 4A).

Fig. 2. Biophysical characterization of (GluN1)₂-(GluN2B(P533T))₂channel properties. (**A**) Representative whole-cell currents evoked by rapid application of 1 mM glutamate + 50 μM glycine (0.5-s duration; −60 mV) in HEK-293T cells expressing GluN1-GluN2B (black trace) or GluN1-GluN2B(P533T) (red trace) receptors. n = 19 and 21 cells from six and five experiments, respectively. (**B**) Average of raw peak currents from HEK-293T cells expressing GluN2B and GluN2B(P533T). n = 19 and 21 cells from six and five experiments, respectively. ***P < 0.001 by Mann-Whitney U test. (**C**) Normalized peak currents (in pA/pF) in HEK-293T cells expressing GluN1-GluN2B and GluN1-GluN2B(P533T), with values from a representative experiment superimposed. Data are from six and five experiments, respectively. ****P < 0.0001 by Mann-Whitney U test. (**D**) Traces recorded at −60 mV in an HEK-293T cell expressing GluN1-GluN2B(P533T) with Mg²⁺ block of the NMDAR. Data are representative of five and seven cells from three independent cultures. (**E**) Percentage of current blocked at −60 mV by Mg²⁺ (1 mM) for GluN2Bwt- and GluN2B(P533T)-containing NMDARs. Single-value experiments are denoted as open circles for each condition. n = 5 and 7 cells, respectively, from three independent experiments per condition. n.s. (not significant) by Mann-Whitney U test. wt, wild-type. (**F**) Current-voltage relationship for GluN2B- and GluN2B(P533T)-containing NMDARs. n = 3 and 4, respectively, from two independent experiments. (**G**) Representative peak-scaled responses to 1 mM glutamate + 50 μM glycine (0.5-s agonists application; −60 mV) for GluN1-GluN2B (black trace) and GluN1-GluN2B(P533T) (red trace). n = 16 and 17 cells from six and five experiments, respectively. (**H**) Average deactivation time constant (τ_w; fitted to a double exponential) fitted from tail currents for GluN1-GluN2B and GluN1-GluN2B(P533T). Values from a representative experiment are shown as open circles for each condition. n = 16 and 17 cells from six and five independent experiments per condition, respectively. ****P < 0.0001 and n.s. by Mann-Whitney U test. (**I**) Representative peak-scaled responses to 1 mM glutamate + 50 μM glycine (long jumps of 5-s duration; −60 mV) in HEK-293T cells expressing GluN1-GluN2B or GluN1-GluN2B(P533T), for the comparison of desensitization rates. n = 14 cells from three independent experiments. (**J**) Desensitization weighted time constant (τ_w) for GluN2Bwt and GluN2B(P533T). Values from a representative experiment are shown as open circles for each condition. n = 14 from three independent experiments. **P < 0.01 by Mann-Whitney U test. (**K** and **L**) Whole-cell currents activated by rapid application of 1 mM glutamate + 50 μM glycine (0.5 s; −60 mV) from HEK-293T cells expressing GluN1-GluN2Bwt (K) or GluN1-GluN2B(P533T) (L). Gray traces represent single responses, and black lines are the average of 69 (wild-type) or 33 (P533T) responses. Insets: Current variance versus mean current plot calculated from the deactivating tail current. (**M** and **N**) Bar graph showing single-channel conductance values (M) and peak open probability (N) in GluN1-GluN2Bwt– and GluN1-GluN2B(P533T)–containing NMDARs expressed in HEK-293T cells. n = 12 and 9 cells, respectively, from four independent experiments. *P < 0.05 by Mann-Whitney U test. Single cells are shown as open circles superimposed to bar graph.
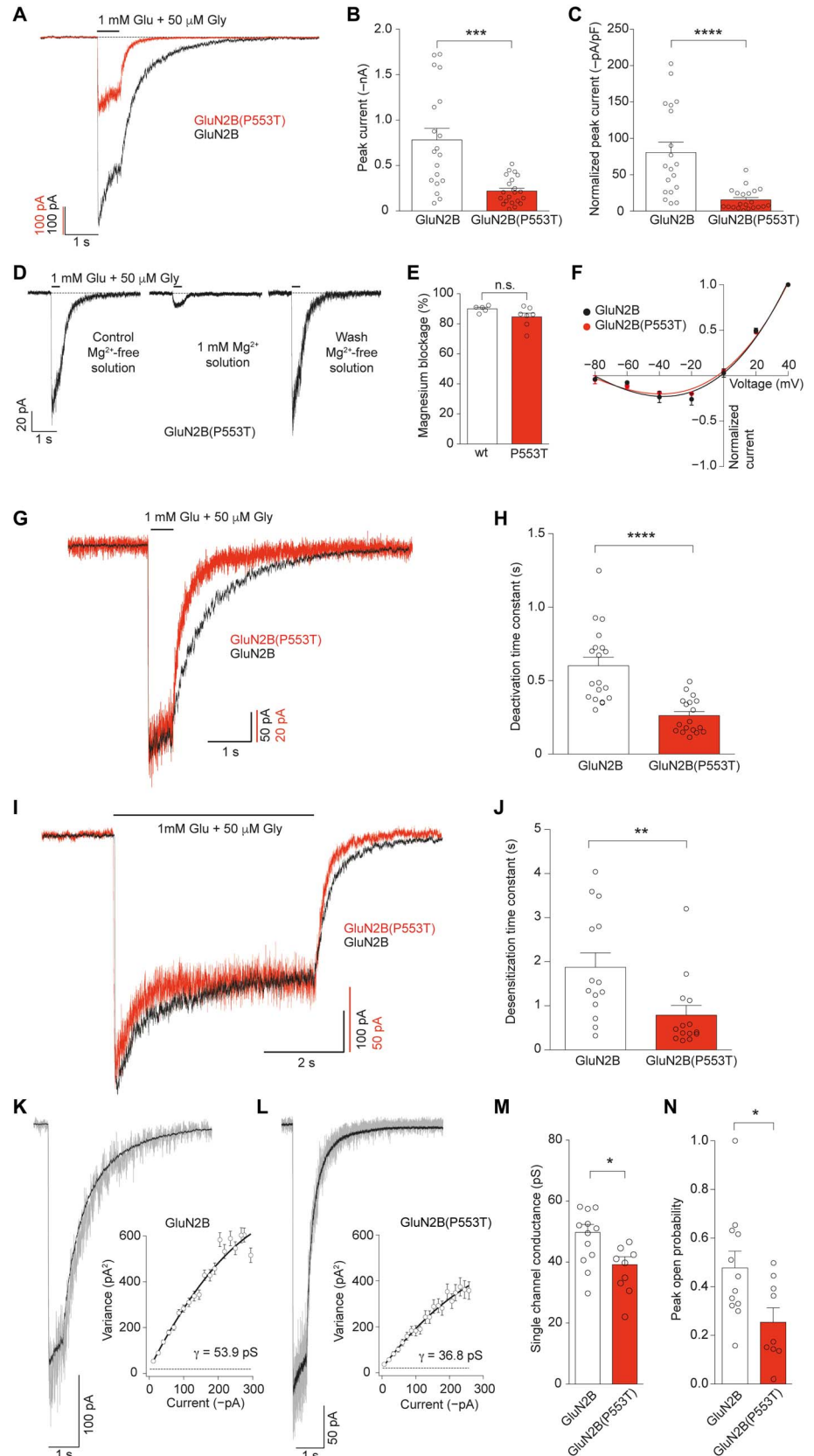
Fig. 3. D-Serine coapplication effect on wild-type and mutant (GluN1)₂-[GluN2B(P533T)]₂NMDARs.
(**A**) Representative traces evoked by physiological concentrations of 1 mM glutamate + 1 μM glycine (0.5 s; −60 mV) from GluN1-GluN2Bwt– or GluN1-GluN2B(P553T)–expressing HEK-293T cells, either in the absence (black traces) or in the presence (red traces) of D-serine at different concentrations. $n \geq 6$ cells from at least two independent experiments. (**B**) Average peak current evoked in transfected HEK-293T cells by application of 1 mM glutamate + 1 μM glycine in the presence of different D-Ser concentrations (gray bars) normalized to that of 1 mM glutamate + 1 μM glycine without D-Ser (white bars). Numbers inside the bars denote the recordings for each condition, from at least two independent experiments. *$P < 0.05$ and **$P < 0.01$ by Mann-Whitney U test. (**C**) Raw peak current responses from data shown in (B), indicating the percentage increase in current due to 100 μM D-Ser. $n = 10$ cells from at least two experiments. (**D**) Representative recordings in HEK-293T cells expressing GluN1-GluN2Bwt or GluN1-GluN2B(P553T) receptors evoked by physiological applications (5 s; −60 mV) of 1 mM glutamate + 1 or 100 μM glycine. $n = 8$ cells per condition from five independent experiments. (**E**) Bar graph representing peak current potentiation induced by high glycine concentration (100 μM versus 1 μM) with coapplication of 1 mM glutamate. $n = 8$ from five independent experiments for each condition. *$P < 0.05$ and n.s. by Student's t test. (**F**) D-Serine concentration-response curves recorded in GluN1-GluN2Bwt and GluN1-GluN2B(P553T) NMDARs expressed in HEK-293T cells, constructed from responses to 1 mM glutamate + the specified D-serine concentration in the absence of glycine. $n = 5$ cells per construct from two independent experiments. (**G**) Glutamate concentration-response curves recorded in GluN1-GluN2Bwt and GluN1-GluN2B(P553T) NMDARs expressed in HEK-293T cells. The dose-response curve was constructed from responses to 1 mM D-serine plus the specified glutamate concentration in the absence of glycine. $n = 5$ and 7 cells, respectively, from two independent experiments.

Nevertheless, spine density was significantly reduced in neurons expressing GluN2B(P553T), resulting from a decrease in the different spine subtypes (Fig. 4A). Further, immunofluorescence analysis of the GluA1 AMPA receptor (AMPAR) subunit, which is overexpressed in RTT murine models (*28*), revealed a significant increase in GluA1 in DIV11 neurons overexpressing GluN2B(P553T) (fig. S3). Overall, these morphological and molecular changes indicated deficient spine development in hippocampal neurons expressing GluN2B(P553T).

Patch-clamp recordings revealed a decrease in the amplitude of spontaneous excitatory postsynaptic currents (EPSCs) mediated by NMDARs in neurons overexpressing mutant GluN2B(P553T) compared with GluN2Bwt (Fig. 4B, top traces and left bar graph), directly demonstrating an effect of this mutation in synaptic NMDARs. Because D-serine
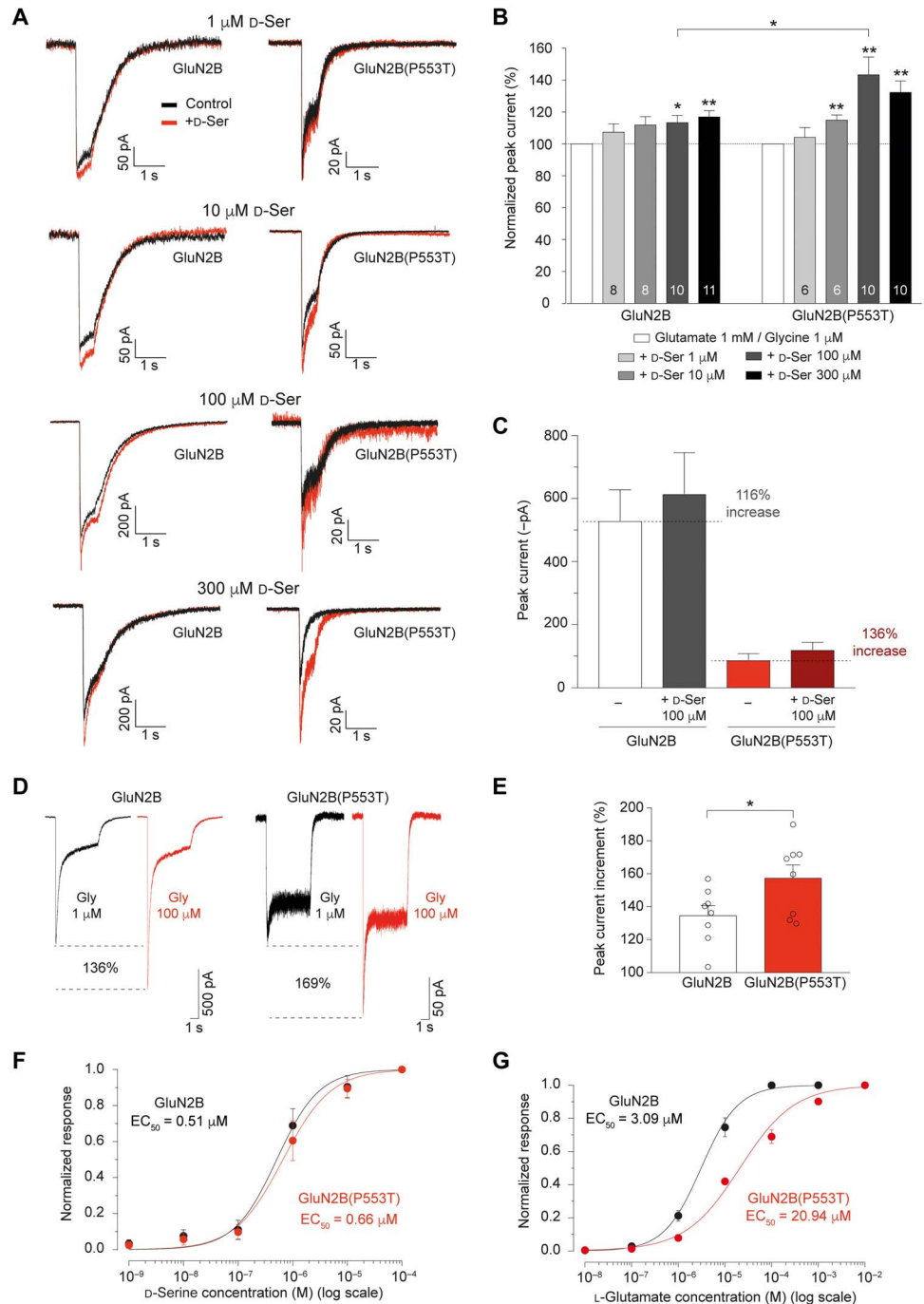
administration enhanced the activity of GluN2B(P553T)-containing NMDARs in heterologous cells (see above), we assessed its effect in primary neurons. The addition of 100 μM D-serine similarly increased EPSCs frequency in GluN2Bwt- and GluN2B(P553T)-overexpressing neurons (measured as a shortening of the interevent interval; Fig. 4B, bottom traces and right bar graph). In contrast to heterologous cell lines data, 100 μM D-serine addition did not increase EPSC amplitudes (Fig. 4B, left bar graph), perhaps due to the recruitment of new synapses or increased desensitization at higher frequencies, thus masking a putative effect on EPSC amplitudes. The rate of recovery from desensitization for NMDARs is quite slow, spanning several seconds (*29*).
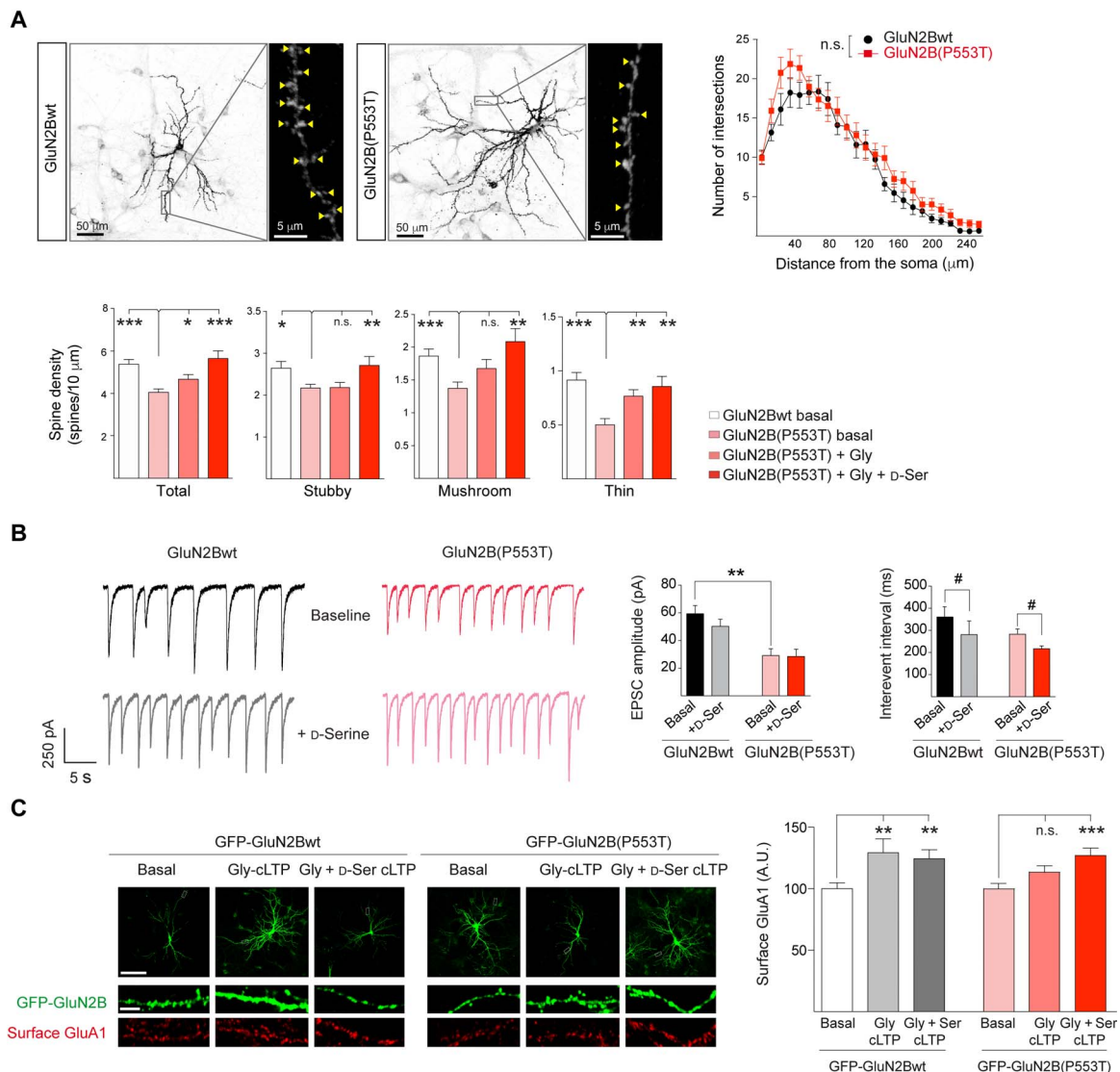
Fig. 4. Synaptic outcomes and D-serine effects on Gly-induced chemical long-term potentiation (Gly-cLTP) in GluN2B(P553T)-expressing primary hippocampal neurons. (**A**) Top left: Representative images of murine primary hippocampal neurons transfected with GFP-GluN2Bwt or GFP-GluN2B(P553T). Insets: Immunodecoration to visualize spines, indicated by yellow arrowheads. Top right: Immunofluorescence detection of GFP-GluN2B to analyze dendritic arborization by Sholl analysis. $n = 16$ to 18 neurons per condition from three independent experiments; $F = 0.71$, $P = 0.884$ by repeated measures two-way analysis of variance (ANOVA) and Bonferroni post hoc test. Bottom: Quantification of spine density and morphology in basal neurons and neurons treated with glycine alone or glycine and 100 μM D-Ser. $n = 27$ to 48 dendrites per condition from three independent experiments. *$P < 0.05$, **$P < 0.01$, ***$P < 0.001$, and n.s. by Student's t test or Mann-Whitney U test for parametric or nonparametric analyses, respectively. (**B**) Representative traces from spontaneous activity–dependent NMDAR-mediated EPSCs recordings from GluN2Bwt- or GFP-GluN2B(P553T)–transfected murine hippocampal neuronal cultures, recorded at −70 mV in the presence of 50 μM NBQX (2,3-dihydroxy-6-nitro-7-sulfamoylbenzo[f]quinoxaline 6-nitro-7-sulfamoylbenzo[f]quinoxaline-2,3-dione) and 10 μM picrotoxin and in the absence of tetrodotoxin, both under basal conditions (top traces) or after 100 μM D-serine application (bottom traces). Graphs show mean amplitudes (left) and mean time of interevent intervals (right) of the EPSCs recorded. $n = 8$ and 6 neurons, respectively, from three independent experiments. **$P < 0.01$ and #$P < 0.05$ by Mann-Whitney U test. (**C**) Representative images and immunofluorescence analysis of surface abundance of the AMPAR subunit GluA1 (red) in murine primary hippocampal neurons (green) at DIV16 that had been transiently transfected at DIV11 with GFP-GluN2Bwt or with GFP-GluN2B(P553T) assessed under basal conditions, after Gly-cLTP, and after simultaneous Gly-cLTP induction and 100 μM D-serine application (Gly + D-Ser cLTP). A.U., arbitrary units. Data are presented relative to the basal condition as means ± SEM from $n = 30$ to 40 spines per dendrite from 14 to 40 dendrites and three to seven neurons per condition, obtained from three independent experiments. **$P < 0.01$ and ***$P < 0.001$ by Student's t test.

Assessment of the effect of high-dose D-serine in GluN2B(P553T)-expressing neurons

Sustained activation of synaptic NMDARs modifies postsynaptic biochemical content (synaptic recruitment of AMPARs), induces morphological changes (synapse enlargement), and elicits LTP (30–32). Therefore, we assessed the ability of GluN2B(P553T)-expressing neu-

rons to support this form of synaptic plasticity. Transfected primary hippocampal cultures were treated either with 200 μM glycine ("Gly-cLTP") or simultaneously with 200 μM glycine and 100 μM D-serine ("Gly + D-Ser cLTP"). The analysis of dendritic spines density showed a slight significant increase in Gly-cLTP condition (Fig. 4A). Coapplication of 100 μM D-serine resulted in a more significant increase in spine

density in GluN2B(P553T)-expressing neurons, with a number of stubby, mushroom, and thin-shape spines similar to neurons expressing GluN2Bwt under basal conditions (Fig. 4A). Immunofluorescence analysis showed that Gly-cLTP significantly increased surface GluA1 abundance at spine-like structures in GluN2Bwt-transfected neurons (Fig. 4C, left images and bar graph). In contrast, GluA1 surface abundance was not significantly increased in GluN2B(P553T)-expressing neurons (Fig. 4C). These defects were rescued by simultaneous administration of glycine and D-serine (Fig. 4C), indicating that D-serine can also facilitate a major potentiation of NMDAR-dependent plasticity in the context of GluN2B(P553T) mutation.

Evaluation of biochemical and clinical effects of L-serine dietary supplementation in pediatric patient with GluN2B(P553T) variant

The partial restoration of mutant NMDAR function by D-serine prompted us to translate the therapeutic strategy to the clinical practice. Because D-serine use was still under investigation at the beginning of the study, the patient was supplemented with L-serine, an approved nutraceutical amino acid acting as the endogenous D-serine precursor. We hypothesized that L-serine supplement might increase serine racemase substrate in the brain (33, 34), raising D-serine brain levels that might potentiate hypofunctional NMDARs. At 5 years and 10 months of age, the patient was administered L-serine (500 mg/kg per day) and continued to date (17 months at the time of writing this report). Ultraperformance liquid chromatography–tandem mass spectrometry (UPLC-MS/MS) analysis showed that L-serine treatment was associated with a 4.4-fold increase in the abundance of D-serine in the patient's plasma (Fig. 5A), whereas D-enantiomers of branched-chain amino acids (valine, isoleucine, and leucine) and plasma amino acids with a potential NMDAR modulatory role (such as glycine, taurine, and cysteine) showed no notable alterations (Fig. 5A). Furthermore, considering that L-serine is involved in sphingolipid biosynthesis, an untargeted UPLC-MS lipidomic analysis was conducted and revealed a strong alteration of the sphingolipidomic profile of the patient, which was not altered by L-serine dietary supplementation (table S1). Because D-serine racemase is strongly expressed in neurons (33), we reasoned that the increased D-serine plasma levels
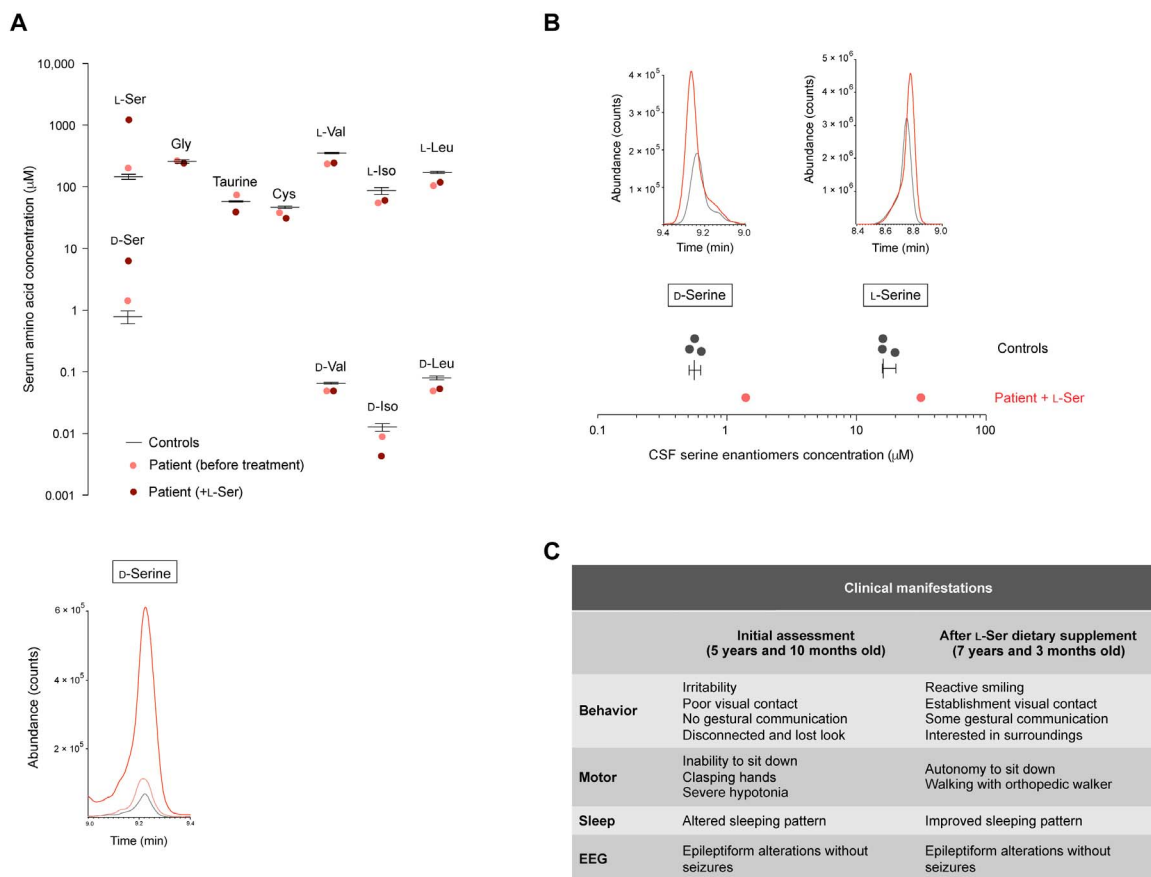
Fig. 5. Biochemical and behavioral assessment of GRIN2B(P553T) patient after L-serine dietary supplementation. (**A**) Top: Analysis of amino acid plasma concentration of D-L-serine, D-L-valine, D-L-isoleucine, D-L-leucine, glycine, taurine, and cysteine. Plasma samples analyzed correspond to the patient before and after L-serine treatment (light red and dark red dots, respectively) and the mean of controls (black lines; whiskers representation of mean-min-max values). Bottom: Chromatographic profiles of D-serine and L-serine enantiomers in plasma samples from the control individual (gray trace), the patient before treatment (light red trace), and the patient with L-serine dietary supplementation (dark red trace). (**B**) Top: Overlapping chromatographic profiles of D-serine and L-serine enantiomers (left and right, respectively) in CSF from a control (gray trace) and from the patient with GRIN2B(P553T) mutation, after L-serine dietary supplementation (red trace). Bottom: Serine enantiomers concentration analysis in CSF of controls (gray dots; whiskers representation of mean-min-max values; gray traces in the chromatogram) and the patient with L-serine dietary supplement (red dots and traces). (**C**) Clinical manifestations of the patient harboring a de novo GRIN2B(P553T) mutation, before and after 17 months of L-serine dietary supplementation.

most probably reflect increased D-serine abundance in the brain of the patient. UPLC-MS analysis showed highly increased D-serine levels in cerebrospinal fluid (CSF) of the treated patient (Fig. 5B).

Together with the biochemical profiling, a neuropsychological assessment was performed. Before treatment, the patient (5 years and 10 months old) had few communication skills, poor eye contact, did not pay attention to the activities of the parents, teachers, and schoolmates, did not have verbal language (any words or sounds), did not show the use of symbolic play, and could not move from the prone position to the sitting position, although she could then sit without support. The Vineland standard score (SS) test before treatment were 42 for communication, 36 for daily living skills, 49 for socialization, and 31 for motor skills (mean SS of 100 with an SD of 15), with an overall SS of 38.

After 11 months of L-serine dietary supplementation, although the EEG was still aberrant, the behavior of the patient was notably improved, as shown by the Vineland Adaptive Behavior Scale (VABS). The Vineland SSs were 42 for communication, 34 for daily living skills, 51 for socialization, and 38 for motor skills. This midterm assessment showed that her motor skills were strongly improved; she was able to stand from sitting and started to walk with external help. Behaviorally, the patient started to communicate with gestures (such as by extending her hands to be held), and her display of facial expressions increased. She started to react by turning her head when called by her name, had improved visual contact, and started to smile proactively. Overall, the clinical assessment indicated an attenuation of both motor and cognitive impairments.

After 17 months of treatment, the patient remarkably improved communication, social, and motor skills (Fig. 5C). The Vineland SSs (motor assessment cannot be performed beyond 7 years old) after L-serine treatment in the patient were 48 for communication, 48 for daily living skills, and 50 for socialization. Behaviorally, she was then interested in faces and had a persistent eye contact, followed the activities of surrounding humans with interest, was able to stretch her arms out to be held, turn her head when called, laugh at funny situations, and was generally (by outward assessments) happier. She could then also imitate toys and animal sounds, creep on the floor, and move from a prone to a sitting position, as well as from a sitting to standing position with support. She had also improved her sleeping pattern, was able to sit down without help, and notably could walk using an orthopedic walker. An EEG showed epileptiform alterations, but clinical seizures were not present. Despite pharmacological interventions to target them specifically (valproate first and levetiracetam later), the epileptiform alterations detected in the EEG were still present; thus, these treatments were stopped. Nonetheless, overall, the clinical assessments indicated an improvement in cognitive, communicative, and motor impairments associated with L-serine dietary supplementation.

DISCUSSION

NMDARs are critical players of glutamatergic neurotransmission and are fundamental actors in neuritogenesis, synaptogenesis, and synaptic plasticity processes. Currently, upon the development of next-generation sequencing, there is a growing body of data implicating de novo mutations of iGluRs (7, 8) in mental and behavioral disorders. Several mutations in subunits of the NMDAR have been related to neurodevelopmental diseases (11–13). However, these data require functional validation to unveil whether these mutations are really pathogenic. In the present study, we identified a GRIN2B(P553T) missense de novo mutation of the GluN2B subunit of the NMDAR in a patient with Rett-like syndrome with severe encephalopathy. This

mutation resulted in the exchange of a highly evolutionary conserved Pro into a Thr. A mutation affecting the same amino acid position GluN2B(P553L) was previously described in a patient from a cohort of individuals with ID (16). This patient exhibited phenotypic alterations similar to those of the case in the present study, including severe ID, hypotonia, and no speech. The phenotypic similarity between these two cases provides a strong evidence for a pathogenic role of GluN2B(Pro^{553}) mutations under these neurodevelopmental conditions.

Electrophysiological studies confirmed the in silico structural studies predicting the hypofunctionality of mutant NMDARs. In addition to a reduction of the channel conductance and peak open probability, we found a significant increase in both the desensitization and the deactivation rates of GluN1-GluN2B(P553T) receptors. Whether the P553T mutation located far from the binding site is altering deactivation kinetics, an intrinsic property of the receptor, is an incognita, but electrophysiological concentration-response experiments indicate a decreased glutamate binding affinity of mutant NMDARs, triggering a decreased receptor efficacy that seems to be physiologically relevant. NMDAR function is largely determined by the high amount of Ca^{2+} influx, which is mostly dependent on channel kinetics, particularly the rates of desensitization and deactivation. Thus, we can speculate that kinetics changes detected on GluN2B(P533T) mutant receptors might be limiting Ca^{2+} influx, which in turn would alter Ca^{2+}-mediated signaling pathways and synaptic plasticity.

Overall, these changes markedly reduce NMDAR-mediated currents and might be underlying the severe phenotype of the patient. GluN2B subunits are highly expressed at embryonic and initial postnatal stages, playing a critical role in neurodevelopmental processes (35). Consequently, the hypofunctionality of this major subtype of NMDARs might certainly affect neuritogenesis and synaptogenesis, leading to altered synaptic transmission. This hypothesis is supported by the morphological and biochemical findings, showing a significant decrease in spine density together with increased levels of GluA1 subunit of AMPARs. Pozzo-Miller's group (28, 36) has reported similar synaptic outcomes in patients with RTT and in primary murine neuronal cultures deficient or harboring mutations of MeCP2. Therefore, our data suggest that NMDAR-induced alterations of glutamatergic synapses might be involved in the pathophysiology of classical RTT condition.

In agreement with the proposed functional impact of de novo mutations of GluN2B subunit, previous studies have associated de novo mutations of GRIN2B with severe phenotypic alterations (6, 14, 15, 37). Lemke and collaborators (13, 38) described the functional consequences of GRIN2B mutations in patients with West syndrome and in individuals with ID with focal epilepsy. In the latter study, the patient with ID and focal epilepsy had a missense mutation in the extracellular glutamate–binding domain. De novo GRIN2B mutations lead to a gain of function, either significantly reducing Mg^{2+} block and increasing Ca^{2+} permeability (N615I and V618G mutations, affecting the M2 domain in the pore of the channel) or increasing the apparent glutamate binding affinity (R540H mutation, within the extracellular S1 domain). These gain-of-function mutations point out the important role of facilitated NMDAR signaling in epileptogenesis, with further therapeutic strategies consisting on the selective blockade of mutant leak/hyperactive channels. In contrast, loss-of-function mutations might be causing a hypoglutamatergic function that could be potentially rescued by increasing NMDAR activity with a therapeutic purpose.

The glutamatergic synapse is an extremely sophisticated system where a plethora of molecular actors reside and interact to finely tune neurotransmission. However, under pathological conditions,

the dysregulation of critical players might compromise glutamatergic neurotransmission, resulting on an enhancement or a reduction of glutamate signaling (8). In the present work, in silico and in vitro experiments concluded that GluN2B(P553T)-containing NMDARs are hypofunctional. Thus, we envisioned that enhancing NMDAR activity might recover normal glutamatergic neurotransmission and attenuate clinical manifestations. To this end, we evaluated the effect of D-serine, a coagonist of the GluN1 subunit, coapplied with physiological glycine concentrations (39). Our findings indicate an enhancement of mutant GluN1-GluN2B receptor activity, suggesting that the structural changes induced by the mutation are not transduced to GluN1 ligand-binding domain. The ability of D-serine to activate wild-type GluN1-GluN2B receptors (shown in this work) and all NMDAR subtypes (40, 41) should have a general effect on glutamatergic function. Because L-serine is a nutraceutical serine enantiomer already used in pediatric care, the patient was treated with L-serine dietary supplementation. This dietary supplement resulted in increased D-serine concentration in the patient's plasma, concomitant with strongly increased D-serine amounts in the CSF, in agreement with a previous report (42). Because L-serine is the substrate of serine racemase in the brain (34), our data support the hypothesis that L-serine supplement increases L-serine availability in the brain, which in turn promotes L-serine conversion to D-serine in the brain (43), likely potentiating hypofunctional NMDARs. The beneficial effect of D-serine in healthy individuals has been described in a clinical trial (44). In that work, Heresco-Levy and colleagues showed the procognitive effects of D-serine through NMDAR function and, as we propose in the present study, intended the development of NMDAR glycine site strategies for treating synaptopathies. In agreement with this, D-serine deficits have been associated with aging in rats, with functional rescue observed after exogenous D-serine administration (45, 46). In addition, serine deficiency disorders also provoke neurological phenotypes (psychomotor retardation, microcephaly, and seizures in newborns and children) that can be safely treated by serine oral replenishment (47). Together, these works and ours indicate that, independent of the molecular etiology (whether serine racemase deficit or NMDAR hypofunctionality), serine-potentiated NMDAR activity can partially rescue hypoglutamatergic function. In addition to the beneficial effect of L-serine–mediated increase in D-serine levels, the effect of some other L-serine metabolites and the neurodevelopmental factors might be considered. Regarding the former, our biochemical studies have shown that additional L-serine–derived amino acids and sphingolipids that potentially modulate the NMDAR were not modified by L-serine dietary supplementation. Regarding the neurodevelopmental aspects, the improved patient's condition might also be influenced by the developmental changes in GluN2 subunit expression, increasing the GluN2A:GluN2B ratio during development (9). Our findings indicate that mutant heterotrimeric NMDARs are less affected than heterodimeric mutant receptors. Therefore, in addition to the NMDAR-potentiating effect of L-serine treatment, GluN2 subunits, the developmental switch might also contribute to improve the clinical symptoms of the patient to some extent.

In summary, our data represent a proof-of-concept study to identify the pathogenicity of de novo mutations of NMDARs and the development of precision therapeutic strategies. The methodological pipeline developed along this study might be further implemented to functionally stratify de novo iGluR mutations associated with synaptic dysfunctions and to define therapeutic strategies. Moreover, they support the use of L-serine as a dietary supplement for the enhancement of glutamatergic neurotransmission and/or excitatory or inhibitory neurotransmitter imbalance that are associated with a large spectrum of neurological disorders.

MATERIALS AND METHODS

Patient neurodevelopmental and adaptive behavior assessments before and after dietary L-serine supplement

The study was approved by the appropriate informed consent of the patient's parents. The VABS-II (48) semistructured interview, allowing the assessment of four domains of adaptive behavior (communication, daily living skills, socialization, and motor skills), was conducted by a trained neuropsychologist before (at 5 years 10 months old) and after 11 and 17 months of L-serine supplementation (at 6 years and 9 months old and 7 years and 3 months old, respectively). Initially, L-serine dose started at 250 mg/kg per day (for 4 weeks), and upon the confirmation of a lack of side effects, the dose was increased to 500 mg/kg per day (divided into three dietary supplements of L-serine powder, mixed with food and/or drinks) and maintained along the extent of the trial.

Whole-exome sequencing

Coding regions were captured using the TruSeq DNA Sample Preparation and Exome Enrichment Kit (Illumina, San Diego, CA, USA), and paired-end 100×2 sequences were sequenced with the Illumina HiScanSQ system at National Center for Genomic Analysis in Barcelona (Catalonia, Spain). The overall coverage statistics for the trio are 381.451, 433.847, and 31.635 for the patient, the mother, and the father, respectively.

Bioinformatic pipeline

Sequence reads were aligned to the Genome Reference Consortium Human Genome Build 37 (GRCh37) hg19 using the Burrows-Wheeler Aligner (49). Properly mapped reads were filtered with SAMtools (1, 2), which was also used for sorting and indexing mapping files. Genome Analysis Toolkit (GATK) (3) was used to realign the reads around known indels and for base quality score recalibration. Once a satisfactory alignment was achieved, identification of single-nucleotide variants (SNVs) and indels was performed using GATK standard multisample variant calling protocol, including variant recalibration (4). For the final exome sequencing analysis report, the Annotate Variation (ANNOVAR) (5) tool was used to provide additional variant information to ease the final selection of candidates. In particular, minor allele frequency (MAF), obtained from dbSNP (Single-Nucleotide Polymorphism Database) (50, 51) and 1000 Genomes Project (6–8), was provided to help to select previously undescribed variants in healthy population.

De novo SNVs and small insertion or deletion events

To identify de novo SNVs and small insertion and/or deletion events, the patient's variants were filtered first against parental variants and then against a pool of controls made up by all healthy parents included in the study. SIFT (52) and PolyPhen-2 (Polymorphism Phenotyping v2) (53) damage scores were computed to predict putative impact over protein structures. The successive application of quality control filters and the prioritization by the parameters with potential functional impact was used to construct a list of candidate genes (and variants) ranked by its uniqueness in the cases (or very low frequency in the control population, as derived from the MAFs) and the putative potential impact.

Sanger sequencing

The variants were validated by Sanger sequencing using BigDye Terminator v3.1 Cycle Sequencing Kit (Life Technologies, Grand Island, NY, USA) in an Applied Biosystems 3730/DNA Analyzer (Applied Biosystems, Life Technologies, Grand Island, NY, USA) using the following set of primers: 5′-TACAATCTAACCTAGGCCCTGG-3′ (forward) and 5′-TGGATATGCTAGGGAAAATGCAG-3′ (reverse). The raw data were analyzed with CodonCode Aligner software (CodonCode Corporation, Centerville, MA, USA).

In silico prediction of mutation impact

The following four in silico prediction tools of functional mutation impact were used: SIFT, PolyPhen-2, Protein Variation Effect Analyzer (PROVEAN) (54), and MutationTaster2 (55). SIFT is a sequence homology–based tool that predicts variants as neutral or deleterious using normalized probability scores. Variants at position with a normalized probability score less than 0.05 are predicted to be deleterious, and a score greater than 0.05 is predicted to be neutral (56). PolyPhen-2 uses a combination of sequence and structure-based attributes and naive Bayesian classifier for the identification of an amino acid substitution and the effect of mutation. The output results of probably damaging and possibly damaging were classified as deleterious ($\geq$0.5) and the benign level being classified as tolerated ($\leq$0.5). PROVEAN uses a region-based delta alignment score, which measures the impact of an amino acid variation not only based on the amino acid residue at the position of interest but also on the quality of sequence alignment derived from the neighborhood flanking sequences. Variants with a PROVEAN score lower than −2.5 are predicted to be deleterious (57). MutationTaster2 also uses a Bayes classifier to generate predictions but includes all publicly available single-nucleotide polymorphisms and indels from the 1000 Genomes Project, as well as known disease variants from ClinVar (58) and the Human Gene Mutation Database (HGMD) (59). Alterations found more than four times in the homozygous state in 1000 Genomes or in HapMap (60) are automatically regarded as neutral. Variants marked as pathogenic in ClinVar were automatically predicted to be potentially disease causing.

Molecular modeling of wild-type and mutant (GluN1)$_2$-(GluN2B)$_2$ receptors

An initial homology model was constructed for the transmembrane domain of human (GluN1)$_2$-(GluN2B)$_2$ receptor using the coordinates of the crystal structure of rat receptor (PDB ID: 4PE5) (61). MODELLER v16 (62) was used to model the lacking residues of the loop connecting M1 and M3. The side-chain conformations for those residues were positioned according to SCWRL (63). The backbone conformation from residues 551 to 556 was modeled with MODELLER v16 software (62). Protein complexes were embedded in a model membrane containing 1-palmitoyl-2-oleoyl-*sn*-glycero-3-phosphocholine (POPC) lipids, water molecules, and 0.15 M NaCl in a rectangular box (64). The initial system was energy-minimized and then subjected to molecular dynamics equilibration (25 ns). Subsequently, the system was subjected to a production stage, extending 250 ns. All the simulations were performed with GROMACS 4.5 simulation package (65).

Phylogenetic analysis of GluN2B(P553)-containing domain

Genes coding for iGluRs subunits from different species belonging to the phylum metazoan were identified using the BLASTP tool and human iGluRs as queries. Subject sequences with an *E* value below 0.05 were selected as possible homologs. These were reblasted against the National Center for Biotechnology Information "nonredundant protein sequences (nr)" database to establish their correspondence with glutamate receptors. These searches were performed against the Ensembl Metazoa database (http://metazoa.ensembl.org/index.html) for *L. gigantea*, *C. teleta*, *S. maritima*, *A. melifera*, *Nematostella vectensis*, *Mnemiopsis leidyi*, and *Trichoplax adhaerens*; Metazome database (https://metazome.jgi.doe.gov/pz/portal.html) for *S. kowalevskii*; and alternative polyadenylation sites database (APAsdb) (http://genome.bucm.edu.cn/utr/) for *B. belcheri*. Sequences from porifera species were taken from Riesgo's group database (66). All vertebrate sequences were obtained from the Ensembl Metazoa database. A final set of 147 iGluR sequences from 12 metazoan species spanning seven phyla was used in the phylogenetic analysis. Sequence multiple alignment was made using MUSCLE tool (67) included in the MEGA6 software (68). The alignment was made with coding DNA sequences, using "codons" option, which allows maintaining nucleotide triplets coding for amino acids. Using MEGA6, we established that GTR + I + G (general time reversible with gamma rates and a proportion of invariant sites) was the best evolutionary model to use in the phylogenetic tree. The phylogenetic tree was constructed using the Bayesian inference method, with MrBayes 3.2 software (69). *Arabidopsis thaliana* iGluR sequences were obtained from the TAIR (The Arabidopsis Information Resource) database (www.arabidopsis.org/) and used as an external group of the tree. Two simultaneous trees were analyzed, and 3,630,000 iterations were run until both trees converged.

Plasmids

The expression plasmids for rat GluN1 and GFP-GluN2B were provided by S. Vicini (Georgetown University Medical Center, Washington, USA) (70). The plasmids used for the analysis of tri-heteromeric NMDARs were provided by P. Paoletti (École Normale Supérieure Paris, France, EU). Nucleotide change (the mutation of GluN2B serine at amino acid position 553 to a Thr residue) was achieved by oligonucleotide-directed mutagenesis, using the QuikChange site–directed mutagenesis kit according to the manufacturer's instructions (Stratagene). The plasmid generated by site-directed mutagenesis was verified by DNA sequencing.

Coimmunoprecipitation experiments

For immunoprecipitation of heterologously expressed GluN1, HA-GluN2A, and GFP-GluN2B (wild-type or mutant), transfected HEK-293T cells were washed in cold phosphate-buffered saline (PBS) and subsequently solubilized in radioimmunoprecipitation assay buffer supplemented with protease and phosphatase inhibitor cocktail (PPIC), for further immunoprecipitation with anti-GFP. The homogenates were clarified by centrifugation at 4°C for 10 min at 16,000g. After preclearing the soluble lysates for 1 hour at 4°C with equilibrated protein G Sepharose, they were incubated overnight at 4°C with 10 μg of an anti-GFP mouse monoclonal antibody (Ab) (1:200; catalog no. 9777966, Clontech). Nonspecific mouse immunoglobulin G (catalog no. I5381, Sigma-Aldrich) was used as a control for specificity. The immunocomplexes were incubated with protein G Sepharose for 2 hours at 4°C, and the beads were then washed twice with lysis buffer and once with PBS. The bound proteins were eluted in Laemmli's buffer and analyzed by Western blot.

Western blot analysis

For protein extraction, cells were washed once with PBS and scraped off the plate in 400 μl of lysis buffer [50 mM Hepes (pH 7.4), 150 mM NaCl,

2 mM EDTA, 1% NP-40, and PPIC]. After 10 min of incubation at 4°C, the cell debris was pelleted at 15,000g, the solubilized proteins were collected, and the protein concentration was determined using a bicinchoninic acid assay (BCA). Proteins were separated by 8% SDS–polyacrylamide gel electrophoresis and transferred to nitrocellulose membranes (Amersham), which were then blocked with 10% skimmed milk in 10 mM tris-HCl (pH 7.5)/100 mM NaCl [tris-buffered saline (TBS)] plus 0.1% Tween 20 (TBS-T). The membranes were probed overnight at 4°C with the primary Ab of interest (diluted in TBS-T + 5% skimmed milk) directed against GluN1 (1:500; catalog no. 05-432, Millipore), HA epitope (catalog no. MMS-101R-500, Covance Inc.), and GFP (Clontech). Ab binding was detected with an anti-mouse or anti-rabbit Ab coupled to horse-radish peroxidase (Dako) for 1 hour at room temperature (RT), and the immunocomplexes were visualized by chemiluminescence (ECL detection system, Pierce), following the manufacturer's instructions. Immunosignals were analyzed densitometrically with ImageJ software [National Institutes of Health (NIH), USA].

Cell culture and transfection

HEK-293T and COS-7 cell lines were obtained from the American Type Culture Collection and maintained at 37°C in Dulbecco's modified Eagle's medium, supplemented with 10% fetal calf serum and antibiotics [penicillin (100 U/ml) and streptomycin (100 μg/ml)]. Furthermore, D-2-amino-5-phosphonopentanoic acid (Abcam) was added to the medium (final concentrations of 200 or 500 μM for HEK-293T and COS-7 cells, respectively) to avoid excitotoxicity. Transient transfection of HEK-293T cells was achieved by the calcium phosphate method (Clontech), and cell extracts were obtained 48 hours after transfection. COS-7 cells were transfected with Lipofectamine 2000 (Invitrogen), following the manufacturer's instructions, and cells were fixed 24 hours after, for further immunofluorescence analysis.

To prepare dissociated mouse hippocampal neuron cultures, mouse embryos (embryonic day 18) were obtained from pregnant CD1 females, the hippocampi were isolated and maintained in cold Hank's balanced salt solution (HBSS; Gibco) supplemented with 0.45% glucose (HBSS-glucose). After carefully removing the meninges, the hippocampi were digested mildly with trypsin for 17 min at 37°C and dissociated. The cells were washed three times in HBSS and resuspended in Neurobasal medium supplemented with 2 mM GlutaMAX (Gibco) before filtering in 70-μm mesh filters (BD Falcon). The cells were then plated onto glass coverslips (5×10^4 cells/cm^2) coated with poly-L-lysine (0.1 mg/ml; Sigma-Aldrich), and 2 hours after seeding, the plating medium was substituted by complete growth medium, consisting on Neurobasal medium supplemented with 2% B27 (Invitrogen) and 2 mM GlutaMAX, and the coverslips were incubated at 37°C in a humidified 5% CO$_2$ atmosphere. Every 3 to 4 days, half of the conditioned medium was removed and replaced by fresh growth medium. Primary cultures were transfected with 0.8 μg of DNA (Lipofectamine 2000, Invitrogen) on DIV4, DIV7, or DIV11 for further surface expression analysis of GFP-GluN2B constructs and endogenous GluA1. All the experimental procedures were carried out according to European Union guidelines (Directive 2010/63/EU) and following protocols that were approved by the Ethics Committee of the Bellvitge Biomedical Research Institute (IDIBELL).

Immunofluorescence analysis of surface NMDARs

The surface-to-total expression of NMDARs in COS-7 cells was performed as previously described (71). Briefly, cells were washed twice with PBS before they were fixed with 4% paraformaldehyde (PFA).

Surface expression of GFP-GluN2B constructs was detected using an Ab against GFP (1:1000; catalog no. A11122, Life Technologies) that recognizes the extracellular epitope of heterologously expressed receptors and that was visualized with an Alexa Fluor 555–conjugated goat anti-rabbit Ab (1:500; catalog no. A-31851, Thermo Fisher Scientific). The total pool of receptors was detected by the fluorescent signal emitted by the GFP-GluN2B construct.

To analyze the surface expression of the transfected NMDARs in primary hippocampal neuronal cultures, cells were washed twice with PBS and fixed with 4% PFA in PBS containing 4% sucrose. The surface expression of GFP-GluN2B constructs was detected by incubating with anti-GFP (1:1000; catalog no. A11122, Life Technologies) during 1 hour at RT and visualized with an Alexa Fluor 488–conjugated goat anti-rabbit Ab (1:500; catalog no. A-11078, Thermo Fisher Scientific). The intracellular pool of receptors was identified by permeabilizing cells with 0.1% Triton X-100 and labeling them with a rabbit anti-GFP–Alexa Fluor 555–conjugated Ab (1:2000; catalog no. A-31851, Thermo Fisher Scientific).

Fluorescence was visualized with a Leica TCS SL spectral confocal microscope (Leica Microsystems, Wetzlar, Germany) using a Plan-Apochromat 63×/1.4–numerical aperture immersion oil objective (Leica Microsystems) and a pinhole aperture of 114.54 or 202 μm (for surface receptors). To excite the different fluorophores, the confocal system is equipped with excitation laser beams at 488 and 546 nm. In each experiment, the fluorescence intensity was measured in 10 to 15 dendrites from at least two to three pyramidal neurons (or in 10 to 15 COS-7 cells) per condition. Fluorescence was quantified using Adobe Photoshop CS5 software (Adobe Systems Inc.), and the results are represented as the means ± SEM of the ratio of surface:intracellular (primary cell culture) or surface:total (COS-7 cells) GluN2B immunofluorescence signal, analyzing at least three independent experiments.

Morphological analysis of dendritic arborization and spines

GFP-GluN2Bwt– and GFP-GluN2B(P553T)–transfected neurons were immunolabeled, and Z-stack images were acquired. The resulting maximum projections were analyzed using "Sholl analysis" ImageJ plugin (72). Dendrites were manually traced with Neuron Studio software (http://research.mssm.edu/cnic/tools-ns.html). Dendritic spines from tertiary neurites were counted and classified into morphological categories (thin, mushroom, and stubby), using Neuron Studio software automatic analysis, followed by manual revision to discard artifacts and/or spines counts redundancy.

Chemical LTP–induced recruitment of AMPARs in the cell surface and synaptic morphology changes

Gly-cLTP assay was performed at DIV14 on primary hippocampal neurons transiently transfected at DIV11 with either GFP-GluN2Bwt + GFP (4:1 ratio) or GFP-GluN2B(P553T) + GFP (4:1 ratio), adapting the protocols previously described (31, 32). Briefly, basal conditions (nonstimulated neurons) consisted in the incubation of primary cultures with Krebs-Ringer solution supplemented with 1 mM Mg^{2+} and 1 μM tetrodotoxin. For Gly-cLTP induction, cells were briefly washed in 20 μM bicuculline (BIC) + 20 μM strychnine and then incubated for 5 min in Krebs-Ringer solution supplemented with 20 μM BIC + 1 μM strychnine and 200 μM Gly (100 μM D-serine supplement, for Gly + D-Ser condition). The solutions were replaced by a medium supplemented with 20 μM BIC, 20 μM strychnine, and 1 mM Mg^{2+}. After 20 min of incubation at 37°C (GluA1 surface recruitment studies) or 35 min of incubation at 37°C (dendritic spines analysis), cells were fixed

with ice-cold 4% PFA in PBS containing 4% sucrose. For immunofluorescence analysis of GluA1 surface recruitment, neurons were incubated at RT for 30 min with anti-GluA1 Ab (1:200; catalog no. MAB2263, Millipore) and incubated with Alexa Fluor 555–conjugated goat anti-mouse Ab (1:500; catalog no. A31570, Molecular Probes). After permeabilization/blocking, cells were incubated with rabbit anti-GFP (1:1000; catalog no. A11122, Life Technologies) and then with Alexa Fluor 488–conjugated goat anti-rabbit Ab (1:500; catalog no. A-11078, Thermo Fisher Scientific), and washed and mounted for confocal microscopy analysis. Secondary dendritic processes expressing the GFP-GluN2B constructs were analyzed by quantifying the fluorescence intensity of GluA1 puncta with ImageJ software (NIH), and tertiary dendritic processes were included for spines density and morphology analysis.

Electrophysiological recordings of diheteromeric and triheteromeric NMDAR-mediated whole-cell currents in HEK-293T cells

Electrophysiological recordings were obtained 18 to 24 hours after transfection, perfusing the cells continuously at RT with an extracellular physiological bath solution: 140 mM NaCl, 5 mM KCl, 1 mM CaCl$_2$, 10 mM glucose, and 10 mM Hepes, adjusted to pH 7.42 with NaOH. Glutamate (1 mM; Sigma-Aldrich), in the presence of glycine (1, 50, or 100 μM depending the experiment type; Tocris) and D-serine (0 to 300 μM) was applied for 0.5 s by piezoelectric translation (P-601.30; Physik Instrumente) of a theta-barrel application tool made from borosilicate glass (1.5 mm outside diameter; Sutter Instruments), and the activated currents were recorded in the whole-cell configuration at a holding potential of −60 mV, acquired at 5 kHz and filtered at 2 kHz by means of Axopatch 200B amplifier, Digidata 1440A interface, and pClamp10 software (Molecular Devices Corporation). Electrodes with open-tip resistances of 2 to 4 megohms were made from borosilicate glass (1.5 mm outside diameter, 0.86 mm outside diameter; Harvard Apparatus), pulled with a PC-10 vertical puller (Narishige), and filled with intracellular pipette solution containing 140 mM CsCl, 5 mM EGTA, 4 mM Na$_2$ATP, 0.1 mM Na$_3$GTP, and 10 mM Hepes, adjusted to pH 7.25 with CsOH. Glutamate and glycine-evoked currents were expressed as current density (in pA/pF; maximum current divided by input capacitance as measured from the amplifier settings) to avoid differences due to surface area in the recorded cells.

The kinetics of deactivation and desensitization of the NMDAR responses were determined by fitting the glutamate/glycine-evoked responses at V_m − 60 mV to a double-exponential function to determine the weighted time constant ($\tau_{w,des}$)

$$\tau_{w,des} = \tau_f \left(\frac{A_f}{A_f + A_s} \right) + \tau_s \left(\frac{A_s}{A_f + A_s} \right)$$

where A_f and τ_f are the amplitude and time constant of the fast component of desensitization, respectively, and A_s and τ_s are the amplitude and time constant of the slow component of desensitization, respectively.

To infer single-channel conductance values from macroscopic deactivating currents, we used NSFA as previously described (24). The single-channel current (i) was calculated by plotting the ensemble variance against mean current ($\bar{I}$) and fitting with Sigworth parabolic function (73)

$$\sigma^2 = \sigma_B^2 + \left(i\bar{I} - \left(\frac{\bar{I}^2}{N} \right) \right)$$

where σ_B^2 is the background variance and N is the total number of channels contributing to the response. The weighted-mean single-channel conductance was determined from the single-channel current and the holding potential of −60 mV.

NMDAR agonists dose-response experiments

To determine the affinity for D-serine or glutamate in GluN2B- and GluN2B(P553T)-transfected cells, concentration-response curves were constructed from whole-cell currents elicited by rapid jumps of 0.5-s duration at different concentrations of the coagonist D-serine (10^{-9} to 10^{-4} M) in the presence of 1 mM glutamate or at different concentrations of the agonist glutamate (10^{-8} to 10^{-2} M) in the presence of 1 mM D-serine. Concentration-response curves were fitted individually for every cell using the Hill equation

$$I = \frac{I_{max}}{1 + \left(\frac{EC_{50}}{[A]} \right)^{n_H}}$$

where I_{max} is the maximum current, $[A]$ is the concentration of D-serine, n_H is the slope (Hill) coefficient, and EC_{50} is the concentration of D-serine or glutamate that produces a half-maximum response. Each data point was then normalized to the maximum response obtained in the fit. The average of the normalized values with their SEM were plotted together and fitted again with the Hill equation. The minimum and maximum values were constrained to asymptote 0 and 1, respectively.

Electrophysiological recordings of NMDA EPSCs in hippocampal neurons

Spontaneous activity–dependent NMDAR-mediated EPSCs were recorded in cultures of hippocampal neurons (DIV16). Whole-cell recordings were obtained from transfected neurons (at DIV12) with GluN2B-GFP or GluN2B(P553T). Extracellular solution contained 140 mM NaCl, 3.5 mM KCl, 2 mM CaCl$_2$, 20 mM glucose, and 10 mM Hepes, (Mg^{2+}-free) adjusted to pH 7.42 with NaOH. To isolate NMDAR component, 50 μM NBQX and 100 μM picrotoxin were added to block AMPAR and γ-aminobutyric acid type A receptor–mediated PSCs, respectively. Intracellular pipette solution contained 116 mM K-gluconate, 6 mM KCl, 8 mM NaCl, 0.2 mM EGTA, 2 mM MgATP, 0.3 mM Na$_3$GTP, and 10 mM Hepes, adjusted to pH 7.25 with KOH. QX-314 (2.5 mM) was included into the pipette solution to block action potential firing. EPSCs were acquired at 5 kHz and filtered at 2 kHz as described for cell lines at a holding potential of −70 mV. EPSCs were measured in 5-min periods in the presence of NBQX (baseline) and NBQX + D-serine (100 μM), as indicated. After D-serine treatment, 2-amino-5-phosphonopentanoic acid (50 μM) was added to validate that EPSCs recorded were NMDAR-mediated. pClamp10/Clampfit10.6 (Molecular Devices) was used to record, detect, and analyze the amplitude, interevent interval, and charge transfer (as area under the curve, in pA*ms) from single EPSCs.

Quantitative analysis of total and stereoselective amino acids in human samples

Amino acid analysis was performed on an ACQUITY UPLC H-class instrument (Waters Co., Milford, MA, USA) with a reversed-phase C-18 column using water and acetonitrile, 0.1% formic acid as mobile phases (run time, 9 min). The detection was performed with a Xevo TQD triple-quadrupole mass spectrometer (Waters Co., Milford,

MA, USA) using positive electrospray ionization in the multiple reaction monitoring mode. For the quantification of L– and D–amino acids enantiomers of human biological fluids (plasma and CSF), a UPLC-MS/MS–based method was performed, using N-(4-nitrophenoxycarbonyl)-L-phenylalanine 2-methoxyethyl ester [(S)-NIFE method], as previously reported (74). Briefly, EDTA-anticoagulated plasma and CSF samples were collected from control age-matched individuals (normal diet) and from the patient (before and after L-serine dietary supplementation, for plasma analysis; after L-serine supplement, for CSF analysis), as previously described (75). All samples were stored at −80°C until use. Plasma and CSF samples were mixed with internal standard solution. After 10 min of incubation at 4°C, ice-cold acetonitrile was added, and the mixture was incubated for >15 min on ice. Precipitates were removed by centrifugation, and the supernatant was evaporated to dryness under a stream of nitrogen, using a heating block set to 40°C. The residue was dissolved in water, followed by the addition of sodium tetraborate and (S)-NIFE solution in acetonitrile. After 10 min of incubation at RT, the reaction was terminated by hydrogen chloride addition. The derivatized and filtrated samples were immediately separated on a 100 mm by 2.1 mm ACQUITY 1.7-µm BEH C18 column, using an ACQUITY UPLC system coupled to a Xevo tandem MS (Waters Co., Milford, MA, USA).

Untargeted sphingolipidomic studies in human samples

Plasma samples were processed and analyzed as previously described (76). Briefly, total lipid extract was obtained from 100 µl of plasma, using modified Bligh and Dyer extraction (77). Plasma total lipid extracts were separated on an Dionex UltiMate 3000 UPLC system (Thermo Fisher Scientific, San Jose, CA, USA) using a kinetex C_8 150×2.1 mm, 2.6-µm column (Phenomenex, Sydney, NSW, Australia). After injection of the samples (10 µl), the column effluent was directly introduced into the heated electrospray ionization source of an Orbitrap Fusion mass spectrometer (Thermo Fisher Scientific, San Jose, CA, USA), and analysis was performed in positive ionization mode. The relative quantification of lipid species was obtained from the area of their corresponding individual chromatographic peaks.

Statistical analysis

Comparison between experimental groups was evaluated using InStat software (GraphPad Software Inc.), applying a one-way ANOVA, followed by a Bonferroni post hoc test for multiple comparisons or a repeated measures two-way ANOVA for Sholl analysis. For single comparisons, either Student's t test (for parametric data) or Mann-Whitney U test (for nonparametric data) was used. Data are presented as means ± SEM from at least three independent experiments.

SUPPLEMENTARY MATERIALS

stke.sciencemag.org/cgi/content/full/12/586/eaaw0936/DC1

Fig. S1. Protein interactions and cellular trafficking of GluN2Bwt- and GluN2B(P553T)-containing NMDARs.
Fig. S2. Altered biophysical properties of heterotrimeric GluN1-GluN2A-GluN2B(P553T) NMDARs.
Fig. S3. GluN2B(P553T) mutation alters GluA1 abundance in hippocampal neurons.
Fig. S4. Alignment of eumetazoan iGluRs showing the residues conservation of Pro[553] and Phe[653].
Table S1. Untargeted analysis of plasma sphingolipid profile in the GRIN2B(P553T) patient before and after L-serine dietary supplementation.
References (78, 79)

REFERENCES AND NOTES

1. A. Rett, On a unusual brain atrophy syndrome in hyperammonemia in childhood. Wien. Med. Wochenschr. 116, 723–726 (1966).

2. M. Chahrour, H. Y. Zoghbi, The story of Rett syndrome: From clinic to neurobiology. Neuron 56, 422–437 (2007).

3. B. Hagberg, J. Aicardi, K. Dias, O. Ramos, A progressive syndrome of autism, dementia, ataxia, and loss of purposeful hand use in girls: Rett's syndrome: Report of 35 cases. Ann. Neurol. 14, 471–479 (1983).

4. R. E. Amir, I. B. Van den Veyver, M. Wan, C. Q. Tran, U. Francke, H. Y. Zoghbi, Rett syndrome is caused by mutations in X-linked MECP2, encoding methyl-CpG-binding protein 2. Nat. Genet. 23, 185–188 (1999).

5. J. L. Neul, H. Y. Zoghbi, Rett syndrome: A prototypical neurodevelopmental disorder. Neuroscientist 10, 118–128 (2004).

6. F. F. Hamdan, J. Gauthier, Y. Araki, D.-T. Lin, Y. Yoshizawa, K. Higashi, A.-R. Park, D. Spiegelman, S. Dobrzeniecka, A. Piton, H. Tomitori, H. Daoud, C. Massicotte, E. Henrion, O. Diallo, M. Shekarabi, C. Marineau, M. Shevell, B. Maranda, G. Mitchell, A. Nadeau, G. D'Anjou, M. Vanasse, M. Srour, R. G. Lafrenière, P. Drapeau, J. C. Lacaille, E. Kim, J.-R. Lee, K. Igarashi, R. L. Huganir, G. A. Rouleau, J. L. Michaud, Excess of de novo deleterious mutations in genes associated with glutamatergic systems in nonsyndromic intellectual disability. Am. J. Hum. Genet. 88, 306–316 (2011).

7. D. Soto, X. Altafaj, C. Sindreu, À. Bayés, Glutamate receptor mutations in psychiatric and neurodevelopmental disorders. Commun. Integr. Biol. 7, e27887 (2014).

8. L. Volk, S.-L. Chiu, K. Sharma, R. L. Huganir, Glutamate synapses in human cognitive disorders. Annu. Rev. Neurosci. 38, 127–149 (2015).

9. H. Monyer, N. Burnashev, D. J. Laurie, B. Sakmann, P. H. Seeburg, Developmental and regional expression in the rat brain and functional properties of four NMDA receptors. Neuron 12, 529–540 (1994).

10. T. Kutsuwada, K. Sakimura, T. Manabe, C. Takayama, N. Katakura, E. Kushiya, R. Natsume, M. Watanabe, Y. Inoue, T. Yagi, S. Aizawa, M. Arakawa, T. Takahashi, Y. Nakamura, H. Mori, M. Mishina, Impairment of suckling response, trigeminal neuronal pattern formation, and hippocampal LTD in NMDA receptor epsilon 2 subunit mutant mice. Neuron 16, 333–344 (1996).

11. N. Burnashev, P. Szepetowski, NMDA receptor subunit mutations in neurodevelopmental disorders. Curr. Opin. Pharmacol. 20, 73–82 (2015).

12. C. Hu, W. Chen, S. J. Myers, H. Yuan, S. F. Traynelis, Human GRIN2B variants in neurodevelopmental disorders. J. Pharmacol. Sci. 132, 115–121 (2016).

13. K. Platzer, H. Yuan, H. Schütz, A. Winschel, W. Chen, C. Hu, H. Kusumoto, H. O. Heyne, K. L. Helbig, S. Tang, M. C. Willing, B. T. Tinkle, D. J. Adams, C. Depienne, B. Keren, C. Mignot, E. Frengen, P. Strømme, D. Biskup, T. M. Strom, H. C. Mefford, C. T. Myers, A. M. Muir, A. LaCroix, L. Sadleir, I. E. Scheffer, E. Brilstra, M. M. van Haelst, J. J. van der Smagt, L. A. Bok, R. S. Møller, U. B. Jensen, J. J. Millichap, A. T. Berg, E. M. Goldberg, I. De Bie, S. Fox, P. Major, J. R. Jones, E. H. Zackai, R. Abou Jamra, A. Rolfs, R. J. Leventer, J. A. Lawson, T. Roscioli, F. E. Jansen, E. Ranza, C. M. Korff, A.-E. Lehesjoki, C. Courage, T. Linnankivi, D. R. Smith, C. Stanley, M. Mintz, D. McKnight, A. Decker, W.-H. Tan, M. A. Tarnopolsky, L. I. Brady, M. Wolff, L. Dondit, H. F. Pedro, S. E. Parisotto, K. L. Jones, A. D. Patel, D. N. Franz, R. Vanzo, E. Marco, J. D. Ranells, N. Di Donato, W. B. Dobyns, B. Laube, S. F. Traynelis, J. R. Lemke, GRIN2B encephalopathy: Novel findings on phenotype, variant clustering, functional consequences and treatment aspects. J. Med. Genet. 54, 460–470 (2017).

14. J. R. Lemke, R. Hendrickx, K. Geider, B. Laube, M. Schwake, R. J. Harvey, V. M. James, A. Pepler, I. Steiner, K. Hörtnagel, J. Neidhardt, S. Ruf, M. Wolff, D. Bartholdi, R. Caraballo, K. Platzer, A. Suls, P. De Jonghe, S. Biskup, S. Weckhuysen, GRIN2Bmutations in west syndrome and intellectual disability with focal epilepsy. Ann. Neurol. 75, 147–154 (2014).

15. S. Endele, G. Rosenberger, K. Geider, B. Popp, C. Tamer, I. Stefanova, M. Milh, F. Kortüm, A. Fritsch, F. K. Pientka, Y. Hellenbroich, V. M. Kalscheuer, J. Kohlhase, U. Moog, G. Rappold, A. Rauch, H.-H. Ropers, S. von Spiczak, H. Tönnies, N. Villeneuve, L. Villard, B. Zabel, M. Zenker, B. Laube, A. Reis, D. Wieczorek, L. Van Maldergem, K. Kutsche, Mutations in GRIN2A and GRIN2B encoding regulatory subunits of NMDA receptors cause variable neurodevelopmental phenotypes. Nat. Genet. 42, 1021–1026 (2010).

16. J. de Ligt, M. H. Willemsen, B. W. M. van Bon, T. Kleefstra, H. G. Yntema, T. Kroes, A. T. Vulto-van Silfhout, D. A. Koolen, P. de Vries, C. Gilissen, M. del Rosario, A. Hoischen, H. Scheffer, B. B. A. de Vries, H. G. Brunner, J. A. Veltman, L. E. L. M. Vissers, Diagnostic exome sequencing in persons with severe intellectual disability. N. Engl. J. Med. 367, 1921–1929 (2012).

17. B. J. O'Roak, P. Deriziotis, C. Lee, L. Vives, J. J. Schwartz, S. Girirajan, E. Karakoc, A. P. MacKenzie, S. B. Ng, C. Baker, M. J. Rieder, D. A. Nickerson, R. Bernier, S. E. Fisher, J. Shendure, E. E. Eichler, Exome sequencing in sporadic autism spectrum disorders identifies severe de novo mutations. Nat. Genet. 43, 585–589 (2011).

18. J.-P. Mothet, A. T. Parent, H. Wolosker, R. O. Brady Jr., D. J. Linden, C. D. Ferris, M. A. Rogawski, S. H. Snyder, D-serine is an endogenous ligand for the glycine site of the N-methyl-D-aspartate receptor. Proc. Natl. Acad. Sci. U.S.A. 97, 4926–4931 (2000).

19. T. Papouin, L. Ladepeche, J. Ruel, S. Sacchi, M. Labasque, M. Hanini, L. Groc, L. Pollegioni, J.-P. Mothet, S.-H. R. Oliet, Synaptic and extrasynaptic NMDA receptors are gated by different endogenous coagonists. Cell 150, 633–646 (2012).

20. M. Lucariello, E. Vidal, S. Vidal, M. Saez, L. Roa, D. Huertas, M. Pineda, E. Dalfó, J. Dopazo, P. Jurado, J. Armstrong, M. Esteller, Whole exome sequencing of Rett syndrome-like patients reveals the mutational diversity of the clinical phenotype. *Hum. Genet.* **135**, 1343–1354 (2016).

21. M. Alsaloum, R. Kazi, Q. Gan, J. Amin, L. P. Wollmuth, A molecular determinant of subtype-specific desensitization in ionotropic glutamate receptors. *J. Neurosci.* **36**, 2617–2622 (2016).

22. S. F. Traynelis, L. P. Wollmuth, C. J. McBain, F. S. Menniti, K. M. Vance, K. K. Ogden, K. B. Hansen, H. Yuan, S. J. Myers, R. Dingledine, Glutamate receptor ion channels: Structure, regulation, and function. *Pharmacol. Rev.* **62**, 405–496 (2010).

23. V. Vyklicky, B. Krausova, J. Cerny, M. Ladislav, T. Smejkalova, B. Kysilov, M. Korinek, S. Danacikova, M. Horak, H. Chodounska, E. Kudova, L. Vyklicky, Surface expression, function, and pharmacology of disease-associated mutations in the membrane domain of the human GluN2B subunit. *Front. Mol. Neurosci.* **11**, 110 (2018).

24. E. Gratacòs-Batlle, N. Yefimenko, H. Cascos-García, D. Soto, AMPAR interacting protein CPT1C enhances surface expression of GluA1-containing receptors. *Front. Cell. Neurosci.* **8**, 469 (2015).

25. K. R. Tovar, M. J. McGinley, G. L. Westbrook, Triheteromeric NMDA receptors at hippocampal synapses. *J. Neurosci.* **33**, 9150–9160 (2013).

26. D. Stroebel, S. Carvalho, T. Grand, S. Zhu, P. Paoletti, Controlling NMDA receptor subunit composition using ectopic retention signals. *J. Neurosci.* **34**, 16630–16636 (2014).

27. M. P. Regalado, A. Villarroel, J. Lerma, Intersubunit cooperativity in the NMDA receptor. *Neuron* **32**, 1085–1096 (2001).

28. W. Li, X. Xu, L. Pozzo-Miller, Excitatory synapses are stronger in the hippocampus of Rett syndrome mice due to altered synaptic trafficking of AMPA-type glutamate receptors. *Proc. Natl. Acad. Sci. U.S.A.* **113**, E1575–E1584 (2016).

29. M. Benveniste, J. Clements, L. Vyklický Jr., M. L. Mayer, A kinetic analysis of the modulation of *N*-methyl-D-aspartic acid receptors by glycine in mouse cultured hippocampal neurones. *J. Physiol.* **428**, 333–357 (1990).

30. D. Liao, R. H. Scannevin, R. Huganir, Activation of silent synapses by rapid activity-dependent synaptic recruitment of AMPA receptors. *J. Neurosci.* **21**, 6008–6017 (2001).

31. W.-Y. Lu, H.-Y. Man, W. Ju, W. S. Trimble, J. F. MacDonald, Y. T. Wang, Activation of synaptic NMDA receptors induces membrane insertion of new AMPA receptors and LTP in cultured hippocampal neurons. *Neuron* **29**, 243–254 (2001).

32. D. A. Fortin, M. A. Davare, T. Srivastava, J. D. Brady, S. Nygaard, V. A. Derkach, T. R. Soderling, Long-term potentiation-dependent spine enlargement requires synaptic Ca^{2+}-permeable AMPA receptors recruited by CaM-kinase I. *J. Neurosci.* **30**, 11565–11575 (2010).

33. H. Wolosker, D. T. Balu, J. T. Coyle, The rise and fall of the D-serine-mediated gliotransmission hypothesis. *Trends Neurosci.* **39**, 712–721 (2016).

34. H. Wolosker, S. Blackshaw, S. H. Snyder, Serine racemase: A glial enzyme synthesizing D-serine to regulate glutamate-*N*-methyl-D-aspartate neurotransmission. *Proc. Natl. Acad. Sci. U.S.A.* **96**, 13409–13414 (1999).

35. P. Paoletti, C. Bellone, Q. Zhou, NMDA receptor subunit diversity: Impact on receptor properties, synaptic plasticity and disease. *Nat. Rev. Neurosci.* **14**, 383–400 (2013).

36. C. A. Chapleau, G. D. Calfa, M. C. Lane, A. J. Albertson, J. L. Larimore, S. Kudo, D. L. Armstrong, A. K. Percy, L. Pozzo-Miller, Dendritic spine pathologies in hippocampal pyramidal neurons from Rett syndrome brain and after expression of Rett-associated *MECP2* mutations. *Neurobiol. Dis.* **35**, 219–233 (2009).

37. B. J. O'Roak, L. Vives, S. Girirajan, E. Karakoc, N. Krumm, B. P. Coe, R. Levy, A. Ko, C. Lee, J. D. Smith, E. H. Turner, I. B. Stanaway, B. Vernot, M. Malig, C. Baker, B. Reilly, J. M. Akey, E. Borenstein, M. J. Rieder, D. A. Nickerson, R. Bernier, J. Shendure, E. E. Eichler, Sporadic autism exomes reveal a highly interconnected protein network of de novo mutations. *Nature* **485**, 246–250 (2012).

38. J. R. Lemke, R. Hendrickx, K. Geider, B. Laube, M. Schwake, R. J. Harvey, V. M. James, A. Pepler, I. Steiner, K. Hörtnagel, J. Neidhardt, S. Ruf, M. Wolff, D. Bartholdi, R. Caraballo, K. Platzer, A. Suls, P. De Jonghe, S. Biskup, S. Weckhuysen, *GRIN2B* mutations in west syndrome and intellectual disability with focal epilepsy. *Ann. Neurol.* **75**, 147–154 (2014).

39. L. G. Harsing Jr., P. Matyus, Mechanisms of glycine release, which build up synaptic and extrasynaptic glycine levels: The role of synaptic and non-synaptic glycine transporters. *Brain Res. Bull.* **93**, 110–119 (2013).

40. P. E. Chen, M. T. Geballe, E. Katz, K. Erreger, M. R. Livesey, K. K. O'Toole, P. Le, C. J. Lee, J. P. Snyder, S. F. Traynelis, D. J. A. Wyllie, Modulation of glycine potency in rat recombinant NMDA receptors containing chimeric NR2A/2D subunits expressed in *Xenopus laevis* oocytes. *J. Physiol.* **586**, 227–245 (2008).

41. S. M. Dravid, P. B. Burger, A. Prakash, M. T. Geballe, R. Yadav, P. Le, K. Vellano, J. P. Snyder, S. F. Traynelis, Structural determinants of D-cycloserine efficacy at the NR1/NR2C NMDA receptors. *J. Neurosci.* **30**, 2741–2754 (2010).

42. J. Jaeken, M. Detheux, J. P. Fryns, J. F. Collet, P. Alliet, E. Van Schaftingen, Phosphoserine phosphatase deficiency in a patient with Williams syndrome. *J. Med. Genet.* **34**, 594–596 (1997).

43. J. H. Yang, A. Wada, K. Yoshida, Y. Miyoshi, T. Sayano, K. Esaki, M. O. Kinoshita, S. Tomonaga, N. Azuma, M. Watanabe, K. Hamase, K. Zaitsu, T. Machida, A. Messing, S. Itohara, Y. Hirabayashi, S. Furuya, Brain-specific *Phgdh* deletion reveals a pivotal role for L-serine biosynthesis in controlling the level of D-serine, an *N*-methyl-D-aspartate receptor co-agonist, in adult brain. *J. Biol. Chem.* **285**, 41380–41390 (2010).

44. R. Levin, A. E. Dor-Abarbanel, S. Edelman, A. R. Durrant, K. Hashimoto, D. C. Javitt, U. Heresco-Levy, Behavioral and cognitive effects of the *N*-methyl-D-aspartate receptor co-agonist D-serine in healthy humans: Initial findings. *J. Psychiatr. Res.* **61**, 188–195 (2015).

45. F. R. Turpin, B. Potier, J. R. Dulong, P.-M. Sinet, J. Alliot, S. H. R. Oliet, P. Dutar, J. Epelbaum, J.-P. Mothet, J.-M. Billard, Reduced serine racemase expression contributes to age-related deficits in hippocampal cognitive function. *Neurobiol. Aging* **32**, 1495–1504 (2011).

46. J.-M. Billard, D-Serine in the aging hippocampus. *J. Pharm. Biomed. Anal.* **116**, 18–24 (2015).

47. S. N. van der Crabben, N. M. Verhoeven-Duif, E. H. Brilstra, L. Van Maldergem, T. Coskun, E. Rubio-Gozalbo, R. Berger, T. J. de Koning, An update on serine deficiency disorders. *J. Inherit. Metab. Dis.* **36**, 613–619 (2013).

48. S. S. Sparrow, D. V. Cicchetti, Diagnostic uses of the Vineland Adaptive Behavior Scales. *J. Pediatr. Psychol.* **10**, 215–225 (1985).

49. H. Li, R. Durbin, Fast and accurate short read alignment with Burrows-Wheeler transform. *Bioinformatics* **25**, 1754–1760 (2009).

50. À. Bayés, L. N. van de Lagemaat, M. O. Collins, M. D. R. Croning, I. R. Whittle, J. S. Choudhary, S. G. N. Grant, Characterization of the proteome, diseases and evolution of the human postsynaptic density. *Nat. Publ. Group* **14**, 19–21 (2011).

51. À. Bayés, M. O. Collins, C. M. Galtrey, C. Simonnet, M. Roy, M. D. R. Croning, G. Gou, L. N. van de Lagemaat, D. Milward, I. R. Whittle, C. Smith, J. S. Choudhary, S. G. N. Grant, Human post-mortem synapse proteome integrity screening for proteomic studies of postsynaptic complexes. *Mol. Brain* **7**, 88 (2014).

52. P. Kumar, S. Henikoff, P. C. Ng, Predicting the effects of coding non-synonymous variants on protein function using the SIFT algorithm. *Nat. Protoc.* **4**, 1073–1081 (2009).

53. I. A. Adzhubei, S. Schmidt, L. Peshkin, V. E. Ramensky, A. Gerasimova, P. Bork, A. S. Kondrashov, S. R. Sunyaev, A method and server for predicting damaging missense mutations. *Nat. Publ. Group* **7**, 248–249 (2010).

54. Y. Choi, A. P. Chan, PROVEAN web server: A tool to predict the functional effect of amino acid substitutions and indels. *Bioinformatics* **31**, 2745–2747 (2015).

55. J. M. Schwarz, D. N. Cooper, M. Schuelke, D. Seelow, MutationTaster2: Mutation prediction for the deep-sequencing age. *Nat. Methods* **11**, 361–362 (2014).

56. P. C. Ng, S. Henikoff, Predicting the effects of amino acid substitutions on protein function. *Annu. Rev. Genomics Hum. Genet.* **7**, 61–80 (2006).

57. Y. Choi, G. E. Sims, S. Murphy, J. R. Miller, A. P. Chan, Predicting the functional effect of amino acid substitutions and indels. *PLOS ONE* **7**, e46688 (2012).

58. M. J. Landrum, J. M. Lee, G. R. Riley, W. Jang, W. S. Rubinstein, D. M. Church, D. R. Maglott, ClinVar: Public archive of relationships among sequence variation and human phenotype. *Nucleic Acids Res.* **42**, D980–D985 (2014).

59. P. D. Stenson, M. Mort, E. V. Ball, K. Shaw, A. D. Phillips, D. N. Cooper, The Human Gene Mutation Database: Building a comprehensive mutation repository for clinical and molecular genetics, diagnostic testing and personalized genomic medicine. *Hum. Genet.* **133**, 1–9 (2014).

60. International HapMap 3 Consortium, D. M. Altshuler, P. Yu, L. Peltonen, P. E. Bonnen, R. A. Gibbs, P. I. W. de Bakker, P. Deloukas, S. B. Gabriel, R. Gwilliam, S. Hunt, M. Inouye, X. Jia, A. Palotie, M. Parkin, P. Whittaker, K. Chang, A. Hawes, L. R. Lewis, Y. Ren, D. Wheeler, D. M. Muzny, C. Barnes, K. Darvishi, M. Hurles, J. M. Korn, K. Kristiansson, C. Lee, S. A. McCarrol, J. Nemesh, E. Dermitzakis, S. B. Montgomery, S. Pollack, N. Soranzo, C. Gonzaga-Jauregui, A. Keinan, V. Anttila, W. Brodeur, M. J. Daly, S. Leslie, G. McVean, L. Moutsianas, H. Nguyen, S. F. Schaffner, Q. Zhang, M. J. R. Ghori, R. McGinnis, W. McLaren, A. L. Price, F. Takeuchi, S. R. Grossman, I. Shlyakhter, E. B. Hostetter, P. C. Sabeti, C. A. Adebamowo, M. W. Foster, D. R. Gordon, J. Licinio, M. C. Manca, P. A. Marshall, I. Matsuda, D. Ngare, V. O. Wang, D. Reddy, C. N. Rotimi, C. D. Royal, R. R. Sharp, C. Zeng, L. D. Brooks, J. E. McEwen, Integrating common and rare genetic variation in diverse human populations. *Nature* **467**, 52–58 (2010).

61. E. Karakas, H. Furukawa, Crystal structure of a heterotetrameric NMDA receptor ion channel. *Science* **344**, 992–997 (2014).

62. B. Webb, A. Sali, Comparative protein structure modeling using MODELLER. *Curr. Protoc. Bioinformatics* **47**, 5.6.1–5.6.32 (2014).

63. Q. Wang, A. A. Canutescu, R. L. Dunbrack Jr., SCWRL and MolIDE: Computer programs for side-chain conformation prediction and homology modeling. *Nat. Protoc.* **3**, 1832–1847 (2008).

64. A. Cordomí, G. Caltabiano, L. Pardo, Membrane protein simulations using AMBER force field and Berger lipid parameters. *J. Chem. Theory Comput.* **8**, 948–958 (2012).

65. S. Pronk, S. Páll, R. Schulz, P. Larsson, P. Bjelkmar, R. Apostolov, M. R. Shirts, J. C. Smith, P. M. Kasson, D. van der Spoel, B. Hess, E. Lindahl, GROMACS 4.5: A high-throughput and highly parallel open source molecular simulation toolkit. *Bioinformatics* **29**, 845–854 (2013).

66. A. Riesgo, N. Farrar, P. J. Windsor, G. Giribet, S. P. Leys, The analysis of eight transcriptomes from all poriferan classes reveals surprising genetic complexity in sponges. *Mol. Biol. Evol.* **31**, 1102–1120 (2014).

67. R. C. Edgar, MUSCLE: Multiple sequence alignment with high accuracy and high throughput. *Nucleic Acids Res.* **32**, 1792–1797 (2004).

68. K. Tamura, G. Stecher, D. Peterson, A. Filipski, S. Kumar, MEGA6: Molecular evolutionary genetics analysis version 6.0. *Mol. Biol. Evol.* **30**, 2725–2729 (2013).

69. F. Ronquist, M. Teslenko, P. van der Mark, D. L. Ayres, A. Darling, S. Höhna, B. Larget, L. Liu, M. A. Suchard, J. P. Huelsenbeck, MrBayes 3.2: Efficient Bayesian phylogenetic inference and model choice across a large model space. *Syst. Biol.* **61**, 539–542 (2012).

70. S. Vicini, J. F. Wang, J. H. Li, W. J. Zhu, Y. H. Wang, J. H. Luo, B. B. Wolfe, D. R. Grayson, Functional and pharmacological differences between recombinant *N*-methyl-D-aspartate receptors. *J. Neurophysiol.* **79**, 555–566 (1998).

71. C. Grau, K. Arató, J. M. Fernández-Fernández, A. Valderrama, C. Sindreu, C. Fillat, I. Ferrer, S. de la Luna, X. Altafaj, DYRK1A-mediated phosphorylation of GluN2A at Ser(1048) regulates the surface expression and channel activity of GluN1/GluN2A receptors. *Front. Cell. Neurosci.* **8**, 331 (2014).

72. J. Schindelin, C. T. Rueden, M. C. Hiner, K. W. Eliceiri, The ImageJ ecosystem: An open platform for biomedical image analysis. *Mol. Reprod. Dev.* **82**, 518–529 (2015).

73. F. J. Sigworth, The variance of sodium current fluctuations at the node of Ranvier. *J. Physiol.* **307**, 97–129 (1980).

74. W. F. Visser, N. M. Verhoeven-Duif, R. Ophoff, S. Bakker, L. W. Klomp, R. Berger, T. J. de Koning, A sensitive and simple ultra-high-performance-liquid chromatography-tandem mass spectrometry based method for the quantification of D-amino acids in body fluids. *J. Chromatogr. A* **1218**, 7130–7136 (2011).

75. A. Ormazabal, À. García-Cazorla, Y. Fernández, E. Fernández-Álvarez, J. Campistol, R. Artuch, HPLC with electrochemical and fluorescence detection procedures for the diagnosis of inborn errors of biogenic amines and pterins. *J. Neurosci. Methods* **142**, 153–158 (2005).

76. A. Seyer, S. Boudah, S. Broudin, C. Junot, B. Colsch, Annotation of the human cerebrospinal fluid lipidome using high resolution mass spectrometry and a dedicated data processing workflow. *Metabolomics* **12**, 91 (2016).

77. E. G. Bligh, W. J. Dyer, A rapid method of total lipid extraction and purification. *Can. J. Biochem. Physiol.* **37**, 911–917 (1959).

78. A. M. Waterhouse, J. B. Procter, D. M. A. Martin, M. Clamp, G. J. Barton, Jalview version 2—A multiple sequence alignment editor and analysis workbench. *Bioinformatics* **25**, 1189–1191 (2009).

79. D. Ramos-Vicente, J. Ji, E. Gratacòs-Batlle, G. Gou, R. Reig-Viader, D. Burguera, E. Navas-Perez, J. García-Fernández, P. Fuentes-Prior, H. Escriva, N. Roher, D. Soto, À. Bayés, Metazoan evolution of glutamate receptors reveals unreported phylogenetic groups and divergent lineage-specific events. *eLife* **7**, e35774 (2018).

Citation: D. Soto, M. Olivella, C. Grau, J. Armstrong, C. Alcon, X. Gasull, A. Santos-Gómez, S. Locubiche, M. Gómez de Salazar, R. García-Díaz, E. Gratacòs-Batlle, D. Ramos-Vicente, E. Chu-Van, B. Colsch, V. Fernández-Dueñas, F. Ciruela, À. Bayés, C. Sindreu, A. López-Sala, À. García-Cazorla, X. Altafaj, L-Serine dietary supplementation is associated with clinical improvement of loss-of-function *GRIN2B*-related pediatric encephalopathy. *Sci. Signal.* **12**, eaaw0936 (2019).

Science Signaling

l-Serine dietary supplementation is associated with clinical improvement of loss-of-function *GRIN2B*-related pediatric encephalopathy

David Soto, Mireia Olivella, Cristina Grau, Judith Armstrong, Clara Alcon, Xavier Gasull, Ana Santos-Gómez, Sílvia Locubiche, Macarena Gómez de Salazar, Roberto García-Díaz, Esther Gratacòs-Batlle, David Ramos-Vicente, Emeline Chu-Van, Benoit Colsch, Víctor Fernández-Dueñas, Francisco Ciruela, Àlex Bayés, Carlos Sindreu, Anna López-Sala, Àngels García-Cazorla and Xavier Altafaj

Treating NMDA receptor deficiency with a dietary supplement

Patients with Rett-like syndrome show impaired neuronal, motor, cognitive, and social development. Soto *et al.* studied the etiology and treatment of the disorder in a 5-year-old patient who had a mutation in *GRIN2B*, the gene encoding the NMDA receptor subunit GluN2B. Expressing this mutant in cultured neurons impaired both electrophysiological activity and dendritic morphology, but these features were improved with the application of the known NMDA receptor agonist, d-serine. d-Serine administration has some toxicity in rodents, but its stereoisomer l-serine is a natural, nonessential amino acid found in various foods. Adding l-serine powder to the patient's food or drink over the course of more than a year increased the amount of d-serine in the plasma and cerebrospinal fluid and markedly improved all neurodevelopment assessments, suggesting that this rather simple treatment might be extended to various patients with disorders associated with NMDA receptor deficiency.

ARTICLE TOOLS	http://stke.sciencemag.org/content/12/586/eaaw0936
SUPPLEMENTARY MATERIALS	http://stke.sciencemag.org/content/suppl/2019/06/14/12.586.eaaw0936.DC1
RELATED CONTENT	http://stke.sciencemag.org/content/sigtrans/11/542/eaar4481.full http://stke.sciencemag.org/content/sigtrans/10/504/eaan0852.full http://stke.sciencemag.org/content/sigtrans/11/513/eaan8784.full http://science.sciencemag.org/content/sci/355/6331/eaal3729.full http://stke.sciencemag.org/content/sigtrans/12/593/eaau9122.full http://stke.sciencemag.org/content/sigtrans/12/603/eaay0300.full http://stke.sciencemag.org/content/sigtrans/12/603/eaaw9315.full http://stke.sciencemag.org/content/sigtrans/12/603/eaay8960.full http://stke.sciencemag.org/content/sigtrans/13/638/eaaw1519.full
REFERENCES	This article cites 79 articles, 14 of which you can access for free http://stke.sciencemag.org/content/12/586/eaaw0936#BIBL
PERMISSIONS	http://www.sciencemag.org/help/reprints-and-permissions

Use of this article is subject to the Terms of Service

GENERAL ARTICLE

Disease-associated GRIN protein truncating variants trigger NMDA receptor loss-of-function

Ana Santos-Gómez[1], Federico Miguez-Cabello[2,3], Adrián García-Recio[1,4], Sílvia Locubiche-Serra[1,5], Roberto García-Díaz[2,6,7], Víctor Soto-Insuga[8], Rosa Guerrero-López[9], Natalia Juliá-Palacios[10], Francisco Ciruela[1,11], Àngels García-Cazorla[10], David Soto[2,3], Mireia Olivella[12,13,*] and Xavier Altafaj[1,2,3,*,†]

[1]Neuroscience Program, Bellvitge Biomedical Research Institute (IDIBELL), L'Hospitalet de Llobregat, 08908 Barcelona, Spain, [2]Neurophysiology Laboratory, Department of Biomedicine, Faculty of Medicine and Health Sciences, Institute of Neurosciences, University of Barcelona, 08036 Barcelona, Spain, [3]August Pi i Sunyer Biomedical Research Institute (IDIBAPS), Hospital Clínic, University of Barcelona, 08036 Barcelona, Spain, [4]Laboratory of Computational Medicine, 08500 Bellaterra, Spain, [5]ZeClinics SL, Germans Trias i Pujol Research Institute (IGTP), 08916 Badalona, Spain, [6]Chemistry and Biotechnology Research Group (QUIBIO), University of Santiago de Cali, 111321 Cali, Colombia, [7]Protein Research Group, Chemistry Department, Colombia National University, Bogotá, Colombia, [8]Neurology Service, Hospital Niño Jesús, 28009 Madrid, Spain, [9]Instituto de Investigaciones Biomédicas Alberto Sols, CSIC/UAM and Centro de Investigación Biomédica en Red de Enfermedades Raras, CIBERER, 28029 Madrid, Spain, [10]Neurometabolic Unit, Department of Neurology. Hospital Sant Joan de Déu and CIBERER, 08950 Barcelona, Spain, [11]Department of Pathology and Experimental Therapeutics, Faculty of Medicine and Health Sciences, Institute of Neurosciences, University of Barcelona, 08908 Barcelona, Spain, [12]School of International Studies, ESCI-UPF, 08003 Barcelona, Spain and [13]Bioinformatics and Medical Statistics Group. Universitat de Vic-Universitat Central de Catalunya, 08500 Vic, Spain

*To whom correspondence should be addressed. Tel: (+34) 938 815 519; Email: mireia.olivella@esci.upf.edu (M.O.); Tel: (+34) 934 024 519; Email: xaltafaj@ub.edu (X.A.)

Abstract

De novo GRIN variants, encoding for the ionotropic glutamate NMDA receptor subunits, have been recently associated with GRIN-related disorders, a group of rare paediatric encephalopathies. Current investigational and clinical efforts are focused to functionally stratify *GRIN* variants, towards precision therapies of this primary disturbance of glutamatergic transmission that affects neuronal function and brain. In the present study, we aimed to comprehensively delineate the functional outcomes and clinical phenotypes of GRIN protein truncating variants (PTVs)—accounting for ∼20% of disease-associated *GRIN* variants—hypothetically provoking NMDAR hypofunctionality. To tackle this question, we created a comprehensive *GRIN* PTVs variants database compiling a cohort of nine individuals harbouring GRIN PTVs, together with previously identified variants, to build-up an extensive *GRIN* PTVs repertoire composed of 293 unique variants. Genotype–phenotype

correlation studies were conducted, followed by cell-based assays of selected paradigmatic GRIN PTVs and their functional annotation. Genetic and clinical phenotypes meta-analysis revealed that heterozygous *GRIN1*, *GRIN2C*, *GRIN2D*, *GRIN3A* and *GRIN3B* PTVs are non-pathogenic. In contrast, heterozygous *GRIN2A* and *GRIN2B* PTVs are associated with specific neurological clinical phenotypes in a subunit- and domain-dependent manner. Mechanistically, cell-based assays showed that paradigmatic pathogenic GRIN2A and GRIN2B PTVs result on a decrease of NMDAR surface expression and NMDAR-mediated currents, ultimately leading to NMDAR functional haploinsufficiency. Overall, these findings contribute to delineate GRIN PTVs genotype–phenotype association and *GRIN* variants stratification. Functional studies showed that GRIN2A and GRIN2B pathogenic PTVs trigger NMDAR hypofunctionality, and thus accelerate therapeutic decisions for this neurodevelopmental condition.

Introduction

Glutamate is the main excitatory amino acid neurotransmitter in the brain, with about 90% of excitatory synapses using glutamate for neuronal communication. Upon release in the synaptic cleft, glutamate acts on a group of transmembrane receptors functionally separated into metabotropic (mGluRs) and ionotropic glutamate receptors (iGluRs) families. The latter are pharmacologically divided into three main families, namely *N*-methyl D-aspartate (NMDA), AMPA and kainate acid receptors. NMDA receptors (NMDARs) are critical for neuronal survival, circuits formation and synaptic plasticity processes, among others (1). Concomitantly, disturbance of the NMDAR function, by means of pharmacological, genetic or modulation of protein–protein interactions, can alter NMDAR-mediated currents which, in turn, can affect glutamatergic neurons, circuits and brain activity. Indeed, the alteration of NMDAR-dependent circuits have been associated with neurodevelopmental disorders (NDDs), epilepsy, neuropsychiatric diseases as well as neurodegenerative processes (2).

The NMDAR is an heterotetramer resulting from the oligomerization of two GluN1 subunits and a combination of two additional subunits (GluN2A-D, GluN3A, GluN3B) whose distribution is finely regulated in a spatio-temporal manner (1). The subunit composition dictates the cellular and temporal expression pattern, subcellular localization and channel properties of the NMDAR, a coincidence detector of pre- and post-synaptic activities (1,3). With the emergence of next-generation sequencing, a growing number of genetic studies reported the association between genetic variants of *GRIN* genes (encoding for GluN subunits of the NMDAR) and neurological disorders. Initial studies describing *de novo GRIN2A* and *GRIN2B* mutations in discrete individuals with intellectual disability (ID) and/or epilepsy (4–6), together with exome analysis implementation in clinical diagnosis and functional studies, allowed to define GRDs (OMIM # 138 249, 138 253,138 252 and 602 717, for GRIN1-, GRIN2A-, GRIN2B- and GRIN2D-related disorders, respectively).

GRDs are a group of rare paediatric encephalopathies resulting from the presence of pathogenic *GRIN* gene variants. To date, about 500 individuals harbouring likely pathogenic *GRIN* variants have been reported worldwide (www.grin-database.de), although GRD prevalence is probably underestimated as for other NDD of genetic origin. Clinically, this neurodevelopmental condition is manifested by a spectrum of neurological and systemic alterations, including ID, hypotonia, communication impairment, epilepsy, movement and sleep disorders and gastrointestinal disturbances (7–12). A comprehensive analysis of *GRIN* gene variants and associated clinical phenotypes, together with the resulting NMDAR structural modelling and functional annotations of *GRIN* variants, strongly supports the view of subunit- and domain-specificity of *GRIN* variants pathogenicity and clinical outcomes. Genetically, GRD mostly results from the

presence of *GRIN de novo* variants, with an autosomal dominant inheritance pattern. *GRIN* variants are predominantly associated with single nucleotide variations causing missense mutations in particularly sensitive domains of GluN subunits. Besides missense mutations (present in 65% of GRD affected individuals), protein truncating variants (PTVs) have also been detected in 23% of individuals with GRD (13). PTVs are defined as genetic variants (nonsense single-nucleotide variants, frameshift insertions or deletions, large structural variants and splice-disrupting SNVs) disrupting transcription and leading to a shortened or absent protein from the mutated allele. Mechanistically, PTVs are hypothesized to provoke a protein loss of function (decrease of protein amounts) though it could potentially also cause gain-of-function effects. Nevertheless, from our knowledge, the functional consequences of *GRIN* PTVs remain elusive.

Here, we present the first study integrating genetic, clinical and functional data related with *GRIN* pathogenic and non-pathogenic PTVs. Our data sheds light on to gene- and domain-specific features of GRIN PTVs, enabling their pathogenicity stratification. Importantly, the delineation of the functional and clinical outcomes associated with GRD PTVs provides genetic and preclinical insights for the definition of personalized therapies for individuals harbouring GRIN PTVs.

Results

Heterozygous GRIN PTVs pathogenicity is gene-dependent

Truncating variants of *GRIN* genes are predicted to introduce a premature stop codon or to disrupt the open reading frame and trigger a premature stop codon. Compared with missense variants, previously reported *GRIN* PTVs likely pathogenic are relatively less abundant (59 out of 226, from (13)). In the present study, we compiled the genetic and clinical information of 10 clinical cases harbouring novel GRIN PTVs referred to our investigational network and proceeded to the functional annotation of representative *GRIN* PTVs. Remarkably, all pathogenic GRIN PTVs are clinically associated with mild-to-moderate ID and movement disorders (Fig. 1A), a relatively more homogeneous and milder phenotype compared with the heterogeneous and severe GRD phenotypes exhibited by individuals carrying pathogenic *GRIN* missense variants (7,8). Nevertheless, these initial observations were find in a reduced cohort of patients and were limited to PTVs affecting GRIN2A and GRIN2B gene products.

In order to evaluate the GRIN-PTV genotype–phenotype association in a larger patients cohort and the potential impact on GRIN genes family, genetic databases were scanned and 293 unique GRIN PTVs (May 2020) and their related clinical symptoms were retrieved (Supplementary Material, Tables S1–S7). Genotype–phenotype analysis showed that GRIN PTVs are

A.

Clinical case	Gender	Gene	Variant	Genotype	Protein changes	Truncated domain(s)	Clinical symptoms
1	Male	*GRIN2A*	GRIN2A-E182fs22	c.544delG	p.E182Nfs22Ter	NTD-LBD-TMD-CTD	Mild intellectual disability. Focal epilepsy idiopathic pharmaco-resistant, evolving to ECSWS. Without hypotonia signs and absence of ASD traits. ADHD
2	Male	*GRIN2A*	GRIN2A-V452fs11	c.1354insT	p.V452Cfs11Ter	LBD-TMD-CTD	Mild intellectual disability, developmental delay, ECSWS, Psychomotor alterations, disturbance of learning, reading and writing skills
3	Female	*GRIN2B*	GRIN2B-R519ter	c.1555C>T	p.Arg519Ter	LBD-TMD-CTD	Mild intellectual disability. No epilepsy, no hypotonia, no ASD traits
4	Female	*GRIN2B*	GRIN2B-D786Mfs23	c.2355delA	p.D786Mfs23Ter	TMD-CTD	Mild intellectual disability, mild hypotonia, abnormal EEG during sleep without seizures, presence of ASD traits. Sleep and digestive problems
5	Female	*GRIN2B*	GRIN2B-E839ter	c.2515G>T	p.Glu839Ter	TMD-CTD	Mild intellectual disability, fine motor skills deficits, abnormal EEG, ECSWS, no ASD traits. Sleep problems, normal GI tract, early puberty, tall
6	Male	*GRIN2B*	GRIN2B-S34Qfs25	c.99insC	p.S34Qfs25Ter	NTD-LBD-TMD-CTD	Mild intellectual disability
7	Female	*GRIN2B*	GRIN2B-K670Vfs5	c.2010insA	p.K670Vfs5Ter	TMD-CTD	Mild intellectual disability, mild hypotonia
8	Female	*GRIN2B*	GRIN2B-het	p.12p13.1(13940589_14112006) del	Haploinsufficiency	GluN2B	Mild intellectual disability, expressive language deficits
9	Female	*GRIN2B*	GRIN2B-R847ter	c.2539-2540CG>TA	p.R847Ter	CTD	Mild intelectual disability. No hypotonia

B.
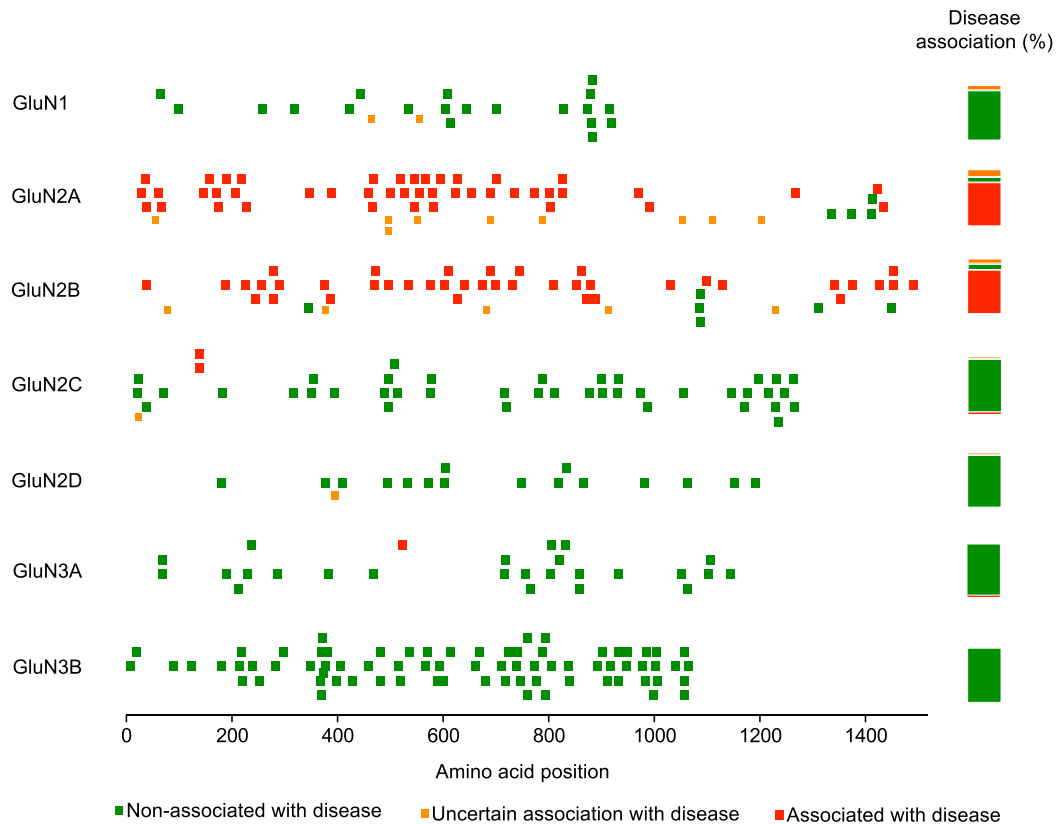
C.

	GRIN1	*GRIN2A*	*GRIN2B*	*GRIN2C*	*GRIN2D*	*GRIN3A*	*GRIN3B*	Total
Associated with disease	0 0,0%	44 77,2%	43 79,6%	2 4,7%	0 0,0%	1 3,8%	0 0,0%	90 30,7%
Uncertain association with disease	2 9,1%	9 15,8%	5 9,3%	1 2,3%	1 5,9%	0 0,0%	0 0,0%	18 6,1%
Non-associated with disease	20 90,9%	4 7,0%	6 11,1%	40 93,0%	16 94,1%	25 96,2%	74 100,0%	185 63,1%
Total	22	57	54	43	17	26	74	293

Figure 1. GRIN PTVs distribution and differential association with neurological disorders. (**A**) Heterozygous *de novo GRIN2A* and *GRIN2B* truncating variants in a European cohort of children with neurological disorders. GI, gastrointestinal tract; EEG, electroencephalogram. GluN subunit domains acronyms: ATD, amino terminal domain; LBD, ligand binding domain; TMD, transmembrane domain; CTD, carboxy terminal domain. (**B**) Scatter plot of PTVs of *GRIN* genes and their distribution along the amino acid sequence (*x*-axis). **Right,** Stacked bars representing the percentage of genetic variants (association, non-association, uncertain association with disease). Green squares: *GRIN* variants non-associated with disease; red squares: disease-associated *GRIN* variants; orange squares: uncertain genetic association and/or functional annotation. (**C**) Summary of *GRIN* truncating variants association with neurological conditions. The table compiles genotype–phenotype correlation of non-pathogenic, disease-associated and uncertain disease-association of *GRIN* truncating variants. *GRIN* PTVs (293) were collected from gnomAD, ClinVar, BCN-GRIN, GRIN-Leipzig and CFERV databases.

scattered along the seven members of the *GRIN* gene family. Disease-association analysis of GRIN PTVs showed that 63.1% are non-associated with neurological disorders (likely non-pathogenic or with recessive inheritance pattern), whereas 30.7% are associated with neurological disorders (pathogenic or likely pathogenic) and 6.1% are of uncertain association with neurological symptoms (PTV conflicting description both in GRD individuals and in healthy population) (Fig. 1 and Supplementary Material, Tables S1–S7).

Remarkably, genotype–phenotype analysis revealed a strong association of GRIN PTVs with neurological disorders in a gene-dependent manner (Fig. 1B and C). Gene-specific analysis showed that *de novo* heterozygous *GRIN1* truncating variants (21) are invariably non-pathogenic. Noteworthy, the two only GRIN1 PTVs (p.R488Afs22Ter and biallelic *GRIN1* (p.Q556Ter/Q556Ter) associated with neurological conditions were inherited, indicating a non-dominant inheritance pattern of these particular variants (Fig. 1, Supplementary Material, Table S1). Conversely, heterozygous GRIN2A and GRIN2B PTVs are mostly associated with neurological disorders (77.2 and 79.6% disease-association versus 7.0 and 11.1% non-disease-association, respectively; Fig. 1, Supplementary Material, Tables S2 and S3). The distribution of disease-associated variants along these genes revealed a high vulnerability of truncations located at the amino terminal (ATD), agonist binding (ABD) and transmembrane (TMD) domains. In contrast, truncations affecting GluN2A and GluN2B carboxy terminal domains (CTDs) were heterogeneously associated with complex neurological disorders (e.g. schizophrenia or autism spectrum disorders (ASDs), for GRIN2A and GRIN2B, respectively). Despite the strong association between truncations affecting the non-CTD domains and neurological conditions, three *GRIN2A* (p.H595Wfs20Ter, p.H595Sfs60Ter and p.E58Ter) and a single *GRIN2B* (p.Q331Sfs5Ter) variants were reported in the gnomAD database. Functional annotation of these variants showed their deficiency to reach the cell surface, leading to a significant reduction of NMDAR-mediated currents (Supplementary Material, Fig. S1). Accordingly, these PTVs were conservatively annotated as variants of uncertain association with neurological conditions.

Genetic analysis showed that *de novo* GRIN2C PTVs are not associated with clinical phenotypes (40 out of 41; Fig. 1C, Supplementary Material, Table S4), with the exception of GRIN2C (p.P132fs192Ter) detected in a subject with schizophrenia. Similarly, *GRIN3A* PTVs are neutral (25 *de novo* variants), with only one inherited *GRIN3A* variant (p.Q508Ter) associated with schizophrenia (Fig. 1B and C, Supplementary Material, Table S6). Truncations of *GRIN2D* and *GRIN3B* genes (16 and 74 variants, respectively) are invariably not associated with neurological disorders (Fig. 1B and C, Supplementary Material, Tables S5 and S7), with the exception of GRIN2D (c.1412G > A) transition potentially affecting GRIN2D splicing site and detected in an individual with schizophrenia (15).

Overall, genetic association studies and variants distribution along NMDAR domains indicate a strong gene-dependent pathogenic effect of heterozygous *GRIN* truncations. In terms of functional annotation, these findings support the pathogenicity of heterozygous *GRIN2A* and *GRIN2B* truncations of the extracellular and transmembrane domains, while the pathogenicity of truncations affecting the CTD of GluN2A or GluN2B subunits is variable and not yet predictable. Moreover, heterozygous PTVs affecting *GRIN1*, *GRIN2C-D* and *GRIN3A-B* genes are almost non-associated with disease, with the exception of discrete cases of schizophrenia.

Clinical phenotypes associated with pathogenic GRIN2A and GRIN2B PTVs

Individuals with GRDs display a spectrum of clinical symptoms not yet completely delineated. In order to establish the genotype–phenotype correlation of pathogenic GRIN PTVs, the clinical annotations for the different variants were manually curated and integrated. The analysis of the clinical symptoms exhibited by individuals harbouring PTVs of GRIN2A and GRIN2B revealed striking clinical hallmarks. Importantly, all pathogenic *GRIN2A* PTVs showed association with different types of epilepsy syndromes, ranging from mild focal epilepsy (benign epilepsy with centro-temporal spikes, BECTS) to epileptic encephalopathies (continuous spike-and-wave during slow-wave sleep, ECSWS; Landau–Kleffner syndrome, LKS), with variable comorbidity with ID (57% of GRIN2A PTVs cases; Fig. 2). In contrast, while seizures are almost absent in subjects harbouring GRIN2B PTVs, genotype–phenotype analysis revealed a higher presence of ID and ASDs traits (85 and 40%, respectively; Fig. 2). Interestingly, GRIN2A and GRIN2B pathogenic truncations are associated with mild-to-moderate forms of ID, in comparison to disease-associated *GRIN2A* and *GRIN2B* missense variants that are associated with more severe ID (7,8).

Heterozygous *GRIN1* truncations do not alter NMDAR-mediated currents

Gene truncations provoke a shortening of the open reading frame, which in turn results in the lack of the corresponding distal domains. In the context of *GRIN* genes, truncations might affect different aspects of the NMDAR biogenesis and/or channel properties, although the pathophysiological mechanisms remain elusive. In order to determine the molecular and biophysical mechanisms underlying *GRIN* gene-dependent vulnerability to truncations, paradigmatic *GRIN* PTV were assessed along cell-based assays. First, we explored the gene dosage effect in *GRIN1* PTVs, by transiently expressing different ratios of *GRIN1* wild-type versus truncated constructs in cellular models.

Electrophysiological experiments were conducted in HEK293T cells transiently expressing wild-type *GRIN2A* and *GRIN1* (wild-type and truncating variants) at different stoichiometric conditions. Electrophysiological studies showed that *GRIN1* truncations do not affect NMDAR-mediated current density in cells co-transfected with HA-Grin1 PTVs and wild-type GFP-Grin2A constructs (P-value > 0.05 for all comparisons; Fig. 3A and B). In contrast, biallelic GRIN1(p.Q556Ter) truncation resulted in the absence of measurable NMDAR-mediated currents in cells expressing GluN2Awt-GluN1(Q556Ter)$_2$ (<0.1 pA/pF NMDAR-mediated currents, $N = 10$ patched cells; data not shown). Further analysis showed that heterozygous *GRIN1* truncations do not alter channel properties (e.g. rise-time, desensitization and deactivation rates) of GluN2Awt-GluN1(wt/trunc) receptors (Fig. 3C–E).

These data suggest that either GluN1 truncated subunits are not assembled into functional NMDARs—and do not affect NMDAR cell surface density—or, alternatively, they form functional NMDARs without interfering channel properties. In order to address these hypotheses, immunofluorescence analysis of NMDAR subunits was conducted. Transient co-transfection of wild-type GFP-GRIN2B and equimolar DNA amounts of HA-GRIN1 (wt:PTV) showed no changes on GFP-GluN2B (NMDARs) surface expression in COS-7 cells ($P > 0.05$; Fig. 3F). In contrast, transfection mimicking biallelic GRIN1(p.Q556Ter) truncation condition resulted in a complete loss of NMDAR surface

A.

	GRIN2A PTVs	*GRIN2B* PTVs
Clinically Reported *	38	29
Developmental delay	20	18
Intellectual disability (ID)	25	27
Mild ID	10	5
Moderate ID	6	6
Severe ID	1	3
ID (% clinically reported cases)	65,8%	93,1%
Epilepsy	21	3
CSWS	5	1
BECT	3	0
LKS	1	0
Focal epilepsy	8	3
Epilepsy events	37	8
EPI (% clinically reported cases)	97,4%	27,6%
Hypotonia	1	2
Speech Disorder	15	0
Speech Disorder (% clinically reported cases)	39,5%	0
ASD traits	0	11
ASD (% clinically reported cases)	0,0%	37,9%
ADHD	1	1
SCZ	0	1

B.
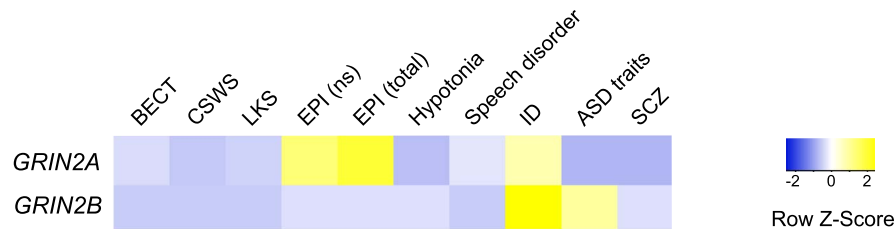
Figure 2. Clinical phenotypes associated with disease-associated *GRIN2A* and *GRIN2B* PTVs. (**A**) Clinical symptoms of individuals harbouring pathogenic GRIN2A or GRIN2B PTVs, represented as the percentage of individuals over the total number of reported clinical cases. (**B**) Phenotype-based heat maps displaying the relative abundance of clinical symptoms in clinically reported individuals harbouring GRIN2A and GRIN2B PTVs. EPI(ns), epilepsy without detailed epileptic symptoms description; EPI (total), individuals with epilepsy symptoms.

expression ($P < 0.0001$; Fig. 3F), in agreement with previous data showing negligible NMDAR-mediated currents in HEK293T cells. The lack of NMDARs surface expression was also observed in cells transiently expressing other biallelic GRIN1 truncations ($P < 0.0001$; Supplementary Material, Fig. S2). Furthermore, a more detailed analysis of the different NMDAR subunits surface expression was conducted, based on the detection

of differentially tagged-GluN subunits resulting from the expression of wild-type GFP-GRIN1 (GFP in the amino terminal domain, (14)), truncated HA-Grin1 and Flag-Grin2b constructs. Immunofluorescence analysis using anti-GFP antibody in non-permeabilized cells showed that GFP-GluN1 wild-type surface expression remains unaltered by the expression of truncated HA-GluN1 subunits ($P > 0.05$; Fig. 3G). In contrast,
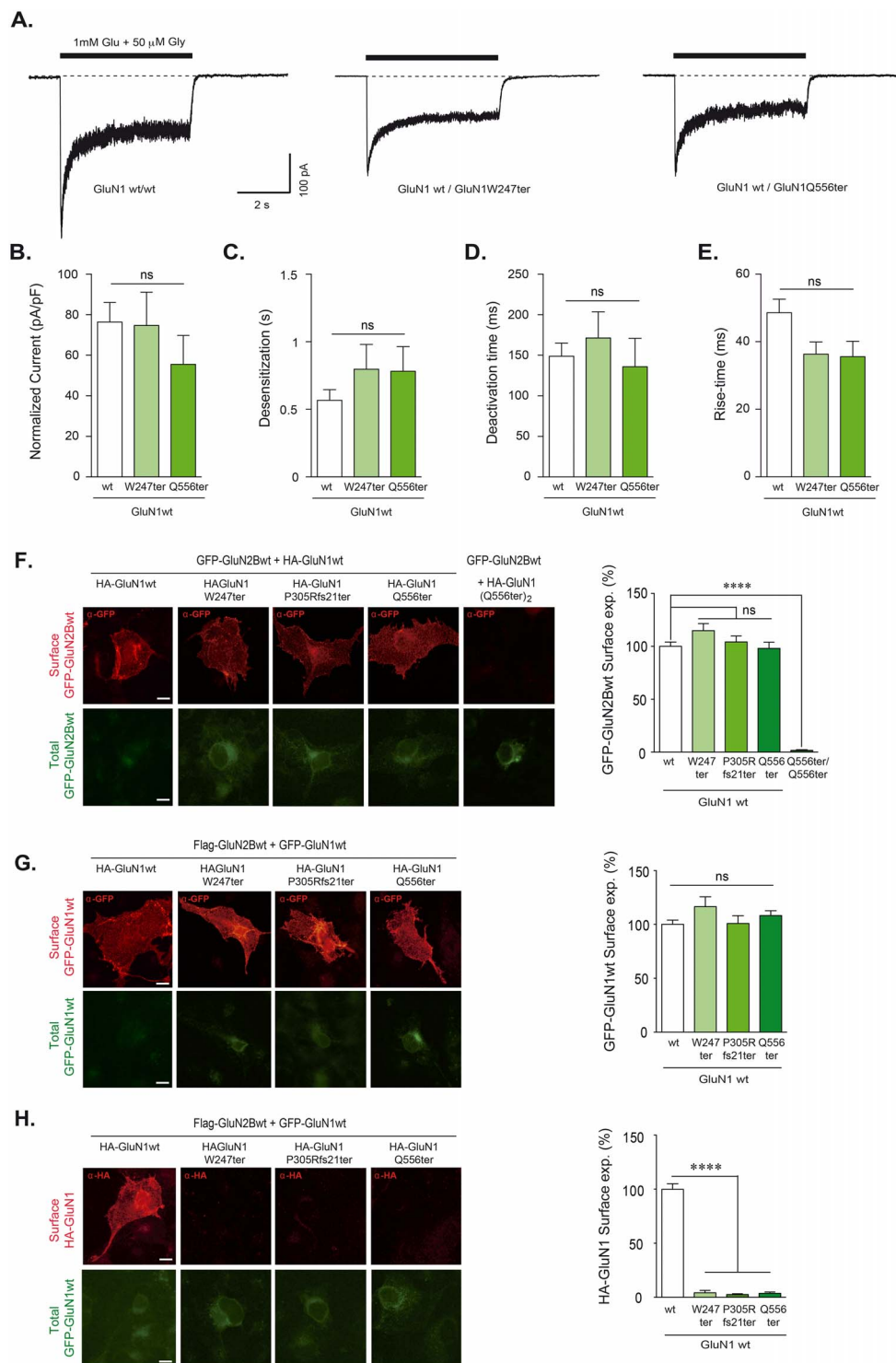
Figure 3. Functional annotation of *GRIN1* PTVs. (**A**) Representative whole-cell currents evoked by rapid application of 1 mM glutamate plus 50 μM glycine (0.5-second duration; −60 mV) in HEK-293 T cells expressing (GluN2Awt)$_2$-(GluN1wt)$_2$ (left trace), (GluN2A)$_2$-GluN1wt/GluN1-PTVs (center and right traces). (**B**) Bar graph representing normalized peak currents of cells transfected with Grin2a together with equimolar amounts of Grin1 constructs (wt/mock/PTVs). (**C–E**) Bar graphs representing mean ± SEM of rise-time (panel C), desensitization (panel D) and deactivation (panel E) rates of NMDAR-mediated currents in HEK293 cells expressing (GluN2A)$_2$-(GluN1wt)$_2$, (GluN2A)$_2$-(GluN1wt/GluN1-PTVs). ns, P-value > 0.05; one-way ANOVA with Dunnett's multiple comparison test or Kruskal–Wallis with Dunn's multiple comparison test. (**F–H**) **Left,** Immunofluorescence analysis of NMDAR surface expression in COS-7 cell line co-transfected with GFP-Grin2b and HA-Grin1 (wild-type and/or truncated) constructs (panel F) or Flag-Grin2b, GFP-Grin1 and HA-Grin1 (wild-type and/or truncated) constructs (panels G, H); scale bar: 10 μm; **Right,** Bar graphs representing the mean ± SEM of cell surface expression of NMDAR (N = 16–38 cells per condition, from 3 to 4 independent experiments; ns, P-value > 0.05; ****, P-value < 0.0001, one-way ANOVA with Bonferroni's *post hoc* test).

non-permeabilized cells incubated with anti-HA showed a lack of truncated HA-GluN1 subunit surface expression ($P < 0.0001$; Fig. 3H). Overall, these data suggest that truncated GluN1 subunits are unable to assemble and, consequently, do not reach the plasma membrane. Together with this observation, our findings showing that heterozygous *GRIN1* truncations do not disturb overall NMDARs surface expression and NMDAR-mediated currents indicate that *GRIN1* monoallelic truncation is not limiting for NMDAR biogenesis in heterologous expression systems. These data are in agreement with the abovementioned genotype–phenotype correlations, showing no association between heterozygous *GRIN1* truncations and neurodevelopmental conditions.

Disease-associated GRIN2A PTVs functionally recapitulate *GRIN2A* haploinsufficiency

Genotype–phenotype studies indicate a strong relationship between truncating *GRIN2A* variants and NDDs. In order to shed light into the genetic dominant effect of *GRIN2A* PTVs, their potential pathophysiological impact was evaluated using cell-based assays. Electrophysiological experiments were conducted in HEK293T cells transiently expressing different Grin2a wt:PTV stoichiometric ratios. Normalized current density analysis showed that disease-associated GRIN2A PTVs drastically reduce NMDAR-mediated peak current (P-value < 0.001 for all comparisons; Fig. 4A and B) without disturbing NMDAR activation, desensitization or deactivation rates ($P > 0.05$ for all comparisons) in cells expressing GluN1(wt)$_2$-(GluN2Awt/PTV), recapitulating GRIN2A haploinsufficiency condition (Fig. 4C–E). These data suggested the absence of GRIN2A PTVs dominant negative effect on the NMDARs wild-type pool, and further cell surface expression experiments were conducted to evaluate this hypothesis. Immunofluorescence analysis of COS-7 cells transiently co-transfected with HA-Grin1 and equimolar DNA ratios of GFP-tagged GRIN2A wild-type and Grin2a truncated constructs, showed a significant decrease of total HA-GluN1 surface expression ($P < 0.0001$; Fig. 4F). These data indicate that heterozygous expression of GRIN2A-PTV, together with one GRIN2A wild-type allele, significantly decreases the surface expression of total NMDARs. Furthermore, in order to specifically determine GluN2A wild-type and GluN2A truncated subunits surface expression, COS-7 cells were co-transfected with GRIN1, GFP-GRIN2Awt and HA-GRIN2A wt/PTV (E182Nfs23ter or V452Cfs11ter) constructs. Immunofluorescence analysis showed that GRIN2A PTV allele resulted in a net reduction of surface expression of wild-type GluN2A subunit ($P < 0.0001$; Fig. 4G), and no surface expression was detected for the truncated GluN2A subunits ($P < 0.0001$; Fig. 4H). Interestingly, the lack of surface expression was confirmed in COS-7 co-transfected with GRIN1 and biallelic GRIN2A truncations affecting the NTD, LBD and TMD domains, while those affecting the CTD exhibited a normal surface trafficking (Supplementary Material, Fig. S2). Overall, these findings support the view that GRIN2A PTVs of the non-CTD functionally recapitulate GRIN2A haploinsufficiency condition, rather than exerting a dominant negative effect on wild-type *GRIN2A* allele.

Disease-associated GRIN2B PTVs functionally recapitulate *GRIN2B* haploinsufficiency

Despite the clustering of clinical symptoms with *GRIN2A* and *GRIN2B* PTVs (Fig. 2), we hypothesized that heterozygous GRIN2B PTVs pathophysiologic mechanisms would be similar to GRIN2A

PTVs. Hence, cell-based functional annotation of representative *GRIN2B* truncations associated with GRD was conducted. Electrophysiological experiments were performed in HEK293T cells transiently expressing the combinations of *GRIN1* and *GRIN2B* constructs (wild-type, R519Ter, D786Mfs23Ter, E839Ter) at different stoichiometric conditions (wt/wt versus wt/trunc). As for GRIN2A PTVs, disease-associated GRIN2B PTVs showed a significant reduction of NMDAR-mediated peak currents in whole-cell patch clamp experiments ($P < 0.001$; Fig. 5A and B) without disturbing NMDAR gating parameters (e.g. rise time, activation and deactivation rates; Fig. 5C–E).

Immunofluorescence studies were performed in COS-7 cells transiently co-transfected with HA-GRIN1wt and equimolar GFP-GRIN2Bwt and GFP-GRIN2Bwt/PTV ratios. Immunolabelling of surface HA-GluN1 subunit showed a significant decrease of total NMDARs surface expression ($P < 0.0001$; Fig. 5E). In order to specifically evaluate potential alterations on GluN2B PTVs surface expression, HA-GRIN1, flag-GRIN2Bwt and GFP-GRIN2Bwt/PTV (R519Ter, D786Mfs23Ter or E839Ter) were co-transfected in COS-7 cells. Immunofluorescence analysis showed an almost negligible detection of truncated GluN2B subunits surface expression ($P < 0.0001$; Fig. 5F), indicating GluN2B PTVs deficiency to assemble and/or to reach the plasma membrane. Interestingly, the lack of surface expression was confirmed in COS-7 cells co-transfected with Grin1 and biallelic Grin2b truncations affecting the NTD, LBD and TMD domains, while those affecting the CTD (non-related with neurological disorders) exhibited a normal surface trafficking (Supplementary Material, Fig. S2).

Previous reports have described the modulatory effect of the GluN subunits domain CTD for a proper trafficking and retention of NMDARs in cell lines (16,17). In order to evaluate whether GRIN2B-CTD truncation might have an impact on surface density of the NMDAR in a neuronal context, disease-associated GRIN2B PTVs disrupting the TMD4 (E839Ter) and the proximal part of the CTD (R847Ter) were generated and expressed either in COS-7 cell line (together with GluN1 subunits) or in primary mouse neuronal cultures. Surface expression analysis of transfected GRIN2B PTVs revealed that, despite the CTD of GluN2B subunit is not required for surface expression of the NMDAR in COS-7 cells ($P < 0.0001$; Supplementary Material, Fig. S3A), truncation of the CTD results in a significant reduction of GluN2B(R847Ter) ($P < 0.001$ or < 0.0001 for neurons transfected with Grin2b versus Grin2b-E839Ter or Grin2b-R847Ter, respectively; Supplementary Material, Fig. S3B). Overall, these results support an haploinsufficiency-like effect of GRD-associated GRIN2B PTVs, rather than form a dominant negative effect on Grin2b wild-type alleles expressed in primary neurons.

Discussion

In the present study, we performed a comprehensive genotype–phenotype analysis of *GRIN* PTVs, delineating *GRIN PTV* pathogenicity scenario. Our findings indicate that GRIN PTVs' pathogenicity is both subunit- and domain-specific, with clinical outcomes dictated by the identity of the truncated *GRIN* gene. Briefly, while heterozygous *GRIN1*, *GRIN2C*, *GRIN2D*, *GRIN3A* and *GRIN3B* truncations are not associated with autosomal dominant neurodevelopmental conditions, non-CTD PTVs of *GRIN2A* and *GRIN2B* genes are invariably related with NDDs, mostly associated with ID, epilepsy (*GRIN2A* PTVs) and/or autism traits (*GRIN2B* PTVs). Mechanistically, our data indicate that disease-associated *GRIN2A* and *GRIN2B* PTVs result in a reduction of
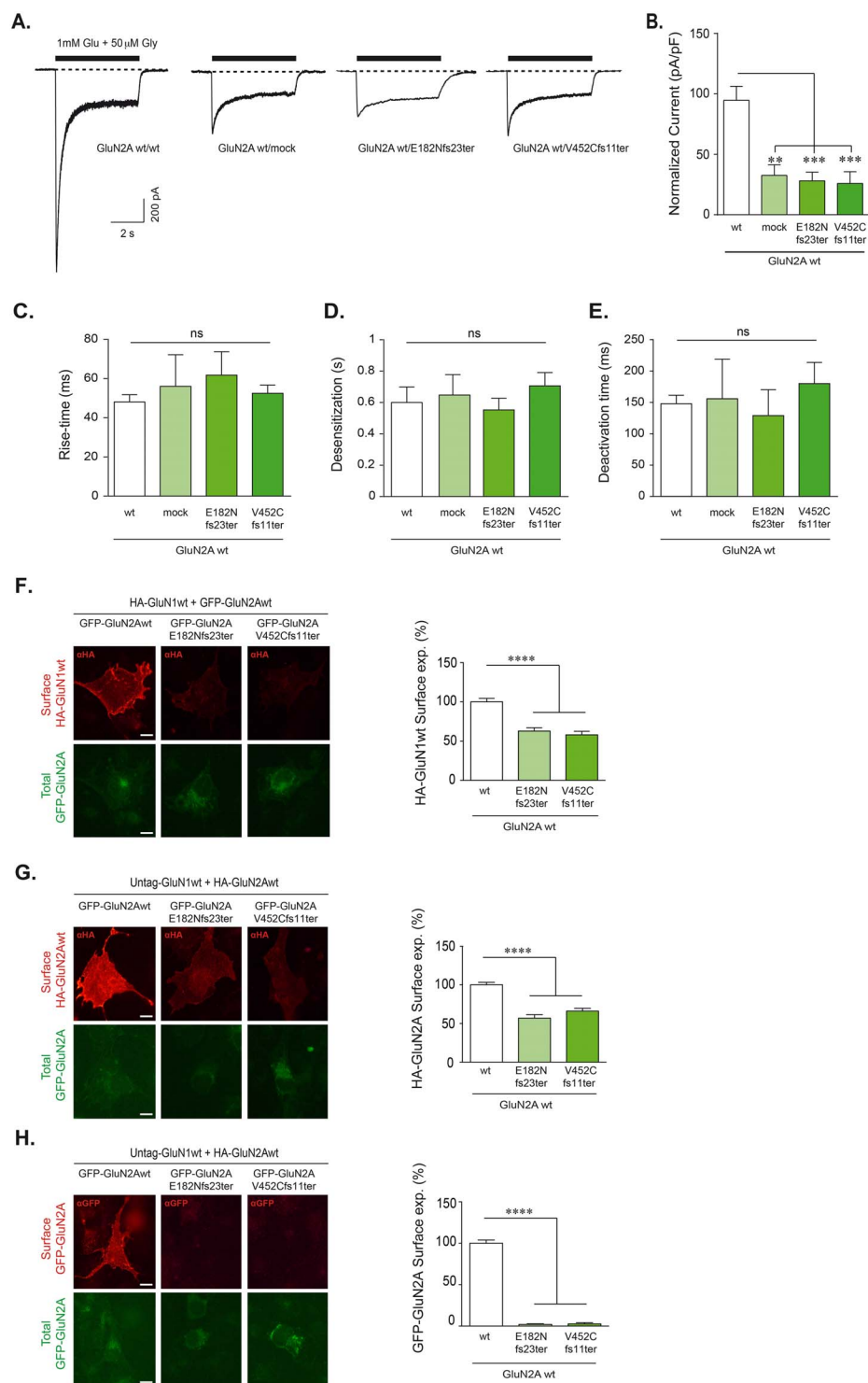
Figure 4. Functional annotation of representative *de novo* GRIN2A PTVs associated with neurological conditions. **(A)** Representative whole-cell currents evoked by rapid application of 1 mM glutamate plus 50 μM glycine (0.5-second duration; −60 mV) in HEK-293 T cells expressing (GluN1)$_2$-(GluN2Awt)$_2$ (left trace), (GluN1)$_2$-GluN2Awt (hemizygous, 'mock' condition), (GluN1)$_2$-GluN2Awt/PTVs. **(B)** Bar graph representing mean ± SEM normalized peak currents of cells transfected with Grin1 together with different stoichiometric amounts of Grin2a constructs (wt/mock/PTVs). **(C–E) Left,** Bar graphs representing mean ± SEM of rise-time (panel C), desensitization (panel D) and deactivation (panel E) rates of NMDAR-mediated currents in HEK293 cells expressing (GluN1)$_2$-(GluN2Awt)$_2$, (GluN1)$_2$-GluN2Awt/− and (GluN1)$_2$-GluN2Awt/PTVs. ns, P-value > 0.05; **, P-value < 0.01; ***, P-value < 0.001; ****, P-value < 0.0001; one-way ANOVA with Dunnett's multiple comparison test or Kruskal–Wallis with Dunn's multiple comparison test. **(F–H)** Immunofluorescence analysis of NMDAR surface expression in COS-7 cell line co-transfected with HA-Grin1 and GFP-Grin2a (wild-type and/or truncated) constructs (panel F) or Untag-Grin1, HA-Grin2a and GFP-Grin2a (wild-type and/or truncated) constructs (panels G, H); scale bar: 10 μm; **Right,** Bar graph representing the mean ± SEM of cell surface expression of NMDAR (N = 21–66 cells per condition, from 3 to 4 independent experiments; ns, P-value > 0.05; ****, P-value < 0.0001; one-way ANOVA with Bonferroni's *post hoc* test).
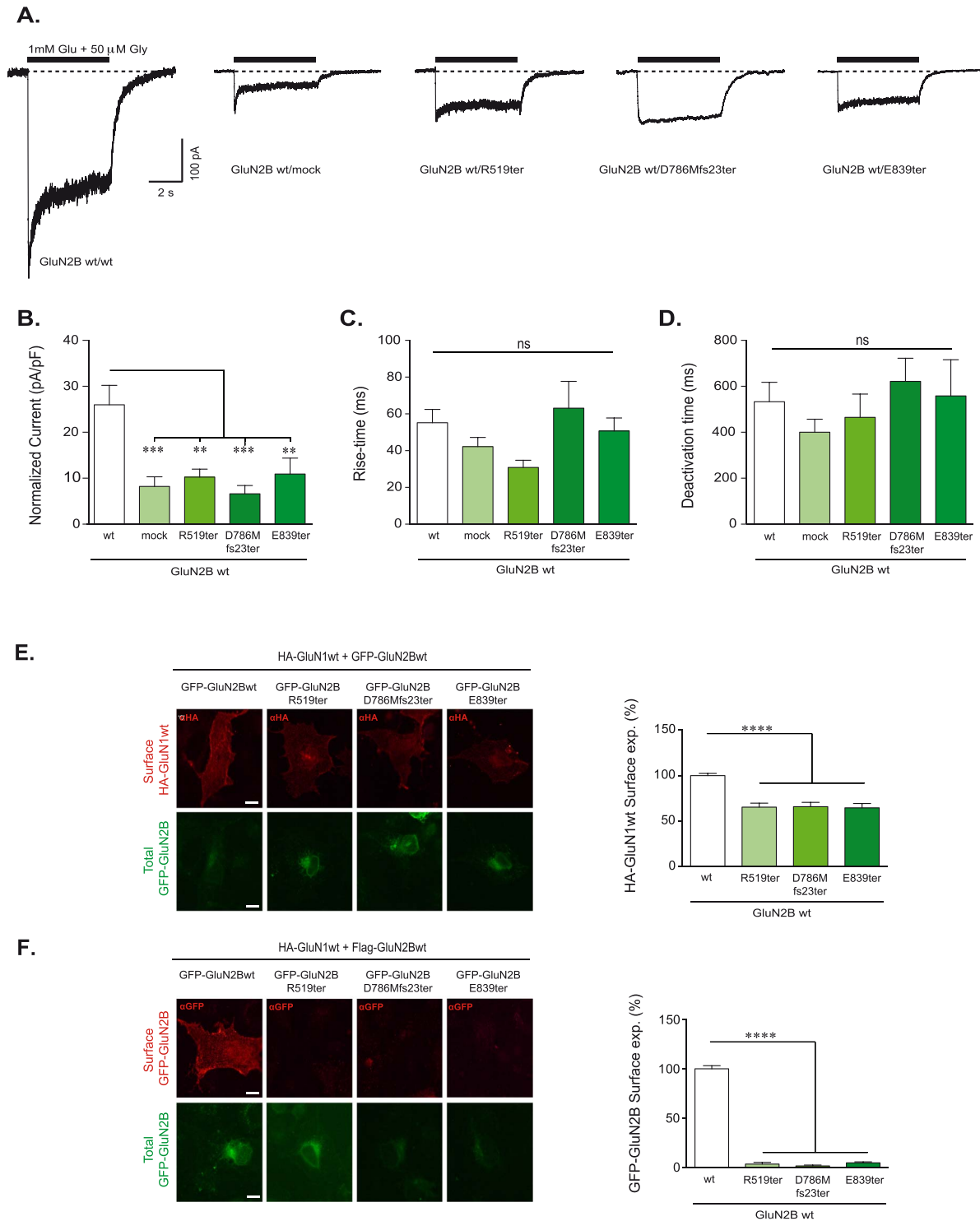
Figure 5. Functional annotation of representative *de novo GRIN2B* PTVs associated with neurological conditions. (**A**) Representative whole-cell currents evoked by rapid application of 1 mM glutamate plus 50 μM glycine (0.5-second duration; −60 mV) in HEK-293 T cells expressing $(GluN1)_2$-$(GluN2Bwt)_2$ (left trace), $(GluN1)_2$-GluN2Bwt (hemizygous, 'mock' condition), $(GluN1)_2$-GluN2Bwt/PTVs. (**B**) Bar graph representing mean ± SEM normalized peak currents of cells transfected with Grin1 together with different equimolar amounts of Grin2b constructs (wt/mock/PTVs). (**C** and **D**) Bar graphs representing mean ± SEM of rise-time (panel C) and deactivation (panel D) rate of NMDAR-mediated currents in HEK293 cells expressing $(GluN1)_2$-$(GluN2Bwt)_2$, $(GluN1)_2$-GluN2Bwt/− and $(GluN1)_2$-GluN2Bwt/PTVs. ns, P-value > 0.05; **, P-value < 0.01; ***, P-value < 0.001; one-way ANOVA with Dunnett's multiple comparison test or Kruskal–Wallis with Dunn's multiple comparison test. (**E** and **F**) **Left,** Immunofluorescence analysis of NMDAR surface expression in COS-7 cell line co-transfected with HA-Grin1 and GFP-Grin2b (wild-type and/or truncated) constructs (panel E) or HA-Grin1, Flag-Grin2b and GFP-Grin2b (wild-type and/or truncated) constructs (panel F); scale bar: 10 μm; **Right,** Bar graphs representing the mean ± SEM of cell surface expression of NMDAR ($N = 20$–86 cells per condition, from 3 to 4 independent experiments; P-value > 0.05; ****, P-value < 0.0001, ns; one-way ANOVA with Bonferroni's *post hoc* test).

NMDARs pool surface density, which invariably causes an overall loss of function.

In general, PTVs lead to a nonsense-mediated decay, a cellular mechanism resulting in loss of function of the truncated protein. Nevertheless, our data showed that with the exception of two non-dominant *GRIN1* variants (c.1342del/p.R448fs22Ter allele from maternal origin, uncertain pathogenicity; p.Q556Ter biallelic variant, reported by Lemke's group (9)), all reported heterozygous *GRIN1* PTVs (20 variants) are not associated with neurological conditions. Theoretically, these findings would indicate that either *GRIN1* gene expression is not critical or, alternatively, wild-type *GRIN1* allele would be sufficient to overcome GRIN1 PTV. GluN1 subunit is invariably present in the NMDAR, which plays a critical role in excitatory glutamatergic neurotransmission (1). Accordingly, *GRIN1* gene product is widely considered a key element in excitatory neurotransmission and brain function. Therefore, the lack of association between *GRIN1* functional haploinsufficiency and clinical outcomes might be attributed to wild-type *GRIN1* allele ability to guarantee physiological NMDAR surface density. In line with this, our data showed that representative GRIN1 PTVs do neither affect NMDAR surface expression nor NMDAR-mediated currents. These findings are in agreement with elegant biochemistry experiments showing GluN1 subunit as a non-limiting subunit for NMDAR biogenesis, whereas GluN2 subunits play a limiting rate (18). Furthermore, $Grin1^{+/-}$ heterozygous mice do not display phenotypic abnormalities, indicating that Grin1 haploinsufficiency—mimicking *Grin1* heterozygous PTVs—is non-pathogenic (19). On the contrary, *GRIN1* missense mutations are strongly linked with NDDs (9,13). This might be due to a dominant negative effect of *GRIN1* missense mutations that result in the incorporation of aberrant amino acids in the GluN1 subunits and abnormal functioning of the mutant GluN1 subunit-containing NMDARs.

Genotype–phenotype correlation studies of GRIN2A and GRIN2B truncations showed similar pathogenicity patterns. Indeed, without considering non-consistent variants, an almost complete pathogenicity versus non-pathogenicity association was detected for *GRIN2A* (37 versus 0 cases, for GluN2A truncations upstream the non-CTD) and *GRIN2B* (24 versus 1 cases for GluN2B truncations upstream the non-CTD) genes. Interestingly, GRIN2A/B PTVs pathogenicity was variable in truncations affecting the CTD, similarly to *GRIN2A* and *GRIN2B* missense mutations (7,8) whose pathogenicity is concentrated at the ABD and TMD, while the CTD is less vulnerable to genetic variation. Mechanistically, our findings strongly suggest that GRIN2A- and GRIN2B-related pathophysiological alterations might result from similar dysfunctions. Indeed, surface expression studies showed that non-CTD GRIN2A and GRIN2B PTVs trigger a decrease of NMDARs surface density, probably due to a defect on subunits assembly and/or a reduction of trafficking to the cell surface. In agreement with this hypothesis, immunofluorescence data showed a strong perinuclear immunosignal (density) of GluN2A or GluN2B PTVs, suggesting the inability of GluN2A and GluN2B truncating variants to exit the endoplasmic reticulum. GluN subunits retention in the ER results from the presence of a retention mechanism that has been proposed as a protein quality control for the NMDAR (20).

PTVs affecting the CTD of GluN2A or GluN2B subunits were found to be heterogeneously associated with NDDs. Functionally, the CTDs of GluN2A and GluN2B subunits are involved in receptor trafficking, docking to plasma membrane and coupling receptors to signalling cascades (3,21,22). Theoretically, GluN2A and GluN2B subunits CTD truncations would neither interfere with GluN subunits assembly nor with NMDAR trafficking to the plasma membrane. Nevertheless, the lack of the PDZ-binding domain (in CTD-truncated GluN2 subunits) would weaken mutant NMDARs-PSD scaffolding proteins interaction, as well as perturbing downstream signalling cascades. In this interactome scenario, we may hypothesize that gene variants affecting NMDAR-interacting proteins (structural) or proteins functionally regulating NMDAR-mediated signalling cascades (upstream and/or downstream) can have synergic/antagonistic effects, dictating the clinical outcome. Further whole exome analysis of gene variants in individuals harbouring *GRIN2A* and *GRIN2B* CTD truncations will contribute to identify potential protective and/or risk genes.

While pathogenic *GRIN* missense variants lead to a continuum of functional outcomes, roughly stratified into gain-of-function, loss-of-function and complex alterations, our study strongly support a pathophysiological scenario in which GRIN PTVs would be invariably associated with NMDAR hypofunctionality. Clinically, individuals harbouring GRIN2A and GRIN2B PTVs exhibit a global developmental delay (DD) and mild-to-moderate ID. In the context of GRD clinical spectrum, these mild cognitive and motor phenotypes might be explained by the reduction of *GRIN2A* and *GRIN2B* PTVs surface expression and NMDAR-mediated currents, without wild-type NMDARs interference. The reduction detected on current density was similar to the haploinsufficiency condition and roughly corresponded to a 50% reduction of current density. This percentage would be in agreement with the observed lack of surface delivery of GRIN2A truncated alleles products, according to an expected Mendelian inheritance pattern. This functional stratification (e.g. pathogenic GRIN2A and GRIN2B PTVs trigger NMDAR hypofunctionality) is critical for the selection of GRD personalized therapies. Despite no rescue experiments have been performed, we can hypothesize that *GRIN2A* and *GRIN2B* PTV could be attenuated by potentiating the NMDAR pool at the cell surface, by means of positive allosteric modulator(s) (PAMs) administration and/or L-serine nutraceutical supplementation, respectively (23,24).

In summary, the present study comprehensively delineates genetic and clinical data associated with GRIN PTVS. Data analysis and functional studies allowed to functional stratify GRIN PTVs, showing that disease-associated *GRIN2A* and *GRIN2B* PTVs result in an haploinsufficiency-like condition potentially treatable with NMDAR potentiators (e.g. nutraceutical L-serine supplementation, PAMs). Overall, these findings contribute to delineate GRDs and unequivocally accelerate *GRIN* variants functional annotation and decision-making of personalized therapeutic interventions.

Materials and Methods

Subjects

Genetic report and clinical information from individuals harbouring GRIN PTVs were provided by referring physicians. All legal guardians provided informed written consent for genetic testing in accordance with the respective national ethics guidelines and with approval of the local ethics committees in the participating study centers.

Database of GRIN PTVs and clinical phenotypes

GRIN PTVs were compiled from ClinVar (www.ncbi.nlm.nih.gov/clinvar), gnomAD (gnomad.broadinstitute.org), GRIN variants databases (lmc-uab.es/grindb/truncations, www.gri

n-database.de, http://functionalvariants.emory.edu/database/index.html) and Pubmed. Nucleotide change, predicted protein sequence, clinical annotation and disease-association were automatically retrieved and integrated under unique entries. Pathogenic and likely pathogenic mutations were classified as disease-associated, while gnomAD variants were classified as non-pathogenic. Furthermore, a conservative annotation was applied and *GRIN* variants inconsistently annotated as pathogenic/non-pathogenic, as well as disease-associated *GRIN* variants with no clinical phenotypes described, were classified as GRIN variants of 'Uncertain Pathogenesis'. Data are compiled in Supplementary Material, Tables S1–S7, and the updated repository accessible at lmc.uab.es/grindb/truncations.

Mice

Adult male and female CD-1 mice (IDIBELL Animal Facilities) were used. The IDIBELL Committee on Animal Use and Care and Autonomous Government (Generalitat de Catalunya) approved the protocol (number: 9108). Following the approved experimental protocol, all animals were supervised daily. Animals were housed and tested in compliance with the guidelines provided by the Guide for the Care and Use of Laboratory Animals and following the European Union guidelines (2010/63/EU). Mice were housed in groups of four in standard cages with ad libitum access to food and water and maintained under a 12 h dark/light cycle (starting at 7:30 a.m.), 22°C temperature and 66% humidity (standard conditions).

Plasmids

The expression plasmids for rat GluN1, GFP-GluN2A and GFP-GluN2B were kindly provided by Dr Vicini (14). Dr Nakanishi provided HA-GluN1 and HA-GluN2A plasmids (25,26), Dr Sanz-Clemente the Flag-GluN2B vector and GFP-GluN1 plasmid was obtained from Dr. Barria (27). Nucleotide changes for the production of *GRIN* variants were achieved by oligonucleotide-directed mutagenesis, using the QuikChange II XL site-directed mutagenesis kit according to the manufacturer's instructions (Stratagene, La Jolla, CA, USA), and verified by Sanger sequencing. All GRIN constructs were generated using rat GRIN cDNA as template, providing a perfect match for all the truncating variants except three human GRIN2A variants (E182Nfs22Ter, H595Wfs20Ter and H595Sfs60Ter) that showed mild changes in the corresponding constructs generated from rat cDNA templates (Grin2a-E182Nfs23Ter, Grin2a-H595Rfs28Ter, Grin2a-H595Lfs60Ter and respectively).

Cell culture and transfection

HEK-293 T and COS-7 cell lines were obtained from the American Type Culture Collection and maintained at 37°C in Dulbecco's modified Eagle's medium, supplemented with 10% fetal calf serum and antibiotics (100 units/ml penicillin and 100 mg/ml streptomycin). Furthermore, D-2-amino-5-phosphonopentanoic acid (D-AP5, Abcam, Cambridge, UK) was added to the medium (0.5-1 mM final concentrations, for HEK-293 T and COS-7 cells, respectively) to avoid excitotoxicity. Transient transfection of HEK-293 T cells was achieved by the calcium phosphate method (Clontech, France) and cell extracts were obtained 48 hours after transfection. COS-7 cells were transfected with Lipofectamine™ 2000 (Invitrogen, Carlsbad, CA, USA) following the manufacturer's instructions, and cells were fixed 24 hours post-transfection, for further immunofluorescence analysis. HEK-293 T were transfected with equimolar amounts of plasmids

encoding for GluN1 and GluN2A/GluN2B subunits, whereas COS-7 cells were transfected with different combinations of tagged subunits, upon the considered allelic (heterozygous or biallelic) conditions. To analyze biallelic expression of GRIN PTV, cells were transfected with equimolar amounts of HA-GluN1 and GFP-GluN2A/GluN2B subunits (1:1), while heterozygous condition was achieved by transfecting equimolar amounts of the wild-type and the truncated variants of the *GRIN* gene of interest (1:0.5:0.5).

Expression experiments in dissociated mouse hippocampal neuron cultures were performed as previously described (24). Briefly, mouse embryos (embryonic day E18) were obtained from pregnant CD1 females; their hippocampi were isolated and maintained in cold Hank's Balanced Salt Solution (HBSS, Gibco, Carlsbad, CA, USA) supplemented with 0.45% glucose (HBSS-Glucose). After carefully removing the meninges, the hippocampi were digested mildly with trypsin, washed in HBSS and resuspended in Neurobasal medium supplemented with 2 mM Glutamax (Gibco, Carlsbad, CA, USA) before filtering in 70-mm mesh filters (BD Falcon, Vaud, Switzerland). The cells were then plated onto glass coverslips (5×10^4 cells/cm^2) coated with 0.1 mg/ml poly-L-lysine (Sigma-Aldrich, St. Louis, MO, USA), and 2 h after plating, the medium was substituted by complete growth medium (Neurobasal medium supplemented with 2% B27 and 2 mM Glutamax). Primary cultures were incubated at 37°C in a humidified 5% CO_2 atmosphere. Every 3–4 days, half of the conditioned medium was removed and replaced by fresh growth medium. Primary cultures were transfected with Lipofectamine™ 2000 (Invitrogen, Carlsbad, CA, USA) on day *in vitro* 11 (DIV11) for further surface expression analysis of GFP-GluN2B constructs.

Immunofluorescence analysis

Transiently transfected COS-7 cells were washed in PBS and fixed with 4% paraformaldehyde (PFA). Surface expression of NMDARs was achieved by immunolabelling the extracellular tags (GFP and HA, inserted in the ATD of the GluN subunits) and incubating the corresponding antibody (anti-GFP, Clontech, France; anti-HA, Covance Inc., Princeton, NJ, USA respectively) for 1 h at RT, under non-permeabilizing conditions. After washing, cells were incubated with secondary antibodies (anti-rabbit IgG or anti-mouse IgG, respectively) conjugated to Alexa fluorochromes (Life Technologies, Carlsbad, CA, USA), for 1 h at RT. The total amount of GFP-tagged GluN subunits was detected by the GFP endogenous fluorescent signal emitted by the GFP-GluN2A/GluN2B construct. Coverslips were mounted in ProLong antifade mounting medium (Life Technologies, Carlsbad, CA, USA) and images were acquired in a Nikon Eclipse 80i microscope (63×/1.4 N.A. immersion oil objective).

To analyze heterologous GluN2B subunit surface expression in primary neuronal cultures, at DIV14, neurons were washed and fixed with 4% PFA in PBS containing 4% sucrose. Surface expression of GFP-GluN2B was detected by incubating with anti-GFP (Life Technologies, Carlsbad, CA, USA) during 1 hour at RT and visualized with an Alexa 488-conjugated goat anti-rabbit Ab (Molecular Probes, Carlsbad, CA, USA). The intracellular pool of GluN2B subunits was identified by permeabilizing cells with 0.1% Triton X-100 and labelling them with anti-GFP-Alexa 555-conjugated Ab (Molecular Probes, Carlsbad, CA, USA), as previously described (28). Images were acquired in a Leica TCS-SL spectral confocal microscope (Leica Microsystems, Wetzlar, Germany) using a Plan-Apochromat 63×/1.4 N.A. immersion oil objective (Leica Microsystems, Wetzlar, Germany) and a pinhole

aperture of 114.54 or 228 μm (for surface receptors). To excite fluorophores, confocal system is equipped with excitation laser beams at 488 and 546 nm. In each experiment, fluorescence intensity was measured in 5–15 COS-7 cells or 1–15 dendrites from at least 7 pyramidal neurons per condition. Fluorescence was quantified using Adobe Photoshop CS5 software (Adobe Systems Inc., San José, CA, USA) and the results are represented as the mean ± standard errors of the mean (SEM) of the surface immunofluorescent signal, analyzing at least three independent experiments.

Electrophysiological recordings of NMDA whole-cell currents in HEK293T cells

Electrophysiological recordings were obtained 38–48 hours after transfection, perfusing the cells continuously at RT with extra-cellular physiological bath solution (in mM): 140 NaCl, 5 KCl, 1 CaCl$_2$, 10 glucose and 10 HEPES, adjusted to pH 7.42 with NaOH. Glutamate (1 mM, Sigma-Aldrich, St. Louis, MO, USA), in the presence of glycine (50 μM; Tocris, Bristol, UK), was applied for 5 seconds by piezoelectric translation (P-601.30; Physik Instrumente, Karlsruhe, Germany) of a theta-barrel application tool made from borosilicate glass (1.5 mm o.d.; Sutter Instruments, Novato, CA, USA), and the activated currents were recorded in the whole-cell configuration at a holding potential of −60 mV, acquired at 5 kHz and filtered at 2 kHz by means of Axopatch 200B amplifier, Digidata 1440A interface and pClamp10 software (Molecular Devices Corporation, San José, CA, USA). Electrodes with open-tip resistances of 2–4 MΩ were made from borosilicate glass (1.5 mm o.d., 0.86 mm i.d., Harvard Apparatus, Holliston, MA, USA), pulled with a PC-10 vertical puller (Narishige, Tokyo, Japan) and filled with intracellular pipette solution containing (in mM): 140 CsCl, 5 EGTA, 4 Na$_2$ATP, 0.1 Na$_3$GTP and 10 HEPES, adjusted to pH 7.25 with CsOH. Glutamate and glycine-evoked currents were expressed as current density (−pA/pF; maximum current divided by input capacitance as measured from the amplifier settings) to avoid differences due to surface area in the recorded cells. The kinetics of deactivation and desensitization of the NMDAR responses were determined by fitting the glutamate/glycine-evoked responses at V_m − 60 mV to a double-exponential function in order to determine the weighted time constant ($\tau_{w,\text{des}}$)

$$\tau_{w,\text{des}} = \tau_f \left(\frac{A_f}{A_f + A_s} \right) + \tau_s \left(\frac{A_s}{A_f + A_s} \right),$$

where A_f and τ_f are the amplitude and time constant of the fast component of desensitization and A_s and τ_s are the amplitude and time constant of the slow component of desensitization.

Statistical analysis

Comparison between experimental groups was evaluated using Prism (GraphPad Software, Inc., San Diego, CA, USA), applying a one-way analysis of variance (ANOVA) followed by a Bonferroni *post hoc* test (cell surface expression experiments) or Dunn's multiple comparison (electrophysiology experiments). For single comparisons, either Student's *t* test (for parametric data) or Mann–Whitney *U*-test (for non-parametric data) was used. Data are presented as the means ± SEM from at least three independent experiments.

Supplementary Material

Supplementary Material is available at *HMG* online.

Acknowledgements

Funding

References

1. Paoletti, P., Bellone, C. and Zhou, Q. (2013) NMDA receptor subunit diversity: impact on receptor properties, synaptic plasticity and disease. *Nat. Rev. Neurosci.*, **14**, 383–400.

2. Lau, C.G. and Zukin, R.S. (2007) NMDA receptor trafficking in synaptic plasticity and neuropsychiatric disorders. *Nat. Rev. Neurosci.*, **8**, 413–426.

3. Traynelis, S.F., Wollmuth, L.P., McBain, C.J., Menniti, F.S., Vance, K.M., Ogden, K.K., Hansen, K.B., Yuan, H., Myers, S.J. and Dingledine, R. (2010) Glutamate receptor ion channels: structure, regulation, and function. *Pharmacol. Rev.*, **62**, 405–496.

4. de Ligt, J., Willemsen, M.H., van Bon, B.W.M., Kleefstra, T., Yntema, H.G., Kroes, T., Vulto-van Silfhout, A.T., Koolen, D.A., de Vries, P., Gilissen, C. *et al.* (2012) Diagnostic exome sequencing in persons with severe intellectual disability. *N. Engl. J. Med.*, **367**, 1921–1929.

5. Tarabeux, J., Kebir, O., Gauthier, J., Hamdan, F.F., Xiong, L., Piton, A., Spiegelman, D., Henrion, É., Millet, B., team, S2.D. *et al.* (2011) Rare mutations in N-methyl-D-aspartate glutamate receptors in autism spectrum disorders and schizophrenia. *Transl. Psychiatry*, **1**, e55–e55.

6. Endele, S., Rosenberger, G., Geider, K., Popp, B., Tamer, C., Stefanova, I., Milh, M., Kortüm, F., Fritsch, A., Pientka, F.K. *et al.* (2010) Mutations in GRIN2A and GRIN2B encoding regulatory subunits of NMDA receptors cause variable neurodevelopmental phenotypes. *Nat. Genet.*, **42**, 1021–1026.

7. Platzer, K., Yuan, H., Schütz, H., Winschel, A., Chen, W., Hu, C., Kusumoto, H., Heyne, H.O., Helbig, K.L., Tang, S. *et al.* (2017) GRIN2B encephalopathy: novel findings on phenotype, variant clustering, functional consequences and treatment aspects. *J. Med. Genet.*, **54**, 460–470.

8. Strehlow, V., Heyne, H.O., Vlaskamp, D.R.M., Marwick, K.F.M., Rudolf, G., de Bellescize, J., Biskup, S., Brilstra, E.H., Brouwer,

O.F., Callenbach, P.M.C. *et al.* (2019) GRIN2A-related disorders: genotype and functional consequence predict phenotype. *Brain*, **142**, 80–92.

9. Lemke, J.R., Geider, K., Helbig, K.L., Heyne, H.O., Schütz, H., Hentschel, J., Courage, C., Depienne, C., Nava, C., Heron, D. *et al.* (2016) Delineating the GRIN1 phenotypic spectrum: a distinct genetic NMDA receptor encephalopathy. *Neurology*, **86**, 2171–2178.

10. Lemke, J.R., Hendrickx, R., Geider, K., Laube, B., Schwake, M., Harvey, R.J., James, V.M., Pepler, A., Steiner, I., Hörtnagel, K. *et al.* (2014) GRIN2B mutations in west syndrome and intellectual disability with focal epilepsy. *Ann. Neurol.*, **75**, 147–154.

11. Carvill, G.L., Regan, B.M., Yendle, S.C., O'Roak, B.J., Lozovaya, N., Bruneau, N., Burnashev, N., Khan, A., Cook, J., Geraghty, E. *et al.* (2013) GRIN2A mutations cause epilepsy-aphasia spectrum disorders. *Nat. Genet.*, **45**, 1073–1076.

12. Lesca, G., Rudolf, G., Bruneau, N., Lozovaya, N., Labalme, A., Boutry-Kryza, N., Salmi, M., Tsintsadze, T., Addis, L., Motte, J. *et al.* (2013) GRIN2A mutations in acquired epileptic aphasia and related childhood focal epilepsies and encephalopathies with speech and language dysfunction. *Nat. Genet.*, **45**, 1061–1066.

13. Xiang Wei, W., Jiang, Y. and Yuan, H. (2018) De novo mutations and rare variants occurring in NMDA receptors. *Curr. Opin. Physiol.*, **2**, 27–35.

14. Vicini, S., Wang, J.F., Li, J.H., Zhu, W.J., Wang, Y.H., Luo, J.H., Wolfe, B.B. and Grayson, D.R. (1998) Functional and pharmacological differences between recombinant N-methyl-D-aspartate receptors. *J. Neurophysiol.*, **79**, 555–566.

15. Yu, Y., Lin, Y., Takasaki, Y., Wang, C., Kimura, H., Xing, J., Ishizuka, K., Toyama, M., Kushima, I., Mori, D. *et al.* (2018) Rare loss of function mutations in N-methyl-D-aspartate glutamate receptors and their contributions to schizophrenia susceptibility. *Transl. Psychiatry*, **8**, 12.

16. Stroebel, D., Carvalho, S., Grand, T., Zhu, S. and Paoletti, P. (2014) Controlling NMDA receptor subunit composition using ectopic retention signals. *J. Neurosci.*, **34**, 16630–16636.

17. Tovar, K.R., McGinley, M.J. and Westbrook, G.L. (2013) Tri-heteromeric NMDA receptors at hippocampal synapses. *J. Neurosci.*, **33**, 9150–9160.

18. Horak, M., Chang, K. and Wenthold, R.J. (2008) Masking of the endoplasmic reticulum retention signals during assembly of the NMDA receptor. *J. Neurosci.*, **28**, 3500–3509.

19. Mohn, A.R., Gainetdinov, R.R., Caron, M.G. and Koller, B.H. (1999) Mice with reduced NMDA receptor expression display behaviors related to schizophrenia. *Cell*, **98**, 427–436.

20. Horak, M. and Wenthold, R.J. (2009) Different roles of C-terminal cassettes in the trafficking of full-length NR1 subunits to the cell surface. *J. Biol. Chem.*, **284**, 9683–9691.

21. Sanz-Clemente, A., Nicoll, R.A. and Roche, K.W. (2013) Diversity in NMDA receptor composition: many regulators, many consequences. *Neuroscientist*, **19**, 62–75.

22. Lussier, M.P., Sanz-Clemente, A. and Roche, K.W. (2015) Dynamic regulation of N-methyl-d-aspartate (NMDA) and α-Amino-3-hydroxy-5-methyl-4-isoxazolepropionic acid (AMPA) receptors by posttranslational modifications. *J. Biol. Chem.*, **290**, 28596–28603.

23. Perszyk, R.E., Swanger, S.A., Shelley, C., Khatri, A., Fernandez-Cuervo, G., Epplin, M.P., Zhang, J., Le, P., Bülow, P., Garnier-Amblard, E. *et al.* (2020) Biased modulators of NMDA receptors control channel opening and ion selectivity. *Nat. Chem. Biol.*, **16**, 188–196.

24. Soto, D., Olivella, M., Grau, C., Armstrong, J., Alcon, C., Gasull, X., Santos-Gómez, A., Locubiche, S., de Salazar, M.G., García-Díaz, R. *et al.* (2019) L-serine dietary supplementation is associated with clinical improvement of loss-of-function GRIN2B-related pediatric encephalopathy. *Sci. Signal.*, **12**, eaaw0936.

25. Tezuka, T., Umemori, H., Akiyama, T., Nakanishi, S. and Yamamoto, T. (1999) PSD-95 promotes Fyn-mediated tyrosine phosphorylation of the N-methyl-D-aspartate receptor subunit NR2A. *Proc. Natl. Acad. Sci. U. S. A.*, **96**, 435–440.

26. Taniguchi, S., Nakazawa, T., Tanimura, A., Kiyama, Y., Tezuka, T., Watabe, A.M., Katayama, N., Yokoyama, K., Inoue, T., Izumi-Nakaseko, H. *et al.* (2009) Involvement of NMDAR2A tyrosine phosphorylation in depression-related behaviour. *EMBO J.*, **28**, 3717–3729.

27. Barria, A. and Malinow, R. (2002) Subunit-specific NMDA receptor trafficking to synapses. *Neuron*, **35**, 345–353.

28. Grau, C., Arató, K., Fernández-Fernández, J.M., Valderrama, A., Sindreu, C., Fillat, C., Ferrer, I., la Luna de, S. and Altafaj, X. (2014) DYRK1A-mediated phosphorylation of GluN2A at Ser (1048) regulates the surface expression and channel activity of GluN1/GluN2A receptors. *Front. Cell. Neurosci.*, **8**, 331.

DATABASES

Human Mutation   HGVS   WILEY

GRIN database: A unified and manually curated repertoire of GRIN variants

Adrián García-Recio[1,2] | Ana Santos-Gómez[1,3] | David Soto[3,4] |
Natalia Julia-Palacios[5] | Àngels García-Cazorla[5] | Xavier Altafaj[1,3] |
Mireia Olivella[6,7] ⓘ

[1]Bellvitge Biomedical Research Institute (IDIBELL), L'Hospitalet de Llobregat, Barcelona, Spain

[2]Laboratori de Medicina Computacional, Unitat de Bioestadística, Facultat de Medicina, Universitat Autònoma de Barcelona, Bellaterra, Spain

[3]Neurophysiology Laboratory, Department of Biomedicine, Institute of Neurosciences, Faculty of Medicine and Health Sciences, University of Barcelona, Barcelona, Spain

[4]August Pi i Sunyer Biomedical Research Institute (IDIBAPS), Hospital Clínic, University of Barcelona, Barcelona, Spain

[5]Neurometabolic Unit, Department of Neurology, Hospital Sant Joan de Déu and CIBERER, Barcelona, Spain

[6]School of International Studies, ESCI-UPF, Barcelona, Spain

[7]Bioinfomatics and Medical Statistics Group, University of Vic–Central University of Catalonia, Vic, Spain

Correspondence
Xavier Altafaj, PhD, Bellvitge Biomedical Research Institute (IDIBELL), L'Hospitalet de Llobregat, 08908 Barcelona, Spain.
Email: xaltafaj@ub.edu

Mireia Olivella, PhD, School of International Studies, ESCI-UPF, 08003 Barcelona, Spain.
Email: mireia.olivella@uvic.cat

Abstract

Glutamatergic neurotransmission is crucial for brain development, wiring neuronal function, and synaptic plasticity mechanisms. Recent genetic studies showed the existence of autosomal dominant de novo GRIN gene variants associated with GRIN-related disorders (GRDs), a rare pediatric neurological disorder caused by N-methyl-D-aspartate receptor (NMDAR) dysfunction. Notwithstanding, GRIN variants identification is exponentially growing and their clinical, genetic, and functional annotations remain highly fragmented, representing a bottleneck in GRD patient's stratification. To shorten the gap between GRIN variant identification and patient stratification, we present the GRIN database (GRINdb), a publicly available, non-redundant, updated, and curated database gathering all available genetic, functional, and clinical data from more than 4000 GRIN variants. The manually curated GRINdb outputs on a web server, allowing query and retrieval of reported GRIN variants, and thus representing a fast and reliable bioinformatics resource for molecular clinical advice. Furthermore, the comprehensive mapping of GRIN variants' genetic and clinical information along NMDAR structure revealed important differences in GRIN variants' pathogenicity and clinical phenotypes, shedding light on GRIN-specific fingerprints. Overall, the GRINdb and web server is a resource for molecular stratification of GRIN variants, delivering clinical and investigational insights into GRDs. GRINdb is accessible at http://lmc.uab.es/grindb.

KEYWORDS
disease-associated mutations, epilepsy, intellectual disability, NMDA receptors

1 | INTRODUCTION

N-methyl-D-aspartate receptors (NMDARs) are ligand-gated ion channels mediating excitatory neurotransmission (Paoletti et al., 2013). Neuronal signaling via the NMDAR plays important roles in brain development, wiring, and high cognitive and motor functions, among others (Traynelis et al., 2010). NMDARs are heterotetramers mostly composed of the assembly of two glycine/D-serine-binding GluN1 subunits (encoded by GRIN1 gene) and two glutamate-binding subunits GluN2A/GluN2B (encoded by GRIN2A and GRIN2B genes, respectively; Flores-Soto & Chaparro-Huerta, 2012). In addition to the predominantly expressed GluN1, GluN2A, and GluN2B subunits, NMDARs can also have the presence of GluN2C, GluN2D, GluN3A, and/or GluN3B subunits at particular developmental stages and in precise neuronal subtypes. For proper neuronal function and brain connectivity, NMDAR heteromeric channels require a precise spatio–temporal expression pattern, in an NMDAR heteromer-dependent manner. Functionally, the NMDAR acts as a coincident detector responding to sustained glutamate release. Following NMDAR activation, NMDAR-mediated calcium influx activates signaling cascades, leading to neuronal responses. Besides neurotransmitter-mediated regulation, the molecular composition of the NMDAR is critical for NMDAR-mediated neurotransmission.

The structure of NMDAR has been recently determined (Karakas & Furukawa, 2014; Lee et al., 2014; Tajima et al., 2016) and showed a topological organization of this receptor into four functionally related domains. The extracellular amino-terminal and ligand-binding domains (ATD and LBD, respectively) are mechanically linked to the transmembrane domain (TMD) that constitutes the pore of the channel, and a cytoplasmic carboxy-terminal domain (CTD) with no determined structure. Functionally, the NMDAR acts as a coincident detector of postsynaptic membrane depolarization (removing Mg^{2+} blockade) and glutamate release. In this context, the simultaneous binding of NMDAR coagonists (glutamate and glycine/D-serine) is mechanically transduced, allowing the channel pore opening and Na^+ and Ca^{2+} influx (Mayer et al., 1984; Nowak et al., 1984). In addition to the subunit composition, which determines NMDAR intrinsic biophysical properties, the receptor activity is regulated by small ions and molecules, such as protons, zinc, spermine (Paoletti et al., 2013), membrane lipids (Korinek et al., 2015), and proteins, involved in posttranslational modifications (Lussier et al., 2015) and protein–protein interactions (Frank & Grant, 2017).

As aforementioned, NMDAR-mediated signaling is crucial for fundamental neuronal processes. Concomitantly, the dysregulation of the NMDAR function can cause synaptic dysfunction and disturb neuronal activity, which ultimately can lead to neurological conditions. Less than 10 years ago, the initial genetic reports describing the association between de novo mutations of GRIN genes associated and neurological disorders were released (de Ligt et al., 2012; O'Roak et al., 2011; Tarabeux et al., 2011). Since then, third-generation deep sequencing has accelerated the identification of novel GRIN variants in individuals affected by neurodevelopmental and psychiatric disorders and allowed to initiate pioneer studies toward the delineation of a clinical spectrum genetically defined as GRIN-related disorders (GRDs; Burnashev & Szepetowski, 2015; Lemke et al., 2014, 2016; Lesca et al., 2013; Platzer et al., 2017). GRDs are a group of rare neurological disorders (Lemke, 2020) with a genetic etiology, namely de novo GRIN mutation (with almost exclusively autosomal dominant inheritance pattern), a primary cause of NMDAR-mediated dysfunction of excitatory neurotransmission. Clinically, GRDs' clinical spectrum includes intellectual disability, epilepsy, movement disorders, development delay, autism spectrum disorder, and schizophrenia, among others.

In addition to genetic data, several functional studies have been conducted to characterize the direct impact of de novo GRIN variants gene products on NMDAR biogenesis and activity. Altogether, genetic and functional studies showed the need to stratify disease-associated GRIN variants and dichotomically dissect those functionally, causing either a gain-of-function (GoF) or a loss-of-function (LoF). This stratification, as well as gene-dependent functional and clinical outcomes definition, is critical to define precise NMDARs functional rescue, ultimately leading to GRDs personalized medicine, a clinical and investigational priority. Therapeutic approaches for GRDs have focused on the potential use of direct NMDAR modulators, potentially counteracting either GoF or LoF GRIN variants effects on NMDARs, for example, reducing or potentiating NMDARs activity, respectively. Regarding GRIN-GoF variants, the FDA-approved drug memantine (low-affinity NMDAR antagonist) has been evaluated for GRD associated with GRIN-GoF variants (Ogden et al., 2017; Pierson et al., 2014; Platzer et al., 2017). Similarly, radiprodil (GluN2B selective negative allosteric modulator) has been recently evaluated and constitutes a promising drug for the treatment of NMDARs containing GluN2B GoF mutations (Auvin et al., 2020; Mullier et al., 2017). The potential rescue of GRIN LoF variants has also been evaluated in preclinical and clinical studies, using both NMDARs orthosteric and allosteric modulators. In this line, a pilot clinical study showed that L-serine (precursor of D-serine, endogenous NMDAR coagonist) dietary supplement results in a clinical improvement in a patient harboring a GRIN2B LoF variant (Soto et al., 2019).

As for many rare conditions with a genetic origin, GRD translational research shows a gap between growing genetic data (e.g., GRIN variants identification) and their evaluation toward functional stratification and therapeutic approaches evaluation. Further, GRIN variants genetic, clinical, and functional data are highly fragmented, redundant, and show certain inconsistencies, making both clinical and genetic advice arduous. In this scenario, we have developed the GRIN database (GRINdb), a clinical and investigational resource, with more than 4000 unique GRIN variants that constitute the largest public repository of GRIN variants and related data. More importantly, GRINdb provides a unique, nonredundant, curated, and updated GRIN variants database. Together with the genetic data, GRINdb delivers all available functional and clinical annotations of the GRIN variant of interest, which, in turn, might accelerate the patient's stratification and therapeutic decisions. Further, GRINdb allowed delineating important differences in GRIN pathogenesis and clinical phenotypes, shedding light on GRIN-specific fingerprints and GRDs' pathophysiology.

2 | METHODS

2.1 | GRINdb

For GRINdb creation, all available *GRIN* variants information (gene, nucleotide change, amino acid position, mutated amino acid, pathogenicity, clinical information, and functional annotations) were retrieved from the following sources: ClinVar (only pathogenic and likely pathogenic variants), LOVD (https://www.lovd.nl), Uniprot Database (UniProt Consortium, 2019), GnomAD (Karczewski & Francioli, 2017), "GRIN-Leipzig" (http://www.grin-database.de), CFERV (http://functionalvariants.emory.edu/database/), and BCN-GRIN (http://lmc.uab.es/grindb/) and from previously published data. The genetic information was used to classify the variants into the following categories: missense, truncating (nonsense, frameshift), and others (amino acid insertions and deletions, large DNA duplications, deletions and translocations, and chromosomal aberration). The amino acid position was used to locate the mutation into the corresponding topological domain (see Table S1 for domain positions), with the TMD positions assigned according to OPM Database (Lomize et al., 2012). Finally, redundant entries (identical *GRIN* variant) were unified under the same entry, while keeping clinical- and functional-associated information.

2.2 | GRIN variants data curation and functional classification

Based on genetic, clinical, and functional data, *GRIN* variants pathogenicity was classified as "Disease-associated," "Neutral," or "Uncertain pathogenicity," according to the following criteria. *GRIN* variants with reported functional alterations (LoF/GoF) were classified as disease-associated, while those not affecting NMDAR activity were classified as neutral variants. For *GRIN* variants devoid of functional annotations, their pathogenicity was defined according to the associated genetic and clinical data. *GRIN* variants associated with neurological disorders (ClinVar, LOVD, GRIN-Leipzig, BCN-GRIN, and CFERV *GRIN* variants with associated phenotypes) were classified as "Disease-associated," while those variants exclusively reported in the GnomAD database were considered as neutral. Finally, *GRIN* variants with conflicting annotations (e.g., described as disease-associated and neutral variants in different databases) were classified as variants of uncertain pathogenicity.

In addition to pathogenic categories, the available functional information was manually curated and used for *GRIN* variants functional stratification into "loss-of-function" (LoF), "gain-of-function" (GoF), "Complex," or "Not affected" categories. *GRIN* variants impact on receptor biogenesis (surface expression of mutant NMDARs) and biophysical changes (electrophysiological properties of mutant NMDARs) allowed to define LoF variants, based on the presence of a reduction of surface expression and/or reduced NMDAR-mediated currents resulting from diminished ion channel conductance, open probability, agonist(s) affinity(ies), and desensitization and/or deactivation rates. On the contrary, *GRIN* variants were annotated as GoF when the

surface expression was increased and/or NMDAR-mediated currents were increased as a result of changes in the gating/affinity properties mentioned previously. *GRIN* variants exhibiting both LoF- and GoF-associated changes were classified as "Complex" variants of uncertain functional classification, while those with not showing functional alterations in heterologous cell systems were defined as "Not affected." Based on our recent findings (Santos-Gómez et al., 2020), *GRIN2A* and *GRIN2B* protein-truncating variants of the ATD, LBD, and TMD were classified as LoF variants. Thus, the classification of variants as GoF, LoF, or complex was entirely based on experimental information and not in a prediction algorithm.

2.3 | Phenotypes associated with GRIN variants

The available clinical information allowed to group *GRIN* variants phenotypic traits into the following phenotype categories: intellectual disability, developmental delay, epilepsy, schizophrenia, autism spectrum disorders, attention-deficit and hyperactivity disorder, cortical visual impairment, hypotonia, speech disorder, movement disorders, and microcephaly. While all these phenotypes categories were automatically retrieved from available clinical information on reference databases and research articles, "epilepsy" phenotype category was grouping epilepsies and epileptic syndromes, such as epilepsy with continuous spike and wave during sleep, benign childhood epilepsy with centro-temporal spikes, Landau–Kleffner syndrome of childhood, focal epilepsy, and discrete epileptic seizures.

2.4 | NMDA receptor molecular model

A molecular model for the triheteromeric NMDA receptor (GluN1)2-GluN2A-GluN2B was generated from 4PE5 X-ray crystal structure (Karakas & Furukawa, 2014). Modeller 9.20 (Webb & Sali, 2016) was used to model the lacking regions of the receptor and Scwrl4 (Krivov et al., 2009) to position the nondetermined side chains. The initial model was energy-minimized using GROMACS 5 (Hess et al., 2008). The CTDs were not modeled, as there is no available determined structure. Pathogenesis and functional annotations for all *GRIN* variants with available information were mapped on the NMDA receptor structural model using Pymol 2 (DeLano, 2002).

2.5 | Web server

GRINdb is a freely available web application tool relying on Python 3.6.6 backend with Flask 1.0.2 framework (http://flask.pocoo.org). Python scripts monthly access data from ClinVar, LOVD, Uniprot, GnomAD, CFERV, GRIN-Leipzig, and BCN-GRINdbs. All data are stored in a MySQL database. The NMDAR molecular model containing the query *GRIN* variant is shown with an NGL Viewer (Rose & Hildebrand, 2015), allowing an interactive rotation in the *x/y/z* axes, together with zoom options (Rose & Hildebrand, 2015).

TABLE 1 Summary of variants in *GRIN* database

	GRIN1	GRIN2A	GRIN2B	GRIN2C	GRIN2D	GRIN3A	GRIN3B	Total
Missense	313	803	592	602	364	596	738	4008
Truncations	22	57	54	43	17	26	74	293
Others	12	14	12	20	11	6	37	112
Total	347	874	658	665	392	628	849	4413

Note: GRIN variants collected from ClinVar, SwissVar, GnomAD, GRIN-Leipzig, CFERV, and BCN-GRIN and bibliography including missense, truncating (nonsense, frameshift), and other variants (amino acid insertions and deletions, large DNA insertions, deletions and translocations, and chromosomal aberration).

3 | RESULTS AND DISCUSSION

3.1 | GRINdb

The increasing number of identified *GRIN* genetic variants associated with neurological and psychiatric disorders deals with high fragmentation and redundancy of the corresponding data, which is split into several databases and research articles. We have constructed GRINdb, a unified, manually curated, nonredundant, and updated database containing all available genetic, clinical, functional, and structural information on *GRIN* variants. GRINdb currently contains 4415 unique *GRIN* variants (May 2020), classified into different genetic categories: 4008 missense variants, 295 protein-truncating variants (frameshift, nonsense, splice site), and 112 other variants (duplications, deletions, translocations; see Table 1). The database can be freely accessed at http://lmc.uab.es/grindb/grindbdata.

3.2 | GRINdb web server

To provide a user-friendly computational tool to retrieve all available information for the *GRIN* variant of interest, we have developed the GRINdb Web Server (http://lmc.uab.es/grindb/). In this *GRIN* variants explorer, the user is invited to introduce the gene name (*GRIN1, GRIN2A, GRIN2B, GRIN2C, GRIN2D, GRIN3A, GRIN3B*) and amino acid position as a query input. Optionally, the user can also select the mutated amino acid (in three- or one-letter code), for missense variants. Following *GRIN* variant query, *GRIN* web server explores GRINdb and retrieves—upon data availability—all associated functional and clinical data: reference database, mutation domain, and category (missense, truncation, other), as well as available functional annotations and clinical information with the corresponding bibliographic references (PubMed links). Classification into GoF/LoF/Complex, phenotype categories, and pathogenicity (disease-associated, neutral, and uncertain association to disease) is also shown (see Section 2). This descriptive information is completed with a molecular model of the NMDAR showing the topological location of the mutated amino acid, displayed with an interactive NGL Viewer (Rose & Hildebrand, 2015; see Figure 1).

3.3 | GRIN variants and disease association

The integration of functional and clinical information (disease-associated or neutral *GRIN* variants) into GRINdb was used to provide the first comprehensive analysis of *GRIN* variant-related pathogenesis. To this end, we analyzed the association of *GRIN* variants with neurological conditions and classified them in three different categories. Disease-associated *GRIN* variants are *GRIN* variants unequivocally associated with GRD, with an autosomal dominant pattern and GRD clinical symptoms described. On the contrary, those *GRIN* variants described as genetic polymorphisms (neutral variants present in gnomAD and/or no functional changes associated) were considered as neutral. The third category of *GRIN* variants is constituted by those genetic variants with contradictory annotations facing the autosomal dominant inheritance pattern described in GRD and was thus classified as *GRIN* variants of uncertain pathogenicity (Table 2). Further, functional data and clinical phenotypes analysis of all collected *GRIN* missense variants (4008, scattered along the seven members of the *GRIN* gene family) revealed striking gene-dependent pathogenicity association. Interestingly, *GRIN1*, *GRIN2A*, and *GRIN2B* genes (encoding for GluN subunits, most widely expressed in excitatory neurons (Paoletti et al., 2013) present a significant percentage of variants associated with disease (ranging from 14.2% to 23.6%). Contrastingly, *GRIN2C, GRIN2D, GRIN3A,* and *GRIN3B* (encoding for GluN subunits expressed in specific excitatory neuron subpopulations; Paoletti et al., 2013) association with pathogenicity is scarce (from 0.2% to 2.5%), with 17 missense disease-associated variants that are randomly located across all domains. Interestingly, following database integration and curation, the originally reported 118 initial total disease-associated variants were reduced to 26, suggesting that genetic variation of *GRIN2C, GRIN2D, GRIN3A,* and *GRIN3B* genes could be more tolerated and less prone to cause neurological phenotypes. *GRIN1, GRIN2A,* and *GRIN2B* genes pathogenicity were further analyzed toward the potential identification of GluN1, GluN2A, and GluN2B domains differential sensitivity to amino acid variation (Figure 2 and Table S2).

Among *GRIN* genes most prevalently associated with the disease, *GRIN1* presents the lowest number of reported *GRIN* variants (313 *GRIN1* vs. 803 and 592 variants, for *GRIN1, GRIN2A,* and *GRIN2B,* respectively) but the highest percentage of disease-associated variants (23.6%). On the contrary, *GRIN2A* presents the highest number
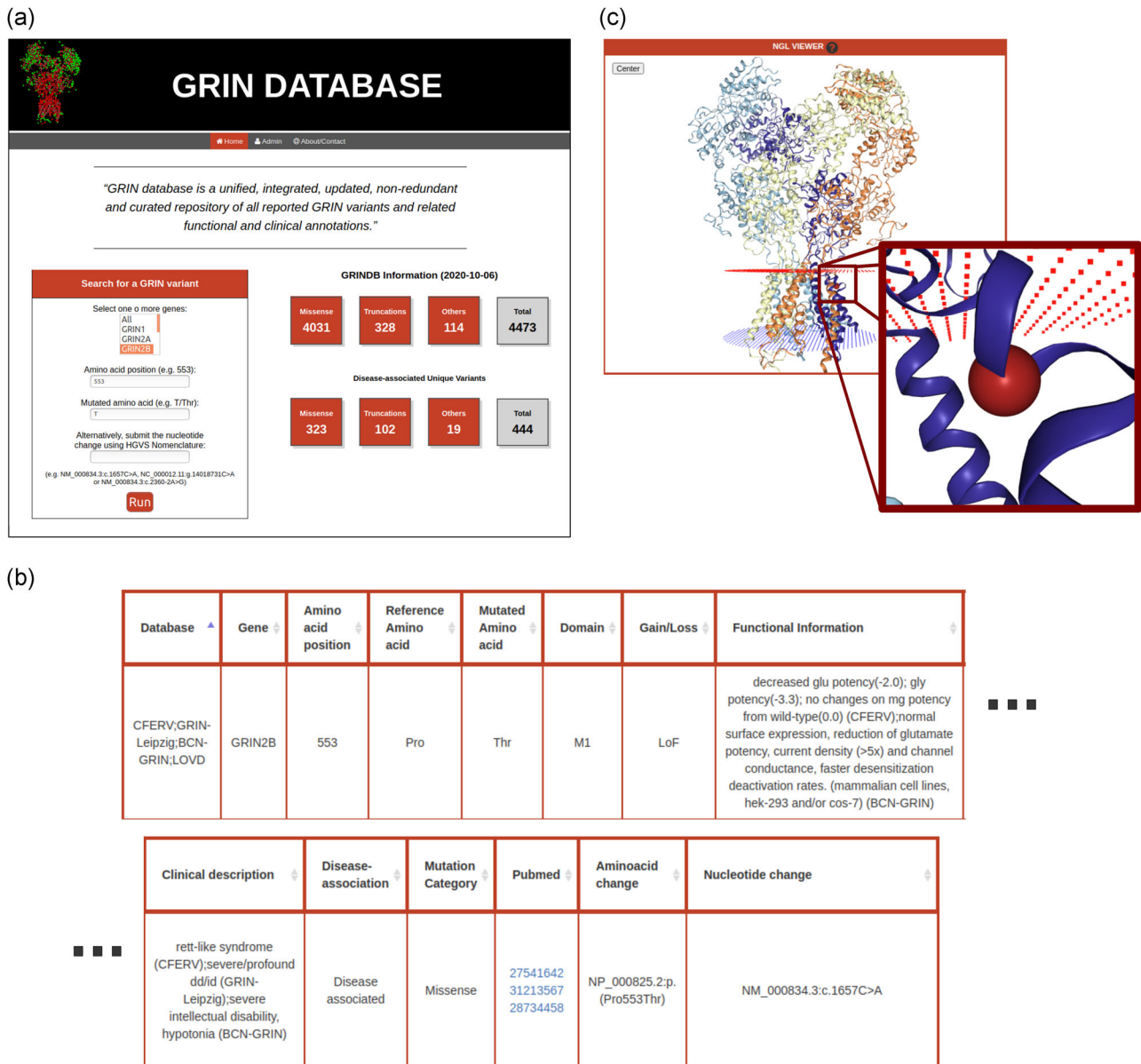
FIGURE 1 GRIN database web server example of use. (a) Input: the user can search for a specific *GRIN* variant (gene, amino acid position, and mutated amino acid); (b) output: the corresponding genetic, clinical, and functional information is displayed. (c) Additionally, the mutated amino acid is mapped on the *N*-methyl-D-aspartate receptor structural model with an NGL Viewer 2015. Variant GRIN2B Pro553Thr (NP_000825.2:p.Pro553Thr) has been used as an example. By integrating the fragmented information collected from databases and research articles, the variant can finally be annotated as loss-of-function (LoF) and the corresponding clinical phenotype is displayed

TABLE 2 Summary of *GRIN* missense variants classification into disease-association categories

	GRIN1	GRIN2A	GRIN2B	GRIN2C	GRIN2D	GRIN3A	GRIN3B	Total
Associated with disease	74 (23.6%)	114 (14.2%)	111 (18.8%)	4 (0.7%)	9 (2.5%)	1 (0.2%)	3 (0.4%)	316
Neutral	222 (71.0%)	647 (80.5%)	445 (75.2%)	575 (95.5%)	347 (95.3%)	573 (96.1%)	704 (95.4%)	3513
Uncertain	17 (5.4%)	42 (5.2%)	36 (6.0%)	23 (3.8%)	8 (2.2%)	22 (3.7%)	31 (4.2%)	179
Total missense	313	803	592	602	364	596	738	4008

Note: Functional and clinical data of *GRIN* variants allowed their classification into variants with disease association, neutral, or with uncertain pathogenesis (see Section 2 for additional information on the criteria used for variants pathogenesis classification).

(a)

(b)   (c)
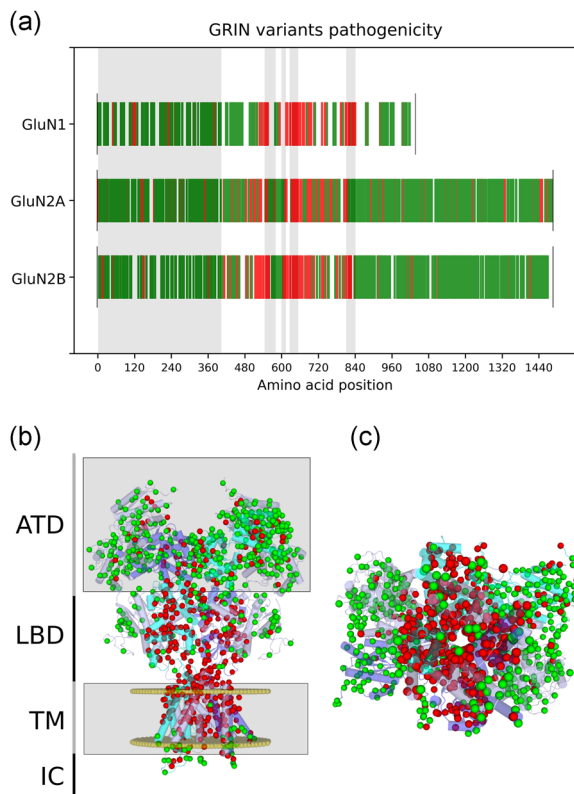
FIGURE 2 *GRIN* variants pathogenicity. (a) Scatter plot representing *GRIN1*, *GRIN2A*, and *GRIN2B* variants' disease association and distribution along the GluN1, GluN2A, and GluN2B protein sequence. Spikes undefined color code: disease-associated GRIN variants in red; not associated with disease in green; no reported variant in white. Juxtaposed topological domains are represented in alternate colors (amino-terminal domain [ATD], M1, M2, M3, and M4 highlighted in gray) and the protein termination with a black spike. (b) *GRIN1*, *GRIN2A*, and *GRIN2B* variants pathogenicity mapped on the structural model of the trihetromeric (GluN1)2-GluN2A/GluN2B NMDA receptor. Lateral view of the structural model of the NMDAR, composed of two GluN1 (pale blue), one GluN2A (cyan), and one GluN2B (purple) subunits. Note the high density of disease-associated *GRIN* variants in the ligand-binding domain (LBD) and transmembrane domain (TMD). (c) Molecular model of the *N*-methyl-D-aspartate receptor (cytosolic side view). The pore channel and the GluN subunit interfaces are highly pathogenic. A position is considered as associated with disease (in red) if at least one disease-associated mutation is found. Neutral variants (in green) are those not reported as disease-associated; TM, transmembrane

of variants, but the lowest percentage of disease-associated variants (14.2%), suggesting a differential tolerance of *GRIN* genes in front of genetic variation, with a *GRIN1* > *GRIN2B* > *GRIN2A* pathogenicity scaling.

Topologically, the majority (about 80%) of *GRIN1*, *GRIN2A*, and *GRIN2B* disease-associated variants are located within TMD and LBD (see Figure 2 and Table S2). This result is in accordance with previous reports compiling the data from around 100 *GRIN* variants (Amin et al., 2020; XiangWei et al., 2018). This differential domain sensitivity is exhibited by all GluN subunits, in line with the high

TABLE 3 Functional annotation of *GRIN1*, *GRIN2A*, and *GRIN2B* variants

	GRIN1	*GRIN2A*	*GRIN2B*
GoF variants	13 (39.4%)	23 (42.5%)	16 (25.4%)
LoF variants	20 (60.6%)	31 (57.4%)	47 (74.6%)
Variants with functional annotation	33 (44.6%)	54 (47.3%)	63 (56.8%)
Variants with no functional annotation	41 (55.4%)	60 (52.6%)	48 (43.2%)
Total	74	114	111

Note: Percentages are shown over reported annotations. Half of the *GRIN* variants contain a functional annotation, and LoF variants are more frequent than GoF variants.

Abbreviations: GoF, gain-of-function; LoF, loss-of-function.

(a)

(b)   (c)
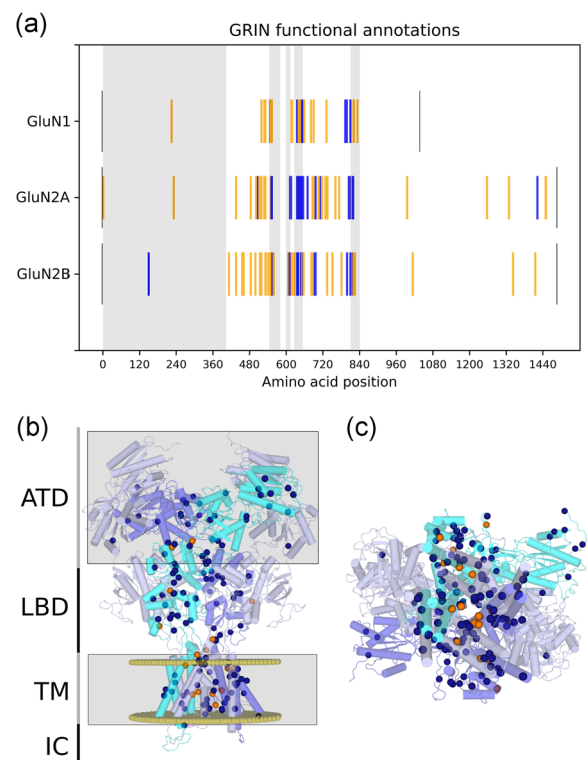
FIGURE 3 *GRIN* variants functional annotations. (a) *GRIN1*, *GRIN2A*, and *GRIN2B* variants functional annotations along the GluN1, GluN2A, and GluN2B sequence (proteins are limited by gray lines). Disease-associated GRIN missense variants causing a loss-of-function are represented by orange lines in the corresponding amino acid position, while GoF variants are represented in blue lines. The domains ATD, M1, M2, M3, and M4 are highlighted in gray. (b) *GRIN1*, *GRIN2A*, and *GRIN2B* variants functional annotations mapped on the structural model of the *N*-methyl-D-aspartate (NMDA) receptor. The structural molecular model is composed of two GluN1 (pale blue), one GluN2A (cyan), and one GluN2B (purple) subunits. LBD and TM domains concentrate most of the disease-associated variants. (c) NMDA receptor molecular model view from the cytosolic side. GoF mutations are mainly around the magnesium-binding site at the pore channel. ATD, amino-terminal domain; GoF, gain-of-function; IC, intracellular; LBD, ligand-binding domain

phylogenetic conservation degree and structural constraints of the NMDAR channel pore. A more detailed analysis of *GRIN* disease-associated variants distribution along NMDAR subdomains revealed several hotspots. These subdomains highly vulnerable to genetic variance correspond to functionally crucial elements of the NMDARs, namely the agonist/coagonist binding pockets (LBD), the inner side of NMDAR channel pore, and the interface between GluN subunits in accordance with the rolling motion between subunits that is necessary to activate the receptor (Esmenjaud et al., 2019). Conversely, the ATD presents a low association with neurological conditions, with occasional disease-associated variants located close to positive and negative allosteric binding sites. These sites are involved in NMDAR channel activity fine-tuning (Zhu et al., 2016), controlling NMDAR open probability and deactivation rate (Gielen et al., 2009; Yuan et al., 2009). Similarly, the CTD domains of GluN1, GluN2A, and GluN2B present a reduced number of disease-associated variants, suggesting that these intracellular domains are mainly neutral. Noteworthy, the presence of inherited *GRIN* variants within the CTD, both in asymptomatic carriers and in GRD individuals, was suggestive of a recessive inheritance pattern, potentially acting as a risk factor of complex disorders.

3.4 | GRIN variants stratification and NMDAR dysfunction

Recently, several efforts have been conducted toward the evaluation of potential GRD therapies, aiming to rescue NMDAR dysfunctions in a personalized manner. While memantine (Ogden et al., 2017; Pierson et al., 2014; Platzer et al., 2017) and radiprodil (Auvin et al., 2020;

Mullier et al., 2017) have been prescribed for patients with *GRIN1* and *GRIN2B* GoF variants, respectively, the L-serine dietary supplement has been investigated in a single individual harboring a *GRIN2B* LoF variant (Soto et al., 2019). Nevertheless, before the therapeutic intervention, the functional annotation of the *GRIN* variant of interest is compulsory and constitutes the bottleneck in patient stratification and personalized therapies. Indeed, the molecular phenotyping of *GRIN* variants is a time-consuming process that can be shortened by the use of already existing data. Unfortunately, these data are spread among databases and the literature, together with data duplication and/or conflicting annotations, making their retrieval and interpretation difficult. To accelerate *GRIN* variants annotation and patient stratification, GRINdb offers a curated repertoire of available *GRIN* variants functional annotations.

GRINdb analysis showed that disease-associated *GRIN1*, *GRIN2A*, and *GRIN2B* variants are similarly functionally annotated (44.6%, 47.3%, and 56.8%, respectively), with a higher number of LoF variants compared with GoF variants (Table 3). Importantly, GRIN variants mapping revealed no specific association between functional alterations (GoF or LoF) and topological domains, with the exception of a certain enrichment of GoF variants location at the Mg^{2+}-binding site at the transmembrane pore channel (see Figure 3 and Table S3). The analysis of *GRIN* variants functional annotations revealed striking fingerprints of both LoF and GoF disease-associated variants. LoF variants mostly result from a decrease of NMDAR surface expression and/or a reduction of charge transfer across the mutant NMDAR. In contrast, *GRIN*-GoF variants are frequently associated with the presence of the following alterations, either individually or combined: reduction or abolishment of magnesium blockade, increase of agonist(s) potency(ies), and decrease of deactivation rate.

TABLE 4 Clinical phenotypes of disease-associated *GRIN1*, *GRIN2A*, and *GRIN2B* variants

	GRIN1			GRIN2A			GRIN2B		
	GoF	LoF	Total	GoF	LoF	Total	GoF	LoF	Total
Reported phenotypes	7	16	56	18	26	99	12	40	91
Autism spectrum disorder	0	6% (1)	18% (10)	0	4% (1)	6% (6)	0	40% (16)	29% (26)
Cortical visual impairment	57% (4)	19% (3)	25% (14)	0	0	0	42% (5)	3% (1)	7% (6)
Developmental delay	86% (6)	81% (13)	71% (40)	83% (15)	46% (12)	38% (38)	100% (12)	75% (30)	68% (62)
Epilepsy (ECSWS, FE, BECTS, LKS)	57% (4)	56% (9)	57% (32)	83% (15)	100% (26)	89% (88)	83% (10)	40% (16)	47% (43)
Hypotonia	43% (3)	38% (6)	30% (17)	11% (2)	4% (1)	3% (3)	8% (1)	38% (15)	21% (19)
Intellectual disability	71% (5)	100% (16)	82% (46)	89% (16)	46% (12)	49% (49)	100% (12)	100% (40)	93% (85)
Microcephaly	0	6% (1)	4% (2)	0	0	1% (1)	50% (6)	8% (3)	14% (13)
Movement disorder	0	31% (5)	13% (7)	6% (1)	0	1% (1)	0	13% (5)	9% (8)
Schizophrenia	0	0	5% (3)	0	0	4% (4)	0	5% (2)	5% (5)
Speech disorder	0	19% (3)	7% (4)	50% (9)	73% (19)	57% (56)	0	0	0

Note: Percentages are shown over reported clinical phenotypes. Also, note that the clinical phenotypes are subunit- and GoF/LoF-dependent.
Abbreviations: BECTS, benign childhood epilepsy with centro-temporal spikes; ECSWS, epilepsy with continuous spike and wave during sleep; FE, focal epilepsy; GoF, gain-of-function; LKS, Landau–Kleffner syndrome of childhood; LoF, loss-of-function.

Clinical phenotypes
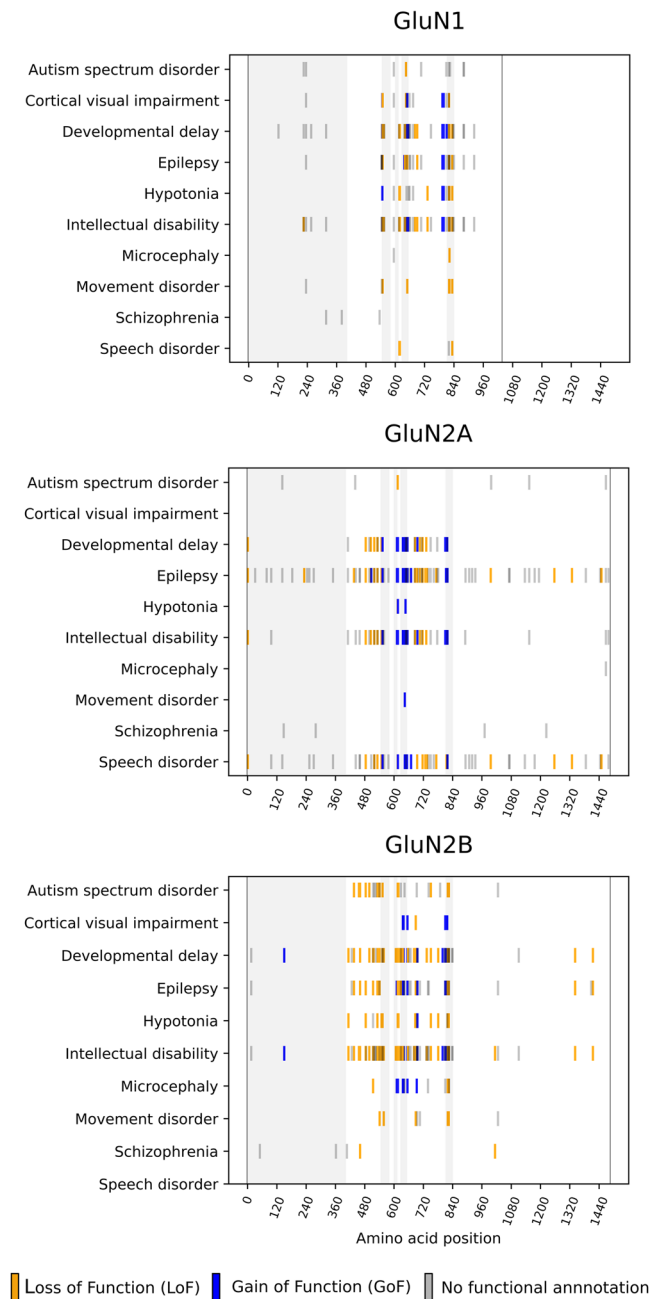
FIGURE 4 GRIN variants clinical phenotypes. Scatter plot of *GRIN1*, *GRIN2A*, and *GRIN2B* loss-of-function (LoF) and gain-of-function (GoF) genetic variants associated with clinical phenotypes. The spikes represent disease-associated GRIN variants (LoF, orange spike; GoF, blue spike) distribution along GluN1, GluN2A, and GluN2B proteins (GluN protein terminus, black spike). The domains ATD, M1, M2, M3, and M4 are highlighted in gray. Note that the clinical phenotypes are subunit- and GoF/LoF-dependent

Noteworthy, along with this analysis, we noticed a nonsystematic analysis of NMDAR surface expression. As this aspect is crucial to determine the overall functional outcome of *GRIN* GoF, these incomplete (pending) variant annotations were indicated as GoF(P) in GRINdb.

3.5 | GRIN variants clinical phenotypes analysis

Following GRINdb construction, *GRIN* variants-associated clinical phenotypes were compiled toward the delineation of the GRDs' clinical spectrum and the exploration of putative genotype- and domain-specific clinical symptoms. Further analysis of the most prevalent GRD-associated *GRIN* genes (*GRIN1*, *GRIN2A*, and *GRIN2B*) showed that disease-associated *GRIN1* variants are generally clinically manifested by developmental delay (71%), intellectual disability (82%), and epilepsy (57%), although the scarce clinical data hampered the determination of putative clinical phenotypes correlation with *GRIN* variants GoF/LoF functional categories (Table 4 and Figure 4).

GRINdb analysis showed that *GRIN2A* variants are almost invariably associated with epilepsy (89%), with frequent speech disturbance (57%) and, to less extent, intellectual disability (49%) and developmental delay (38%). Importantly, intellectual disability and development delay are more frequently associated with *GRIN2A* GoF variants (89% and 83%, respectively) than with *GRIN2A* LoF variants (46% in both cases), while speech disorder is more frequently associated with *GRIN2A* LoF variants, compared with *GRIN2A* GoF variants (73% vs. 50%). Interestingly, the domain-based analysis showed a strong presence of speech disorders in individuals harboring *GRIN2A* variants affecting the ATD. Genotype–phenotype analysis showed that ATD is the less vulnerable domain of GluN subunits, suggesting that speech disorder might not be recorded in databases for those individuals with severe developmental delay and/or intellectual disability.

Regarding *GRIN2B*, disease-associated missense mutations are almost invariably associated with intellectual disability (93%) and development delay (68%). The occurrence of epilepsy is variable (47%) and more frequently associated with GoF than with LoF variants (83% vs. 40%). GRINdb analysis also showed that *GRIN2B* variants are frequently associated with the presence of autism spectrum disorders phenotypic traits in *GRIN2B* LoF but not *GRIN2B* GoF variants (40% vs. 0%). *GRIN2B* variants functional alterations were also associated with additional clinical traits, such as hypotonia (38% in LoF vs. 8% in GoF *GRIN2B* variants) and microcephaly (0% in LoF vs. 50% in GoF *GRIN2B* variants).

4 | CONCLUSIONS

The GRINdb research resource constitutes an updated, manually curated, and nonredundant database comprising genetic, clinical, functional, and structural information of the largest repertoire of *GRIN* variants, with more than 4400 unique *GRIN* variants entries. From a clinical angle, the comprehensive data compiled in the GRINdb represents a valuable bioinformatic resource shortening the gap between the growing number of *GRIN* variants identification (resulting from the implementation of deep genomic sequencing data in the clinical practice) and patient stratification. Noteworthy, the query of individual *GRIN* variants throughout the *GRIN* web server

provides important molecular diagnosis insights of *GRIN* variants' functional outcomes (disease-association and functional annotation, e.g., GoF/LoF), which is compulsory for GRD personalized medicine.

The analysis of more than 4000 missense *GRIN* variants sheds light on the pathogenesis map almost completely covering GluN subunits amino acid positions, revealing their weighted association with neurological conditions in a gene-, subunit- and region-dependent manner. For *GRIN1*, *GRIN2A*, and *GRIN2B* genes, around 18% of its variants are disease-associated and mainly concentrated in the LBDs and TMDs. Contrastingly, reported *GRIN2C*, *GRIN2D*, *GRIN3A*, and *GRIN3B* variants have a very limited association with neurological conditions. Indeed, about 95% of the reported missense variants affecting these genes are neutral. Further, the variants of these genes are homogeneously distributed across all domains, in contrast to *GRIN1*, *GRIN2A* and *GRIN2B* mutations hotspots present in the agonist-binding domain and the channel pore. In summary, these association studies suggest that although the variants affecting these genes could be involved in complex neurological diseases (schizophrenia, attention deficit hyperactivity disorder), the majority of the variants are neutral and not disease-causing. This reduced vulnerability is indicative of a weaker pathophysiological impact on glutamatergic neurotransmission-related processes, which might result from their intrinsic spatio–temporal expression patterns (restrained to a small set of glutamatergic synapses), a putative functional redundancy with other gene products and/or asymptomatic conditions. Despite the pathogenic map of *GRIN* variants being extensive, the functional annotations are still fragmented. Indeed, about half of disease-associated *GRIN* variants lack functional annotation and concomitantly their classification into LoF or GoF remains elusive. In the context of GRD, this annotation is essential toward patient stratification and personalized medicine (e.g., positive or negative allosteric modulators and subunit specificity) and thus further efforts are required to achieve this critical task.

The number of reported phenotypes brings the opportunity to characterize the clinical phenotype and suggests that clinical phenotype is subunit-, domain- and LoF/GoF-dependent. In addition, the clinical phenotypes are in accordance with *GRIN* protein-truncating variants-associated clinical phenotypes, which represent a paradigmatic genetic condition of NMDAR LoF (Santos-Gómez et al., 2020). However, GRINdb data analysis presents some intrinsic limitations resulting from the partial functional annotations of *GRIN* variants and the heterogeneous and not comprehensive clinical description of GRD individuals. Therefore, there is an urgent need to fully report the clinical phenotypes of each domain in each subunit and according to LoF and GoF and to homogenize and extensively assess the clinical phenotypes of GRD individuals. This would lead to delineate GRD genetic and functional determinants, as well as defining GRD patient stratification and prognosis.

The enrichment of the database with new *GRIN* variants, which is daily growing, will allow to also improve the predictive model of *GRIN* pathogenesis and clinical phenotype and the effect of disease-associated variants on receptor structure and function, thus shortening even more the gap between variant identification and personalized medicine.

CONFLICT OF INTERESTS
The authors declare that there are no conflict of interests.

AUTHOR CONTRIBUTIONS
Xavier Altafaj, Mireia Olivella, and David Soto designed the study. Adrián García-Recio generated GRINdb. Natalia Julia-Palacios and Àngels García-Cazorla curated the clinical data. Xavier Altafaj and Ana Santos-Gómez curated the functional annotations. Mireia Olivella and Adrián García-Recio compiled and analyzed genetic, functional, and clinical information. Xavier Altafaj and Mireia Olivella wrote the manuscript that was proofread by all authors.

DATA AVAILABILITY STATEMENT
The data that support the findings of this study are openly available at http://lmc.uab.es/grindb/grindbdata and the database is accessible at http://lmc.uab.es/grindb.

WEB RESOURCES
The following web resources were used: ClinVar (https://www.ncbi.nlm.nih.gov/clinvar/), LOVD (https://www.lovd.nl), Uniprot Database (https://www.uniprot.org), GnomAD (https://gnomad.broadinstitute.org), GRIN-Leipzig (http://www.grin-database.de), and CFERV (http://functionalvariants.emory.edu/database/).

ORCID
Mireia Olivella https://orcid.org/0000-0002-6035-3399

REFERENCES
Amin, J. B., Moody, G. R., & Wollmuth, L. P. (2020). From bedside-to-bench: What disease-associated variants are teaching us about the NMDA receptor. *The Journal of Physiology*. Advance online publication. https://doi.org/10.1113/JP278705

Auvin, S., Dozières-Puyravel, B., Avbersek, A., Sciberras, D., Collier, J., Leclercq, K., Mares, P., Kaminski, R. M., & Muglia, P. (2020). Radiprodil, a NR2B negative allosteric modulator, from bench to

bedside in infantile spasm syndrome. *Annals of Clinical and Translational Neurology*, 7(3), 343–352.

Burnashev, N., & Szepetowski, P. (2015). NMDA receptor subunit mutations in neurodevelopmental disorders. *Current Opinion in Pharmacology*, 20, 73–82.

DeLano, W. L. (2002). PyMOL: An open-source molecular graphics tool. *CCP4 Newsletter on Protein Crystallography*, 40(1), 82–92.

de Ligt, J., Willemsen, M. H., van Bon, B. W. M., Kleefstra, T., Yntema, H. G., Kroes, T., Vulto-Van Silfhout, A. T., Koolen, D. A., de Vries, P., Gilissen, C., del Rosario, M., Hoischen, A., Scheffer, H., de Vries, B. B. A., Brunner, H. G., Veltman, J. A., & Vissers, L. E. L. M. (2012). Diagnostic exome sequencing in persons with severe intellectual disability. *The New England Journal of Medicine*, 367(20), 1921–1929.

Esmenjaud, J.-B., Stroebel, D., Chan, K., Grand, T., David, M., Wollmuth, L. P., Taly, A., & Paoletti, P. (2019). An inter-dimer allosteric switch controls NMDA receptor activity. *The EMBO Journal*, 38(2):e99894. https://doi.org/10.15252/embj.201899894

Flores-Soto, M. E., Chaparro-Huerta, V., Escoto-Delgadillo, M., Vazquez-Valls, E., González-Castañeda, R. E., & Beas-Zarateaf, C. (2012). Structure and function of NMDA-type glutamate receptor subunits. *Neurología (English)*, 27, 301–310. https://www.sciencedirect.com/science/article/pii/S2173580812000739

Frank, R. A., & Grant, S. G. (2017). Supramolecular organization of NMDA receptors and the postsynaptic density. *Current Opinion in Neurobiology*, 45, 139–147.

Gielen, M., Siegler Retchless, B., Mony, L., Johnson, J. W., & Paoletti, P. (2009). Mechanism of differential control of NMDA receptor activity by NR2 subunits. *Nature*, 459(7247), 703–707.

Hess, B., Kutzner, C., van der Spoel, D., & Lindahl, E. (2008). GROMACS 4: Algorithms for highly efficient, load-balanced, and scalable molecular simulation. *Journal of Chemical Theory and Computation*, 4(3), 435–447.

Karakas, E., & Furukawa, H. (2014). Crystal structure of a heterotetrameric NMDA receptor ion channel. *Science*, 344(6187), 992–997.

Karczewski, K., & Francioli, L. (2017). The Genome Aggregation Database (gnomAD). *MacArthur Lab*. https://ibg.colorado.edu/cdrom2019/nealeB/Gnomad/boulder_190307.pdf

Korinek, M., Vyklicky, V., Borovska, J., Lichnerova, K., Kaniakova, M., Krausova, B., Krusek, J., Balik, A., Smejkalova, T., Horak, M., & Vyklicky, L. (2015). Cholesterol modulates open probability and desensitization of NMDA receptors. *The Journal of Physiology*, 593(10), 2279–2293.

Krivov, G. G., Shapovalov, M. V., Dunbrack, R. L., Jr. (2009). Improved prediction of protein side-chain conformations with SCWRL4. *Proteins*, 77(4), 778–795.

Lee, C.-H., Lü, W., Michel, J. C., Goehring, A., Du, J., Song, X., & Gouaux, E. (2014). NMDA receptor structures reveal subunit arrangement and pore architecture. *Nature*, 511(7508), 191–197.

Lemke, J. R. (2020). Predicting incidences of neurodevelopmental disorders. *Brain: A Journal of Neurology*, 143(4), 1046–1048.

Lemke, J. R., Geider, K., Helbig, K. L., Heyne, H. O., Schütz, H., Hentschel, J., Courage, C., Depienne, C., Nava, C., Heron, D., Møller, R. S., Hjalgrim, H., Lal, D., Neubauer, B. A., Nürnberg, P., Thiele, H., Kurlemann, G., Arnold, G. L., Bhambhani, V., ... Syrbe, S. (2016). Delineating the GRIN1 phenotypic spectrum: A distinct genetic NMDA receptor encephalopathy. *Neurology*, 86(23), 2171–2178.

Lemke, J. R., Hendrick, R., Geider, K., Laube, B., Schwake, M., Harvey, R. J., James, V. M., Pepler, A., Steiner, I., Hörtnagel, K., Neidhardt, J., Ruf, S., Wolff, M., Bartholdi, D., Caraballo, R., Platzer, K., Suls, A., De Jonghe, P., Biskup, S., & Weckhuysen, S. (2014). GRIN2B mutations in West syndrome and intellectual disability with focal epilepsy. *Annals of Neurology*, 75(1), 147–154.

Lesca, G., Rudolf, G., Bruneau, N., Lozovaya, N., Labalme, A., Boutry-Kryza, N., Salmi, M., Tsintsadze, T., Addis, L., Motte, J., Wright, S., Tsintsadze, V., Michel, A., Doummar, D., Lascelles, K., Strug, L., Waters, P., de Bellescize, J., Vrielynck, P., ... Szepetowski, P. (2013). GRIN2A mutations in acquired epileptic aphasia and related childhood focal epilepsies and encephalopathies with speech and language dysfunction. *Nature Genetics*, 45(9), 1061–1066.

Lomize, M. A., Pogozheva, I. D., Joo, H., Mosberg, H. I., & Lomize, A. L. (2012). OPM database and PPM web server: Resources for positioning of proteins in membranes. *Nucleic Acids Research*, 40(Database issue), D370–D376.

Lussier, M. P., Sanz-Clemente, A., & Roche, K. W. (2015). Dynamic regulation of *N*-methyl-D-aspartate (NMDA) and α-amino-3-hydroxy-5-methyl-4-isoxazolepropionic acid (AMPA) receptors by posttranslational modifications. *The Journal of Biological Chemistry*, 290(48), 28596–28603.

Mayer, M. L., Westbrook, G. L., & Guthrie, P. B. (1984). Voltage-dependent block by Mg^{2+} of NMDA responses in spinal cord neurones. *Nature*, 309(5965), 261–263.

Mullier, B., Wolff, C., Sands, Z. A., Ghisdal, P., Muglia, P., Kaminski, R. M., & André, V. M. (2017). GRIN2B gain of function mutations are sensitive to radiprodil, a negative allosteric modulator of GluN2B-containing NMDA receptors. *Neuropharmacology*, 123, 322–331.

Nowak, L., Bregestovski, P., Ascher, P., Herbet, A., & Prochiantz, A. (1984). Magnesium gates glutamate-activated channels in mouse central neurones. *Nature*, 307(5950), 462–465.

O'Roak, B. J., Deriziotis, P., Lee, C., Vives, L., Schwartz, J. J., Girirajan, S., Karakoc, E., MacKenzie, A. P., Ng, S. B., Baker, C., Rieder, M. J., Nickerson, D. A., Bernier, R., Fisher, S. E., Shendure, J., & Eichler, E. E. (2011). Exome sequencing in sporadic autism spectrum disorders identifies severe de novo mutations. *Nature Genetics*, 43(6), 585–589.

Ogden, K. K., Chen, W., Swanger, S. A., McDaniel, M. J., Fan, L. Z., Hu, C., Tankovic, A., Kusumoto, H., Kosobucki, G. J., Schulien, A. J., Su, Z., Pecha, J., Bhattacharya, S., Petrovski, S., Cohen, A. E., Aizenman, E., Traynelis, S. F., & Yuan, H. (2017). Molecular mechanism of disease-associated mutations in the Pre-M1 helix of NMDA receptors and potential rescue pharmacology. *PLOS Genetics*, 13(1), e1006536.

Paoletti, P., Bellone, C., & Zhou, Q. (2013). NMDA receptor subunit diversity: Impact on receptor properties, synaptic plasticity and disease. *Nature Reviews Neuroscience*, 14(6), 383–400.

Pierson, T. M., Yuan, H., Marsh, E. D., Fuentes-Fajardo, K., Adams, D. R., Markello, T., Simeonov, D. R., Holloman, C., Tankovic, A., Karamchandani, M. M., Schreiber, J. M., Mullikin, J. C., Tifft, C. J., Toro, C., Boerkoel, C. F., Traynelis, S. F., & Gahl, W. A. (2014). GRIN2A mutation and early-onset epileptic encephalopathy: Personalized therapy with memantine. *Annals of Clinical and Translational Neurology*, 1(3), 190–198.

Platzer, K., Yuan, H., Schütz, H., Winschel, A., Chen, W., Hu, C., Kusumoto, H., Heyne, H. O., Helbig, K. L., Tang, S., Willing, M. C., Tinkle, B. T., Adams, D. J., Depienne, C., Keren, B., Mignot, C., Frengen, E., Strømme, P., Biskup, S., ... Lemke, J. R. (2017). GRIN2B encephalopathy: Novel findings on phenotype, variant clustering, functional consequences and treatment aspects. *Journal of Medical Genetics*, 54(7), 460–470.

Rose, A. S., & Hildebrand, P. W. (2015). NGL Viewer: A web application for molecular visualization. *Nucleic Acids Research*, 43(W1), W576–W579.

Santos-Gómez, A., Miguez-Cabello, F., García-Recio, A., Locubiche, S., García-Díaz, R., Soto, V., Guerrero-López, R., Juliá-Palacios, N., Ciruela, F., García-Cazorla, À., Soto, D., Olivella, M., & Altafaj, X. (2020). Disease-associated GRIN protein truncating variants trigger NMDA receptor loss-of-function. *Human Molecular Genetics*. Advance online publication. https://doi.org/10.1093/hmg/ddaa220

Soto, D., Olivella, M., Grau, C., Armstrong, J., Alcon, C., Gasull, X., Santos-Gómez, A., Locubiche, S., Gómez de Salazar, M., García-Díaz, R., Gratacòs-Batlle, E., Ramos-Vicente, D., Chu-Van, E., Colsch, B., Fernández-Dueñas, V., Ciruela, F., Bayés, À., Sindreu, C., López-Sala, A., … Altafaj, X. (2019). L-Serine dietary supplementation is associated with clinical improvement of loss-of-function GRIN2B-related pediatric encephalopathy. *Science Signaling*, 12(586), eaaw0936. https://doi.org/10.1126/scisignal.aaw0936

Tajima, N., Karakas, E., Grant, T., Simorowski, N., Diaz-Avalos, R., Grigorieff, N., & Furukawa, H. (2016). GluN1b-GluN2B NMDA receptor structure in non-active-2 conformation. https://doi.org/10.2210/pdb5fxi/pdb

Tarabeux, J., Kebir, O., Gauthier, J., Hamdan, F. F., Xiong, L., Piton, A., Spiegelman, D., Henrion, É., Millet, B., Fathalli, F., Joober, R., Rapoport, J. L., DeLisi, L. E., Fombonne, É., Mottron, L., Forget-Dubois, N., Boivin, M., Michaud, J. L., Drapeau, P., … Krebs, M. O. (2011). Rare mutations in *N*-methyl-D-aspartate glutamate receptors in autism spectrum disorders and schizophrenia. *Translational Psychiatry*, 1, e55.

Traynelis, S. F., Wollmuth, L. P., McBain, C. J., Menniti, F. S., Vance, K. M., Ogden, K. K., Hansen, K. B., Yuan, H., Myers, S. J., & Dingledine, R. (2010). Glutamate receptor ion channels: Structure, regulation, and function. *Pharmacological Reviews*, 62(3), 405–496.

UniProt Consortium. (2019). UniProt: A worldwide hub of protein knowledge. *Nucleic Acids Research*, 47(D1), D506–D515.

Webb, B., & Sali, A. (2016). Comparative protein structure modeling using MODELLER. *Current Protocols in Protein Science*, 86, 2.9.1–2. 9.37.

XiangWei, W., Jiang, Y., & Yuan, H. (2018). De novo mutations and rare variants occurring in NMDA receptors. *Current Opinion in Physiology*, 2, 27–35.

Yuan, H., Hansen, K. B., Vance, K. M., Ogden, K. K., & Traynelis, S. F. (2009). Control of NMDA receptor function by the NR2 subunit amino-terminal domain. *The Journal of Neuroscience: The Official Journal of the Society for Neuroscience*, 29(39), 12045–12058.

Zhu, S., Stein, R. A., Yoshioka, C., Lee, C.-H., Goehring, A., Mchaourab, H. S., & Gouaux, E. (2016). Mechanism of NMDA receptor inhibition and activation. *Cell*, 165(3), 704–714.

SUPPORTING INFORMATION

Additional Supporting Information may be found online in the supporting information tab for this article.

How to cite this article: García-Recio A, Santos-Gómez A, Soto D, et al. *GRIN* database: A unified and manually curated repertoire of *GRIN* variants. *Human Mutation*. 2020;1–11. https://doi.org/10.1002/humu.24141

2.

Supplementary tables

GRIN1 disease-associated variants

GRIN variant	Type of variant	Domain	Clinical description	Functional impact
V27G	Missense	ATD	NA	NA
R217W	Missense	ATD	Severe ID, movement disorder, autism, epilepsy, language problems, sleep problems, constipation	Increased Zn^{2+} inhibition
D227H	Missense	ATD	ID, autism, language problems, stereotypies, hypotonia, brain alterations	NA
R306Q	Missense	ATD	NA	NA
A349T	Missense	ATD	Schizophrenia	NA
A370T	Missense	ATD	Schizophrenia	NA
R397S	Missense	ATD	NA	NA
P532H	Missense	LBD	NA	NA
S549G	Missense	LBD-TM	NA	NA
S549R	Missense	LBD-TM	Epilepsy, severe ID, movement disorder, seizures	NA
L551P	Missense	LBD-TM	DD, stereotypies, epilepsy, hypotonia	
D552E	Missense	LBD-TM	ID, epilepsy, movement disorder, seizures, CVI, myoclonus, oculogyric crises, chorea, dyskinesia, stereotypies, brain alterations, quadriplegia	Reduced current amplitude, reduced surface expression, reduced glutamate and glycine potency
S553L	Missense	LBD-TM	Polymicrogyria, DD, hypotonia	NA
Q556*	Nonsense	LBD-TM	Severe epileptic encephalopathy	NA
P557R	Missense	LBD-TM	ID, epilepsy	Reduced current amplitude, reduced surface expression
S560dup	Indel	LBD-TM	Severe ID, hypotonia, partial epilepsy, CVI, seizures	Reduced current amplitude
G618R	Missense	TM	DD, ID, hypotonia, language alterations	Reduced current amplitude
G620R	Missense	TM	DD, ID, hypotonia, dysmorphism, language alterations, behavior alterations, stereotypies	Enhanced proton inhibition, decreased Mg^{2+} blockade, reduced current amplitude, decreased glutamate potency, decreased glycine potency, decreased Ca^{2+} permeability
G638A	Missense	TM	NA	NA
G638V	Missense	TM	NA	NA
M641I	Missense	TM	Epilepsy, severe ID, movement disorder, seizures, stereotypies, sleep problems, brain alterations	NA
A645S	Missense	TM	Epilepsy, severe ID, CVI, seizures	NA
Y647C	Missense	TM	NA	Increased glutamate potency, increased glycine potency, increased Mg^{2+} blockade,
Y647S	Missense	TM	Spasms, DD, severe ID, epilepsy, hypotonia, seizures	Reduced current amplitude
N650I	Missense	TM	DD, epilepsy, hypotonia	NA
N650K	Missense	TM	Epilepsy, severe ID, movement disorder, seizures, feeding problems, dyskinesia, stereotypies, chorea, sleep problems, brain alterations	NA
A653G	Missense	TM	NA	NA
R659W	Missense	TM	Polymicrogyria, DD, microcephaly, CVI, epilepsy	Increased glutamate potency, increased glycine potency
E662K	Missense	TM	Mild-moderate ID	Increased current amplitude
N674I	Missense	LBD	Polymicrogyria, DD, microcephaly, CVI, epilepsy, hypotonia	Reduced glycine potency, reduced proton inhibition

S688Y	Missense	LBD	Encephalopathy, DD, hypotonia, oculogyric-like movements	Reduced glycine affinity, decreased Ca^{2+} permeability, slow desensitization and reduced surface expression in GluN3A-containing receptors
M706V	Missense	LBD	NA	NA
D789N	Missense	LBD	Polymicrogyria, DD, microcephaly, CVI, epilepsy, hypotonia, language problems	Reduced current amplitude
R794Q	Missense	LBD	Polymicrogyria, DD, microcephaly, CVI, epilepsy, hypotonia	Increased glutamate potency, increased glycine potency
A814D	Missense	TM	NA	NA
G815R	Missense	TM	Epilepsy, severe ID, movement disorder, CVI, seizures, oculogyric crises, myoclonus, chorea, brain alterations	Reduced current amplitude, reduced glutamate potency
G815V	Missense	TM	ID, movement disorder, seizures	NA
F817L	Missense	TM	Severe ID, movement disorder	Reduced current amplitude
G827R	Missense	TM	Epilepsy, severe ID, DD, movement disorder, encephalopathy, hypotonia, oculogyric-like movements, seizures	Unstable structure and assembly
R844C	Missense	CTD	Epilepsy, severe ID, movement disorder, seizures	NA

Supplementary table 1. Summary list of *GRIN1* reported variants accompanied by a description of the type of variant (missense, frameshift/nonsense, nonsense, indel), the associated clinical symptoms and functional annotation (from: Hamdan FF. et al, 2011; Burnashev N. et al., 2015; Ohba C. et al., 2015; Lemke JR. et al., 2016; Chen W. et al., 2017; Odgen KK. Et al., 2017; Rossi M. et al., 2017; Xu XX. and Luo J-H, 2017; Zehavi Y. et al., 2017; Fry AE. et al., 2018; Yu Y. et al., 2018; Li J. et al., 2019; Skrenkova K. et al., 2020; Amin JB. et al., 2021). Abbreviations: ID, intellectual disability; DD, developmental delay; CVI, cortical visual impairment; ATD, amino-terminal domain; LBD, ligand-binding domain; TMD, transmembrane domain; CTD, carboxy-terminal domain; NA, not available. Splice-site variants are not included.

GRIN2A disease-associated variants

GRIN variant	Type of variant	Domain	Clinical description	Functional impact
M1T	Missense	ATD	LKS, ID	NA
P31Sfs*107	Frameshift/nonsense	ATD	RE	NA
P31T	Missense	ATD	Epilepsy	NA
W55*	Nonsense	ATD	NA	NA
P79R	Missense	ATD	CSWS, RE, ID, ADHD, seizures	Reduced Zn^{2+} inhibition, reduced surface expression, reduced current amplitude, reduced glutamate potency, reduced glycine potency
P140A	Missense	ATD	Schizophrenia	NA
T141M	Missense	ATD	Epilepsy	NA
T143I	Missense	ATD	NA	NA
A149V	Missense	ATD	Schizophrenia	NA
Q163*	Nonsense	ATD	NA	NA
F183I	Missense	ATD	RE, cognitive problems	NA
I184S	Missense	ATD	CSWS, aphasia, ID	Reduced current amplitude, increased activation and deactivation time, reduced surface expression
T189N	Missense	ATD	NA	NA
W198*	Nonsense	ATD	Partial epilepsy, ID, hypotonia, language problems, seizures	NA
Q218*	Nonsense	ATD	Mild-moderate ID, seizures, epilepsy, hypotonia	NA
C231R	Missense	ATD	Partial epilepsy	NA

C231Y	Missense	ATD	LKS, ID, language problems, hypotonia	Reduced surface expression, reduced current amplitude, reduced glutamate potency, reduced glycine potency
A243V	Missense	ATD	RE, learning difficulties	Reduced Zn^{2+} inhibition
A290V	Missense	ATD	RE	NA
G295S	Missense	ATD	RE	NA
L334*	Nonsense	ATD	CSWS, ID, motor problems, language problems	NA
P336S	Missense	ATD	NA	NA
K346*	Nonsense	ATD	ID, DD, hypotonia	NA
R370W	Missense	ATD	RE	Increased Zn^{2+} inhibition
C436R	Missense	LBD	Partial epilepsy, DD, language problems, seizures	Reduced surface expression, reduced current amplitude, increased glutamate potency, reduced glycine potency
K441N	Missense	LBD	Autism	NA
N447K	Missense	LBD	RE	Increased current amplitude, increased glutamate potency, decreased Mg^{2+} blockade
V452M	Missense	LBD	Schizophrenia, seizures	Increased glutamate potency
C455Y	Missense	LBD	Partial epilepsy	NA
G483R	Missense	LBD	CSWS, RE, aphasia, ID, seizures	Reduced glutamate potency, reduced glycine potency, reduced current amplitude, reduced surface expression, faster deactivation
R504W	Missense	LBD	CSWS, aphasia, ADHD, ID	Reduced surface expression, slow deactivation
V506A	Missense	LBD	Focal seizures	Increased glutamate potency, increased surface expression
R518C	Missense	LBD	NA	NA
R518H	Missense	LBD	CSWS, LKS, RE, seizures, apraxia, ID	Reduced current amplitude, increased activation and deactivation time, reduced surface expression, increased open time, reduced close time
P522R	Missense	LBD	NA	NA
F528Gfs*22	Frameshift/nonsense	LBD	CSWS, seizures,	NA
V529Wfs*22	Frameshift/nonsense	LBD	Epilepsy, RE, mild ID	NA
T531M	Missense	LBD	CSWS, ID, language problems, seizures	Increased open state, reduced current amplitude
S538*	Nonsense	LBD	ID, DD, dysarthria, ataxia, seizures	NA
S545L	Missense	LBD-TM	NA	NA
S547del	Indel	LBD-TM	CSWS, partial epilepsy, ID	NA
A548T	Missense	LBD-TM	LKS, seizures, ID, ADHD, language problems	Reduced current amplitude, reduced glutamate potency, reduced glycine potency
P552R	Missense	LBD-TM	Seizures, severe ID, language alterations, DD, gray matter reduction	Slow rise time, slow deactivation, increased glutamate and glycine potency, increased mean open time, increased Zn^{2+} inhibition
A555T	Missense	LBD-TM	NA	NA
R586K	Missense	LBD-TM	Encephalopathy	NA
K590N	Missense	LBD-TM	Autism	NA
W606*	Nonsense	TM	Partial epilepsy, seizures	NA
L611Q	Missense	TM	Epilepsy, DD, ID	Increased glutamate potency, reduced proton inhibition, decreased Mg^{2+} blockade, reduced conductance
N614S	Missense	TM	Epilepsy, DD, ID, autism and language alterations, seizures	Increased glutamate potency, reduced proton inhibition, reduced current amplitude

N615K	Missense	TM	Severe ID, DD, autism, language alterations, epilepsy, seizures, hypotonia, spasms, myoclonus, dysmorphism	Loss of Mg^{2+} blockade and decreased Ca^{2+} permeability, increased glutamate potency, reduced conductance
A643D	Missense	TM	DD, moderate ID, language problems, dystonia, dyskinesia, strabismus, sleep problems	Increased glutamate potency, increased glycine potency, reduced Mg^{2+} blockade, reduced proton inhibition, reduced Zn^{2+} inhibition, decreased current amplitude
S644G	Missense	TM	Epilepsy, language alterations	Enhanced glutamate potency, slow deactivation
T646A	Missense	TM	Epilepsy, seizures, spasms, myoclonus	NA
L649V	Missense	TM	Seizures, severe ID, aphasia, feeding alterations, dysmorphism, hypothyroidism	NA
F652V	Missense	TM	CSWS, autism	Increased open time and decreased close time
K669N	Missense	LBD	CSWS, seizures	Increased glutamate potency, increased glycine potency, slower deactivation
G760S	Missense	LBD	LKS	NA
R681*	Nonsense	LBD	LKS, ID, partial epilepsy, language problems, ADHD	NA
V685G	Missense	LBD	Severe epilepsy, DD	Reduced current amplitude, reduced glutamate potency, reduced surface expression, faster deactivation
I694T	Missense	LBD	LKS, seizures, language problems	Reduced current amplitude, reduced glutamate potency, reduced surface expression, reduced open probability
Y698*	Nonsense	LBD	Language problems, ID, epileptic encephalopathy	NA
P699S	Missense	LBD	RE	Increased glutamate potency, reduced surface expression
M705V	Missense	LBD	RE, seizures, language problems	Reduced glutamate potency, reduced glycine potency, reduced surface expression, reduced open probability
E714K	Missense	LBD	CSWS	Reduced surface expression
A716T	Missense	LBD	RE, apraxia, LKS, hypotonia, motor alterations, ID, seizures, ADHD	Reduced glutamate potency, reduced surface expression, faster deactivation
G723S	Missense	LBD	NA	NA
A727T	Missense	LBD	RE	Reduced glutamate potency, reduced surface expression, reduced open probability
D731N	Missense	LBD	RE, LKS, apraxia, DD, hypotonia, seizures, ID, motor alterations	Reduced glutamate potency, reduced glycine potency, increased Zn^{2+} inhibition, increased proton inhibition, reduced current amplitude, fast deactivation, decreased open probability, reduced surface expression
V734L	Missense	LBD	RE	Reduced glutamate potency, fast deactivation
T749I	Missense	LBD	NA	NA
K772E	Missense	LBD	Partial epilepsy, ID	Reduced glutamate potency, reduced current amplitude, reduced surface expression
D776Y	Missense	LBD	ID	NA

L779Sfs*5	Frameshift/nonsense	LBD	CSWS, epilepsy	NA
E803*	Nonsense	LBD-TM	LKS, seizures	NA
L812M	Missense	LBD-TM	Epilepsy, DD, ID, motor alterations, seizures, hypotonia, hypertonia, myoclonus, brain alterations	Increased open probability, increased glutamate potency, increased glycine potency, decreased Zn^{2+} inhibition, reduced proton inhibition, reduced Mg^{2+} blockade, slow deactivation
I814T	Missense	LBD-TM	RE	NA
M817T	Missense	TM	NA	NA
M817V	Missense	TM	Seizures, DD	Increased glutamate potency, increased glycine potency, decreased Zn^{2+} inhibition, reduced proton inhibition, reduced Mg^{2+} blockade
I840F	Missense	CTD	Autism	NA
V865G	Missense	CTD	Seizures	NA
I876T	Missense	CTD	Epilepsy, autism	NA
D884N	Missense	CTD	Schizophrenia	NA
I904F	Missense	CTD	RE, cognitive problems	NA
A922V	Missense	CTD	NA	NA
D933N	Missense	CTD	LKS	NA
Y943*	Nonsense	CTD	CSWS	NA
Q964E	Missense	CTD	Schizophrenia	NA
V967L	Missense	CTD	Epilepsy	NA
N976S	Missense	CTD	Partial epilepsy, CSWS	NA
A978T	Missense	CTD	Schizophrenia	NA
V998M	Missense	CTD	NA	NA
V1000M	Missense	CTD	Autism	NA
E1055Q	Missense	CTD	DD, ID, language problems, motor alterations, dystonia, abnormal gait, hyperkinetic movements, brain alterations	NA
T1064A	Missense	CTD	Schizophrenia, epilepsy	NA
N1076K	Missense	CTD	Epilepsy, LKS	NA
H1129R	Missense	CTD	Schizophrenia	NA
R1159P	Missense	CTD	NA	NA
T1229S	Missense	CTD	NA	NA
D1251N	Missense	CTD	RE	NA
A1276G	Missense	CTD	CSWS	NA
I1295T	Missense	CTD	NA	NA
R1376C	Missense	CTD	NA	NA
I1379V	Missense	CTD	Absence epilepsy	NA
D1385Y	Missense	CTD	Partial epilepsy	NA
Y1387*	Nonsense	CTD	CSWS, autism	Removal of phosphorylation site
S1459G	Missense	CTD	Epilepsy	Removal of phosphorylation site, decreased interaction with PSD95 and SNX27, decreased surface expression, decreased spine density and mEPSC frequency

Supplementary table 2. Summary list of *GRIN2A* reported variants accompanied by a description of the type of variant (missense, frameshift/nonsense, nonsense, indel), the associated clinic, and the functional impact (from: Endele S. et al., 2010; Tarabeux J. et al, 2011; Lemke JR. et al., 2013; Lesca G. et al., 2013; Pierson TM. et al., 2014; Yuan H. et al., 2014; Burnashev N. et al, 2015; Serraz B. et al., 2016; Swanger SA. et al., 2016; Addis L. et al., 2017; Gao K. et al., 2017; Odgen KK. Et al., 2017; von Stülpnagel C. et al., 2017; Xu XX. et al., 2017; Xu XX. and Luo J-H, 2017; Yang X. et al., 2017; Fernández-Marmiesse A. et al., 2018; Strehlow V. et al., 2018; XiangWei W. et al., 2018; Yu Y. et al., 2018; Li J. et al., 2019; Marwick KFM. Et al., 2019; Nicotera A. et al., 2019; Amador A. et al., 2020; Li X. et al., 2020; Mora Viera M. et al., 2020; Amin JB. et al., 2021). Abbreviations: ADHD, attention deficit, hyperactivity disorder; ID, intellectual disability; DD, developmental delay; CSWS, continuous spike and wave during sleep; LKS, Landau-Kleffner syndrome; RE, rolandic epilepsy; ATD, amino-terminal domain; LBD, ligand-binding domain; TMD, transmembrane domain; CTD, carboxy-terminal domain ; NA, not available. Splice-site variants and/or chromosomal translocations are not included.

GRIN2B disease-associated variants

GRIN variant	Type of variant	Domain	Clinical description	Functional impact
S34Qfs*25	Frameshift/nonsense	ATD	ID, autism	NA
E47G	Missense	ATD	Epilepsy	NA
I50N	Missense	ATD	NA	NA
V65I	Missense	ATD	Schizophrenia	NA
I150V	Missense	ATD	DD, ID	NA
Q180*	Nonsense	ATD	Moderate ID, seizures	NA
Q217*	Nonsense	ATD	ID, DD	NA
S246*	Nonsense	ATD	Mild ID, DD	NA
T268Sfs*15	Frameshift/nonsense	ATD	Moderate ID, behavior alterations	NA
A271V	Missense	ATD	Schizophrenia	NA
L362M	Missense	ATD	NA	NA
V363Gfs*2	Frameshift/nonsense	ATD	ID, DD	NA
E370K	Missense	ATD	Epilepsy	NA
W373*	Nonsense	ATD	Severe ID, autism, seizures, DD, motor alterations	NA
E413G	Missense	LBD	Severe ID, DD, behavior alterations	Reduced glutamate potency, reduced current amplitude, fast deactivation, reduced surface expression
C436R	Missense	LBD	Epilepsy, ID, autism, seizures	Reduced current amplitude, decreased surface expression
	Missense	LBD	Autism, epilepsy, ID	Enhanced glutamate potency, reduced glycine potency, reduced current amplitude, decreased surface expression
C461F	Missense	LBD	Lennox-Gastaut syndrome, autism, ID, epilepsy	Reduced current amplitude, decreased surface expression, reduced glutamate potency, increased glycine potency, fast deactivation, EPSC with fast decay
G499R	Missense	LBD	Moderate ID, autism	NA
T514A	Missense	LBD	Severe ID, seizures, brain alterations	NA
N516S	Missense	LBD	Mild ID	NA
D524N	Missense	LBD	Autism, ID, epilepsy	NA
F525V	Missense	LBD	Autism, ID	NA
G533D	Missense	LBD	NA	NA
R540H	Missense	LBD	ID, focal epilepsy, autism, seizures	Decreased Mg^{2+} blockade. increased Ca^{2+} permeability, increased glutamate potency, increased glycine potency, decreased surface expression, fast deactivation
S541R	Missense	LBD-TM	Severe ID, autism, seizures, motor alterations	Decreased glutamate potency, decreased glycine potency
P553L	Missense	LBD-TM	Severe ID/DD, hypotonia, language alterations, dysmorphism	Reduced glutamate potency, increased desensitization, reduced EPSC amplitude, EPSC with fast decay, reduced current amplitude
P553T	Missense	LBD-TM	Severe encephalopathy, motor, cognitive and language problems	NA
S555I	Missense	LBD-TM	Severe ID	NA
V558I	Missense	TM	ID	Decreased glutamate potency, increased desensitization, reduced open probability
W559*	Nonsense	TM	Autism, ID	NA
A590T	Missense	TM	ID, ADHD, autism	NA

W607C	Missense	TM	DD, ID, dysmorphism, autism, ADHD	Enhanced proton inhibition, decreased Mg^{2+} blockade, reduced current amplitude, decreased mean open time, reduced open probability, reduced glutamate potency, reduced glycine potency
G611V	Missense	TM	ID, epilepsy, seizures, dysmorphism, ADHD, autism, brain alterations	Reduced current amplitude, decreased mean open time, decreased Mg^{2+} blockade
N615I	Missense	TM	ID, epilepsy, seizures, autism, hypotonia, West syndrome, severe DD, autism, ADHD	Decreased Mg^{2+} blockade, reduced current amplitude, reduced Ca^{2+} permeability, EPSC with fast decay, reduced glutamate potency
N615K	Missense	TM	DD, ID	Decreased Mg^{2+} blockade, reduced current amplitude
N615L	Missense	TM	West syndrome, DD, ID	Decreased Mg^{2+} blockade and increased Ca^{2+} permeability
N616K	Missense	TM	ID, epilepsy, hypertonia, dysmorphism	Increased glutamate potency, decreased Mg^{2+} blockade
V618G	Missense	TM	West syndrome, epilepsy, seizures, ID, hypotonia, severe DD, autism, ADHD	Decreased Mg^{2+} inhibition, increased Ca^{2+} permeability, enhanced proton inhibition, reduced current amplitude, decreased mean open time, reduced open probability, reduced desensitization
V620M	Missense	TM	DD, ID, hypotonia, autism, ADHD	Reduced proton inhibition, decreased Ca^{2+} permeability
S628C	Missense	TM	Severe ID, autism, seizures, DD	NA
S628F	Missense	TM	ID, ADHD, autism, DD, epileptic encephalopathy	Reduced surface expression, reduced current amplitude
A636P	Missense	TM	Mild ID, myoclonus, abnormal EEG, behavior alterations, autism, ADHD	NA
A636V	Missense	TM	Severe ID, ADHD, autism, epilepsy, seizures, CVI, brain alterations	NA
A639V	Missense	TM	Severe ID, ADHD, autism, seizures, CVI, brain alterations	NA
L643P	Missense	TM	DD, motor alterations, language problems, sleep problems, stereotypies, epilepsy,	NA
I655F	Missense	TM	Severe ID, epilepsy, seizures, brain alterations, CVI	Decreased glutamate potency, decreased Mg^{2+} blockade, reduced proton inhibition
Q656*	Nonsense	LBD-TM	Moderate ID, seizures	NA
E657G	Missense	LBD-TM	ID, DD	Reduced current amplitude, increased glutamate potency, reduced glycine potency
Q662P	Missense	LBD	Severe ID, myoclonus, DD, autism, CVI, epilepsy, seizures	NA
D668Y	Missense	LBD	Severe ID, seizures	NA
F671-Q672del	Indel	LBD	West syndrome	NA
R682C	Missense	LBD	Mild/moderate ID, behavior alterations, DD, autism, CVI, epilepsy	Increased glutamate potency, increased glycine potency, slow deactivation
G684E	Missense	LBD	NA	NA
G684R	Missense	LBD	NA	NA
T685P	Missense	LBD	Severe ID, DD, autism, CVI, epilepsy	NA
P687L	Missense	LBD	ID, DD	NA
P687R	Missense	LBD	Severe ID, DD, autism, CVI, epilepsy	NA

G689C	Missense	LBD	Severe DD, brain alterations, language problems, strabismus, constipation, reflux, dyskinesia, hypotonia	Reduced glutamate potency, reduced glycine potency, reduced surface expression, reduced current amplitude, reduced proton inhibition, reduced EPSC time course
G689S	Missense	LBD	Severe ID, DD, autism, CVI, epilepsy, seizures, motor alterations, myoclonus/spasms, brain alterations, language problems, dyskinesia, hypertonia	Reduced glutamate potency, reduced proton inhibition
S690N	Missense	LBD	NA	NA
R693S	Missense	LBD	Severe ID, epilepsy, seizures, brain alterations	NA
I695T	Missense	LBD	Moderate ID	NA
R696H	Missense	LBD	Severe ID, DD, hypotonia, autism, CVI, epilepsy, seizures	Increased glutamate potency, reduced current amplitude, fast deactivation
M706V	Missense	LBD	Severe ID, DD, autism, CVI, epilepsy, seizures	NA
Q711*	Nonsense	LBD	Severe ID, DD, autism, CVI, epilepsy	NA
G724*	Nonsense	LBD	Autism, ID, language problems	Reduced surface expression, increased pruning of dendritic branches
A734V	Missense	LBD	ID, DD	NA
I751T	Missense	LBD	ID, autism, DD	NA
M789K	Missense	LBD	NA	NA
E807K	Missense	LBD-TM	ID, DD	NA
S810N	Missense	LBD-TM	ID, seizures, epilepsy, brain alterations	NA
S810R	Missense	LBD-TM	ID, seizures, brain alterations	Increased glutamate potency, increased glycine potency, reduced proton inhibition
M818L	Missense	TM	ID, DD	NA
M818T	Missense	TM	Seizures, epilepsy, DD, CVI	Increased glutamate potency, increased glycine potency, reduced proton inhibition
A819T	Missense	TM	ID, DD, seizures	Increased glutamate potency, increased glycine potency, reduced proton inhibition
G820A	Missense	TM	ID, DD, epilepsy, dyskinesia, autism, brain alterations	Reduced current amplitude
G820E	Missense	TM	ID, brain alterations	Increased surface expression, reduced current amplitude
G820V	Missense	TM	ID, DD	NA
M824R	Missense	TM	Epilepsy, ID, DD, brain alterations, motor alterations, autism	Reduced current amplitude
L825V	Missense	TM	Autism, ID	Reduced open probability
G826E	Missense	TM	Moderate ID	NA
R847*	Nonsense	CTD	Severe ID, DD, autism	NA
I864Sfs*20	Frameshift/nonsense	CTD	ID, DD	NA
K976del	Indel	CTD	ID, DD	NA
Y1004*	Nonsense	CTD	Moderate ID, autism	NA
F1037L	Missense	CTD	NA	NA
Q1014R	Missense	CTD	NA	NA
G1026S	Missense	CTD	NA	NA
R1111H	Missense	CTD	ID, DD	NA
T1228M	Missense	CTD	NA	NA
A1267S	Missense	CTD	NA	NA
T1273K	Missense	CTD	NA	NA
K1292R	Missense	CTD	NA	NA
K1293R	Missense	CTD	NA	NA
M1331I	Missense	CTD	NA	NA
M1339V	Missense	CTD	NA	NA
M1342R	Missense	CTD	NA	NA

S1415L	Missense	CTD	Autism	Impaired MAGUK binding, reduced surface expression, spines density reduction
L1424F	Missense	CTD	Schizophrenia	Impaired MAGUK binding, slight decrease of glutamate potency
S1446T	Missense	CTD	NA	NA
S1452F	Missense	CTD	Schizophrenia	Impaired MAGUK binding, slight increase of glycine potency

Supplementary table 3. Summary list of *GRIN2B* reported variants accompanied by a description of the type of variant (missense, frameshift/nonsense, nonsense, indel), the associated clinic, and the functional impact (from: Endele S. et al., 2010; Tarabeux J. et al, 2011; Lemke JR. et al., 2013; Burnashev N. et al, 2015; Hu C. et al., 2016; Swanger SA. et al., 2016; Liu S. et al., 2017; Mullier B. et al., 2017; Platzer K. et al., 2017; Xu XX. and Luo J-H, 2017; Fedele L. et al., 2018; Kyriakopoulos P. et al., 2018; Vyklicky V. et al., 2018; Wells G. et al., 2018; XiangWei W. et al., 2018; Li J. et al., 2019; Sceniak MP. et al., 2019; Bahry JA. et al., 2021; Kellner S. et al., 2021; Amin JB. et al., 2021). Abbreviations: ADHD, attention deficit, hyperactivity disorder; ID, intellectual disability; DD, developmental delay; CVI, cortical visual impairment; ATD, amino-terminal domain; LBD, ligand-binding domain; TMD, transmembrane domain; CTD, carboxy-terminal domain; NA, not available. Splice-site variants and/or chromosomal translocations are not included.

3.

Figures and tables index

Figures index

Results

Chapter 1 – Recruitment of patients with GRIN-related disorders and *GRIN* variants annotation

Chapter 2 – Phenotypic assessment of haploinsufficient Grin2b$^{+/-}$ mouse model

Discussion

Tables index